THE RELATIONSHIPS BETWEEN THE VOLUMETRIC DEFORMATION MODULI OF UNSATURATED SOILS

DAVID YIP-FEI HO

1988

UNIVERSITY OF SASKATCHEWAN
Saskatoon, Saskatchewan

THE RELATIONSHIPS BETWEEN THE VOLUMETRIC DEFORMATION MODULI OF UNSATURATED SOILS

A Thesis

Submitted to the Faculty of Graduate Studies and Research

in Partial Fulfilment of the Requirements

For the Degree of

Doctor of Philosophy

in the

Department of Civil Engineering

University of Saskatchewan

Saskatoon, Canada

by

David Yip-Fei Ho

1988

COLLEGE OF
GRADUATE STUDIES
AND RESEARCH
UNIVERSITY OF
SASKATCHEWAN
SASKATOON, CANADA
S7N 0W0

UNIVERSITY OF SASKATCHEWAN
COLLEGE OF GRADUATE STUDIES AND RESEARCH

Saskatoon

CERTIFICATION OF THESIS WORK

We, the undersigned, certify that David Yip-Fei Ho candidate for the degree of Doctor of Philosophy has presented a thesis with the following title: "The Relationships Between the Volumetric Deformation Moduli of Unsaturated Soils". We consider that the thesis is acceptable in form and content, and that a satisfactory knowledge of the field covered by the thesis was demonstrated by the candidate through an oral examination held on December 6, 1988.

External Examiner: Dr. N. R. Morgenstern,
University of Alberta

[redacted]

Internal Examiner:

[redacted]

[redacted] 1988

OFFICE OF THE DEAN
PHONE 306-966-5751
FAX 306-373-6088
TELEX 074-2659

COLLEGE OF
GRADUATE STUDIES
AND RESEARCH
UNIVERSITY OF
SASKATCHEWAN
SASKATOON, CANADA
S7N 0W0

UNIVERSITY OF SASKATCHEWAN
COLLEGE OF GRADUATE STUDIES AND RESEARCH

Saskatoon

RECOMMENDATION FOR THE AWARD OF DOCTOR OF PHILOSOPHY

I hereby certify that David Yip-Fei Ho candidate for the degree of Doctor of Philosophy in the Department of Civil Engineering has met all the requirements for this award.

On behalf of the Advisory Committee, I recommend that the candidate's name go forward to the Faculty of the College of Graduate Studies and Research for award of this degree.

[redacted]

Barry D. McLennan, Ph.D.
Associate Dean

December 6, 1988

BDM/ph

OFFICE OF THE DEAN
PHONE 306-966-5751
FAX 306-373-6088
TELEX 074-2659

ABSTRACT

The International Conference on Soil Mechanics and Foundation Engineering in 1936 was perhaps the first international forum which brought unsaturated soil problems to the attention of geotechnical engineers. Since then, the understanding of unsaturated soil behaviour has been improved considerably. The theory for the volume change and shear strength behaviour of unsaturated soils has now developed to the point of potential application in geotechnical practice. A complete understanding of the volume change behaviour of an unsaturated soil requires a knowledge of volumetric deformation moduli on four state planes. These moduli must be determined in either a direct or indirect manner in order to solve practical problems involving volume change, moisture movement, bearing capacity and slope stability analysis. The measurement of these moduli generally requires modification to conventional laboratory equipment. The solution of unsaturated soil problems would be greatly facilitated if the relationships between the various moduli were known. Then it would be possible for all moduli to be determined by a few established conventional soil tests.

The main objective of this dissertation is to develop and measure the relationships between the various

volume change moduli. The study began with a literature review on the volume change constitutive relations for the soil structure and water phase of an unsaturated soil. Attempts were made to gather information pertinent to the relationships between different moduli. The theory chapter started with an examination of the most acceptable form for the soil structure and water phase constitutive surfaces on both arithmetic and semi-logarithmic scales. Approximate semi-logarithmic constitutive surfaces were then proposed. The geometry of the approximate semi-logarithmic constitutive surfaces is used to relate the moduli associated with a particular phase (i.e., the soil structure or water phase).

When a soil is saturated, the soil structure and water phase moduli with respect to the logarithm of net total stress are related by the relative density, G_s, of the soil. The inter-relationship of the three remaining moduli was then studied. A laboratory test program was designed to obtain experimental data showing the characteristic form of the semi-logarithmic constitutive surfaces on the net total stress and matric suction planes. Two soils, a uniform silt and a glacial till were tested. Specimens were formed by static compaction at half standard Proctor compaction effort with either dry of optimum or at optimum initial water contents. The investigation included specimens being loaded and unloaded under K_o and isotropic

conditions. The results were analyzed and used to evaluate the relationships between the moduli.

The knowledge of four moduli is needed to completely describe the volume change behaviour of an unsaturated soil in a monotonic volume change process. Special tests are required to determine these four moduli in the laboratory. For instance, the one-dimensional or isotropic compression test, the suction and unconfined shrinkage tests are necessary for solving settlement problems.

The use of an approximate semi-logarithmic constitutive surface as a means to relate moduli for the same phase appears to be viable only for the soil structure. The geometry of the approximate soil structure constitutive surfaces is identifiable by two characteristic stress states namely the corrected swelling pressure (i.e., P_s') and the initial stress state translated to the matric suction plane following a constant volume stress path (i.e., $(u_a - u_w)_i^e$). Relationships between soil structure moduli can be written in terms of log P_s' and $\log(u_a - u_w)_i^e$. The experimental data has revealed empirical relationships between moduli for the water phase. As a whole, six relationships for the eight moduli associated with monotonic volume decrease and increase are suggested. The compressive and swelling indices with respect to the net total stress (i.e., C_t and C_{ts} respectively) can be measured using conventional

oedometer or triaxial equipment. These two are regarded as "basic" moduli. The remaining moduli can be estimated from the proposed relationships with the knowledge of the basic moduli and the characteristic stress states, P_s' and $(u_a - u_w)_i^e$.

ACKNOWLEDGEMENTS

The author is grateful to the Faculty of Graduate Studies, University of Saskatchewan for providing financial assistance in the form of a scholarship for the first four years of my Ph. D. program. Without the scholarship, I would not have been able to continue my studies.

My primary obligation is to Professor D. G. Fredlund, my staff supervisor. For those who know him, no words are necessary; for those who do not know him, no words will suffice. It is my blessing to have the privilege to be his student. He is a teacher whom I shall ever remember and be indebted to.

The author received excellent cooperation from the staff of the Central Shop, University of Saskatchewan during the many hours of equipment development. This integral part does not go unrecognized. In particular, the assistance of Mr. H. Bartsch, Mr. G. Belle, Mr. J. DeGoede, Mr. F. Schnabel and Mr. B. Woodward is greatly appreciated.

The author acknowledge the laboratory assistance received from Mr. D. Wong during the final stage of the test program. I received quality help from Mr. V. Lam in preparing the figures. His assistance is appreciated.

The completion of this research work has been greatly facilitated through the constant cooperation and

encouragement from my wife, Georgina. She has been my source of strength throughout the study. Her magnificent job of typing and editing the manuscript is vital to the preparation of this dissertation. To her, this thesis is sincerely dedicated.

It has been a long trial period for me during this doctoral study. Several verses in the Scripture are perhaps the best summary of my feeling as this study comes to an end.

" ... if you call out for insight
and cry aloud for understanding,
and if you look for it as for silver
and search for it as for hidden treasure,
then you will understand the fear of the Lord
and find the knowledge of God.
For the Lord gives wisdom,
and from his mouth come
knowledge and understanding. "

Proverbs 2:3-6

For my parents

who showed me the dream,

for my teacher

who showed me the way,

for my wife

who shared my endeavour,

for my Maker

who blessed me with the opportunity.

TABLE OF CONTENTS

	Page
Title Page	i
Approval Sheet	ii
Abstract	iii
Acknowledgements	vii
Table of Contents	x
List of Tables	xvii
List of Figures	xxi
CHAPTER I INTRODUCTION	1
1.1 General	1
1.2 Scope of The Thesis	3
CHAPTER II LITERATURE REVIEW	5
2.1 Introduction	5
2.2 Constitutive Relations for Volume Change in Unsaturated Soils	5
2.2.1 Constitutive relation for the soil structure	7
2.2.2 Constitutive relation for the water phase	52
2.3 Relationships between Volumetric Deformation Moduli of Unsaturated Soils	75

TABLE OF CONTENTS (continued)

		Page
CHAPTER II	continued	
2.3.1	Importance of the shrinkage and swelling tests	75
2.3.2	Other research	90
CHAPTER III	THEORY	100
3.1	Introduction	100
3.2	Characteristic Forms for The Soil Structure and Water Phase Constitutive Surfaces Based on Published Experimental Evidence	101
3.3	Theoretical Development Pertinent to The Use of Semi-logarithmic Constitutive Surfaces	130
3.4	The Adopted Semi-logarithmic Volume Change Constitutive Relations for The Soil Structure and Water Phase	141
3.4.1	Numerical presentation of the adopted semi-logarithmic constitutive relations	142
3.4.2	Graphical presentation of the adopted semi-logarithmic constitutive relations	150
3.5	Relationships between The Moduli	155
3.5.1	Relationships between moduli of the same phase with respect to different constitutive relations using different pairs of stress state variables	156

TABLE OF CONTENTS (continued)

	Page
CHAPTER III continued	
3.5.2 Relationships between moduli of the same phase	158
3.5.3 Relationships between moduli of the soil structure and water phase with respect to the same stress variable change	160
3.5.3.1 Relationships between moduli of the soil structure and water phase with respect to $\log(\sigma - u_a)$	161
3.5.3.2 Relationships between moduli of the soil structure and water phase with respect to $\log(u_a - u_w)$	161
3.5.4 Summary	166
3.6 Conceptual Adaptation for Collapsing Soils	173
CHAPTER IV TEST PROGRAM	180
4.1 General	180
4.2 Soils	180
4.2.1 Soil preparation	185
4.3 Testing Equipment	190
4.3.1 Modified Anteus consolidometer	190
4.3.2 Stress controlled isotropic cell	199
4.3.3 Plumbing layout and data collecting system	211
4.4 Program	214

TABLE OF CONTENTS (continued)

		Page
CHAPTER IV	continued	
4.4.1	Zero lateral expansion loading and unloading conditions	215
4.4.2	Isotropic loading and unloading conditions	228
CHAPTER V	PRESENTATION OF TEST RESULTS	234
5.1	Introduction	234
5.2	Tests to Evaluate the Initial Suction of the Specimens	234
5.3	Tests to Establish the Water Content versus Increasing Matric Suction Relation	238
5.4	Unconfined Shrinkage Tests	242
5.5	One-Dimensional Constant Volume Loading and Unloading Tests	256
5.6	One-Dimensional Free Swell Tests	262
5.7	Isotropic Constant Volume Loading and Unloading Tests	274
5.8	Isotropic Free Swell Test	278
5.9	Summary	284
CHAPTER VI	ANALYSIS AND DISCUSSION OF RESULTS	287
6.1	Introduction	287
6.2	Analysis of Results from The Test Program	287

TABLE OF CONTENTS (continued)

		Page
CHAPTER VI	continued	
6.2.1	Tests to evaluate the initial matric suction	288
6.2.2	Tests to establish the water content versus increasing matric suction relation	290
6.2.3	Unconfined shrinkage tests	298
6.2.4	One-dimensional constant volume loading and unloading tests	303
6.2.5	One-dimensional free swell tests	304
6.2.6	Isotropic constant volume loading and unloading tests	310
6.2.7	Isotropic free swell tests	315
6.3	The Form of The Semi-Logarithmic Soil Structure and Water Phase Constitutive Surfaces	316
6.3.1	The form of the semi-logarithmic soil structure and water phase constitutive surfaces for loading conditions	318
6.3.2	The form of the semi-logarithmic soil structure and water phase constitutive surfaces for unloading conditions	334
6.4	Relationships between The Moduli	345
6.4.1	Relationships between moduli of the same phase under loading conditions	348

TABLE OF CONTENTS (continued)

		Page
CHAPTER VI	continued	
6.4.2	Relationships between moduli of the same phase under unloading conditions	356
6.4.3	Summary	364
CHAPTER VII	CONCLUSIONS AND RECOMMENDATIONS	367
7.1	Conclusions	367
7.2	Recommendations	371
LIST OF REFERENCES		374
APPENDIX A	Listings of Programs for Sensor Calibration and Data Processing	A1
APPENDIX B-1	Equipment Preparation for The Null Pressure Plate Tests	B1
APPENDIX B-2a	Equipment Preparation for The Suction Tests	B7
APPENDIX B-2b	Estimation of Equalization Time for Suction Tests	B10
APPENDIX B-3	Equipment Preparation for The One-Dimensional Constant Volume Loading and Unloading Tests	B13
APPENDIX B-4	Equipment Preparation for The One-Dimensional Free Swell Tests	B17

TABLE OF CONTENTS (continued)

		Page
APPENDIX B continued		
APPENDIX B-5	Equipment Preparation for The Isotropic Free Swell and Constant Volume Loading and Unloading Tests	B23

LIST OF TABLES

Table		Page
2.1	Effect of Suction Pressure on Compressibility (Barden et. al., 1969)	22
2.2	Functions Used for State Surface Approximation (Lloret and Alonso, 1985)	47
2.3	Test Program for The Verification of The Various Constitutive Functions (Lloret and Alonso, 1985)	49
2.4	Soils Used in the Prism Tests (Haines, 1923)	77
2.5	Classification Test Results for Regina Clay (Gilchrist, 1963)	91
2.6	Summary of The Initial Properties of The Samples Tested in The Selected Sequences of Constant Volume and Free Swell Tests on Regina Clay (Gilchrist, 1963)	92
2.7	Summary of Free Swell Test Results on Compacted Regina Clay (Gilchrist, 1963)	93
3.1	Adopted Sign Convention for The Moduli and The Stress State Variables Used in the Constitutive Relations	149
4.1	Index Properties of the Silt and Glacial Till Used in the Test Program	181
4.2	Results of the Salinity Analyses on Silt and Till Samples	184

LIST OF TABLES (continued)

Table		Page
4.3	Layout of The Sub-Program I	216
4.4	Layout of The Sub-Program II	229
5.1a	Summary of Suction Test Results on the Water Content Changes	239
5.1b	Summary of Suction Test Results on Dimensional Changes	240
5.2	Calibration Checks for the Direct Measurement Method Using a Stainless Steel Plug	257
5.3	Summary of One-Dimensional Free Swell Test Data	272
5.4	Summary of Isotropic Free Swell Test Data	282
5.5	A Summary of All Tests Performed	286
6.1	A summary of Results from Null Pressure Plate Tests on Silt Specimens	289
6.2	A Summary of The Moduli Determined from The Average Water Content Versus Increasing Matric Suction Curves	299
6.3	A Summary of The Moduli Determined from The Linear Portions of The Average One-Dimensional Loading and Unloading Cuves	309
6.4	A Summary of The Moduli Determined from The One-Dimensional Free Swell Test Results	312
6.5	A Summary of The Moduli Determined from The Isotropic Constant Volume Loading and unloading Test Results	314

LIST OF TABLES (continued)

Table		Page
6.6	A Summary of The Moduli Determined from The Isotropic Free Swell Test Results	317
6.7	A Summary of Moduli Determined from The Average Loading Curves for Silt and Till	326
6.8	A Summary of The Characteristic Stress States for Silt and Till	328
6.9	A Summary of The Net Total Stress and Matric Suction at The Projected Points of Convergence of The Silt and Till Soil Structure Constitutive Surfaces for Monotonic Volume Decrease	331
6.10	A summary of The Average Swelling Indices with Respect to The Net Total Stress and Matric Suction at The Points of Convergence of The Silt and Till Soil Structure Constitutive Surfaces for Monotonic Volume Increase	344
6.11	A Comparison between The Measured Moduli Ratio, C_m / C_t and Those Predicted According to The Proposed Relationships	351
6.12	A Comparison between The Measured Water Content Index with Respect to Net Total Stress and The Proportioned Water Content Index with Respect to Matric Suction	355

LIST OF TABLES (continued)

Table		Page
6.13	A Comparison between The Measured Moduli Ratio, C_{ms}/C_{ts} and Those Predicted According to The Proposed Relationships	358
6.14	A Comparison between The Measured Water Content Index with Respect to Net Total Stress and The Reduced Rebound Water Content Index with Respect to Matric Suction	363
6.15	A Summary of Tests Needed to Determine the Necessary Moduli to Describe the Volume Change Behaviour of An Unsaturated Soil	365

LIST OF FIGURES

Figure		Page
2.1	Volume Changes under Equal All-Round Pressure Plotted in Void Ratio-Stress State Space (Bishop and Blight, 1963)	13
2.2	Plots Showing the Variation of Void Ratio in (e, $\sigma - u_a$, $u_a - u_w$) Space for A Quartz and Kaolin Mixture (Matyas and Radhakrishna, 1968)	14
2.3	Volume Change Curves for a Blank Earth from Adelaide, Australia (Aitchison & Woodburn, 1969)	16
2.4	Stress Paths for Test Groups 2 to 11 (Barden, et.al., 1969)	17
2.5	Compression Curves for Specimens with Monotonic Increases in Degree of Saturation and Decreases in Strain (Barden, et.al., 1969)	19
2.6	Compression Curves for Specimens with Monotonic Increases in Degree of Saturation and Strain Reversals (Barden, et.al., 1969)	20
2.7	Compression Curves for Group II specimens with Both Degree of Saturation and Strain Reversals (Barden, et.al., 1969)	21
2.8	Typical Consolidation Curves Throughout the Suction Range (Aitchison and Woodburn, 1969)	23
2.9	Constant Water Content Compression Curves for a South African Clay (Brackley, 1971)	24

LIST OF FIGURES (continued)

Figure		Page
2.10	Rectilinear Plots of Comparative Effects of Applied Pressure, Matric and Solute Suction for A Pleistorene Clay from Adelaide, South Australia (Aitchison and Martin, 1973)	28
2.11	Constitutive Surfaces for the Various Phases of an Unsaturated Soil (Fredlund, 1982)	31
2.12	Arithmetic Plot of Void Ratio Versus Stress State Variables (Fredlund, 1980)	33
2.13	Void Ratio Versus Logarithm of Stress State Variables (Fredlund, 1979)	34
2.14	Relationships Between Surcharge Pressure, Specimen Thickness and Volume Increase for Constant Density and Water Content Specimens (Chen, 1975)	35
2.15	Relationships Between Initial Water Content, Degree of Saturation and Volume Increase for Constant Density and Water Content Specimens (Chen, 1975)	36
2.16	Effects of Varying Density on Swelling Pressure for Constant Water Content Specimens (Chen, 1975)	38
2.17	State Surface for the Soil Structure (Data Taken from Matyas and Radhakrishna, 1968) (LLoret and Alonso, 1980)	40

LIST OF FIGURES (continued)

Figure		Page
2.18	Vertical Strain Versus Matric Suction Plots for Black Earth and Pleistocene Clays (Richards, Peter and Martin, 1984)	42
2.19	Vertical Strain Versus Solute Suction Plots for Pleistocene Clays (Richards, Peter and Martin, 1984)	43
2.20	Core Shrinkage Test Results for an O'Halloran Hill Clay (Mitchell and Avalle, 1984)	45
2.21	Constitutive Curve of the O'Halloran Hill Clay with respect to Total Suction (Mitchell and Avalle, 1984)	46
2.22	Schematic Representation of the Optimum Soil Structure Volume Change Constitutive Relation for Unsaturated Soils (Lloret and Alonso, 1985)	51
2.23	Relationships between Suction and Water Content for Samples of Hard and Soft Chalk (Croney and Coleman, 1954)	54
2.24	Relationships between Suction and Water Content for Three Mixes of Plaster of Paris: drying condition (Croney and Coleman, 1954)	55
2.25	Relationships between Suction and Water Content for a Silty Sand at Two Densities (Croney and Coleman, 1954)	56

LIST OF FIGURES (continued)

Figure		Page
2.26	Suction/Water Content and Shrinkage relationships for a Heavy Clay Soil (Croney and Coleman, 1954)	57
2.27	Suction/Water Content and Shrinkage Relationships for a Heavy Clay Soil (Croney and Coleman, 1954)	58
2.28	Plots Showing the Variation of Degree of Saturation in (S , $\sigma - u_a$, $u_a - u_w$) Space for a Quartz and Kaolin Mixture (Matyas and Radhakrishna, 1968)	60
2.29	Degree of Saturation Change Curves for Illite Spacimens with Monotonic Increases in Degree of Saturation and Decreases in Strain (Barden et.al., 1969)	61
2.30	Arithmetic Presentation of Water Content Versus Stress State Variables (Fredlund, 1979)	64
2.31	Water Content Versus Logarithm of Stress State Variables (Fredlund, 1979)	65
2.32	Relation Between Pore-Water Pressure Head and Volumetric Water Content for Two Sands (McWhorter and Nelson, 1979)	67
2.33	The Degree of Saturation Versus Matric Suction Relation (Seker, 1983)	70

LIST OF FIGURES (continued)

Figure		Page
2.34	Water Content Versus Total Suction Relations for Australian Soils (Mitchell and Avalle, 1984)	71
2.35	Schematic Representation of The Optimum Water Phase Constitutive Relation for Unsaturated Soils (Lloret and Alonso, 1985)	73
2.36	Unconfined Shrinking and Swelling Curves from Prism Tests (Haines, 1923)	78
2.37	Conceptual Diagrams of The Swelling and Shrinking Phenomena (Wooltorton, 1954)	80
2.38	Hypothetical Shrinkage Curves for Remoulded Soils (Wooltorton, 1954)	81
2.39	Hypothetical Shrinkage Curves for Undisturbed Soils (Wooltorton, 1954)	82
2.40	Hypothetical Shrinkage and Swelling Curves for Saturated Remoulded Soils (Wooltorton, 1954)	83
2.41	Hypothetical Shrinkage and Swelling Curves for Desiccated Compacted Soils (Wooltorton, 1954)	84
2.42	Experimental Density Change and Shrinking-Swelling Curves (Wooltorton, 1954)	85
2.43	Shrinkage Curves of a Romania Clay with Different Crumb Size Fractions (Popescu, 1980)	87
2.44	Test Arrangement (Beal, 1984)	88

LIST OF FIGURES (continued)

Figure		Page
2.45	Swelling and Shrinkage Curves of a Dalby Clay (Beal, 1984)	89
2.46	Void Ratio Versus Pressure Curve for Specimen III-2C-(CV) (After Gilchrist, 1963)	94
2.47	Void Ratio Versus Pressure Curve for Specimen IV-IC-(CV) (After Gilchrist, 1963)	95
2.48	Swelling Curves for Compacted El Arahal Clay Specimens (Justo el.al., 1984)	98
3.1	The Logarithm of Effective Stress Versus Vertical Strain Relation for An Arizona Clay (Holtz and Gibbs, 1956)	103
3.2	The Logarithm of Effective Stress Versus Void Ratio Relations for Compacted Regina Clay (Gilchrist, 1963)	105
3.3	The Logarithm of Effective Stress Versus Volume Change Relations for Remoulded Regina Clay (Noble, 1966)	106
3.4	The Logarithm of Matric Suction Versus The Percent of Swelling Relations for Remoulded Madrid Clay (Escario, 1969)	108
3.5a	The Matric Suction Versus Swelling Pressure Relation on An Arithmetic Scale for A Remoulded Madrid Clay Undergoing Constant Volume Stress Changes (Escario, 1969)	109

LIST OF FIGURES (continued)

Figure		Page
3.5b	The Matric Suction Versus Swelling Pressure Relation on A Logarithmic Scale for A Remoulded Madrid Clay Undergoing Constant Volume Stress Changes (Escario, 1969)	109
3.6	The Logarithm of Effective Stress Versus Void Ratio Relations for Compacted Glacial Till (Lidgren, 1970)	111
3.7	The Logarithm of Matric Suction Versus Vertical Strain Relations for An Adelaide Clay Undergoing Monotonic Volume Increase (Aitchison and Martin, 1973)	112
3.8	The Logarithm of Matric Suction Versus Vertical Strain Relations for An Adelaide Clay Undergoing Monotonic Volume Decrease (Aitchison and Martin, 1973)	113
3.9	The Logarithm of Decreasing Effective Stress Versus The Percent of Swelling for Denver Claystone Shale (Chen, 1975)	115
3.10	The Logarithm of Increasing Total Suction Versus Vertical Strain Relation for O'Halloran Hill Clay (Mitchell and Avalle, 1984)	116
3.11	The Logarithm of Matric Suction Versus Vertical Strain Relations for Athelstone Park Clay (Richards, Peter and Martin, 1984)	118

LIST OF FIGURES (continued)

Figure		Page
3.12a	A Schematic Diagram of The Soil Structure Constitutive Surfaces for Monotonic Volume Changes on An Arithmetic Scale	121
3.12b	A Schematic Diagram of The Soil Structure Constitutive Surfaces for Monotonic Volume Changes on A Semi-Logarithmic Scale	121
3.13	The Logarithm of Matric Suction Versus Water Content Relation for A Heavy Clay Soil (Croney and Coleman, 1954)	123
3.14	Comparison of Recompression Branches for Suction and One-Dimensional Consolidation Tests for Regina Clay (Fredlund, 1964)	124
3.15	The Logarithm of Matric Suction Versus Volumetric Water Content Relation for Two Sands (McWhorter and Nelson, 1979)	125
3.16	The Logarithm of Total Suction Versus Water Content Relation for O'Halloran Hill Clay (Mitchell and Avalle, 1984)	127
3.17a	A Schematic Diagram of The Water Phase Constitutive Surfaces for Monotonic Volume Changes on An Arithmetic Scale	129
3.17b	A Schematic Diagram of The Water Phase Constitutive Surfaces for Monotonic Volume Changes on A Semi-logarithmic Scale	129

LIST OF FIGURES (continued)

Figure		Page
3.18a	The Soil Structure Constitutive Surface for Monotonic Volume Decrease	132
3.18b	The Approximated Form for The Soil Structure Constitutive Surface for Monotonic Volume Decrease	132
3.19a	Constant Volume Stress Path on An Arithmetic Scale	134
3.19b	Constant Volume Stress Path on A Logarithmic Scale	134
3.20	Actual and Approximated Constant Volume Stress Paths for Soils with The $\frac{p'_s}{(u_a - u_w)^e_i}$ Ratio Being 1	136
3.21	Actual and Approximated Constant Volume Stress Paths for Soils with The $\frac{p'_s}{(u_a - u_w)^e_i}$ Ratio Being 0.5774	137
3.22	Actual and Approximated Constant Volume Stress Paths for Soils with The $\frac{p'_s}{(u_a - u_w)^e_i}$ Ratio Being 0.268	138
3.23a	Geometry of The Orthogonal Planes I and III Approximating The Soil Structure Constitutive Surface for Monotonic Volume Decrease	139
3.23b	Geometry of The Transition Plane II Approximating The Soil Structure Constitutive Surface for Monotonic Volume Decrease	139
3.24	Geometrical Characteristics of The Approximated	143

Figure		Page
	Soil Structure Constitutive Surface for Monotonic Volume Decrease	
3.25a	Graphical Presentation of The Adopted Soil Structure Constitutive Surface for Monotonic Volume Increase	151
3.25b	Graphical Presentation of The Adopted Soil Structure Constitutive Surface for Monotonic Volume Decrease	151
3.26a	Graphical Presentation of The Adopted Water Phase Constitutive Surface for Monotonic Water Content Increase	152
3.26b	Graphical Presentation of The Adopted Water Phase Constitutive Surface for Monotonic Water Content Decrease	152
3.27a	Geometrical Relationship between Moduli of The Same Phase Undergoing Monotonic Volume Increase	159
3.27b	Geometrical Relationship between Moduli of The Same Phase Undergoing Monotonic Volume Decrease	159
3.28	Unconfined Shrinking and Swelling Curves for Durham Clay (Haines 1923)	164
3.29	Unconfined Shrinking and Swelling Curves for A Compacted Clay	165

LIST OF FIGURES (continued)

Figure		Page
3.30a	Three-Dimensional Presentation of The Relationship between Moduli of The Soil Structure Undergoing Monotonhic Volume Decrease	168
3.30b	Two-Dimensional Presentation of The Relationship between Moduli of The Soil Structure Undergoing Monotonic Volume Decrease	169
3.31a	Three-Dimensional Stress Plot Representing The Insitu Swelling of A Soil at Constant Load	171
3.31b	Two-Dimensional Stress Plot Representing The Insitu Swelling of A Soil at Constant Load	172
3.32a	The Soil Structure Constitutive Surface of A Collapsing Soil for Monotonic Volume Decrease on An Arithmetic Scale	175
3.32b	The Soil Structure Constitutive Surface of A Collapsing Soil for Monotonic Volume Decrease on A Semi-Logarithmic Scale	175
3.33	The Approximated Form for The Soil Structure Constitutive Surface of a Collapsing Soil Undergoing Monotonic Volume Decrease	177
3.34a	A Schematic Diagram Showing The Transition between The Constitutive Surfaces of A Swelling Soil to A Collapsing Soil on An Arithmatic Plot	178

LIST OF FIGURES (continued)

Figure		Page
3.34b	A Schematic Diagram Showing The Transition between The Constitutive Surfaces of A Swelling Soil to A Collapsing Soil on A Semi-Logarithmic Plot Semi-Logarithmic Plot	178
4.1	Grain Size Distribution Curve for Silt	182
4.2	Grain Size Distribution Curve for Glacial Till	183
4.3	Compaction Curve for Silt	186
4.4	Compaction Curve for Glacial Till	187
4.5	Schematic Layout of the 6.3 cm Diameter Compaction Mould	188
4.6	Schematic Layout of the 10.2 cm Diameter Compaction Mould	189
4.7	Modified Anteus Consolidometer (Pufahl, 1970)	191
4.8a	Loading Cap Complex for the Modified Anteus Consolidometer - Front View	193
4.8b	Loading Cap Complex for the Modified Anteus Consolidometer - Top View	194
4.9	Schematic Layout of the Modified Anteus Consolidometer	195
4.10	Water Volume Change Indicator (Fredlund, 1973)	197
4.11	Diffused Air Volume Indicator (Fredlund, 1975)	198
4.12	Modified Triaxial Cell (Fredlund, 1973)	200
4.13	Lateral Displacement Indicator (Fredlund, 1973)	201

LIST OF FIGURES (continued)

Figure		Page
4.14	General Assembly of the Stress Controlled Isotropic Cell	202
4.15	Cross Section of the Cylindrical Cover	204
4.16	Top View of the Cylinderical Cover	205
4.17	Base Plate of The Stress Controlled Isotropic Cell	206
4.18a	Front View of the Loading Cap Complex for the Stress Controlled Isotropic Cell	207
4.18b	Top View of the Loading Cap Complex for the Stress Controlled Isotropic Cell	208
4.19	Schematic Layout for the Strain Measuring Devices inside the Stress Controlled Isotropic Cell	210
4.20	Schematic Diagram of Plumbing Layout for the Modified Anteus Consolidometer and Stress Controlled Isotropic Cell	212
4.21	Schematic Diagram of Plumbing Layout for the Hypodermic Water Injection Line	213
4.22	University of Saskatchewan Pressure Plate Apparatus (Blocking and Fredlund, 1980)	217
4.23	Stress Path of the Suction Test, ST in Terms of the Water Content, w	218
4.24	Multi-Layered Pressure Plate Apparatus (Fredlund, 1964)	219

LIST OF FIGURES (continued)

Figure		Page
4.25	Pressure Membrane Apparatus (Fredlund, 1964)	220
4.26	Stress Path of the One-Dimensional Constant Volume Loading Test, CVT	224
4.27	Stress Path of the One-Dimensional Free Swelling Test, FST	226
5.1	Null Pressure Plate Test Results for Specimen PP3DS	236
5.2	Null Pressure Plate Test Results for Specimen PP2OS	237
5.3	Results for Unconfined Shrinkage Tests SLTM2DS and SLTM3DS	243
5.4	Results for Unconfined Shrinkage Tests SLTR2DS and SLTR3DS	244
5.5	Results for Unconfined Shrinkage Tests SLTD1DS, SLTD2DS, and SLTD3DS	246
5.6	Results for Unconfined Shrinkage Test SLTD4DS	247
5.7	Results for Unconfined Shrinkage Test SLTD5DS	248
5.8	Results for Unconfined Shrinkage Tests, SLTD1OS, SLTD2OS, and SLTD3OS	250
5.9	Results for Unconfined Shrinkage Test SLTD4OS	251
5.10	Results for Unconfined Shrinkage Test SLTD5OS	252
5.11	Results for Unconfined Shrinkage Test SLTDM1OS	253
5.12	Results for Unconfined Shrinkage Tests SLTD1DT and SLTDM1DT	254

LIST OF FIGURES (continued)

Figure		Page
5.13	Results for Unconfined Shrinkage Test SLTDM20T	255
5.14	Comparsion between Volumes Measured by the Direct Measurement and Mercury Submersion Method	258
5.15	Results for One-Dimensional Constant Volume Loading and Unloading Tests CVT1DS to CVT6DS	260
5.16	Results for One-Dimensional Constant Volume Loading and Unloading Tests CVT10S to CVT40S	261
5.17	Results for One-Dimensional Constant Volume Loading and Unloading Tests CVT1DT To CVT3DT	263
5.18	Results for One-Dimensional Constant Volume Loading and Unloading Tests CVT10T to CVT30T	264
5.19	Specimen Volume and Water Volume Equilibrium Curves for Stage I of One-Dimensional Free Swell Test FST3DS	266
5.20	Specimen Volume and Water Volume Equilibrium Curves for Stage II of One-Dimensional Free Swell Test FST3DS	267
5.21	Specimen Volume and Water Volume Equilibrium Curves for Stage III of One-Dimensional Free Swell Test FST3DS	268
5.22	Results for One-Dimensional Free Swell Test FST3DS	270
5.23	Results for One-Dimensional Free Swell Test FST4DS	271

LIST OF FIGURES (continued)

Figure		Page
5.24	Results for One-Dimensional Free Swell Test FST10S	273
5.25	Results for One-Dimensional Free Swell Test FST1DT	275
5.26	Results for One-Dimensional Free Swell Test FST10T	276
5.27	Results for The Isotropic Constant Volume Loading and Unloading Tests TCVT3DS and TCVT4DS	279
5.28	Results for The Isotropic Constant Volume Loading and Unloading Test TCVT10S	280
5.29	Results for The Isotropic Free Swell Test TFST2DS	283
5.30	Results for The Isotopic Free Swell Test TFST10S and TFST20S	285
6.1	Matric Suction Versus Water Content Curve for Glacial Till (Krahn, 1970)	291
6.2	Average Water Content Versus Increasing Matric Suction Curve for Silt with Dry of Optimum Initial Water Content	293
6.3	Average Water Content Versus Increasing Matric Suction Curve for Silt with Optimum Initial Water Content	294
6.4	Matric Suction Versus Water Content for Glacial	295

LIST OF FIGURES (continued)

Figure		Page
	Till with Various Installation Methods (Lee and Fredlund, 1984)	
6.5	Average Water Content Versus Increasing Matric Suction Curve for Till with Dry of Optimum Initial Water Content	296
6.6	Average Water Content Versus Increasing Matric Suction Curve for Till with Optimum Initial Water Content	297
6.7	A Comparison between Void Ratios Determined by Direct Volume Measurements With and Without Surface Indentation	301
6.8	A Comparison between Void Ratios Determined by Mercury Submersion and Direct Measurements	302
6.9	Mean Void Ratio Versus The Logarithm of Net Total Stress Curve for Silt Dry of Optimum under One-Dimensional Conditions	305
6.10	Mean Void Ratio Versus The Logarithm of Net Total Stress Curve for Silt at Optimum under One-Dimensional Conditions	306
6.11	Mean Void Ratio Versus The Logarithm of Net Total Stress Curve for Till Dry of Optimum under One-Dimensional Conditions	307
6.12	Mean Void Ratio Versus The Logarithm of Net	308

LIST OF FIGURES (continued)

Figure		Page
	Total Stress Curve for Till at Optimum under One-Dimensional Conditions	
6.13	Average One-Dimensional Void Ratio and Water Content Versus Matric Suction Unloading Curves for Silt with Dry of Optimum Initial Water Content	311
6.14	Constitutive Relations for Silt Dry of Optimum under One-dimensional Loading Conditions	320
6.15	Constitutive Relations for Silt at Optimum under One-dimensional Loading Conditions	321
6.16	Constitutive Relations for Till Dry of Optimum under One-dimensional Loading Conditions	322
6.17	Constitutive Relations for Till at Optimum under One-dimensional Loading Conditions	323
6.18	A Comparison between The One-Dimensional and Isotropic Void Ratio Versus Net Total Stress Loading and Unloading Curves for Silt with Dry of Optimum Initial Water Content	324
6.19	A Comparision between The One-Dimensional and Isotropic Void Ratio Versus Net Total Stress Loading and Unloading Curves for Silt with Optimum Initial Water Content	325
6.20	Determination of The Stress State at The Projected Point of Convergence of The Soil	330

Figure		Page
	Structure Constitutive Surface for Silt with Dry of Optimum Initial Water Content under Isotropic Loading Conditions	
6.21	The Divergence of The Water Content Loading Curves for Silt with Dry of Optimum Initial Water Content under One-Dimensional Loading	333
6.22	Determination of The Stress State at The Soil Structure Constitutive Surface Point of Convergence for Silt with Dry of Optimum Initial Water Content under One-Dimensional Unloading Conditions	338
6.23	Determination of The Stress State at The Soil Structure Constitutive Surface Point of Convergence for Silt with Optimum Initial Water Content under One-Dimensional Unloading Conditions	339
6.24	Determination of The Stress State at The Soil Structure Constitutive Surface Point of Convergence for Till with Dry of Optimum Initial Water Content under One-Dimensional Unloading Conditions	340
6.25	Determination of The Stress State at The Soil Structure Constitutive Surface Point of Convergence for Till with Optimum Initial Water	341

LIST OF FIGURES (continued)

Figure		Page
	Content under One-Dimensional Unloading Conditions	
6.26	Determination of The Stress State at The Soil Structure Constitutive Surface Point of Convergence for Silt with Dry of Optimum Initial Water Content under Isotropic Unloading Conditions	342
6.27	Determination of The Stress State at The Soil Structure Constitutive Surface Point of Convergence for Silt with Optimum Initial Water Content under Isotropic Unloading Conditions	343
6.28	Relations between The Characteristic Stress States and Initial Soil Condition of An Unconfined Unsaturated Soil	346
6.29	The Divergence of The Water Content Unloading Curves for Till at Dry of Optimum Initial Water Content Under One-Dimensional Unloading	347

CHAPTER I

INTRODUCTION

1.1 General

The development of unsaturated soil mechanics consists of several primary areas of study, namely, volume change, moisture movement and shear strength behaviour. Theory and technology developed in these areas form the basis for geotechnical engineering practice involving volume change, seepage, bearing capacity and slope stability analysis. The volume change theory is relevant when solving these practical problems. Volume change for an unsaturated soil is described in terms of constitutive relations. The material properties in such relations can be called volumetric deformation moduli.

The prediction of volume change in an unsaturated soil becomes a direct application of the volume change constitutive relations in conjunction with the constraint of various boundary conditions. The flow laws and volume change constitutive relations provide the necessary physical relations for formulations related to seepage problems. Both bearing capacity and slope stability analysis involve the shear strength equation for unsaturated soils. The shear strength equation relates shear strength to stress state variables such as the net total stress (i.e.,

$(\sigma - u_a))$ and matric suction (i.e., $(u_a - u_w)$) (Fredlund, Morgenstern and Widger, 1978). The pore-air, u_a, and and pore-water, u_w, pressure are stress components of the stress state variables. A change in the boundary conditions causes the pore-air and pore-water pressure to change. This, in turn, leads to a change in the shear strength. The change in pore-air and pore-water pressure due to environmental changes can be described by the transient flow equations for the air and water phases. The transient flow equations are written in terms of the volume change constitutive relations and the air and water flow laws. Pore-air and pore-water pressure changes for undrained loading conditions are described using pore pressure parameters. The pore pressure parameters can be written in terms of the volume change constitutive relations and the density and compressibility equations for air-water mixtures.

A knowledge of four independent moduli is required in order to completely describe the volume change behaviour of an unsaturated soil in a monotonic volume change process. The development of the relationships between the moduli is regarded as an area of much needed research to enhance the volume change theory for unsaturated soils.

1.2 Scope of The Thesis

The main objective of this dissertation is the development of relationships between the various volumetric deformation moduli. Attempts are made to find relationships between the moduli in order that all required moduli can be determined from a few basic conventional soil tests. An experimental program is used to gather data to test the proposed relationships. The methodology used in the study is as follows.

Chapter II provides a summary of existing information on the volume change behaviour of unsaturated soils. Pertinent literature on the volume change constitutive relations for the soil structure and water phase is presented and criticized. An attempt is made to gather information pertaining to the relationships between the different moduli. Theory surrounding possible relationships between the moduli is developed in Chapter III. The form of the soil structure and water phase constitutive surfaces is examined on both an arithmetic and a semi-logarithmic scale. Approximate semi-logarithmic constitutive surfaces are proposed. The geometry of the approximate constitutive surfaces is used to relate the various moduli. A brief discussion is presented on the adaptation of the proposed theory for unsaturated collapsing soils. However, a complete consideration of collapsing soils is outside the scope of this thesis.

Chapter IV describes the test program used to experimentally verify the form of the constitutive surfaces for K_o and isotropic loading and unloading conditions. The results from the test program are presented in Chapter V. The analysis of the experimental results and an evaluation of the proposed relationships between the moduli are provided in Chapter VI. Final conclusions and recommendations of the study are presented in Chapter VII.

CHAPTER II

LITERATURE REVIEW

2.1 Introduction

This chapter presents existing information on the volume change behaviour of unsaturated soils. Literature on the constitutive relations for volume change in the soil structure and water phase is reviewed. The form of the constitutive surfaces is discussed. Attempts are made to gather information pertaining to the relationships between the different volumetric deformation moduli. There are three sections in this chapter. Section 2.1 describes the layout of the chapter. Section 2.2 reviews literature on the constitutive relations for volume change in unsaturated soils. Section 2.3 presents and discusses previous research done on the relationships between the different volumetric deformation moduli.

2.2 Constitutive Relations for Volume Change in Unsaturated Soils

A volume change constitutive relation relates the stress and strain variables of a continuum through material constants known as volumetric deformation moduli. The same

mathematical equations can be represented graphically as a constitutive surface in three dimensional plots.

An unsaturated soil consists of four phases - the soil solids, pore-water, pore-air and contractile skin (i.e. air-water interphase) (Fredlund, 1979). Assuming the soil solids are incompressible and the volume change of the contractile skin is internal to the soil element, the continuity requirement (i.e. conservation of mass) can be expressed as follows (Fredlund, 1973).

$$\varepsilon = \theta_w + \theta_a \qquad (2.1)$$

where

$\varepsilon = \frac{\Delta V}{V}$, the volumetric strain of the soil structure

$\theta_w = \frac{\Delta V_w}{V}$, the volumetric strain of the pore-water

$\theta_a = \frac{\Delta V_a}{V}$, the volumetric strain of the pore-air

V = total volume of an unsaturated soil element

ΔV_w = change in volume of water in the soil element

ΔV_a = change in volume of air in the soil element

It follows that any two of the three constitutive relations are required for complete description of volume changes sustained by an unsaturated soil undergoing stress changes. These relations pertain to the volume change of the soil structure and pore-water in terms of the total stress, σ, pore-air, u_a and pore-water pressure, u_w.

Section 2.2.1 and 2.2.2 present volume change

constitutive relations of the soil structure and pore-water respectively.

2.2.1 Constitutive relation for the soil structure

In 1941, Biot presented volume change constitutive relations for an unsaturated soil. The deformation of the soil structure was mathematically related to the stress variables, $(\sigma - u_w)$ and u_w. The soil structure was assumed to behave as a linear, reversible, isotropic and elastic material. Provision was made for soils "not completely saturated with water and containing air bubbles". The proposed constitutive relations are as follows.

$$\varepsilon_x = \frac{(\sigma_x - u_w)}{E} - \frac{\mu}{E}(\sigma_y + \sigma_z - 2u_w) + \frac{u_w}{3H} \qquad (2.2a)$$

$$\varepsilon_y = \frac{(\sigma_y - u_w)}{E} - \frac{\mu}{E}(\sigma_x + \sigma_z - 2u_w) + \frac{u_w}{3H} \qquad (2.2b)$$

$$\varepsilon_z = \frac{(\sigma_z - u_w)}{E} - \frac{\mu}{E}(\sigma_x + \sigma_y - 2u_w) + \frac{u_w}{3H} \qquad (2.2c)$$

$$\varepsilon_{xy} = \frac{\tau_{xy}}{G} \qquad (2.2d)$$

$$\varepsilon_{yz} = \frac{\tau_{yz}}{G} \qquad (2.2e)$$

$$\varepsilon_{zx} = \frac{\tau_{zx}}{G} \qquad (2.2f)$$

where

ε = strain

σ = total stress

τ = shear stress

u_w = pore-water pressure

E = elastic modulus with respect to a change in $(\sigma - u_w)$

μ = Poisson's ratio

H = material parameter, physical constant

$G = \frac{E}{2(1 + \mu)}$, shear modulus

The soil coefficient, 1/H was interpreted as "a measure of the compressibility of the soil for a change in water pressure, u_w". No experimental verification was presented. The choice of the stress and strain variables was not justified or discussed. However, the proposed constitutive relations are similar to those suggested some thirty years later (Fredlund and Morgenstern, 1976). In 1976, the following equations were presented by Fredlund and Morgenstern as the constitutive relations for volume change of the soil structure in an unsaturated soil element (i.e., with a continuous air phase) which behaves as a linear, elastic, isotropic material.

$$\varepsilon_x = \frac{(\sigma_x - u_w)}{E} - \frac{\mu}{E}(\sigma_y + \sigma_z - 2u_w) + \frac{(u_a - u_w)}{H^*} \qquad (2.3a)$$

$$\varepsilon_y = \frac{(\sigma_y - u_w)}{E} - \frac{\mu}{E}(\sigma_x + \sigma_z - 2u_w) + \frac{(u_a - u_w)}{H^*} \qquad (2.3b)$$

$$\varepsilon_z = \frac{(\sigma_z - u_w)}{E} - \frac{\mu}{E}(\sigma_x + \sigma_y - 2u_w) + \frac{(u_a - u_w)}{H^*} \qquad (2.3c)$$

where

$(u_a - u_w)$ = soil matric suction

H^* = an elastic modulus with respect to a change in $(u_a - u_w)$

A comparison between the two sets of equations (i.e., equation set (2.2) and (2.3)) indicates that the choice of stress variables used in forming the equations is the main difference between these two formulations. Fredlund and Morgenstern (1977) showed by the principle of superimposition of coincident equilibrium stress fields that any two of the three stress variables, $(\sigma - u_a)$, $(\sigma - u_w)$ and $(u_a - u_w)$ can completely define the stress state of an unsaturated soil. For soils with interconnected air voids open to atmospheric pressure, the stress state variable, $(u_a - u_w)$ equals the pore-water stress component, $-u_w$. The Biot (1941) equations were given little heed until the mid 1970's.

In 1936, Terzaghi presented the effective stress concept. The success of using a single stress variable, $(\sigma - u_w)$ in describing the mechanical behaviour of saturated soils lead researchers to seek for a similar formulation for unsaturated soils. In 1959, Bishop proposed his effective stress equation for an unsaturated soil.

$$\sigma' = \sigma - [\chi u_w + (1 - \chi)u_a] \qquad (2.4)$$

or $$= (\sigma - u_w) + \chi(u_a - u_w)$$

where

σ' = effective stress

u_a = pore-air pressure

u_w = pore-water pressure

$(u_a - u_w)$ = matric suction

χ = a soil parameter related to the degree of saturation

In the 1960 Research Conference on "Pore Pressure and Suction in Soil" at London, Bishop's effective stress was widely accepted. However, in 1962, Jennings and Burland used experimental results to qualitatively illustrate the shortcomings of considering Bishop's effective stress as the stress variable fully accountable for the volume change characteristics of unsaturated soils. A series of oedometer and isotropic compression tests were carried out on unsaturated and saturated soils ranging from silty sands to silty clays. It was shown that the soil structure of silts and silty sands would collapse when being saturated. In order to maintain a constant volume of the specimens upon saturation, a decrease in the stress variable, $(\sigma - u_w)$ was required. Such findings contradicted Bishop's suggestion of a single valued stress state variable. This conclusion led to a search for other more appropriate stress state variables that better describe the volume change behaviour of unsaturated soils.

In the same year, 1962, Coleman separated the components of Bishop's effective stress equation and proposed a constitutive relation for soil structure volume change as follows.

$$-\frac{dV}{V} = -C_{21}(du_w - du_a) + C_{22}(d\sigma - du_a) + C_{23}(d\sigma_1 - d\sigma_3) \qquad (2.5)$$

where

dV = the change in the overall volume of the soil structure

V = current overall volume of a soil element

C_{21}, C_{22}, C_{23} = soil parameters depend solely upon the current values of $(u_w - u_a)$, $(\sigma - u_a)$ and $(\sigma_1 - \sigma_3)$ and the stress history of the soil.

Coleman (1962) did not present details of the formulation for the proposed constitutive relation or explain how the stress variables, $(u_w - u_a)$, $(\sigma - u_a)$ and $(\sigma_1 - \sigma_3)$ were selected. No experimental verification was presented.

In 1963, Bishop and Blight acknowledged the problems of using one stress variable to describe the volume change behaviour of unsaturated soils. The authors wrote, "A change in value of the term, $(u_a - u_w)$ does not correspond directly to a change in neutral stress since the term represents a pressure difference due to surface tension acting in general over only a part of the surface area of the soil particles. A change in the value of $(u_a - u_w)$ is almost invariably accompanied by a significant change in the value of χ. Furthermore, the presence of large surface tension forces within the soil leads to differences in soil structure in samples following apparently similar effective stress paths. These differences have proved to be of particular significance with regard to volume change ... ". Bishop and Blight (1963) proposed that, "... results of any test measuring volume change under all round pressure may be expressed as a path in space with the axes being the void

ratio, e, stress difference, $(\sigma - u_a)$ and $(u_a - u_w)$ ... " (Figure 2.1). This was perhaps the first time the suggestion was made that the constitutive relation could be graphically represented as a constitutive surface. However, no experimental verification was presented.

In 1968, Matyas and Radhakrishna used the concepts of state and state parameters from continuum mechanics in studying the volume change behaviour of unsaturated soils. Attempts were made to establish the "stress point functions" and "state surfaces" which are the constitutive relations and surfaces, respectively. The stress variables, $(\sigma - u_a)$ and $(u_a - u_w)$ were chosen as the "state parameters" whereas the void ratio, e and degree of saturation, S were selected as "stress dependent quantities". Experimental data illustrating the constitutive surface of the soil structure were presented (Figure 2.2). Statically compacted specimens prepared from a mixture of 80% grounded quartz and 20% kaolin were used. A predominantly collapsing behaviour was observed.

In an attempt to establish a systematic approach to foundation design on desiccated clays, Aitchison and Woodburn (1969) advocated the idea of separate consideration of each component of Bishop's effective stress (i.e. equation 2.4). The total stress, σ and matric suction, $(u_a - u_w)$ were used as stress variables in describing ground movements. It was proposed that modified oedometer tests

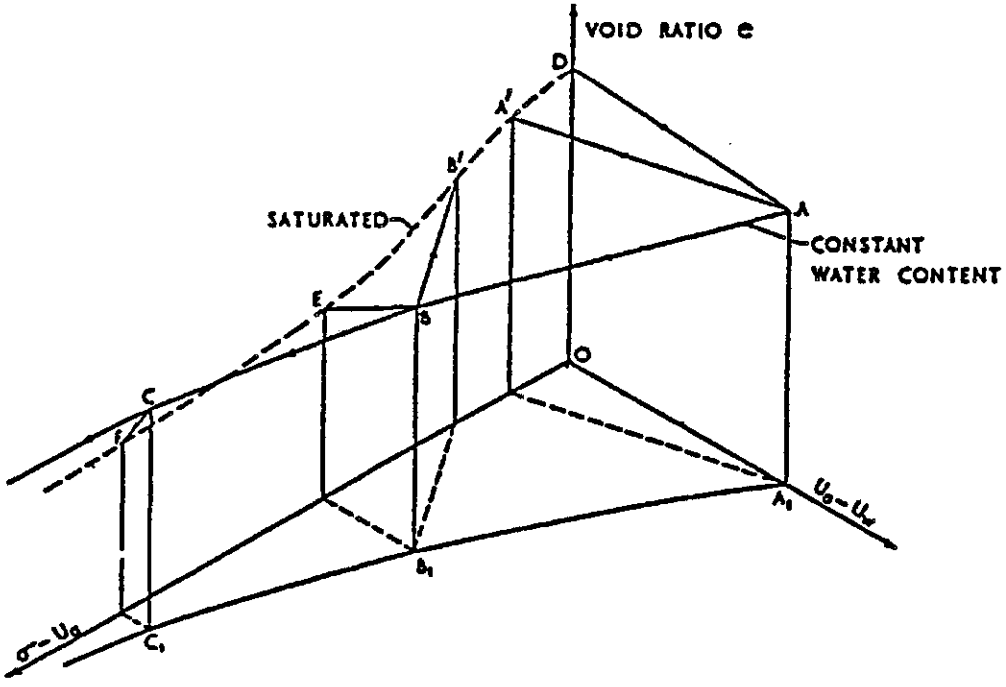

Figure 2.1 Volume Changes under Equal All-Round Pressure Plotted in Void Ratio-Stress State Space (Bishop and Blight, 1963)

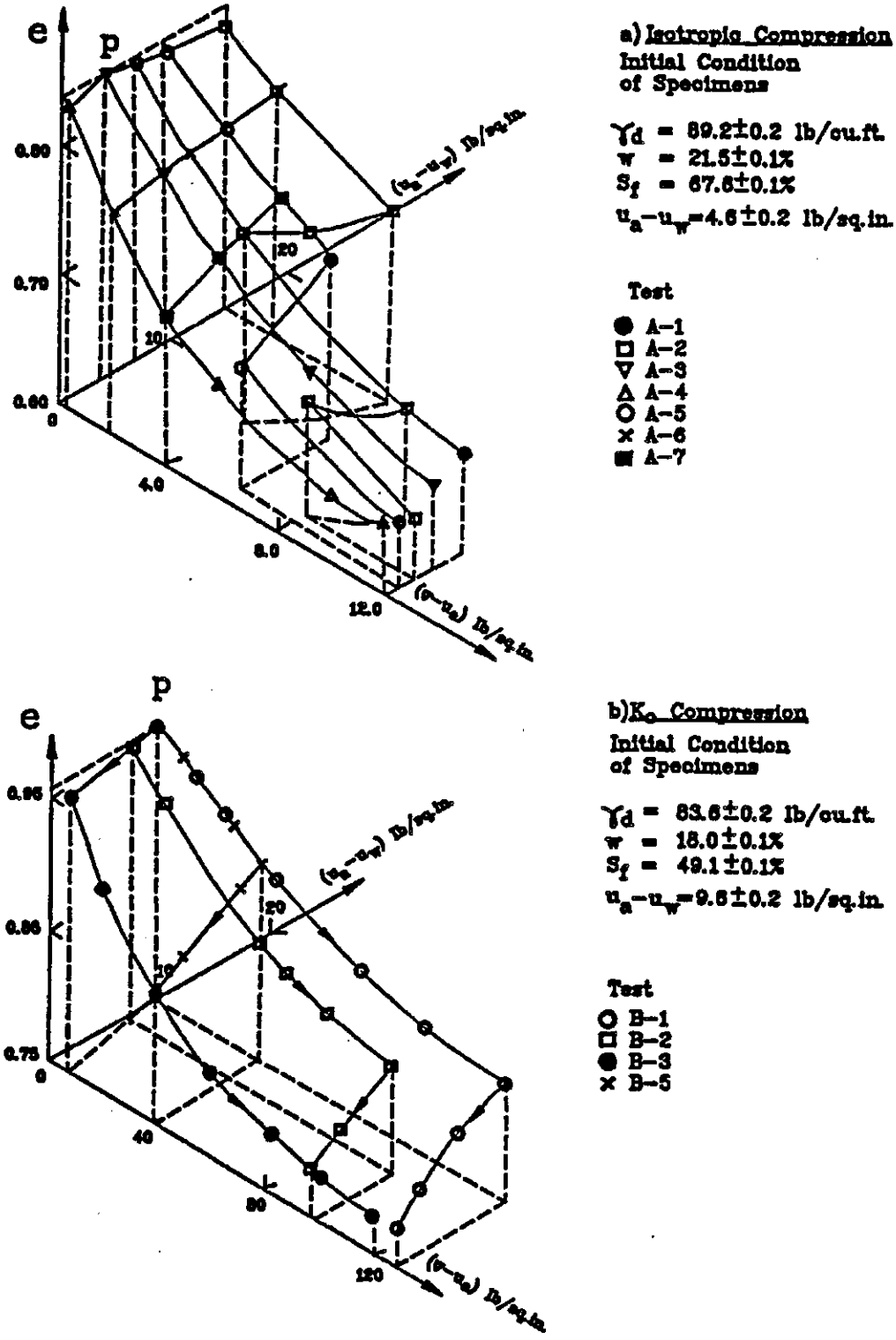

Figure 2.2 Plots Showing the Variation of Void Ratio in (e, $e - u_a$, $u_a - u_w$) Space for A Quartz and Kaolin Mixture (Matyas and Radhakrishna, 1968)

with independent control of suction and applied load be run in accordance with the anticipated field stress path. The resulting volume change curves were proposed to be used for predicting ground movement. Volume change curves of an expansive black earth from Adelaide in south Australia were presented (Figure 2.3). The presented experimental data illustrates the diminishing effect of increasing suction to reduce the volume of a soil and a near linear semi-logarithm relation between suction and strain in the unloading phase.

Barden, Madedor and Sides (1969) conducted a test program to experimentally investigate the volume change behaviour of unsaturated soils under K_o conditions. Coleman's (1962) proposed constitutive relation for studying soil structure volume change under one-dimensional compression was used in the study.

$$\varepsilon_v = C_1 d(\sigma - u_a) + C_2 d(u_a - u_w) \qquad (2.6)$$

where

ε_v = volumetric strain of the soil structure

C_1, C_2 = compressibility moduli with respect to $(\sigma - u_a)$ and $(u_a - u_w)$ respectively

$(\sigma - u_a)$ = net total axial stress

$(u_a - u_w)$ = matric suction

Compacted, low to high plasticity illite specimens were tested. These specimens were subjected to suction and total stress changes of 80 and 450 kPa respectively (Figure 2.4). Specimens in Group 2,3,4,5 underwent monotonic increases in

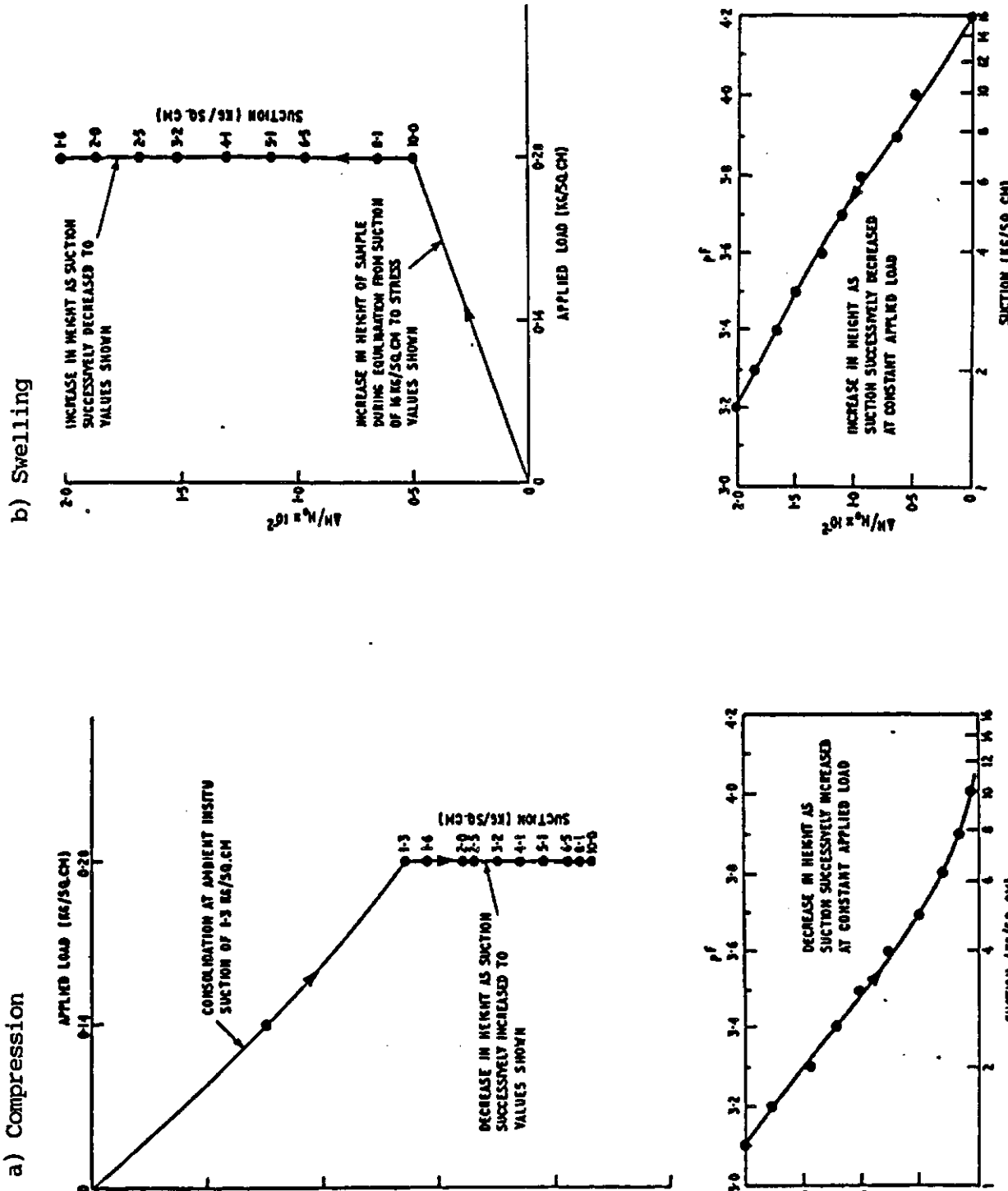

Figure 2.3 Volume Change Curves for a Blank Earth from Adelaide, Australia (Aitchison & Woodburn, 1969)

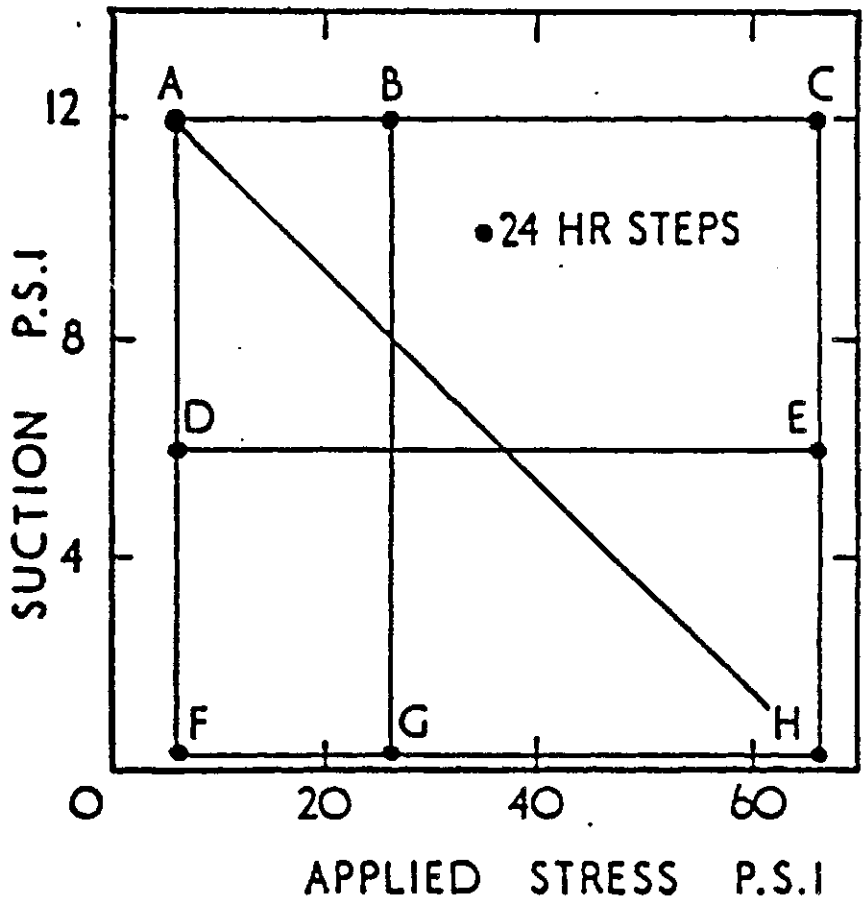

Figure 2.4 Stress Paths for Test Groups 2 to 11 (Barden, et.al., 1969)

degree of saturation and decreases in strain. The test results indicated a unique constitutive surface for soil structure volume change under K_o conditions (Figure 2.5). Specimens in Group 6 and 7 underwent a monotonic increase in the degree of saturation but strain reversals. The test results showed hysteresis in volume changes (Figure 2.6). Group 11 specimens were subjected to both degree of saturation and strain reversals. The test results showed significant stress path dependence in the soil structure deformation (Figure 2.7). The authors reported a gradual decrease in the compressibility modulus, C_1 as the matric suction, $(u_a - u_w)$ increased (Table 2.1). This finding agrees with the "typical family" of soil structure volume change curves (Figure 2.8) presented by Aitchison and Woodburn (1969). Fredlund (1979) later suggested a constitutive model which possessed a similar feature.

In 1971, Brackley used Bishop's effective stress (i.e., equation 2.4) to study unsaturated soil volume change behaviour. Oedometer and triaxial tests on compacted expansive South African clay specimens were performed. The observed collapsing behaviour upon saturation was used to illustrate soil structure volume change behaviour that was inconsistent with Bishop's effective stress equation (Figure 2.9). No definite mathematical equation was proposed for the soil structure volume change constitutive relation.

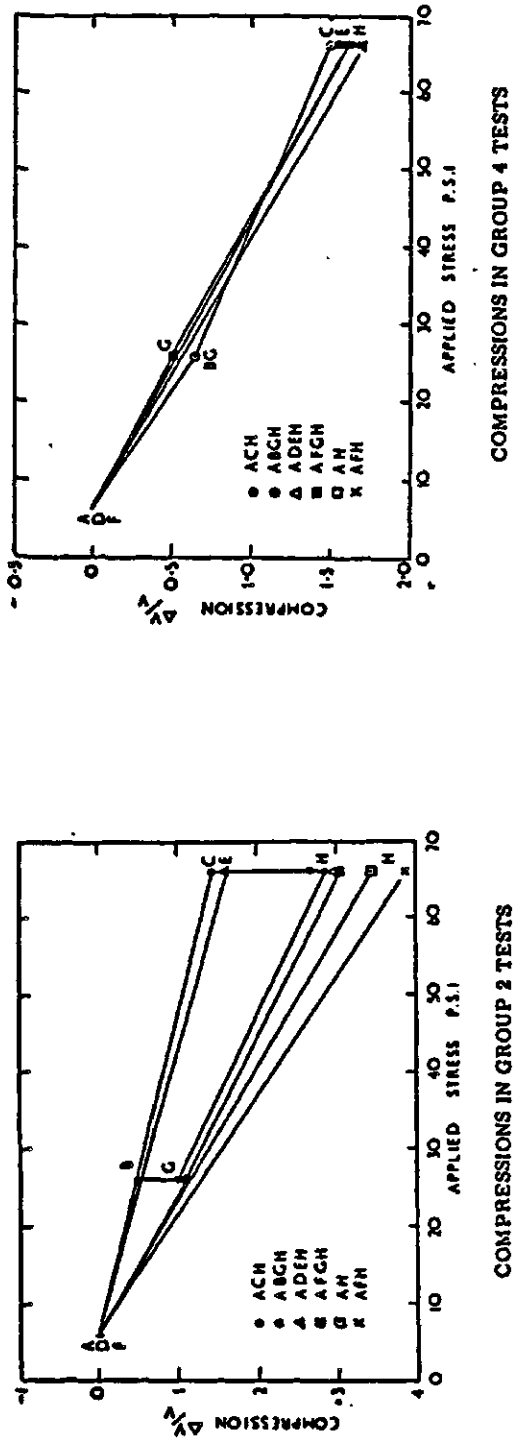

Figure 2.5 Compression Curves for Specimens with Monotonic Increases in Degree of Saturation and Decreases in Strain (Barden, et.al., 1969)

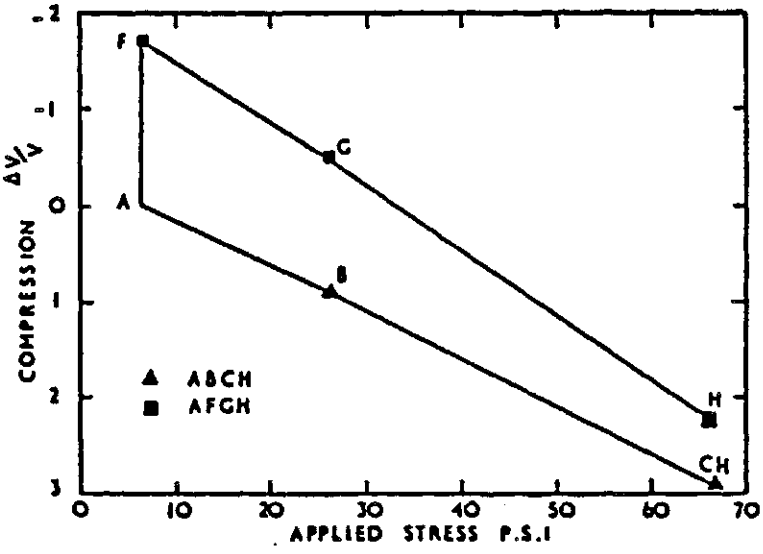

COMPRESSIONS IN GROUP 6 TESTS

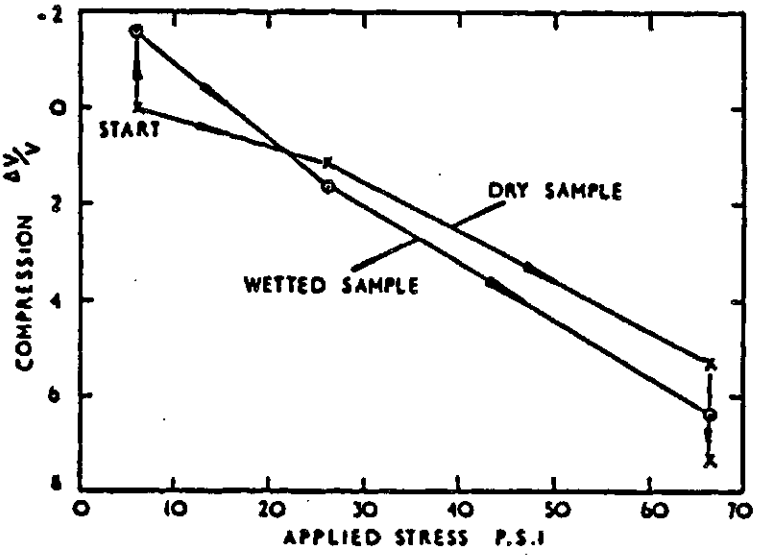

COMPRESSIONS IN GROUP 7 TESTS

Figure 2.6 Compression Curves for Specimens with Monotonic Increases in Degree of Saturation and Strain Reversals (Barden, et.al., 1969)

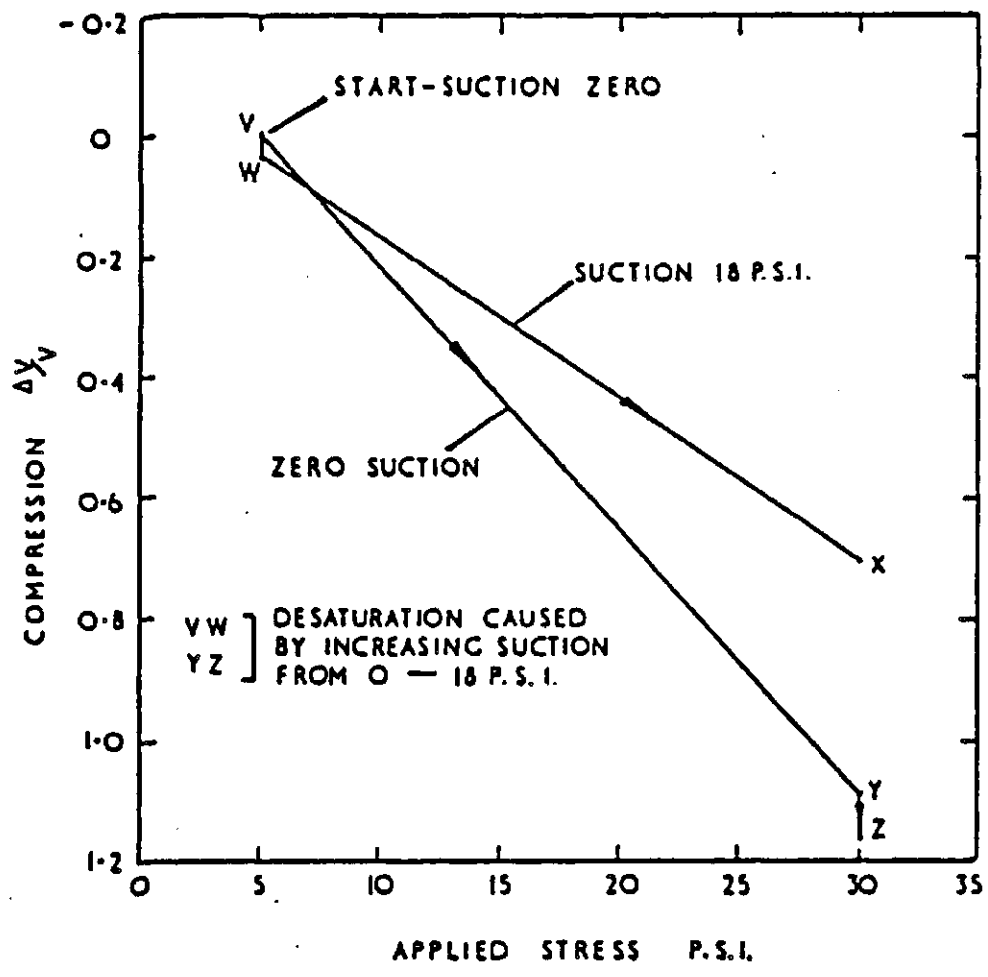

Figure 2.7 Compression Curves for Group II specimens with Both Degree of Saturation and Strain Reversals (Barden, et.al., 1969)

Table 2.1 Effect of Suction Pressure on Compressibility (Barden et. al., 1969)

Group number (1)	Stress path (2)	Suction, in pounds per square inch (3)	C_1, in square inches, per pound (4)
2	AC	12	2.38×10^{-4}
	DE	6	2.67
	FH	0	5.00
4	AC	12	2.64×10^{-4}
	DE	6	2.83
	FH	0	2.69
5	AC	12	5.26×10^{-4}
	DE	6	7.34
	FH	0	13.77
6	AC	12	4.89×10^{-4}
	FH	0	6.60
11	WX	18	2.80×10^{-4}
	VY	0	4.36

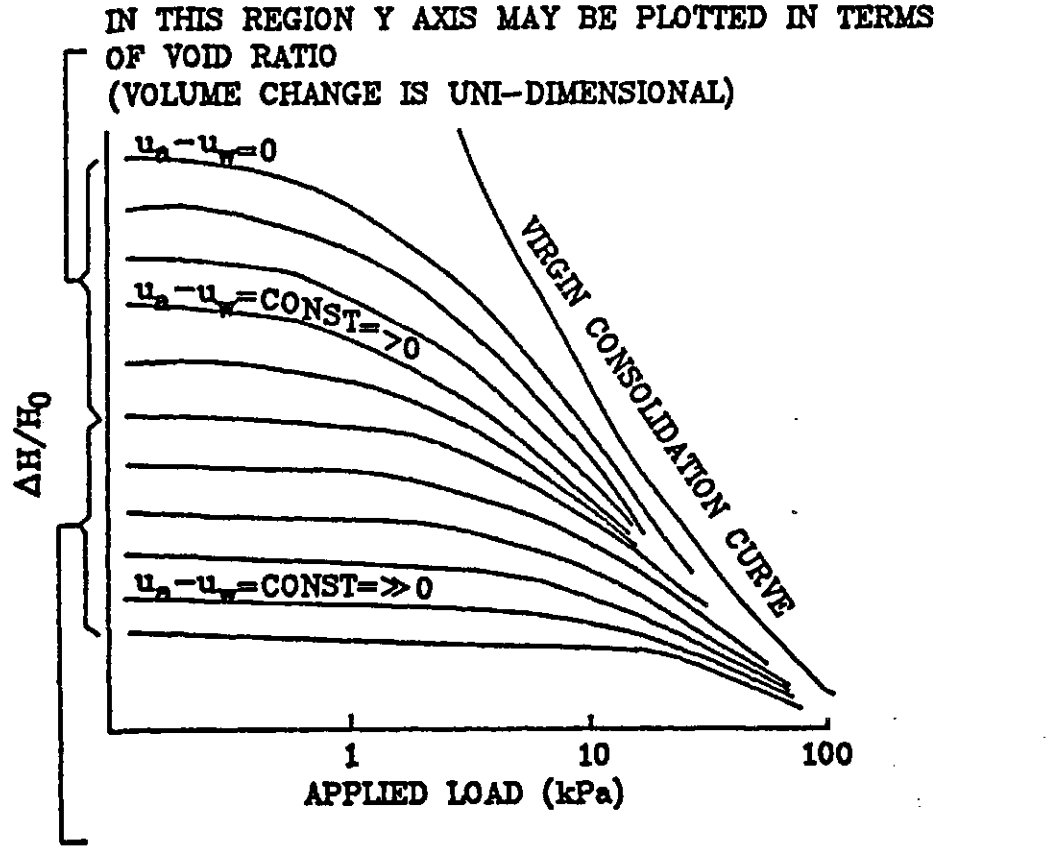

Figure 2.8 Typical Consolidation Curves Throughout the Suction Range (Aitchison and Woodburn, 1969)

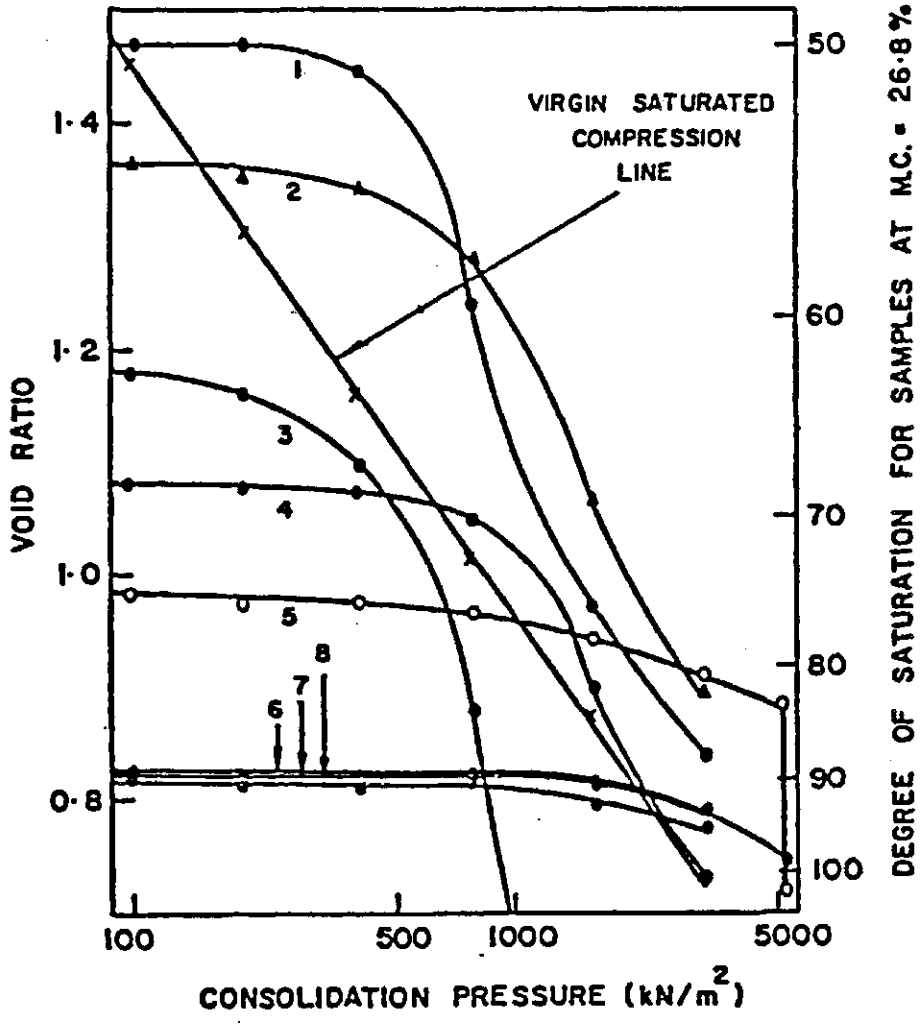

Figure 2.9 Constant Moisture Content Compression Curves for a South African Clay (Brackley, 1971)

During the Third International Conference on Expansive Soils at Haifa in 1973, Aitchison and his co-workers presented a series of papers on the "quantitive description of the stress-deformation behaviour of expansive soils". An effective stress equation (Aitchison, 1965) similar in form to that of Bishop's (1959) was presented.

$$\sigma' = \sigma + \chi_m(u_a - u_w) + \chi_s\pi \qquad (2.7)$$

where

σ' = effective stress

σ = total stress

$(u_a - u_w)$ = matric suction

π = solute suction

χ_m, χ_s = soil parameters within the range 0 to 1 and are stress path dependent

Aitchison (1973) reported that "... it is rarely possible to quantify the operative effective stress (although each stress component may be known) and one must be content with a quantitative soil response to a quantitative change in one or more of the components of effective stress". It was suggested that "stress path studies be adopted in studying the volume change behaviour of unsaturated soils. It was proposed that "... stress path studies give rise to sets of 'behavioral laws' in which the soil response is quantified against a single stress variable with each other stress components remaining constant ... to define sets of simple laws governing relationships between soil properties and individual stress components ...". The following

constitutive relations were suggested for the soil structure volume change of an unsaturated soil (Aitchison et.al., 1973).

$$\varepsilon_\sigma = C_c' (\log\sigma_2 - \log\sigma_1) \quad (2.8)$$

$$\varepsilon_m = I_m . N_m \quad (2.9)$$

$$\varepsilon_s = I_s . N_s \quad (2.10)$$

where

ε_σ = soil structure volumetric strain due to changes in the total stress component, σ

C_c' = compression index at specified values of matric, $(u_a - u_w)$ and solute, π suction

σ_2, σ_1 = total stress

ε_m = soil structure volumetric strain due to changes in the matric suction, $(u_a - u_w)$ component

I_m = matric instability index at specified values of total stress, σ and solute suction, π

N_m = matric suction environmental control, $[\log(u_a - u_w)_2 - \log(u_a - u_w)_1]$

ε_s = soil structure volumetric strain due to changes in the solute suction, π component

I_s = solute instability index at specified values of total stress, σ and matric suction, $(u_a - u_w)$

N_s = solute suction environmental control, $[\log \pi_2 - \log \pi_1]$

A linear variation between the soil structure volumetric strain and the logarithm of the stress variables, σ, $(u_a - u_w)$ and π was assumed. The soil compression and instability indices are basically volume change moduli with respect to the different stress variables. Combining equation (2.8), (2.9) and (2.10) gives an overall constitutive relation for soil structure volume change as

follows.

$$\varepsilon_s = C_c' \log\left(\frac{\sigma_2}{\sigma_1}\right) + I_m \log\left[\frac{(u_a - u_w)_2}{(u_a - u_w)_1}\right] + I_s \log\left[\frac{\pi_2}{\pi_1}\right] \qquad (2.11)$$

where

ε_s = overall volumetric strain of the soil structure

Such an equation is similar in form (but extended) to the conventional constitutive relation for volume change in saturated soils (Terzaghi and Peck, 1967)

$$\varepsilon_s = \frac{C_c}{1+e_o} \log\left(\frac{\sigma_2'}{\sigma_1'}\right) \qquad (2.12)$$

where

C_c = compression index

e_o = initial void ratio

Graphically, the proposed constitutive relation (equation 2.11) represents a family of parallel planar constitutive surfaces using the logarithm of the stress variables, σ, $(u_a - u_w)$ and π as abscissas and contouring variables in the third dimension respectively. Experimental data demonstrating the form of the composite constitutive surface was presented by Aitchison and Martin (1973) (Figure 2.10). The proposed soil structure volume change constitutive relation resembles that presented by Fredlund and Morgenstern (1976) when the pore-air pressure, u_a is atmospheric and there is a constant solute suction environment.

Up to the mid 1970's, considerable experimental work had been conducted to study the soil structure volume

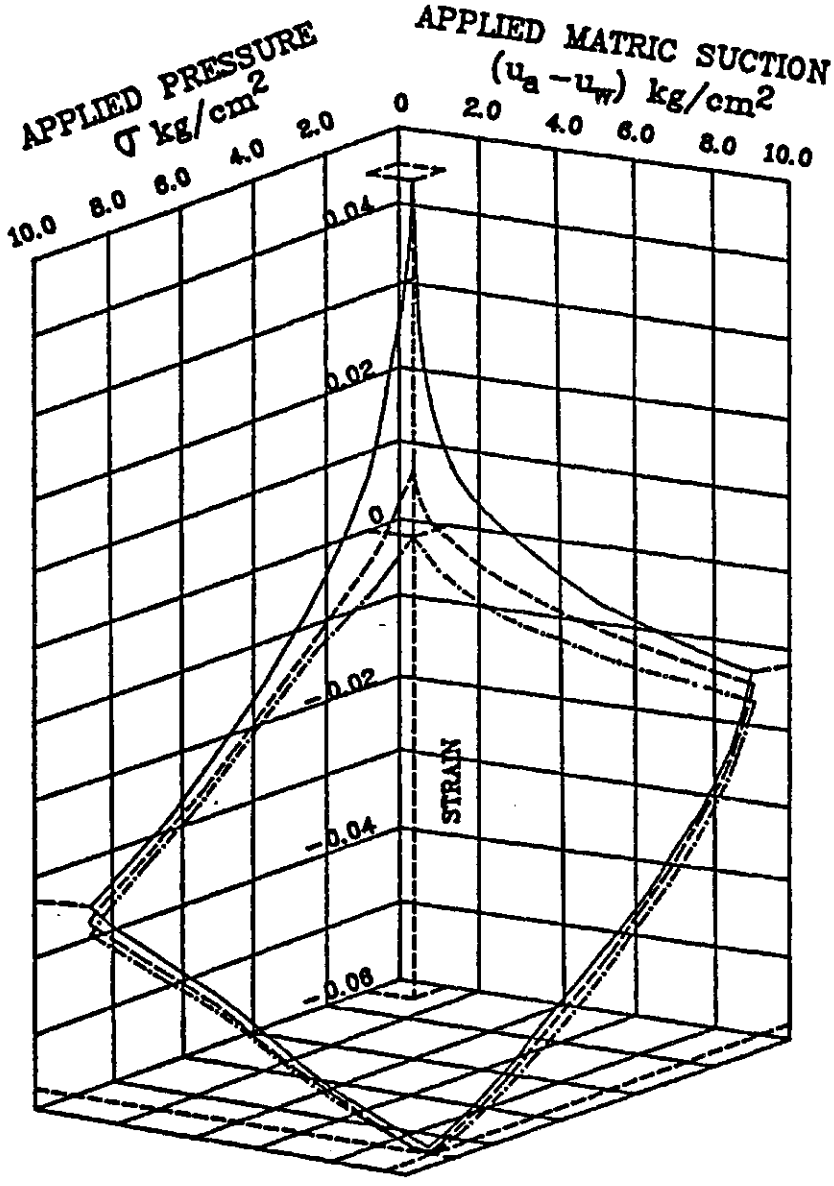

APPLIED SOLUTE SUCTION

———— π = 0.10 kg/cm²

---------- π = 4.00 kg/cm²

———— π = 40.0 kg/cm²

Figure 2.10 Rectilinear Plots of Comparative Effects of Applied Pressure, Matric and Solute Suction for A Pleistorene Clay from Adelaide, South Australia (Aitchison and Martin, 1973)

change characteristics but there was little agreement on how best to formulate the constitutive relation. There was experimental evidence that the independent stress variables, $(\sigma - u_a)$ and $(u_a - u_w)$ together are more appropriate than a single-valued "effective stress", σ' for describing the volume change behaviour (Jennings and Burland, 1962) (Coleman, 1962) (Bishop and Blight, 1963) (Matyas and Radhakrishna, 1968) (Aitchison and Woodburn, 1969) (Barden et.al., 1969) (Brackley, 1971) (Aitchison, 1973). There were suggestions that two volume change constitutive relations, one for the soil structure and one for the pore-water were required to define the volumetric behaviour of an unsaturated soil (Biot, 1941) (Coleman, 1962) (Matyas and Radhakrishna, 1968). Little further explanation was presented. It was apparent that research progress in this area was awaiting a better understanding of the fundamental physical behaviour (Aitchison, 1973).

In 1973, Fredlund identified the governing independent stress (i.e., $(\sigma - u_a)$, $(\sigma - u_w)$ and $(u_a - u_w)$) and deformation (i.e., ε, θ_w and θ_a) state variables for an unsaturated soil. Semi-empirically formulated volume change constitutive relations linking the independent stress and deformation state variables were proposed for the soil structure, pore-water and pore-air phases (Fredlund and Morgenstern, 1976). These constitutive relations were also presented graphically as constitutive surfaces in three

dimensional plots with the stress state variables as abscissas (Figure 2.11). Any two of these three constitutive relations were shown to be required for a complete description of volume change. The volume change constitutive relation of the soil structure was presented as follows.

$$\varepsilon = \frac{1}{V}\frac{\partial V}{\partial(\sigma - u_a)} d(\sigma - u_a) + \frac{1}{V}\frac{\partial V}{\partial(u_a - u_w)} d(u_a - u_w) \qquad (2.13)$$

where

$\frac{1}{V}\frac{\partial V}{\partial(\sigma - u_a)} = m_1^S$, volume change coefficient of the soil structure when $d(u_a - u_w)$ is zero

$\frac{1}{V}\frac{\partial V}{\partial(u_a - u_w)} = m_2^S$, volume change coefficient of the soil when $d(\sigma - u_a)$ is zero

The above relation was presented in a different format to retain consistency with conventional saturated soil mechanics analyses (Fredlund, 1979).

$$de = a_t d(\sigma - u_a) + a_m d(u_a - u_w) \qquad (2.14)$$

where

de = change in void ratio

$a_t = \frac{-de}{d(\sigma - u_a)}$, coefficient of compressibility with respect to the net total stress, $(\sigma - u_a)$

$a_m = \frac{-de}{d(u_a - u_w)}$, coefficient of compressibility with respect to matric suction, $(u_a - u_w)$

It was suggested that the constitutive surface could be linearized over a wider range of stress changes using the logarithm of the stress state variables.

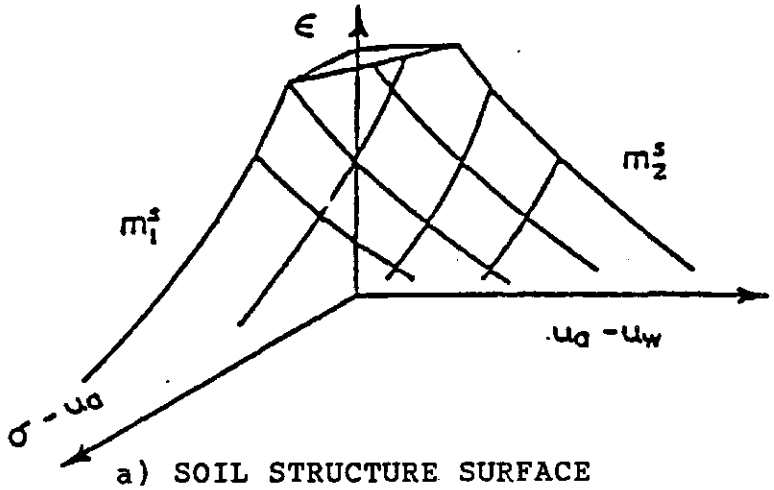

a) SOIL STRUCTURE SURFACE

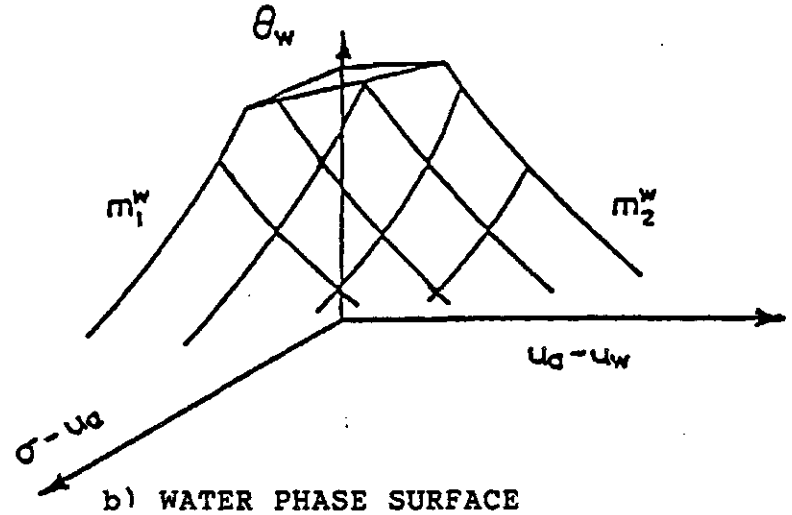

b) WATER PHASE SURFACE

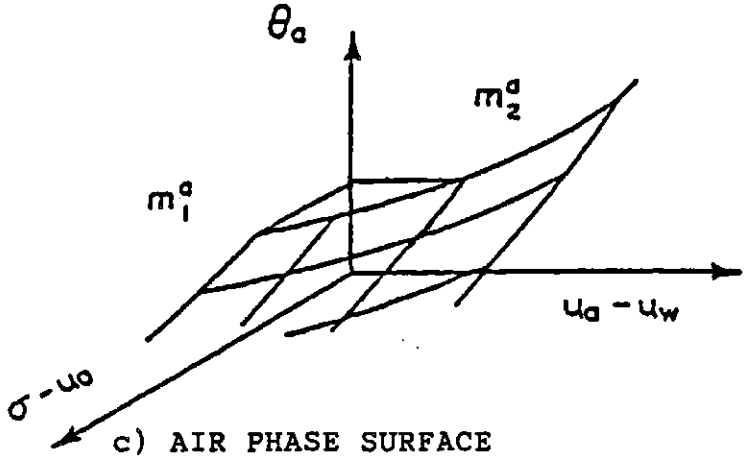

c) AIR PHASE SURFACE

Figure 2.11 Constitutive Surfaces for the Various Phases of an Unsaturated Soil (Fredlund, 1982)

$$e = e_o - C_t \log \frac{(\sigma - u_a)_f}{(\sigma - u_a)_o} - C_m \log \frac{(u_a - u_w)_f}{(u_a - u_w)_o} \qquad (2.15)$$

where

C_t = compressive index with respect to the net total stress,

$$\frac{+\Delta e}{\log \frac{(\sigma - u_a)_f}{(\sigma - u_a)_o}}$$

C_m = compressive index with respect to matric suction,

$$\frac{+\Delta e}{\log \frac{(u_a - u_w)_f}{(u_a - u_w)_o}}$$

Laboratory results demonstrating the validity and uniqueness of the proposed constitutive relations near a stress point, for isotropic and K_o loading conditions, with monotonic deformation were presented. It should be noted that the proposed constitutive relations are similar in form to those suggested by Coleman in 1962. A linear variation between the stress variables on the horizontal planes (i.e., the e = constant, planes) is suggested (Figure 2.12 and 2.13) (Fredlund, 1979 and 1980). The semi-logarithmic constitutive surface is presented as a planar surface.

Chen (1975) performed series of one-dimensional free swell tests on claystone shale specimens. The effect of surcharge pressure, initial specimen thickness, water content, degree of saturation and dry density on swelling pressure was investigated. The test results (Figure 2.14 and 2.15) indicate the swelling pressure is independent of

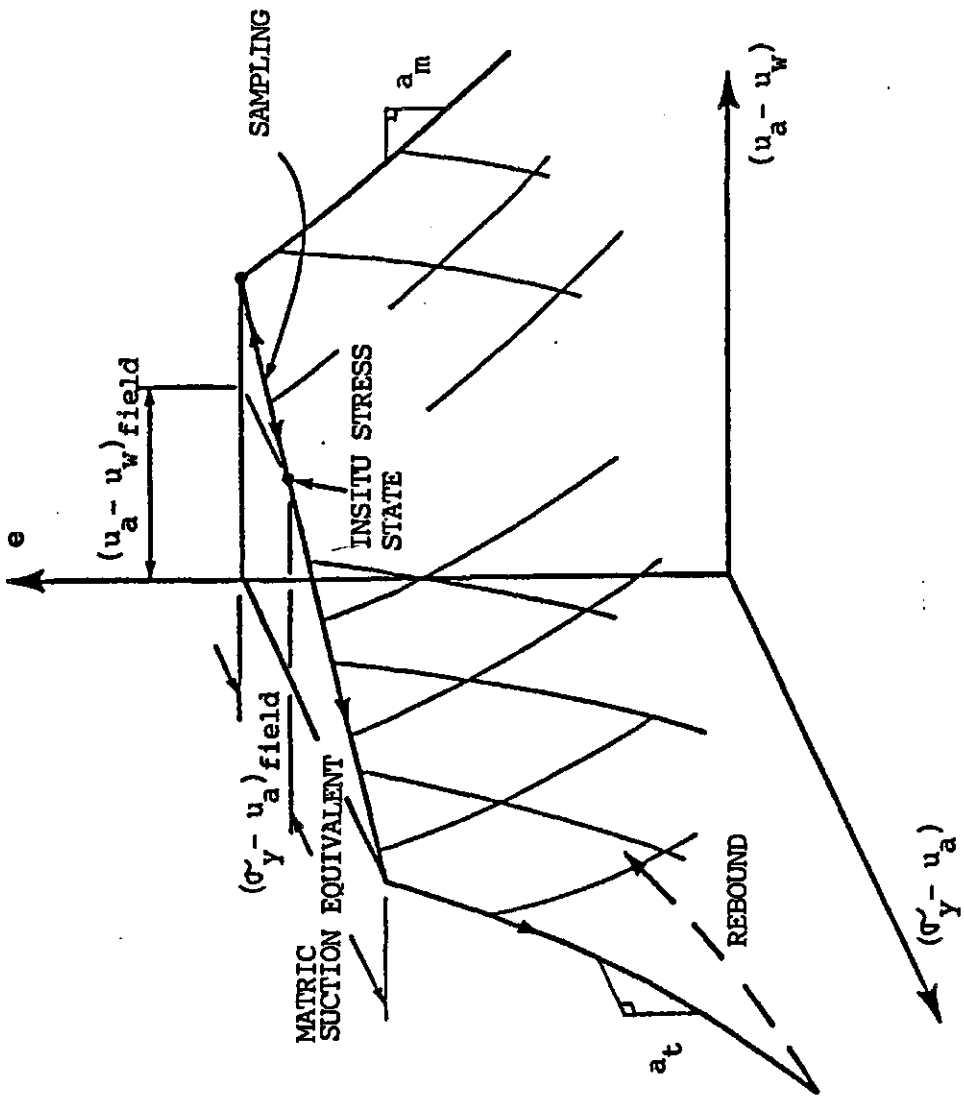

Figure 2.12 Arithmetic Plot of Void Ratio Versus Stress State Variables (Fredlund, 1980)

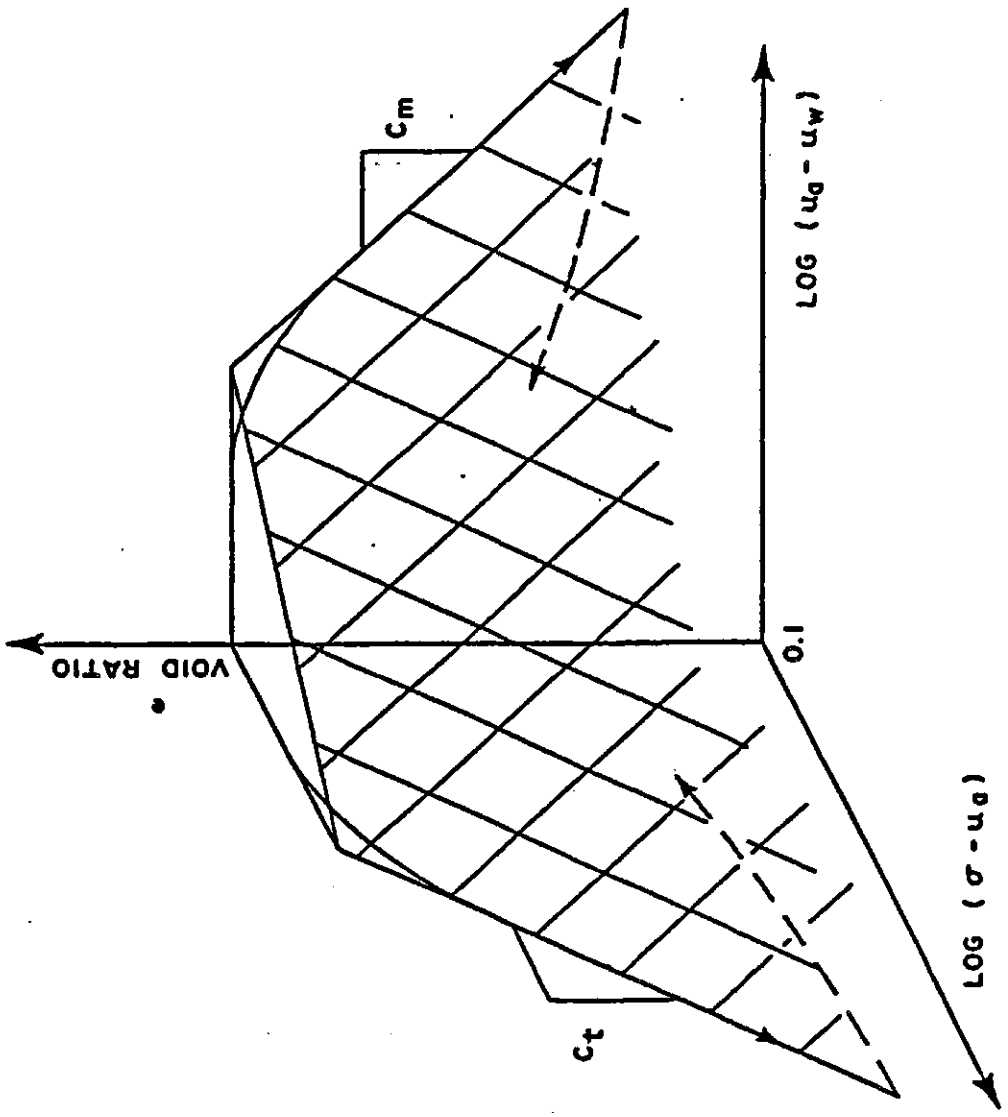

Figure 2.13 Void Ratio Versus Logarithm of Stress State Variables (Fredlund, 1979)

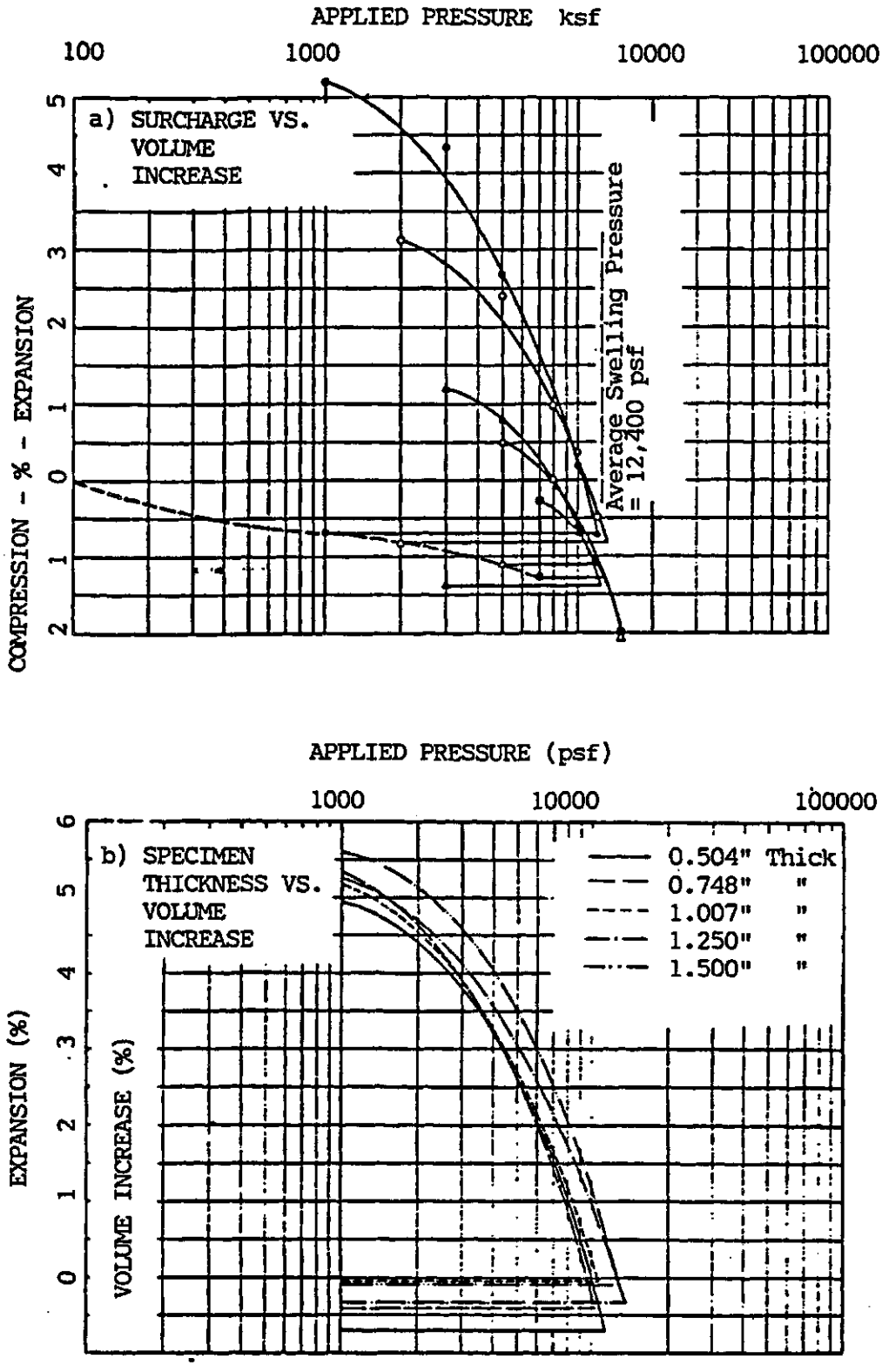

Figure 2.14 Relationships Between Surcharge Pressure, Specimen Thickness and Volume Increase for Constant Density and Water Content Specimens (Chen, 1975)

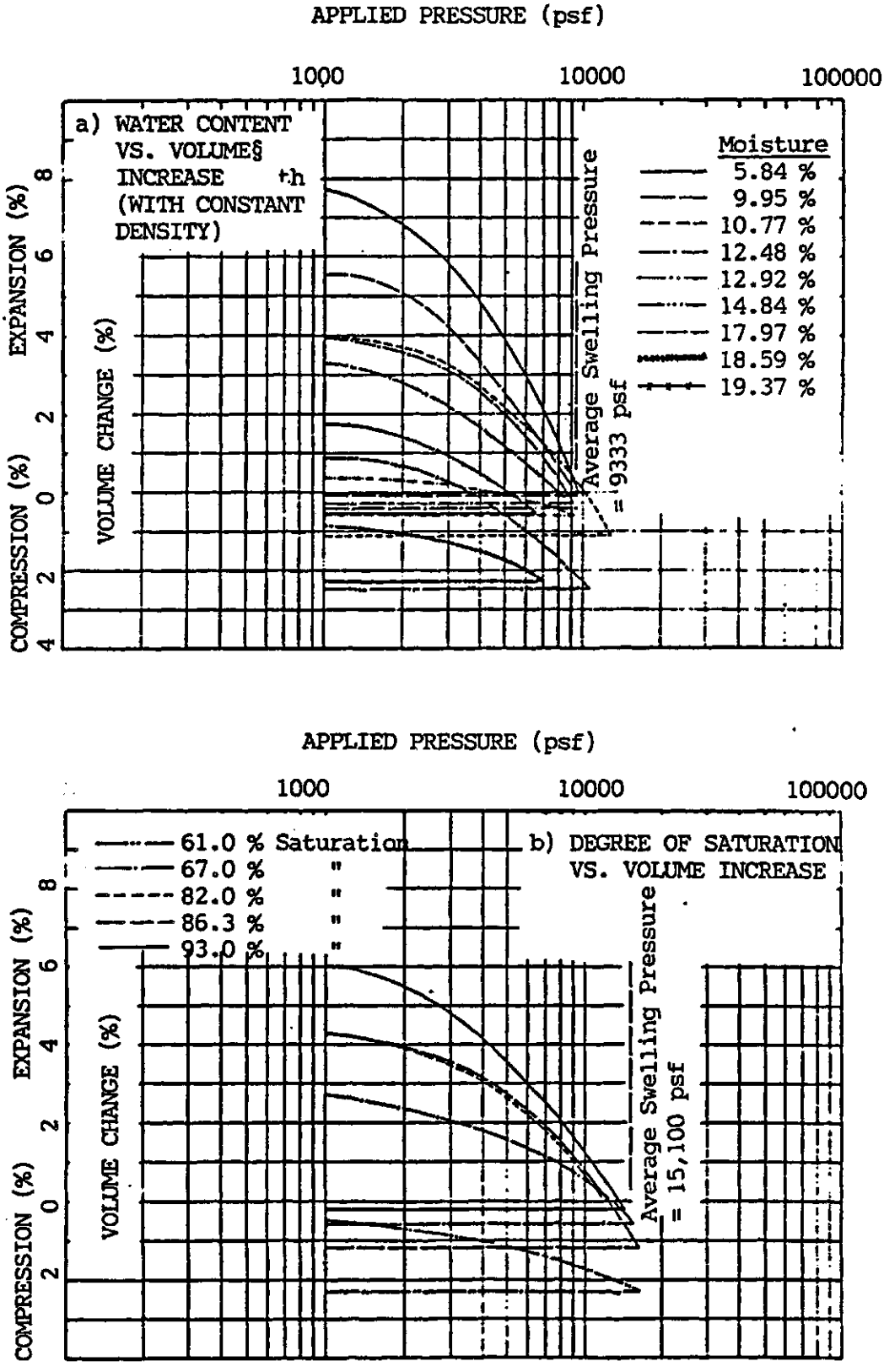

Figure 2.15 Relationships Between Initial Water Content, Degree of Saturation and Volume Increase for Constant Density and Water Content Specimens (Chen, 1975)

the surcharge pressure, initial specimen thickness, water content and degree of saturation. There exists a linear relation between the swelling pressure and dry density in a semi-log scale (Figure 2.16). The relation is exponential in an arithmetic plot (Figure 2.16). This experimental data illustrates some of the characteristics of the soil structure volume change constitutive curve with respect to total stress.

Llorett and Alonso (1980) used a cubic spline interpolation technique (Burden, Faires and Reynolds, 1978) to approximate the volume change constitutive surfaces of the different phases of an unsaturated soil from discrete experimental data points. The volume change constitutive surface of the soil structure was approximated using the soil parameter, porosity, n, as the dependent variable and the stress variables, $(\sigma - u_a)$ and $(u_a - u_w)$ as independent variables. Smooth constitutive curves with respect to either one of the stress variables were defined by third degree polynomials satisfying the following conditions.

1) $n'_{j+1}(x_{j+1}) = n'_j(x_{j+1})$ for each j = 0,1,2...,n-2.

2) $n''_{j+1}(x_{j+1}) = n''_j(x_{j+1})$ for each j = 0,1,2...,n-2.

where

$$x = (\sigma - u_a) \text{ or } (u_a - u_w)$$

Experimental results from one-dimensional and isotropic compression tests presented by Matyas and Radhakrishna (1968) were used in approximating the soil structure volume

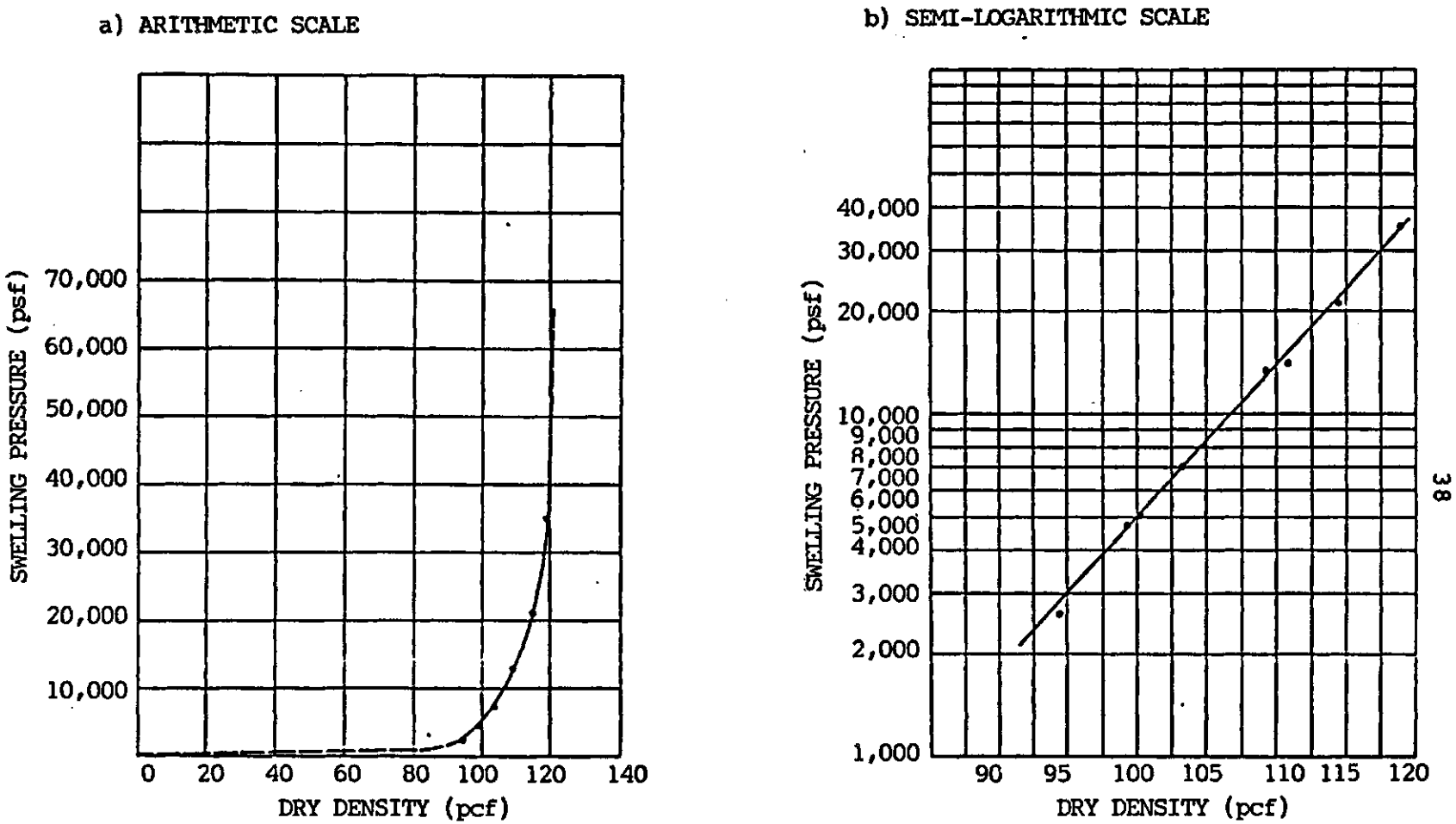

Figure 2.16 Effects of Varying Density on Swelling Pressure for Constant Water Content Specimens (Chen, 1975)

change constitutive surface illustrated in Figure 2.17. The approximated constitutive surface indicates two continuous concave constitutive curves on the two principal planes of $(\sigma - u_a)$ and $(u_a - u_w)$ versus the porosity, n. The mathematical functions representing these curves were not shown. The presented constitutive surface shows a reverse in the direction of deformation with respect to changes in suction, as the total stress increases. This anomaly was not explained. Nevertheless, the paper tends to add more evidence for a unique soil structure constitutive surface with respect to the stress variables, $(\sigma - u_a)$ and $(u_a - u_w)$.

In 1984, Richards, Peter and Martin studied the effect of suction on the soil structure volume change of unsaturated soils under one-dimensional loading conditions. Soil suction was suggested to be composed of two components with the "true soil suction", S defined as follows.

$$S = (u_a - u_w) + \pi \qquad (2.16)$$

where

$(u_a - u_w)$ = matric suction

π = solute suction

Specimens of a Pleistocene clay and a Black Earth from Australia were tested in suction controlled consolidometers and conventional pressure membrane apparatuses. The vertical strain of the specimens under different vertical total stress, matric and solute suction was measured (Figure

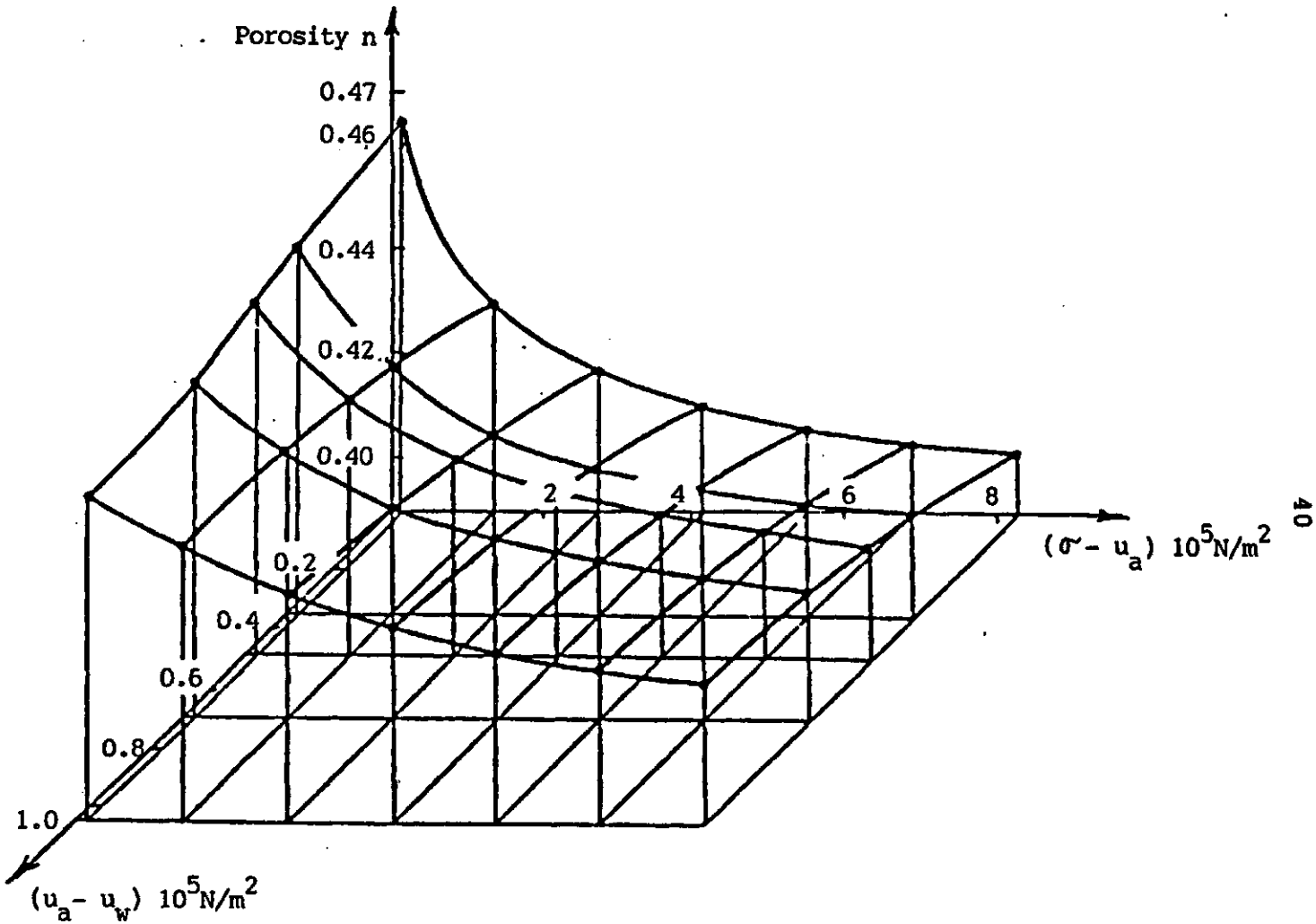

Figure 2.17 State Surface for the Soil Structure (Data Taken from Matyas and Radhakrishna, 1968) (LLorett and Alonso, 1980)

2.18 and 2.19). The presented test data shows the geometry of the soil structure volume change constitutive curves with respect to suction. There exists a "S" shape relation between the soil structure vertical strain and the logarithm of increasing matric suction (Figure 2.18). The curvatures of these "S" shape curves are found to be diminishing to near linear with increasing total vertical stress. The same observation can be made for the constitutive curves of the soil structure with respect to the logarithm of decreasing solute suction (Figure 2.19).

Michell and Avalle (1984) presented the results of another study on soil structure volume change with respect to suction. The one-dimensional soil structure volume change constitutive relation was described as follows.

$$\varepsilon_{vert} = I_{pt}\Delta u_T \qquad (2.17)$$

where

ε_{vert} = vertical strain

I_{pt} = "total" instability index, a soil constant

Δu_t = change in total soil suction, $\Delta[(u_a - u_w)+\pi]$

The "total" instability index is a volume change modulus with respect to total suction. The authors suggested that the instability index, I_{pt} be determined experimentally by dimensional measurements on undisturbed soil cores exposed to surface evaporation. The "core shrinkage test" was introduced. It involved measuring the linear strain versus water content ratio, $\frac{\varepsilon_{vert}}{\Delta w}$ and the "moisture character-

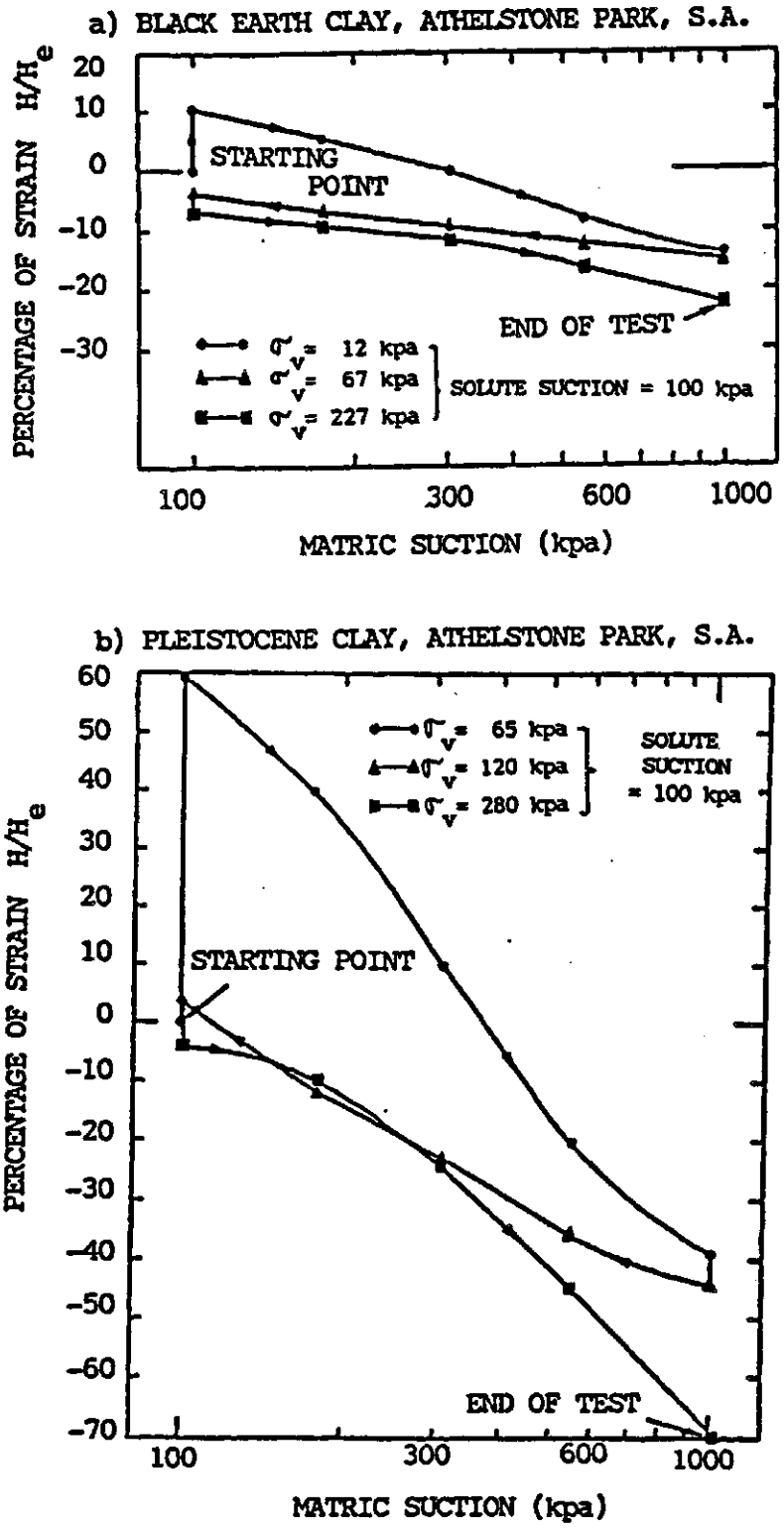

Figure 2.18 Vertical Strain Versus Matric Suction Plots for Black Earth and Pleistocene Clays (Richards, Peter and Martin, 1984)

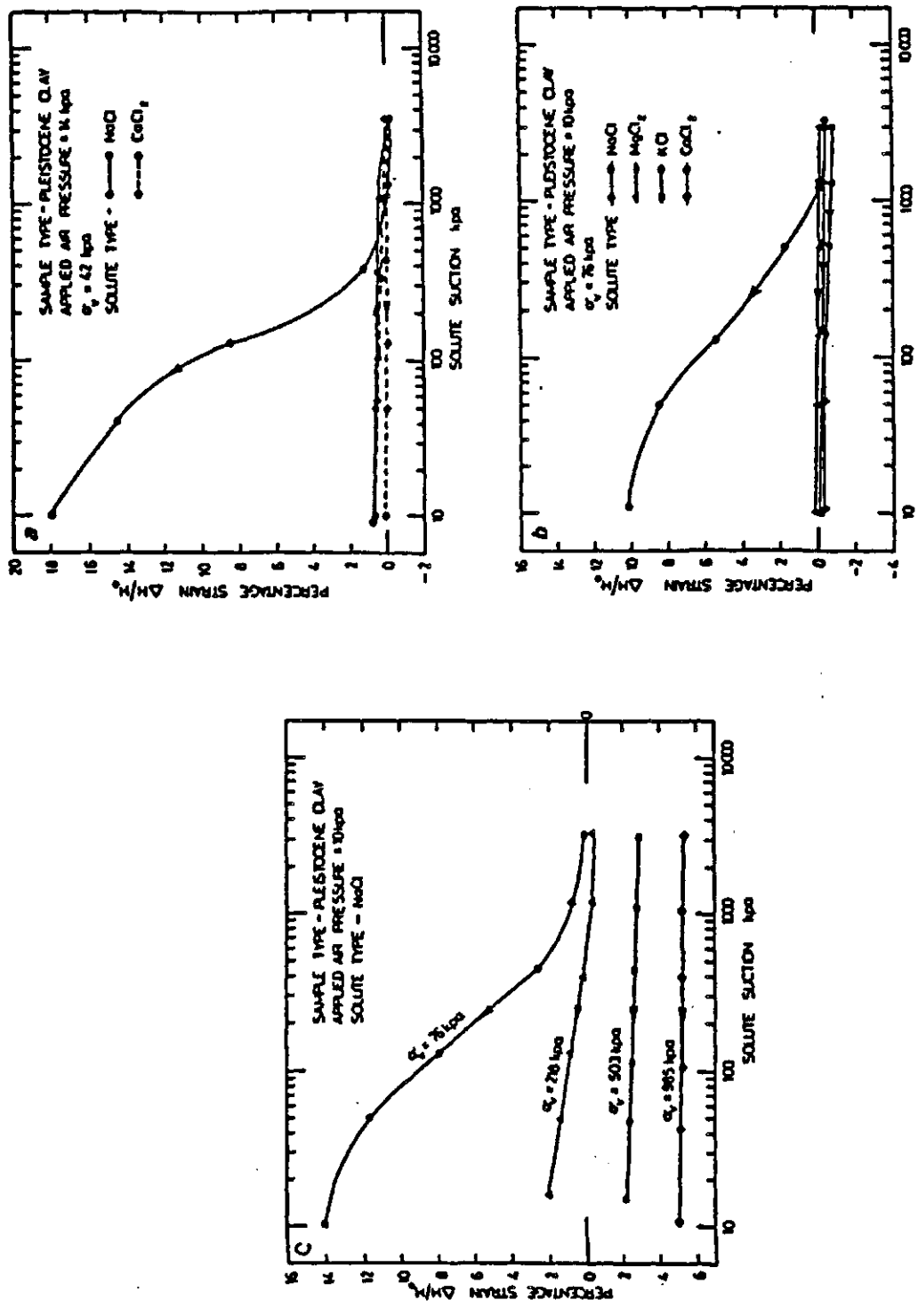

Figure 2.19 Vertical Strain Versus Solute Suction Plots for Pleistocene Clays (Richards, Peter and Martin, 1984)

istics", $\frac{\Delta w}{\Delta u_t}$ of unconfined undisturbed specimens dried from a water content above the shrinkage limit. Thermocouple psychrometers were used to measure the soil suction of the specimens. The "total" instability index was determined as follows.

$$I_{pt} = \frac{\varepsilon_{vert}}{\Delta u_t} = (\frac{\varepsilon_{vert}}{\Delta w}).(\frac{\Delta w}{\Delta u_t}) \qquad (2.18)$$

Test results for a highly plastic O'Halloran Hill clay were presented (Figure 2.20). The procedure was used for heave calculations to predict the field behaviour. Comparisons were made between the predicted and observed amount of heave. The instability index obtained by the method of core shrinkage were shown to be applicable for both shrinking and swelling analyses. Cross-plotting the presented data gives the constitutive curve the soil structure with increasing suction (Figure 2.21). On an arithmetic scale, the data shows the vertical strain at the shrinkage limit to be the lower asymptotic boundary of the constitutive curve. On a semi-logarithmic scale, the relation is essentially bi-linear.

Lloret and Alonso (1985) sought analytical expressions to describe the volume change constitutive surfaces of unsaturated soils subjected to confined or isotropic compression, through optimization techniques. Mathematical functions (Table 2.2) including those published in the literature as proposed volume change constitutive

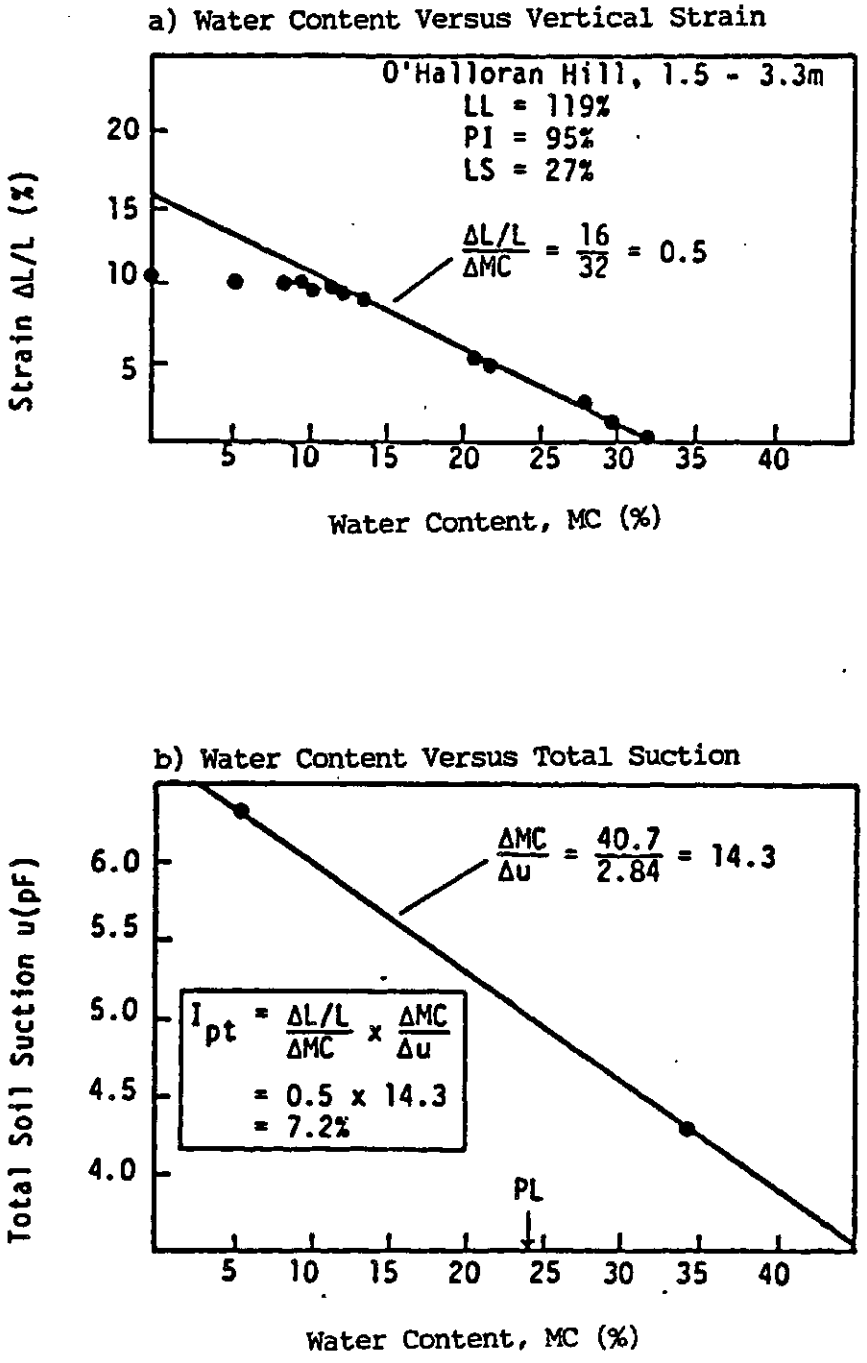

Figure 2.20 Core Shrinkage Test Results for an O'Halloran Hill Clay (Mitchell and Avalle, 1984)

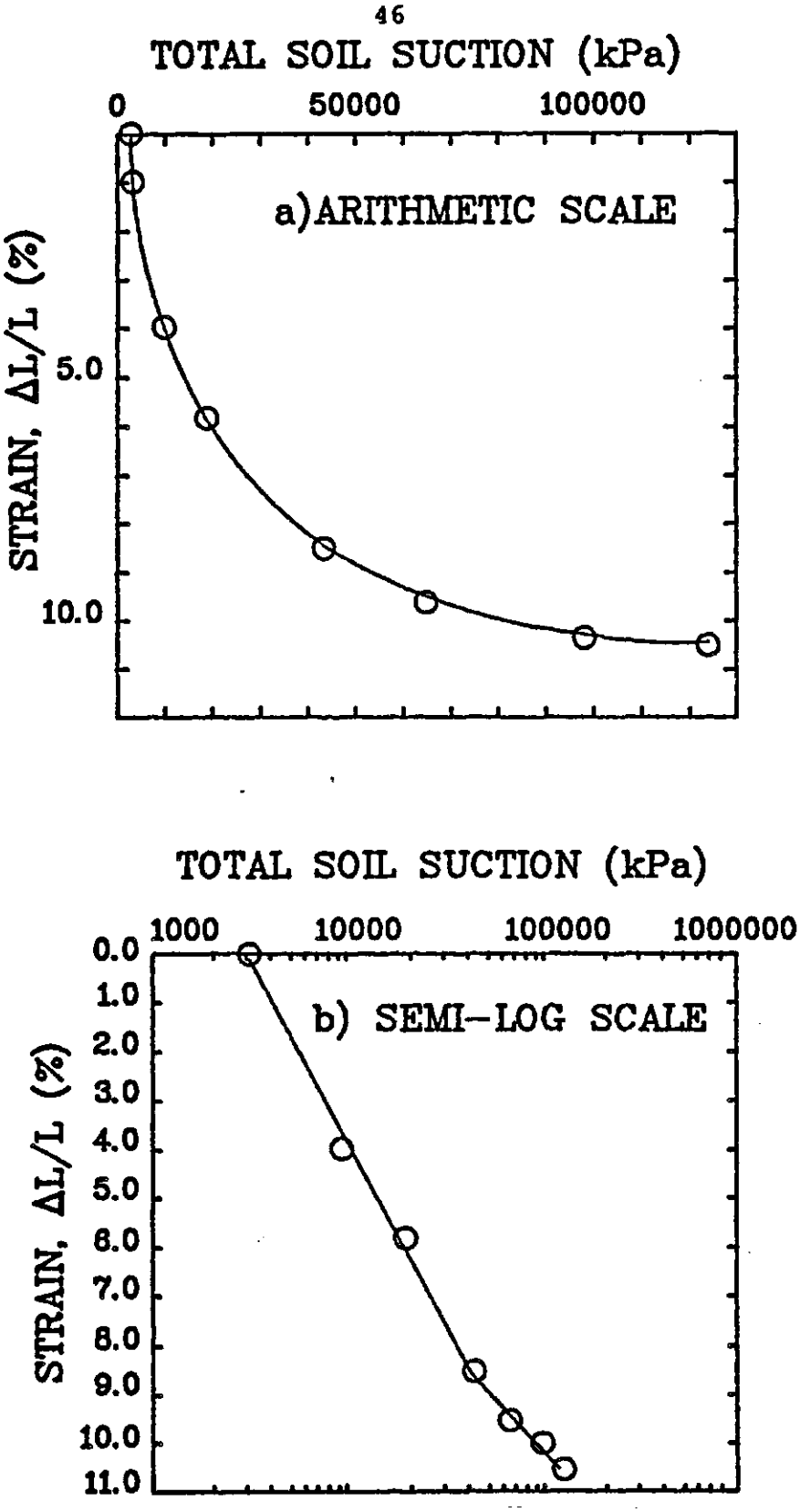

Figure 2.21 Constitutive Curve of the O'Halloran Hill Clay with respect to Total Suction (Mitchell and Avalle, 1984)

Table 2.2 Functions Used for State Surface Approximation (Lloret and Alonso, 1985)

CASE	FUNCTION
1	$e_{S_r} = a + b(\sigma - u_a) + c(u_a - u_w)$
2	$e_{S_r} = a + b \log(\sigma - u_a) + c(u_a - u_w)$
3	$e_{S_r} = a + b(\sigma - u_a) + c \log(u_a - u_w)$
4	$e_{S_r} = a + b \log(\sigma - u_a) + c \log(u_a - u_w)$
5	$e_{S_r} = a + b(\sigma - u_a) + c(u_a - u_w) + d(\sigma - u_a)(u_a - u_w)$
6	$e_{S_r} = a + b \log(\sigma - u_a) + c(u_a - u_w) + d \log(\sigma - u_a)(u_a - u_w)$
7	$e_{S_r} = a + b(\sigma - u_a) + c \log(u_a - u_w) + d(\sigma - u_a)\log(u_a - u_w)$
8	$e_{S_r} = a + b \log(\sigma - u_a) + c \log(u_a - u_w) + d \log(\sigma - u_a) \log(u_a - u_w)$
9	$S_r = a - Th[b(u_a - u_w)] [c + d(\sigma - u_a)]$
10	$S_r = a - [1 - e^{-b(u_a - u_w)}] [c + d(\sigma - u_a)]$

relations were analyzed. Theoretical predictions using these analytical functions were compared with the test results on different soil types (Table 2.3). An analysis of the applicability of the different expressions was made and the optimum functions were selected on the basis of minimum fitting errors. The following conclusions were drawn for the soil structure volume change constitutive relation.

(a) "For a limited variation range of total external stress, a suitable analytical expression for the state surface of void ratio is,

$$e = a + b(\sigma-u_a) + c \log(u_a- u_w) + d(\sigma-u_a)\log(u_a-u_w) \quad (2.19)$$

(b) If the range of significant stress variation is larger a more suitable state function for void ratio is given by,

$$e = a + b \log(\sigma-u_a) + c \log(u_a- u_w) + d \log(\sigma-u_a)\log(u_a-u_w) \quad (2.20)$$

where a,b,c and d are all soil constants".

These two equations are of the same form being,

$$z = a + bx + cy + dxy \quad (2.21)$$

where

z = the void ratio, e

x = the net total stress, $(\sigma - u_a)$ for equation (2.19); the logarithm of the net total stress, $(\sigma - u_a)$ for equation (2.20)

and y = the logarithm of matric suction, $(u_a- u_w)$ for both equations (2.19) and (2.20)

Table 2.3 Test Program for The Verification of The Various Constitutive Functions (Lloret and Alonso, 1985)

Characteristics of Soils Analyzed

Type of Soil (Reference)	W_L (%)	W_P (%)	I_P (%)	% < #200	Unified Classification	G_s	Composition	Sample Preparation
1. Silty Clay (Jennings and Burland, 1962)	56.4	21.2	35.2	23	CH	2.75	80% quart site 20% Wyoming bentonite	Formed in moulds and brought to equilibrium
2. Kaolin (Matyas and Radhakrishna, 1968)	29	25	4	8	ML	2.63	80% flint powder 20% Peerless Clay	Statically compacted
3. West Water Clay (Barden et.al., 1969)	20	16	4	10	CL	2.66	Illite	Half Proctor compacted
4. Kaolin (Lloret, 1982)	41	29	12	4	ML	2.65	Kaolin	Statically compacted
5. "Pinolem" Clayey sand	32.2	18.5	13.7	3	SC	2.72	-------	Kneading compacted

Characteristics of Test Series Analyzed

Test series	Type of test[a]	Type of soil (Table above)	Initial void ratio	Initial degree of saturation	Suction range (10^5 N/m^2)	Range of Applied Load (10^5 N/m^2)	No. of points to define state surface e/S_r	Type of stress path[b]
1	A	4	0.934	0.517	0 - 1	0.05 - 8	41/36	C
2	B	4	0.934	0.517	0.2 - 1	0.1 - 2	8/8	D
3	A	5	0.474	0.433	0 - 1	0.05 - 8	25/25	D
4	B	2	0.825	0.676	0 - 1.03	0.14 - 8.27	31/31	C
5	A	2	0.963	0.491	0 - 0.64	0.14 - 8.27	29/29	C
6	B	1	0.838	0.504	0 - 31.02	0.1 - 30.6	21/12	D
7	A	3	0.475	0.400	0.02 - 0.82	0.41 - 4.5	15/-	C

Notes: a) A: One-dimensional deformation
B: Isotropic compression
b) C: Loading under constant suction alternating with suction decrease with suction decrease
D: Loading under constant suction

A schematic illustration of the constitutive surface representing the optimum state function for wide stress range (i.e., equation 2.20) is presented in Figure 2.22. The constitutive curves on the net total stress and matric suction planes are essentially linear on a semi-logarithmic scale. One a semi-logarithmic plot of net total stress and matric suction versus void ratio, the constitutive surface resembles a quarter section of the convex surface of a vertical cone.

After the mid 1970's, there was experimental evidence that there exists a unique soil structure volume change constitutive surface with respect to the stress variables, $(\sigma - u_a)$ and $(u_a - u_w)$ (Fredlund and Morgenstern, 1976) (Llorett and Alonso, 1980). If the volume change process involves changes in ion concentration of the soil water, the solute suction, π was suggested to be considered as a component of the changing stress state (Richard, Peter and Martin, 1984).

There were test results indicating that the soil structure volume change constitutive curve with respect to the logarithm of increasing suction is bi-linear and becoming asymptotic towards the void ratio at the shrinkage limit (Mitchell and Avalle, 1984). On a semi-logarithmic scale, the soil structure constitutive surface was suggested to be planar (Fredlund, 1979). There were indications that the same surface could be curved (Llorett and Alonso, 1985).

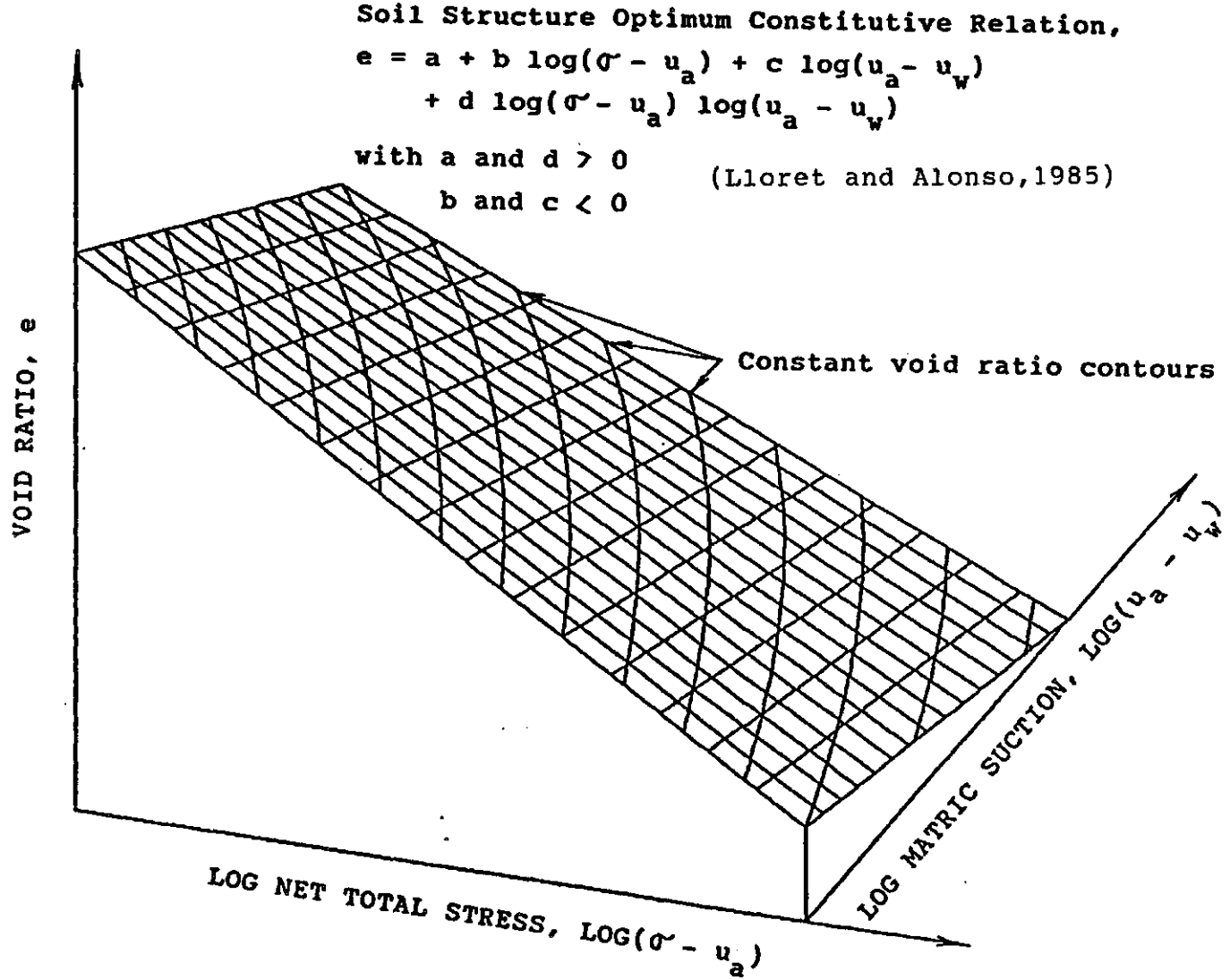

Figure 2.22 Schematic Representation of The Optimum Soil Structure Volume Change Constitutive Relation for Unsaturated Soils

2.2.2 Constitutive relation for the water phase

Biot (1941) presented a mathematical formula as the water phase volume change constitutive relation for a soil "not completely saturated with water and containing air bubbles".

$$\theta_w' = \frac{(\sigma_x + \sigma_y + \sigma_z - 3u_w)}{3H_1} + \frac{u_w}{R^*} \qquad (2.22)$$

where

θ_w' = increment of water volume per unit volume of soil

H_1 and R^* = soil parameters, physical constants

The coefficients, $\frac{1}{H_1}$ and $\frac{1}{R^*}$ were identified as measures of the changes in net volume of pore-water in a soil element for a given change in the mean effective stress and water pressure, respectively. No experimental verification was presented. This formulation is of interest although it was not derived for soils with a continuous air phase. Fredlund and Morgenstern (1977) showed that any two of the three stress variables, $(\sigma - u_a)$, $(\sigma - u_w)$ and $(u_a - u_w)$ are sufficient to completely define the stress state of an unsaturated soil. For soils with interconnected air voids at atmospheric pressure, $(u_a - u_w)$ equals the pore-water pressure, $-u_w$. The Biot (1941) formulation is nevertheless a legitimate water phase volume change constitutive relation for soils with a continuous air phase at atmospheric pressure.

In 1954, Croney and Coleman studied the suction versus water content relation. A wide variety of soils ranging from heavy clays to sands were tested. The suction versus water content curves of these soils under increasing and decreasing suction were presented (Figure 2.23 to 2.27). These are basically water phase volume change constitutive curves on the matric suction principal plane. No constitutive relation was proposed based on the experimental data. Nevertheless, the results illustrate the characteristics of the water phase volume change constitutive curve with respect to suction.

Coleman (1962) suggested a constitutive relation for the net water volume change in an unsaturated soil.

$$-\frac{dV_w}{V} = -C_{11}(du_w - du_a) + C_{12}(d\sigma - du_a) + C_{13}(d\sigma_1 - d\sigma_3) \quad (2.23)$$

or

$$-\frac{dV_w}{V} = -C_{11}(du_w - du_a) + C_{12}(d\sigma - du_a) + C_{13}(d\sigma_1 - d\sigma_3) \quad (2.24)$$

where

dV_w = the change in the volume of water held in the soil

V = current overall volume of a soil element

C_{11}, C_{12}, C_{13} = soil parameters depend upon the current values of $(u_w - u_a)$, $(\sigma - u_a)$ and $(\sigma_1 - \sigma_3)$ and the stress history of the soil

Experimental verification was not presented. However, for an isotropic elastic soil under one-dimensional or isotropic stress conditions, the proposed constitutive relation becomes,

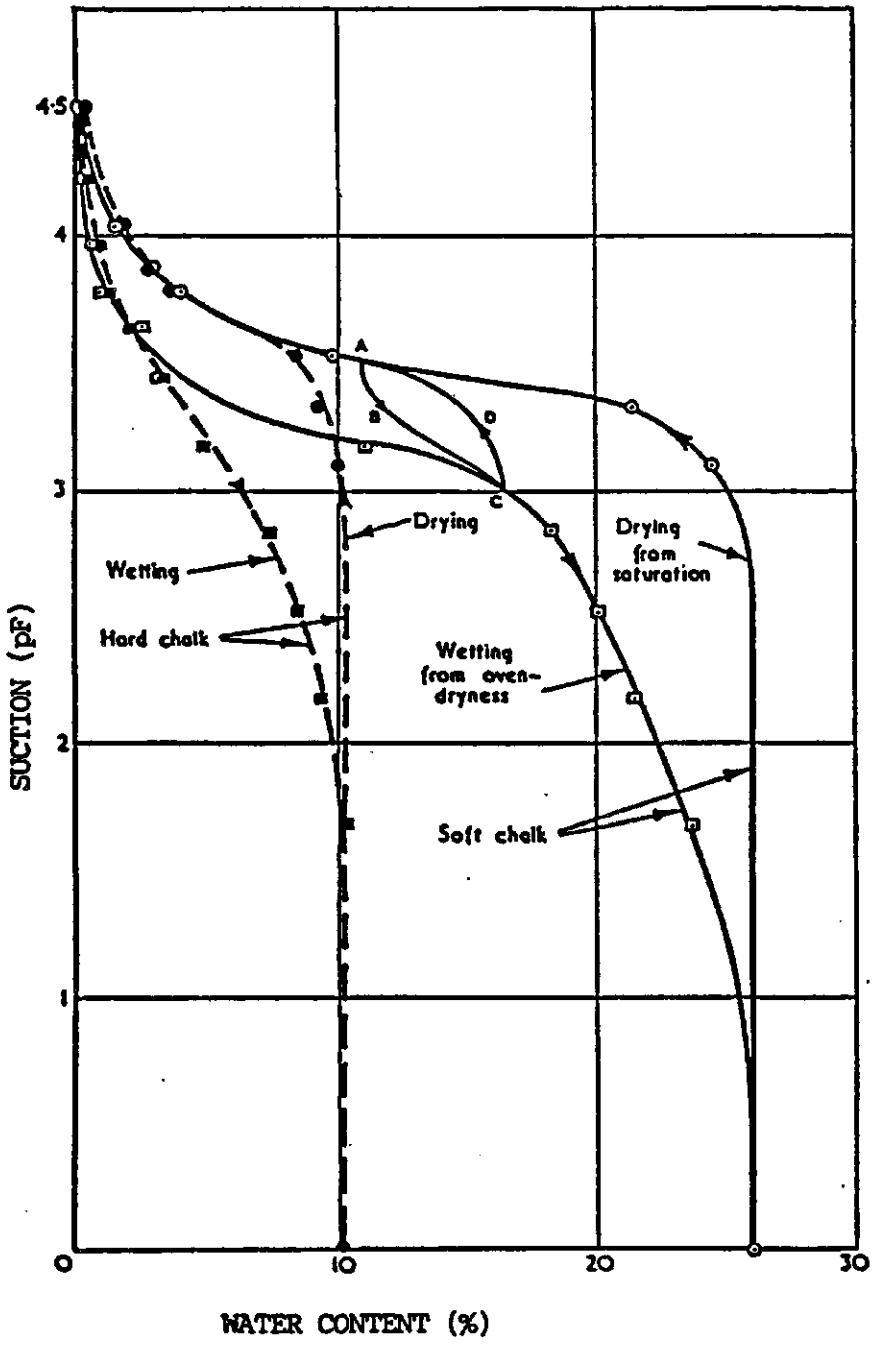

Figure 2.23 Relationships between Suction and Water Content for Samples of Hard and Soft Chalk (Croney and Coleman, 1954)

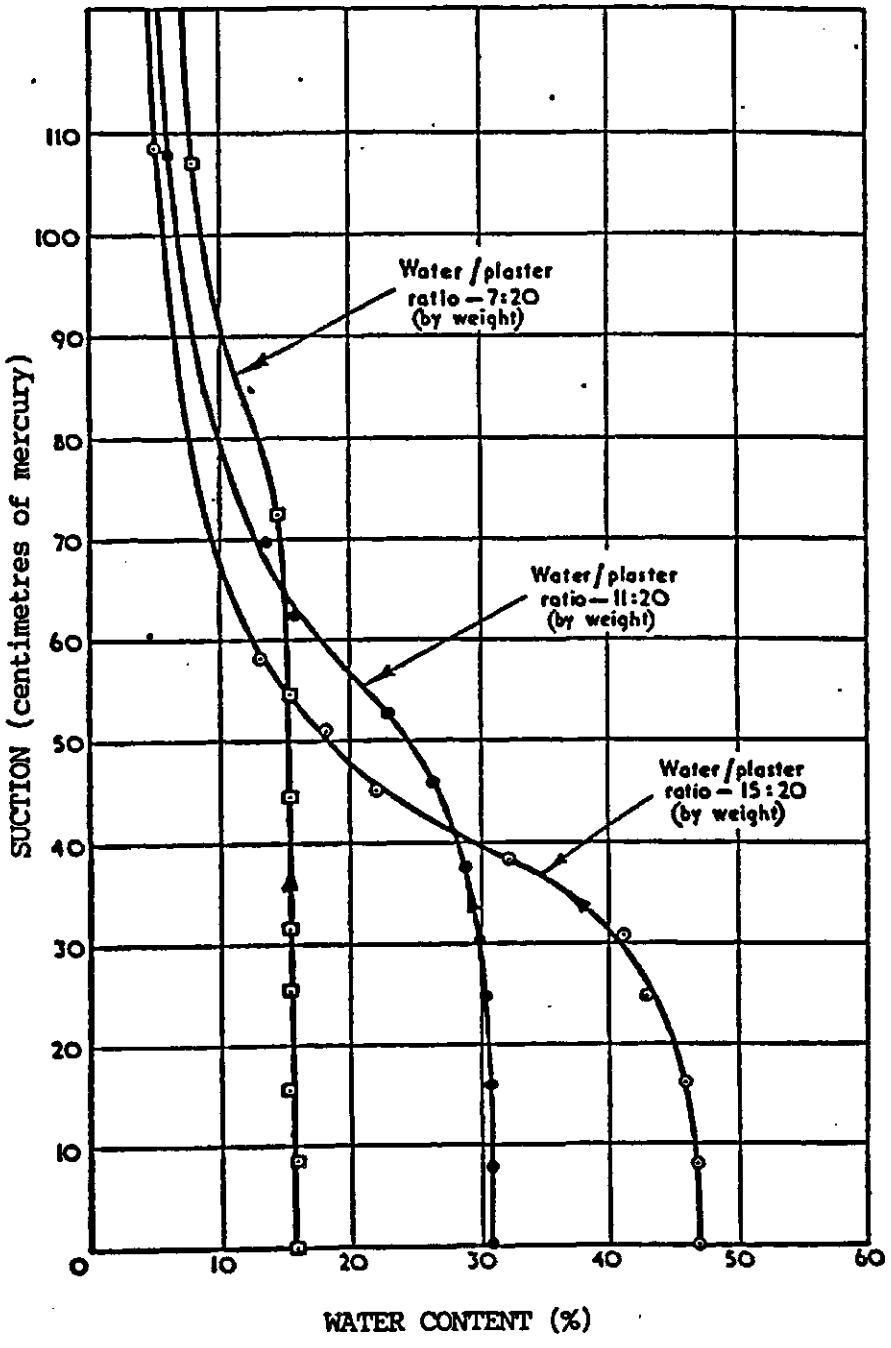

Figure 2.24 Relationships between Suction and Water Content for Three Mixes of Plaster of Paris: drying condition (Croney and Coleman, 1954)

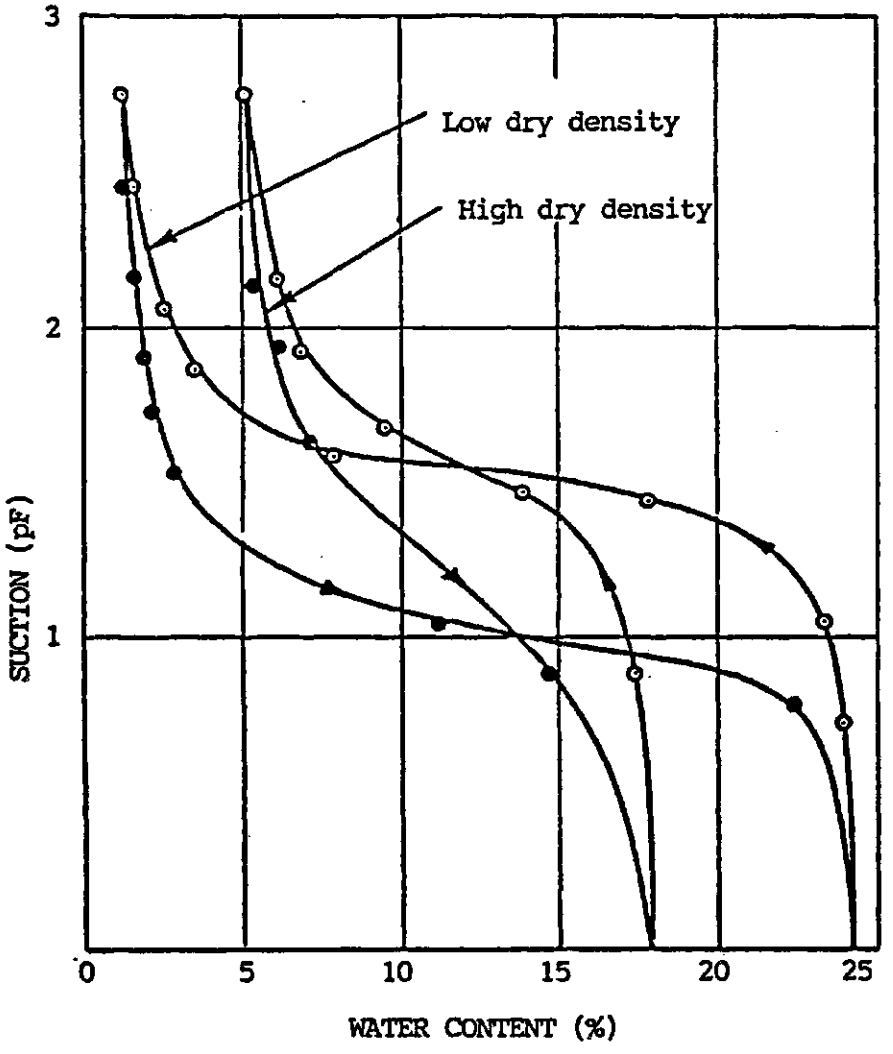

Figure 2.25 Relationships between Suction and Water Content for a Silty Sand at Two Densities (Croney and Coleman, 1954)

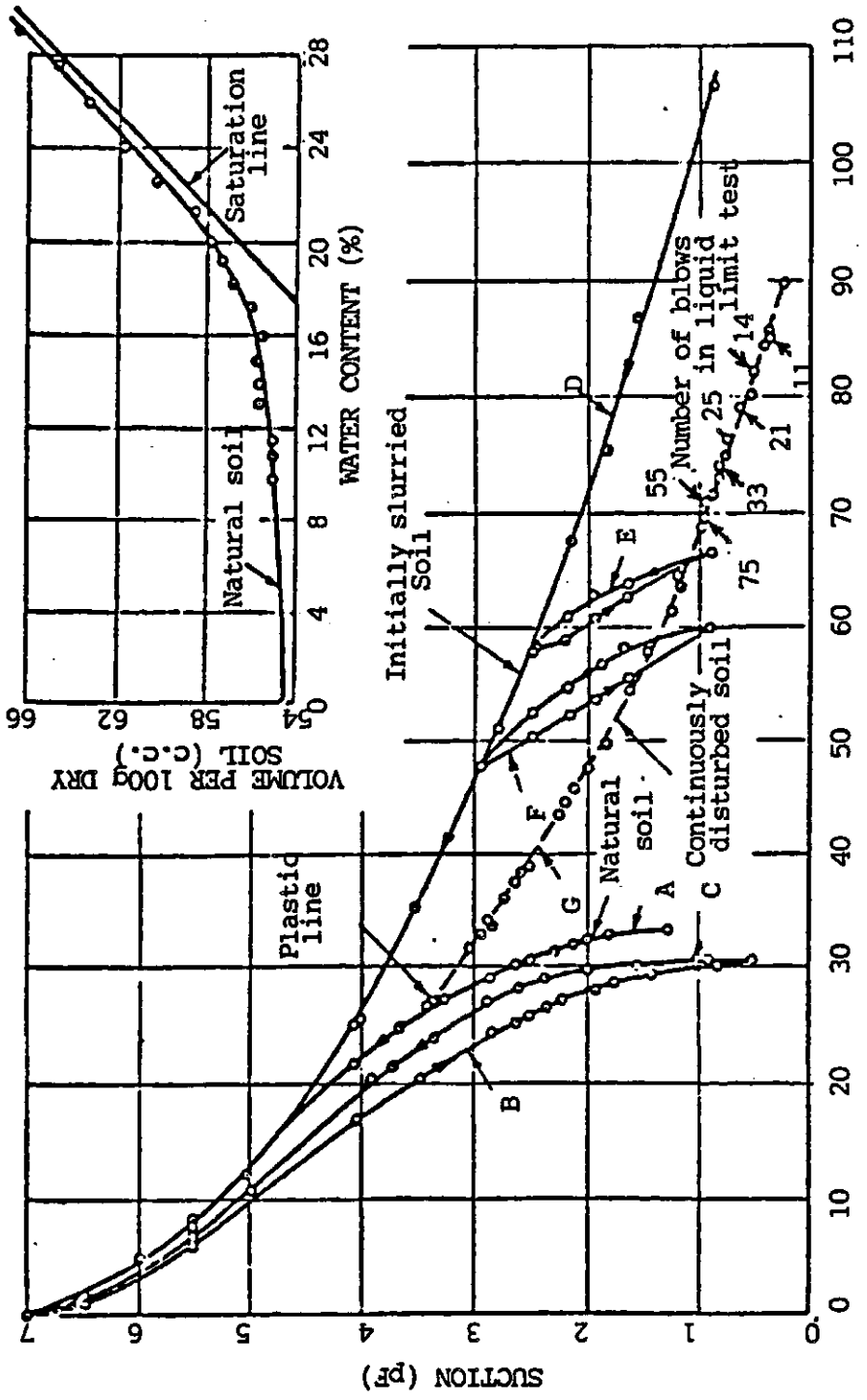

Figure 2.26 Suction/Water Content and Shrinkage Relationships for a Heavy Clay Soil (Croney and Coleman, 1954)

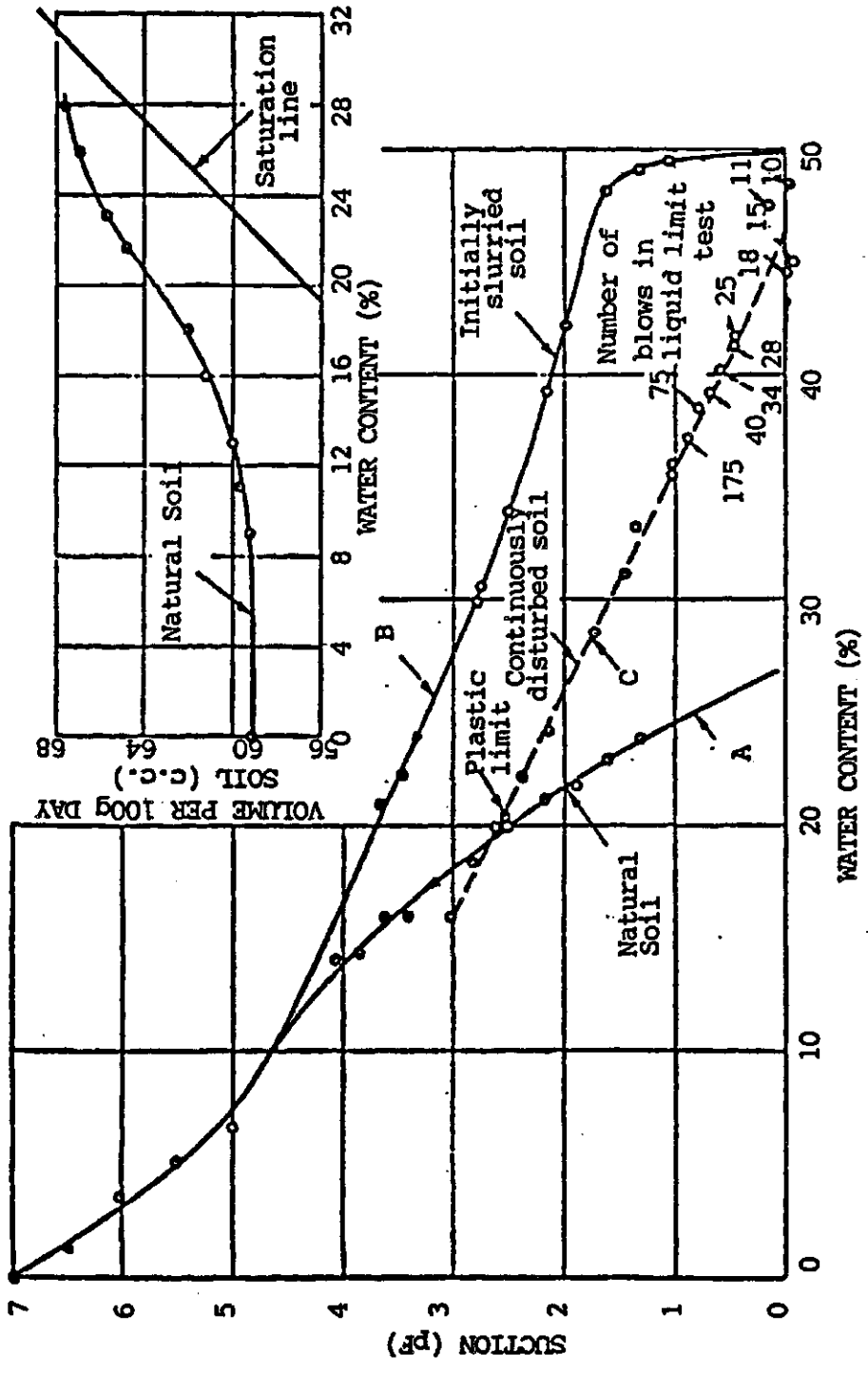

Figure 2.27 Suction/ Water Content and Shrinkage Relationships for a Heavy Clay Soil (Croney and Coleman, 1954)

$$-\frac{dV_w}{V} = C_{11}d(u_a - u_w) + C_{12}d(\sigma - u_a) \qquad (2.25)$$

A similar relation was later proposed by Fredlund and Morgenstern (1976).

In 1968, Matyas and Radhakrishna used the state and state parameter concept from continuum mechanics in describing the volume change behaviour of unsaturated soils. Series of one-dimensional and isotropic compression tests were performed on statically compacted soil specimens of a mixture of quartz and kaolin. Test results in terms of the degree of saturation, S, and the stress variables, $(\sigma - u_a)$ and $(u_a - u_w)$ were presented. If the degree of saturation, S is considered as a measure of net water volume change, the results indicate a unique constitutive surface for the water phase under monotonic deformation (Figure 2.28). No mathematical constitutive relation was presented. However, the water volume change constitutive surface appears to compose of two families of congruent constitutive curves for the stress range indicated.

Barden, Madedor and Sides (1969) studied the volume change behaviour of an unsaturated soil under K_o conditions. Compacted illite specimens were subjected to suction and total stress changes of 80 and 450 kPa respectively (see Figure 2.4). The water phase volume change of the specimens in one group of the tests was monitored using the degree of saturation as the stress dependent soil parameter (Figure 2.29). The results

a) Isotropic Compression

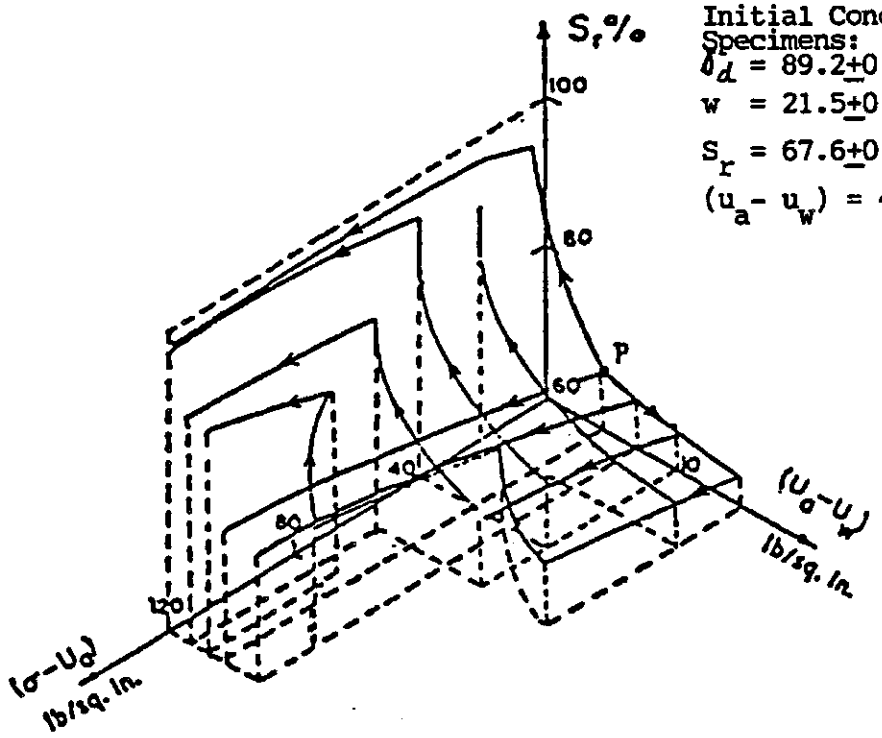

Initial Condition of Specimens:
γ_d = 89.2±0.2 lb/cu.ft.
w = 21.5±0.1 %
S_r = 67.6±0.1 %
$(u_a - u_w)$ = 4.6±0.2 psi

b) K_o Compression

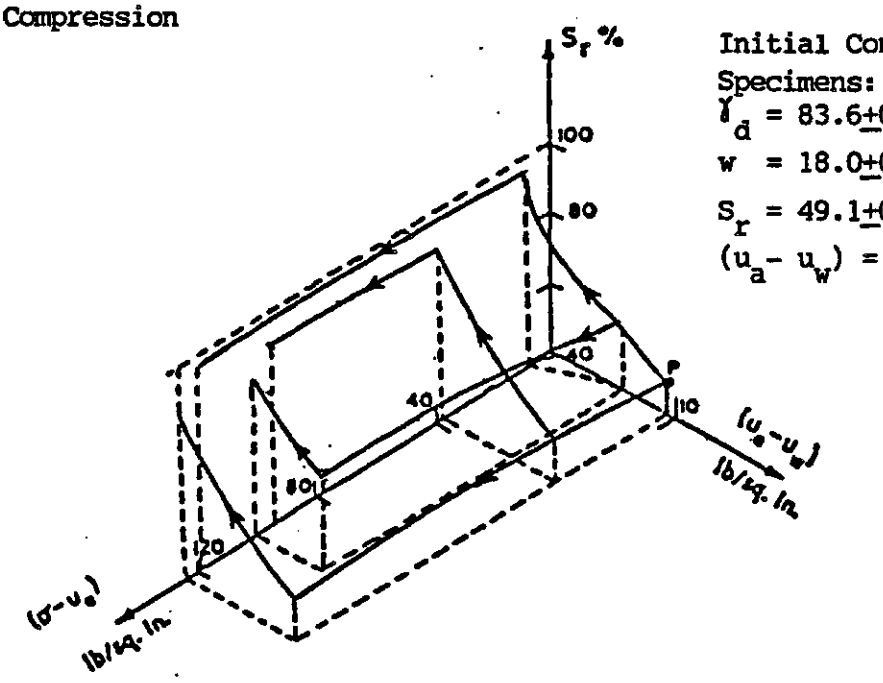

Initial Condition of Specimens:
γ_d = 83.6±0.2 lb/cu.ft.
w = 18.0±0.1 %
S_r = 49.1±0.1 %
$(u_a - u_w)$ = 9.6±0.2 psi

Figure 2.28 Plots Showing the Variation of Degree of Saturation in (S_r, $\sigma - u_a$, $u_a - u_w$) Space for a Quartz and Kaolin Mixture (Matyas and Radhakrishna, 1968)

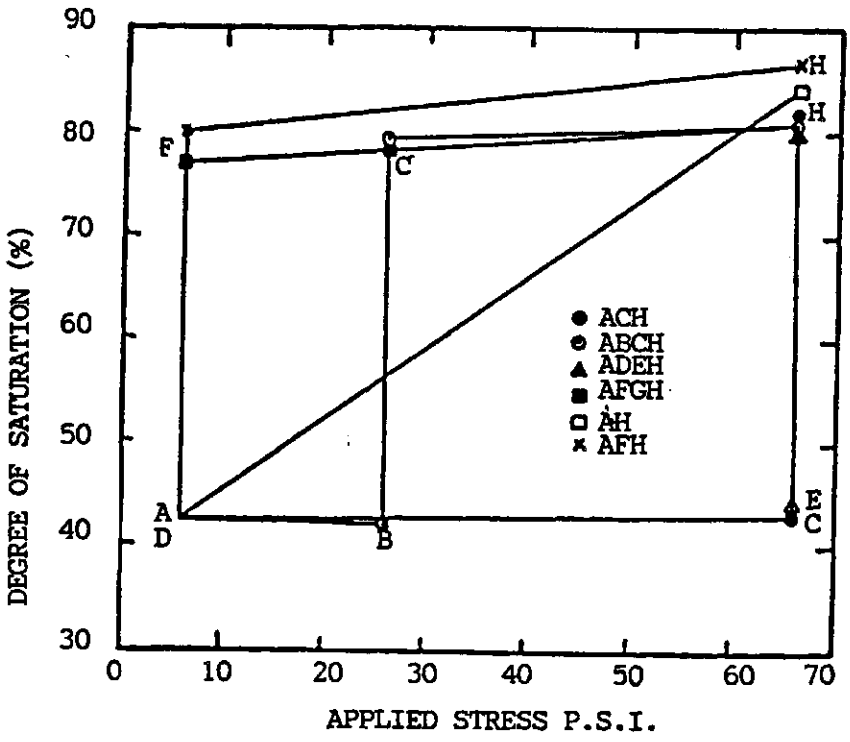

Figure 2.29 Degree of Saturation Change Curves for Illite Spacimens with Monotonic Increases in Degree of Saturation and Decreases in Strain (Barden et.al., 1969)

indicate a unique water phase volume change constitutive surface with near parallel constitutive curves with respect to the stress variables, $(\sigma - u_a)$ and $(u_a - u_w)$.

Fredlund (1973) identified the governing stress and deformation state variables for unsaturated soils. The constitutive relation for water volume change of an unsaturated soil was formulated as follows (Fredlund and Morgenstern, 1976).

$$\theta_w = \frac{1}{V}\frac{\partial V_w}{\partial(\sigma - u_a)} d(\sigma - u_a) + \frac{1}{V}\frac{\partial V_w}{\partial(u_a - u_w)} d(u_a - u_w) \qquad (2.26)$$

where

$\frac{1}{V}\frac{\partial V_w}{\partial(\sigma - u_a)} = m_1^w$, volume change coefficient of the water phase when $d(u_a - u_w)$ is zero

$\frac{1}{V}\frac{\partial V_w}{\partial(u_a - u_w)} = m_2^w$, volume change coefficient of the water phase when $d(\sigma - u_a)$ is zero

An alternate form consistent with conventional saturated soil mechanics was presented (Fredlund, 1979).

$$dw = b_t d(\sigma - u_a) + b_m d(u_a - u_w) \qquad (2.27)$$

where

dw = change in gravimetric water content

$b_t = \frac{-dw}{d(\sigma - u_a)}$, coefficient of water content with respect to net total stress, $(u_a - u_w)$

$b_m = \frac{-dw}{d(u_a - u_w)}$, coefficient of water content with respect to matric suction, $(u_a - u_w)$

It was suggested that the nonlinear constitutive curves of water content versus the stress state variables could be

linearized on a logarithm scale over a limited stress range. A linearized form of the water phase volume change constitutive relation was presented as follows.

$$w = w_o - D_t \log\frac{(\sigma-u_a)_f}{(\sigma-u_a)_o} - D_m \log\frac{(u_a-u_w)_f}{(u_a-u_w)_o} \qquad (2.20)$$

where

D_t = water content index with respect to net total stress,

$$\frac{\Delta w}{\log\frac{(\sigma-u_a)_f}{(\sigma-u_a)_o}}$$

D_m = water content index with respect to matric suction,

$$\frac{\Delta w}{\log\frac{(u_a-u_w)_f}{(u_a-u_w)_o}}$$

These constitutive relations were also presented graphically as constitutive surfaces composed of families of congruent constitutive curves (Figure 2.30 and 2.31). Experimental verification for the uniqueness of the proposed form of water phase constitutive surface was presented. The suggestion that the constitutive surface is planar in a logarithmic plot offers a convenient way to relate the volume change moduli through the characteristic curves on the principal planes with respect to the individual stress state variables.

In 1979, McWhorter and Nelson studied an empirical function between pore-water pressure head and volumetric water content for unsaturated soils presented by Brooks and Corey (1966).

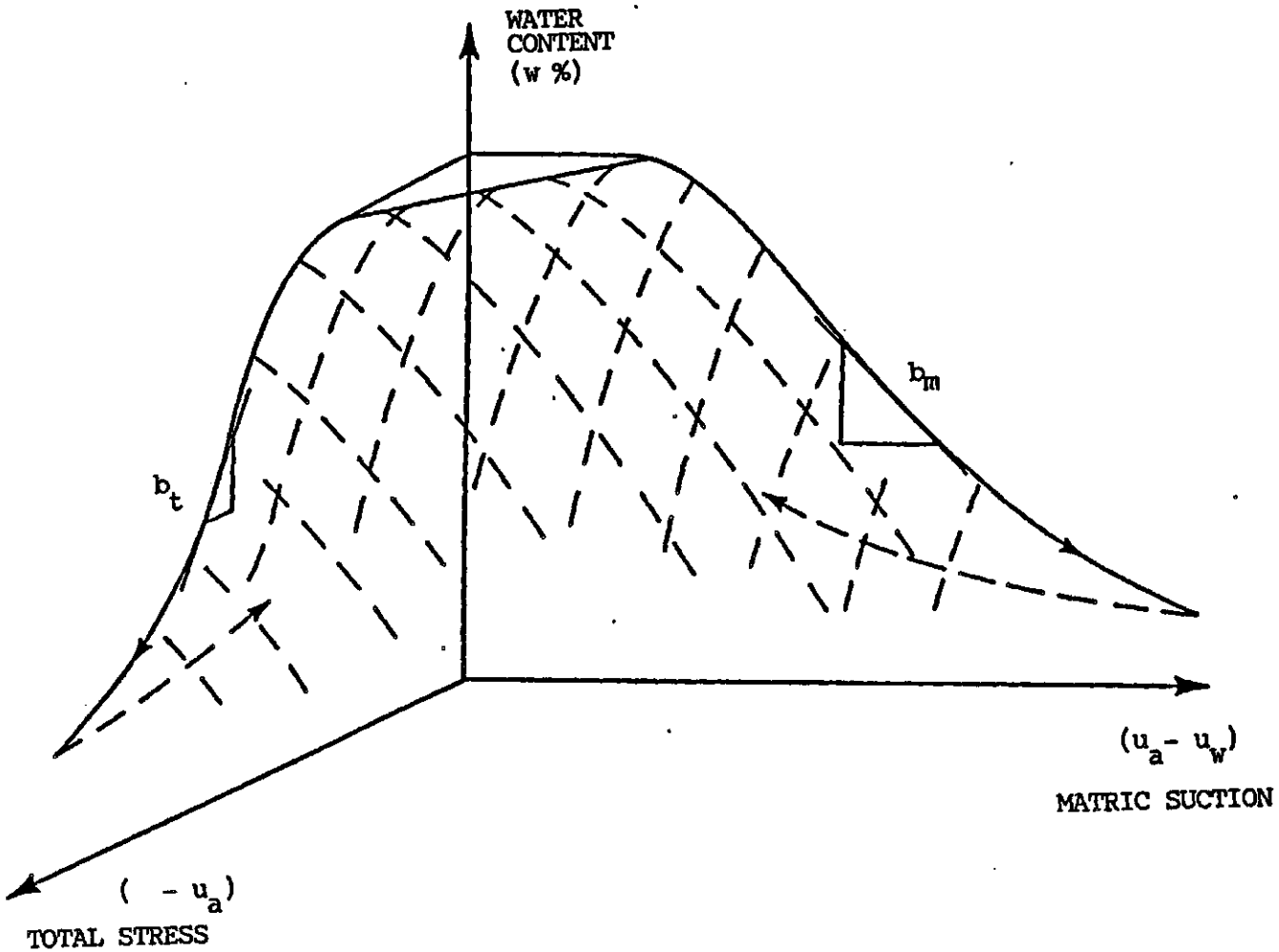

Figure 2.30 Arithmetic Presentation of Water Content Versus Stress State Variables (Fredlund, 1979)

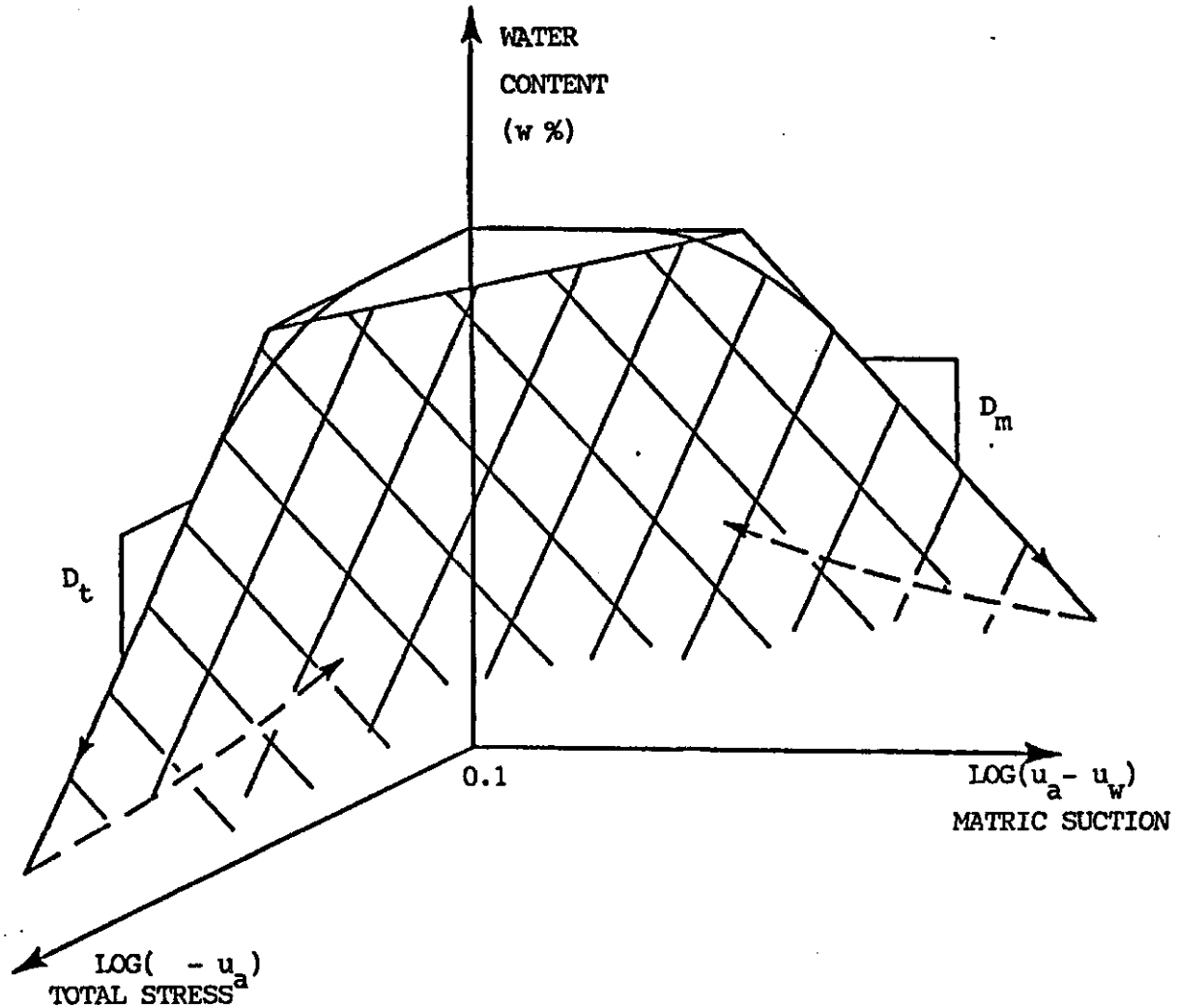

Figure 2.31 Water Content Versus Logarithm of Stress State Variables (Fredlund, 1979)

$$\theta_w = (n - \theta_r)\left(\frac{h}{h_d}\right)^{-\lambda} + \theta_r \; ; \quad h \leq h_d \tag{2.29}$$

where

θ_w = volumetric water content, volume of water per unit total volume of porous medium

n = porosity

θ_r = volumetric residual water content below which the volumetric water content is "very difficult" to be reduced by mechanical means

h = pore-water pressure head

h_d = displacement pressure head, pore-water pressure head below which (i.e. more negative) air will become continuous in an unsaturated soil

λ = pore size distribution index, a recommended value of 2 for most soils

Experimental data for two different sands were presented as verification (Figure 2.32). An empirically correlated expression was proposed for the evaluation of the displacement pressure head, h_d based on published test results in the literature (McWhorter and Nelson, 1980)

$$h_d = -9.66\left(\frac{k}{n - \theta_r}\right)^{-0.401}, \text{ (cm of water)} \tag{2.30}$$

where

k = saturated hydraulic conductivity (cm/sec)

A common name for the displacement pressure head, h_d is the air entry value of a soil. If the air voids within a soil is continuous and open to the atmosphere, the pore-water pressure, u_w equals the stress state variable, $(u_a - u_w)$. Accordingly, the presented pore-water pressure versus

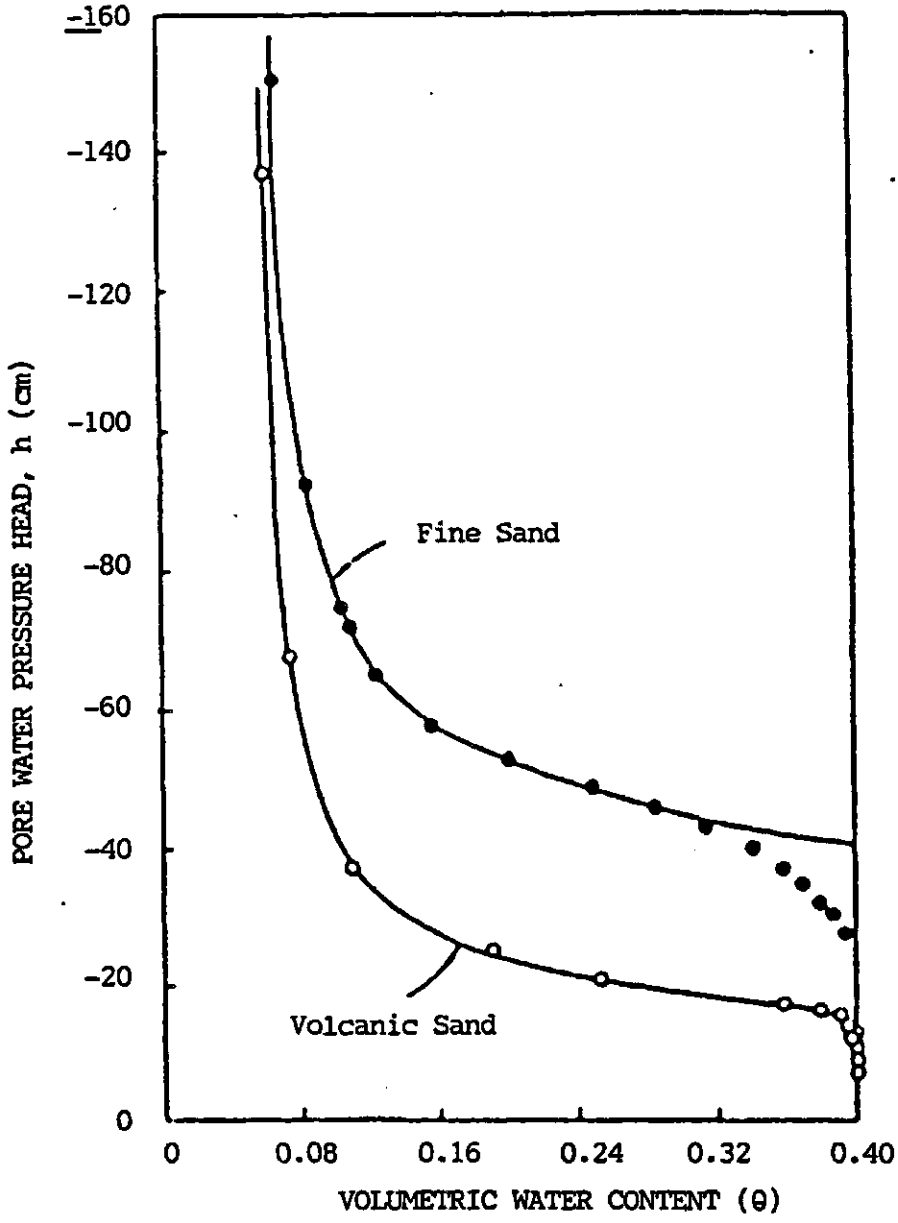

Figure 2.32 Relation Between Pore-Water Pressure Head and Volumetric Water Content for Two Sands (McWhorter and Nelson, 1979)

volumetric water content curves are volume change constitutive curves of the water phase with respect to matric suction, $(u_a - u_w)$. The presented empirical function (i.e., equation 2.29) is a constitutive relation for the water phase when the total stress is zero. It should noted that another empirically formulated water phase volume change constitutive relation of similar form was later presented by Seker (1983).

In 1983, Seker presented a volume change constitutive relation for the water phase with respect to matric suction, $(u_a - u_w)$ as follows.

$$p^F = \Psi_o \left(\frac{1-S}{S}\right)^{\Psi_1} \tag{2.31}$$

where

$$p^F = \log H_c \tag{2.32}$$

$$H_c = \frac{(u_a - u_w)}{\gamma_w} \tag{2.33}$$

$$m = 4\Psi_o\Psi_1 \tag{2.34}$$

H_c = capillary rise (cm)

γ_w = unit of water

S = degree of saturation

m = the slope of the p^F versus S curve of the soil at S equals 50%

Ψ_o = a soil parameter, the p^F value at S equals 50% on the p^F versus S curve of the soil

Ψ_1 = a soil parameter, $\frac{1}{4\Psi_o} \cdot \frac{d(pF)}{dS}$ at S = 50%

This relation was based on the correlation of published test data on a wide variety of soils ranging from clay to sand (Figure 2.33). It is a mathematical description of the water volume change constitutive curve on the matric suction principal plane. Based on the presented information, the proposed relation shows promise in modelling the water volume change constitutive curve with respect to matric suction.

Mitchell and Avalle (1984) presented a summary of water content versus soil suction characteristic curves for a number of Australian soils (Figure 2.34). The slope of these "moisture characteristic curves" were defined as,

$$C = \frac{\Delta w}{\Delta \log u_t} \qquad (2.35)$$

where

C = "moisture characteristic"

Δw = change in water content

$\Delta \log u_t$ = change in total suction, $[(u_a - u_w) + \pi]$ in a logarithmic scale.

The "moisture characteristic" defined by the authors is the water volume change modulus with respect to total suction over a wide stress range. The "moisture characteristic curves" are linear approximation of the generally "S" shape water volume change constitutive curves on the total suction plane. The authors reported that a value of total suction at zero water content can be taken as pF 6.8 (i.e., 6.2×10^6 kPa) for practical purposes. The same conclusion

Nos	ψ_0	ψ_1	Auteurs
1	1.680	0.100	NARASIMHAN et Al. (1978)
2	1.660	0.166	VACHAUD et Al. (1974)
3	3.100	0.180	VERBRUGGE (1974)
4	4.449	0.240	ESSAIS (ISRF) (1983)

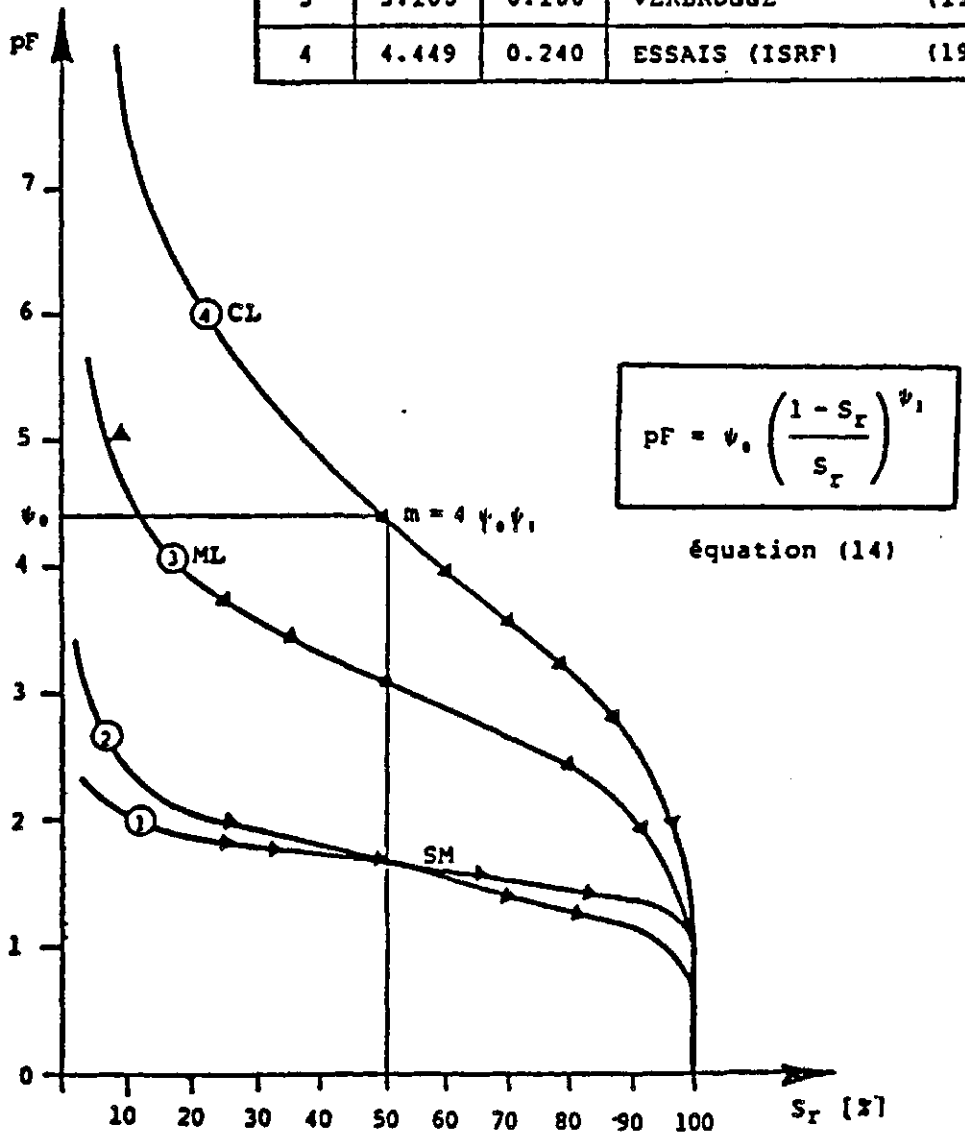

$$pF = \psi_0 \left(\frac{1 - S_r}{S_r} \right)^{\psi_1}$$

équation (14)

Figure 2.33 The Degree of Saturation Versus Matric Suction Relation (Seker, 1983)

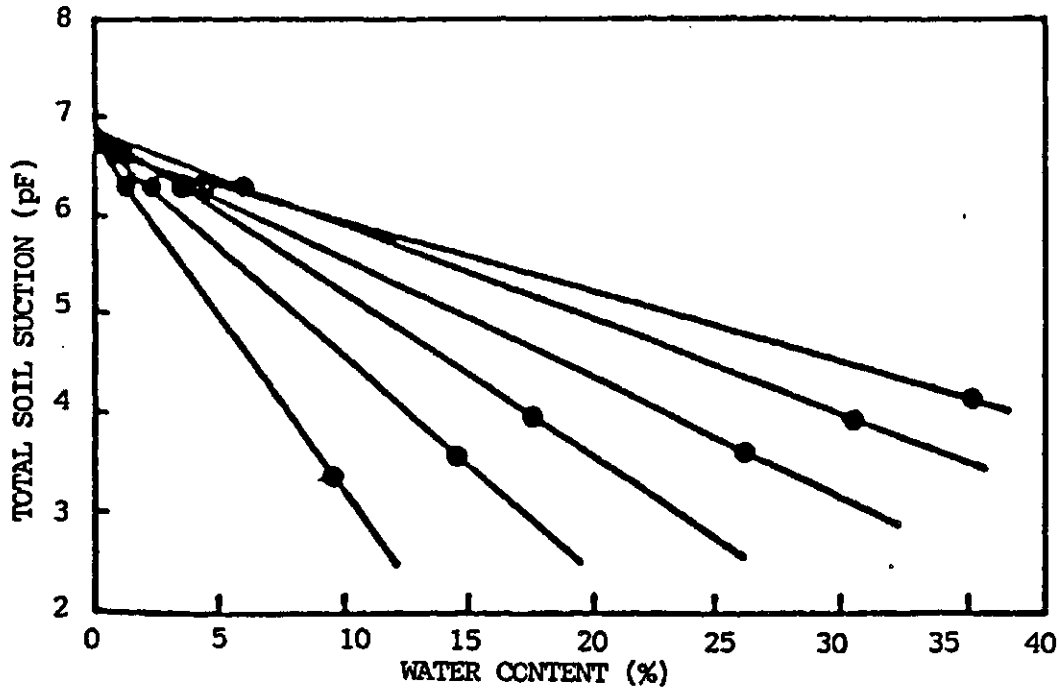

Figure 2.34 Water Content Versus Total Suction Relations for Australian Soils (Mitchell and Avalle, 1984)

was presented by Arnold (1983). This finding is valuable in providing a lower boundary for approximating water volume change constitutive curves with respect to suction.

Lloret and Alonso (1985) studied different analytical expressions to identify the appropriate types of functions for describing the volume change constitutive surfaces of the different phases of an unsaturated soil. Published test results were used in the optimization process based on minimum fitting errors. The degree of saturation, S was chosen as the soil parameter describing the water volume change. Two functions were presented as optimum water phase volume change constitutive relations.

$$S = a - \text{Tanh}[b(u_a - u_w)][c + d(\sigma - u_a)] \qquad (2.36a)$$

or

$$= a - \left\{\frac{e^{b(u_a - u_w)} - e^{-b(u_a - u_w)}}{e^{b(u_a - u_w)} + e^{-b(u_a - u_w)}}\right\}[c + d(\sigma - u_a)] \qquad (2.36b)$$

and

$$S = a - \{1 - e^{-b(u_a - u_w)}\}[c + d(\sigma - u_a)] \qquad (2.37)$$

where

a,b,c,d = soil constants

A schematic illustration of the constitutive surface representing equation 2.36 is presented in Figure 2.35. The constitutive curves on the net total stress planes are essentially linear whereas the constitutive curves on the matric suction planes are generally exponential. On an arithmetic plot of net total stress and

Water Phase Optimum Constitutive Relation,

$S = a - \tanh[b(u_a - u_w)][c + d(\sigma - u_a)]$

(Lloret and Alonso,1985)

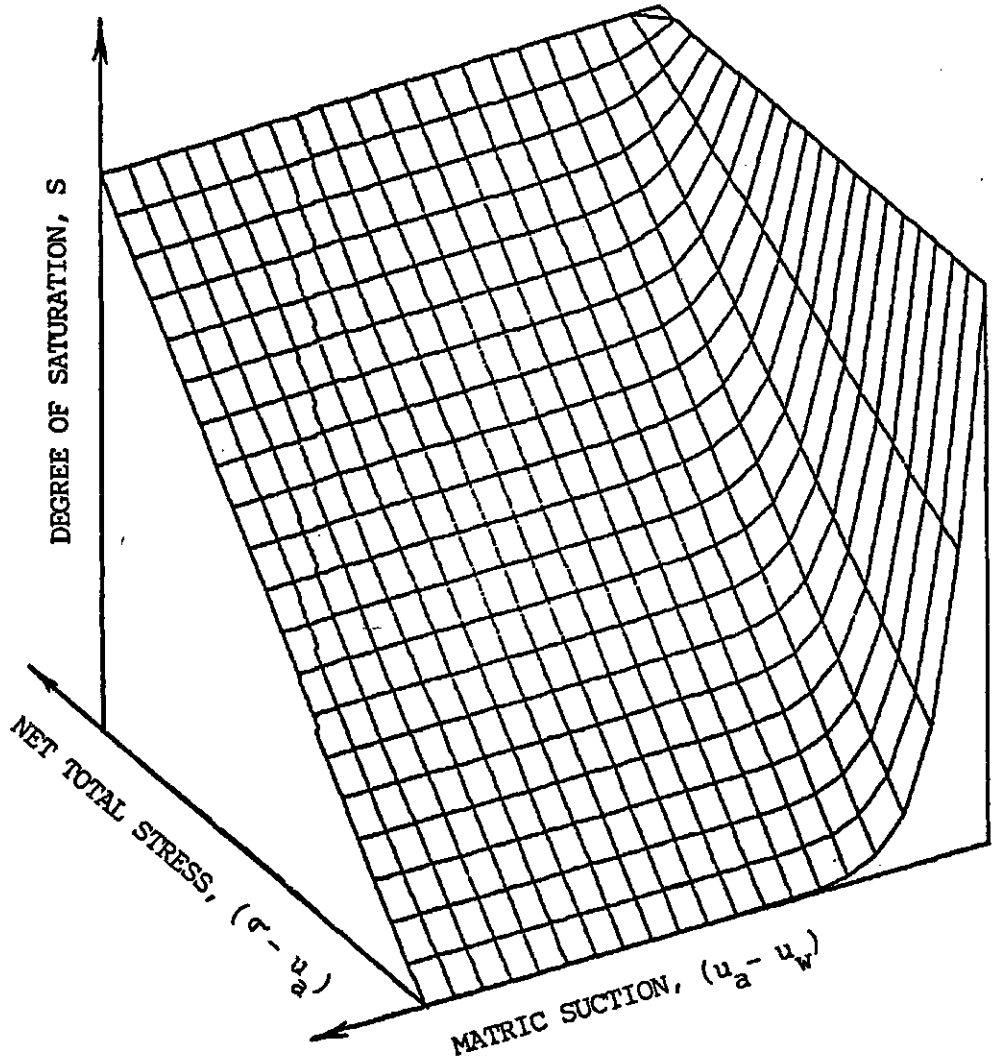

Figure 2.35 Schematic Representation of The Optimum Water Phase Constitutive Relation for Unsaturated Soils

matric suction versus the degree of saturation, the constitutive surface is a continuous warping concave surface.

There are suggestions in the literature for the formulation of the volume change constitutive relation for the water phase of an unsaturated soil. The volume change behaviour of the water phase was suggested to be best described by considering changes in the stress variables, $(\sigma - u_a)$ and $(u_a - u_w)$ (Coleman, 1962) (Matyas and Radhakerishna, 1968) (Barden et. al., 1969) (Fredlund, 1973 and 1979) (Fredlund and Morgenstern, 1976) (Llorett and Alonso, 1985). Both water content and degree of saturation were proposed to be used to describe the water volume change. The use of graphical representation of the constitutive relation as a three-dimensional surface is common (Matyas and Radhakrishna, 1968) (Fredlund and Morgenstern, 1976) (llorett and Alonso, 1985). Empirical functions have been suggested for describing the constitutive curve with respect to matric suction (McWhorter and Nelson, 1979) (Seker, 1983). There is experimental evidence that the water phase constitutive surface is unique (Matyas and Radhakrishna, 1968) (Barden et.al.,1969) (Fredlund and Morgenstern, 1976) (Lloret and Alonso, 1985). On a semi-logarithmic plot of net total stress and matric suction versus the water content, the constitutive surface

was suggested to be planar (Fredlund, 1979). On an arithmetic plot of net total stress and matric suction versus the degree of saturation, the constitutive surface was suggested to be a continuous concave surface (Lloret and Alonso, 1985).

2.3 Relationships between Volumetric Deformation Moduli of Unsaturated Soils

Limited information is available in the literature on the relationships between the various volumetric deformation moduli of unsaturated soils. There are published test results on the shrinkage and swelling behaviour of different soils. Section 2.3.1 discusses the importance of this data to developing the relationship between the soil structure and water phase moduli with respect to matric suction. Section 2.3.2 reviews literatures with relevant information for establishing the other relationships between the different moduli.

2.3.1 Importance of the shrinkage and swelling tests

At the beginning of the nineteenth century, agricultural researchers studied the soil volume change behaviour associated with water content changes. Attempts

were made to understand the soil water interaction in order to estimate the water retention capacity of soils for agricultural purposes (Hardy, 1923). Haines (1923) conducted a comprehensive study on a wide variety of soils (Table 2.4). Soil prisms of the size 6x1x1 cm were prepared from samples at liquid limits. The investigation involved measuring the volume changes which the soil prisms experienced during a slow drying and wetting process. Volume measurements were made by displacement of mercury from a constant volume bottle. The shrinkage and swelling curves in terms of the soil and water volume were presented (Figure 2.36). Results of this type of tests give the relative variation in volume of the soil structure to the water phase per unit matric suction change. This experimental data can be re-analyzed to provide the relationship between the volumetric deformation moduli of the soil structure and water phase with respect to matric suction changes (See Chapter III). There are several publications with this type of test results in the literature.

In 1954, Wooltorton attempted to develop a qualitative theory for the swelling and shrinking behaviour of unsaturated soils. Effort was made to establish empirical equations to estimate the maximum swelling and shrinking of a soil based on the Atterberg limits. Conceptual diagrams of the swelling and shrinking phenomena

Table 2.4 Soils Used in The Prism Tests (Haines, 1923)

Soil	Fine sand	Silt	Fine Silt I	Fine Silt II*	Clay	Loss on ignition
A Clay separate	---	--	--	--	90.5	9.5
B Kaolin	___	__	__	11.7	52.8	12.4
C Clay (Sudan)	16.2	11.8	4.7	4.8	42.3	11.4
D Clay subsoil (Durham)	16.1	14.5	13.3	9.7	33.8	9.6
E Harpenden Common	17.8	32.0	9.0	8.3	25.2	10.5
F Loam (Rothamsted)	28.6	33.8	10.0	4.9	14.8	8.3
G Sandy (Norfolk)	60.5	12.3	5.1	3.3	5.3	8.3
H Peaty	---	--	--	--	--	27.0

* The clay fraction on the American system of mechanical analysis = fine silt II + clay of the above table

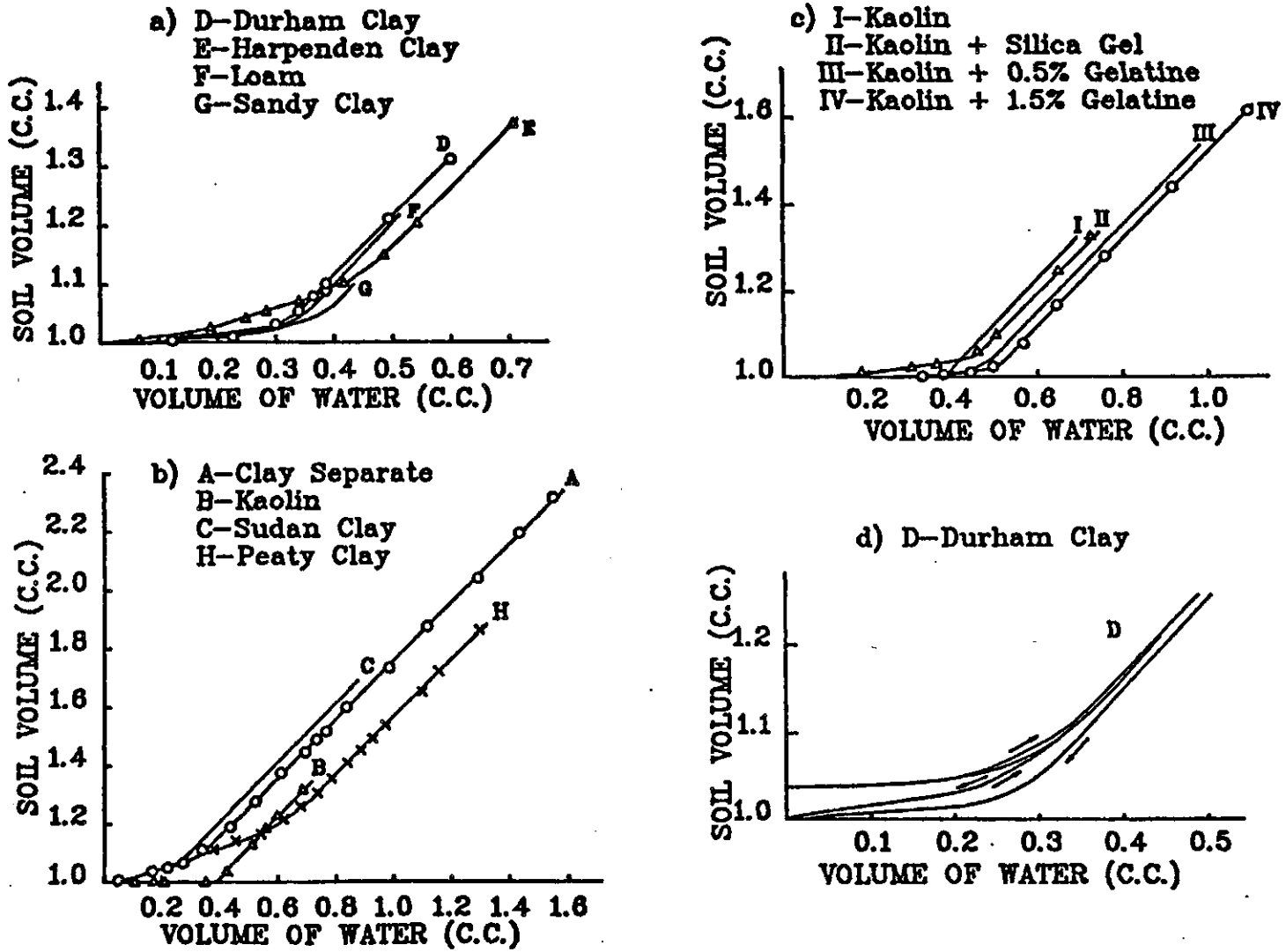

Figure 2.36 Unconfined Shrinking and Swelling Curves from Prism Tests (Haines, 1923)

were presented (Figure 2.37). The amount of entrapped air and the resistance of the soil structure to slaking were suggested to be the two governing factors affecting the swelling and shrinking behaviour of a soil. Shrinkage curves for initially saturated and unsaturated remoulded and undisturbed soils were hypothesized (Figure 2.38 and 2.39). The amount of entrapped air in the soil was suggested to be the reason for the deviation of the shrinkage curves away from the saturation line. Hypothesized swelling and shrinkage curves of initially saturated remoulded and desiccated compacted soils were also presented (Figure 2.40 and 2.41). It was suggested that a soil with stable structure highly resistant against slaking would possess a "zigmoid" type of swelling curve (Figure 2.41). Soils susceptible to slaking were said to have "lunar" type of swelling curves. Experimental "density change curves" of four different soils were presented as verification for the hypotheses (Figure 2.42). The author appears to have unintentionally conducted perhaps the first comprehensive study on the relationship between the volumetric deformation moduli of the soil structure and water phase with respect to matric suction changes.

Popescu (1980) studied expansive soils with a crumb structure to define the "interrelationship" between the "principal variables" controlling the water retention

a) Phase Diagram

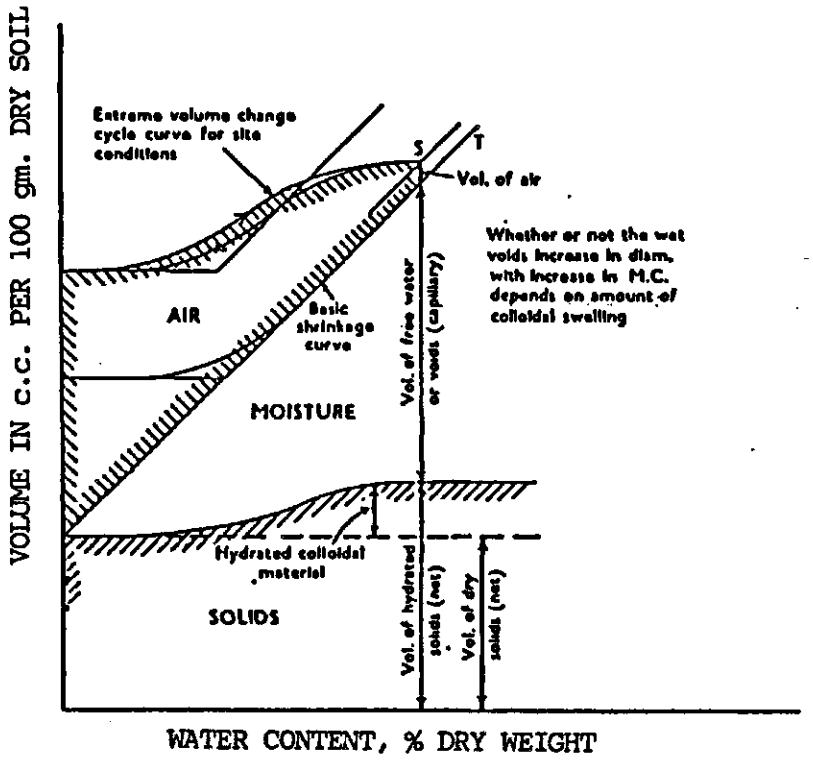

b) Plasticity Diagram

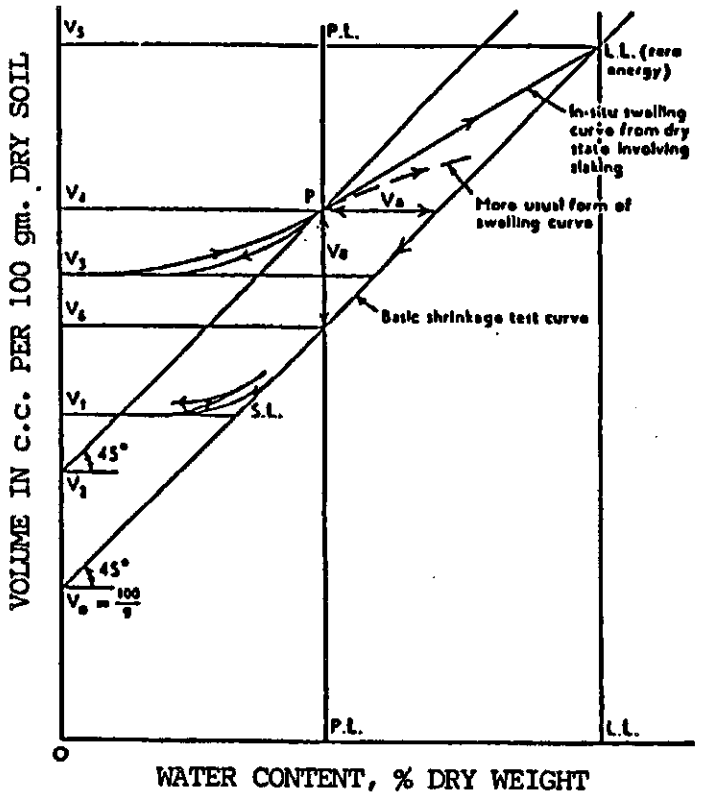

Figure 2.37 Conceptual Diagrams of The Swelling and Shrinking Phenomena (Wooltorton, 1954)

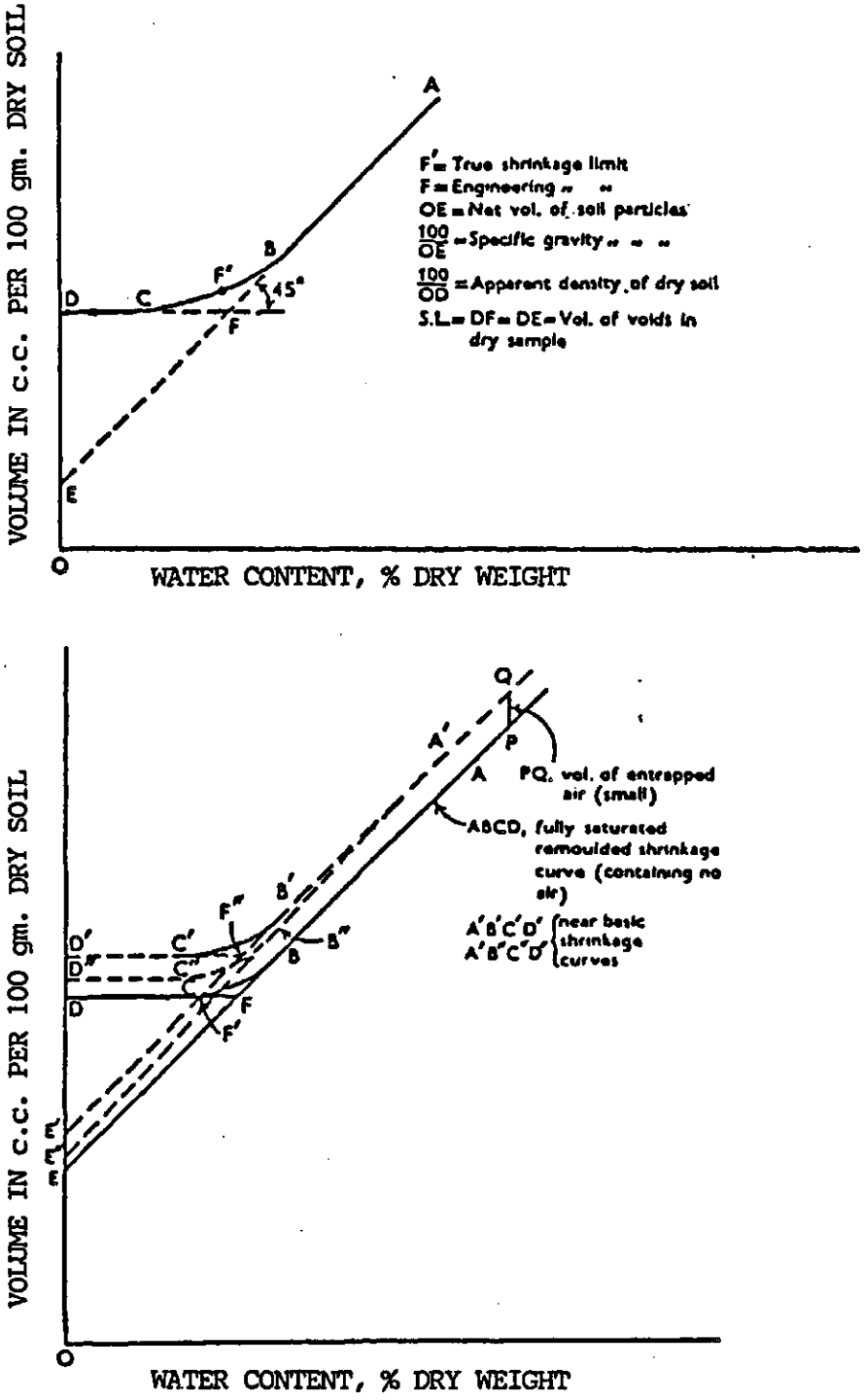

Figure 2.38 Hypothetical Shrinkage Curves for Remoulded Soils (Wooltorton, 1954)

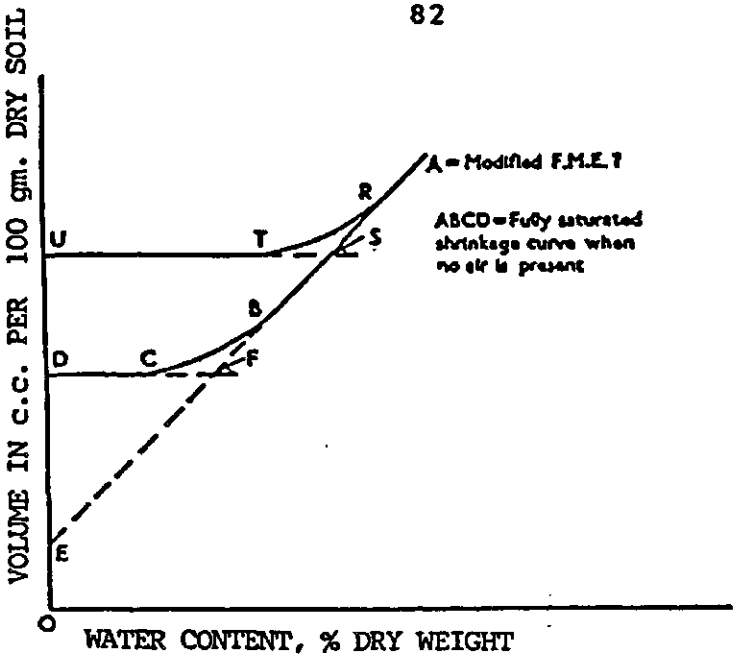

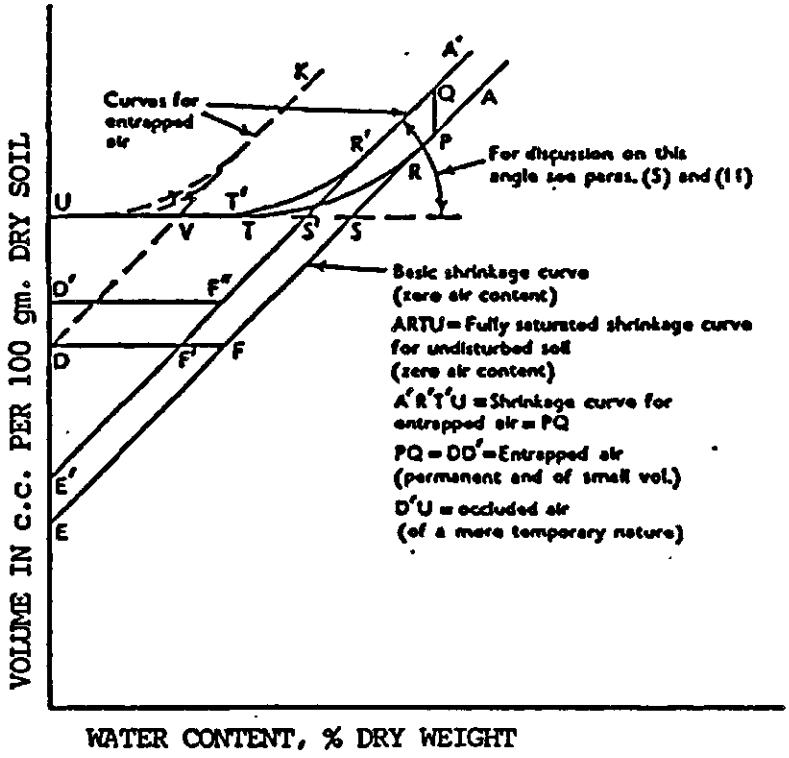

Figure 2.39 Hypothetical Shrinkage Curves for Undisturbed Soils (Wooltorton, 1954)

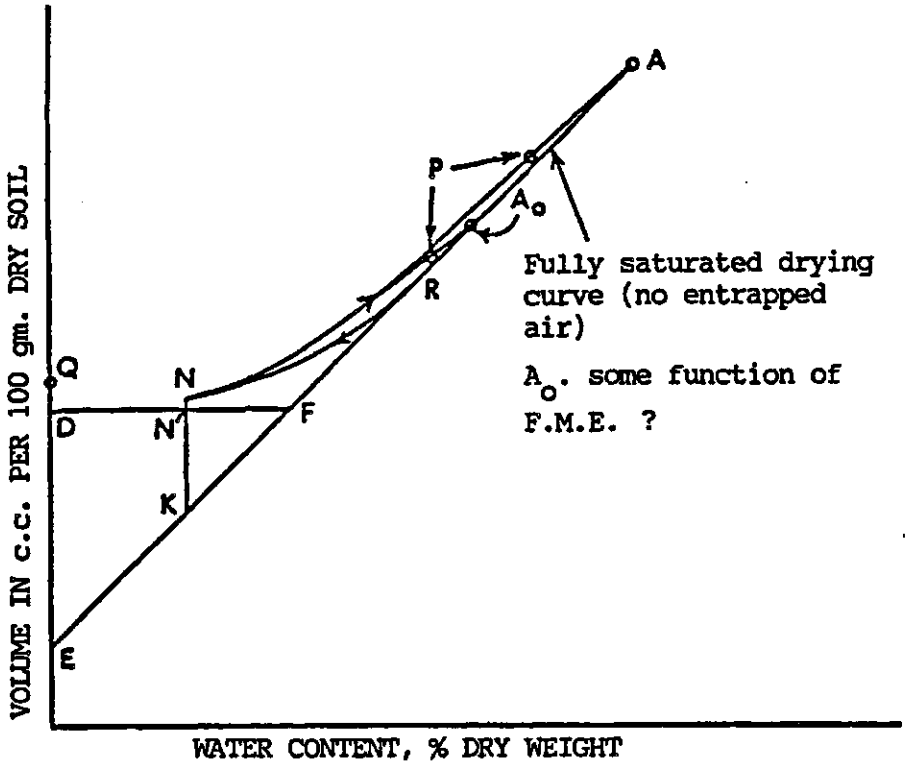

Drying and Rewetting Curves for Remoulded Soils when no Air is Entrapped. (Not to scale)

Figure 2.40 Hypothetical Shrinkage and Swelling Curves for Saturated Remoulded Soils (Wooltorton, 1954)

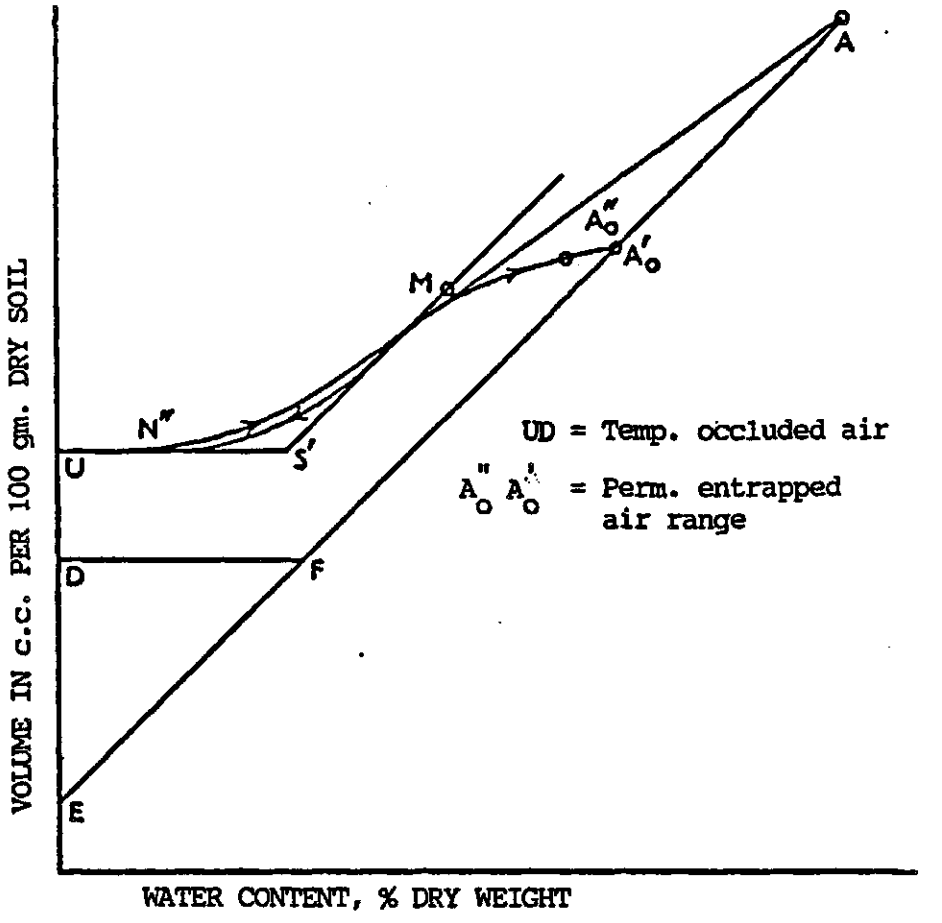

Drying and Rewetting Curves for Undisturbed Desiccated Soils. (Not be scale)

Figure 2.41 Hypothetical Shrinkage and Swelling Curves for Desiccated Compacted Soils (Wooltorton, 1954)

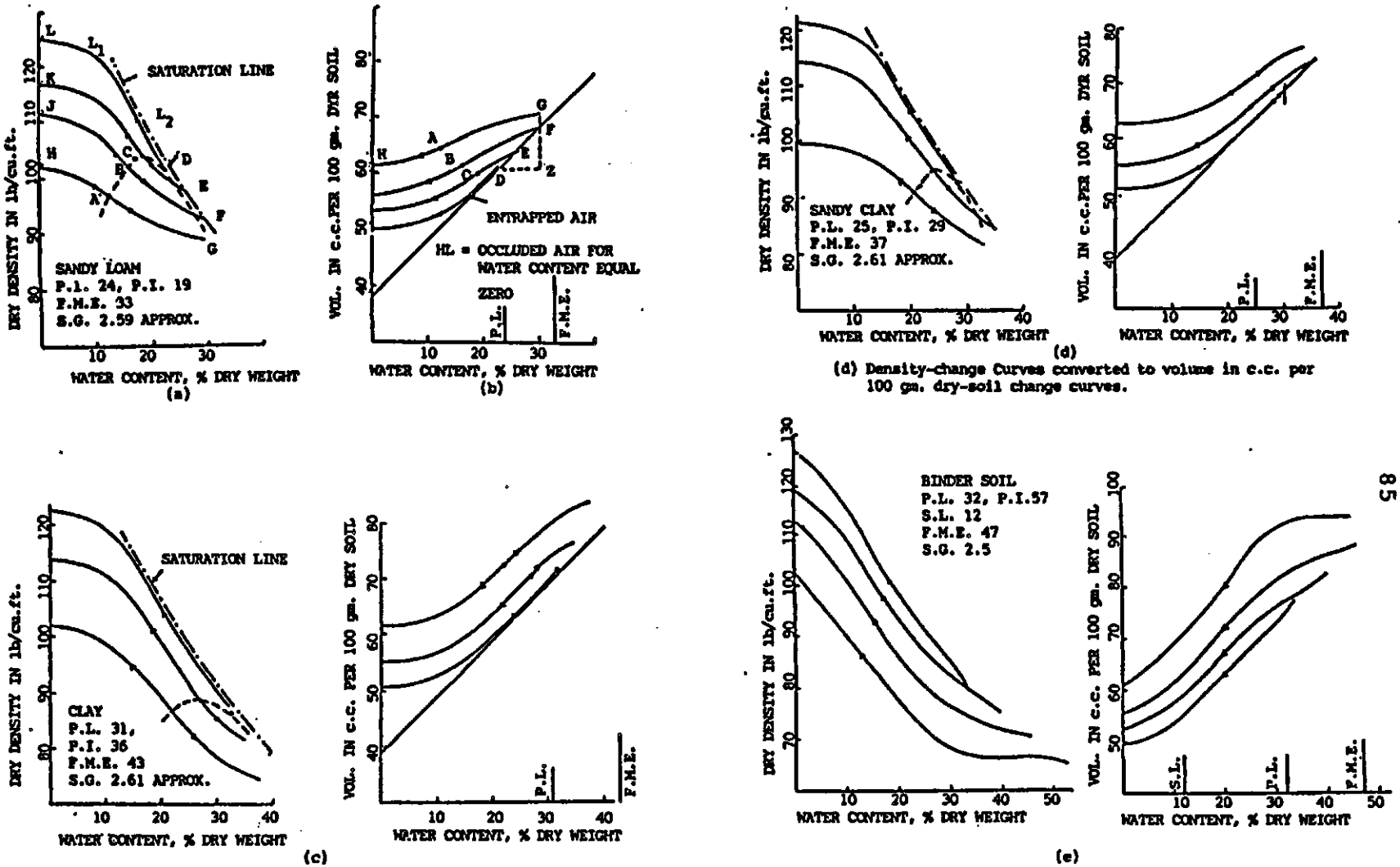

Figure 2.42 Experimental Density Change and Shrinking-Swelling Curves (Wooltorton, 1954)

and shrinkage-swell phenomena. An active South Romania clay loam was tested. Shrinkage curves for soil specimens with different crumb size fraction were presented (Figure 2.43). The slopes of these shrinkage curves are the ratios between the soil structure and water volume change moduli with respect to increasing matric suction.

Beal (1984) proposed a test method for direct determination of the water content and linear dimensional changes of a soil specimen under applied vertical loads. The general arrangement of the test apparatus was presented (Figure 2.44). The test involved wetting or drying a soil specimen under different applied vertical loads. The vertical strain and change in water content of the specimen were monitored during the test. The specimen was wrapped laterally by polythene sheets and tissue paper wick. Consequently, the lateral confining stresses applied during the test were indeterminate. Test results of remoulded and undisturbed specimens of a clay from Dalby, Queensland were presented (Figure 2.45). The slopes of these swelling and shrinkage curves are ratios between the soil structure and water volume change moduli with respect to matric suction.

Index properties of the investigated active clay

Characteristic specification		Experimental range	Active clay range according to Romainian Standard 9262 - 73
Clay content < 2μ	(%)	23 - 27	18 - 35
Plasticity index	(%)	32 - 36	25 - 40
Free swell in a 100 cc graduate	(%)	90 - 110	75 - 100
Shrinkage limit	(%)	8 - 10	12 - 10
Moistening heat	(cal/g)	8 - 9	6 - 8
Moisture content at 15 bar suction	(%)	3 - 4	5 - 10

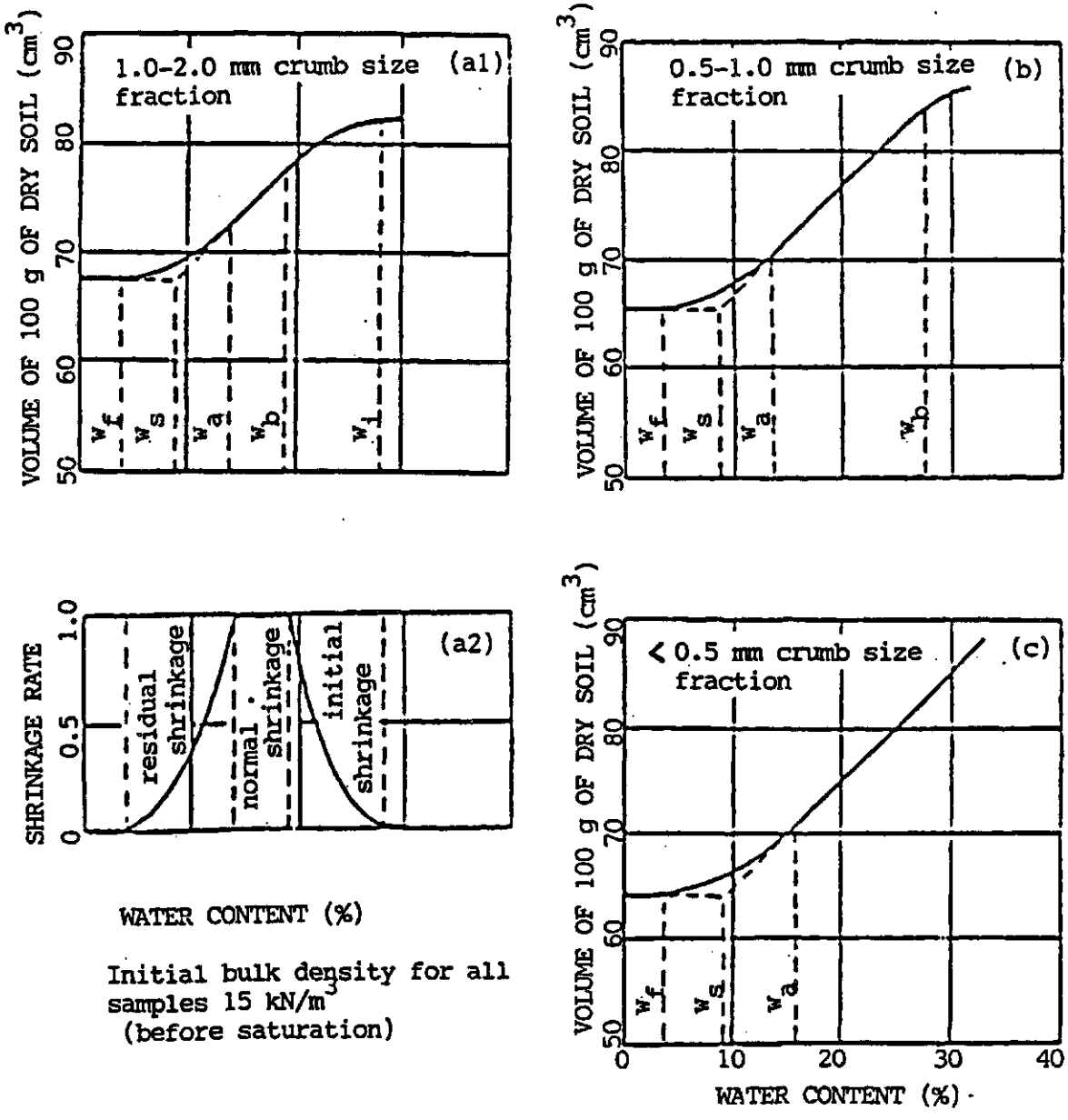

Initial bulk density for all samples 15 kN/m^3 (before saturation)

Figure 2.43 Shrinkage Curves of a Romania Clay with Different Crumb Size Fractions (Popescu, 1980)

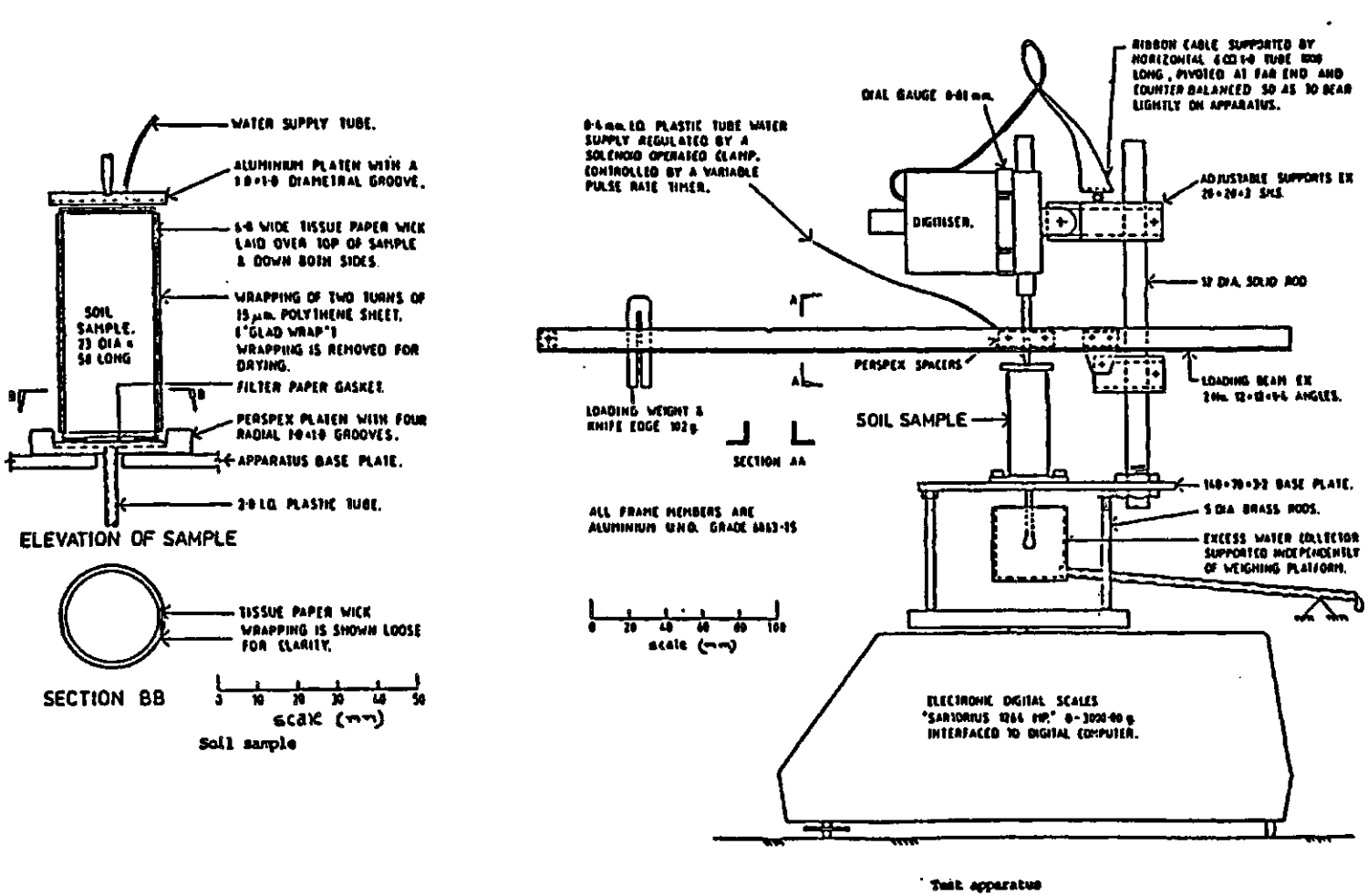

Figure 2.44 Test Arrangement (Beal, 1984)

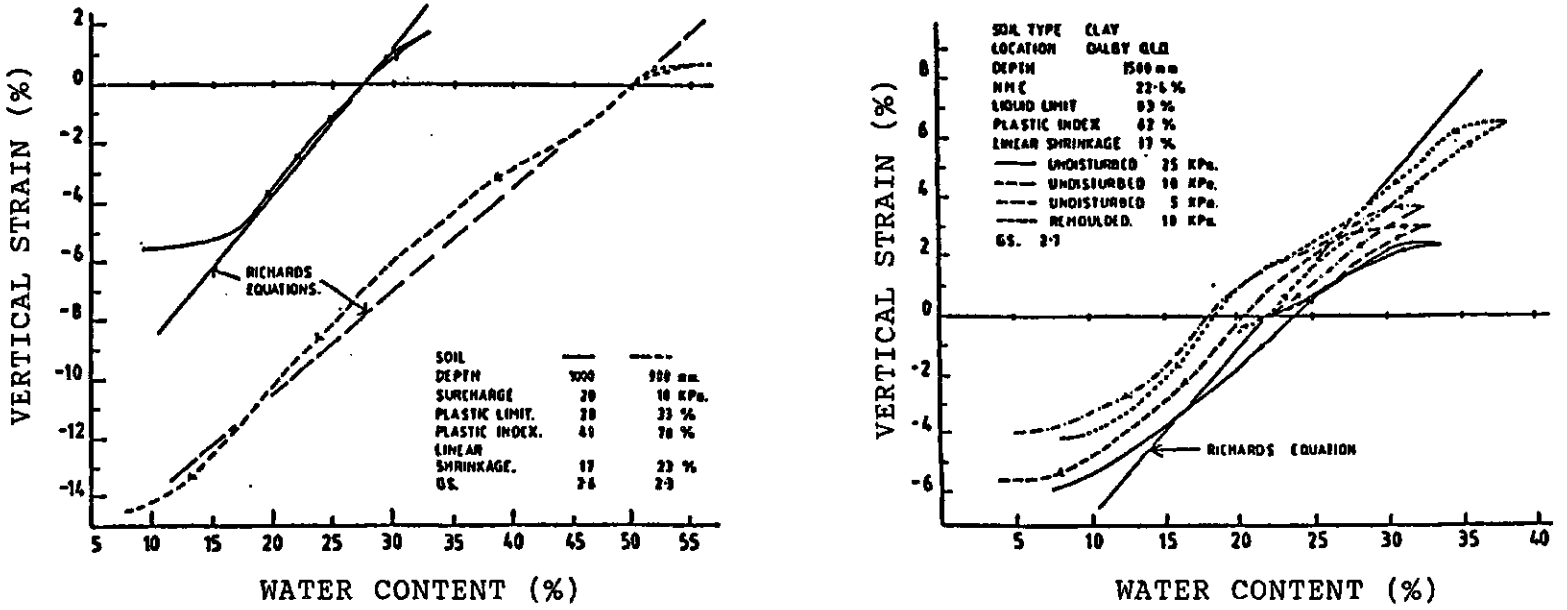

Figure 2.45 Swelling and Shrinkage Curves of a Dalby Clay (Beal, 1984)

2.3.2 Other research

In 1963, Gilchrist performed series of one-dimensional constant volume and free swell tests on statically compacted Regina clay specimens. Conventional lever type consolidometers were used. Classification test results on the clay sample were presented (Table 2.5). There were sequences of constant volume and free swell tests on pairs of specimens of near identical initial states (Table 2.6). Test results from these sequences of tests (Figure 2.46, 2.47 and Table 2.7) can be re-analyzed to give the relationship between the soil structure volume change moduli with respect to decreasing total stress and suction.

Richards (1967) reported that soils at seventeen road sites in Australia remained saturated to over 9800 kPa of suction. Consequently, based on the general volume-mass relation for soils, $Se = wG_s$, a mathematical relation was derived to relate the soil volume and water content changes per unit change in matric suction.

$$\frac{\Delta V}{V_1} = \frac{(w_2 - w_1)\, G_s}{(100 + w_1 G_s)} \qquad (2.38)$$

where

ΔV = change in volume of the soil structure

V_1 = initial volume of the soil structure

w_1 = initial water content

Table 2.5 Classification Test Results for Regina Clay (Gilchrist, 1963)

Atterberg Limits	Undried	Air Dried
Liquid Limit (L.L)	88%	76%
Plastic Limit (P.L.)	33%	30%
Shrinkage Limit (S.L.)	14%	15%
Plastic Index (P.I.)	55%	46%
Specific Gravity (Gs)	2.83	2.83

Table 2.6 Summary of The Initial Properties of The Samples Tested in The Selected Sequences of Constant Volume and Free Swell Tests on Regina Clay (Gilchrist, 1963)

Sample No.	Initial water content (%)	Initial void ratio	Initial degree of saturation, (%)
III-2C-(CV)	32.9	0.937	0.994
III-8A-(FS)	33.0	0.943	0.992
IV-IC-(CV)	38.2	1.086	0.995
IV-4A-(FS)	38.1	1.092	0.987

(CV) - Data obtained from constant volume, (CV) tests

(FS) - Data obtained from free swell, (FS) tests

Table 2.7 Summary of Free Swell Test Results on Compacted Regina Clay (Gilchrist, 1963)

Sample No.	Initial void ratio	Final void ratio	Final water content, * (%)
III-8A-(FS)	0.943	1.232	43.5
IV-4A-(FS)	1.092	1.262	44.6

* is calculated according to the general volume-weight relation, $Se = wGs$ with $S = 100\%$ and $Gs = 2.83$ for Regina clay

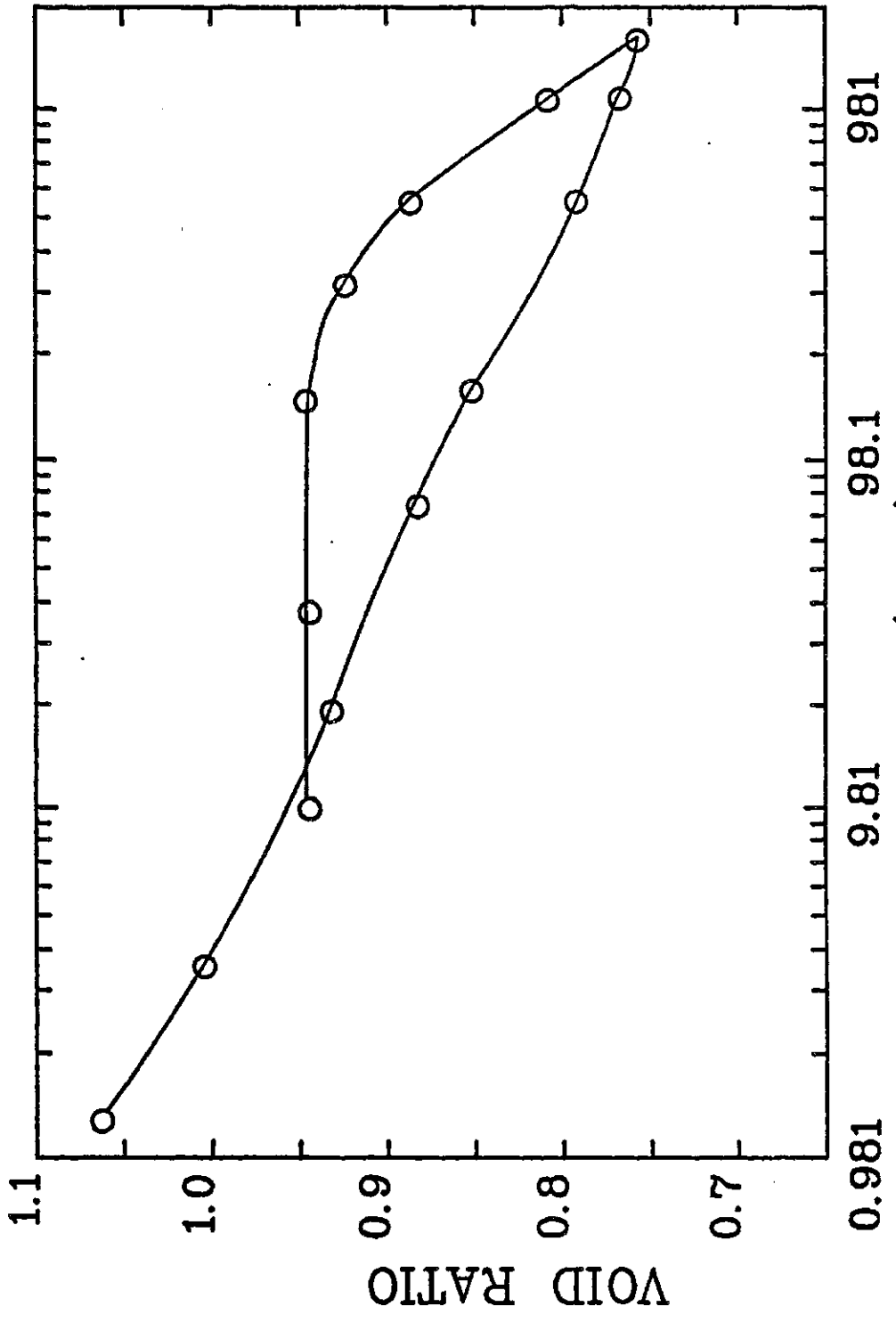

Figure 2.46 Void Ratio Versus Pressure Curve for Specimen III-2C-(CV) (After Gilchrist, 1963)

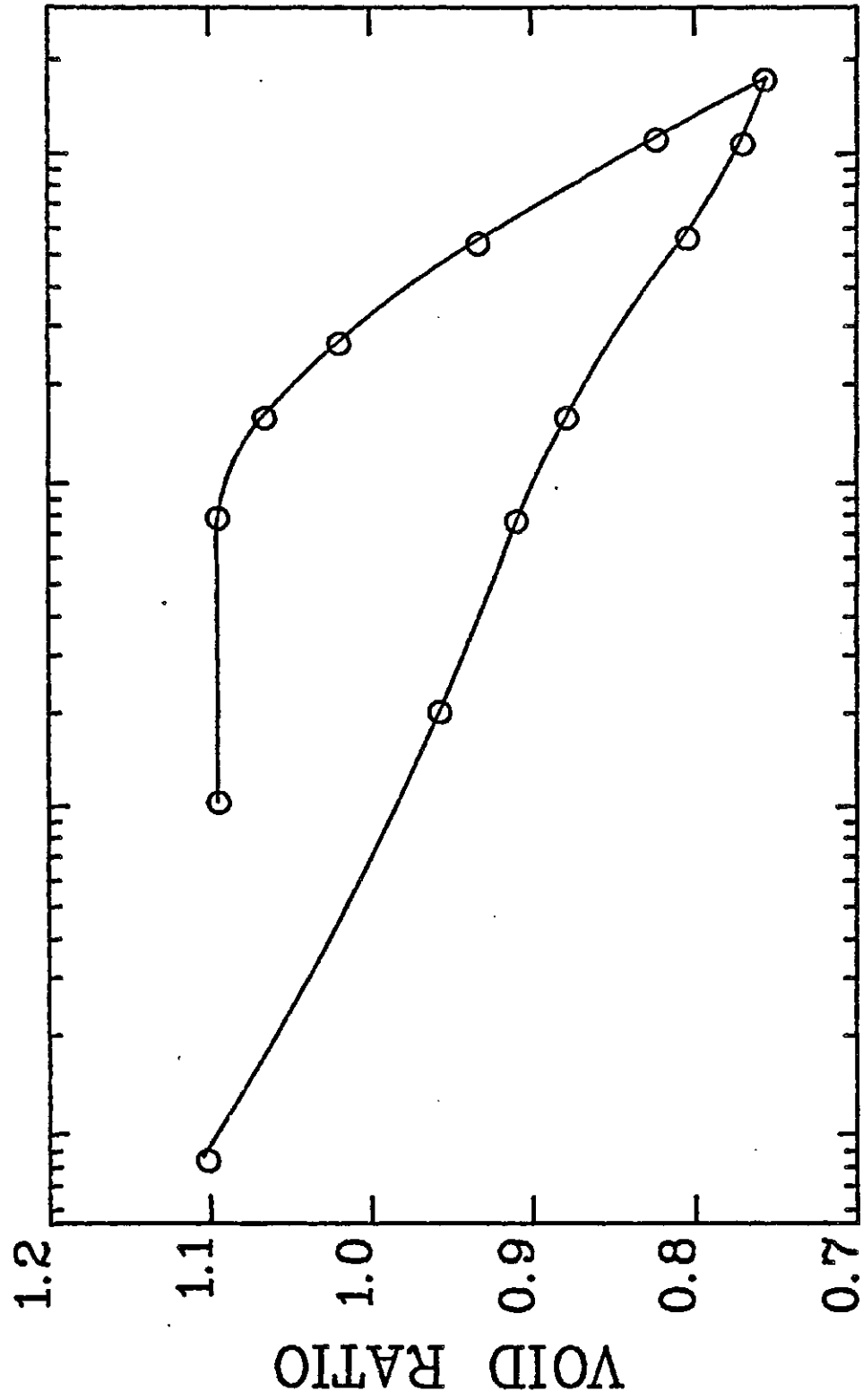

Figure 2.47 Void Ratio Versus Pressure Curve for Specimen IV-IC-(CV) (After Gilchrist, 1963)

w_2 = final water content

Assuming equal volume changes in the vertical and horizontal directions, the fractional height change was suggested to be as follows.

$$\frac{\Delta H}{H_1} = \frac{\Delta V}{3V_1} = \frac{(w_2 - w_1)\, G_s}{(100 + w_1 G_s)} \qquad (2.39)$$

where

ΔH = change in height of the soil element

H_1 = initial height of the soil element

The presented equation is a relationship between the soil structure and water phase deformation moduli with respect to matric suction.

In 1979, Fredlund presented a qualitative discussion on the relationships between the various deformation moduli. The moduli were suggested to be "different for increases and decreases of the stress state variables" and converging "towards one value for a saturated soil". The general soil volume-mass relation was suggested to be the continuity requirement for volume changes among the various phases of an unsaturated soil. It was reported that "little or no information is available on the relative effects of the two stress state variables, $(\sigma - u_a)$ and $(u_a - u_w)$ on the volume change behaviour of the various phases in an unsaturated soil". Such a problem was posed as an area of much needed research.

Justo, Delgodo and Ruiz (1984) studied the

influence of stress path to the collapsing and swelling behaviour of soils under no lateral strain conditions. Compacted El-Arahal clay specimens were tested. Both common and suction controlled oedometers were used. Amongst the presented test results, there were swelling curves for specimens under different total stress and matric suction (Figure 2.48). This test data can be re-analyzed to provide the relationship between the soil structure moduli with respect to total stress and matric suction when the stress variables are decreasing.

In 1985, Lloret and Alonso suggested analytical expressions as optimum functions to be used as volume change constitutive relations for the soil structure and water phase of unsaturated soils subjected to confined or isotropic compression. The relationships between the different moduli under the specified conditions can be derived from these functions. However, such an undertaking involves complicated and hypothetical equations.

Information in the literature on the relationships between the different moduli is scarce and incomplete. There are published swelling and shrinking test results which can be re-analyzed to give the relationship between the soil structure and water volume change moduli with respect to matric suction (Haines, 1923) (Wooltorton, 1954) (Popescu, 1980) (Beal, 1984). Limited experimental data is available to be analyzed to show the relationship between

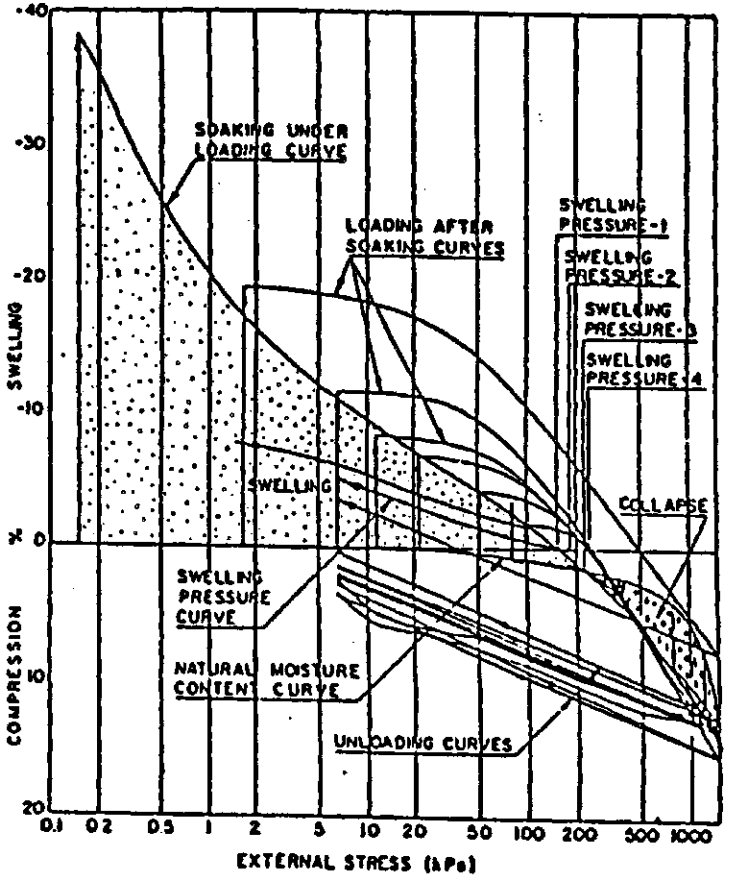

Soaking tests on compacted samples of El Arahal

Clay of El Arahal (Seville)
Sand 14%, silt 36%, clay 50%
w_L = 55-75 I_p = 30-44 w_s = 20-23
CEC 21,8 meq./100 g
Mineralogical analysis of clay:
kaolinite 14%
illite 34%
montmorillonite 52%
CO_3 Ca 27.8%

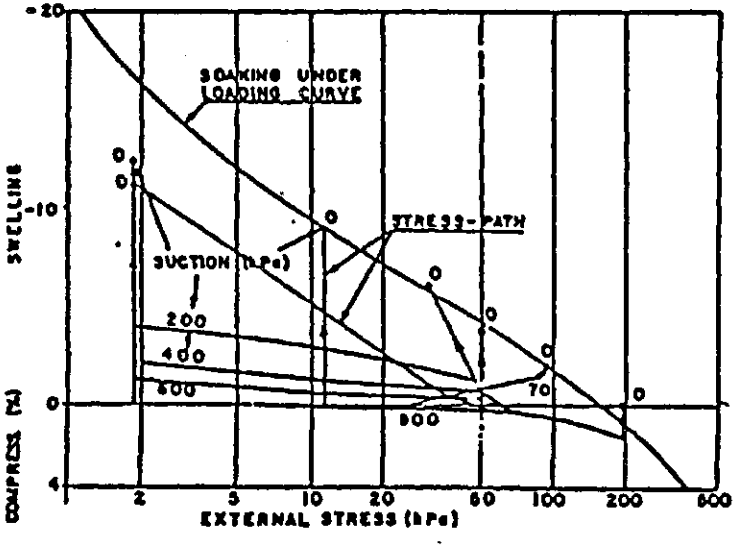

Suction-controlled tests on compacted samples from El Arahal

Figure 2.48 Swelling Curves for Compacted El Arahal Clay Specimens (Justo el.al., 1984)

the soil structure moduli with respect to decreasing total stress and matric suction (Gilchrist, 1963) (Justo, Delgado and Ruiz, 1984). The general soil volume-mass relation (i.e., $Se = wG_s$), was suggested to be the volume change continuity requirement among the various phase (Richards, 1967) (Fredlund and Morgenstern, 1976). There are analytical expressions which can be developed to give relationships between moduli of the same phase with respect to different stress variables (Llorett and Alonso, 1985). However, such undertaking involves complicated mathematics. The resulting relationships are also limited to K_o and isotropic compression conditions. There is no comprehensive study on the relationships between the moduli for both compression and expansion conditions. The lack of knowledge on this subject has prompted the research described in this dissertation.

CHAPTER III

THEORY

3.1 Introduction

This chapter presents the theory of possible relationships between the various moduli. The form of the soil structure and water phase constitutive surfaces is examined on both an arithmetic and a semi-logarithmic scale. Approximate semi-logarithmic constitutive surfaces are proposed. The geometry of the approximate constitutive surfaces is used as a basis for developing relationships between the moduli.

The chapter is divided into six sections. Section 3.1 describes the layout of the chapter. Section 3.2 presents the form of the soil structure and water phase constitutive surfaces based on published experimental evidence. The form on an arithmetic scale and its alternate on a semi-logarithmic scale are both discussed. Section 3.3 explains the theory development for the relationships between the various moduli. Approximate semi-logarithmic constitutive surfaces with planar suctions are proposed. The methodology of mathematically relating the moduli through the geometry of the approximate constitutive surfaces is discussed. Section 3.4 identifies the soil structure and water phase volume change constitutive

relations adapted to approximate the curved constitutive surfaces. The geometrical characteristic of the associated planar, semi-logarithmic constitutive surfaces are shown. Section 3.5 develops and presents proposed relationships between the moduli based on the geometry of the approximated constitutive surfaces. Section 3.6 discusses how the proposed theory can be adapted for unsaturated collapsing soils. However, a complete consideration of collapsing soil is outside the scope of this thesis.

3.2 Characteristic Forms for The Soil Structure and Water Phase Constitutive Surfaces Based on Published Experimental Evidence

The continuity requirement (i.e., equation 2.1) justifies that the soil structure and water phase constitutive relations are sufficient to completely describe all volume change properties of an unsaturated soil (see Section 2.2). This section attempts to identify the nature of these relations based on published experimental evidence. The form of the soil structure constitutive surface is discussed first, followed by the form of the water phases constitutive surface.

Soil Structure Constitutive Surface

In 1956, Holtz and Gibbs presented results of "load-expansion tests" on undisturbed expansive Arizona clay specimens. Each specimen was tested by measuring the load required to restrain the specimen during saturation and measuring the expansion produced by reducing the load increments to approximately one pound per square inch. Results of four specimens with different initial conditions were presented (Figure 3.1). A linear vertical strain versus the logarithm of decreasing effective stress relation was observed. A free swell test was performed on a specimen with initial conditions similar to one of the specimens used for the "load expansion tests". The vertical strain versus the logarithm of decreasing effective stress and matric suction lines are found to be converging. This limited data illustrates that the soil structure constitutive surface for the unloading mode is unique.

In 1963, Gilchrist presented results of one-dimensional constant volume and free swell tests on near identical statically compacted Regina clay specimens. Results of two series of tests on two groups of specimens with different initial void ratios and water contents are re-analyzed. The rebound curve obtained from the constant volume compression test is assumed to be the same as the effective stress unloading curve from the corrected swelling pressure, P_s' (Fredlund, 1983). The void ratio versus the

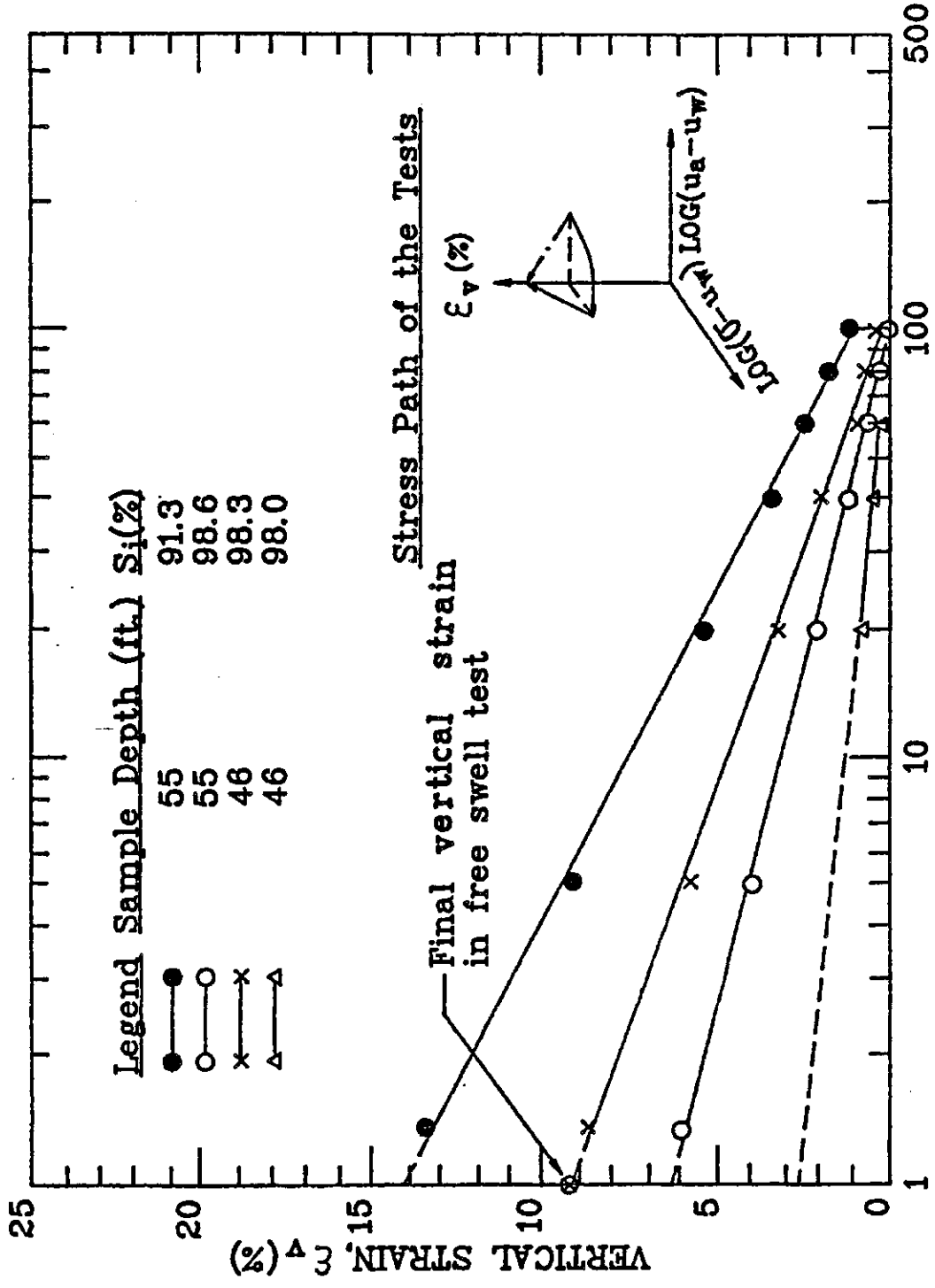

Figure 3.1 The Logarithm of Effective Stress Versus Vertical Strain Relation for An Arizona Clay (Holtz and Gibbs, 1956)

logarithm of decreasing effective stress and matric suction lines are found to be converging (Figure 3.2). This illustrates the soil structure constitutive surface for the unloading mode is unique.

In 1966, Noble presented results of constant load swelling tests on undisturbed and remoulded Regina clay specimens. These tests were part of the test program conducted by Gilchrist in 1963. Each specimen was subjected to a constant load and was then given free access to water and allowed to swell. The time between the application of the load and the completion of the flooding was maintained near thirty seconds with "zero" time for volume change phenomena considered to be when the addition of water was completed. Results for five groups of remoulded specimens with similar initial conditions are re-analyzed and presented (Figure 3.3). The amount of swelling is plotted against the logarithm of the applied load. The volume change versus the logarithm of decreasing effective stress relations are shown to be essentially linear. The swelling moduli with respect to decreasing effective stress (i.e., C_{ts}) for group III, IV and V are found to be 0.099, 0.090 and 0.100 respectively. The rebound moduli or swell indices (i.e., C_s) of the same soils were determined by Gilchrist (1963) to be 0.101, 0.092 and 0.101 respectively. The close agreement illustrates the rebound or unloading curves are approximately parallel to one another.

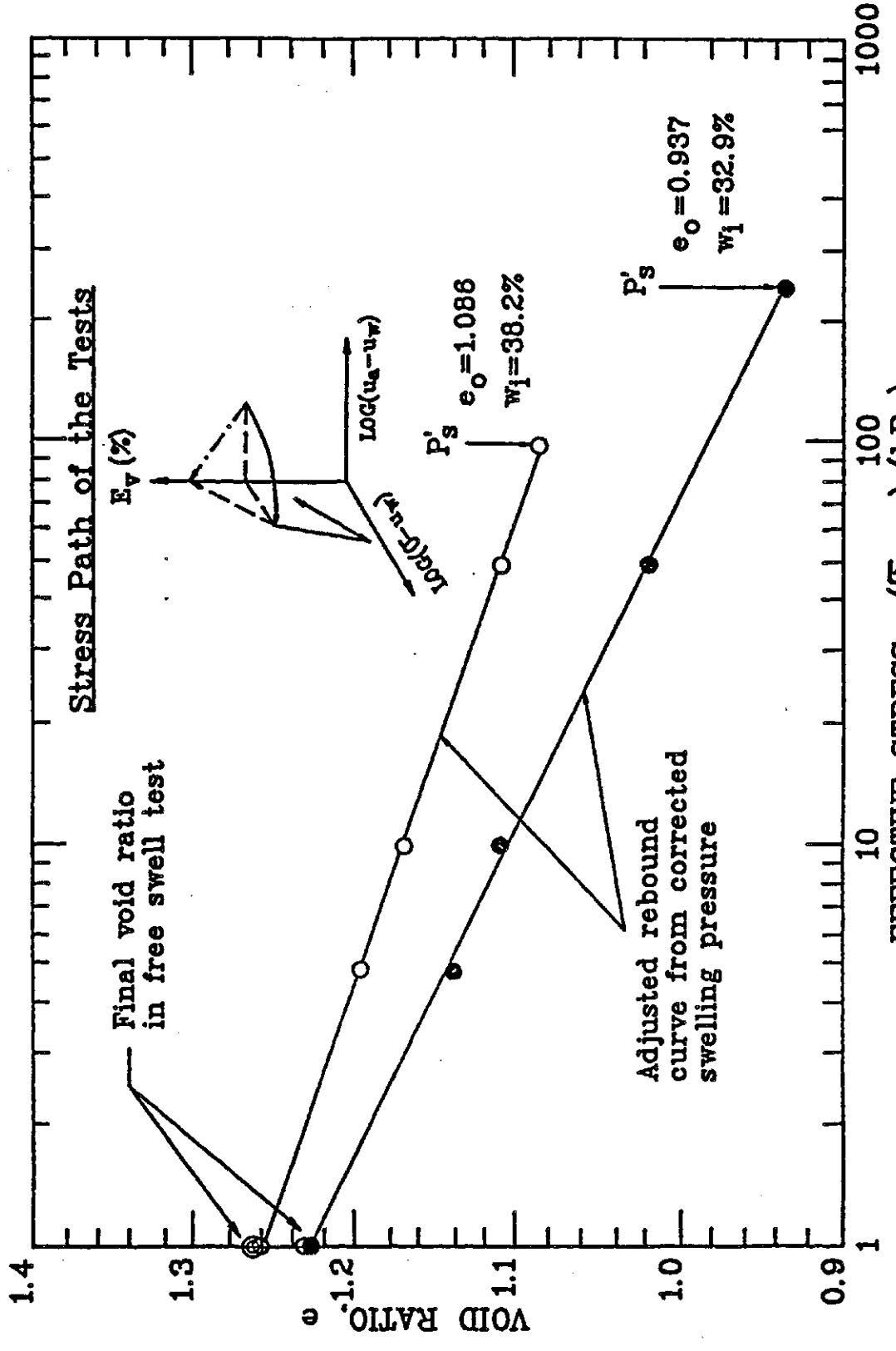

Figure 3.2 The Logarithm of Effective Stress Versus Void Ratio Relations for Compacted Regina Clay (Gilchrist, 1963)

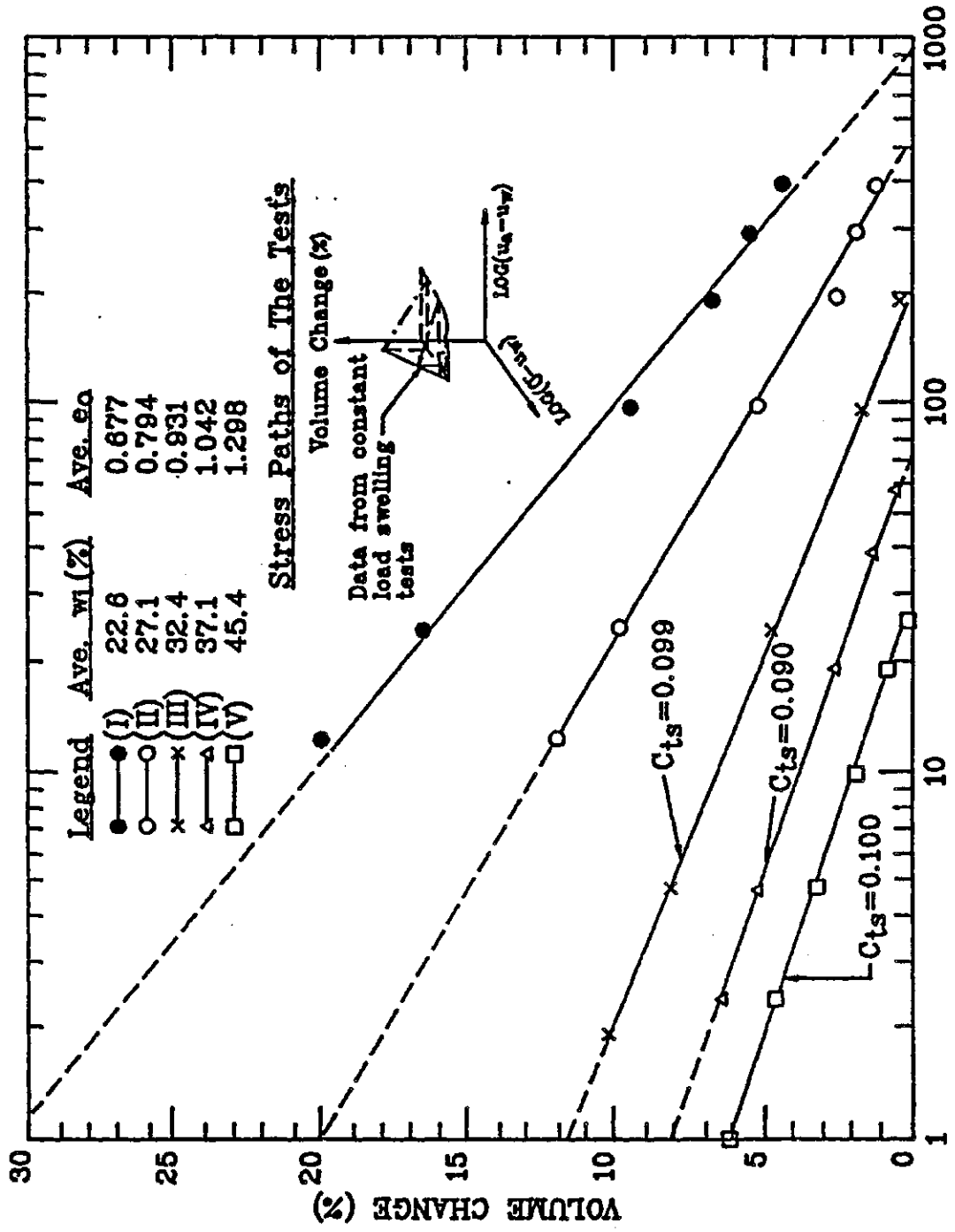

Figure 3.3 The Logarithm of Effective Stress Versus Volume Change Relations for Remoulded Regina Clay (Noble, 1966)

In 1969, Aitchison and Woodburn performed modified oedometer tests on Adelaide Black Earth specimens. Volume change curves under controlled matric suction and surcharge load were presented. The vertical strain versus the logarithm of increasing and decreasing matric suction relations are found to be closely linear (See Figure 2.3).

1969, Escario presented results of free swelling and "swelling pressure" tests on remoulded Madrid clay specimens. Free swelling test results for three specimens of different initial conditions are re-analyzed. The vertical strain versus the logarithm of matric suction relations for these specimens are approximately bilinear (Figure 3.4). The constant volume stress paths of three other different specimens during the "swelling pressure tests" are presented (Figure 3.5). In a "swelling pressure" test, the swelling of the specimen was prevented by increasing and measuring the applied effective stress while water at atmospheric pressure was fed to the soil. These constant volume lines are found to be essentially linear on an arithmetic scale. The same lines are asymptotic curves on a logarithmic scale. The shape of these constant volume stress paths illustrates the form of the soil structure constitutive surfaces in a three-dimensional plot using the stress state variables as the abscissas.

In 1970, Lidgren presented results of one-dimensional constant volume and free swell tests on near

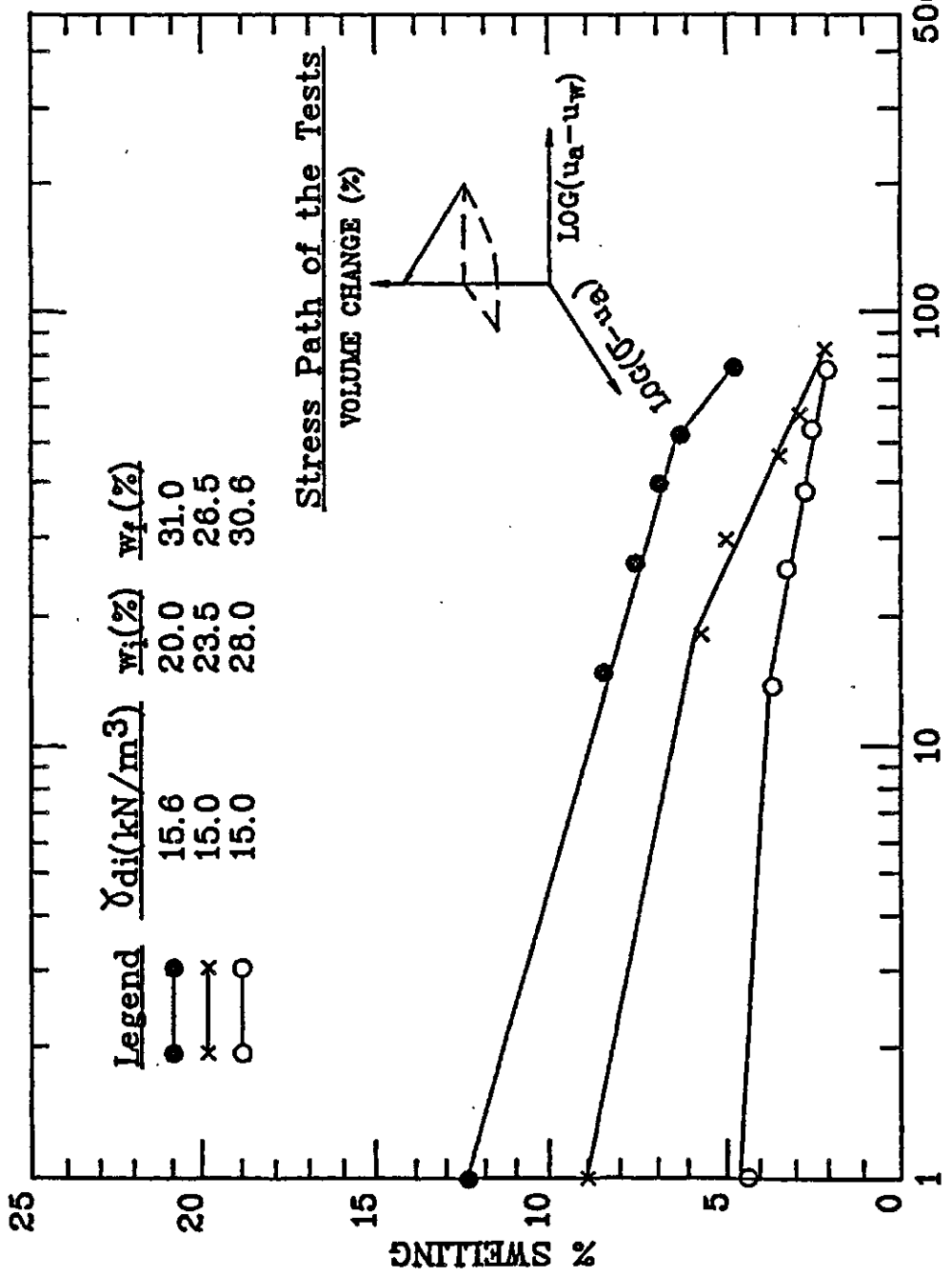

Figure 3.4 The Logarithm of Matric Suction Versus The Percent of Swelling Relations for Remoulded Madrid Clay (Escario, 1969)

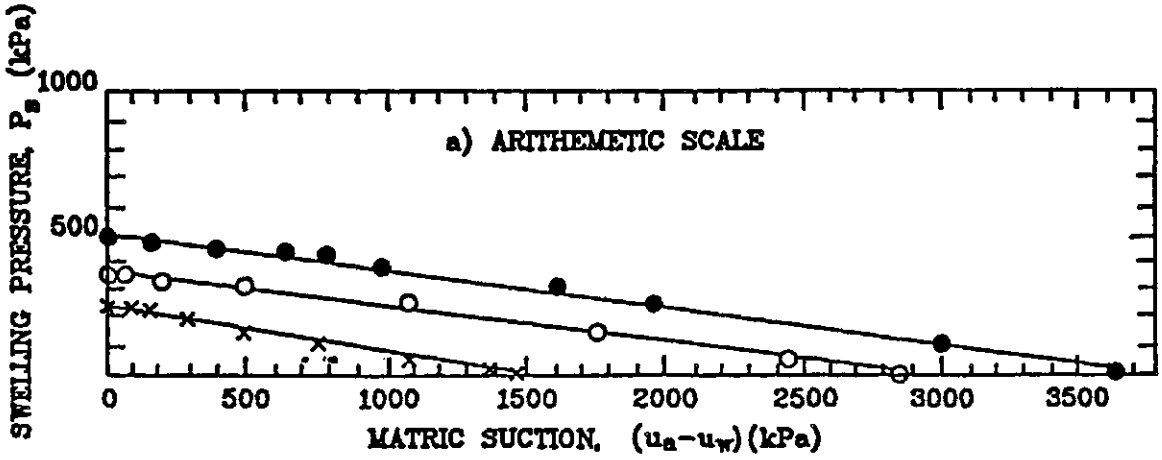

Figure 3.5a The Matric Suction Versus Swelling Pressure Relation on An Arithmetic Scale for A Remoulded Madrid Clay Undergoing Constant Volume Stress Changes (Escario,1969)

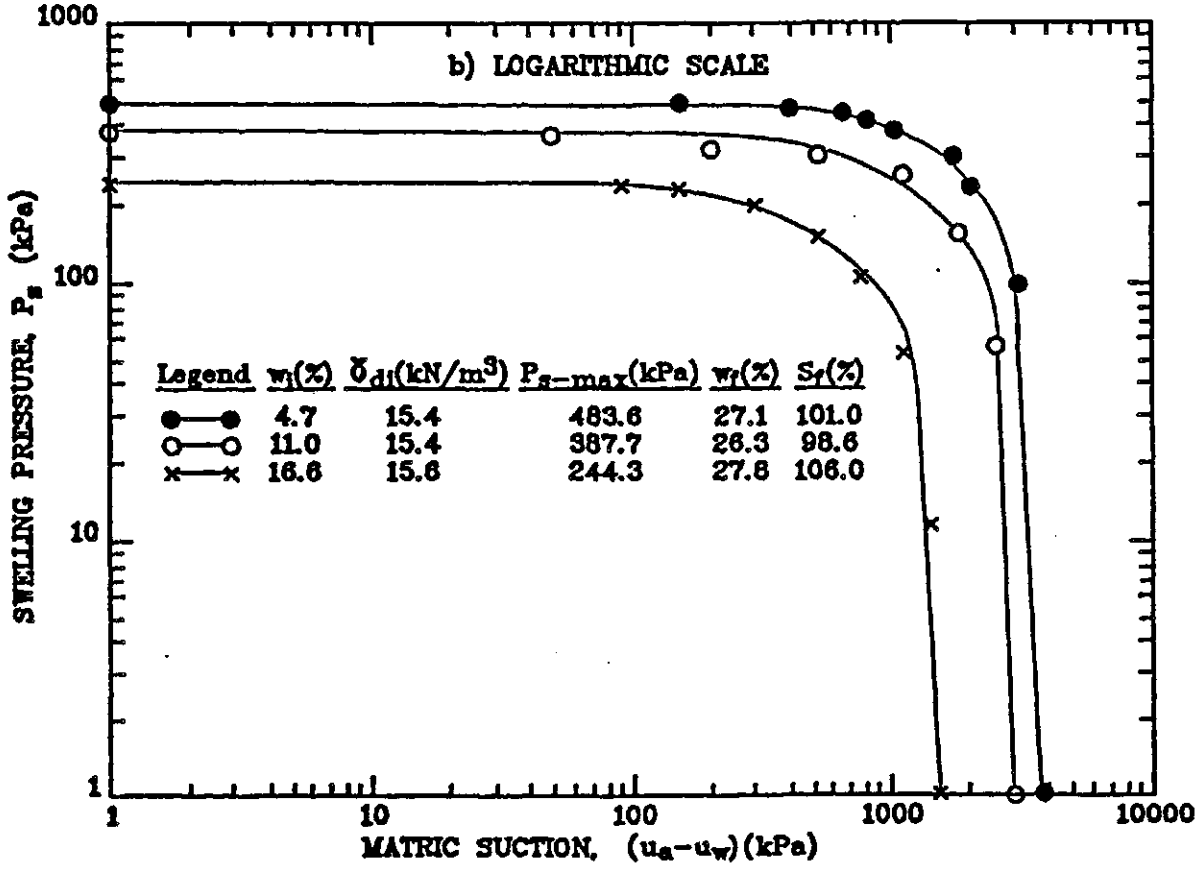

Figure 3.5b The Matric Suction Versus Swelling Pressure Relation on A Logarithmic Scale for A Remoulded Madrid Clay Undergoing Constant Volume Stress Changes (Escario, 1969)

identical compacted glacial till specimens. The results of three series of tests on three groups of specimens with different initial void ratios and water contents are re-analyzed and presented. The void ratio versus the logarithm of decreasing effective stress and matric suction lines are found to be converging (Figure 3.6). It should be noted that it is necessary to correct the swelling pressure for sample disturbance to get the rebound curve to converge with the matric suction unloading curve. This illustrates the uniqueness of the soil structure constitutive surface for the unloading mode.

In 1973, Aitchison and his co-workers reported a linear relation between the soil structure volumetric strain and the logarithm of the total stress (i.e., σ), matric suction (i.e., $(u_a - u_w)$) and solute suction (i.e., π). Modified oedometer test results on an Adelaide clay were presented (Aitchison and Martin, 1973). For monotonic volume increases, the vertical strain versus total stress and matric suction curves are shown to converge towards a single point on the vertical strain axis when both the total stress and matric suction approach zero (see Figure 2.10). The vertical strain versus the logarithm of decreasing matric suction relation appears to be bilinear (Figure 3.7). The vertical strain versus the logarithm of increasing matric suction relation is found to be essentially linear (Figure 3.8).

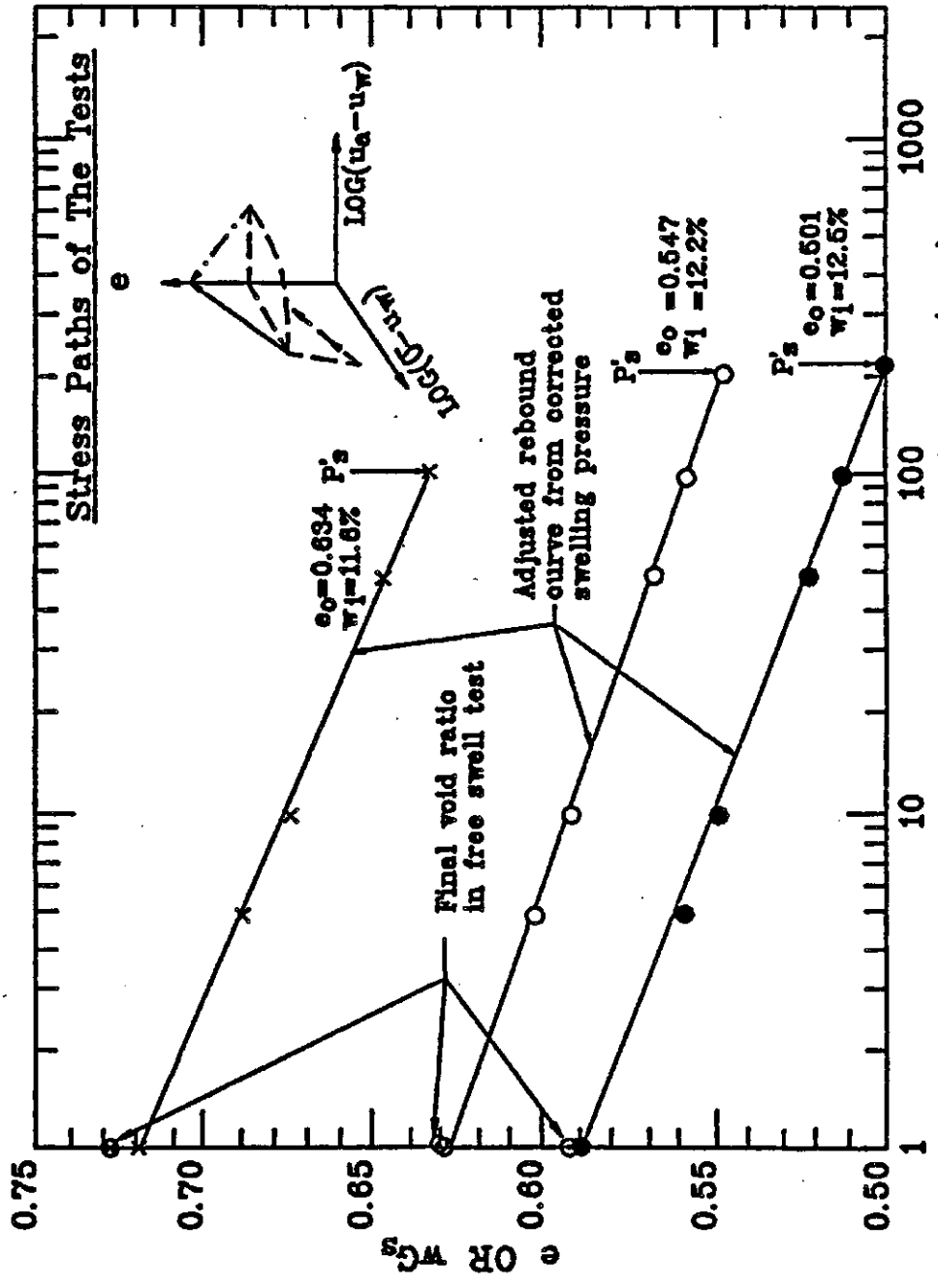

Figure 3.6 The Logarithm of Effective Stress Versus Void Ratio Relations for Compacted Glacial Till (Lidgren, 1970)

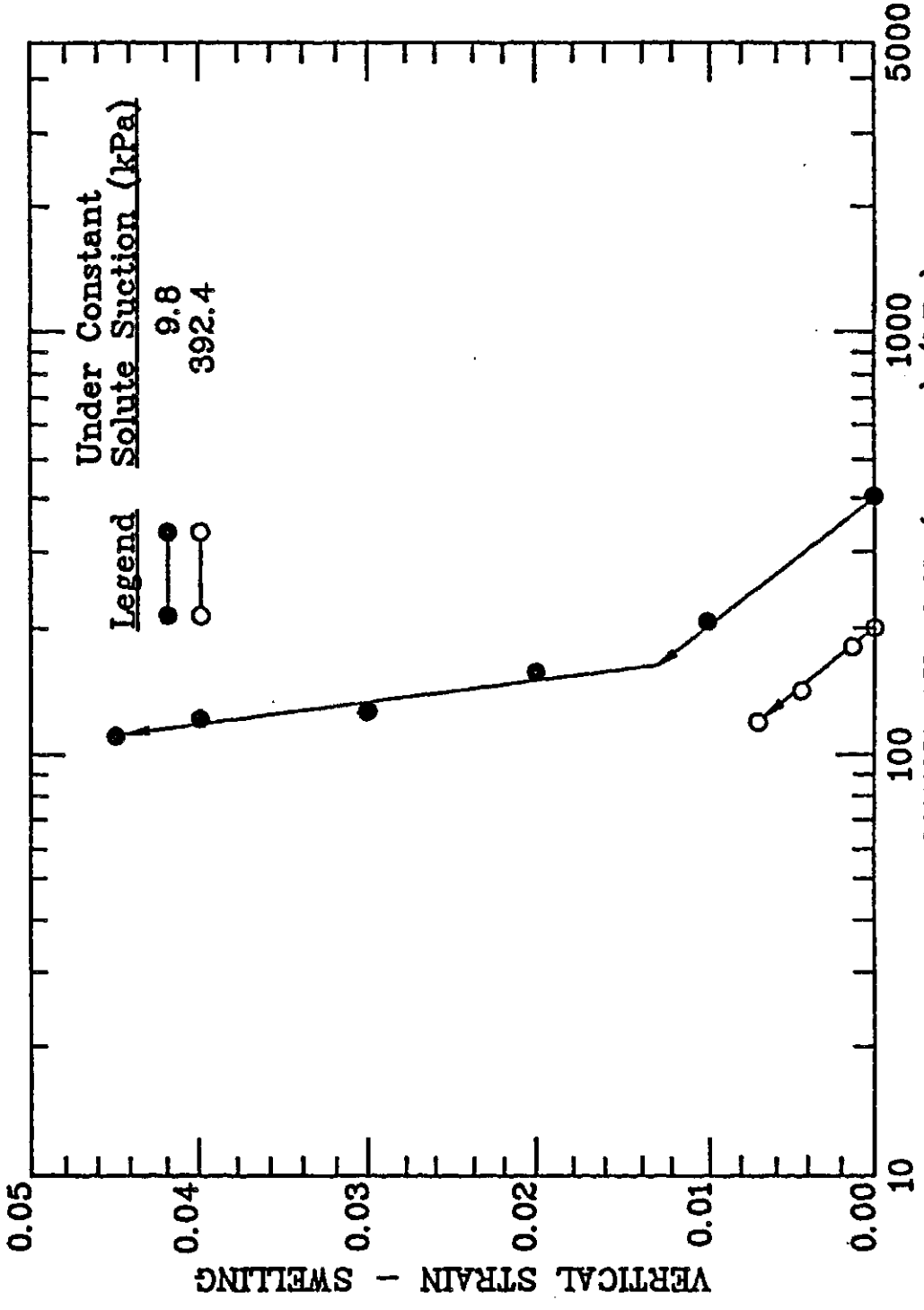

Figure 3.7 The Logarithm of Matric Suction Versus Vertical Strain Relations for An Adelaide Clay Undergoing Monotonic Volume Increase (Aitchison and Martin, 1973)

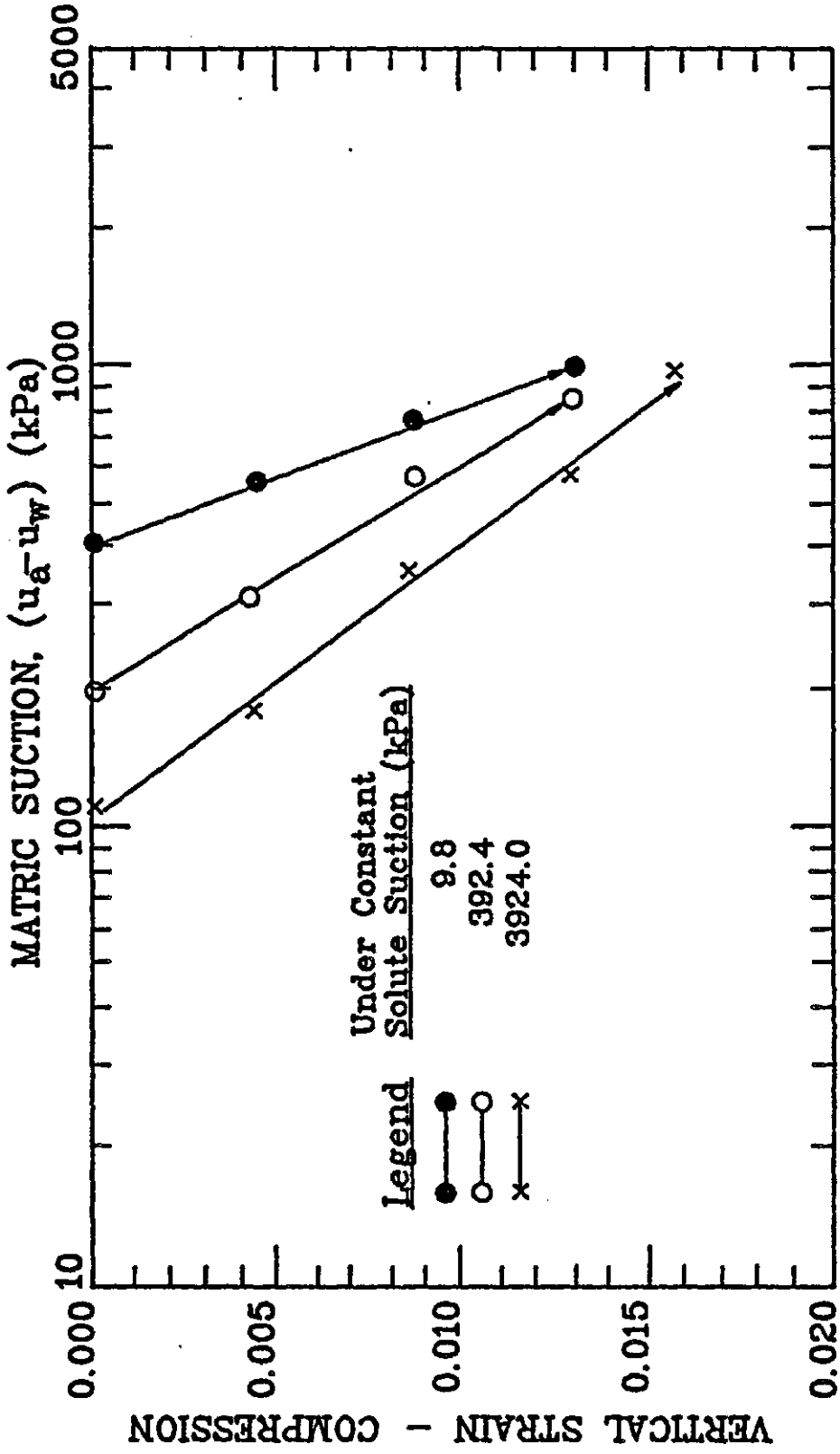

Figure 3.8 The Logarithm of Matric Suction Versus Vertical Strain Relations for An Adelaide Clay Undergoing Monotonic Volume Decrease (Aitchison and Martin, 1973)

In 1975, Chen presented results of "controlled swelling" tests on remoulded Denver claystone shale specimens. Results from a group of five near identical specimens are re-analyzed and presented. Water was added to each specimen under constant volume conditions at different stress levels. The specimen was then allowed to swell under constant applied stress. A linear vertical strain versus the logarithm of decreasing effective stress relation is evident when the soil structure undergoes monotonic volume increases (Figure 3.9). Unfortunately data was not available on the slope of the rebound curve from constant volume loading and unloading tests.

In 1984, Mitchell and Avalle presented "core shrinkage test" results of undisturbed O'Halloran Hill clay specimens. The volume change data of one specimen under increasing total suction is re-analyzed. The vertical strain versus the logarithm of increasing total suction was found to be somewhat bilinear, the slope becoming flatter at suction beyond 60,000 kPa (Figure 3.10).

In 1984, Richards, Peter and Martin presented results of "suction controlled consolidometer tests" on undisturbed Athelstone Park clay specimens. The matric suction of the specimen was increased and then decreased under constant applied total stress. One set of test data is re-analyzed and presented. The results demonstrate linear vertical strain versus the logarithm of matric

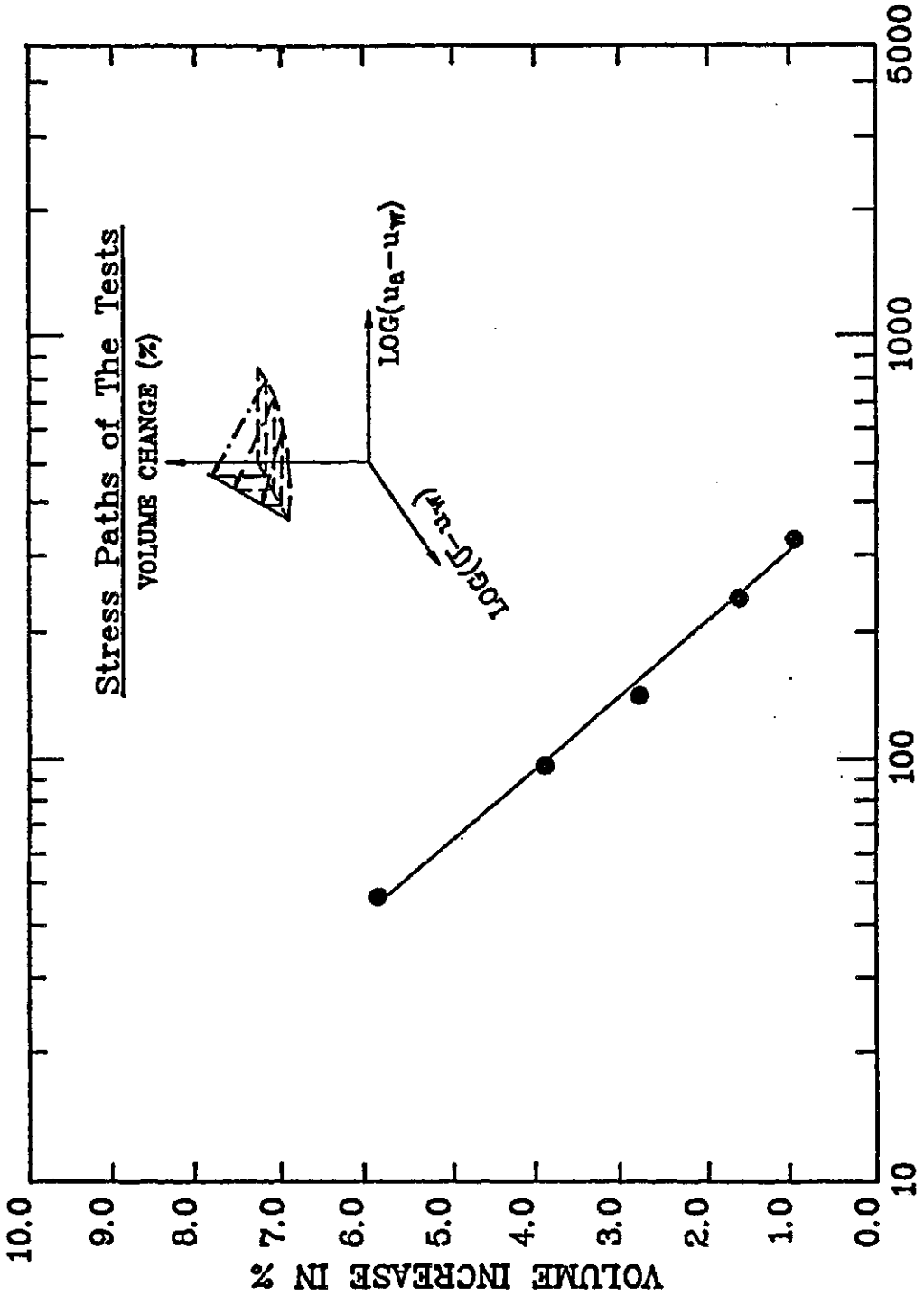

Figure 3.9 The Logarithm of Decreasing Effective Stress Versus The Percent of Swelling for Denver Claystone Shale (Chen, 1975)

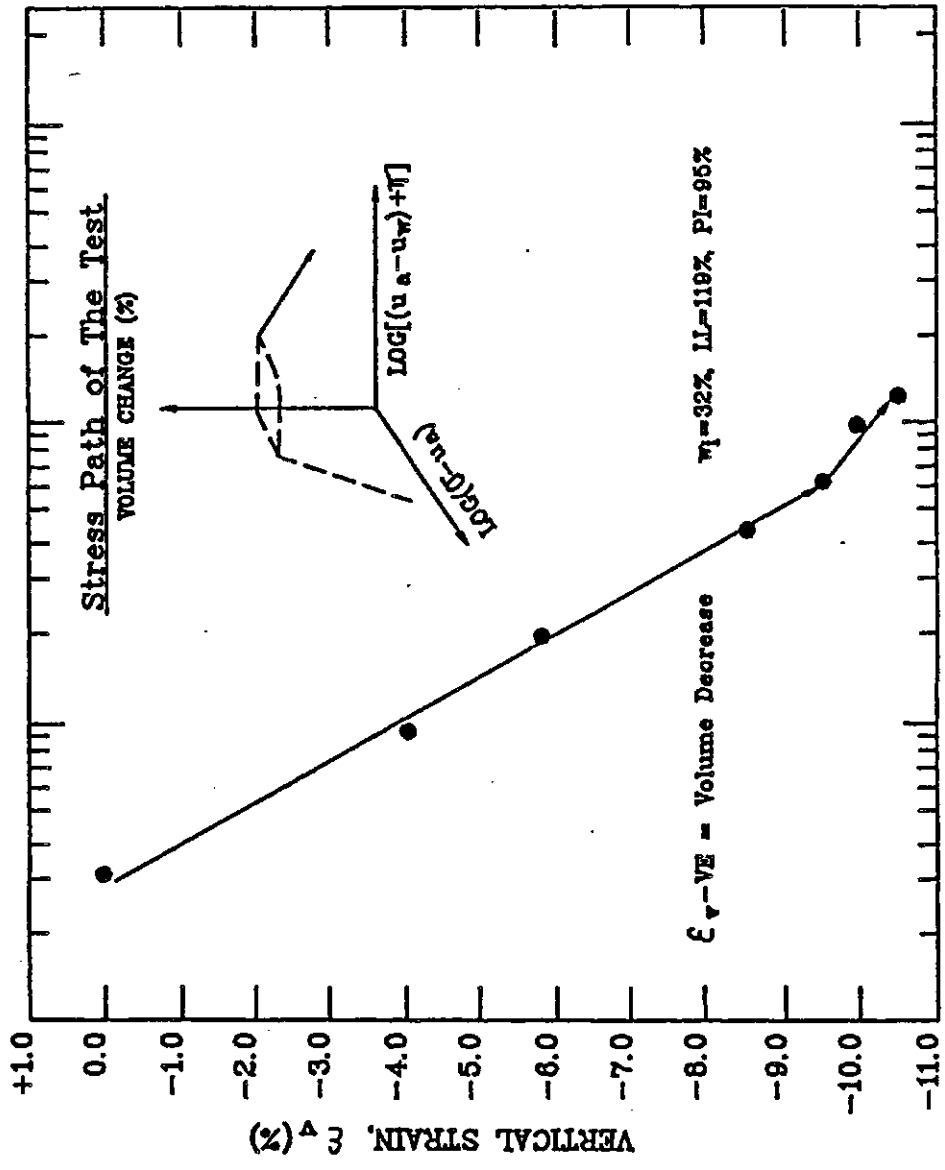

Figure 3.10 The Logarithm of Increasing Total Suction Versus Vertical Strain Relation for O'Halloran Hill Clay (Mitchell and Avalle, 1984)

suction relations for monotonic volume changes under constant total stress (Figure 3.11).

In 1985, Lloret and Alonso presented an optimum soil structure volume change constitutive relation for significant stress variation. A graphical presentation of the proposed constitutive relation was shown in Figure 2.22. On a semi-logarithmic plot of net total stress and matric suction versus void ratio, the constitutive surface resembles a quarter section of the convex surface of a vertical cone.

In addition to the discussed literature, the form of the effective stress versus void ratio relation is well established when matric suction is zero. The compression of a saturated soil consists of two distinct stages, the recompression and virgin compression (Terzaghi and Peck, 1967). The virgin compression curve is exponential on an arithmetic scale and can be linearlized on a semi-logarithmic plot. The rebound curves are approximately parallel to one another and can be linearlized on a semi-logarithmic scale (Lambe and Whitman, 1969). The effective stress equals the net total stress (i.e., $\sigma - u_a$) when a soil is saturated and the pore-water pressure is zero (Fredlund, 1973). Similarly, soils can be over-consolidated by desiccation and rebound due to suction decrease. The compression consists of recompression and virgin compression. The virgin compression branch and rebound curves are essentially linear on a semi-logarithmic scale

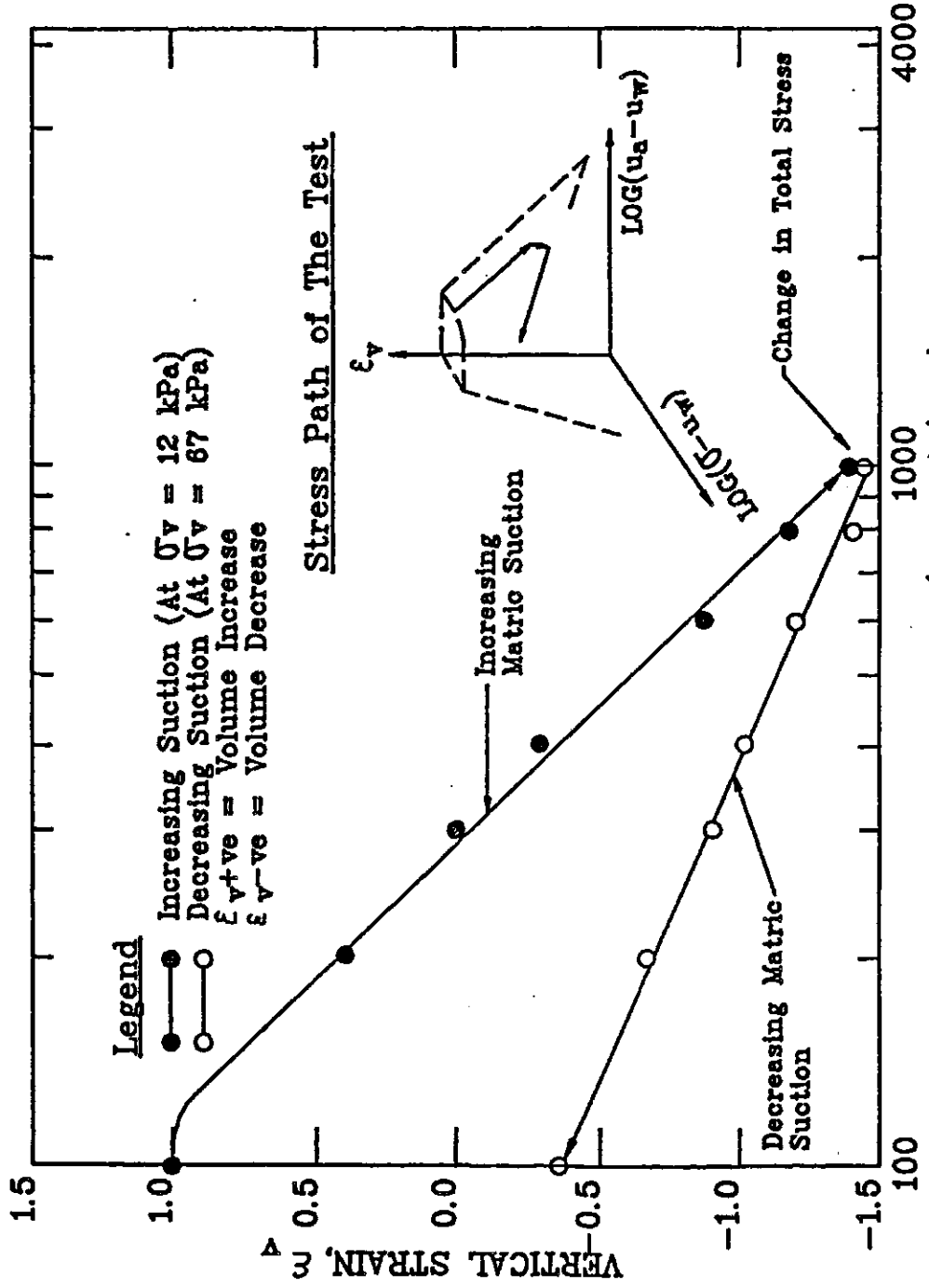

Figure 3.11 The Logarithm of Matric Suction Versus Vertical Strain Relations for Athelstone Park Clay (Richards, Peter and Martin, 1984)

(Fredlund, 1964).

Based on the above studies, the following key observations can be made concerning the form of the soil structure constitutive surfaces for monotonic volume changes.

a) The constitutive curves on the matric suction or net total stress planes are essentially linear on a semi-logarithmic scale. The matric suction and net total stress planes are state planes on which the net total stress and matric suction are at a nominal value respectively. The same curves are therefore exponential on arithmetic plots. There are pressure limits which must be observed. For example, in the suction range of 0 to 60,000 kPa, the above relations will often be linear over a significant portion of this range.

b) A constant volume stress path (i.e., constant void ratio) on the constitutive surface is essentially a straight line on an arithmetic plot. The same path becomes an asymptotic curve on a logarithmic scale.

On an arithmetic plot of void ratio, net total stress and matric suction, the soil structure constitutive surface is a concave, warped surface. The same surface becomes a quarter section of the convex surface of a vertical cone on a void ratio versus the logarithm of net total stress and matric suction plot. A schematic diagram of the soil structure constitutive surfaces for monotonic volume changes is shown

(Figure 3.12). There are four moduli (i.e., a_t, a_{ts}, a_m, a_{ms}) associated with the arithmetic representation. These moduli are defined as follows,

a_t , a_{ts} = coefficient of compressibility and coefficient of swelling with respect to the net total stress for monotonic volume decrease and increase respectively

a_m , a_{ms} = coefficient of compressibility and coefficient of swelling with respect to matric suction for monotonic volume decrease and increase respectively

There are four moduli (i.e., C_t, C_{ts}, C_m, C_{ms}) associated with the semi-logarithmic representation. These moduli are defined as follows,

C_t , C_{ts} = compressive and swelling index with respect to the net total stress for monotonic volume decrease and increase respectively

C_m , C_{ms} = compressive and swelling index with respect to matric suction for monotonic volume decrease and increase respectively

Water Phase Constitutive Surface

There is limited information on the form of the water phase volume change constitutive surface. The following is an attempt to identify its characteristic form based on data from research literature.

In 1954, Croney and Coleman presented the suction versus water content curves for a variety of soils ranging from heavy clays to sands (See Figures 2.23 to 2.27). The water content versus increasing and decreasing matric suction relations are approximately linear or gradually

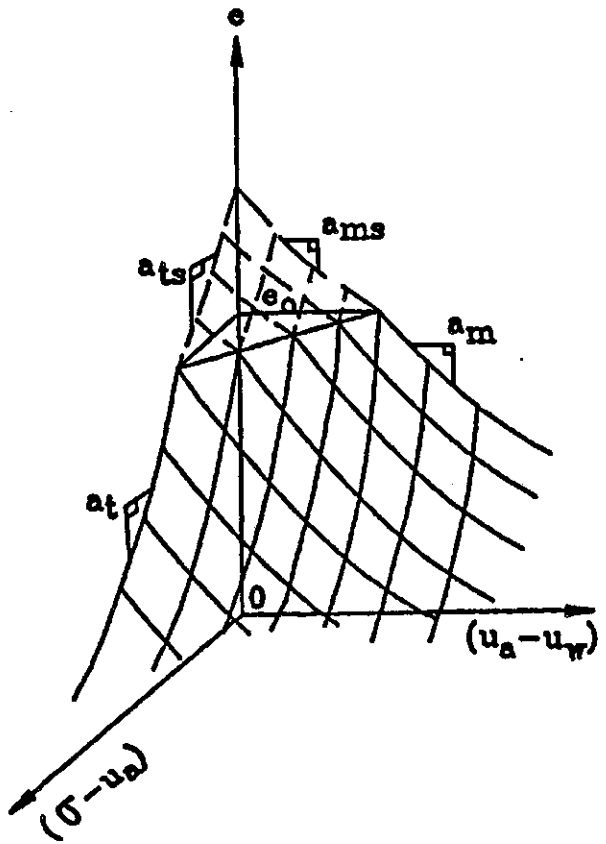

Figure 3.12a A Schematic Diagram of The Soil Structure Constitutive Surfaces for Monotonic Volume Changes on An Arithmetic Scale

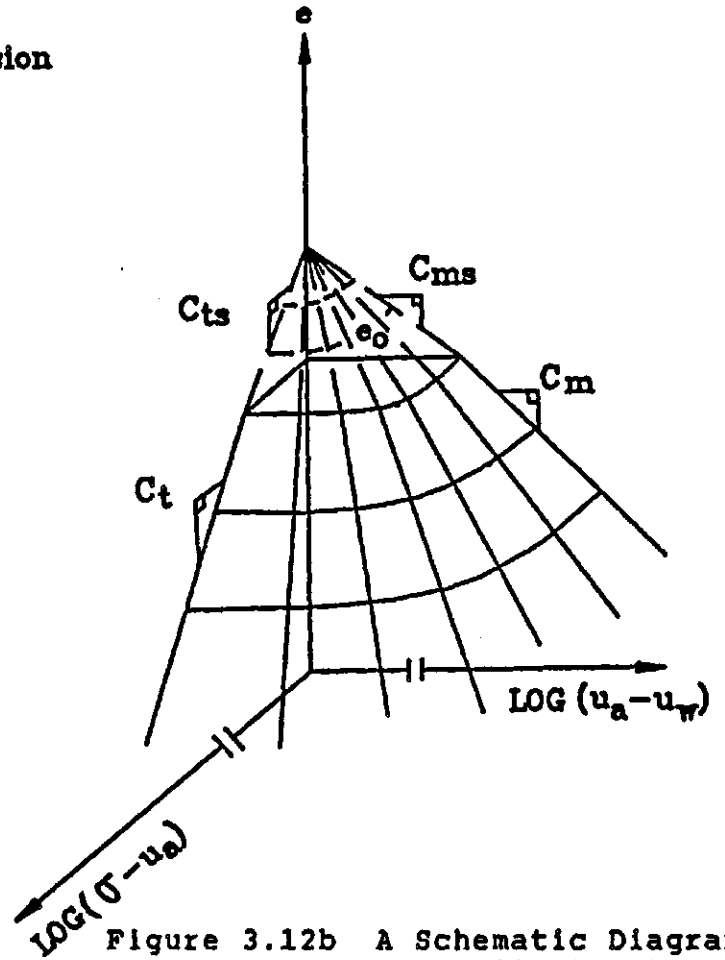

Figure 3.12b A Schematic Diagram of The Soil Structure Constitutive Surfaces for Monotonic Volume Changes on A Semi-Logarithmic Scale

curving on a semi-logarithmic plot. The same relations are approximately exponential on an arithmetic scale. Figure 3.13 shows data which is considered to be characteristic of water content versus matric suction data. The projected matric suction at zero water content from the linear portions of both the drying and wetting curves is approximately equal to 300,000 kPa.

In 1967, Fredlund presented matric suction and one-dimensional consolidation test results on remoulded, slurry Regina clay specimens. The water content versus the logarithm of effective stress and matric suction relations are shown to be essentially linear once the virgin compression branches are reached (Figure 3.14).

In 1979, McWhorter and Nelson presented matric suction versus volumetric water content curves for two sands. The water content versus the logarithm of increasing matric suction relations for both sands are found to be bilinear (Figure 3.15).

Arnold (1983) reported that "a value of total suction at zero water content can be taken as pF 6.8 (i.e., 6.2×10^5 kPa) for practical purposes". In 1984, Mitchell and Avalle presented six water content versus total suction curves for O'Halloran Hill clay specimens of different initial states to support the same conclusion. The data is re-analyzed to show linear water content versus the logarithm of total suction relations converging towards a

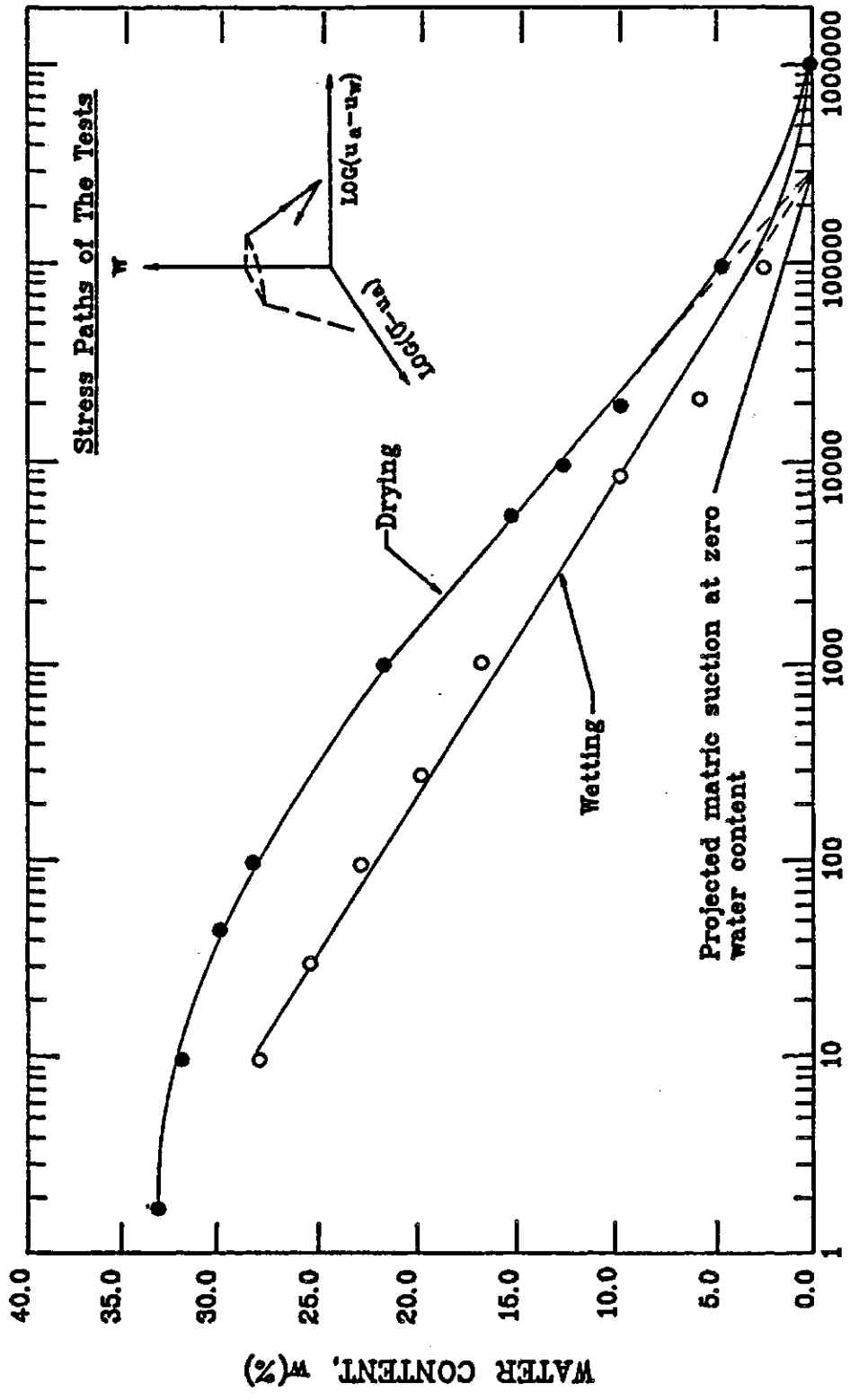

Figure 3.13 The Logarithm of Matric Suction Versus Water Content Relation for A Heavy Clay Soil (Croney and Coleman, 1954)

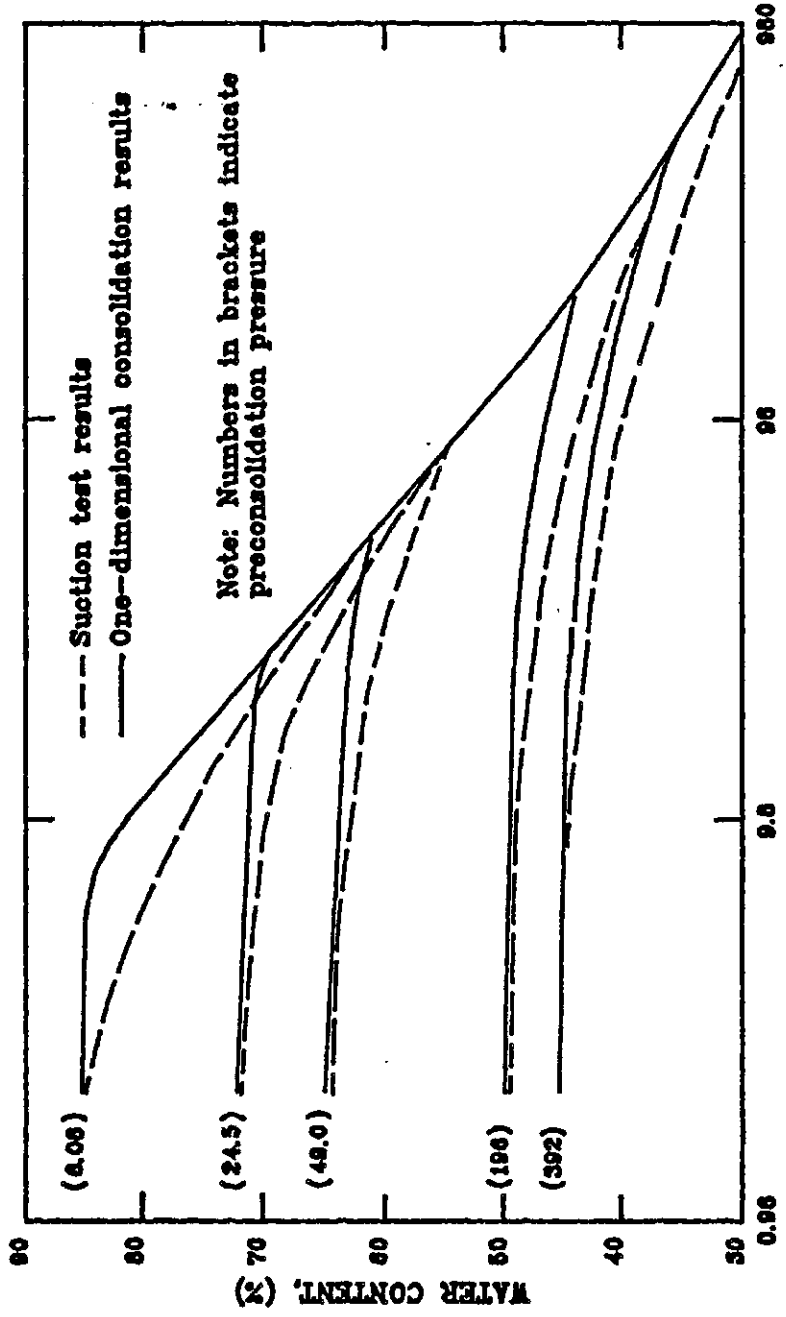

Figure 3.14 Comparison of Recompression Branches for Suction and One-Dimensional Consolidation Tests for Regina Clay (Fredlund, 1964)

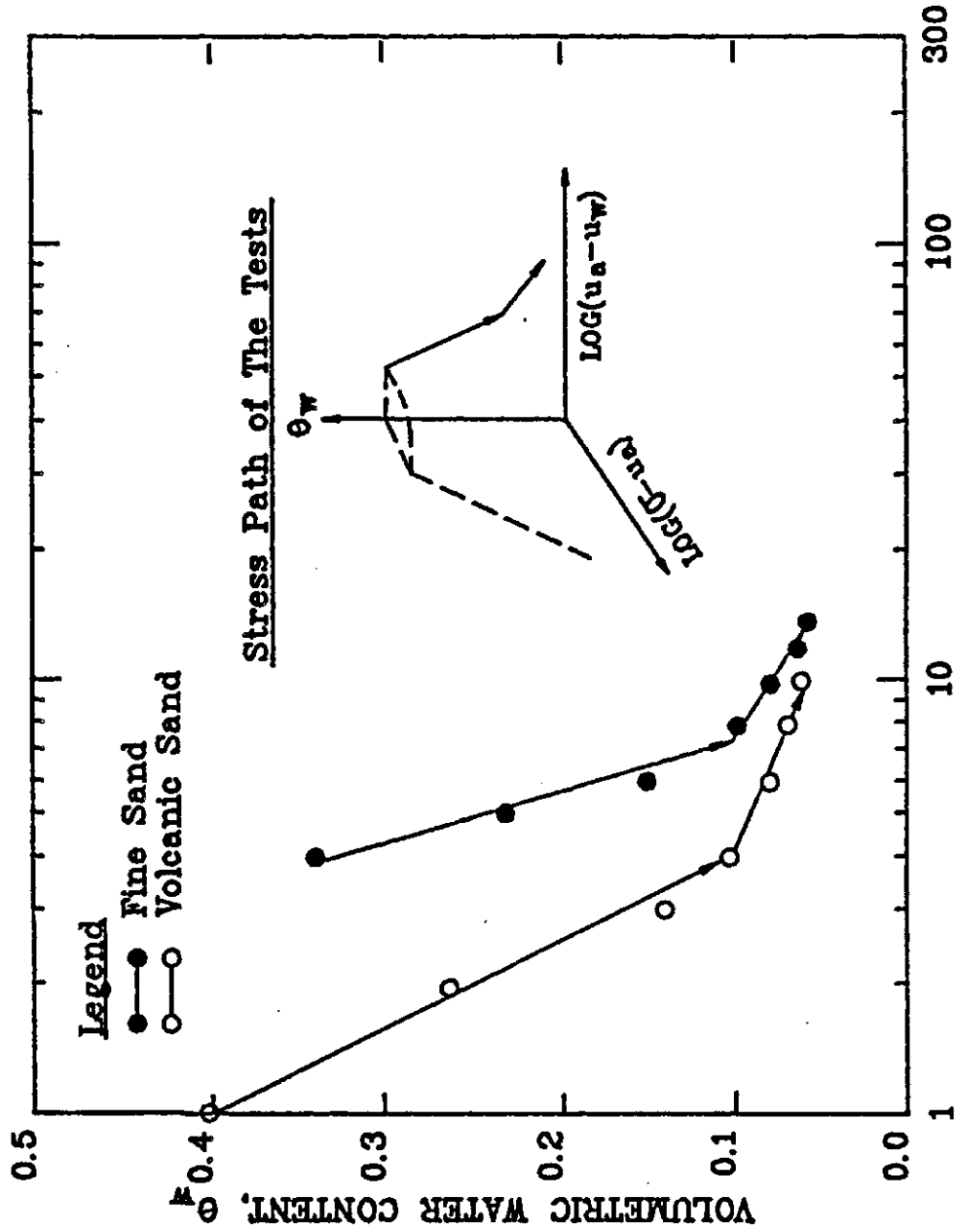

Figure 3.15 The Logarithm of Matric Suction Versus Volumetric Water Content Relation for Two Sands (McWhorter and Nelson, 1979)

limiting value of 6.2×10^5 kPa at zero water content (Figure 3.16). Previously, Croney and Coleman (1954) reported the total suction at zero water content for sands, light and heavy clay soils to be pF 4.5 (i.e., 3.1×10^3kPa) and pF 7.0 (i.e., 9.8×10^5 kPa) respectively. In 1964, Fredlund presented the total suction at zero water content for a remoulded Regina clay to be 8.8×10^5 kPa. One the basis of the above data, it can be concluded that all soils have essentially the same total suction at zero water content. The preferred value appears to be 6.2×10^5 kPa. This provides a fixed point when establishing the water content versus suction relation.

The water content and void ratio constitutive relations are related to each other by the relative density when a soil is saturated. The form of the effective stress versus void ratio constitutive relation is well established and discussed previously in this section. Conclusions arrived at also pertain to the water phase constitutive relation on the net total stress plane.

There is insufficient information in the literature to completely define the form of the water phase volume change constitutive surface. There is evidence that the constitutive curves on the matric suction or net total stress equals to zero planes are essentially linear on a semi-logarithmic scale. There are pressure limits within which the linearity is observed. The same curves are

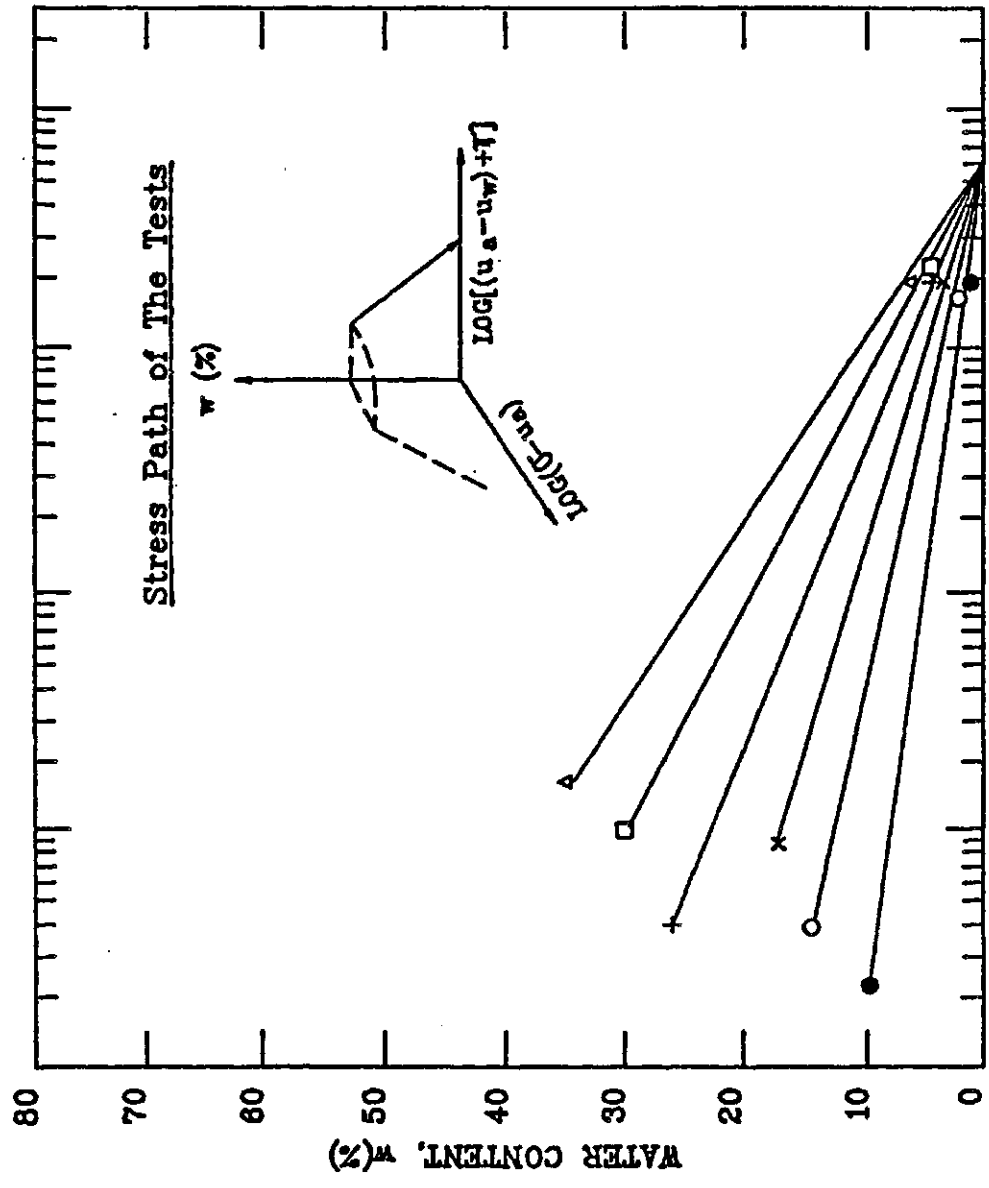

Figure 3.16 The Logarithm of Total Suction Versus Water Content Relation for O'Halloran Hill Clay (Mitchell and Avalle, 1984)

therefore approximately exponential on arithmetic plots. There is no experimental information available on the shape of a constant water content stress path on the constitutive surface. When a soil approaches saturation, a change in net total stress is as effective as a change in matric suction in changing the water content. A constant water content stress path must therefore approach a forty-five degree line towards the matric suction equals to zero plane. This angle forms an upper limit. A constant water content stress path on the water phase constitutive surface must be assumed to be a straight line on an arithmetic plot of water content versus net total stress and matric suction. The angle can be less than forty-five degree. The resulting water phase constitutive surface is a concave surface when water content is increased or decreased. The linear constant water content stress path becomes an asymptotic curve on a logarithmic net total stress and matric suction plot. The resulting water phase constitutive surface therefore resembles a quarter section of the convex surface of a vertical cone on a water content versus the logarithm of net total stress and matric suction plot. A schematic diagram of the water phase constitutive surfaces for monotonic volume changes is presented (Figure 3.17). There are four moduli (i.e., b_t, b_{ts}, b_m, b_{ms}) associated with the arithmetic representation. These moduli are defined as follows,

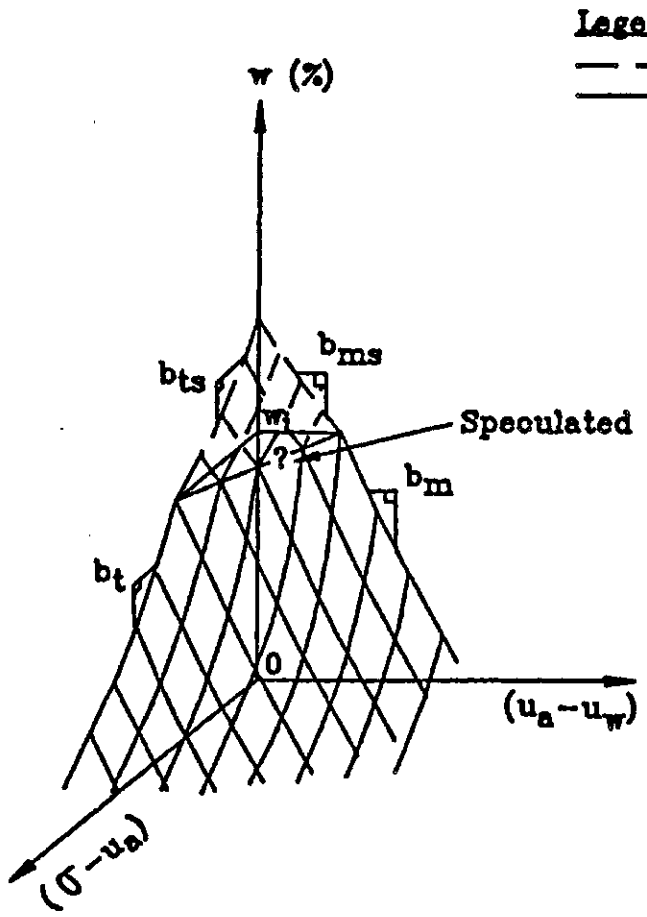

Figure 3.17a A Schematic Diagram of The Water Phase Constitutive Surfaces for Monotonic Volume Changes on An Arithmetic Scale

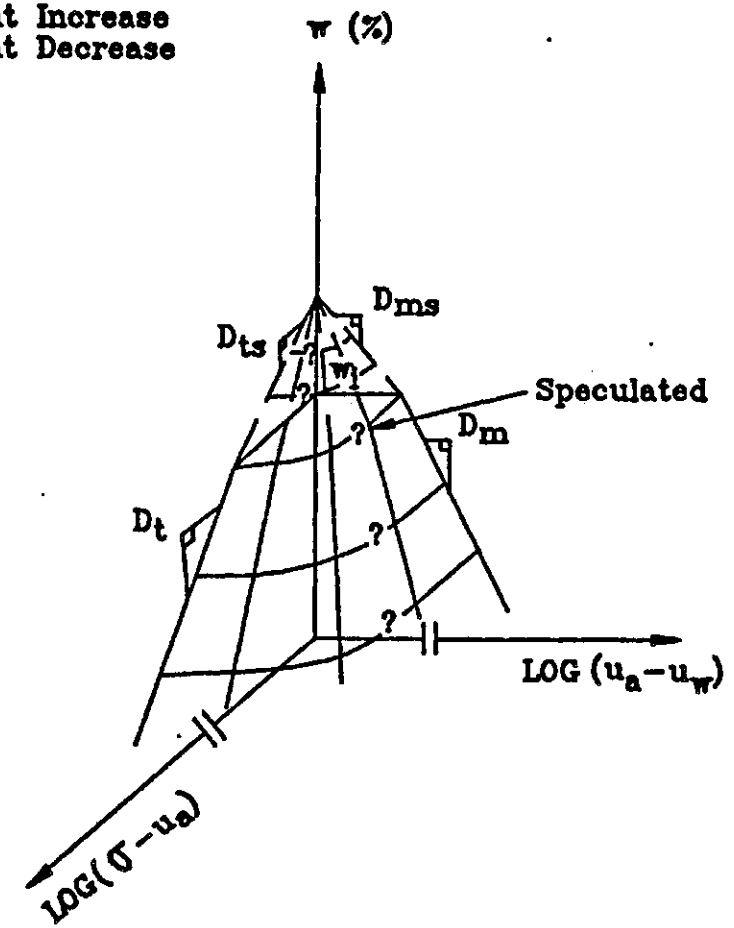

Figure 3.17b A Schematic Diagram of The Water Phase Constitutive Surfaces for Monotonic Volume Changes on A Semi-logarithmic Scale

b_t , b_{ts} = coefficient of water content and rebound coefficient of water content with respect to the net total stress for monotonic water content decrease and increase respectively

b_m , b_{ms} = coefficient of water content and rebound coefficient of water content with respect to matric suction for monotonic water content decrease and increase respectively

There are four moduli (i.e., D_t, D_{ts}, D_m and D_{ms}) associated with the semi-logarithmic representation. These moduli are defined as follows,

D_t , D_{ts} = water content and rebound water content index with respect to the net total stress for monotonic water content decrease and increase respectively

D_m , D_{ms} = water content and rebound water content index with respect to matric suction for monotonic water content decrease and increase respectively

3.3 Theoretical Development Pertinent to The Use of Semi-logarithmic Constitutive Surfaces

Section 3.2 identifies characteristic forms for the soil structure and water phase volume change constitutive surfaces in terms of void ratio, water content, the net total stress and matric suction. This section describes a methodology of formulating relationships between the various moduli through geometric considerations of the semi-logarithmic constitutive surfaces. The case of the soil

structure undergoing monotonic volume decrease is used as an example to explain the proposed theory in the following discussion. Similar logic can be applied to other modes of volume change.

The soil structure volume change constitutive surface is a convex surface on a void ratio versus the logarithm of net total stress and matric suction plot (Figure 3.18). The curved surface resembles a quarter surface section of a vertical cone with an ellipsoid base. The tip of the cone is a projected point of convergence, EL on the void ratio axis. Point EL is assumed to be the point where the two linear void ratio versus the logarithm of net total stress and matric suction constitutive lines meet. Point EL represents the void ratio of a soil under a nominal stress of net total stress and matric suction.

It is proposed that this curved surface can be approximated by three planar surface sections (i.e., planes I, II and III) (Figure 3.18). The boundaries of these planar sections are defined by four stress points (i.e., points u, v, w and x) and point EL which is the projected point of convergence of the constitutive surface. The point u is commonly referred to as the corrected swelling pressure (i.e., P_s') (Fredlund, 1983). Point x represents the matric suction of a soil after being unloaded at constant volume (i.e., $(u_a - u_w)_i^e$). Points v and w are the intersections of plane II with planes I and III (Figure 3.18). A graphical

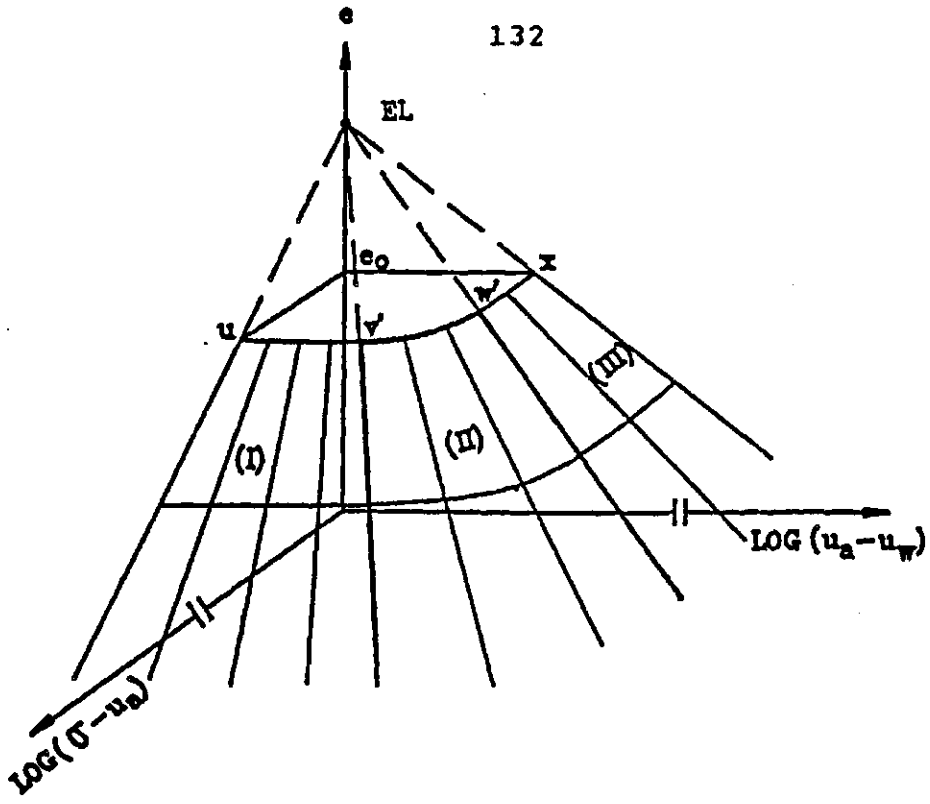

Figure 3.18a The Soil Structure Constitutive Surface for Monotonic Volume Decrease

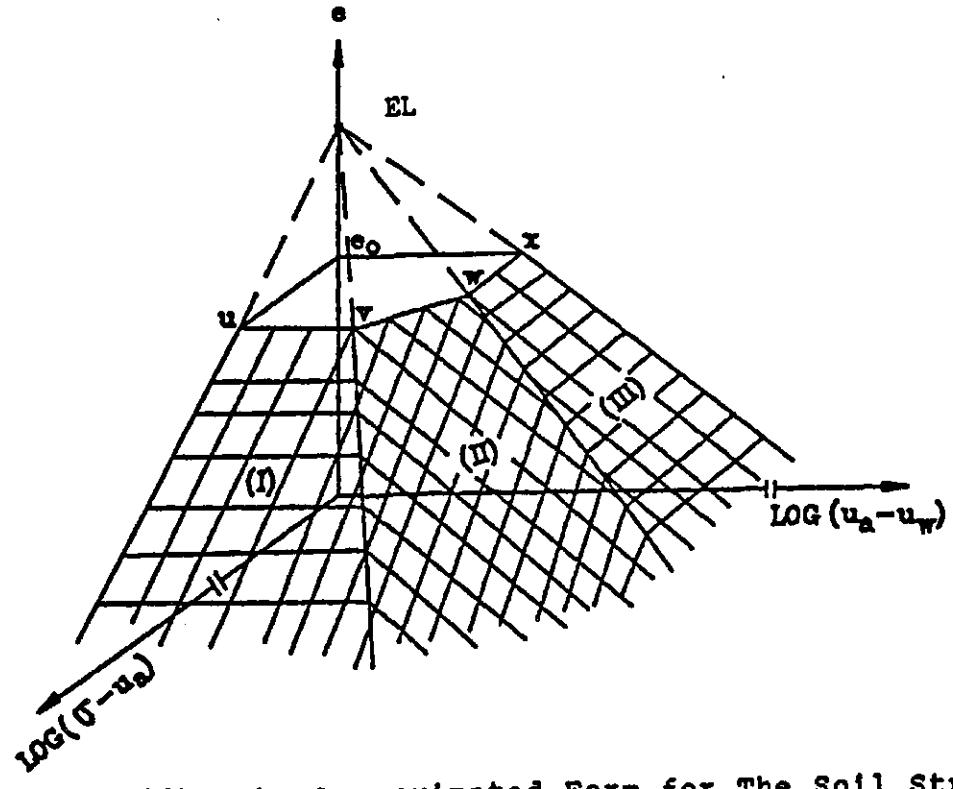

Figure 3.18b The Approximated Form for The Soil Structure Constitutive Surface for Monotonic Volume Decrease

procedure is suggested to locate points v and w in the next paragraph.

The constant volume stress path is essentially a straight line on an arithmetic plot of net total stress versus matric suction. The slope of this line is defined by the corrected swelling pressure (i.e., P'_s or stress point u) and the corresponding matric suction of a soil after being unloaded at constant volume (i.e., $(u_a - u_w)^e_i$ or stress point x) (Figure 3.19). The same constant volume stress path becomes an asymptotic curve on a logarithmic plot of net total stress versus matric suction. It is proposed that this asymptotic stress path can be approximated by three linear segments (i.e., uv, vw and wx). A graphical procedure to locate point v and w is as follows (see Figure 3.19),

i) draw a line AB with a slope of $\frac{\log P'_s}{\log(u_a - u_w)^e_i}$ and tangential to the asymptotic curve;

ii) draw a line parallel to the $\log(u_a - u_w)$ axis through u to intersect line AB, the point of intersection is v;

iii) draw a line parallel to the $\log(\sigma - u_a)$ axis through x to intersect line AB, the point of intersection is w.

(i.e., x coordinate)
If the abscissa of stress point v is denoted by "log a", the ordinate of stress point w would be "$\frac{\log a \log P'_s}{\log(u_a - u_w)^e_i}$". The numerical value of "a" can be found through the graphical procedure discussed. The term, "log a" can also be written mathematically as,

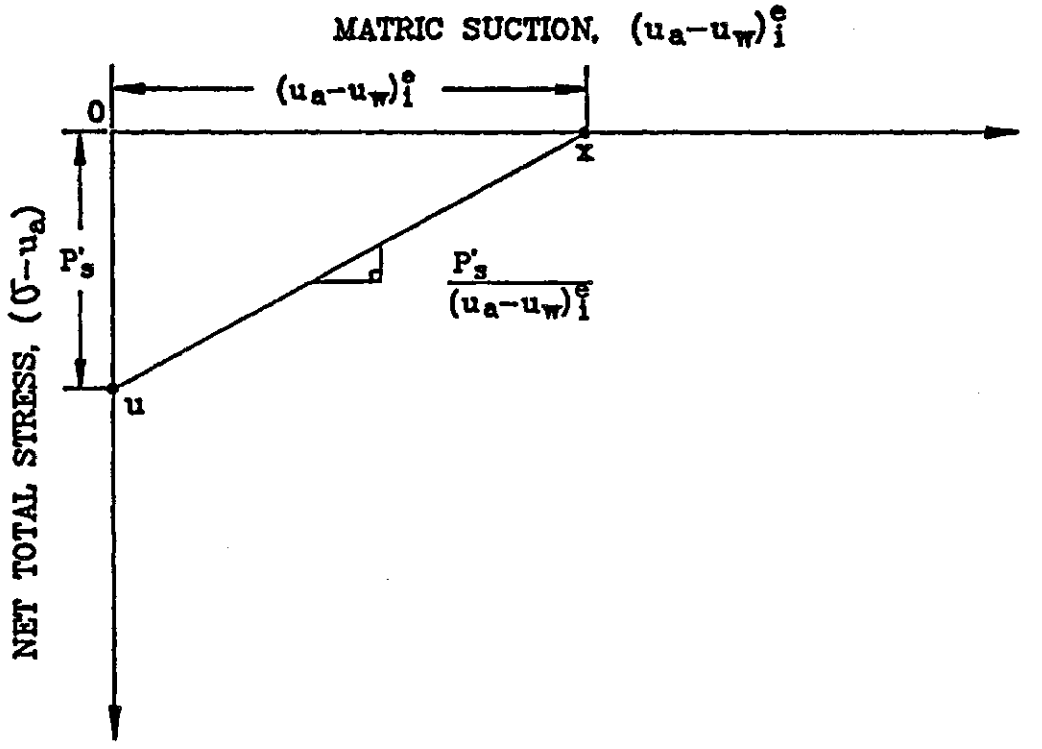

Figure 3.19a Constant Volume Stress Path on An Arithmetic Scale

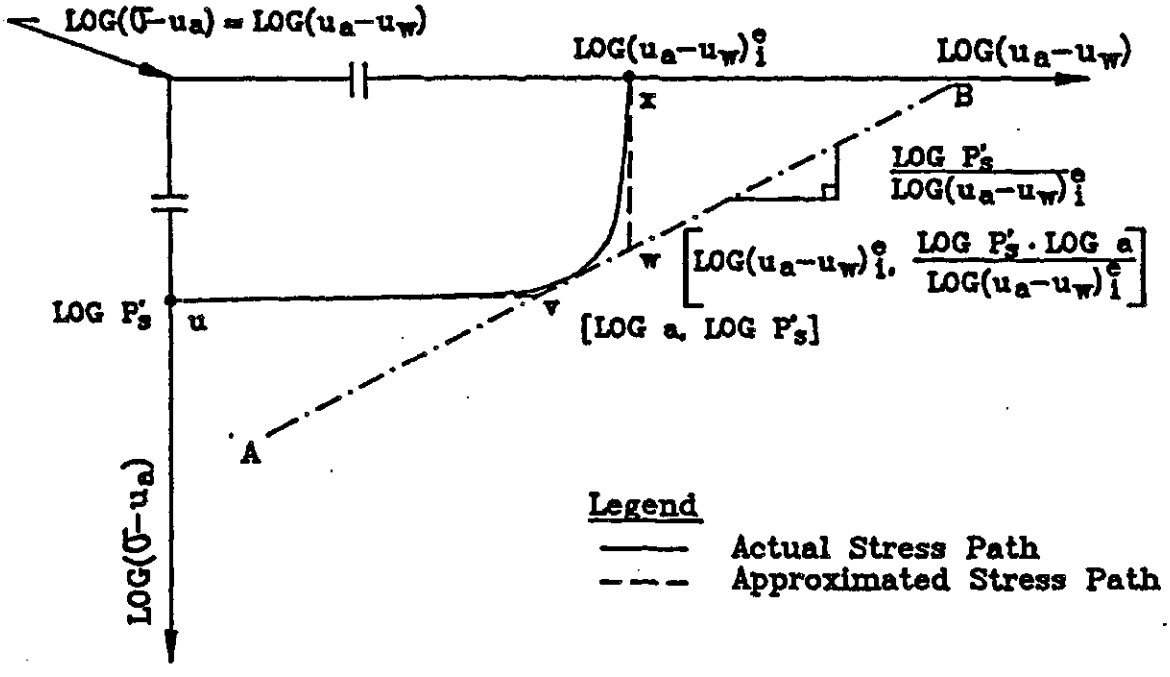

Figure 3.19b Constant Volume Stress Path on A Logarithmic Scale

$$\log a = \log\left[\frac{\log P'_s}{\log(u_a - u_w)^e_i}\right] - \log\left[\frac{P'_s}{(u_a - u_w)^e_i}\right] + \log P'_s - \left[1 + \frac{(u_a - u_w)^e_i}{P'_s}\right] \log\left[1 + \frac{\log P'_s}{\log(u_a - u_w)^e_i}\right] \quad (3.1)$$

Actual and approximated constant volume stress paths for various $\frac{P'_s}{(u_a - u_w)^e_i}$ ratios are presented (Figure 3.20 to 3.22). The proximity of the approximated stress path to the actual stress path is illustrated.

Plane I and III are referred to as the orthogonal planes. The boundaries of plane I are line uv and the projections of lines ELu and ELv (Figure 3.23). Plane I is orthogonal to the void ratio versus the logarithm of the net total stress plane. The slope of plane I is equal to the compressive index with respect to the net total stress (i.e., C_t) (see section 2.2.1) Plane I defines a stress space within which any volume change is defined by one modulus. Plane III is bounded by line wx and the projections of lines ELw and ELx (Figure 3.23). Plane III is orthogonal to the void ratio versus the logarithm of matric suction plane. The slope of plane III is equal to the compressive index with respect to matric suction (i.e., C_m) (see section 2.2.1). One modulus is needed to define volume change resulting from any stress change within the stress space defined by plane III.

Plane II is a transition between planes I and III. Plane II is assumed to be a part of the triangular plane

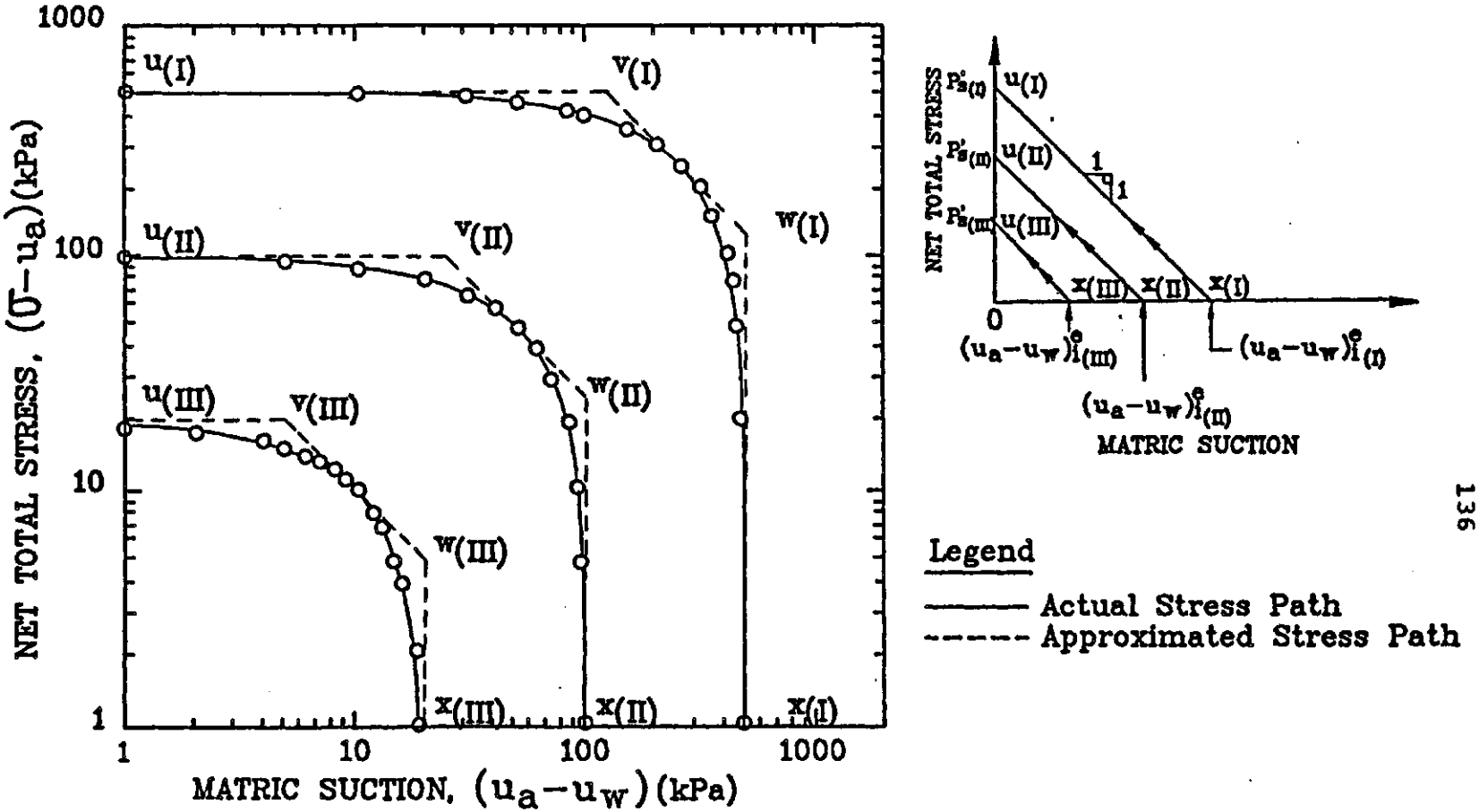

Figure 3.20 Actual and Approximated Constant Volume Stress Paths for Soils with The $\frac{P'_s}{(u_a - u_w)^e_i}$ Ratio Being 1

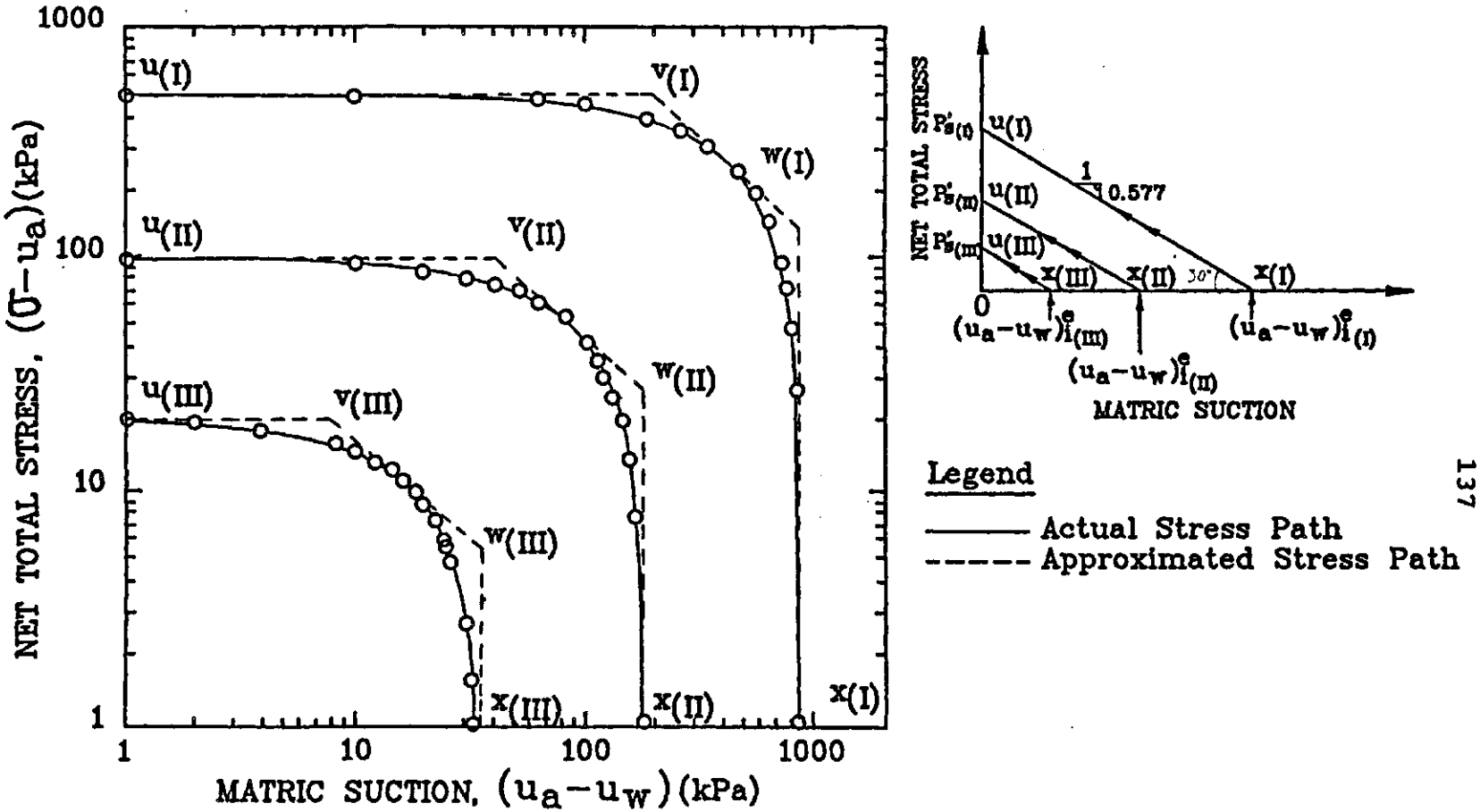

Figure 3.21 Actual and Approximated Constant Volume Stress Paths for Soils with The $\frac{p'_s}{(u_a - u_w)^e_i}$ Ratio Being 0.5774

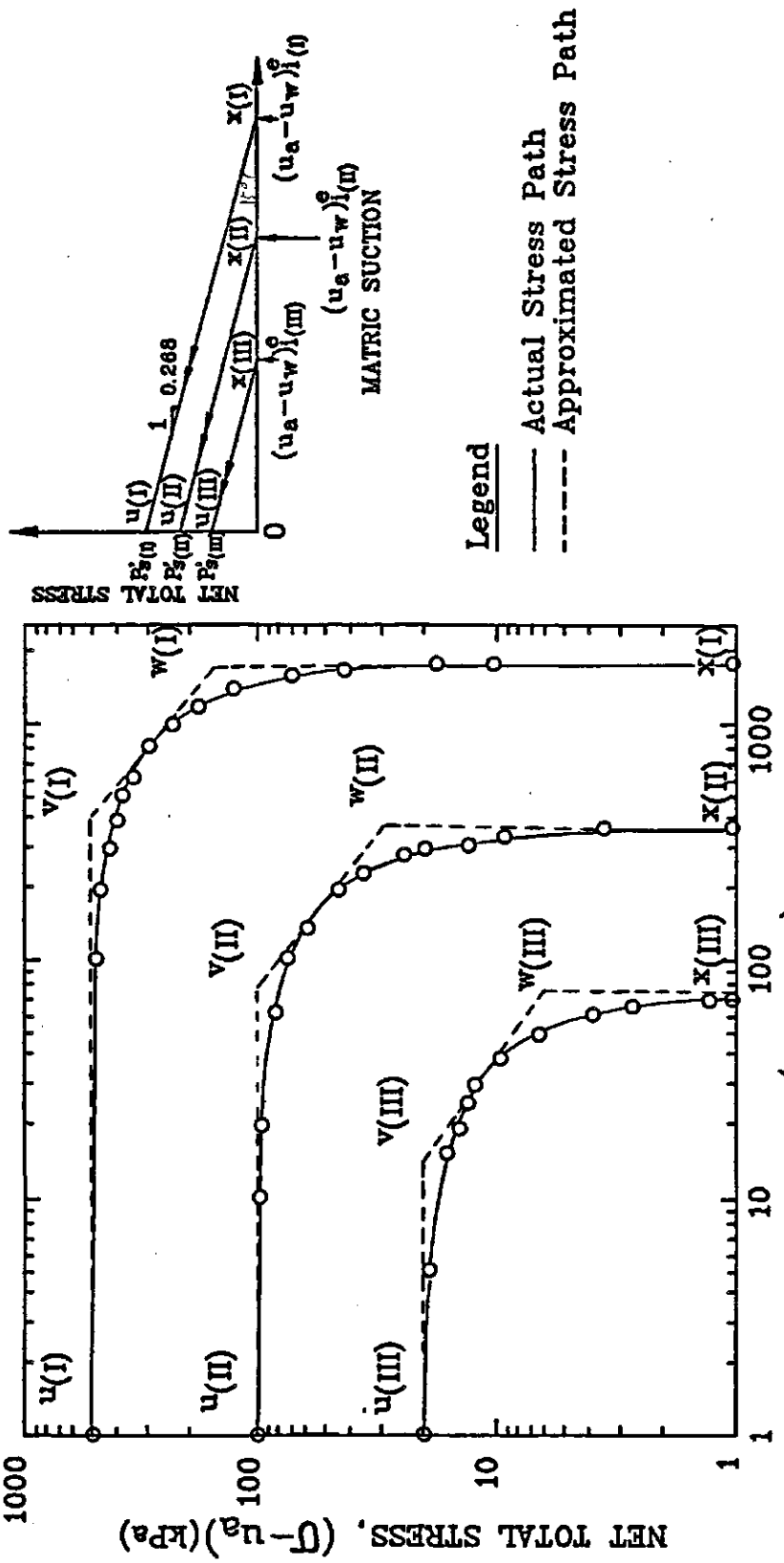

Figure 3.22 Actual and Approximated Constant Volume Stress Paths for Soils with The $\frac{p'_s}{(u_a - u_w)^e_i}$ Ratio Being 0.268

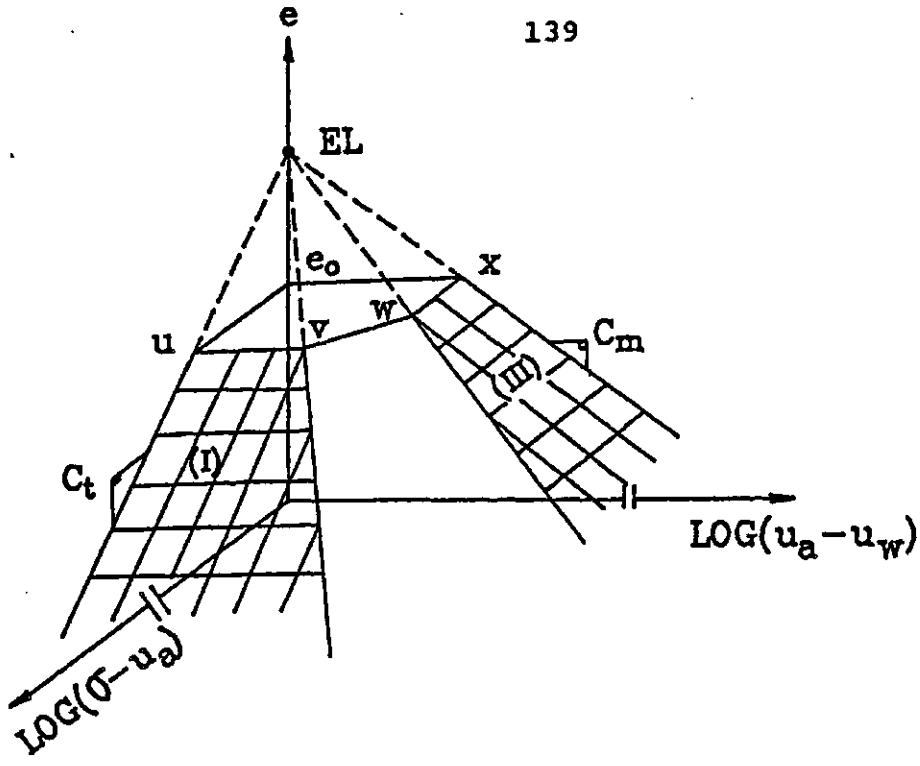

Figure 3.23a Geometry of The Orthogonal Planes I and III Approximating The Soil Structure Constitutive Surface for Monotonic Volume Decrease

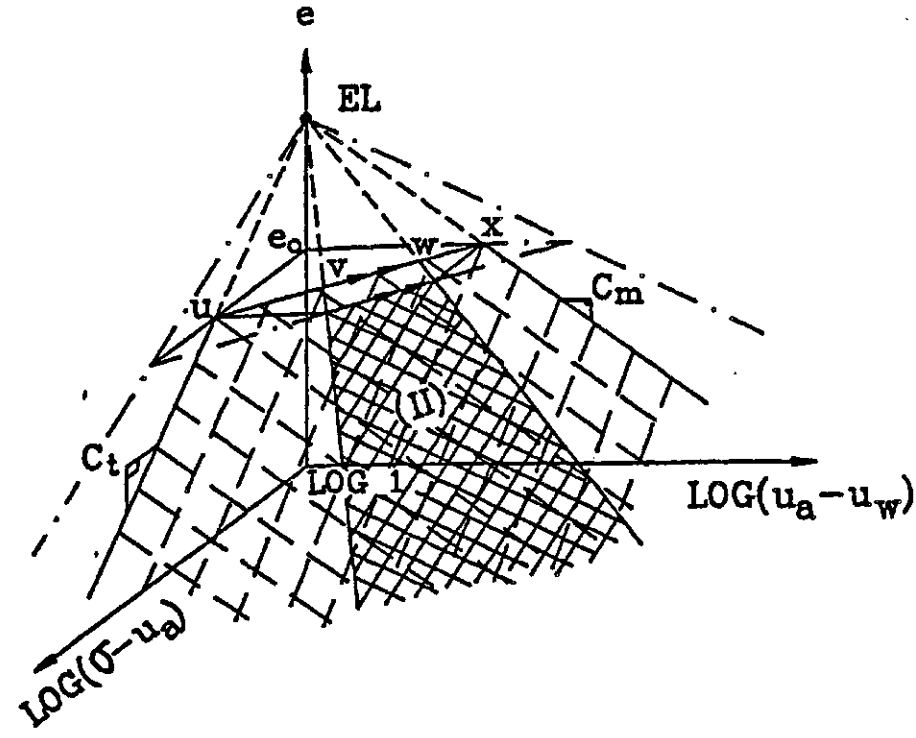

Figure 3.23b Geometry of The Transition Plane II Approximating The Soil Structure Constitutive Surface for Monotonic Volume Decrease

defined by line ELv and ELw (Figure 3.23). The void ratio ordinate is assumed to locate at an intersection of the abscissas where the net total stress is equal to the matric suction. Plane II is bounded by line vw and the projections of line ELv and ELw. Line vw is constructed such that the slope of the line is $\frac{\log P'_s}{\log(u_a - u_w)^e_i}$. Line vw is parallel to line ux, if the logarithm of the stress variables are both equal to zero at the intersections of the abscissas. Planes uELx and vELw are therefore converging planes towards a common point EL on the ordinate. The projected point of convergence, EL and stress points u, v, w and x define a degenerated pyramid. Gradients on plane II with respect to the logarithm of the net total stress and matric suction can be written in terms of the slopes of line ELu and ELx by geometry of the pyramid. The slopes of lines ELu and ELx are the compressive indices with respect to the net total stress (i.e., C_t) and matric suction (i.e., C_m) respectively. Plane II therefore represents a stress space within which any volume change is defined by two moduli which can be written in terms of the compressive indices. The same two compressive indices are related to each other by geometry through the assumed form of the constitutive surface.

The preceding discussion presents an approximate form of the constitutive surface for monotonic volume change. The approximated form is composed of three planar

sections. These planes are assumed to converge towards a single point on the ordinate. Two of these planes are orthogonal planes. A horizontal line on the third transition plane is assumed to have a slope defined by the ratio of the logarithm of the corrected swelling pressure and the corresponding matric suction of a soil after being unloaded at constant volume. This transition plane can be defined by the two moduli with respect to the logarithm of the stress variables of the abscissas. The same two moduli can be related mathematically by geometry of the approximated constitutive surface.

3.4 The Adopted Semi-logarithmic Volume Change Constitutive Relations for The Soil Structure and Water Phase

In section 3.3, geometric surfaces of three planar sections are proposed to approximate the curved soil structure and water phase constitutive surfaces. Each proposed geometric surface is composed of two orthogonal and one transition planes. This section presents constitutive relations which represent these planes. The proposed constitutive relations are presented first numerically and then graphically.

3.4.1 Numerical presentation of the adopted semi-logarithmic constitutive relations

This section derives the equations for the planar sections of the approximated soil structure and water phase constitutive surfaces. The case of the soil structure undergoing monotonic volume decrease is used as an example to show the mathematical derivation. The constitutive relation representing the transition plane is discussed first, followed by the constitutive relations representing the orthogonal planes.

An illustration of the geometrical characteristics of the approximated soil structure constitutive surface for monotonic volume decrease is presented (Figure 3.24). The void ratio ordinate is assumed to locate at an intersection of the abscissas where the net total stress is equal to matric suction. The projected point of convergence, EL of the constitutive surface represents the void ratio of a soil under a nominal stress. The numerical value of the net total stress and matric suction at this projected state is assumed to be unity.

Constitutive Relation for The Transition Plane

The compressive indices with respect to the net total stress and matric suction (i.e., C_t and C_m) can be related through the geometry of the approximate constitutive surface (Figure 3.24). The two right angle triangles, ΔELuQ

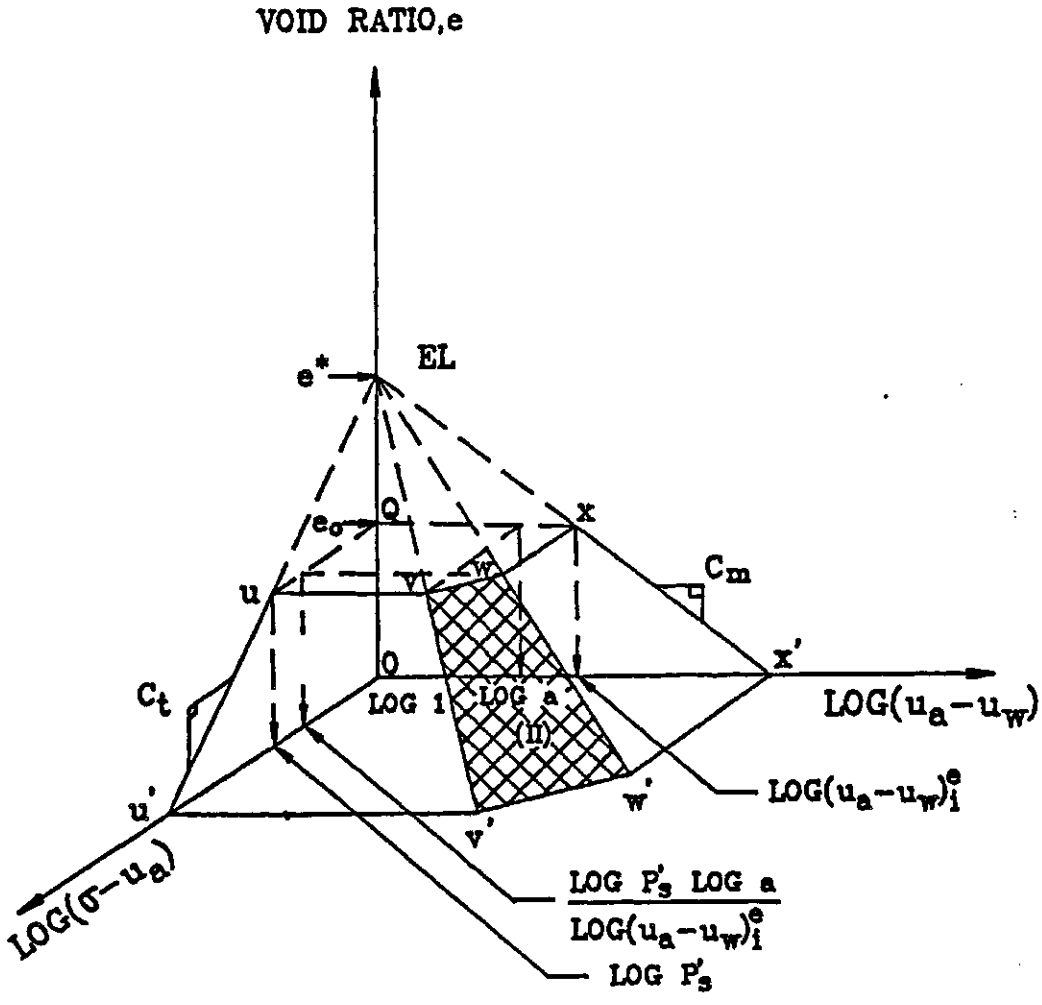

Figure 3.24 Geometrical Characteristics of The Approximated Soil Structure Constitutive Surface for Monotonic Volume Decrease

and $\Delta ELxQ$ share a common vertical side, ELQ.

Mathematically, it follows,

$$e^* = e_o + C_t \log P'_s \tag{3.2a}$$

or

$$e^* = e_o + C_m \log(u_a - u_w)^e_i \tag{3.2b}$$

Vectors $\vec{EL}\vec{v}$ and $\vec{EL}\vec{w}$ lay on the transition plane (II) (i.e., plane ELv'w') be written as,

$$\vec{EL}\vec{v} = [\log P'_s]\vec{i} + [\log a]\vec{j} + [-C_t \log P'_s]\vec{k} \tag{3.3}$$

$$\vec{EL}\vec{w} = [\frac{\log a \log P'_s}{\log(u_a - u_w)^e_i}]\vec{i} + [\log(u_a - u_w)^e_i]\vec{j} + [-C_t \log P'_s]\vec{k} \tag{3.4}$$

A vector normal to the transition plane (II) can be written as,

$$\vec{n} = \vec{EL}\vec{v} \times \vec{EL}\vec{w}$$

$$= n_1\vec{i} + n_2\vec{j} + n_3\vec{k} \tag{3.5a}$$

where

$$n_1 = C_t \log P'_s [\log(u_a - u_w)^e_i - \log a] \tag{3.5b}$$

$$n_2 = \frac{C_t (\log P'_s)^2 [\log(u_a - u_w)^e_i - \log a]}{\log(u_a - u_w)^e_i} \tag{3.5c}$$

$$n_3 = \frac{\log P'_s [\log(u_a - u_w)^e_i - \log a][\log(u_a - u_w)^e_i + \log a]}{\log(u_a - u_w)^e_i} \tag{3.5d}$$

Let P be a point on the transition plane (II). The vector $\vec{EL}\vec{P}$ can be written as,

$$\vec{EL}\vec{P} = [\log(\sigma - u_a)]\vec{i} + [\log(u_a - u_w)]\vec{j} + [e - (e_o + C_t \log P'_s)]\vec{k} \tag{3.6}$$

Since vector $\vec{ELP}$ lays on the transition plane (II), therefore

$$\vec{ELP} \cdot \vec{n} = 0 \tag{3.7a}$$

it follows,

$$n_1 \log(\sigma - u_w) + n_2 \log(u_a - u_w) + n_3[e - (e_o + C_t \log P'_s)] = 0 \tag{3.7b}$$

or

$$e = (e_o + C_t \log P'_s) - \frac{n_1}{n_3} \log(\sigma - u_a) - \frac{n_2}{n_3} \log(u_a - u_w) \tag{3.7c}$$

Combining equations (3.5b),(3.5c),(3.5d) and (3.7c) gives,

$$e = (e_o + C_t \log P'_s) - \left[\frac{C_t \log(u_a - u_w)^e_i}{\log(u_a - u_w)^e_i + \log a}\right] \log(\sigma - u_a) - \left[\frac{C_t \log P'_s}{\log(u_a - u_w)^e_i + \log a}\right] \log(u_a - u_w) \tag{3.8}$$

The same equation can be written in terms of the initial and final void ratio (i.e., e_i and e_f) of a soil before and after a volume decrease.

$$e_f = e_i - \left[\frac{C_t \log(u_a - u_w)^e_i}{\log(u_a - u_w)^e_i + \log a}\right] \log\left[\frac{(\sigma - u_a)_f}{(\sigma - u_a)_i}\right] - \left[\frac{C_t \log P'_s}{\log(u_a - u_w)^e_i + \log a}\right] \log\left[\frac{(u_a - u_w)_f}{(u_a - u_w)_i}\right] \tag{3.9}$$

The same mathematical procedure can be repeated to derive an equation describing a water content change on the transition plane of the approximated water phase constitutive surface for monotonic water content decrease.

$$w_f = w_i - \left[\frac{D_t \log(u_a - u_w)_i^w}{\log(u_a - u_w)_i^w + \log b}\right] \log\left[\frac{(\sigma - u_a)_f}{(\sigma - u_a)_i}\right]$$

$$- \left[\frac{D_t \log P'_w}{\log(u_a - u_w)_i^w + \log b}\right] \log\left[\frac{(u_a - u_w)_f}{(u_a - u_w)_i}\right] \quad (3.10)$$

The term, P'_w is the net total stress of a soil after being saturated at constant water content. The term, $(u_a - u_w)_i^w$ represents the matric suction of a soil after being unloaded at constant water content. The term, log b is the abscissa value of the stress point, v used to approximate the asymptotic constant water content stress path. The numerical value of "b" can be found through the graphical procedure discussed in Section 3.3.

Similar equations can be written for a volume or water content change on the transition planes of the approximated soil structure and water phase constitutive surfaces for monotonic volume increase.

$$e_f = e_i + \left[\frac{C_{ts} \log(u_a - u_w)_i^e}{\log(u_a - u_w)_i^e + \log a}\right] \log\left[\frac{(\sigma - u_a)_i}{(\sigma - u_a)_f}\right]$$

$$+ \left[\frac{C_{ts} \log P'_s}{\log(u_a - u_w)_i^e + \log a}\right] \log\left[\frac{(u_a - u_w)_i}{(u_a - u_w)_f}\right] \quad (3.11)$$

and

$$w_f = w_i + \left[\frac{D_{ts} \log(u_a - u_w)_i^w}{\log(u_a - u_w)_i^w + \log b}\right] \log\left[\frac{(\sigma - u_a)_i}{(\sigma - u_a)_f}\right]$$

$$+ \left[\frac{D_{ts} \log P'_w}{\log(u_a - u_w)_i^w + \log b}\right] \log\left[\frac{(u_a - u_w)_i}{(u_a - u_w)_f}\right] \quad (3.12)$$

Constitutive Relations for The Orthogonal Planes

The mathematical derivation for an equation describing a volume change on the transition plane of the approximated soil structure constitutive surface for monotonic volume decrease was presented. Similar mathematical procedures can be repeated to derive equations describing a volume change on the two orthogonal planes (i.e., plane I-uvu'v' and plane III-wxw'x') of the same constitutive surface (See Figure 3.24).

Plane I (i.e., plane uvu'v') is perpendicular to the void ratio versus the logarithm of the net total stress plane. Plane I defines a stress space within which any volume change is defined by the compressive index with respect to the net total stress. An equation describing a volume change on plane I can be written as,

$$e_f = e_i - C_t \log\left[\frac{(\sigma - u_a)_f}{(\sigma - u_a)_i}\right] \qquad (3.13)$$

Plane III (i.e., plane wxw'x') is perpendicular to the void ratio versus the logarithm of matric suction plane. It defines a stress space within which any volume change is defined by the compressive index with respect to matric suction. An equation describing a volume change on plane III can be written as,

$$e_f = e_i - C_m \log\left[\frac{(u_a - u_w)_f}{(u_a - u_w)_i}\right] \qquad (3.14)$$

Similarly, equations describing a volume change on

the orthogonal planes of the approximated water phase constitutive surface for monotonic water content decrease can be written as,

$$w_f = w_i - D_t \log\left[\frac{(\sigma - u_a)_f}{(\sigma - u_a)_i}\right] \tag{3.15}$$

and

$$w_f = w_i - D_m \log\left[\frac{(u_a - u_w)_f}{(u_a - u_w)_i}\right] \tag{3.16}$$

Similar equations can be written for a volume or water content change on the orthogonal planes of the approximated soil structure and water phase constitutive surfaces for monotonic volume increase.

$$e_f = e_i + C_{ts} \log\left[\frac{(\sigma - u_a)_i}{(\sigma - u_a)_f}\right] \tag{3.17}$$

$$e_f = e_i + C_{ms} \log\left[\frac{(u_a - u_w)_i}{(u_a - u_w)_f}\right] \tag{3.18}$$

$$w_f = w_i + D_{ts} \log\left[\frac{(\sigma - u_a)_i}{(\sigma - u_a)_f}\right] \tag{3.19}$$

and

$$w_f = w_i + D_{ms} \log\left[\frac{(u_a - u_w)_i}{(u_a - u_w)_f}\right] \tag{3.20}$$

The sign convention adopted for the presented constitutive relations (i.e., equation (3.9), (3.10), (3.11), (3.12), (3.13), (3.14), (3.15), (3.16), (3,17), (3.18), (3.19), and (3.20)) is shown in Table 3.1.

Table 3.1 Adopted Sign Convention for The Moduli and The Stress State Variables Used in the Constitutive Relations

DESCRIPTION	SIGN
Increase in void ratio or water content (e.g., de or dw)	Positive (+)
Decrease in void ratio or water content	Negative (-)
Loading (i.e., increase in the stress state variable)	Positive (+)
Unloading (i.e., decrease in the stress state variable)	Negative (-)

3.4.2 Graphical presentation of the adopted semi-logarithmic constitutive relations

This section presents graphically the approximate soil structure and water phase constitutive surfaces (Figure 3.25 and 3.26). The void ratio and water content ordinates are assumed to be located at the intersection of the stress variable abscissas where the net total stress is equal to matric suction. The approximate constitutive surfaces for monotonic volume increase are assumed to have points of convergence on the void ratio (i.e., point EU) and water content ordinates (i.e., point WU). Similarly, the approximate constitutive surfaces for monotonic volume decrease are assumed to have projected points of convergence on the void ratio and water content ordinates as well (i.e., points EL and WL respectively). These points of convergence of the constitutive surfaces represent the void ratio and water content of a soil under a nominal stress. The numerical value of the net total stress and matric suction at this nominal stress state is assumed to be one. The use of a logarithmic scale for the abscissas makes the specification of units for the stress variables unnecessary. A soil is seldom at a stress free state in nature. The assumption of a nominal stress condition as a limiting stress state is therefore considered reasonable. The void ratio and water content of a soil after being unloaded to a nominal stress state is defined as the free swelling void

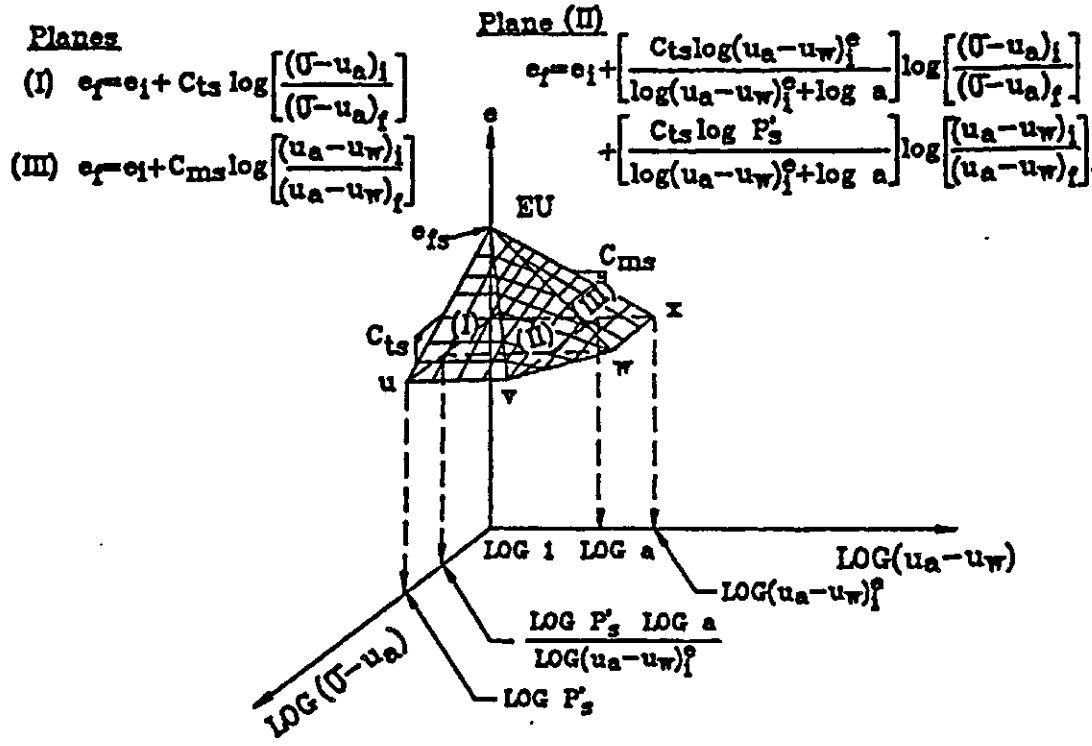

Figure 3.25a Graphical Presentation of The Adopted Soil Structure Constitutive Surface for Monotonic Volume Increase

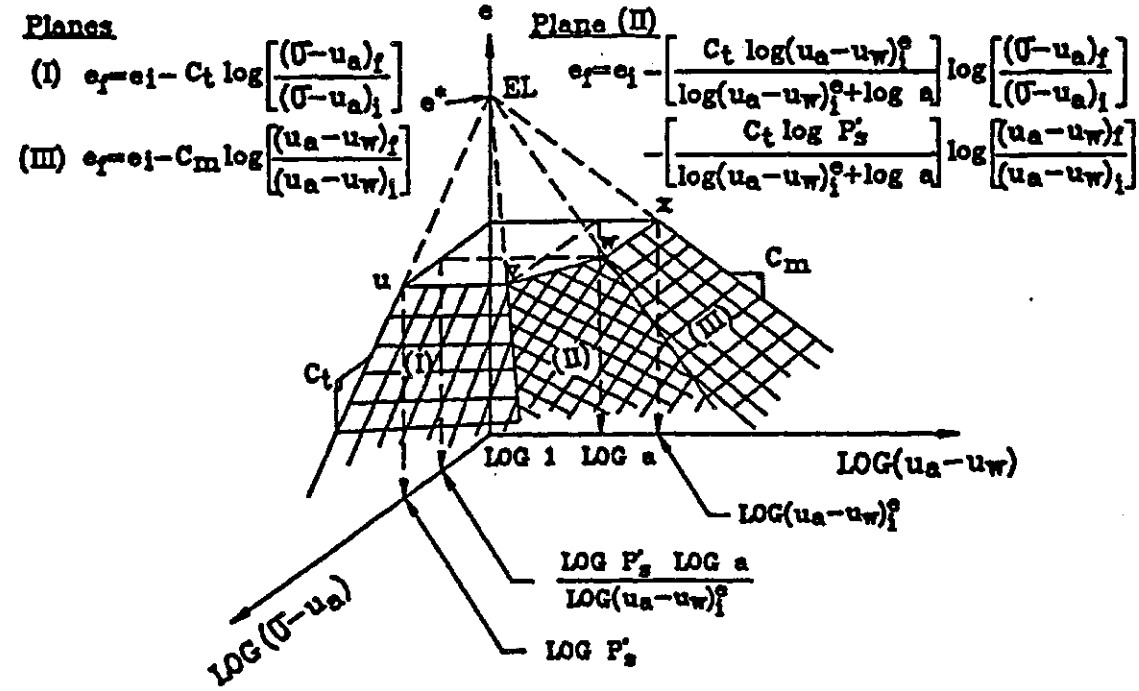

Figure 3.25b Graphical Presentation of The Adopted Soil Structure Constitutive Surface for Monotonic Volume Decrease

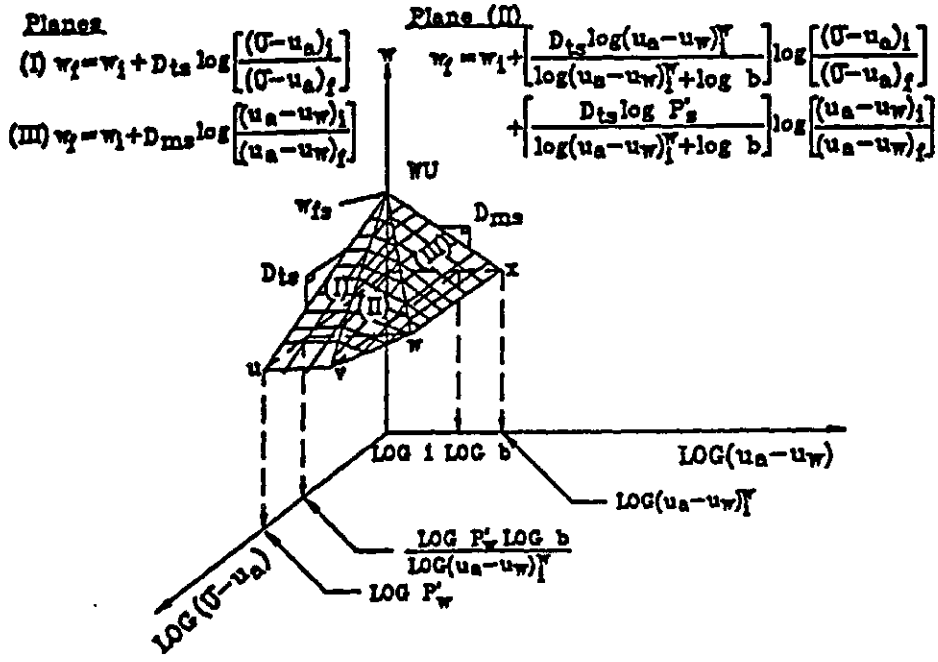

Figure 3.26a Graphical Presentation of The Adopted Water Phase Constitutive Surface for Monotonic Water Content Increase

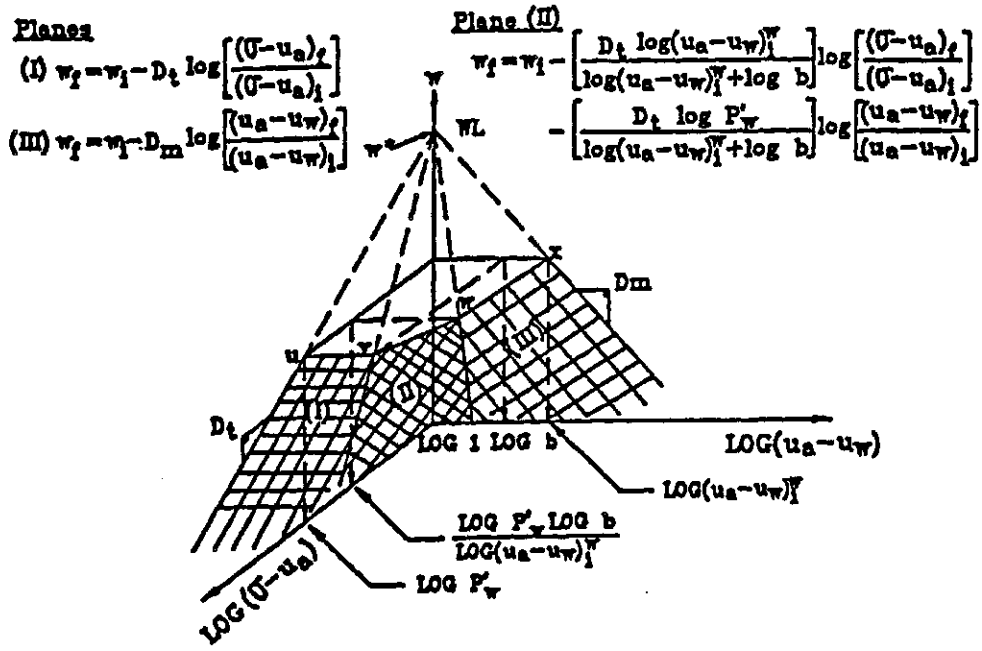

Figure 3.26b Graphical Presentation of The Adopted Water Phase Constitutive Surface for Monotonic Water Content Decrease

ratio and water content respectively (i.e., e_{fs} and w_{fs}). These approximated constitutive surfaces are used as a basis for developing the relationships between the various soil structure and water phase moduli.

The geometry of the approximated constitutive surfaces is identifiable by four characteristic stress states represented by the variables, P_s' , $(u_a - u_w)_i^e$, P_w' and $(u_a - u_w)_i^w$.

The variable, P_s' represents the initial stress state of a soil translated to the net total stress plane following a constant volume stress path (Figure 3.25). It is referred to as the corrected swelling pressure (Fredlund, 1983). The word "corrected" is used to distinguish this stress state from the conventionally determined swelling pressure which normally falls below the corrected value due to sample disturbance (Fredlund, 1983). The corrected swelling pressure is equal to the initial net total stress, $(\sigma - u_a)_i$ plus the initial matric suction, $(u_a - u_w)_i$ translated onto the net total stress plane. The magnitude of the translated matric suction is smaller than the initial matric suction. The difference is because the net total stress is more effective in deforming the soil structure than matric suction.

The stress state, $(u_a - u_w)_i^e$ represents the initial stress state translated to the matric suction plane following a constant volume stress path (Figure 3.25). It

is equal to the initial matric suction plus the initial net total stress translated onto the matric suction plane. The magnitude of the translated net total stress is larger than the initial net total stress because matric suction is less effective in deforming the soil structure than net total stress.

The stress state, P'_w represents the initial stress state of a soil translated to the net total stress plane following a constant water content stress path (Figure 3.26). It is equal to the initial net total stress plus the initial matric suction translated onto the net total stress plane. The magnitude of the translated matric suction is larger than the initial matric suction because matric suction is more effective in changing the water content than net total stress.

The stress state, $(u_a - u_w)^w_i$ represents the initial stress state translated to the matric suction plane following a constant water content stress path (Figure 3.26). It is equal to the initial matric suction plus the initial net total stress translated onto the matric suction plane. The magnitude of the translated net total stress is smaller than the initial net total stress because a change in net total stress is less effective in changing the water content than a same amount of change in the matric suction.

The magnitudes of the four characteristic stress states (i.e., P'_s, $(u_a - u_w)^e_i$, P'_s and $(u_a - u_w)^w_i$) are unique

for a soil. A saturated soil with an overburden acting on it has a corrected swelling pressure, P_s' equal to that of P_w'. The magnitudes of the stress states, $(u_a - u_w)_i^e$ and $(u_a - u_w)_i^w$, of an unconfined unsaturated soil are the same as the initial matric suction of the soil.

3.5 Relationships between The Moduli

There are six volumetric deformation moduli associated with the soil structure, pore-water and pore-air phases in an unsaturated soil. Only four are independent and reference will be made to the soil structure and water phase constitutive relations. Differentiating the basic volume-mass relation (i.e., $Se = wG_s$) with respect to the logarithm of the net total stress gives,

$$\frac{de}{d\log(\sigma - u_a)} - S_a \frac{de}{d\log(\sigma - u_a)} - e \frac{dS_a}{d\log(\sigma - u_a)} = G_s \frac{dw}{d\log(\sigma - u_a)} \qquad (3.21)$$

Differentiating the same volume-mass relation with respect to the logarithm of matric suction gives,

$$\frac{de}{d\log(u_a - u_w)} - S_a \frac{de}{d\log(u_a - u_w)} - e \frac{dS_a}{d\log(u_a - u_w)} = G_s \frac{dw}{d\log(u_a - u_w)} \qquad (3.22)$$

where

$$S_a = 100\% - S$$

S = degree of saturation, (%)

The above two equations are fixed relationships between moduli of the soil structure, pore-water and pore-air phases.

3.5.1 Relationships between moduli of the same phase with respect to different constitutive relations using different paris of stress state variables

Constitutive relations can be formulated by using any two of the three independent stress state variables (i.e., $(\sigma - u_a)$, $(\sigma - u_w)$ and $(u_a - u_w)$). Three equivalent constitutive relations in incremental form can be written to describe a volume change process for any one phase of an unsaturated soil.

$$de \text{ (or } dw) = A_1 d\log(\sigma - u_a) + A_2 d\log(u_a - u_w) \qquad (3.23a)$$

$$\text{or} \qquad = A_3 d\log(\sigma - u_w) + A_4 d\log(u_a - u_w) \qquad (3.23b)$$

$$\text{or} \qquad = A_5 d\log(\sigma - u_w) + A_6 d\log(\sigma - u_a) \qquad (3.23c)$$

where

A_1, A_2 , A_3, A_4 , A_5 , A_6

= volumetric deformation moduli with respect to the specified increasing or decreasing (i.e. loading or unloading) reference stress state variable

Consider a volume change process with the pore-air, u_a, and pore-water pressure, u_w being kept constant while total stress, σ is changed by $d\sigma$. The resulting volume change can be represented by any one of the above three

constitutive relations (i.e., equation 3.23a, 3.23b and 3.23c). Comparing 3.23a to 3.23b shows that,

$$A_1 = A_3 \tag{3.24}$$

Consider a volume change process with the total stress and pore-air pressure being kept constant while the pore-water pressure is changed by du_w. A comparison between equations 3.23a and 3.23c illustrates,

$$A_2 = A_5 \tag{3.25}$$

Similarly, for a volume change process with the total stress and pore-water pressure being kept constant while the pre-air pressure is changed by du_a, a comparison between equations 3.23b and 3.23c shows,

$$A_4 = - A_6 \tag{3.26}$$

Since equations 3.23a, 3.23b and 3.23c are equivalent constitutive relations describing the same volume change, they are mathematically equal to one another. Combining equations 3.23a , 3.23b and 3.24 gives,

$$A_1 = A_2 - A_4 \tag{3.27}$$

Combining equations 3.23a, 3.23c and 3.25 gives,

$$A_1 = A_5 - A_6 \tag{3.28}$$

Combining equations 3.23b, 3.23c and 3.26 gives,

$$A_3 = - A_4 + A_5 \tag{3.29}$$

Four of the six established relationships (i.e. equation 3.24 to 3.29) between the six moduli (i.e. A_1 to A_6) defined by the three equivalent constitutive relations (i.e. equation 3.23a to 3.23c) are independent. It follows

that only two of these six moduli (i.e. A_1 to A_6) are independent variables. Once the moduli with respect to any pair of the three independent stress variables (i.e. $(\sigma - u_a)$, $(\sigma - u_w)$ and $(u_a - u_w)$) are determined experimentally for any one phase, moduli of the same phase with respect to other possible pairs of stress variables can be found by using the above theoretical relationships (i.e. equation 3.24 to 3.29).

3.5.2 Relationships between moduli of the same phase

Section 3.4.2 presented the approximated soil structure and water phase constitutive surfaces. The deformation moduli of the soil structure (i.e., C_t and C_m, C_{ts} and C_{ms}) and those of water phase (i.e., D_t and D_m, D_{ts} and D_{ms}) can be related mathematically to the characteristic stress states (see Section 3.4.2) according to the geometry of the approximated constitutive surfaces (Figure 3.27).

Consider the pyramids, OEUux or OWUux and OELux or OWLux in Figure 3.27,

$$OEU = \Delta e = C_{ts} \log P'_s = C_{ms} \log(u_a - u_w)_i^e \qquad (3.30)$$

or

$$OWU = \Delta w = D_{ts} \log P'_w = D_{ms} \log(u_a - u_w)_i^w \qquad (3.31)$$

and

$$OEL = \Delta e = C_t \log P'_s = C_m \log(u_a - u_w)_i^e \qquad (3.32)$$

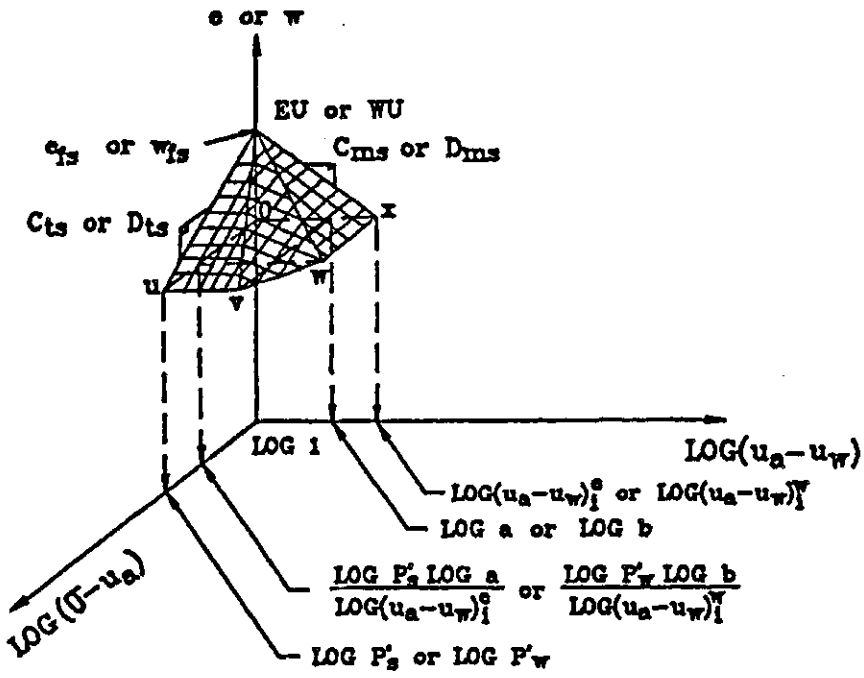

Figure 3.27a Geometrical Relationship between Moduli of The Same Phase Undergoing Monotonic Volume Increase

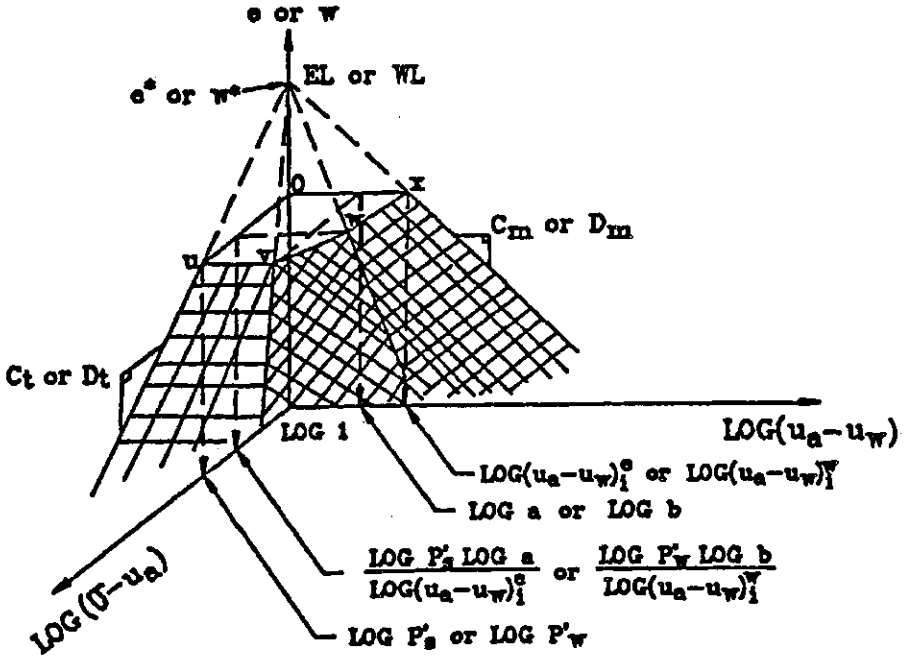

Figure 3.27b Geometrical Relationship between Moduli of The Same Phase Undergoing Monotonic Volume Decrease

or

$$OWL = \Delta w = D_t \log P'_w = D_m \log(u_a - u_w)_i^w \tag{3.33}$$

It follows,

$$\frac{C_{ms}}{C_{ts}} \text{ or } \frac{C_m}{C_t} = \frac{\log P'_s}{\log(u_a - u_w)_i^e} \tag{3.34}$$

and

$$\frac{D_{ts}}{D_{ms}} \text{ or } \frac{D_t}{D_m} = \frac{\log(u_a - u_w)_i^w}{\log P'_w} \tag{3.35}$$

A change in net total stress is more effective in deforming the soil structure than a change in matric suction. The reverse is true when inducing water content change is considered (Fredlund, 1973). As a result,

$$C_{ts} \geq C_{ms} \tag{3.36}$$

$$C_t \geq C_m \tag{3.37}$$

$$D_{ms} \geq D_{ts} \tag{3.38}$$

$$D_m \geq D_t \tag{3.39}$$

Combining equations 3.34 to 3.39 shows the moduli ratios, $\frac{C_{ms}}{C_{ts}}$, $\frac{C_m}{C_t}$, $\frac{D_{ts}}{D_{ms}}$ and $\frac{D_t}{D_m}$ should be less than one.

3.5.3 Relationships between moduli of the soil structure and water phase with respect to the same stress variable change

This section discusses the relationships between moduli of the soil structure and water phase with respect to the same stress state variable change. Moduli with respect

to the logarithm of net total stress (i.e., C_{ts} and D_{ts}, C_t and D_t) are related by the soil volume-mass relation (i.e., $Se = wG_s$). Relationships between moduli with respect to the logarithm of matric suction (i.e., $C_{ms}$and D_{ms}, C_m and D_m) are derived from the relationships previously discussed.

3.5.3.1 Relationships between moduli of the soil structure and water phase with respect to $\log(\sigma - u_a)$

When the degree of saturation of a soil is 100 percent, the soil volume-mass relation states,

$$e = wG_s \tag{3.40}$$

it follows,

$$\frac{de}{d\log(\sigma - u_a)} = G_s \frac{dw}{d\log(\sigma - u_a)} \tag{3.41}$$

and

$$\frac{C_{ts}}{D_{ts}} \text{ or } \frac{C_t}{D_t} = G_s \tag{3.42}$$

In other words, the relative density (i.e., G_s) is a fixed link between the soil structure and water phase moduli with respect to the logarithm of the net total stress when a soil approaches saturation.

3.5.3.2 Relationships between moduli of the soil structure and water phase with respect to $\log(u_a - u_w)$

Equation 3.34 describes the relationships between

moduli, C_{ts} and C_{ms} or C_t and C_m whereas equation 3.35 describes the relationships between moduli, D_{ts} and D_{ms} or D_t and D_m as follows (see Section 3.5.2),

$$\frac{C_{ms}}{C_{ts}} \text{ or } \frac{C_m}{C_t} = \frac{\log P'_s}{\log(u_a - u_w)^e_i}$$

$$\frac{D_{ts}}{D_{ms}} \text{ or } \frac{D_t}{D_m} = \frac{\log(u_a - u_w)^w_i}{\log P'_w}$$

Equation 3.42 describes the relationships between moduli C_{ts} and D_{ts} or C_t and D_t as follows,

$$\frac{C_{ts}}{D_{ts}} \text{ or } \frac{C_t}{D_t} = G_s$$

Combining these relationships (i.e., equations (3.34), (3.35) and (3.42)) gives the relationships between moduli of the soil structure and the water phase with respect to the logarithm of matric suction.

$$\frac{C_{ms}}{D_{ms}} \text{ or } \frac{C_m}{D_m} = \frac{G_s \log P'_s \log(u_a - u_w)^w_i}{\log(u_a - u_w)^e_i \log P'_w} \qquad (3.43)$$

When a soil is saturated (i.e., the degree of saturation equals 100 percent), equation 3.40 describes the relative change in void ratio and water content of a soil subjected to a stress change. It follows,

$$\frac{de}{d\log(u_a - u_w)} = G_s \frac{dw}{d \log(u_a - u_w)} \qquad (3.44)$$

and

$$\frac{C_{ms}}{D_{ms}} \text{ or } \frac{C_m}{D_m} = G_s \qquad (3.45)$$

Unconfined shrinking and swelling tests measure the relative volume change of the soil structure and pore-water phase of a soil subjected to matric suction changes while the total stress is constant. The soil specimen is generally dried or wetted under unconfined conditions. The net total stress acting on the specimen would therefore be constant and equal to the self weight at a nominal value. The test results are commonly presented as void ratio versus water content plots. The slope of these shrinking and swelling curves are therefore the $\frac{C_{ms}}{D_{ms}}$ and $\frac{C_m}{D_m}$ moduli ratios respectively.

In 1923, Haines presented unconfined shrinking and swelling curves of slurry Durham clay specimens. The re-analyzed data is presented (Figure 3.28). A bilinear relation between water content and void ratio is apparent. The slopes of the initial sections of the drying curves and the end sections of the wetting curves are approximately the same as the relative density of the soil when the soil approaches saturation.

In 1954, Wooltorton presented unconfined shrinking and swelling curves of compacted sandy loam, sandy clay and plastic clay specimens (see Figure 2.42). Two identical specimens were prepared for each compaction state. One specimen was dried and the other wetted. Results for six pairs of specimens were presented. The data for the compacted clay specimens are re-analyzed (Figure 3.29). A

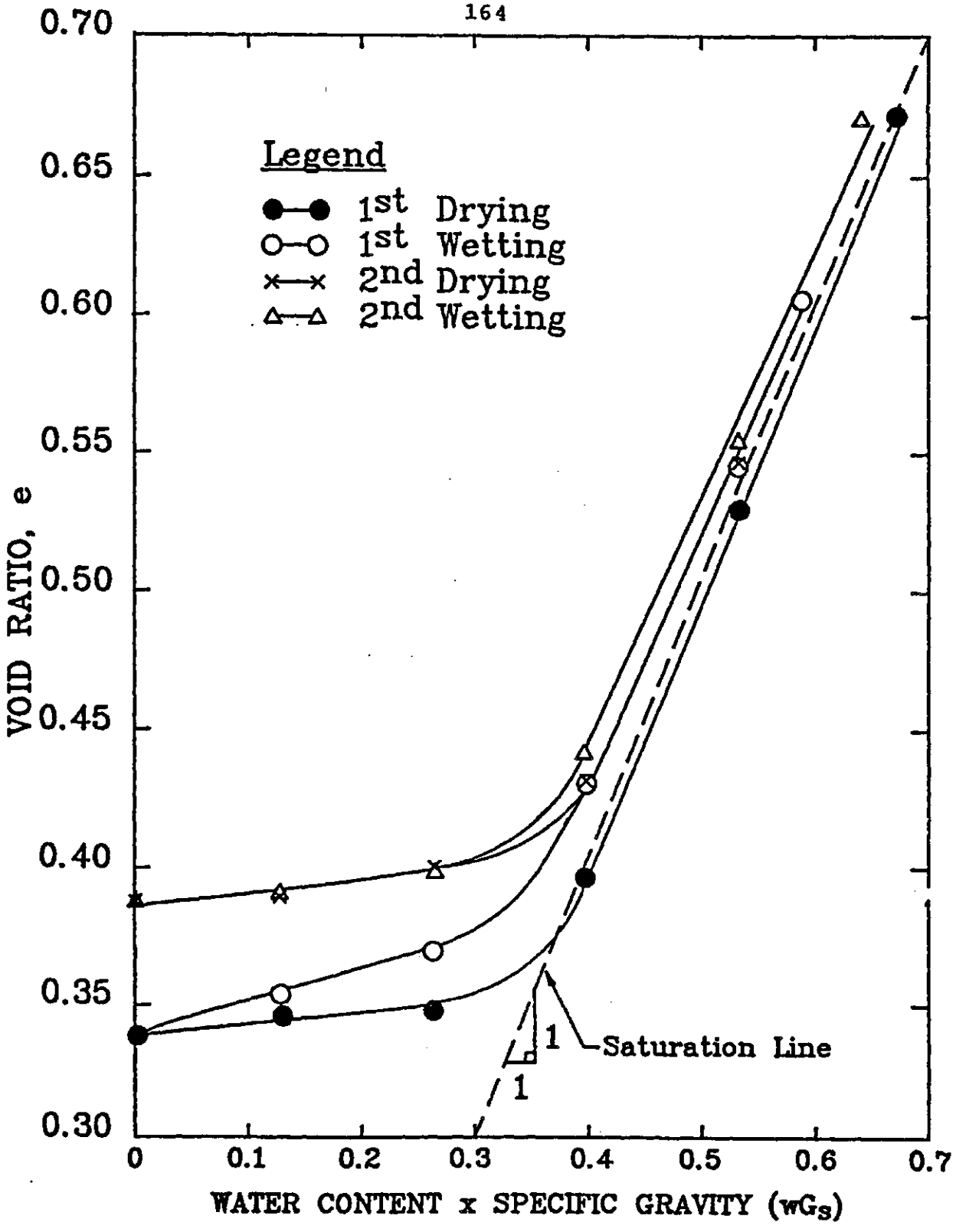

Figure 3.28 Unconfined Shrinking and Swelling Curves for Durham Clay (Haines 1923)

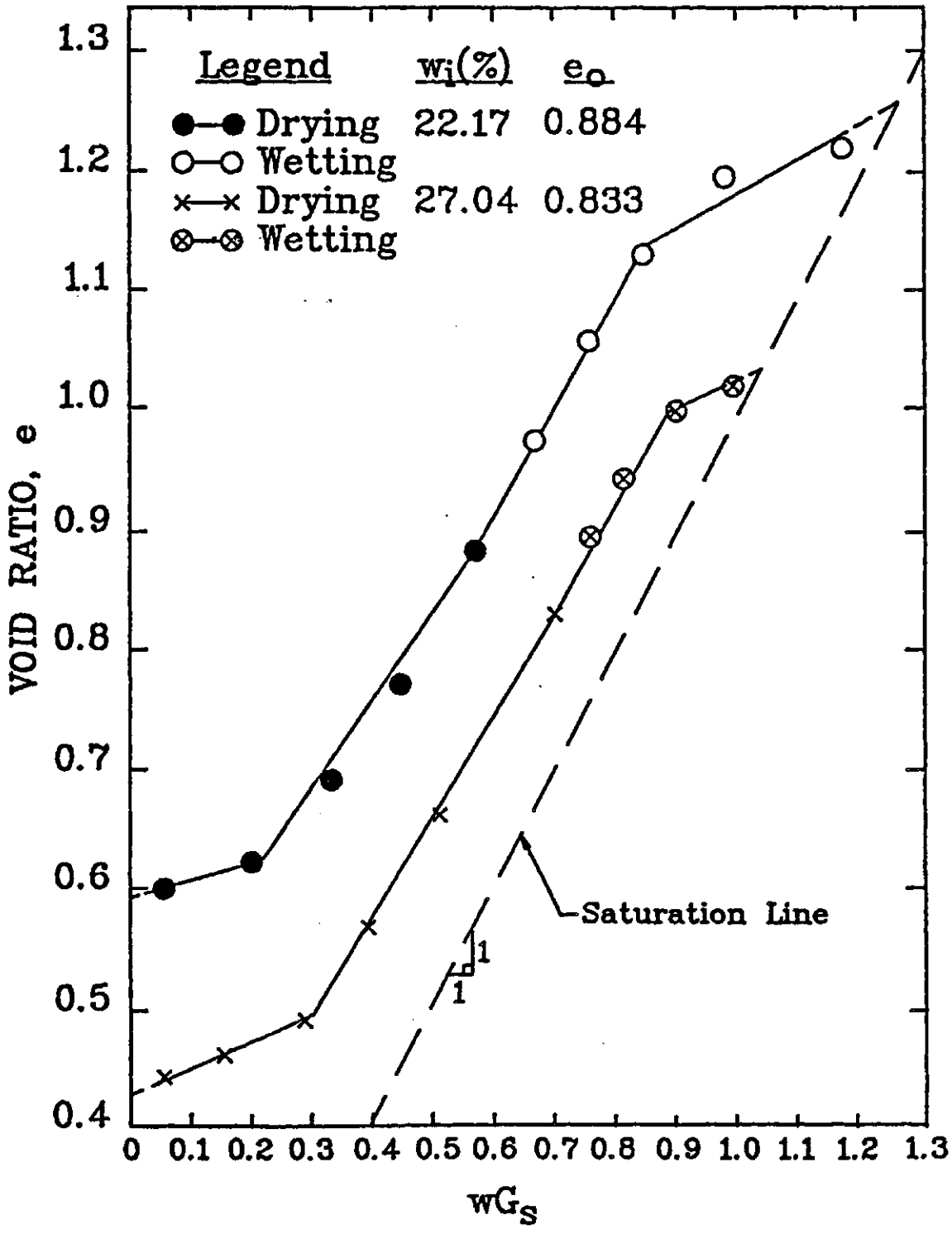

Figure 3.29 Unconfined Shrinking and Swelling Curves for A Compacted Clay

bi-linear relation between water content and void ratio is apparent. The slopes of the initial sections of the wetting curves (i.e., $\frac{C_{ms}}{D_{ms}}$) are approximately the same as the slopes of the initial sections of the drying curves (i.e., $\frac{C_m}{D_m}$). However, the slopes of the end sections of the wetting curves are found to be decreasing rather than approaching unity. This would appear to be a rather unusual soil behaviour. In the original literature, Wooltorton (1954) did not provide any information on how the specimen volumes were measured. If the volumes of the specimens were determined by direct measurements, the resulting void ratio values could have been under-estimated especially when the specimens were wet (see Section 5.4). This could have led to the exhibited unnatural phenomenon.

3.5.4 Summary

Section 3.4 presents approximated soil structure and water phase constitutive surfaces for monotonic volume changes. The assumed geometry of these approximated constitutive surfaces is used as a basis to relate the various soil structure and water phase moduli.

Section 3.5.2 shows the proposed relationships between moduli, C_{ms} and C_{ts}, C_m and C_t, D_{ts} and D_{ms}, D_t and D_m based on the assumed geometry of the approximated constitutive surfaces. The relationships are written in

terms of the characteristic stress states identifiable to the approximated constitutive surfaces. Section 3.5.3 discusses the relationships between moduli, C_{ts} and D_{ts}, C_t and D_t based on the soil volume-mass relation. The between moduli, C_{ms} and D_{ms}, C_m and D_m are subsequently derived in terms of the established preceding relationships.

The relationships between moduli of the soil structure and those between moduli of the water phase can be presented graphically. The case of a soil undergoing monotonic volume decrease is used as an example to explain the method.

Consider a soil under a stress condition of $(\sigma - u_a)_i$ and $(u_a - u_w)_i$ (Figure 3.30). The initial void ratio and water content of the soil are represented by e_o and w_i respectively. The corrected swelling pressure, P_s' and the slope of the virgin compression branch (i.e., C_t) can be established by conventional saturated soil testing techniques (Lambe, 1951). An extension of the virgin compression branch through the corrected swelling pressure gives the projected point of convergence of the approximated constitutive surface on the void ratio ordinate (i.e., point EL). A line extending from this projected point of convergence gives the matric suction of the soil after being unloaded at constant volume (i.e., $(u_a - u_w)_i^e$) or the modulus C_m if either one is known. The modulus, C_t is equal to $D_t G_s$ when a soil is saturated (see equation (3.42)). The

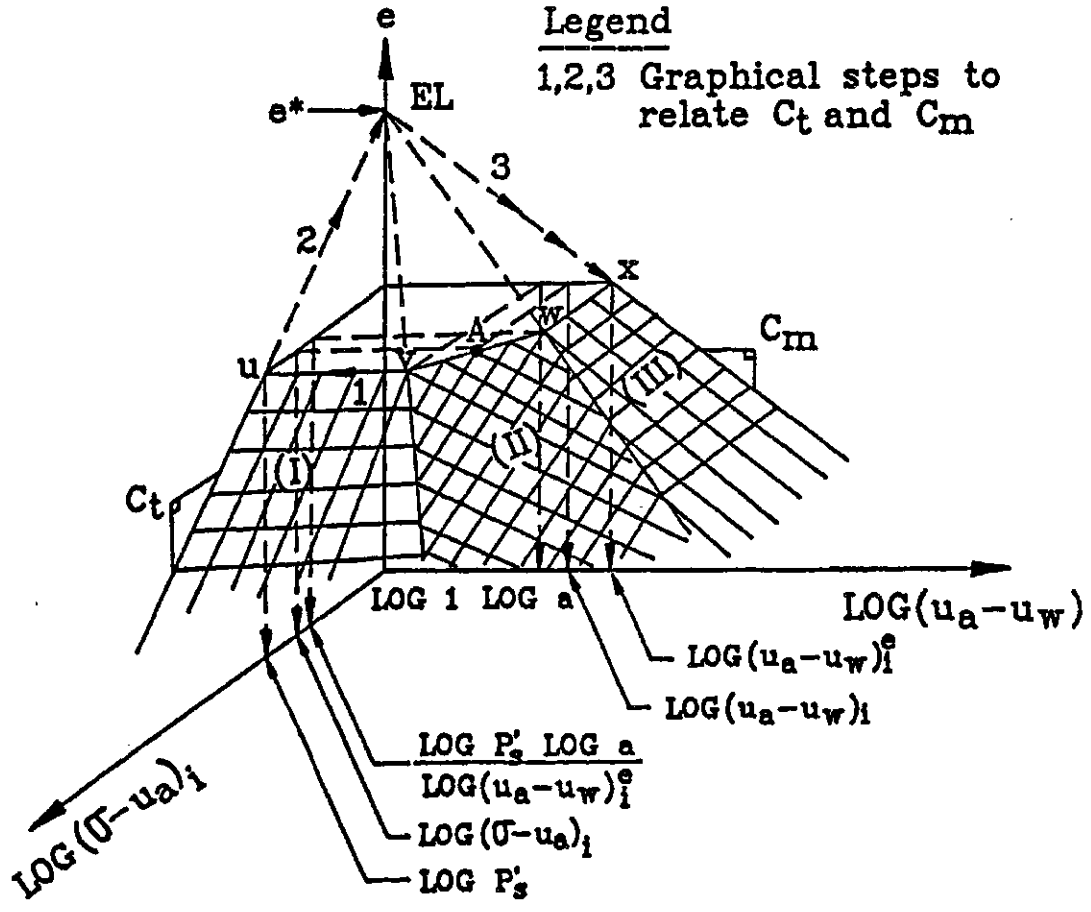

Figure 3.30a Three-Dimensional Presentation of The Relationship between Moduli of The Soil Structure Undergoing Monotonic Volume Decrease

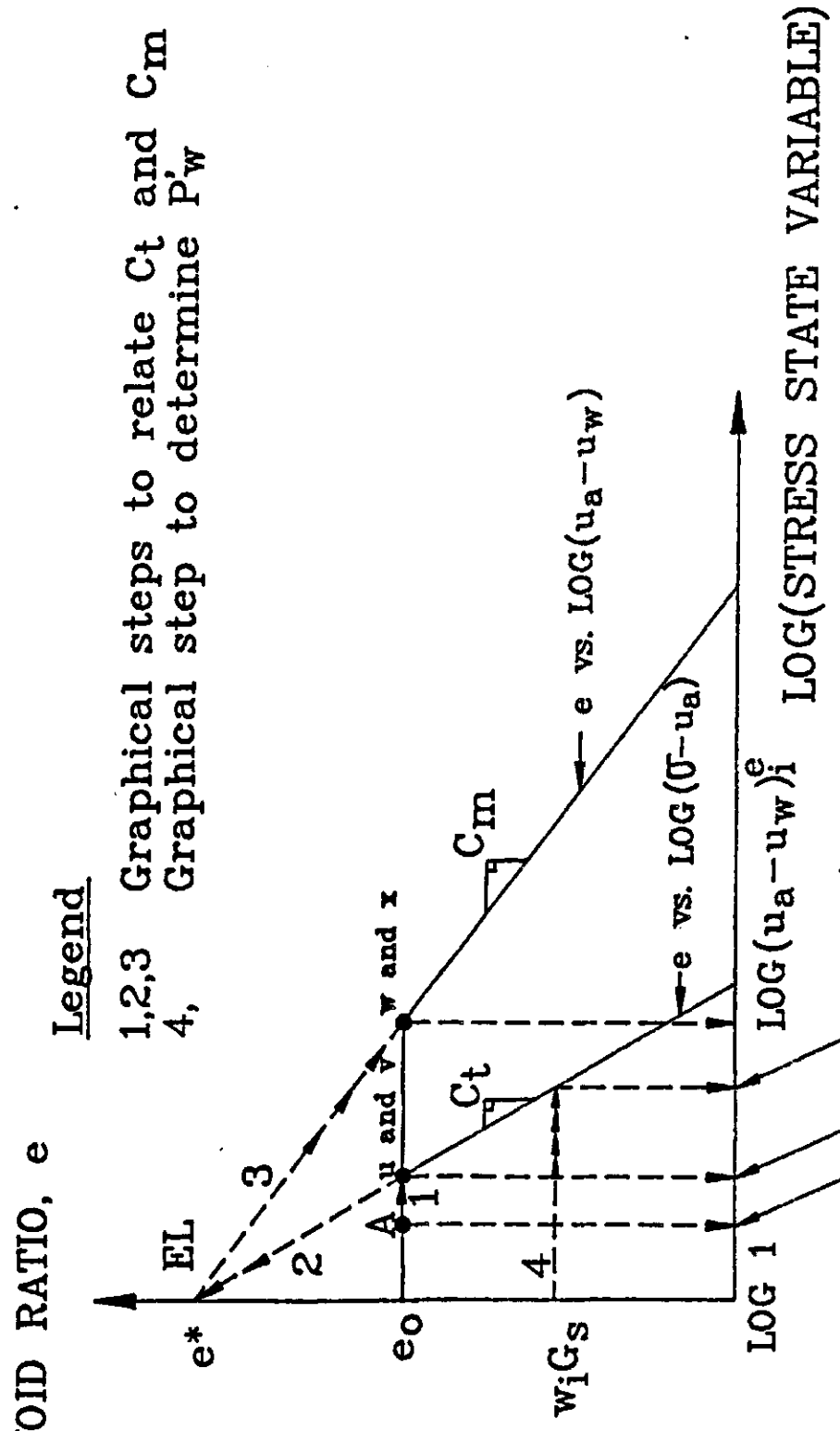

Figure 3.30b Two-Dimensional Presentation of The Relationship between Moduli of The Soil Structure Undergoing Monotonic Volume Decrease

intersection of the virgin compression branch and a horizontal line from the void ratio ordinate at $w_i G_s$ gives the initial stress state of the soil translated to the net total stress plane following a constant water content stress path (i.e., P'_w) (see Figure 3.26). The virgin compression branch of the water phase is therefore established. Similar graphical steps described previously can be followed to locate the projected point of convergence of the approximate water phase constitutive surface. The modulus, D_m or the initial stress state of the soil translated to the matric suction plane following a constant water content stress path (i.e., $(u_a - u_w)_i^w$) (see Figure 3.26) can be found subsequently if either one is known. The graphical procedure is similar to that described for the soil structure earlier.

The approximated constitutive surfaces involve the assumption of a nominal stress state as a limiting stress condition (see Section 3.4.2). The numerical value of the net total stress and matric suction at this nominal stress state is assumed to be one. This assumption does not impose a problem when the approximated constitutive surfaces are used as means to evaluate monotonic volume change. The case for insitu swelling of a soil due to saturation is used as an example to illustrate this point.

Consider a soil under an initial stress condition of $(\sigma - u_a)_i$ and $(u_a - u_w)_i$ (i.e., stress point A) (Figure 3.31). The stress path AB represents the insitu swelling of

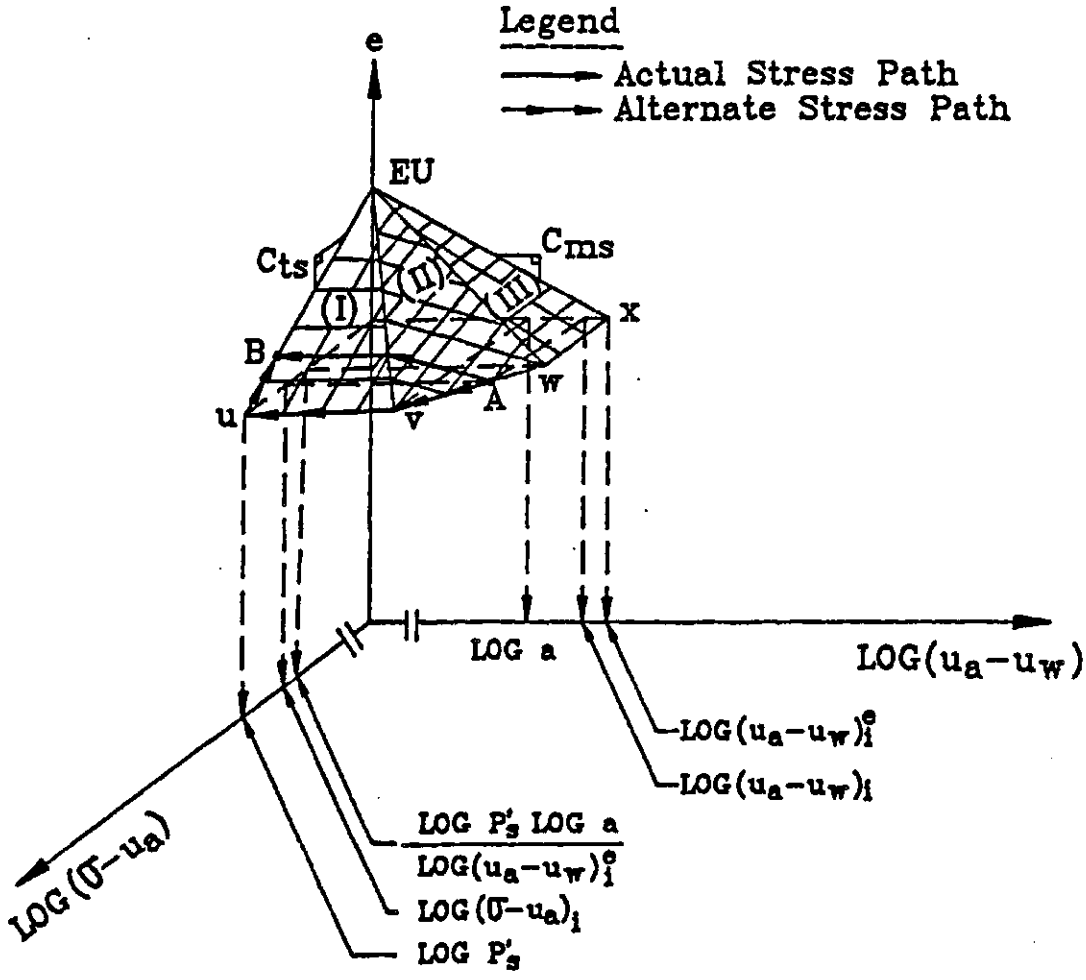

Figure 3.31a Three-Dimensional Stress Plot Representing The Insitu Swelling of A Soil at Constant Load

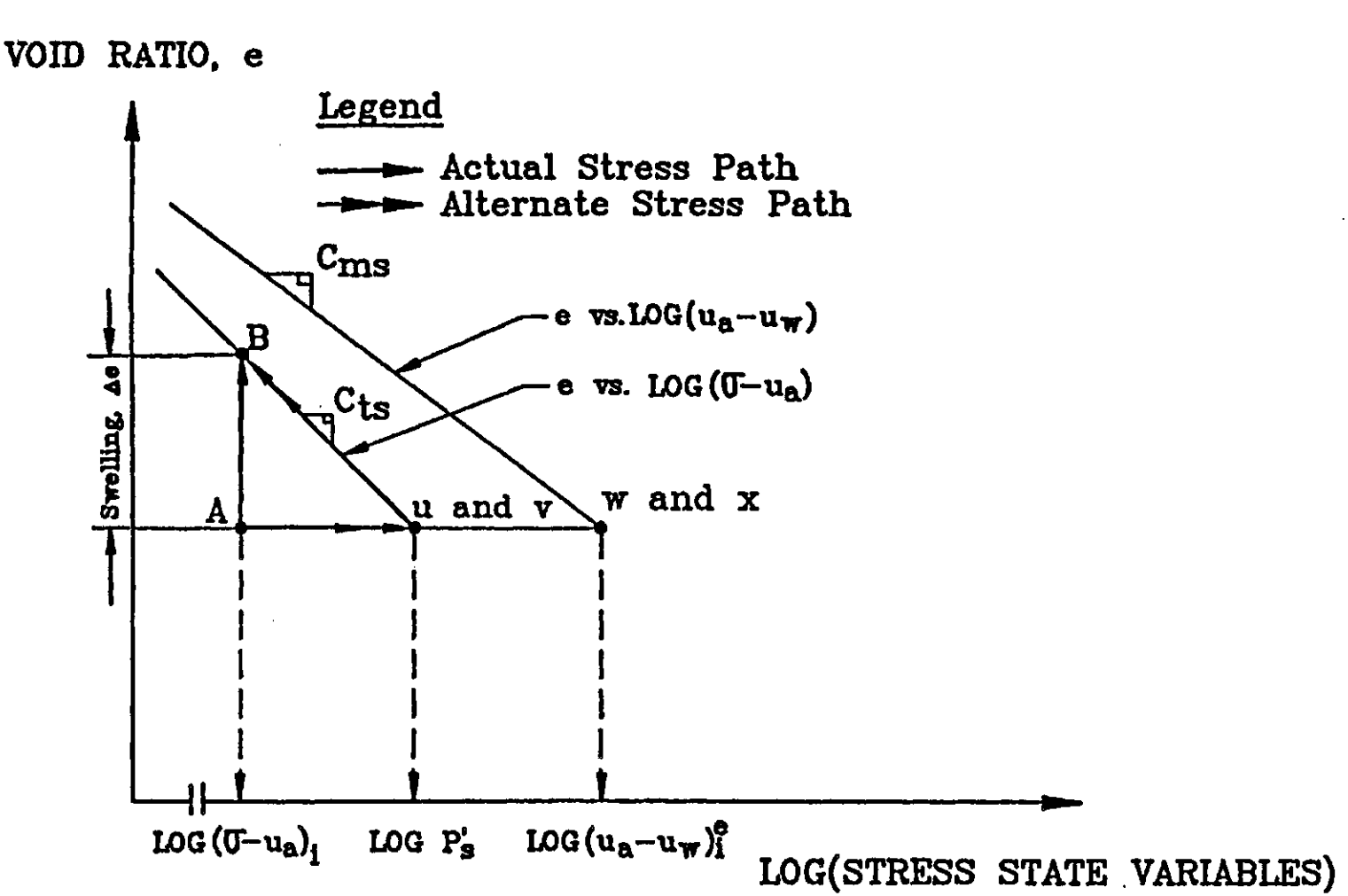

Figure 3.31b Two-Dimensional Stress Plot Representing The Insitu Swelling of A Soil at Constant Load

the soil when it is saturated. The actual stress change is reducing the initial matric suction of the soil to zero at constant net total stress. Zero matric suction is undefined on a logarithmic scale. The soil structure constitutive surfaces for monotonic volume change are unique (Fredlund, 1979). Therefore, following an alternate stress path AvuB should end at the same final state as stress path AB. The resulted insitu swelling can be readily evaluated by knowing the corrected swelling pressure (i.e., P_s') and the swelling index with respect to the net total stress (i.e., C_{ts}).

The proposed theory in this section is limited for monotonic volume changes. Stress changes involving non-monotonic volume changes can be resolved into steps of stress changes producing monotonic volume change only. The discussed concepts can therefore be applied accordingly.

3.6 Conceptual Adaptation for Collapsing Soils

A collapsing soil is generally referred to as an unsaturated soil which exhibits volume decrease upon saturation under a constant applied load. Limited information is available in the literature on the volume change constitutive relation for collapsing soils. The following is a suggestion on how the relationships between

the various moduli of a collapsing soil may be formulated.

The following properties are widely observed for collapsing soils,

a) A decrease in the net total stress is required to maintain a constant volume of a specimen upon saturation (Jennings and Burland, 1962).

b) A collapsing soil becomes normally consolidated following soaking (Burland, 1985).

The volume change constitutive surfaces for a collapsing soil are hypothesized based on these observations.

Little is known about the form of the constant volume stress path of a collapsing soil when it is being wetted. The soil structure constitutive surface for monotonic volume decrease is hypothesized by assuming the stress path (i.e., stress path AM) is a straight line (Figure 3.32). On an arithmetic plot, the constitutive surface is a combination of two concave surfaces, I and II. The two concave surfaces are separated by a ridge defined by the virgin compression curve on the matric suction equals to the initial matric suction (i.e., $(u_a - u_w)_i$) plane. The same constitutive surface becomes a composite of a planar and a convex curved surface on a semi-logarithmic plot. The collapsing curve (i.e., the void ratio versus decreasing matric suction relation at constant net total stress) is assumed to be linear on a semi-logarithmic scale. It is suggested that this composite surface can be

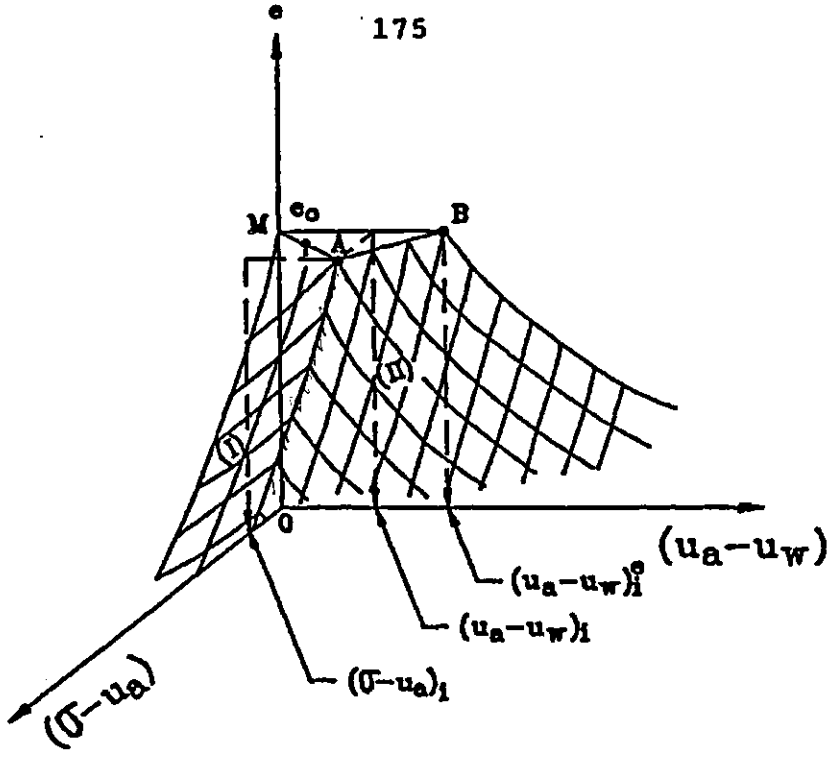

Figure 3.32a The Soil Structure Constitutive Surface of A Collapsing Soil for Monotonic Volume Decrease on An Arithmetic Scale

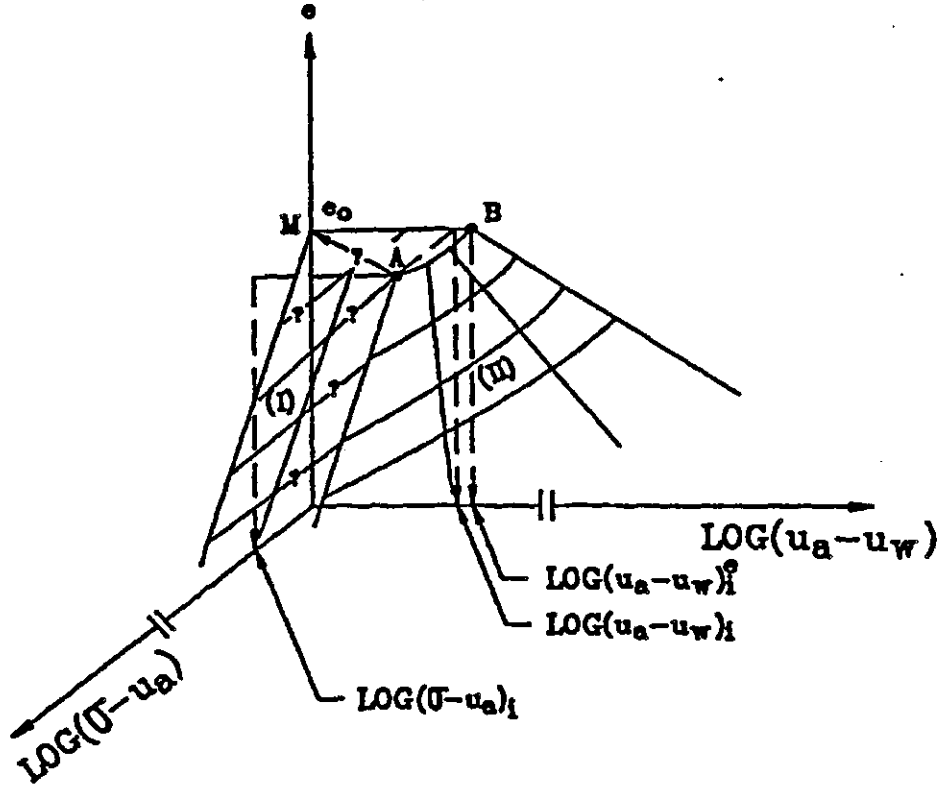

Figure 3.32b The Soil Structure Constitutive Surface of A Collapsing Soil for Monotonic Volume Decrease on A Semi-Logarithmic Scale

approximated by two planar surfaces (Figure 3.33). Planar surface I is defined by the linearlized virgin compression and collapsing curves. Planar surface II is defined by the linearlized virgin compression and void ratio versus increasing matric suction curves. Three moduli are required to define this approximated constitutive surface. The moduli are the compression indices with respect to the net total stress and matric suction (i.e., C_t and C_m), as well as the collapse index (i.e., C_{tc}). The collapse index is defined as the void ratio change per the logarithm of matric suction decrease. The compression index with respect to the net total stress can be related to the collapse index by geometry,

$$C_{tc} = C_t \frac{\log(\sigma - u_a)_i}{\log(u_a - u_w)_i} \qquad (3.46)$$

Other relationships involving the compression index with respect to matric suction may be formulated pending on a better understanding of the form of the constitutive surface.

It is observed that the less swelling that a soil exhibits, the smaller the swelling pressure (Maswosve, 1985). Under K_o condition when the net total stress is small, soaking alone seldom causes a soil to collapse. The constitutive surface for monotonic volume increase can, therefore, be visualized as a sequence of diminishing surfaces as a soil becomes less swelling (Figure 3.34). The limiting case would be that of a collapsing soil under no

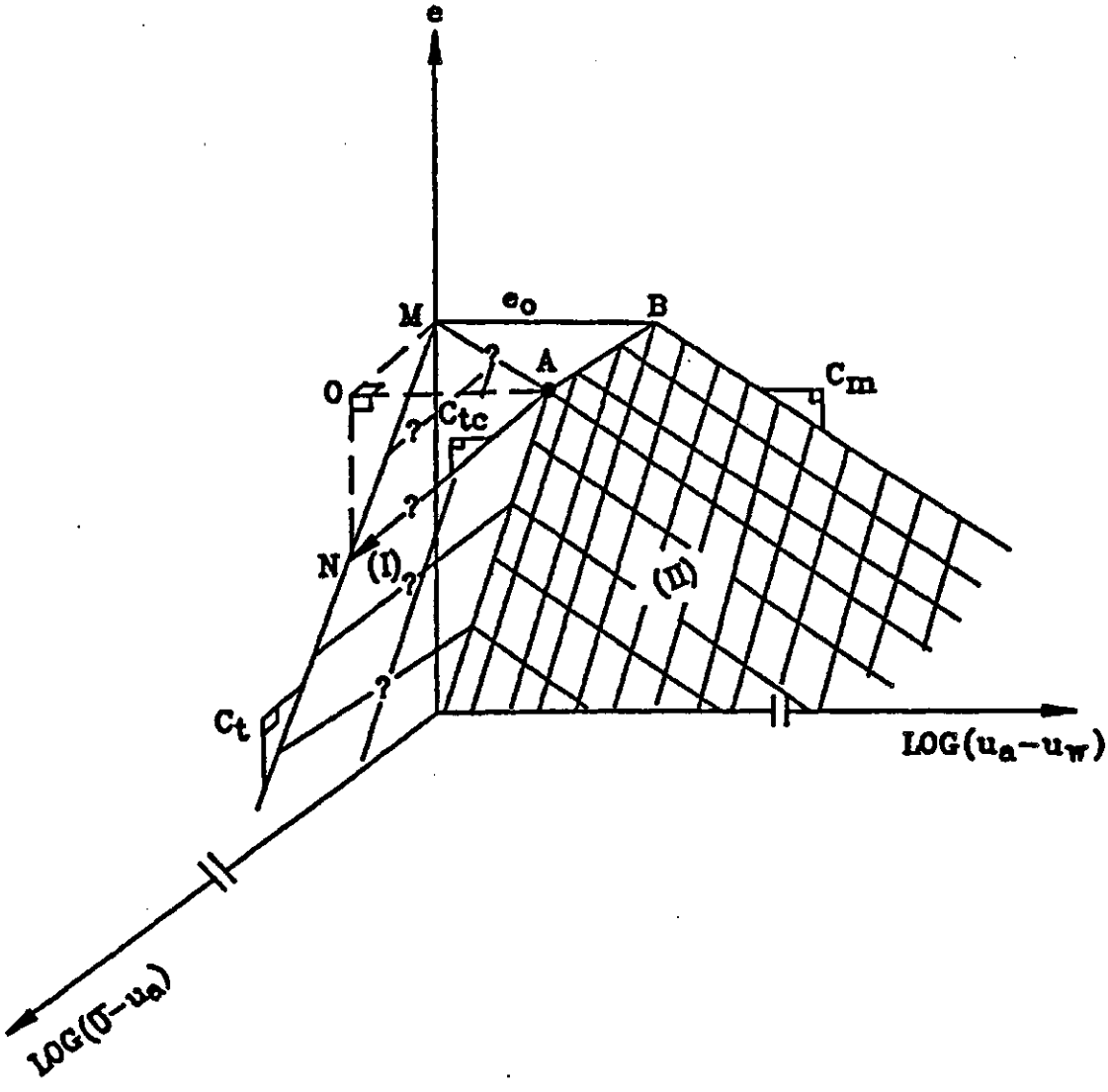

Figure 3.33 The Approximated Form for The Soil Structure Constitutive Surface of a Collapsing Soil Undergoing Monotonic Volume Decrease

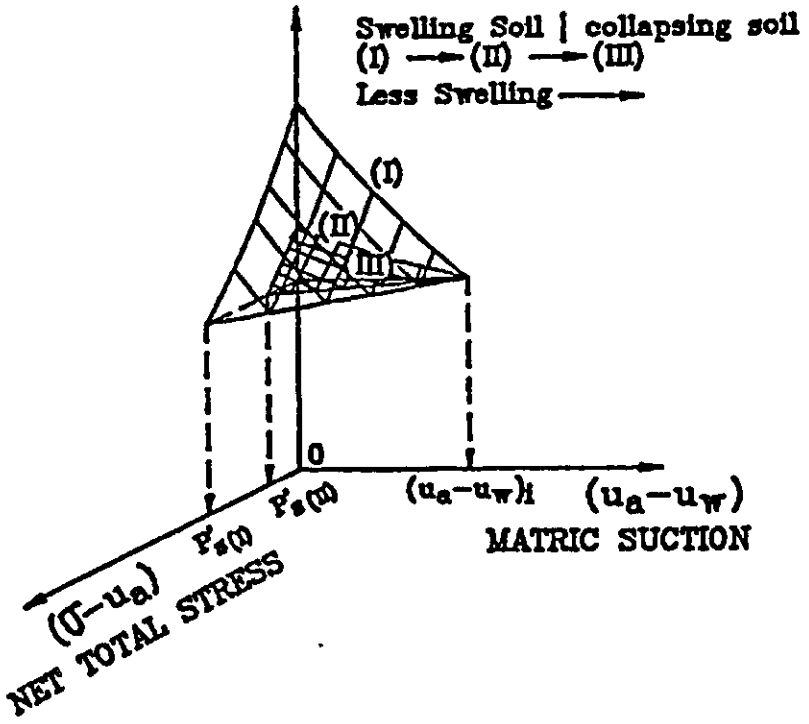

Figure 3.34a A Schematic Diagram Showing The Transition between The Constitutive Surfaces of A Swelling Soil to A Collapsing Soil on An Arithmetic Plot

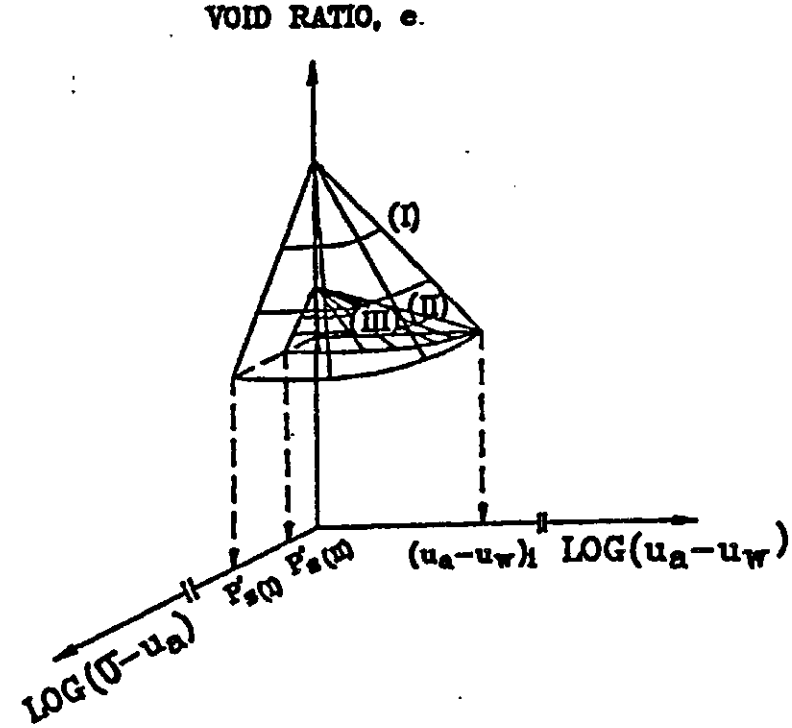

Figure 3.34b A Schematic Diagram Showing The Transition between The Constitutive Surfaces of A Swelling Soil to A Collapsing Soil on A Semi-Logarithmic Plot

net total stress. The constitutive surface should become a horizontal line on the void ratio versus the logarithm of matric suction plane. There is, therefore, a smooth transition between the constitutive surface of a swelling soil to that of a collapsing soil. However, the formulation of relationships between moduli of a collapsing soil awaits further research in order to completely identify the form of the volume change constitutive surfaces.

CHAPTER IV

TEST PROGRAM

4.1 General

The main objective of the test program is to experimentally verify the form of the constitutive surfaces for various loading conditions. The two loading conditions can be described as i) vertical loading with no lateral expansion and ii) isotropic loading. The form of the constitutive surface will provide an understanding of the relationships between relevant moduli.

4.2 Soils

Two soils, a uniform silt and a glacial till, were selected. The silt is from the Pilot Butte area (SW-14-18-18-W2) in Saskatchewan. It was selected for its relatively high permeability. The till is from the Indian Head area (NE-11-18-14-W2) in Saskatchewan. Its volume change behaviour has been documented by Lidgren (1970). The index properties and grain size distribution curves for these soils are presented in Table 4.1, Figure 4.1 and 4.2 respectively. Results of salinity analyses on these soils are given in Table 4.2.

Table 4.1 Index Properties of the Silt and Glacial Till Used in the Test Program

	Silt	Glacial Till
Liquid Limit	26.7%	33.2%
Plastic Limit	14.9%	13.0%
Plasticity Index	11.8%	20.2%
Percent Sand Sizes	25.0%	32.0%
Percent Silt Sizes	52.0%	39.0%
Percent Clay Sizes	23.0%	29.0%
Relative Density of Solids	2.719	2.764

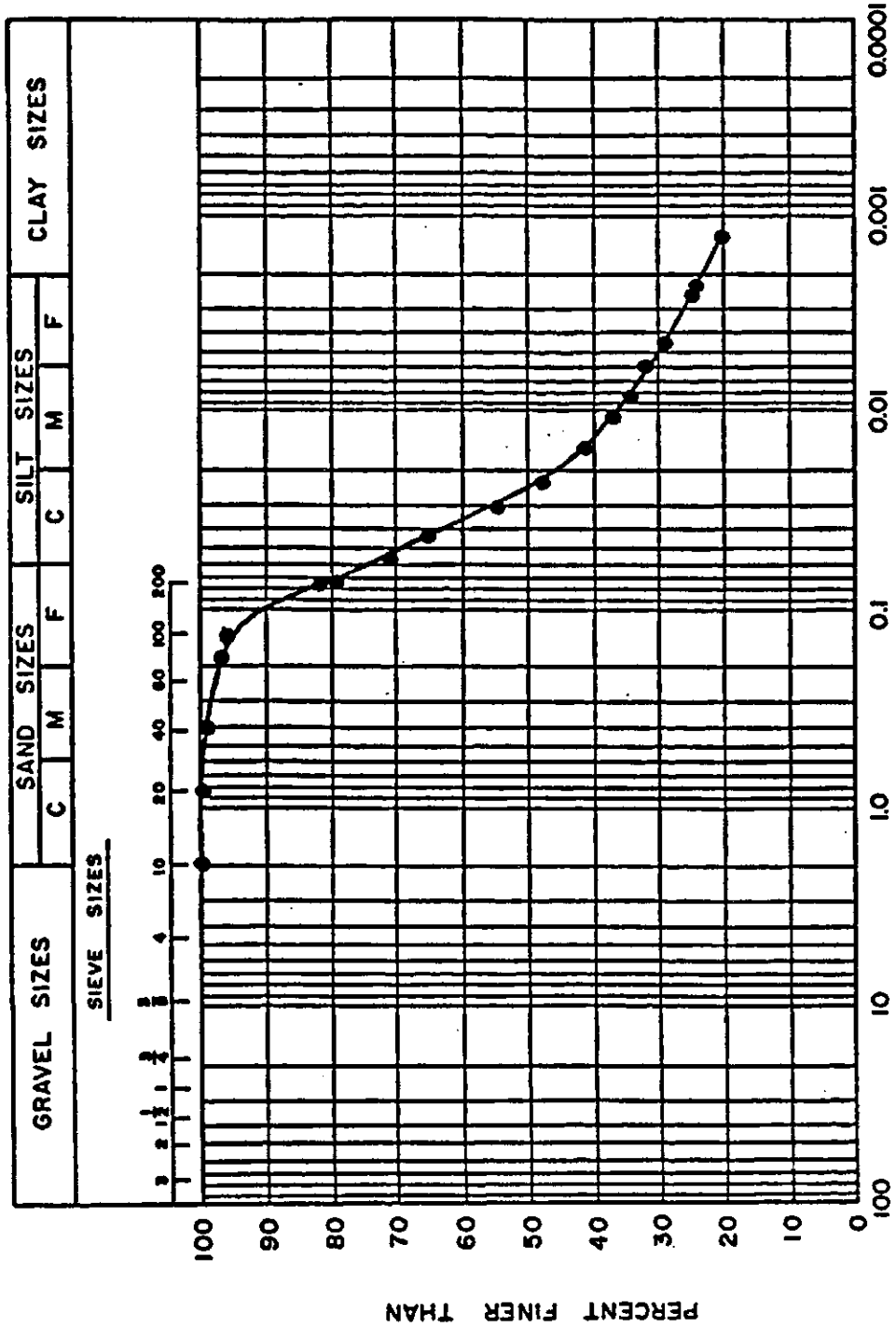

Figure 4.1 Grain Size Distribution Curve for Silt

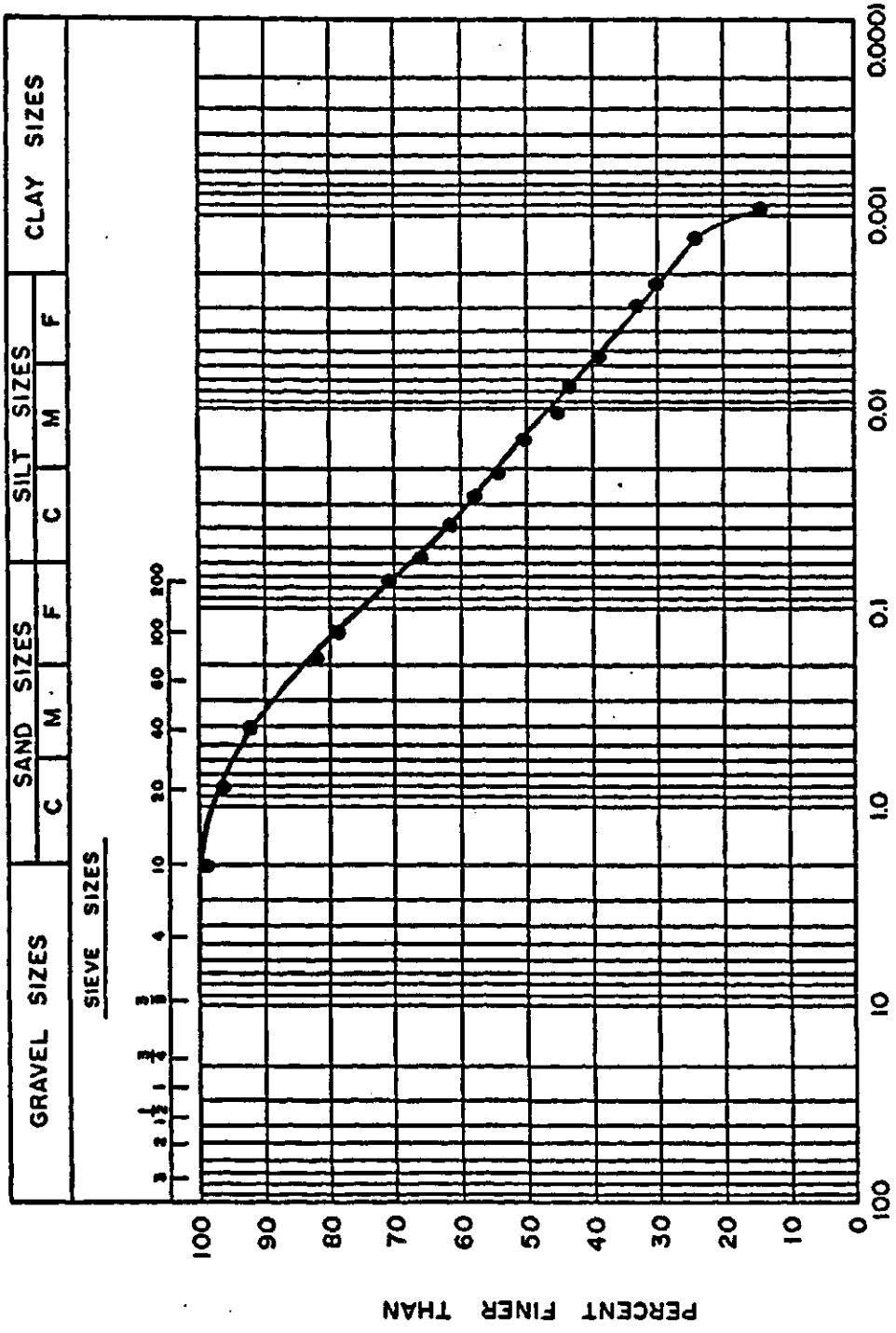

Figure 4.2 Grain Size Distribution Curve for Glacial Till

Table 4.2 Results[a] of the Salinity Analyses on Silt and Till Samples

Test Result	Silt	Glacial Till
Water content of saturation extract	43%	43%
pH	7.5	7.9
Conductivity (mS/cm)[b]	1.6	0.9
Ions in saturation extract ($\mu g/ml$)[c]		
Na^+	96	75
Ca^{++}	207	23
Mg^{++}	43	66
K^+	49	18
Cl^-	43	75
$SO_4^=$	390	65
Sodium Adsorption Ratio $\frac{Na^+}{[(Ca^{++}+Mg^{++})/2]^{\frac{1}{2}}}$ (meq/litre)	1.6	1.8

SAR ≈ 1:1 ESP (endangered certain...) ESP 72%, ...

Note : a) Tests were performed by the Saskatchewan Soil Testing Laboratory, University of Saskatchewan, Saskatoon.

b) "mS/cm" means milli-Siemens per centimeter.

c) "µg/ml" means micro-grams per milli-litre.

4.2.1 Soil preparation

Prepared specimens with near identical initial conditions were desired. Remoulded samples of each soil were compacted at various water contents to different initial dry densities.

Soil used in this study was first air dried for approximately two days. It was then pulverized using a rubber mallet. Only material passing the No. 10 sieve was used in the testing program. The soil was oven-dried for 24 hours and hand mixed with a precalculated quantity of distilled water. The wet soil was placed in a sealed bag consisting of alternate layers of polystyrene bag and aluminum foil and left to cure for about 7 days in a constant humidity and temperature room. The water content of the soil was measured after the curing period. An attempt was made to have a water content control of $\pm$0.5% between batches of the soil.

Specimens were formed by static compaction at half standard Proctor compaction effort to ensure that significant volume changes in response to stress changes would occur. Figure 4.3 and 4.4 show the compaction characteristics of the silt and till, respectively. Two sizes of compaction moulds were used as shown in figure 4.5 and 4.6. Each specimen was statically compressed to a predetermined volume defined by the mould and the caps. The applied load was maintained for at least 48 hours in a

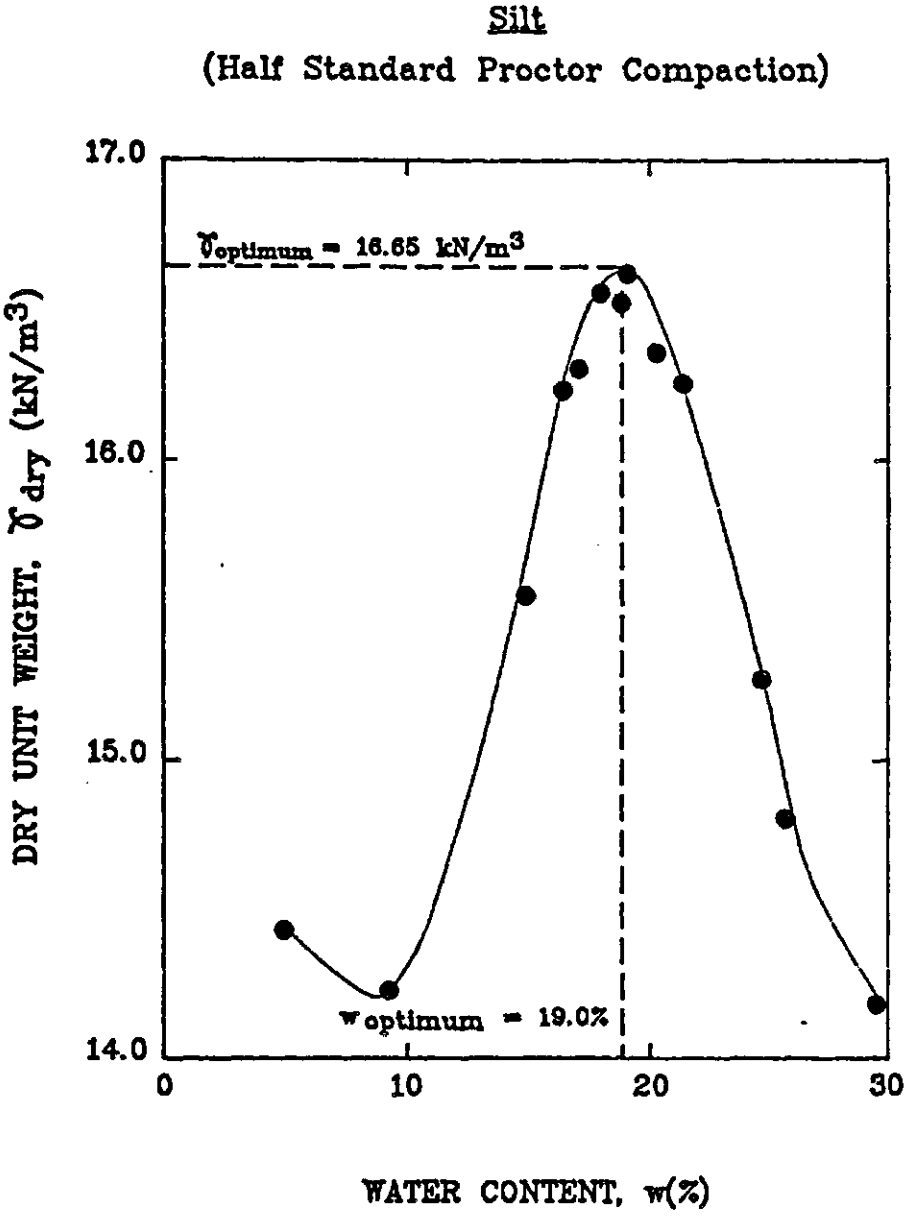

Figure 4.3 Compaction Curve for Silt

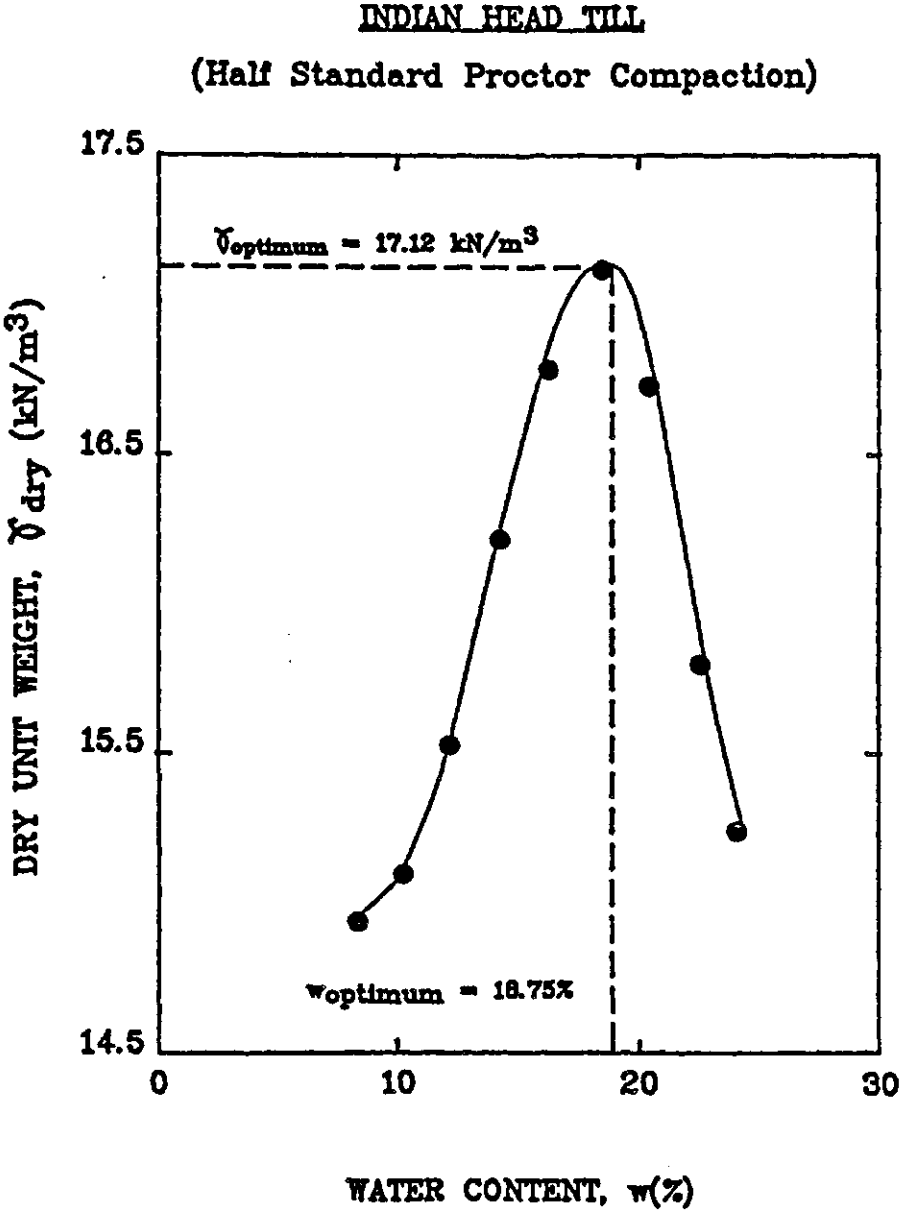

Figure 4.4 Compaction Curve for Glacial Till

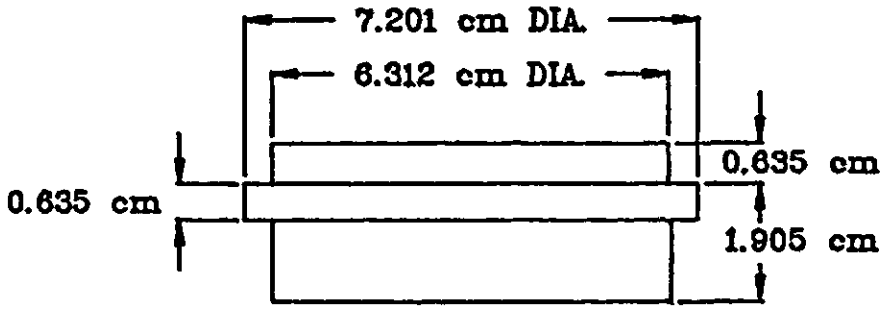

END CAP OF THE SMALL DIAMETER COMPACTION MOULD

NOTE: 1) TWO END CAPS PER MOULD
2) MADE OF STAINLESS STEEL

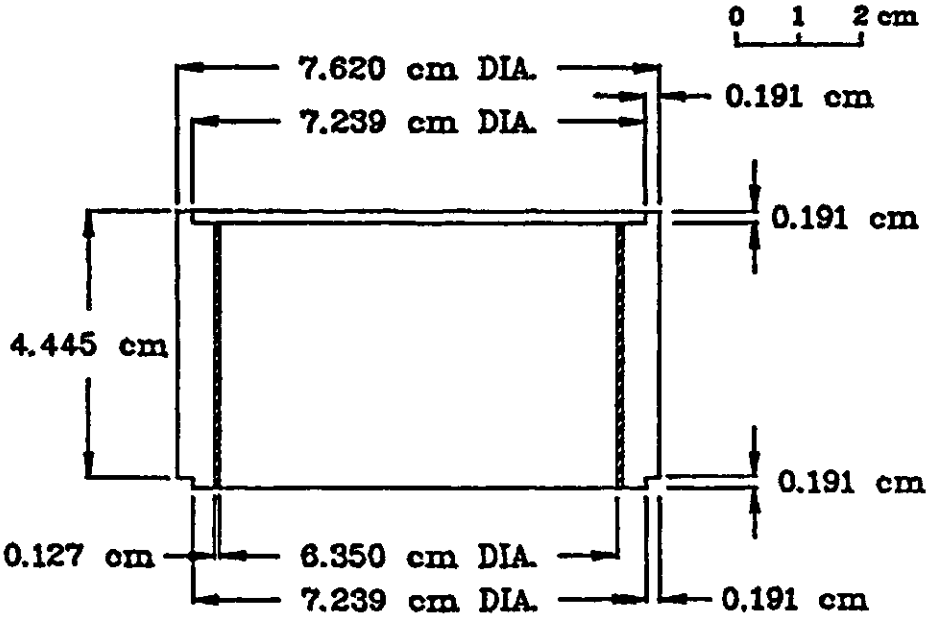

RING OF THE SMALL DIAMETER COMPACTION MOULD

NOTE: 1) BODY OF THE RING IS MADE OF STAINLESS STEEL WITH A 0.127 cm THICK OF TEFLON LINING

Figure 4.5 Schematic Layout of the 6.3 cm Diameter Compaction Mould

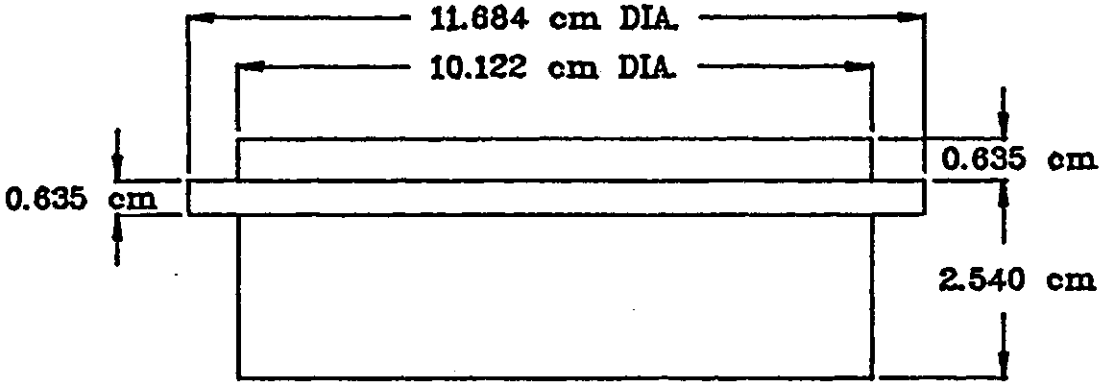

END CAP OF THE LARGE DIAMETER COMPACTION MOULD

NOTE: 1) TWO END CAPS PER MOULD MADE OF STAINLESS STEEL

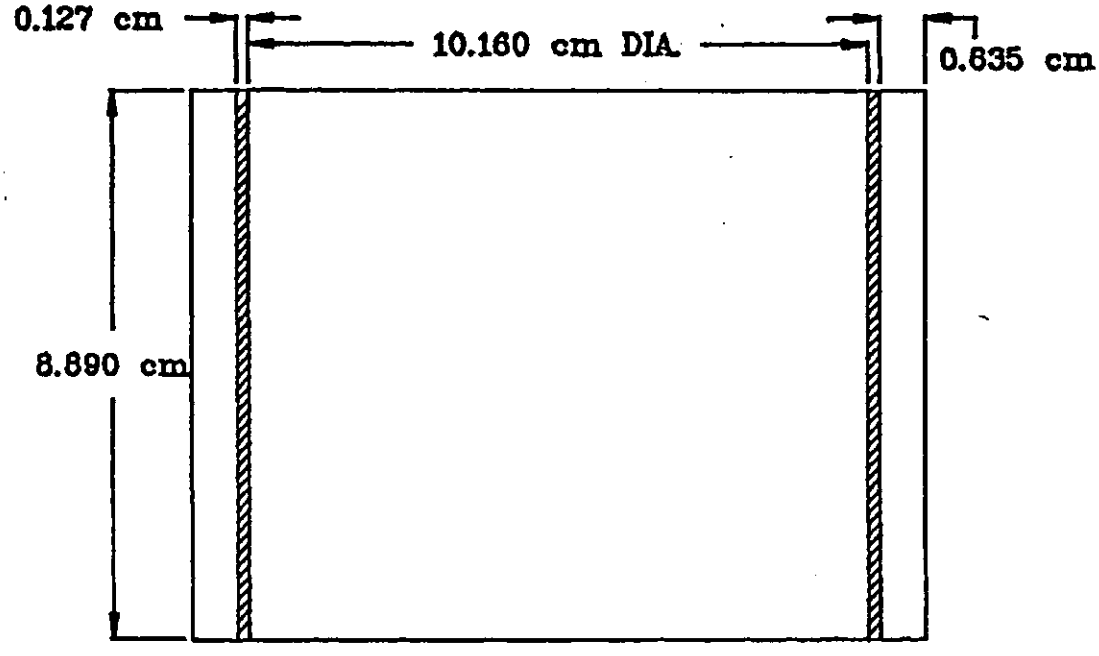

RING OF THE LARGE DIAMETER COMPACTION MOULD

NOTE: 1) BODY OF THE RING IS MADE OF STAINLESS STEEL WITH A 0.127 cm THICK OF TEFLON LINING

Figure 4.6 Schematic Layout of the 10.2 cm Diameter Compaction Mould

constant humidity and temperature room. The specimens were then extruded and tested. Precaution was taken to avoid moisture loss from the specimens during their preparation. The silt and till samples were prepared at either approximately 3% dry of optimum or at optimum water content.

4.3 Testing Equipment

Conventional soil testing equipment was used in the test program whenever possible. However, for some stress paths, it was necessary to develop special equipment. This section will present the unique features of the equipment used in this test program.

4.3.1 Modified Anteus consolidometer

A conventional Anteus consolidometer was modified for the study of one-dimensional volume change behaviour of unsaturated soils (Figure 4.7). Some of the modifications are the same as those used by Pufahl (1970). A high air entry disc was installed in the base pedestal of the consolidometer. This allowed the axis-translation technique (Hilf, 1956) to control the matric suction in the specimen. An axial load was applied using a water pressure actuated rubber diaphragm attached to the loading piston. A dial

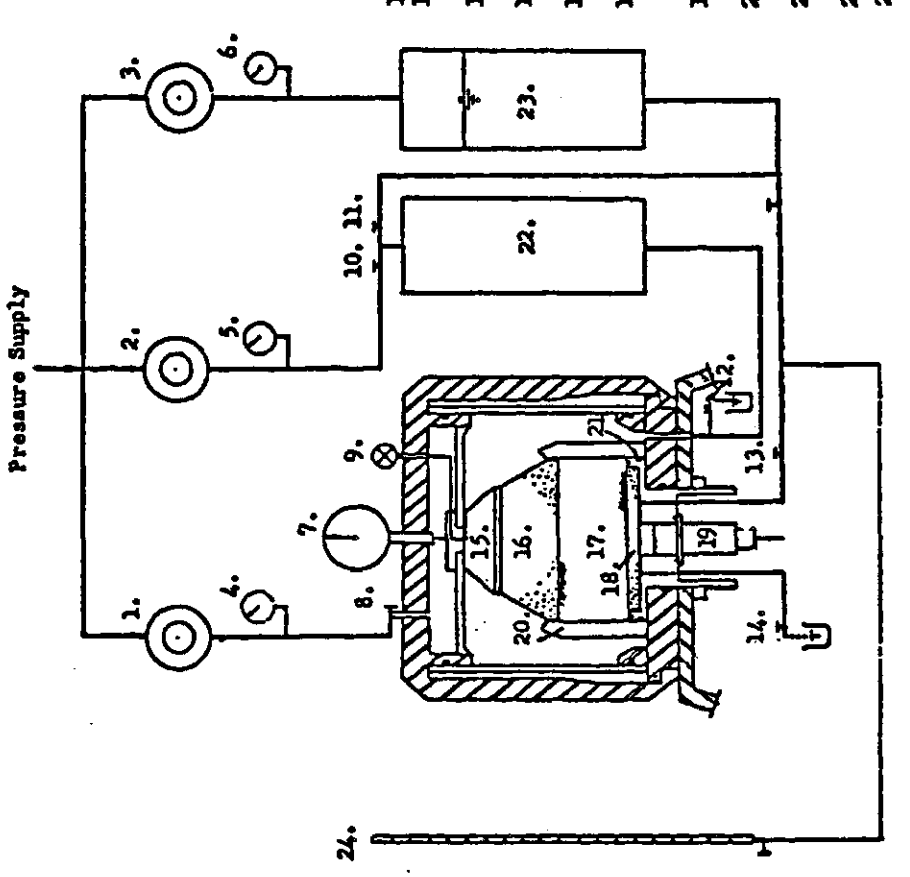

Figure 4.7 Modified Anteus Consolidometer (Pufahl, 1970)

gauge with the plunger resting on top of the loading piston was used to measure vertical displacement of the specimen. The space inside the consolidometer was controlled at a constant air pressure. A coarse porous stone was placed between the loading piston and the specimen. This allowed the control of the pore-air pressure in the specimen. Two drainage lines were connected to the basal compartment beneath the high air entry disc. One drainage line was connected to a water supply tank for the control of the pore-water pressure. The second drainage line was used when flushing diffused air from underneath the high air entry disc (Fredlund, 1975).

The permeability of the high air entry disc is extremely low. Therefore, water moving to the specimen through the base pedestal requires long periods of time (Ho and Fredlund, 1982). The loading cap of the modified Anteus consolidometer was redesigned to enable a more efficient addition of water to the specimen. A composite loading cap was built consisting of an aluminum top and two layers of porous alundum stones. Three 17-gauge (i.e., 1.47 mm O.D. and 1.04 mm I.D.) hypodermic needles were installed through the loading cap (Figure 4.8). The presence of the coarse alundum stones allowed the pore-air pressure of the specimen in the air chamber to be regulated. A polyvinyl chloride (PVC) tube serving as the water injection line was joined to the loading cap through the cell wall (Figure 4.9) to a

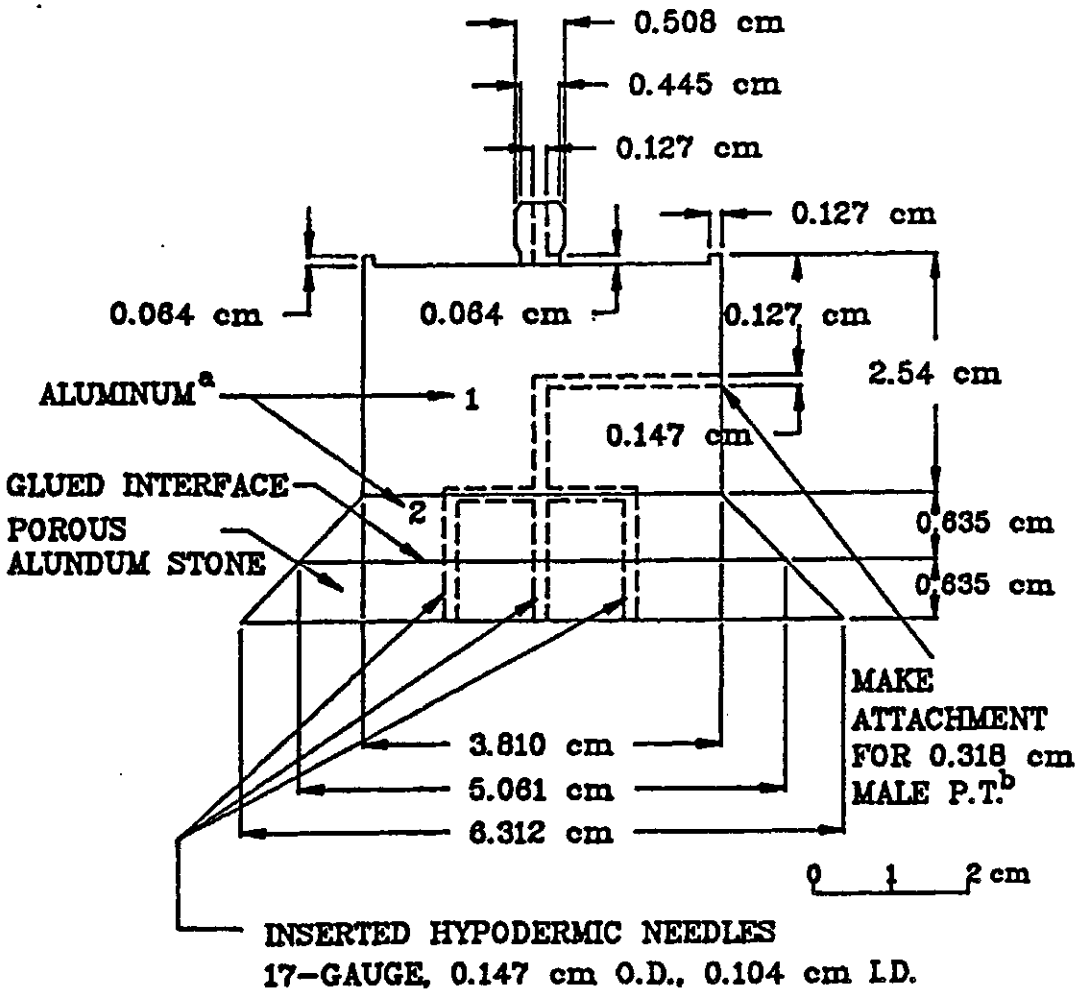

NOTE: a) ALUMINUM BLOCK 1 AND 2 ARE EITHER GLUED OR SCREWED TOGETHER WITH "O" RING SEALS AT THE INTERFACE

b) P.T. MEANS PIPE THREAD

Figure 4.8a Loading Cap Complex for the Modified Anteus Consolidometer - Front View

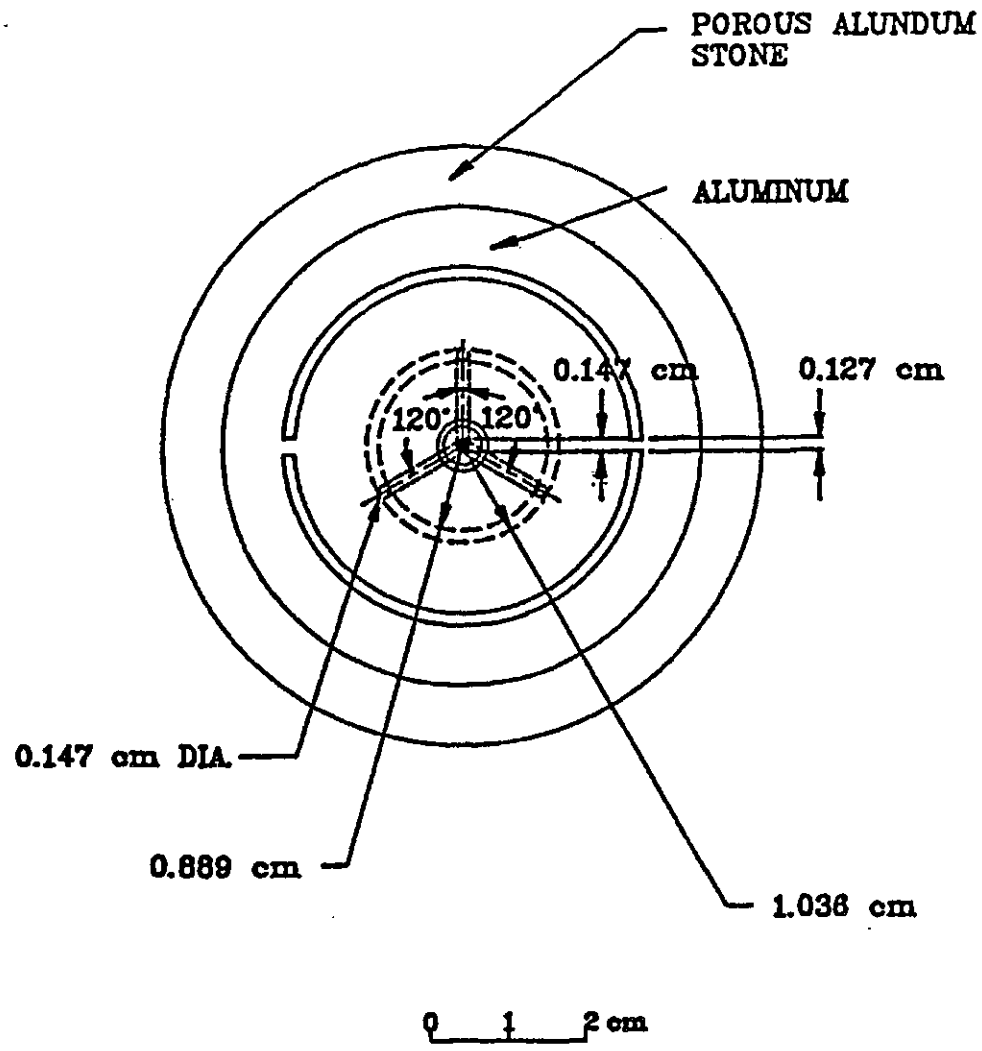

Figure 4.8b Loading Cap Complex for the Modified Anteus Consolidometer - Top View

MAXIMUM EXPANDED POSITION

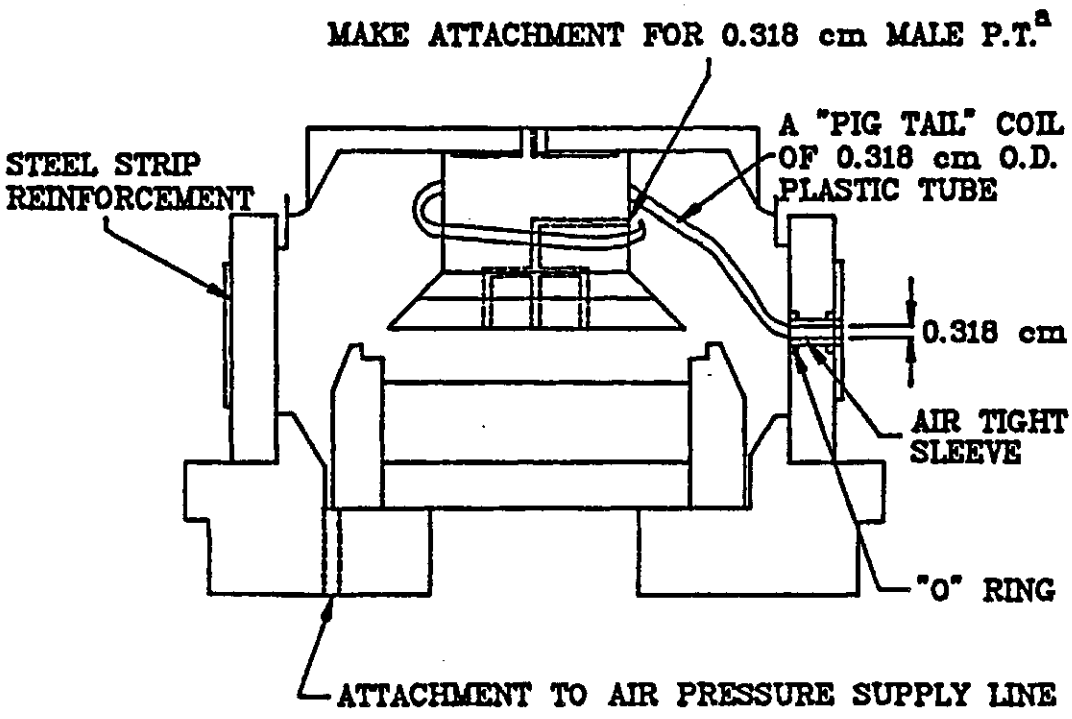

NOTE: a) P.T. MEANS PIPE THREAD

Figure 4.9 Schematic Layout of the Modified Anteus Consolidometer

pressurized water tank via a double burette volume change indicator (Figure 4.10). A two-way valve was installed in the water injection line between the consolidometer and the double burette volume change indicator. This line could be closed when the hypodermic water injection system was not being used. Water movement in or out of the specimen was then restricted to the drainage line through the high air entry disc. The water injection system allowed water to be added to the specimen under any applied total, pore-air and pore-water pressure condition.

A linear variable differential transformer (LVDT) was used to measure the vertical displacement of the specimen. Signals from the LVDT and other pressure transducers monitoring the axial load, cell pressure and pore-water pressure of the specimen were fed to a data acquisition system. Processing of the data was conducted as the test progressed. A double burette volume change indicator was used to monitor the water passing into or out of the specimen. One of the bottom drainage lines was connected to a diffuse air volume indicator (Figure 4.11) (Fredlund, 1975). The volume of diffused air passing through the ceramic high air entry disc was monitored from time to time. The volume of diffused air measured by flushing the basal compartment was applied as a correction to the measured change in the volume of water of the specimen.

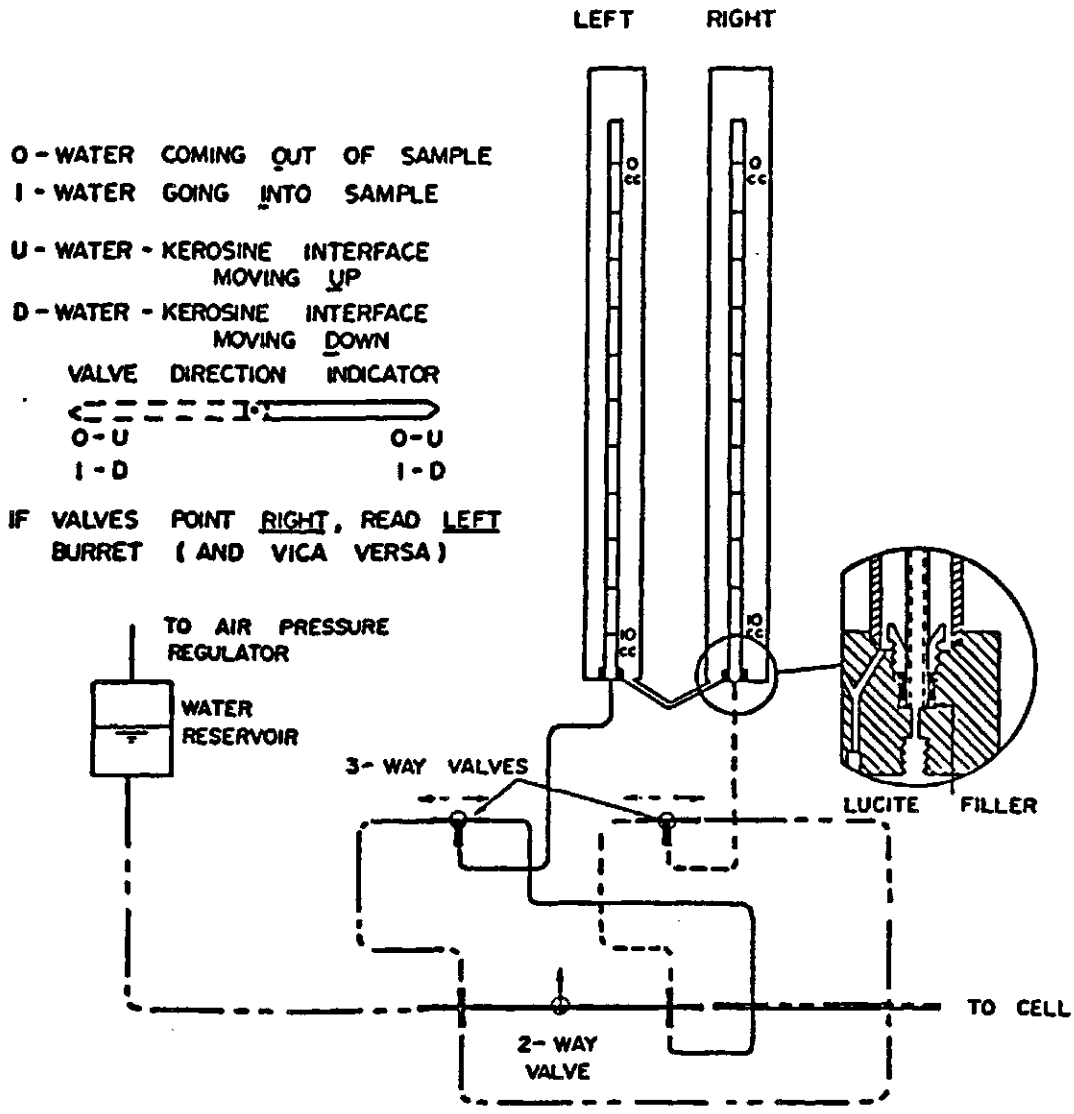

Figure 4.10 Water Volume Change Indicator (Fredlund, 1973)

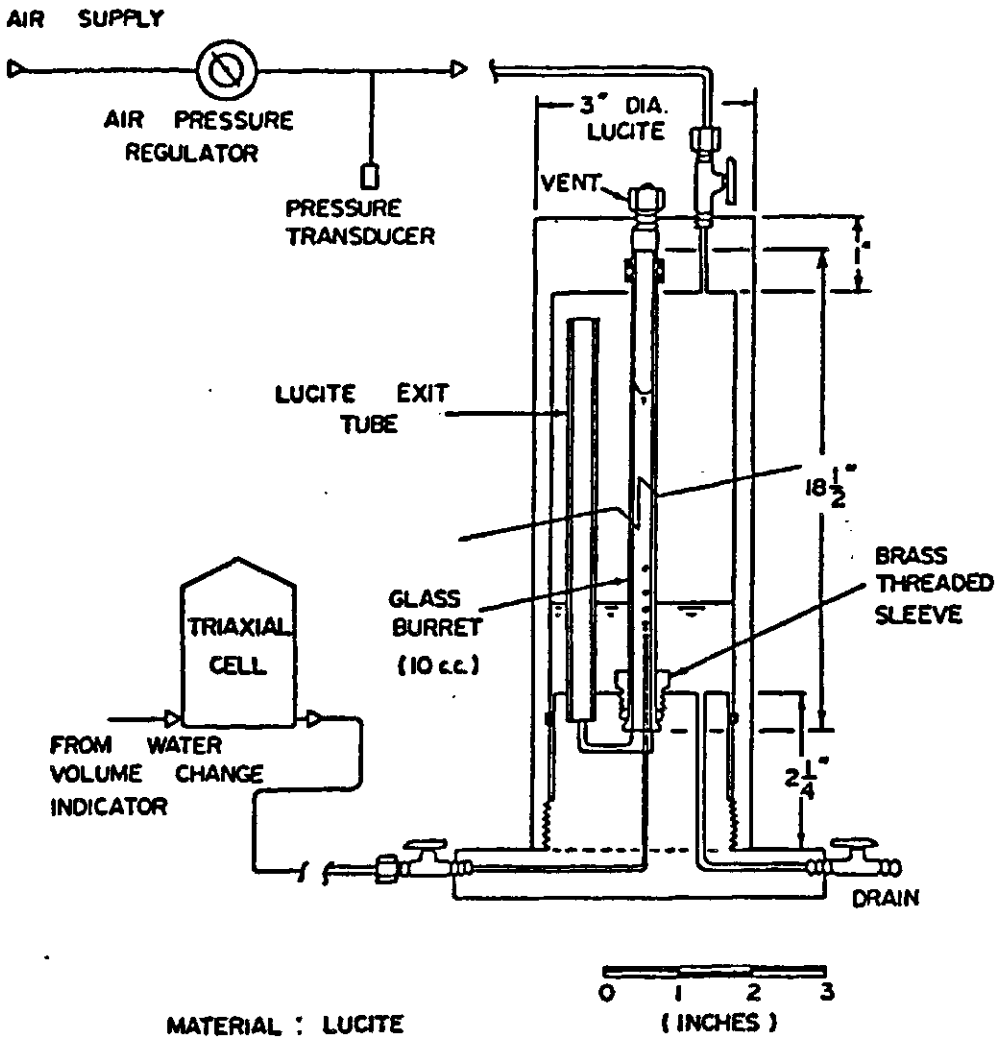

Figure 4.11 Diffused Air Volume Indicator (Fredlund, 1975)

4.3.2. Stress controlled isotropic cell

A Wykeham Farrance triaxial cell was modified to study isotropic volume change. The design was a modification of that used by Fredlund (1973) (Figure 4.12). A brief description of the equipment designed by Fredlund is as follows. The pore-air and pore-water pressure were independently controlled using the axis-translation technique. A high air entry disc was installed in the base pedestal of the cell. The vertical displacement of the specimen was measured using a LVDT with the plunger resting on the top loading cap. The lateral displacement was measured using an LVDT attached to a modified K_o lateral displacement indicator (Figure 4.13). The cell was filled with air and the soil specimen was surrounded with a composite rubber and aluminum foil membrane.

There are two undesirable features of this modified triaxial cell used by Fredlund (1973). The first deals with water movement in the specimen. The pore-water line at the base of the triaxial cell is the only means to pass water into the specimen. However, the high air entry disc greatly impedes the water movement (Ho and Fredlund, 1982). Secondly, the K_o lateral displacement indicator used by Fredlund (1973) is not sufficiently accurate.

The stress controlled isotropic cell developed for the present study followed the basic design principles of Fredlund's (1973) modified triaxial cell (Figure 4.14 to

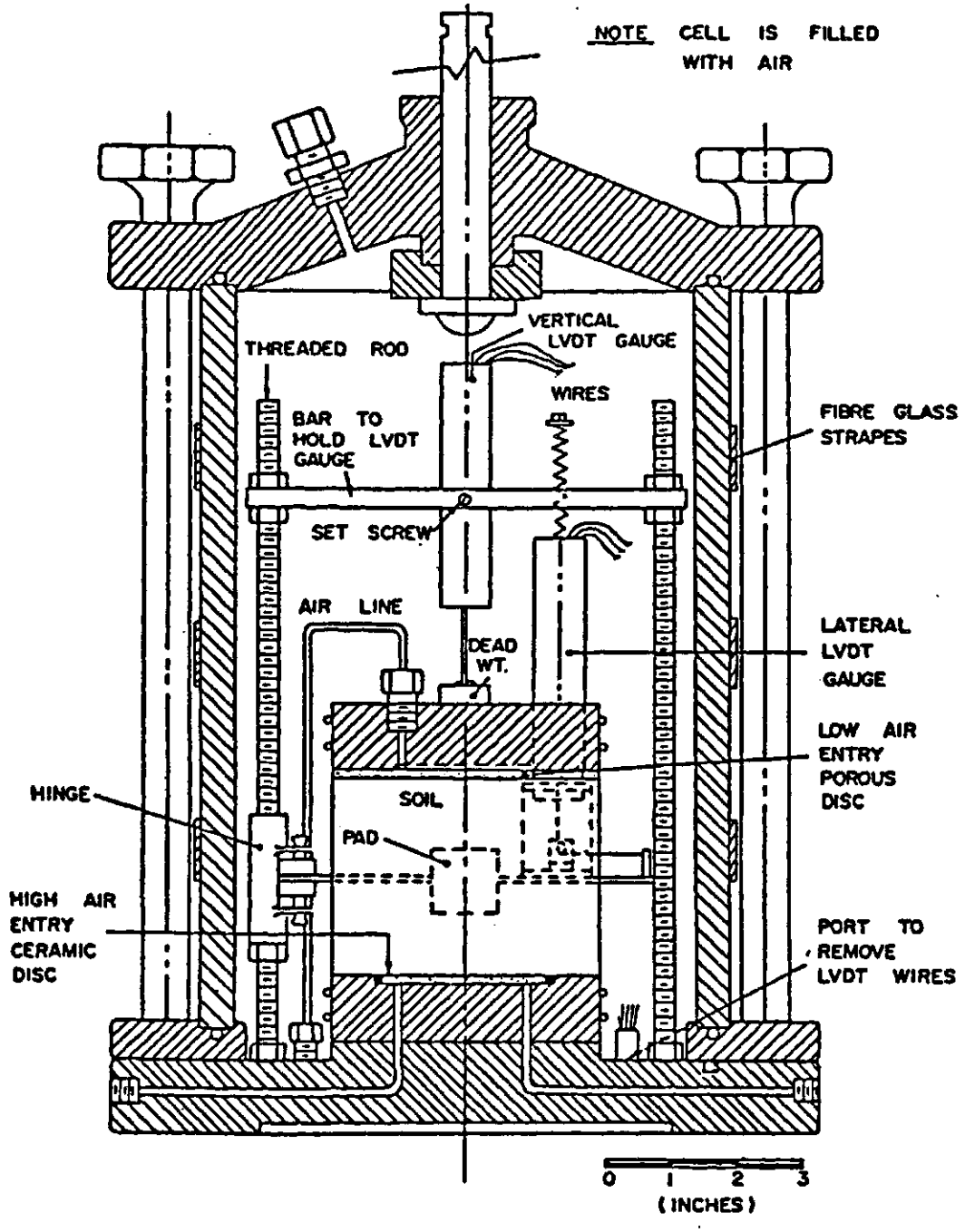

Figure 4.12 Modified Triaxial Cell (Fredlund, 1973)

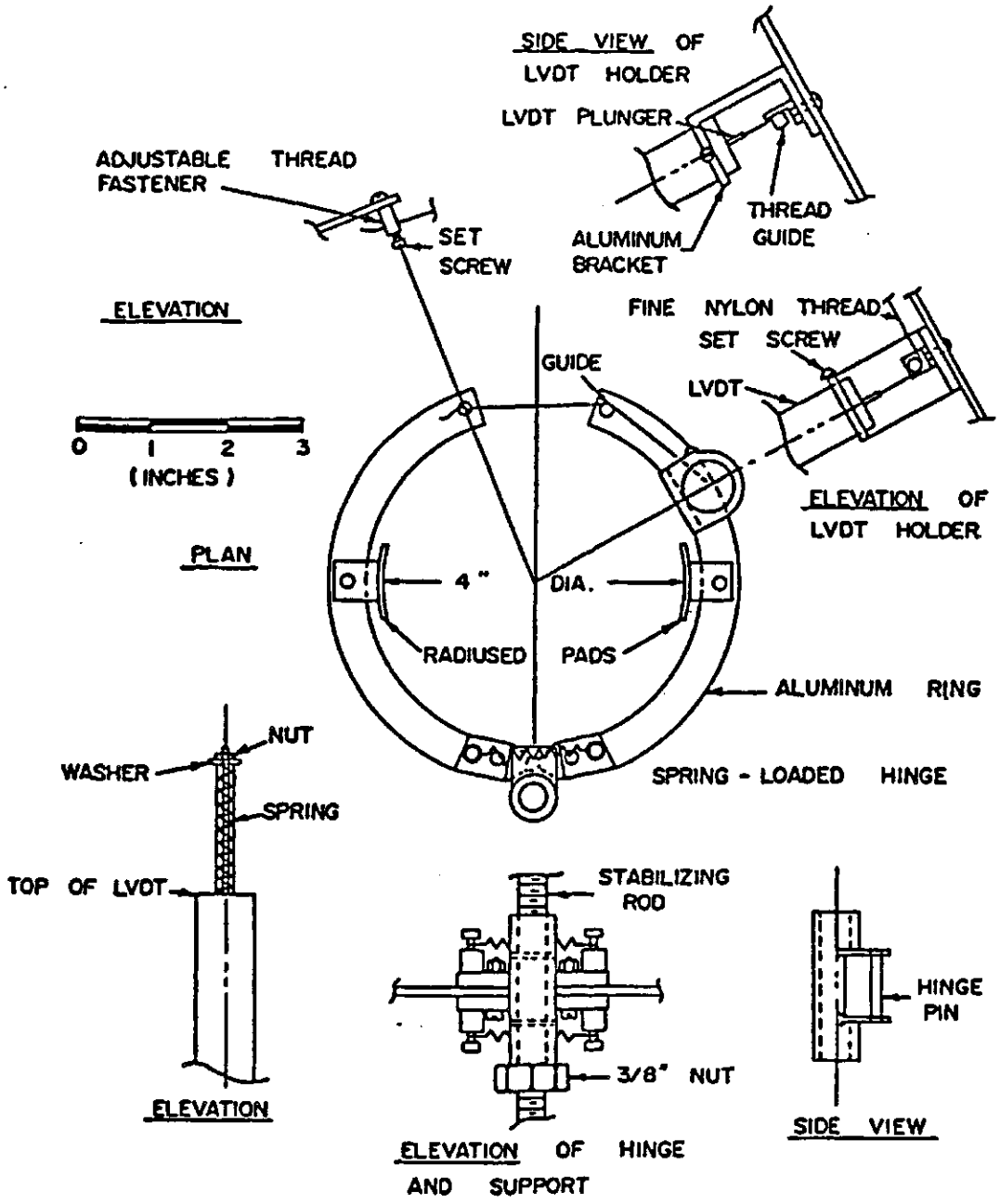

Figure 4.13 Lateral Displacement Indicator (Fredlund, 1973)

NOTE:

a) 0.508 cm THICK OR ADEQUATE THICKNESS TO SUSTAIN AN INSIDE AIR PRESSURE UP TO 1380 kPa
b) TWO KINDS OF STRAIN INDICATORS ARE USED
c) 8 – 0.953 cm BOLTS AROUND THE RIM TO SECURE THE COVER UP TO 1380 kPa AIR PRESSURE WITHIN THE CELL
d) P.T. MEANS PIPE THREAD

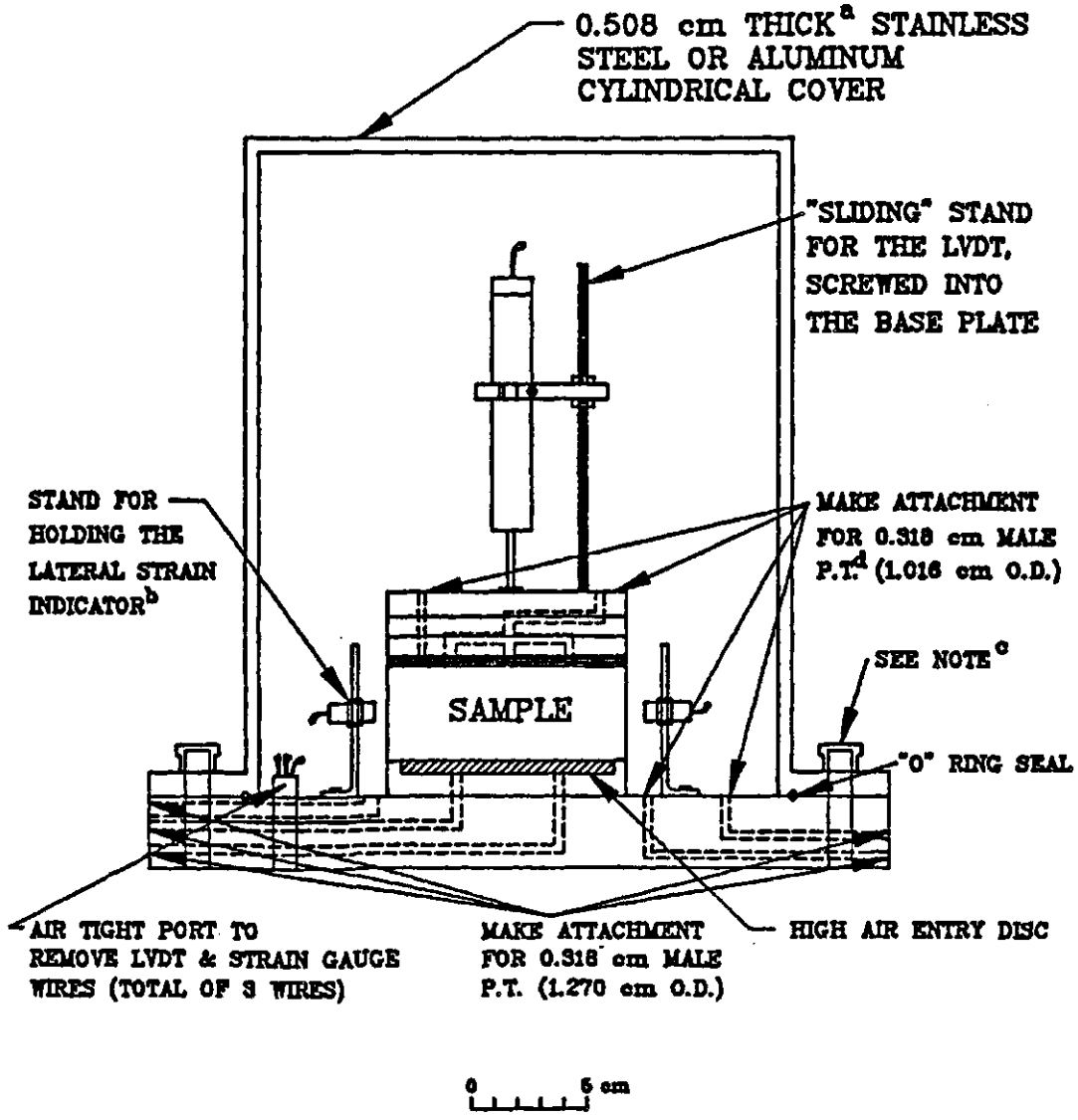

Figure 4.14 General Assembly of the Stress Controlled Isotropic Cell

4.17). A 5 bar high air entry disc, 0.635 cm thick, was installed in the base pedestal of the cell (Figure 4.14). The pore-air pressure was controlled by a line connected to the top of the composite loading cap (Figure 4.18). The pore-water pressure was controlled by a line connected to the base pedestal of the cell (Figure 4.17). The cell was filled with air and regulated by the cell pressure line connected to the base of the cell (Figure 4.17). The pore-water pressure line was connected to a pressurized water tank through a double burette volume change indicator (Fredlund, 1970). A second line was attached to the basal compartment (Figure 4.17) to facilitate the flushing of diffused air from below the high air entry disc. The line was connected to a diffused air volume indicator (Figure 4.11; Fredlund 1975).

The 4 inch (i.e., 101.6 mm) diameter composite loading cap (Figure 4.18) was equipped with a hypodermic water injection system as described in Section 4.3.1 so that water could be added to the specimen under any imposed stress conditions. A PVC tube was connected from the composite loading cap to the base plate (Figure 4.17). The water injection line was connected to a pressurized water tank through a double burette volume change indicator (Fredlund, 1970). The water injection line could be closed using a two-way valve attached to the base plate. Further water movement in or out of the specimen would then be

NOTE: a) THE OUTSIDE DIAMETER OF THE CYLINDRICAL COVER IS FIXED HOWEVER THE INSIDE DIAMETER MAY BE VARIED IF NECESSARY

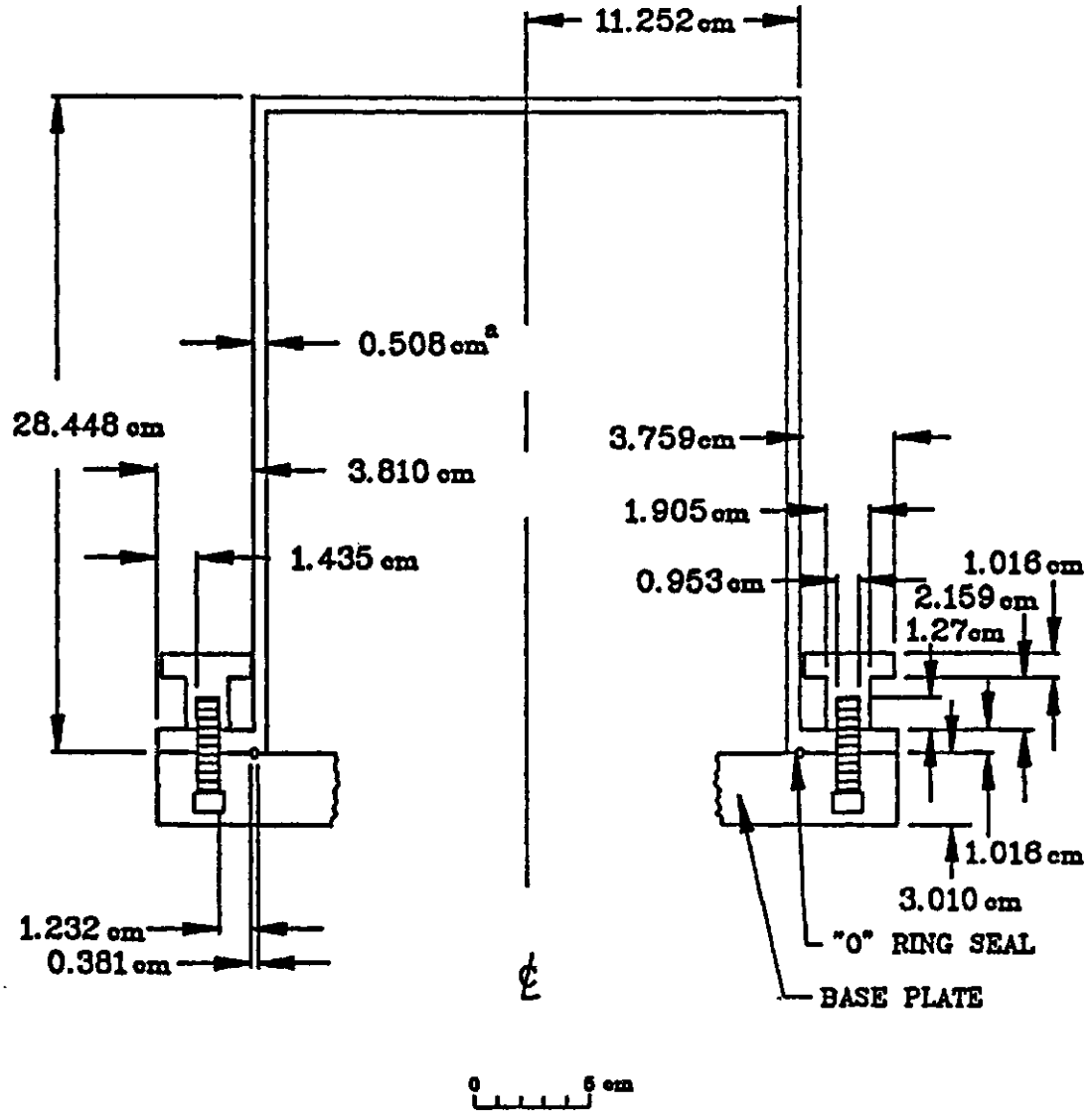

Figure 4.15 Cross Section of the Cylindrical Cover

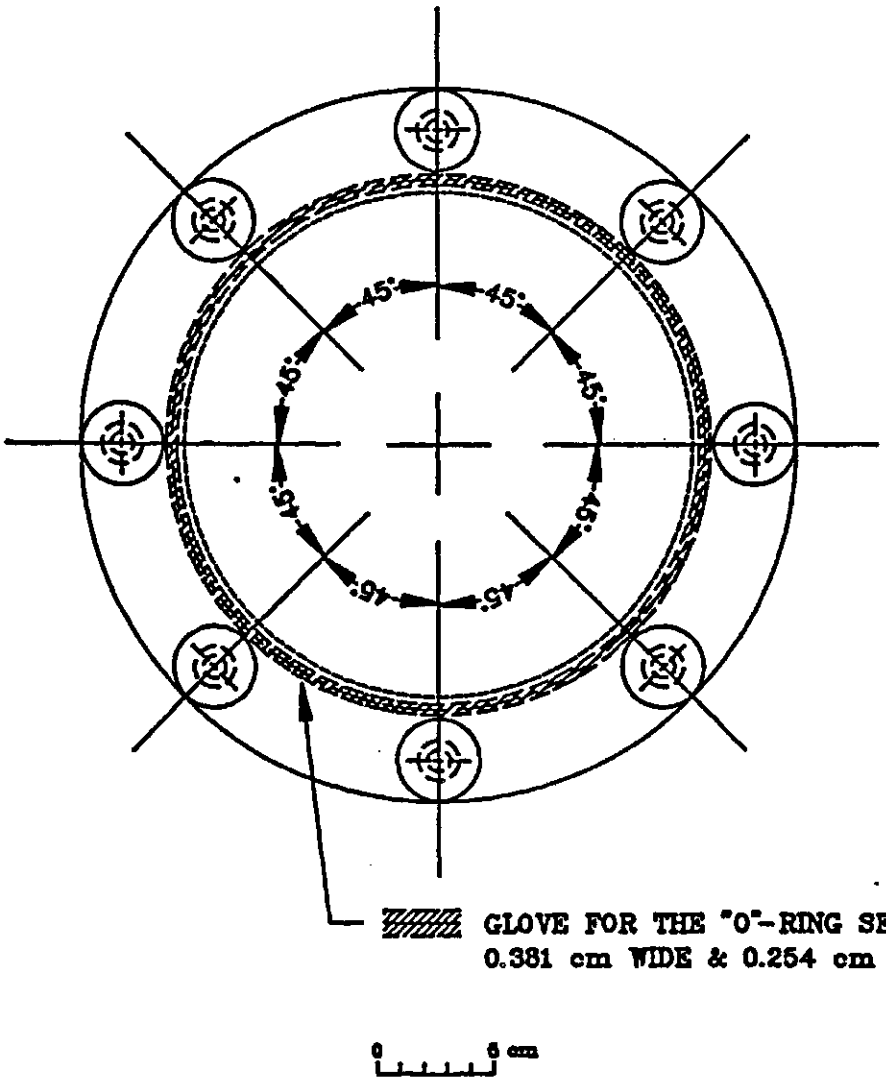

Figure 4.16 Top View of the Cylinderical Cover

NOTE: a) P.T. MEANS PIPE THREAD

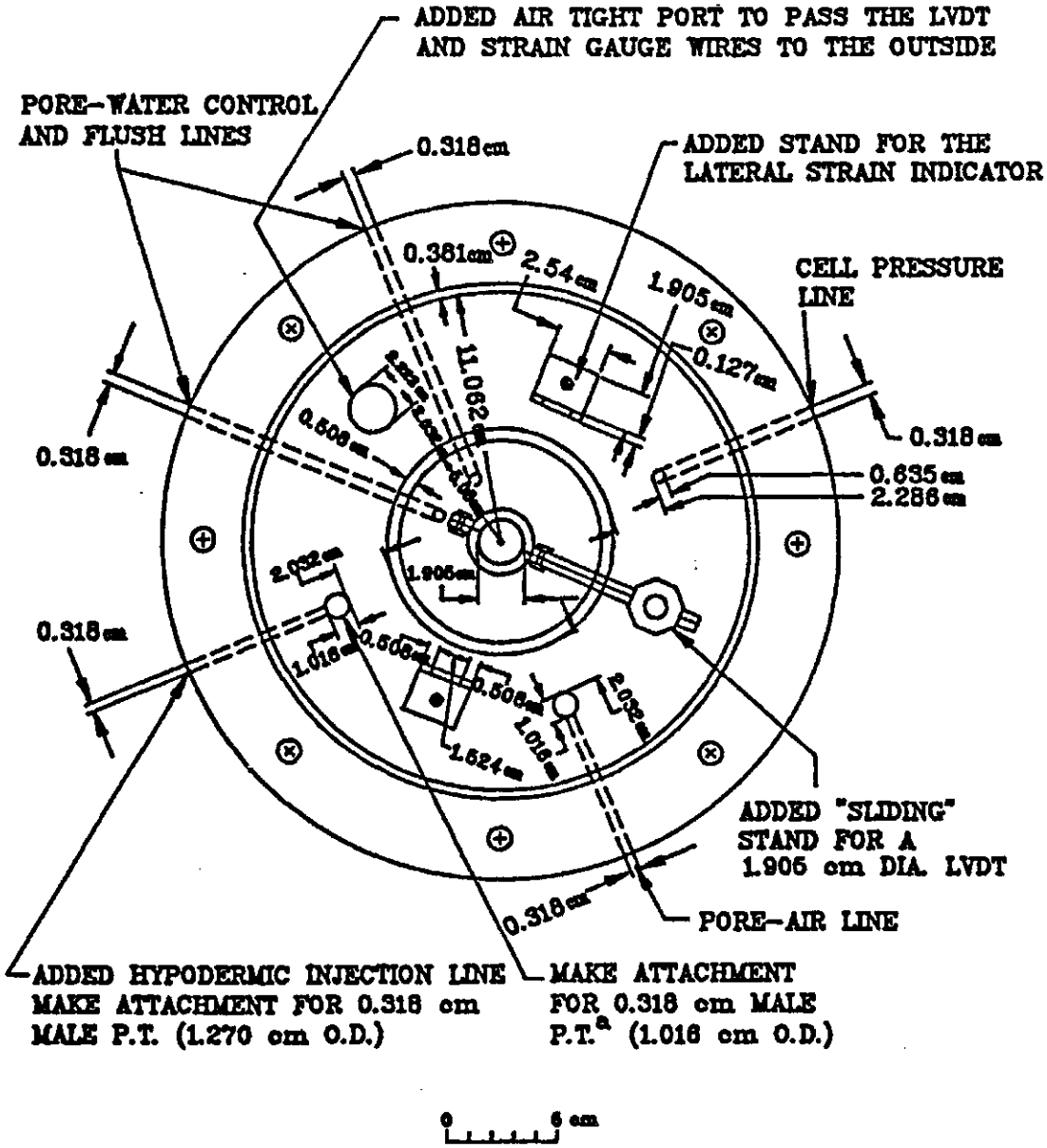

Figure 4.17 Base Plate of the Stress Controlled Isotropic Cell

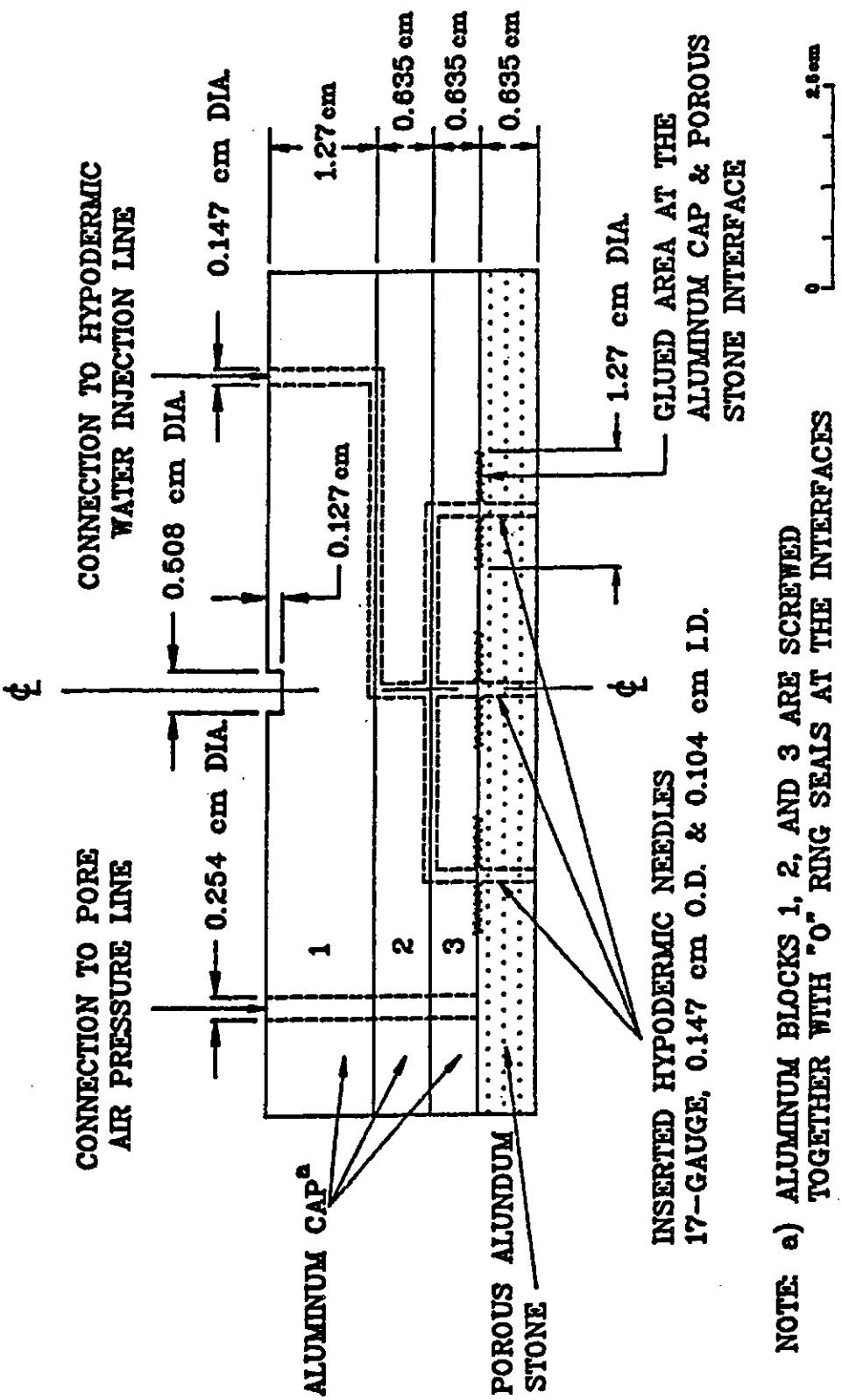

NOTE: a) ALUMINUM BLOCKS 1, 2, AND 3 ARE SCREWED TOGETHER WITH "O" RING SEALS AT THE INTERFACES

Figure 4.18a Front view of the Loading Cap Complex for the Stress Controlled Isotropic Cell

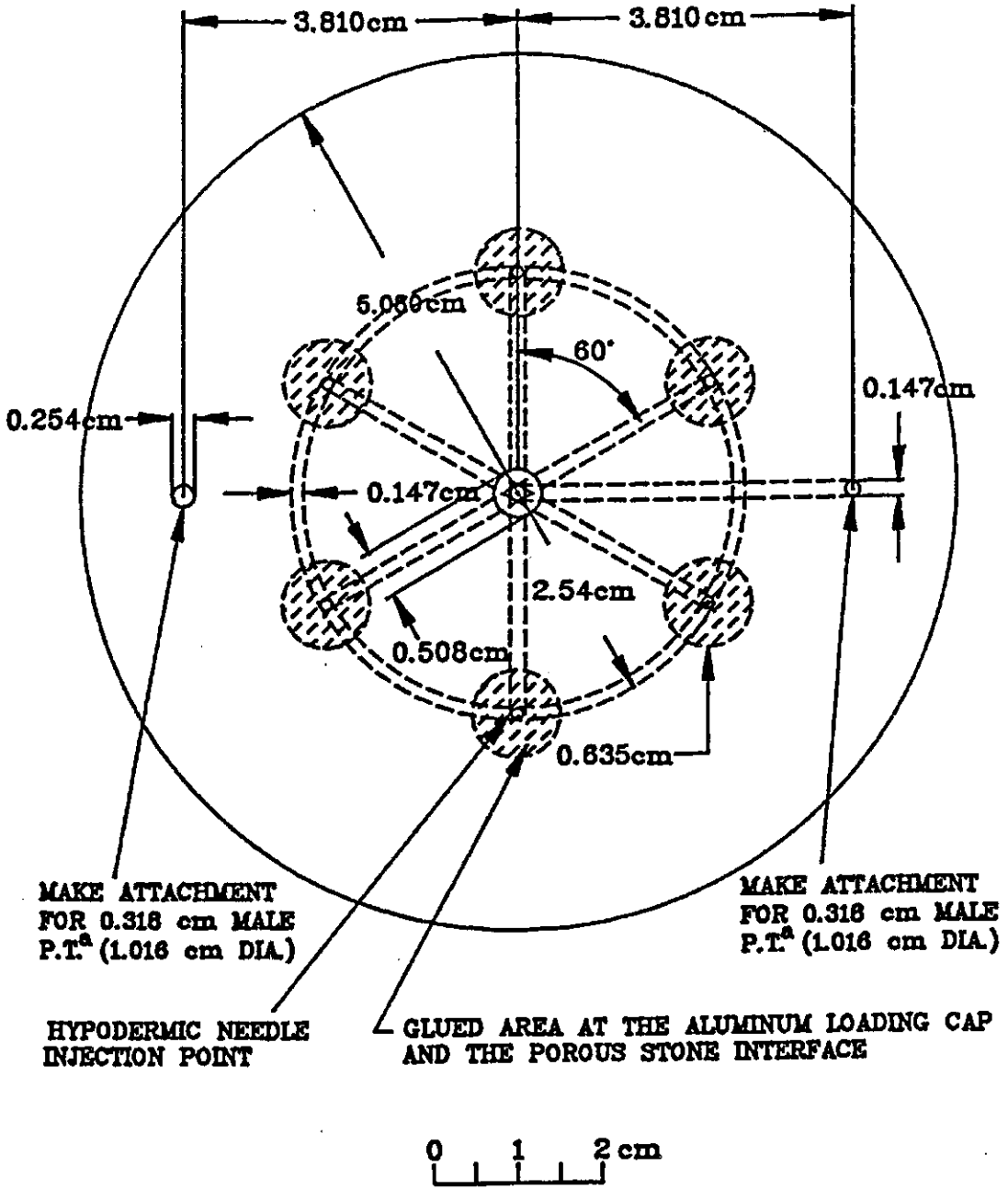

NOTE: a) P.T. MEANS PIPE THREAD

Figure 4.18b Top view of the Loading Cap Complex for the Stress Controlled Isotropic Cell

forced through the high air entry disc.

The vertical displacement of the specimen was measured using a LVDT with the plunger resting on the loading cap (Figure 4.14). The lateral strain of the specimen was measured using a "Non-Contacting Displacement Measuring System" manufactured by the Kaman Sciences Corporation at Colorado Springs, Colorado. Two types of sensors, KD2300-2S and KD2310-6U were used corresponding to different displacement ranges (i.e., 2.5 mm and 6.0 mm). Two sensors were located across the diameter of the specimen (Figure 4.19). Two aluminum targets (i.e., 25.4 mm by 38.1 mm) were attached to the specimen surface opposite the sensors. The aluminum targets were made from four folds of heavy duty commercial aluminum foil, 8×10^{-3} mm thick. The measuring system operates on the eddy-current loss principle between the conductive surfaces of the aluminum targets and the electronic transducers. As the conductive surface moves closer to the transducer, more eddy currents are generated and the losses within the bridge circuit of the oscillator demodulator become greater. When the conductive surface moves away from the transducer, the losses become less. These impedance variations are converted to a DC voltage. The lateral displacement measurements were combined with the vertical displacements so that the total volume of the specimen could be monitored continuously.

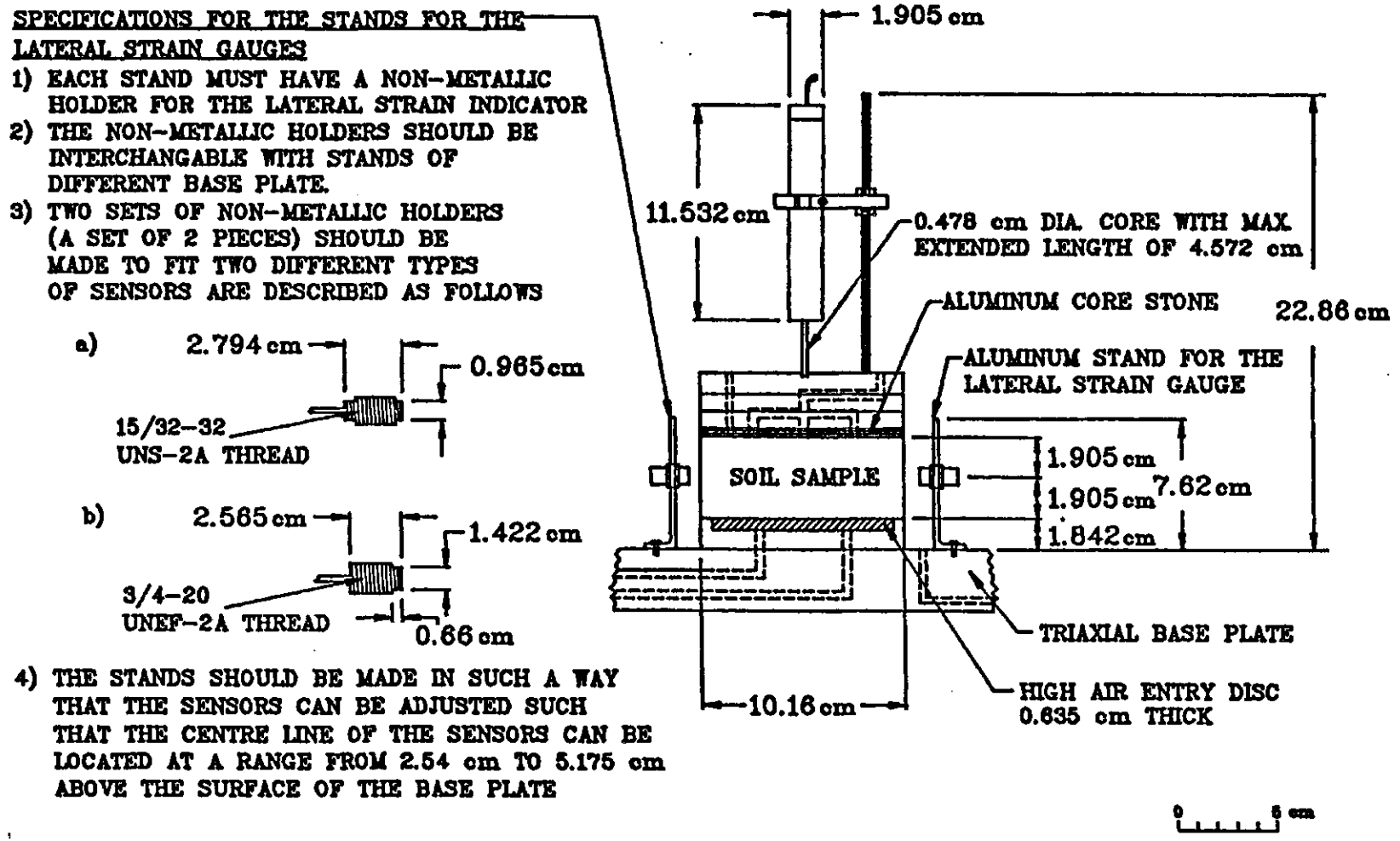

Figure 4.19 Schematic Layout for the Strain Measuring Devices inside the Stress Controlled Isotropic Cell

4.3.3 Plumbing layout and data collecting system

A board of plumbing was required to support the operation of both the modified Anteus consolidometer and the stress controlled isotropic cell (Figure 4.20). The pore-water pressure was controlled through an air-water reservoir, whereas the total stress and the pore-air pressures were regulated directly from an air pressure line. The plumbing allowed for the independent regulation of the total stress, the air and water pressures as well as the back pressure that was applied to the diffused air volume indicator. The hypodermic water injection system operated on a separate pressurized air-water reservoir system with an independent double burette water volume change indicator (Figure 4.21). In addition to mechanical gauges, pressure transducers were used to continuously monitor the cell, pore-air and pore-water pressures.

An electronic data analogue system was used for data collection and processing.* The signals from the transducers were converted to pressures and displacements with the assistance of a modified version of the standard Basic 8082A/Pet/C64 software package that accompanied the

---

* Model 8082A electronic measuring system, manufactured by Sciemetric Instruments, Division of Sheaff and Associates Engineering Inc., P.O. Box 1048, Manotick, Ontario.

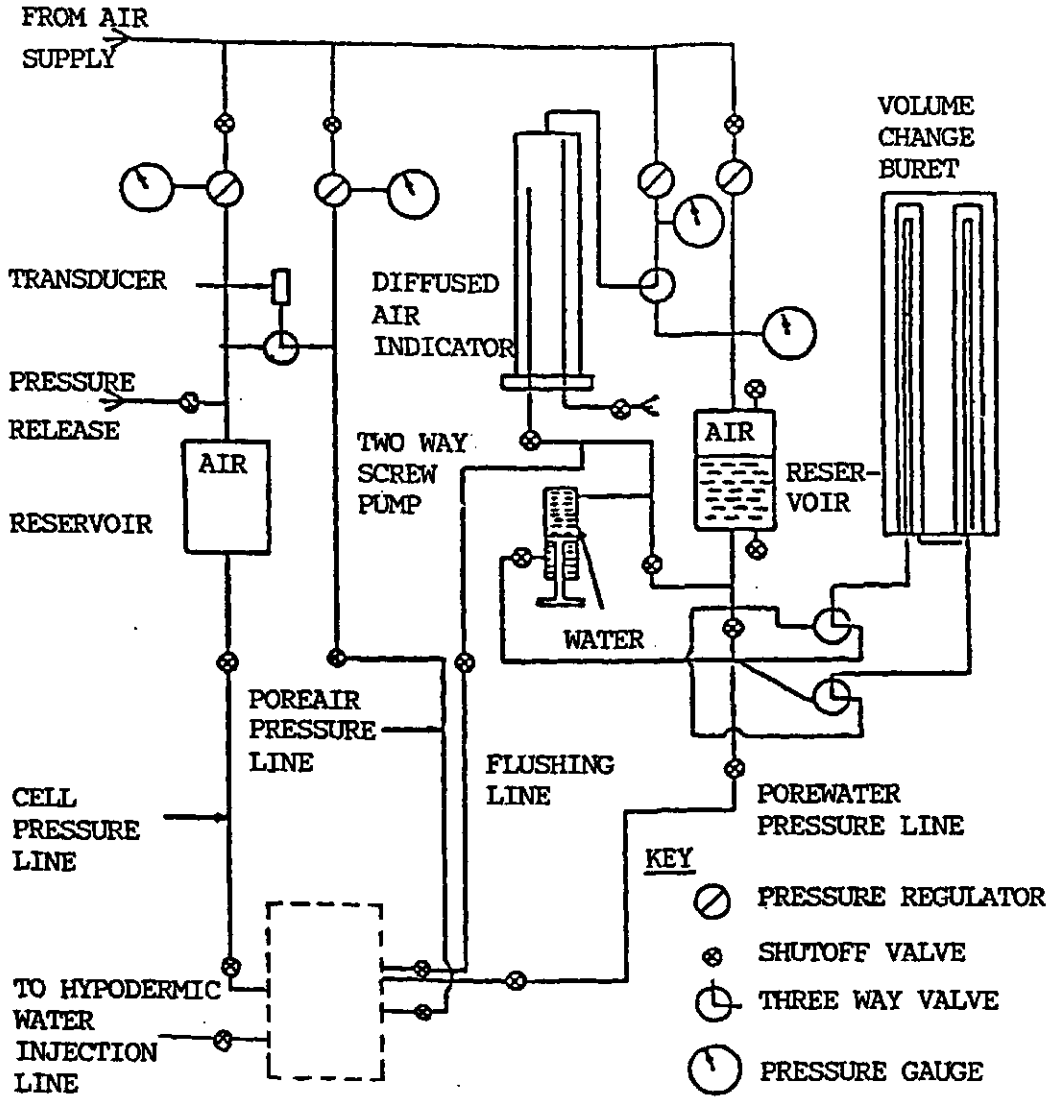

Figure 4.20 Schematic Diagram of Plumbing Layout for the Modified Anteus Consolidometer and Stress Controlled Isotropic Cell

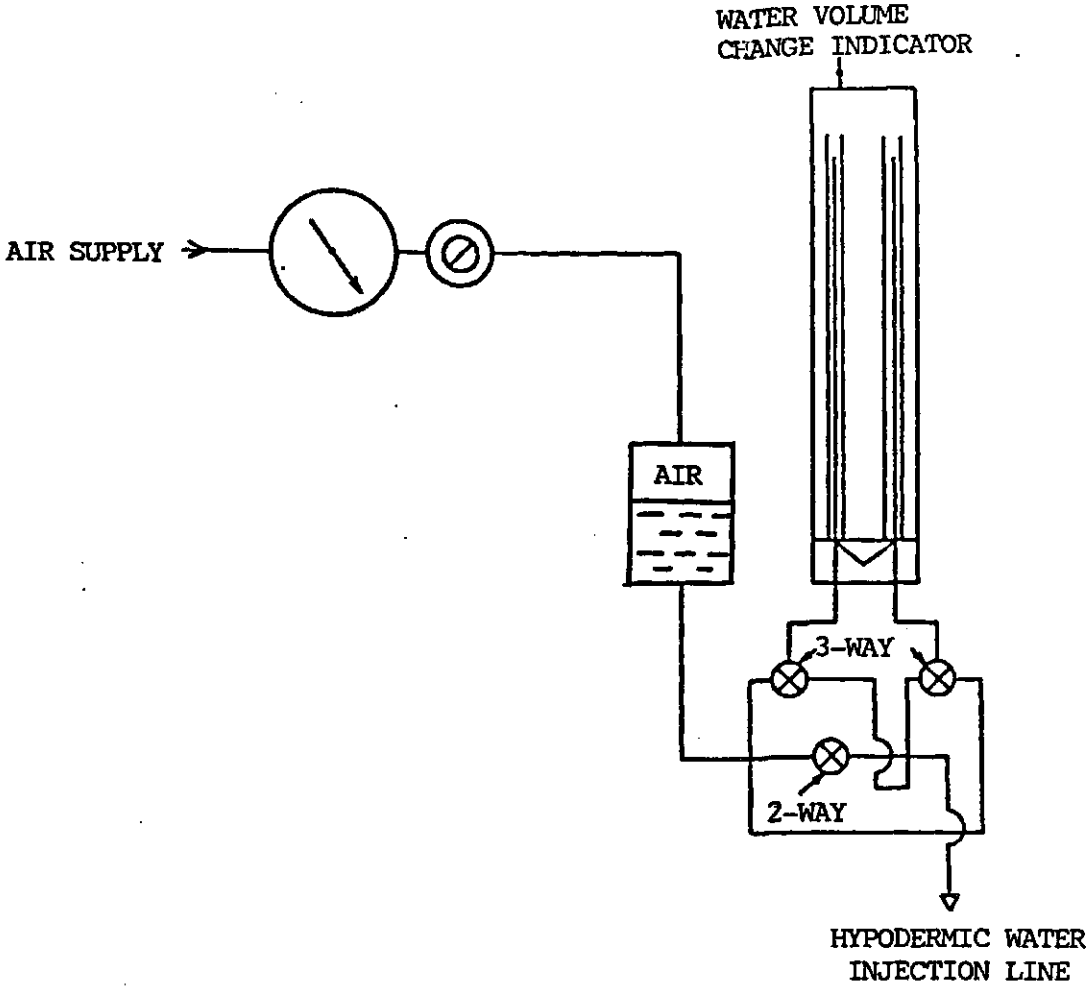

Figure 4.21 Schematic Diagram of Plumbing Layout for the Hypodermic Water Injection Line

8082A electronic measuring system. Listings of the programs for sensor calibrations and data processing are shown in Appendix A. Details concerning the 8082A electronic measuring system can be found in the "Model 8082A Electronic Measurement System Application Notes" published by the manufacturer in 1986.

4.4 Program

The test program was directed towards establishing the form of the constitutive surfaces. Two sub-programs were performed to achieve this purpose. Sub-program I tested soils under stress changes involving no lateral expansion. The term "no lateral expansion", indicates K_o loading conditions as long as there is a tendency for lateral expansion. Since lateral shrinkage can also occur, under this condition, K_o conditions are not always satisfied. Sub-program II tested soils under isotropic changes of total stress and matric suction. In this section, each of the two sub-programs are separately presented. The objective, procedure and analysis of each type of test are highlighted.

4.4.1 Zero lateral expansion loading and unloading conditions

A layout of the sub-program I is shown in Table 4.3. The tests involved in the program are as follows.

1) Null pressure plate test (PPT)

The null pressure plate test was used to establish the initial matric suction, $(u_a - u_w)_i$ of a specimen. The pressure plate apparatus is shown in Figure 4.22. The initial matric suction of a specimen was obtained using the null, axis-translation technique (Hilf, 1956). The testing procedure and method of data analysis are in accordance with those presented by Fredlund (1969); Bocking and Fredlund (1980).

2) Suction test (ST)

The suction test was used to obtain the loading curve of water content versus matric suction. The stress path adhered to in the test is shown in Figure 4.23. The test was conducted in two stages. A 507 kPa multi-layered, pressure plated apparatus (Figure 4.24) was used for the first stage while a 1520 kPa pressure membrane apparatus (Figure 4.25) was used for the second stage. The test procedure is as follows.

a) The specimen was weighed and set onto the 507 kPa pressure plate.

b) The initial matric suction, $(u_a - u_w)_i$, determined previously using the null pressure plate test was

Table 4.3 Layout of The Sub-Program I

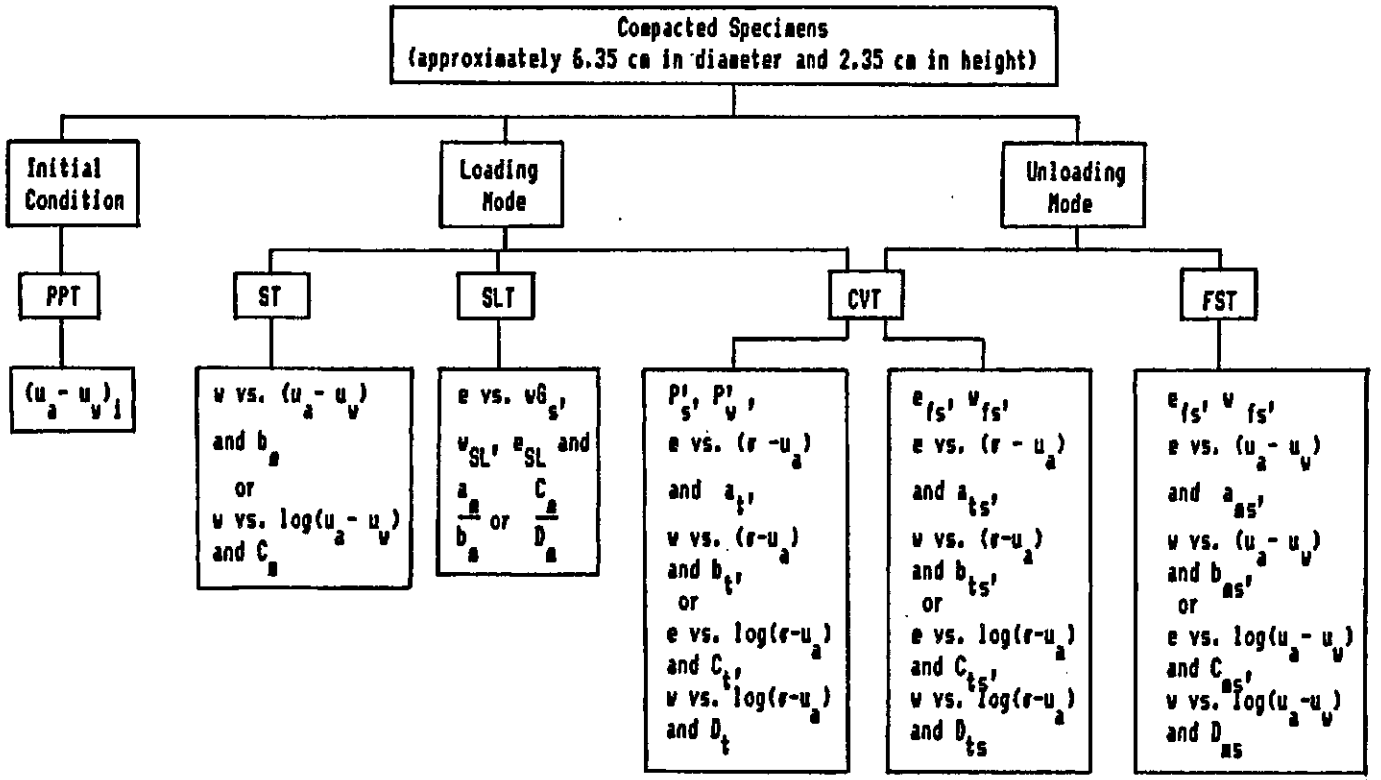

Legend	Description
PPT	Null pressure plate test performed with a 507 kPa pressure plate apparatus
ST	Suction test performed with first a 507 kPa pressure plate apparatus and then a 1520 kPa pressure membrane apparatus
SLT	Unconfined shrinkage test
CVT	Constant volume loading and unloading test performed with a pneumatic oedometer
FST	One-dimensional free swell test performed with a modified anteus consolidometer
Subscript, "SL"	Specific soil parameter at the shrinkage limit "SL"

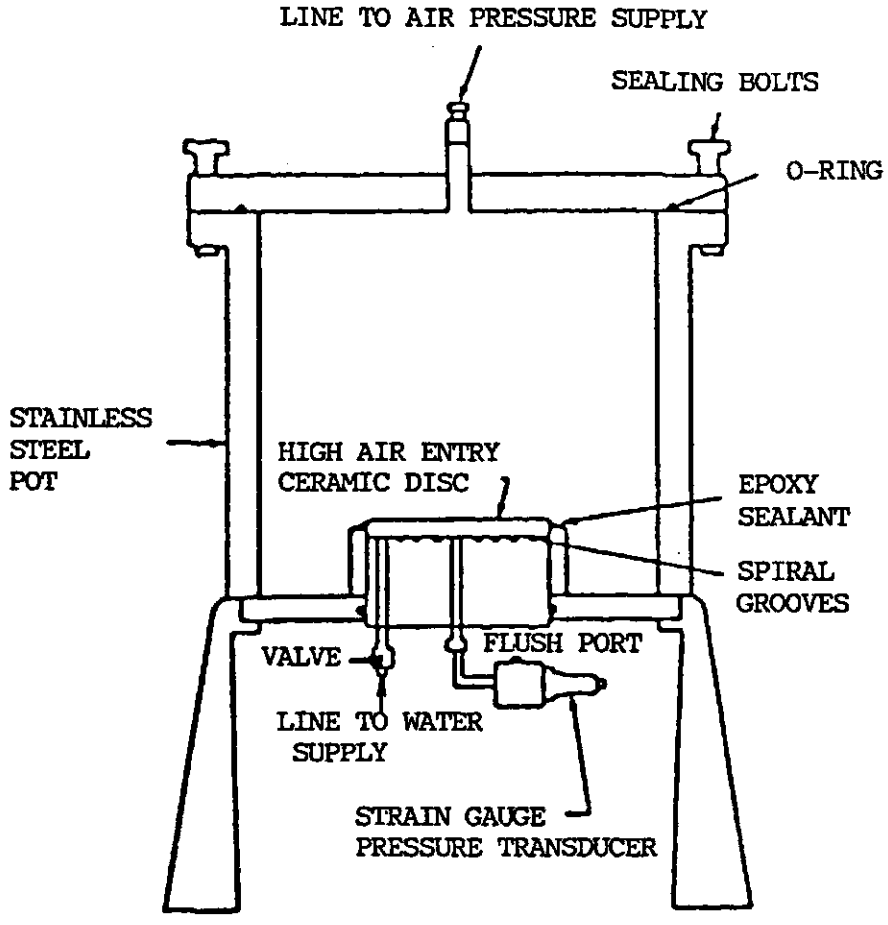

Figure 4.22 University of Saskatchewan Pressure Plate Apparatus (Blocking and Fredlund, 1980)

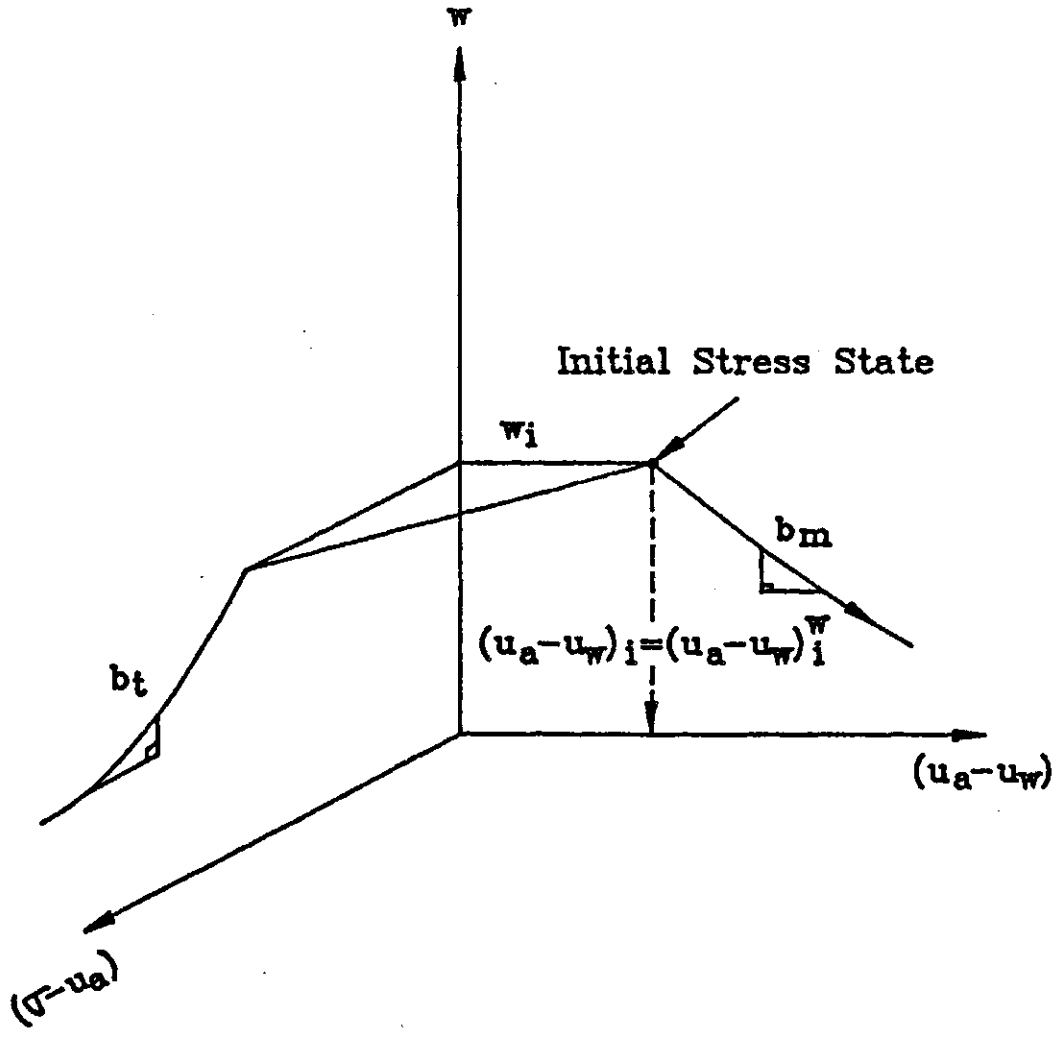

Figure 4.23 Stress Path of the Suction Test, ST in Terms of the Water Content, w

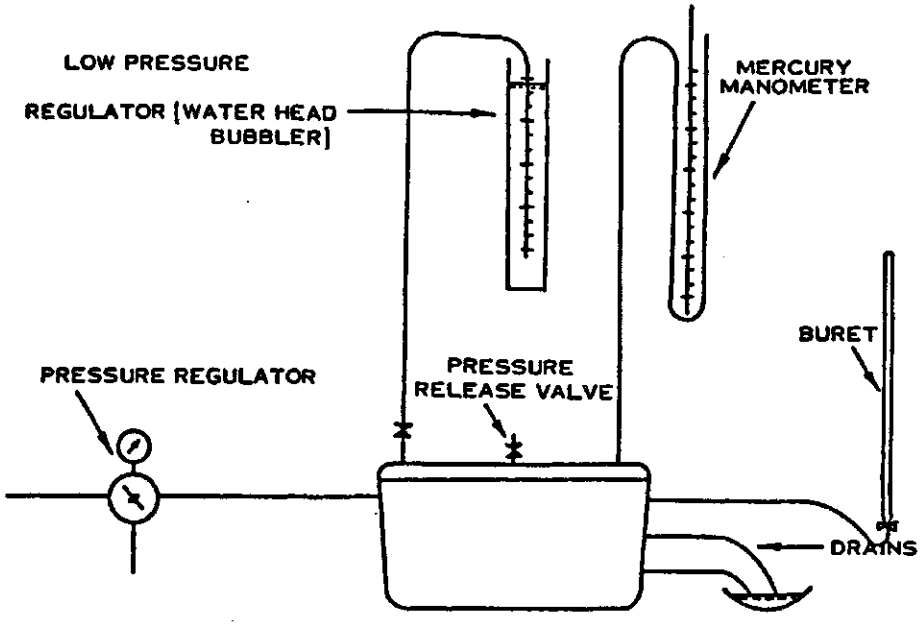

SETUP OF PRESSURE PLATE EXTRACTOR

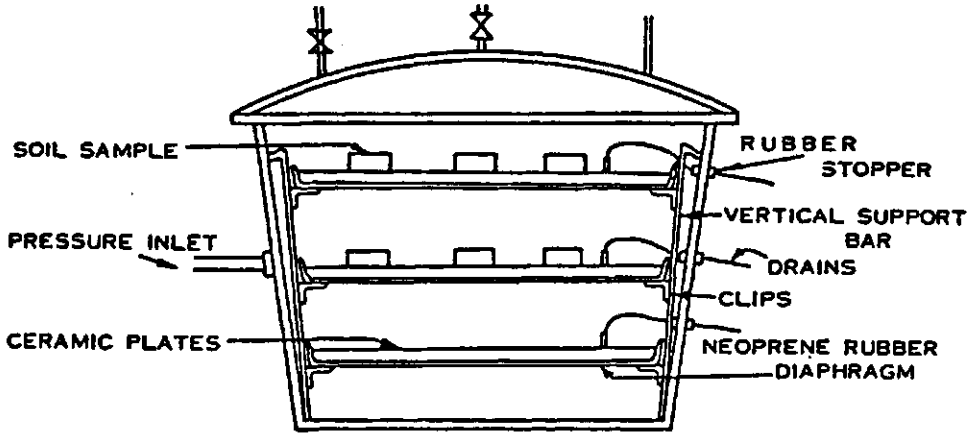

Figure 4.24 Multi-Layered Pressure Plate Apparatus (Fredlund, 1964)

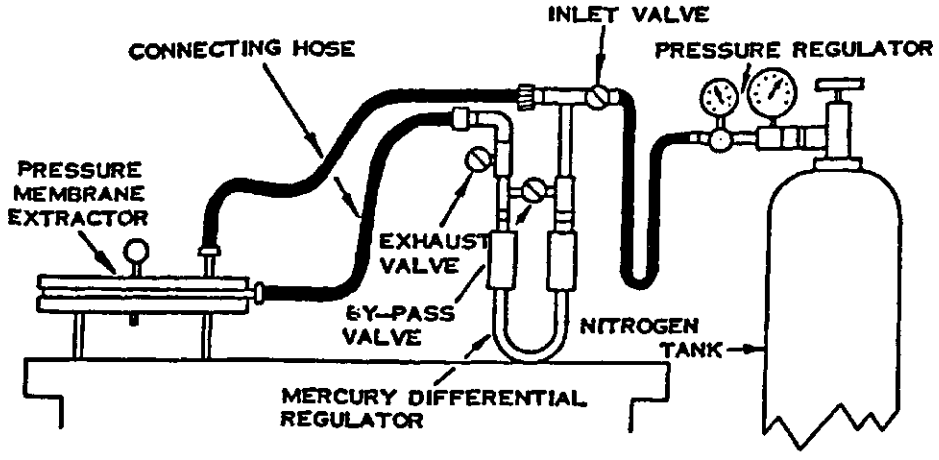

SETUP OF PRESSURE MEMBRANE EXTRACTOR

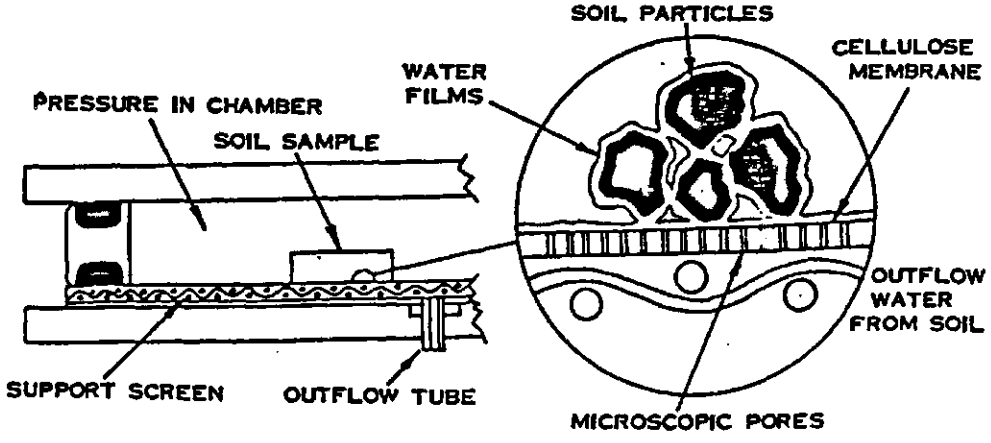

SECTION VIEW OF EXTRACTION PROCESS

Figure 4.25 Pressure Membrane Apparatus (Fredlund, 1964)

applied to the specimen which was left to equalize. The equilibrium time required between matric suction changes was estimated to be 2 and 23 hours for silt and till specimens respectively. A uniform 48 hour equalization period was used. Details are presented in Appendix B-2.

c) Starting from the initial matric suction, $(u_a - u_w)_i$, the specimen was desaturated by increasing the suction, $(u_a - u_w)$ in increments. When the 507 kPa capacity of the pressure plate apparatus was reached, the specimen was transferred to the 1520 kPa pressure membrane apparatus and the desaturation process was continued. Under each new suction, the equilibrium water content was measured. The oven-dried weight of the specimen was then measured.

The water content versus matric suction loading curve is plotted for the specimen (Figure 4.23). As a result, the modulus, b_m or D_m with respect to water content can be computed.

3) Unconfined shrinkage test (SLT)

The unconfined shrinkage test was used to establish the water content versus void ratio curve for a soil undergoing unconfined shrinkage (see Section 3.5.3.2). The standard ASTM procedure and equipment was used. The mercury submersion procedure used to measure the volume of the specimen was checked by using an independent, direct measurement technique and a resin-coating submersion

procedure (Hamberg, 1985). The direct measurement technique involves measuring the specimen diameter using a micrometer, and measuring the thickness of the thin specimen using a dial gauge. Attempts were made to develop a practical alternative to the mercury submersion technique for measuring the volume of a specimen. The test procedure is as follows.

a) A specimen of known initial water content was weighed. The initial volume of the specimen was first determined using one or a combination of the volume measuring technique. The results were recorded.

b) The specimen was then left to air-dry.

c) At regular time intervals, the mass of the specimen was determined as well as the specimen volume. One or a combination of the volume measuring techniques was used.

d) When the air dry process appeared to be ineffective in further reducing the water content, a desiccator was used to further dry the specimen. Once again the specimen was weighed and its volume was measured at regular time intervals.

e) When the desiccator was ineffective in further drying the specimen, the specimen was oven-dried at 125 ^{o}C for 48 hours. The oven-dried mass of the specimen and the corresponding sample volume was determined using one or a combination of the volume measuring techniques.

The water content versus void ratio curve for the

specimen can then be plotted from the test data. The slope of the curve, $\frac{de}{dw}$, gives the moduli ratio, $\frac{a_m}{b_m}$ or $\frac{C_m}{D_m}$, of the soil as the matric suction of the soil increases. Combining this information with the loading curve for the water content versus matric suction, gives the loading curve for the soil structure or the void ratio versus matric suction. In other words, the variation of the modulus, a_m or C_m with increasing suction and decreasing void ratio can be plotted.

4) Constant volume loading and unloading test, CVT

This test is commonly referred to as the "constant volume oedometer test" (Fredlund, 1969). Conventional oedometers were used. The stress paths of the test in terms of void ratio, e, and water content, w, are shown in Figure 4.26. The test procedure is as follows.

a) The specimen was prepared with a known initial water content, w_i and void ratio, e_i. The specimen was placed in the oedometer.

b) The initial matric suction $(u_a - u_w)_i$ of the specimen was reduced by immersing the specimen in water. At the same time, load was applied to the specimen in order to maintain a constant volume.

c) When the specimen exhibited no further tendency to swell, the "uncorrected" swelling pressure had been reached (Fredlund, 1983). The specimen was further loaded to give the loading curve for the soil structure

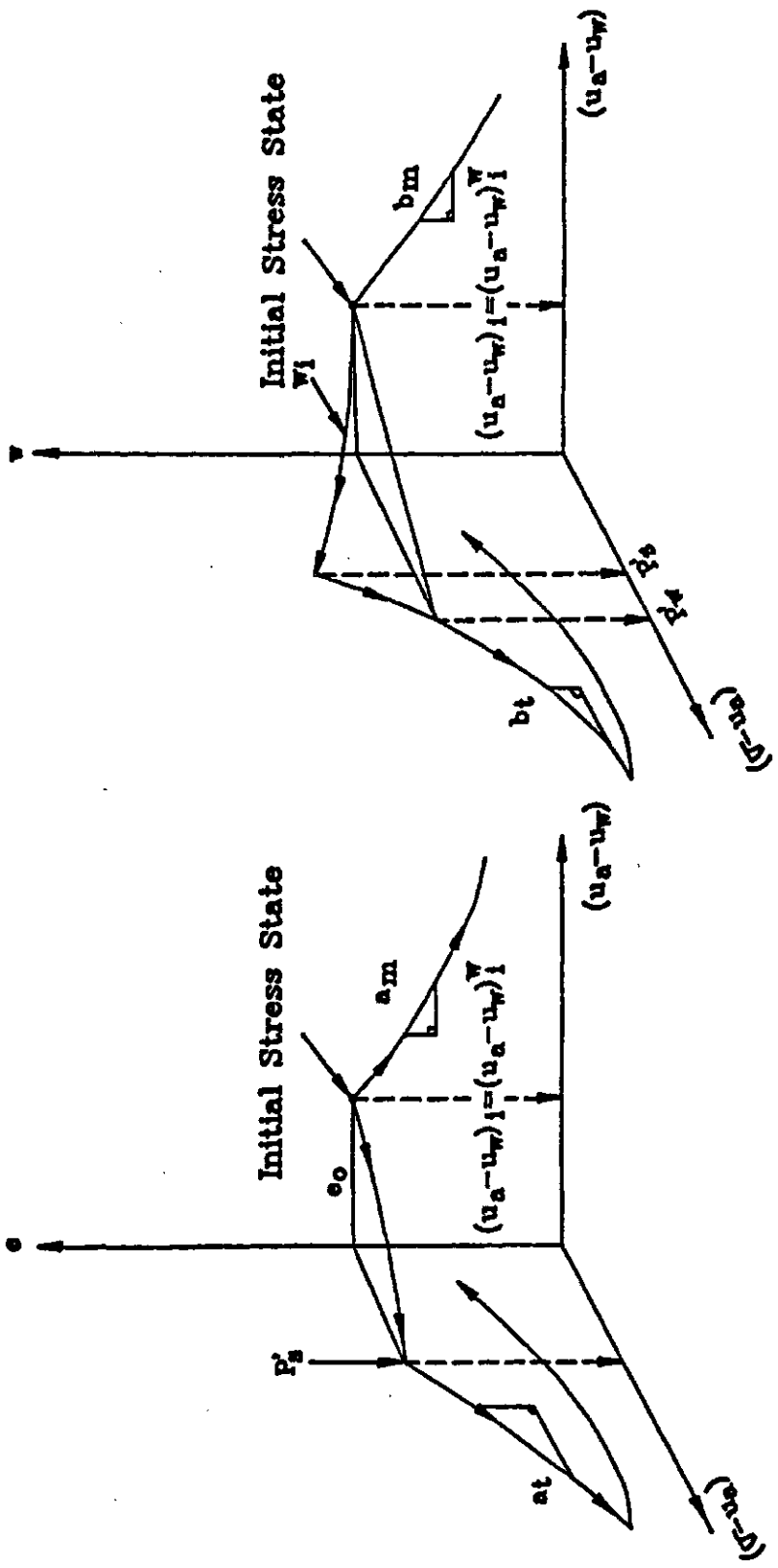

Figure 4.26 Stress Path of the One-Dimensional Constant Volume Loading Test, CVT

and water phase in terms of void ratio, e, and water content, w, versus the stress state variable, $(\sigma - u_a)$.

d) When the specimen was loaded to the capacity of the oedometer, the specimen was unloaded in decrements to a nominal stress.

The corrected swelling pressure, P_s' and the characteristic stress state, P_w' of the specimen can then be established from the test data (Figure 4.26). The variation of the moduli, a_t and b_t or C_t and D_t with void ratio, e, and water content w, can also be computed. Unloading curves with respect to the stress state variable, $(\sigma - u_a)$ are approximately parallel to one another on the saturation plane (Lambe and Whitman, 1969). Therefore, the unloading curve established at the end of the loading sequence, can also be taken as the unloading curve of the specimen from its initial state (Figure 4.26). The free swell void ratio, e_{fs}, and water content, w_{fs}, can be obtained along with the variation of the moduli, a_{ts} and b_{ts} or C_{ts} and D_{ts}, with respect to void ratio and water content.

5) One dimensional free swell test, FST

A modified Anteus consolidometer was used to perform the one dimensional free swell test. The stress paths of the test in terms of void ratio and water content are illustrated in Figure 4.27. The modified Anteus consolidometer allows the simulation of K_o conditions (i.e., no lateral expansion) when the soil swells. The test

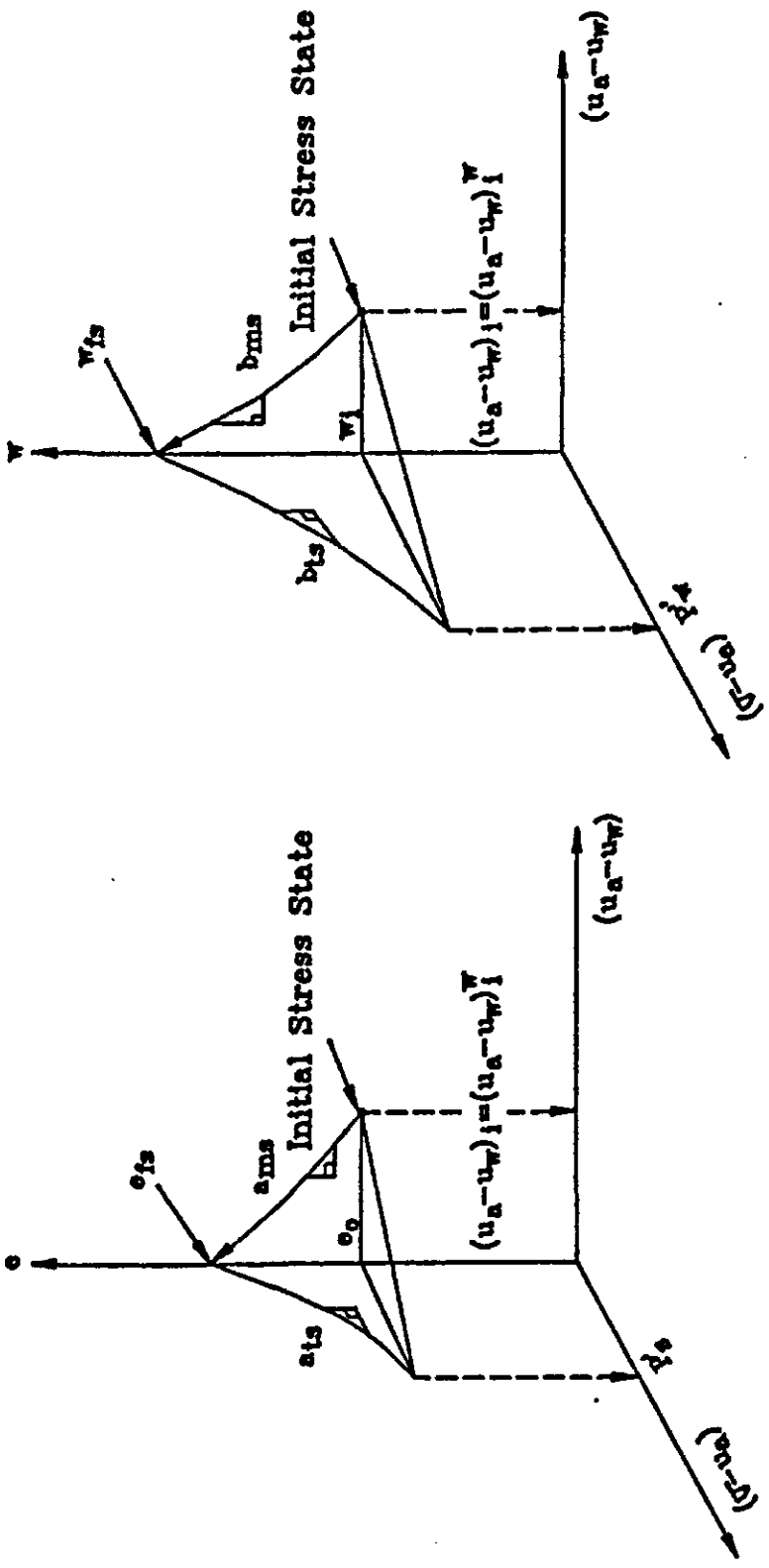

Figure 4.27 Stress Path of the One-Dimensional Free Swelling Test, FST

procedure is as follows.

a) The specimen was placed into a modified Anteus consolidometer. The initial matric suction, $(u_a - u_w)_i$ of the specimen was pre-determined by running a null pressure plate test on a similar specimen. The specimen was left to come to equilibrium under a zero total stress and its initial matric suction.

b) The matric suction of the specimen was gradually reduced by adding water through the hypodermic water injection system.

c) The saturation process was continued until the matric suction was reduced to a nominal value of approximately 5 kPa. During the test, changes in the pore-water pressures, u_w, pore-air pressure, u_a, specimen volume, and the amount of water entering or leaving the specimen were monitored. The volume of diffused air was measured twice daily and applied as a correction to the water volume changes.

The test data provide the unloading curves for void ratio and water content, versus matric suction. The variation of the moduli, a_{ms} and b_{ms}, or C_{ms} and D_{ms} with respect to void ratio and water content, respectively, can be computed. In addition, the free swell void ratio, e_{fs}, and free swell water content, w_{fs}, can also be obtained (Figure 4.27).

Sub-program I as described in the preceding pages

establishes the characteristic stress states, P'_s, P'_w and $(u_a - u_w)_i$ the loading and unloading curves of the soil structure and the water phase on the net total stress, $(\sigma - u_a)$ and matric suction, $(u_a - u_w)$ planes. All tests correspond to zero lateral expansion conditions. The test data will allow the constitutive surfaces of the soil under monotonic loading and monotonic unloading to be defined. Subsequently, the results will establish the variation of the moduli with changing states of stress.

4.4.2 Isotropic loading and unloading conditions

Sub-program II was designed to obtain experimental results indicating the relationships between the various moduli under isotropic loading and unloading conditions. A description of the program is provided in Table 4.4. Three of the five tests in sub-program II are the same as those described in sub-program I. Details concerning the null pressure plate test, PPT, suction test, ST and the unconfined shrinkage test, SLT are described in Section 4.4.1. Other tests involved in the sub-program II are as follows.

1) Isotropic constant volume loading and unloading test, TCVT

A specially equipped stress controlled isotropic cell (see Section 4.3.2) was needed to perform the test. The cell must be capable of accurately measuring the total

Table 4.4 Layout of The Sub-Program II

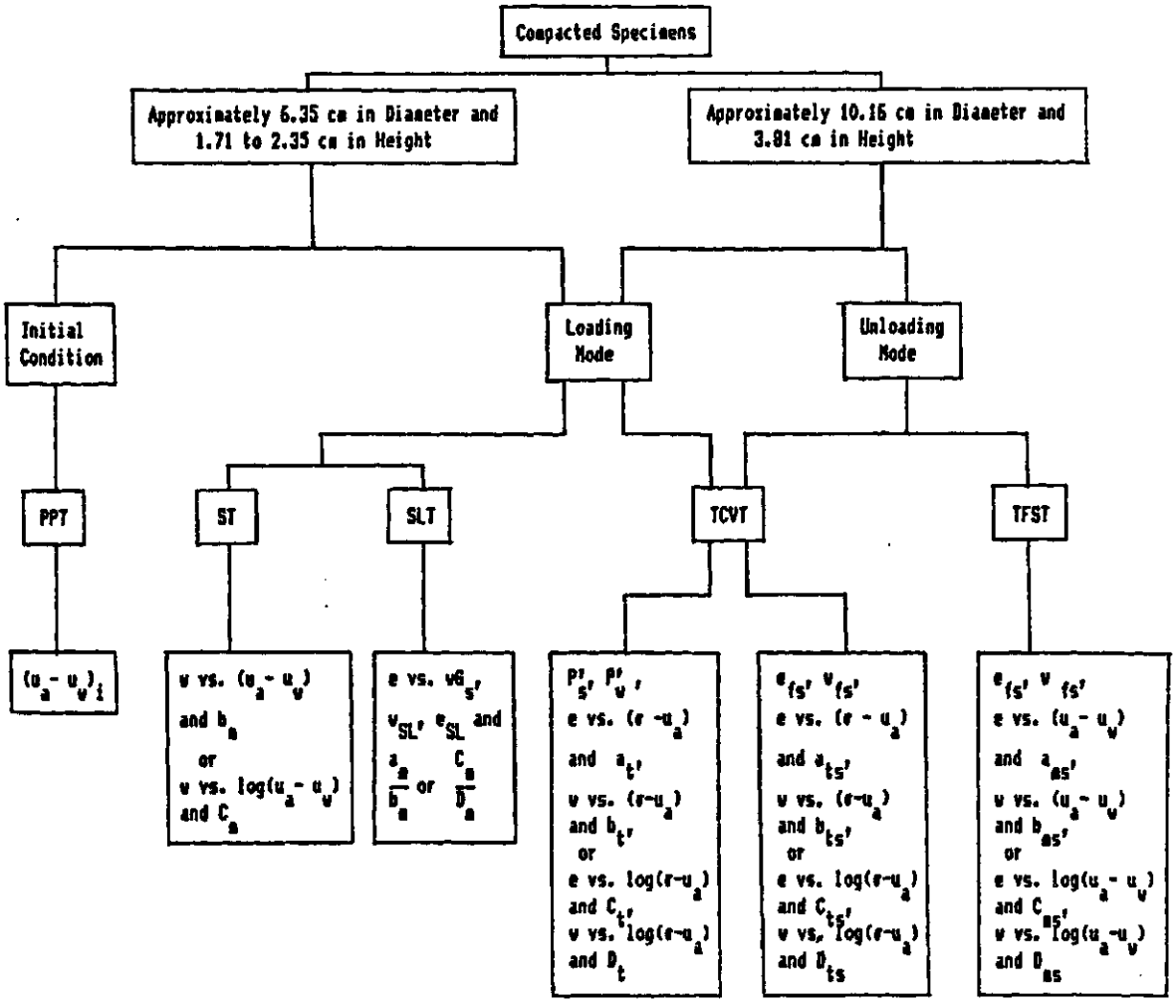

Legend	Description
PPT	Null pressure plate test performed with a 507 kPa pressure plate apparatus
ST	Suction test performed with first a 507 kPa pressure plate apparatus and then a 1520 kPa pressure membrane apparatus
SLT	Unconfined shrinkage test
TCVT	Isotropic constant volume loading and unloading test performed with a stress controlled isotropic cell
TFST	Isotropic free swell test performed with a stress controlled isotropic cell
subscript, "SL"	Specific soil parameter at the shrinkage limit

volume change of the specimen under different applied stress conditions. In order to shorten the flow path for water, a specimen 3.81 cm high was used. The stress paths of the test are the same as those shown for the one-dimensional constant volume loading and unloading test, CVT (Figure 4.26) (see Section 4.4.1). The test procedure is briefly outlined as follows.

a) A specimen was prepared with a known initial void ratio, e_i, water content, w_i and matric suction, $(u_a - u_w)_i$. The specimen was placed into the stress controlled isotropic cell.

b) The amount of water required to saturate the specimen was determined from the volume-mass relations for the soil. The initial matric suction, $(u_a - u_w)_i$ of the specimen was gradually reduced by injecting water into the specimen through the hypodermic water injection system. The water injection process was performed in increments with a simultaneous reduction in the pore-air and pore-water pressures. At the same time, the cell pressure, σ was increased to maintain the specimen at a constant volume.

c) When the specimen exhibited no further tendency to swell, the "uncorrected" swelling pressure, P_s was reached (Fredlund, 1983). The specimen was further loaded isotropically in increments to define the loading curve.

d) When the specimen was loaded to the capacity of the stress-controlled isotropic cell, the specimen was unloaded in decrements to a nominal total stress of 5 to 10 kPa.

e) During the test, the change in volume of the specimen and the amount of water entering or leaving the specimen were monitored. The basal compartment of the stress controlled isotropic cell was flushed twice a day. Diffused air that accumulated underneath the high air entry disc was measured using the diffuse air volume change indicator (see Section 4.3.1).

The corrected swelling pressure, P_s' , and the characteristic stress state, P_w' , of the specimen can be obtained from the test data. Variations of the moduli, a_t or C_t and b_t or D_t with changing void ratio and water content can then be computed. The free swelling void ratio, e_{fs}, and water content, w_{fs}, can be established along with variation of the moduli, a_{ts} or C_{ts} and b_{ts} or D_{ts}, from the unloading portion of the test. The interpretation of the data involves the assumption that the unloading curves on the net total stress plane are approximately parallel to one another (Lambe and Whitman, 1969). Subsequently, the unloading curve established at the end of the loading sequence can be taken as the unloading curve of the specimen from its initial state (Figure 4.26) (see Section 4.4.1).

2) Isotropic free swell test, TFST

The isotropic free swell test was used to determine the unloading curves for the soil structure and the water phase on the matric suction plane. The stress paths are essentially the same as those described for the one-dimensional free swell test, FST (Figure 4.27) (see Section 4.4.1). The stress controlled isotropic cell equipped (see Section 4.3.2) with the lateral strain monitoring system and the hypodermic water injection device was used for this test. The test procedure is as follows.

a) A specimen of approximately 101.6 mm in diameter and 38.1 mm in height with a known initial void ratio, water content and matric suction was prepared and place into a stress controlled isotropic cell.

b) The initial applied stresses on the specimen were set to produce the initial stress state of the specimen (i.e., $(u_a - u_w) = (u_a - u_w)_i$ and $(\sigma - u_a) = 0$). The specimen was allowed to reach equilibrium under the applied stresses.

c) The amount of water required to saturate the specimen was estimated from the volume mass properties of the soil. The suction in the specimen was reduced in three decrements during the saturation process. The volume of water required by the specimen for each decrement was estimated form the total amount of water required to saturate the specimen. At each of the suction reduction stages, the applied cell pressure, air and water

pressures were decreased. The estimated amount of water required to bring the specimen to equilibrium at the new imposed stress state was then added through the hypodermic water injection device. The specimen was then allowed to come to equilibrium.

d) Step (c) was repeated until the specimen was saturated. The specimen volume and the volume of water entering or leaving the specimen were continuously monitored. The volume of diffused air was measured twice daily. Corrections were made to the measure water volume change of the specimen.

From the test data, the free swell void ratio, e_{fs}, and water content, w_{fs}, can be obtained. The variation of the moduli, a_{ms} or C_{ms} and b_{ms} or D_{ms} with changing void ratio and water content can then be established for isotropic free swelling of the soil.

Sub-program II provides test data on the characteristic stress states, P_s' , P_w' and $(u_a - u_w)_i$, the loading and unloading curves for the soil structure and the water phase on both the net total stress and matric suction planes. This data is for isotropic stress conditions.

CHAPTER V

PRESENTATION OF TEST RESULTS

5.1 Introduction

This chapter presents experimental results from tests performed under the test program (Section 4.4). Description of the equipment setup and operation, and results of individual tests are briefly described in this chapter. There is a one to one correspondence between the format for the information presented in this chapter and the outline of the program presented in chapter 4. Details are presented in the appendices as specified.

5.2 Tests to Evaluate the Initial Suction of the Specimens

The null pressure plate test was used to determine the initial matric suction of the soil. The pressure plate apparatuses and accessories used were prepared and tested in accordance to procedures suggested by Fredlund in 1973. The setup of the equipment, the procedures and the results are presented in Appendix B-1.

Three null pressure plate tests (i.e., PP1DS, PP2DS and PP3DS) were performed on silt specimens with water contents dry of optimum, at approximately 15.65%. Test

PP1DS was abandoned shortly after the test started when the data acquisition system failed. A leak through the epoxy seal at the base pedestal was observed during test PP2DS and as a result it was abandoned. Data collected for test PP3DS are presented in Figure 5.1. During the test, diffused air accumulated underneath the high air entry disc continued to increase the pore-water pressure measured at the basal compartment of the pressure plate apparatus. The base was flushed regularly to obtain pore-water measurements representing the stress state of the specimen. The initial matric suction of the specimen is taken as the applied air pressure which produces a zero water pressure measured at the basal compartment. The initial matric suction of the specimen in test PP3DS is 117.5 kPa.

Two null pressure plate tests (i.e., PP10S and PP20S) were carried out on silt specimens with an optimum initial water contents of approximately 19.0%. Shortly after test PP10S started, a leak through the fitting attached to the flush-port was found. The test was abandoned. Data collected for test PP20S are shown in Figure 5.2. The initial matric suction of the specimen is considered to be 100 kPa.

The initial matric suction of the glacial till specimens was determined from published water content versus suction curves (Krahn and Fredlund, 1972). Details of the determination are discussed in Chapter VI.

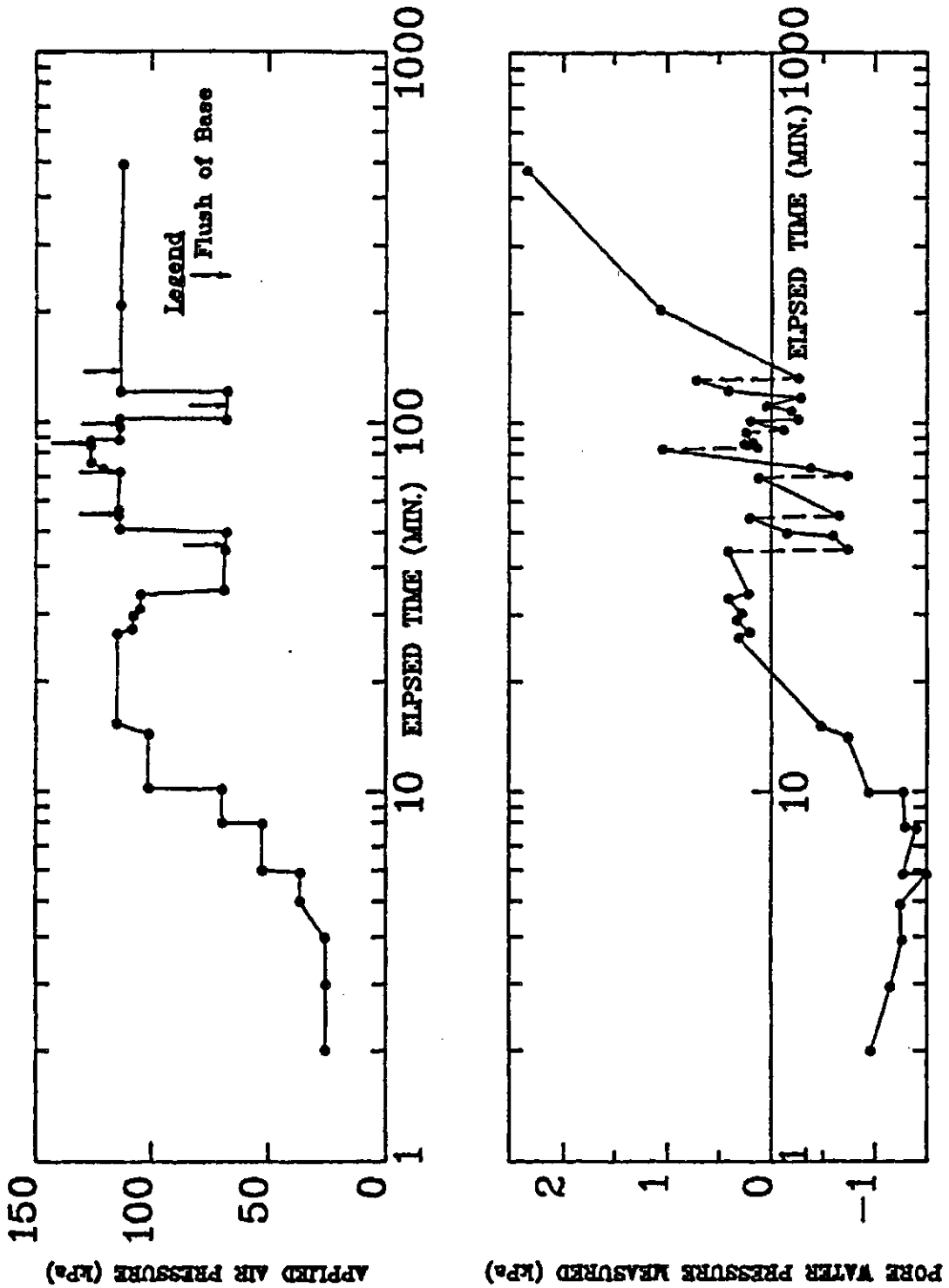

Figure 5.1 Null Pressure Plate Test Results for Specimen PP3DS

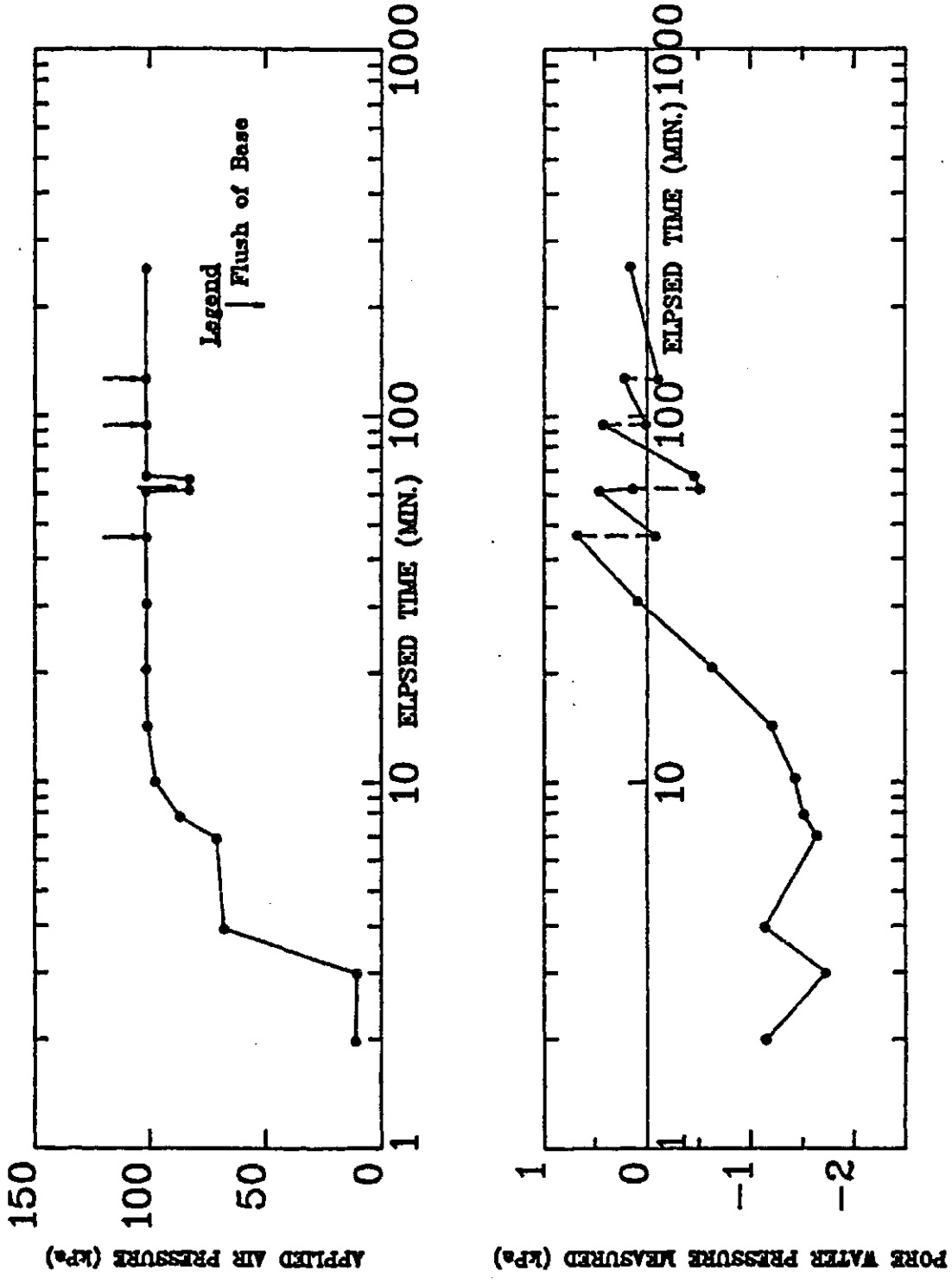

Figure 5.2 Null Pressure Plate Test Results for Specimen PP2OS

5.3 Test to Establish the Water Content versus Increasing Matric Suction Relation

Suction tests were used to establish the water content versus increasing matric suction relation. The multi-layered pressure plate and pressure membrane apparatuses used were prepared as discussed in Appendix B-2a. The equalization time required for each matric suction change was estimated to be 2 and 23 hours for the silt and the glacial till specimens, respectively (see Appendix B-2b). A uniform 48 hour equalization period was used for all tests.

A total of 23 suction tests were performed. A summary of the test results is given in Table 5.1a and 5.1b. Five suction tests (i.e., ST1, ST2, ST3, ST4 and ST5) were conducted on silt specimens with an initial water content dry of optimum, at approximately 15.6%. Tests ST1 and ST2 were trial tests. It was during these tests when it was decided to record the dimensional changes (i.e., changes in diameter and thickness) of the specimen in addition to water content changes. Test specimen ST3 was accidentally disturbed when it was being transferred from the pressure plate to the pressure membrane apparatus. The test was abandoned.

Nine suction tests (i.e., ST6, ST7, ST8, ST9, ST10, ST11,ST12, ST13 and ST14) were performed on silt specimens with an initial water content at optimum, at approximately

Table 5.1a Summary of Suction Test Results on the Water Content Changes

SOIL TYPE	TEST NO.	INITIAL e_o	INITAL $w_i G_s$	wG_s AT $(u_a - u_v)$ 304 kPa	507kPa	1014 kPa	1520 kPa
DS	ST1	*	0.4245	0.3825	0.3769	0.3367	0.3051
DS	ST2	*	0.4205	0.3511	*	0.3263	0.3151
DS	ST3	0.7037	0.4214	0.3945	0.3820	*	*
DS	ST4	0.6965	0.4236	0.3958	0.3817	0.3345	0.3094
DS	ST5	0.6964	0.4243	0.3950	0.3845	0.3340	0.3106
OS	ST6	0.6163	0.5117	0.4626	0.4538	*	*
OS	ST7	0.6140	0.5139	0.4605	0.4509	*	*
OS	ST8	0.6131	0.5161	0.4641	0.4587	*	*
OS	ST9	*	*	ABORTED	*	*	*
OS	ST10	0.6220	0.5172	0.4661	0.4627	0.4255	*
OS	ST11	0.6313	0.5116	0.4460	0.4299	0.3960	0.2973
OS	ST12	0.6200	0.5171	0.4698	*	0.3982	0.3547
OS	ST13	0.6351	0.5164	0.4777	*	0.4144	0.3633
OS	ST14	0.6399	0.5183	0.4695	0.4566	0.4000	0.3485
OS	ST15	0.6832	0.4323	*	ABORTED	*	*
OS	ST16	0.6682	0.4364	*	ABORTED	*	*
OS	ST17	0.6719	0.4286	*	ABORTED	*	*
DT	ST15R	0.6734	0.4291	0.4243	0.4204	0.3839	0.3630
DT	ST16R	0.6713	0.4325	0.4247	0.4202	0.3986	0.3672
DT	ST17R	0.6880	0.4306	0.4206	0.4140	0.3709	0.3330
OT	ST18	0.6135	0.5165	0.4830	0.4752	0.4176	0.3985
OT	ST19	0.5987	0.5226	0.4858	0.4764	0.4287	0.4216
OT	ST20	0.6082	0.5303	0.4896	0.4811	*	*

Note : DS - silt dry of optinum water content

OS - silt at optinum water content

DT - till dry of optinum water content

OT - till at optinum water content

Table 5.1b Summary of Suction Test Results on Dimensional Chnages

SOIL TYPE	TEST NO.	INITIAL THICKNESS (cm)	INITAL DIAMETER (cm)	DIMENSIONS AT $(u_a - u_w)$ 304 kPa t(cm)	304 kPa d(cm)	507kPa t(cm)	507kPa d(cm)	1014 kPa t(cm)	1014 kPa d(cm)	1520 kPa t(cm)	1520 kPa d(cm)	OVEN DRIED t(cm)	OVEN DRIED d(cm)
DS	ST1	*	*	*	*	1.7180	6.3259	1.7069	6.3157	1.7005	6.3068	1.6996	6.2871
DS	ST2	*	*	*	*	1.7308	6.3094	1.7238	6.3030	1.7109	6.2967	1.7119	6.2763
DS	ST3	1.7600	6.3481	1.7609	6.3360	1.7680	6.3310	*	*	*	*	*	*
DS	ST4	1.7132	6.3481	1.7138	6.3386	1.7182	6.3303	1.7178	6.3081	1.6904	6.3017	1.6901	6.2831
DS	ST5	1.7255	6.3386	1.7269	6.3265	1.7297	6.3170	1.7172	6.3068	1.6906	6.2992	1.6865	6.2816
OS	ST6	1.7589	6.3417	1.7646	6.3106	1.7655	6.3005	*	*	*	*	*	*
OS	ST7	1.7091	6.3456	1.7149	6.3062	1.7174	6.2973	*	*	*	*	*	*
OS	ST8	1.7209	6.3379	1.7266	6.3005	1.7284	6.2916	*	*	*	*	*	*
OS	ST9	0.9727	6.3360	*	*	*	*	ABORTED		*	*	*	*
OS	ST10	1.0743	6.3414	1.0792	6.3049	1.0787	6.2950	1.0798	6.2621	1.0835	6.1762	1.0802	6.1722
OS	ST11	1.1252	6.3428	1.1274	6.3002	1.1279	6.2808	1.1279	6.2560	1.1282	6.2103	1.1270	6.1900
OS	ST12	1.0728	6.3458	1.0744	6.3170	*	*	1.0823	6.2598	1.0823	6.2360	1.0858	6.1906
OS	ST13	1.0998	6.3297	1.0983	6.3099	*	*	1.1008	6.2395	1.1005	6.2090	1.1019	6.1537
OS	ST14	1.1256	6.3481	1.1269	6.3151	1.1278	6.3011	1.1304	6.2421	1.1376	6.2160	1.1337	6.1779
OS	ST15	1.1246	6.3441	*	*	*	*	ABORTED		*	*	*	*
OS	ST16	1.0735	6.3487	*	*	*	*	ABORTED		*	*	*	*
OS	ST17	1.0906	6.3341	*	*	*	*	ABORTED		*	*	*	*
DT	ST15R	1.0921	6.3360	1.0939	6.3341	1.0944	6.3284	1.0976	6.2934	1.0981	6.2586	1.0950	6.1938
DT	ST16R	1.0741	6.3487	1.0753	6.3462	1.0767	6.398	1.0789	6.3100	1.0829	6.3214	1.0696	6.2103
DT	ST17R	1.1260	6.3481	1.1294	6.3450	1.1306	6.3348	1.1275	6.2855	1.1290	6.2433	1.1302	6.1957
OT	ST18	1.1236	6.3468	1.1216	6.2954	1.1234	6.2875	1.1180	6.2052	1.1192	6.1770	1.1047	6.0814
OT	ST19	1.0703	6.3468	1.0714	6.2935	1.0720	6.2859	1.0697	6.2122	1.0718	6.1989	1.0538	6.0744
OT	ST20	1.0915	6.3310	1.0898	6.2630	1.0892	6.2554	*	*	*	*	1.0745	6.0141

Note : DS - silt dry of optinum water content

DS - silt at optinum water content

DT - till dry of optinum water content

OT - till at optinum water content

19.0%. The cover of the pressure membrane apparatus was over-tightened during tests ST6, ST7 and ST8 and the specimens were disturbed. The tests were abandoned. After test ST9 was completed, it was discovered that an error in weighing was made during specimen preparation. The specimen was not compacted to the same initial conditions as the other specimens in the same series of tests. These test results were excluded. At the end of the 304 kPa matric suction increment for test ST12 and ST13, the air pressure supply to the pressure plate apparatus failed. The specimens were than transferred to the pressure membrane apparatus. The 507 kPa matric suction increment was therefore omitted.

Six suction tests (i.e., ST15, ST16, ST17, ST15R, ST16R and ST17R) were carried out on glacial till specimens with initial water contents dry of optimum at approximately 15.6%. After specimens of ST15, ST16 and ST17 were placed inside the pressure plate apparatus, water accidentally came in contact with the specimens. These test data were therefore abandoned.

Three suction tests (i.e. ST18 to ST20) were performed on glacial till specimens with an initial water content at optimum, at approximately 18.9%. At the end of the 1014 kPa matric suction increment for test ST20, a hole was found on the cellulose membrane on top of which the specimen sat. The test was abandoned.

5.4 Unconfined Shrinkage Tests

Unconfined shrinkage tests were used to establish the water content versus void ratio curves for specimens under increasing matric suction. Three different methods were tried to measure the specimen volume during the test. The three methods were: mercury submersion, resin-coating submersion and direct measurement of dimensions.

Eleven unconfined shrinkage tests were performed on silt specimens with initial water contents dry of optimum. Three tests (i.e., SLTM1DS, SLTM2DS and SLTM3DS) used the mercury submersion method to measure specimen volumes. Test SLTM1DS was a trial test. The specimen was badly damaged during the test due to inexperience in handling the mercury bath. The test results were ignored. The results of tests SLTM2DS and SLTM3DS are presented in Figure 5.3. Three tests (i.e., SLTR1DS, SLTR2DS and SLTR3DS) were carried out using a resin-coating submersion technique. Test SLTR1DS was abandoned when the resin coating on the specimen was found to be leaking water during the first volume measurement. Test SLTR2DS was stopped part way through the test when leakage was detected. The results of tests SLTR2DS and SLTR3DS are shown in Figure 5.4. Serious leaking problems were encountered with the resin coating during this series of tests. It was subsequently decided against performing further volume measurement using the resin-coating submersion technique. Five tests (i.e

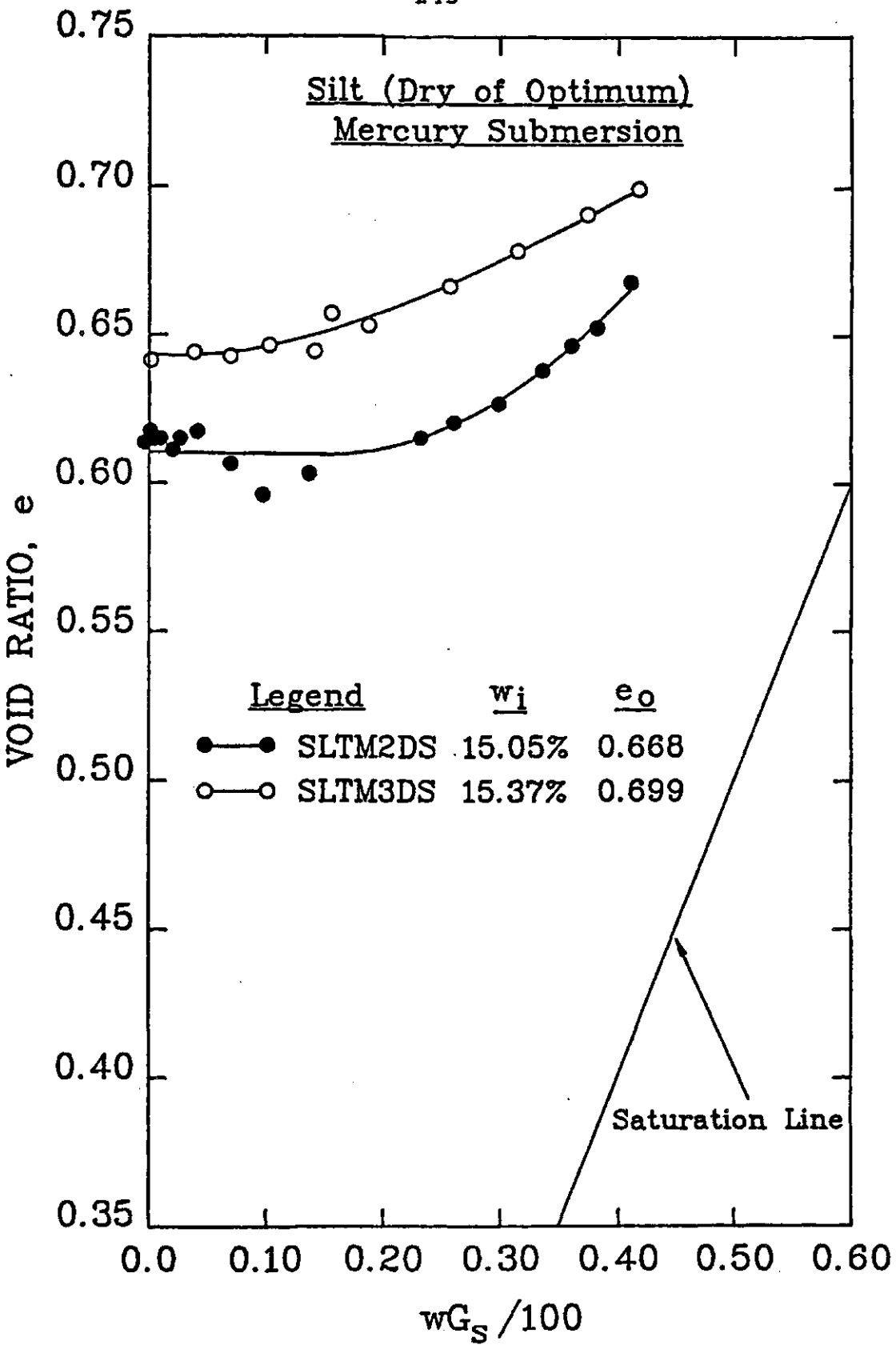

Figure 5.3 Results for Unconfined Shrinkage Tests SLTM2DS and SLTM3DS

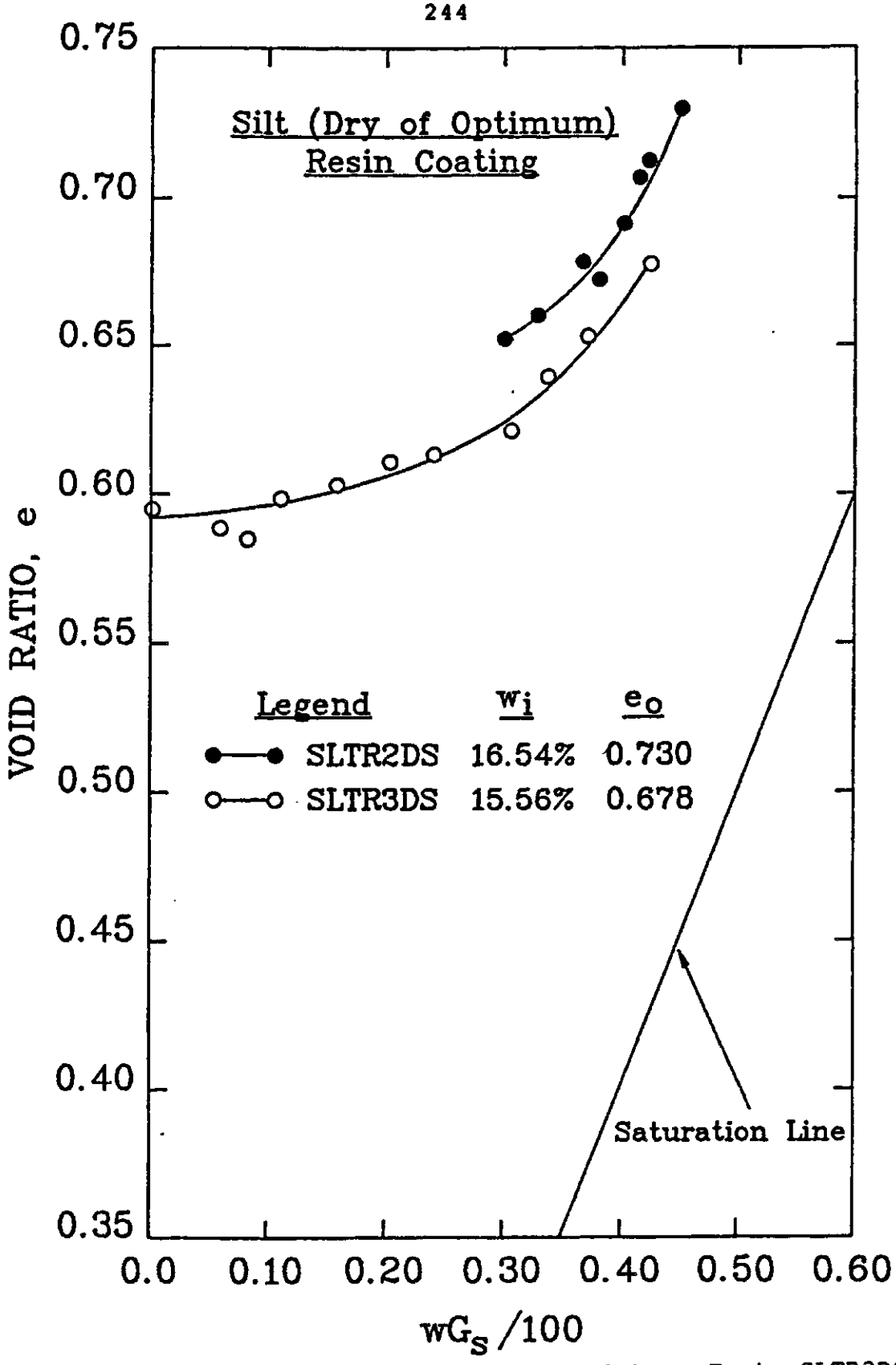

Figure 5.4 Results for Unconfined Shrinkage Tests SLTR2DS and SLTR3DS

SLTD1DS, SLTD2DS, SLTD3DS, SLTD4DS and SLTD5DS) were run using the direct measurement method for volume measurements. The specimen was placed on a stationary surface and a dial gauge was carefully lowered onto the specimen surface to measure its thickness. The tip of the dial gauge was found to indent the specimen surface slightly before coming to equilibrium and giving a stable thickness reading. The thickness readings for specimens SLTD1DS, SLTD2DS and SLTD3DS were taken with the indentation. Dual sets of thickness readings were taken for specimens of tests SLTD4DS and SLTD5DS; one with and one without allowing the indentation. The results are shown in Figure 5.5, 5.6 and 5.7.

Six unconfined shrinkage tests were performed on silt specimens with initial water contents close to optimum. Five tests (i.e. SLTD10S, SLTD20S, SLTD30S, SLTD40S and SLID50S) were performed using the direct measurement method to determine the specimen volumes. The thickness readings of specimens SLTD10S, STLD20S and SLTD30S were taken allowing indentation of the dial gauge tip. Two sets of thickness measurements were taken for specimens SLTD40S and SLTD50S, one with and one without indentation. Two methods were used to measure the volume for specimen SLTDM10S. The specimen volume was first determined by the direct measurement method without allowing the dial gauge tip to indent the specimen surface. The specimen volume was then

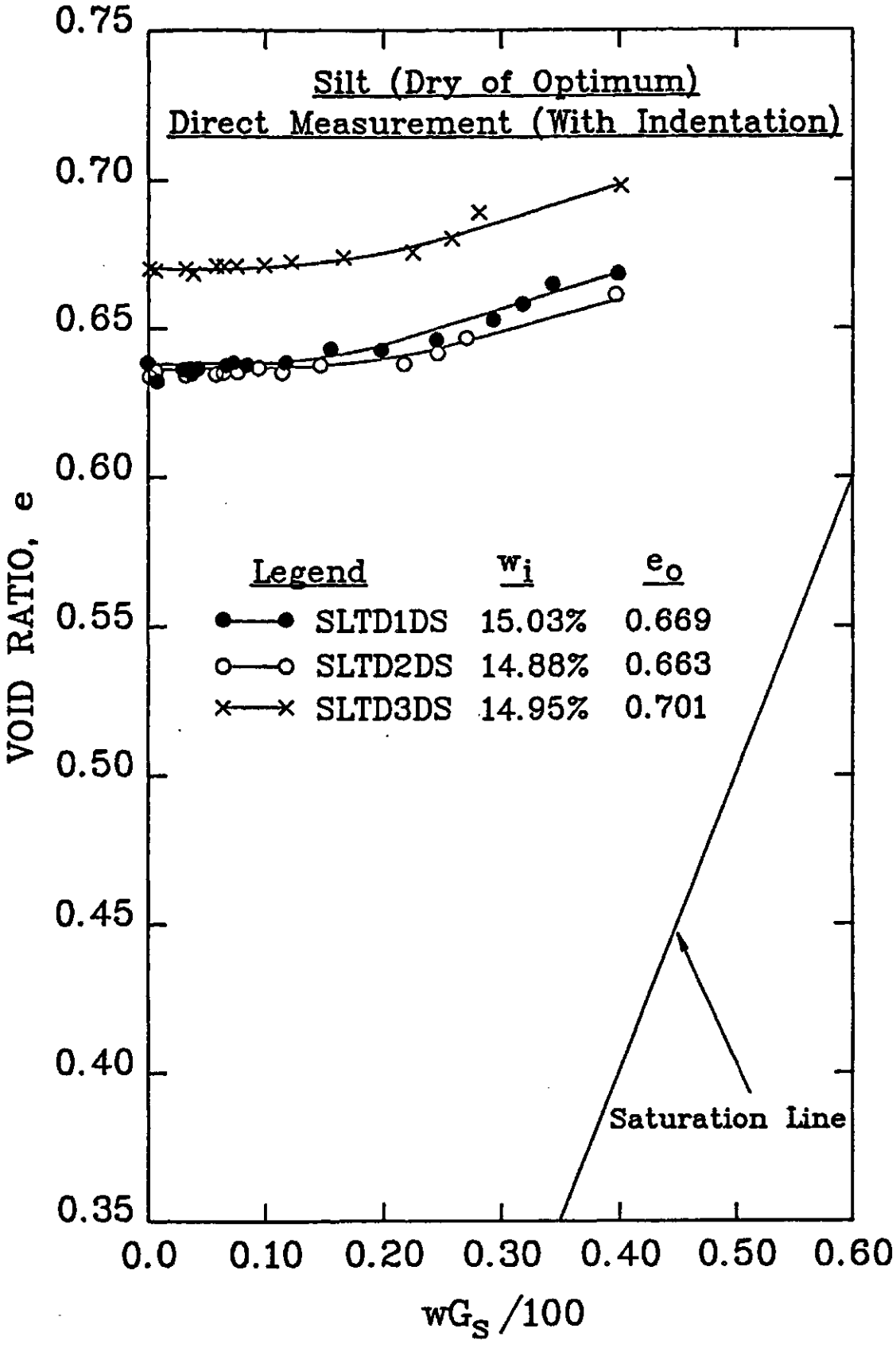

Figure 5.5 Results for Unconfined Shrinkage Tests SLTD1DS, SLTD2DS, and SLTD3DS

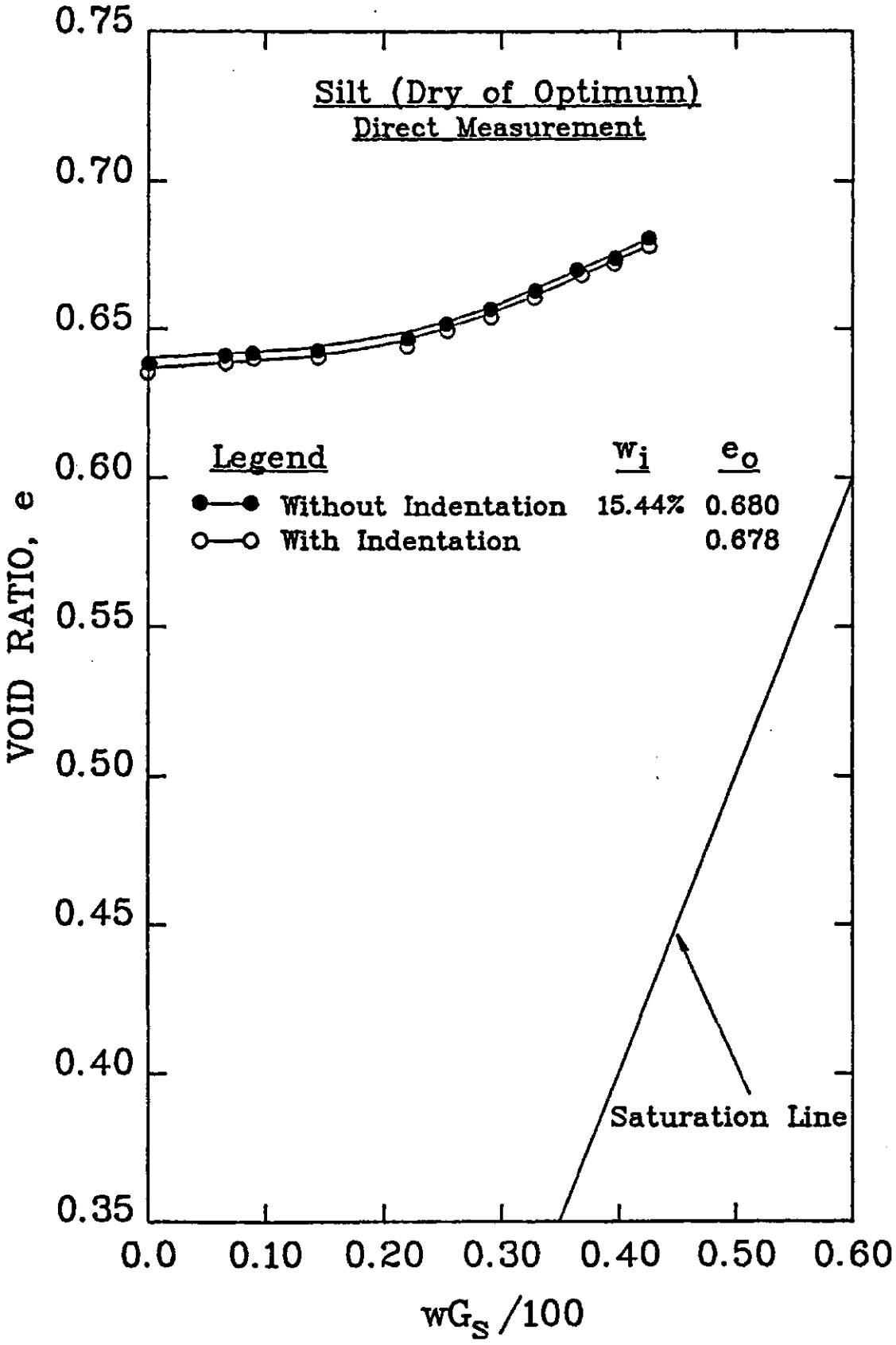

Figure 5.6 Results for Unconfined Shrinkage Test SLTD4DS

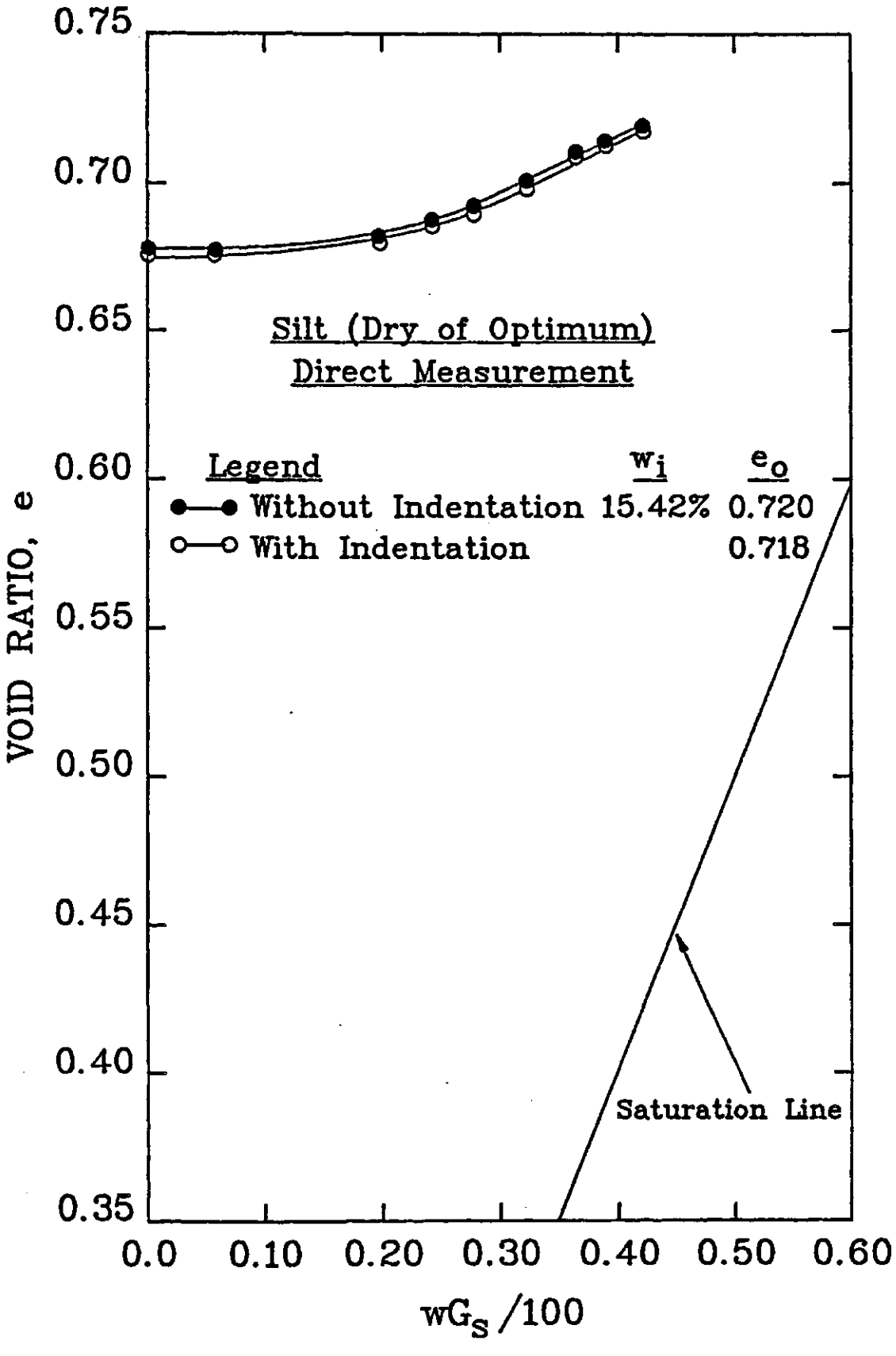

Figure 5.7 Results for Unconfined Shrinkage Test SLTD5DS

re-measured using the mercury submersion method. The resulted shrinkage curves for all the above tests are presented in Figure 5.8 to 5.11.

Two unconfined shrinkage tests were carried out on glacial till specimens with dry of optimum initial water contents. Test SLTD1DT was run using the direct measurement method to determine specimen volumes. Both direct measurement and mercury submersion methods were used for test SLTDM1DT. Thickness readings for the specimens of both tests (i.e. SLTD10T and SLTDM10T) were taken without allowing the tip of the dial gauge to indent the specimen surface. The resulted shrinkage curves are presented in Figure 5.12.

Two unconfined shrinkage tests were performed on glacial till specimens with initial water contents close to optimum. Both direct measurement and mercury submersion methods were used for volume measurements for both tests. Thickness readings were taken by dial gauge without allowing indentation of the specimen surfaces. Specimen SLTDM10T was found to be too soft to support the wire prongs attached to the glass plate used to press the specimen into the mercury bath. The test was abandoned. The wire prongs were replaced by plastic studs with diameters approximately 0.5 cm. The change allowed test SLTDM20T to be completed successfully. The plot of wG_s versus void ratio for test SLTDM20T is presented in Figure 5.13.

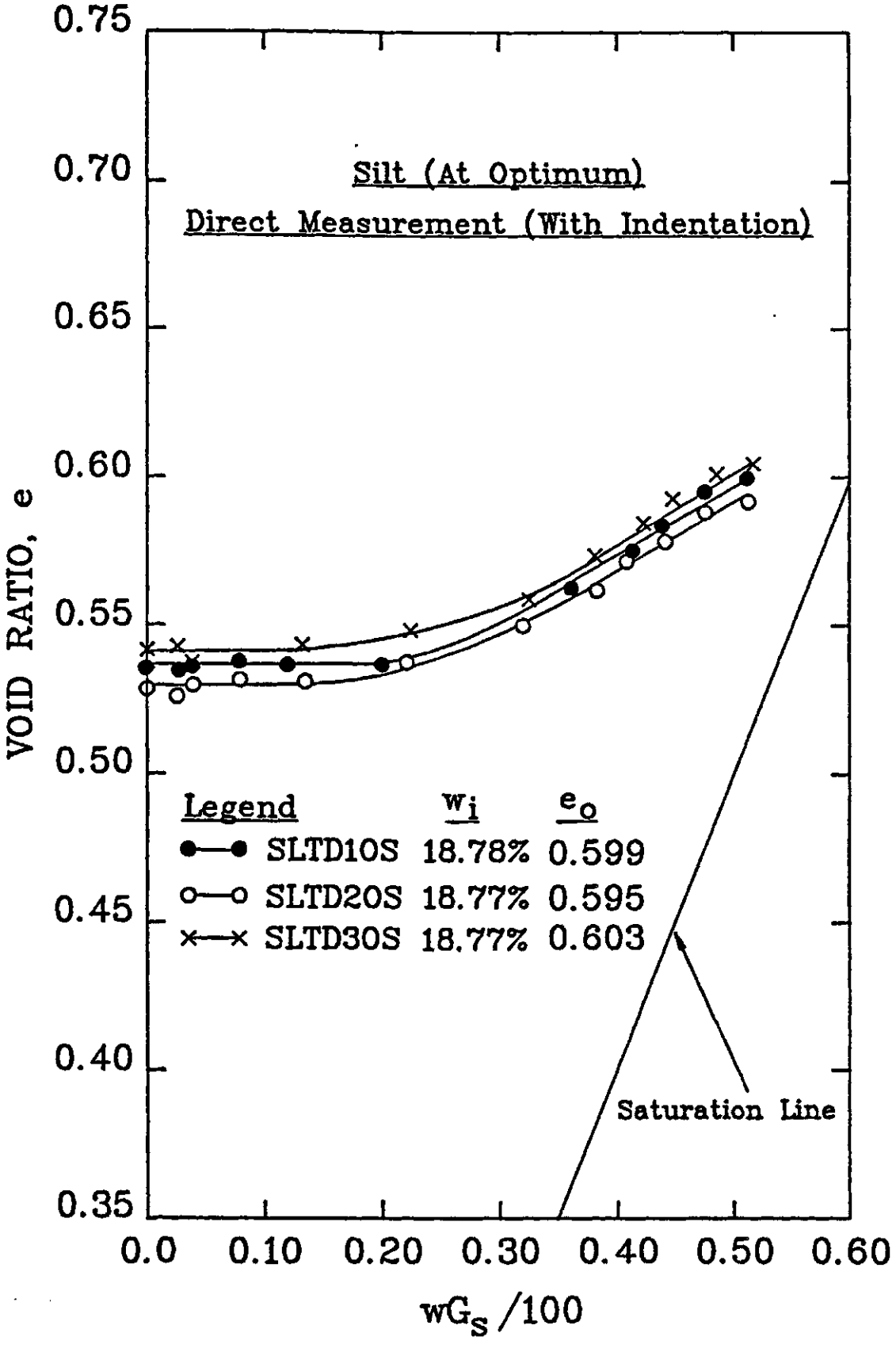

Figure 5.8 Results for Unconfined Shrinkage Tests, SLTD10S, SLTD20S, and SLTD30S

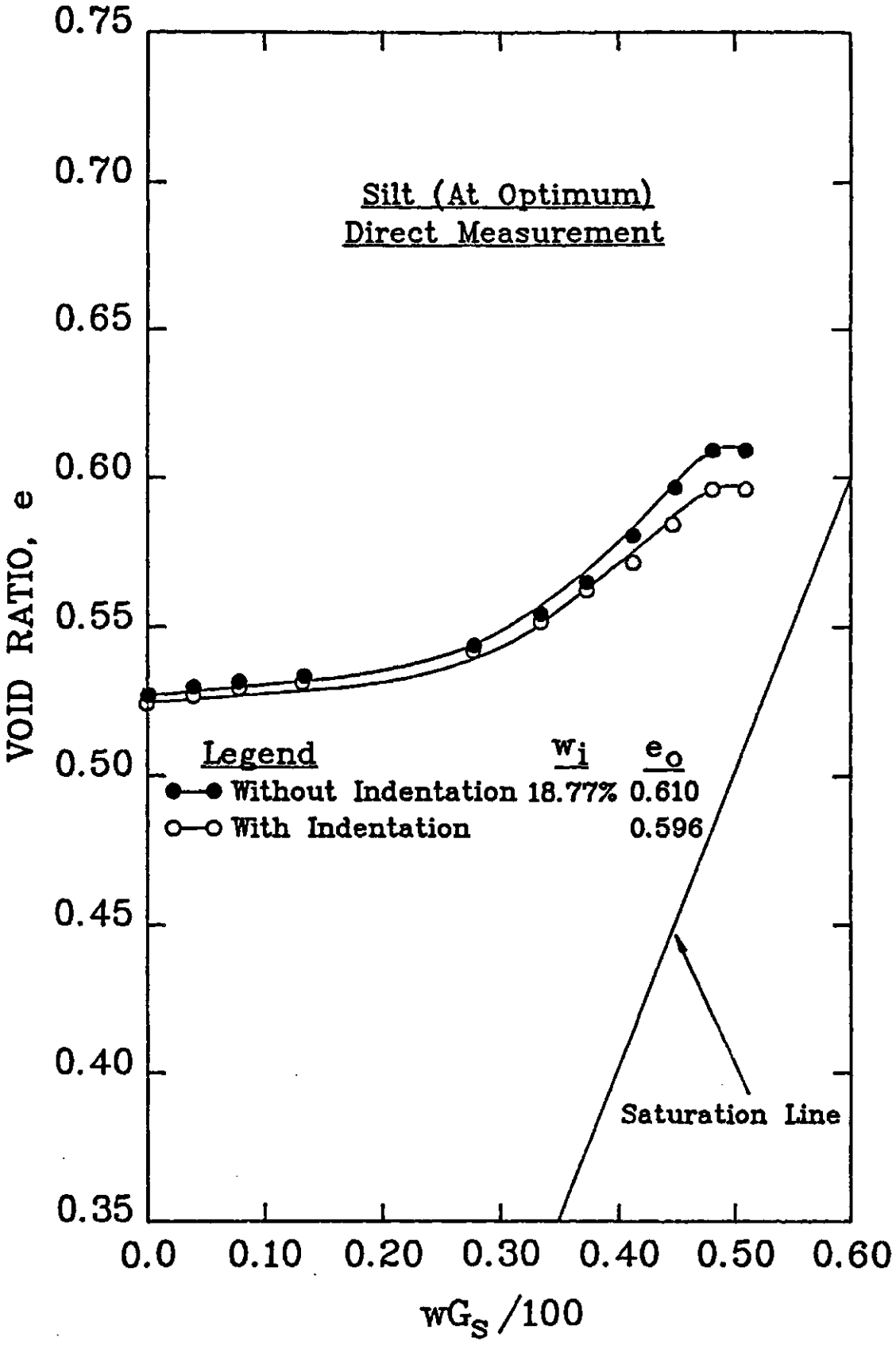

Figure 5.9 Results for Unconfined Shrinkage Test SLTD40S

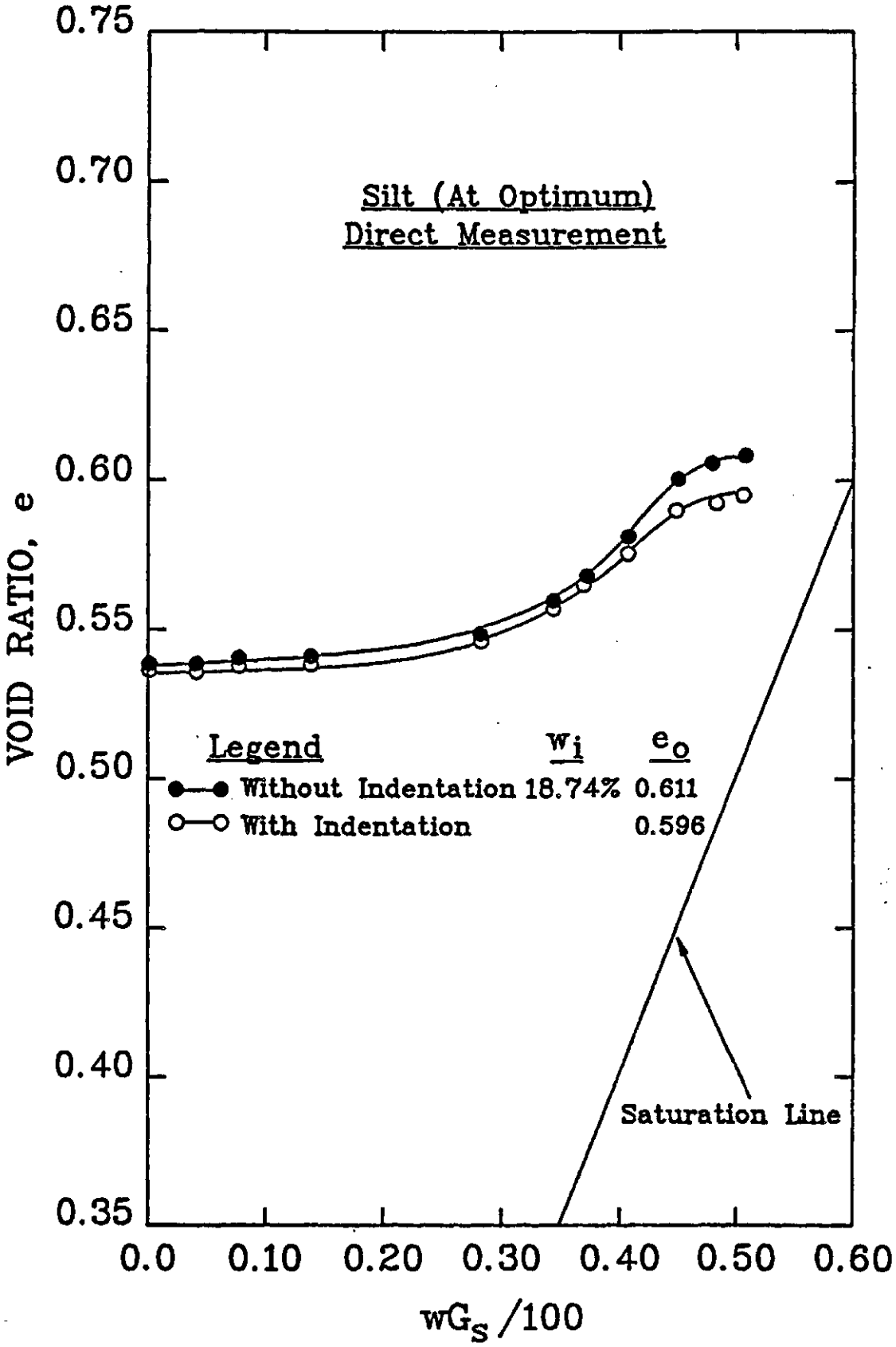

Figure 5.10 Results for Unconfined Shrinkage Test SLTD50S

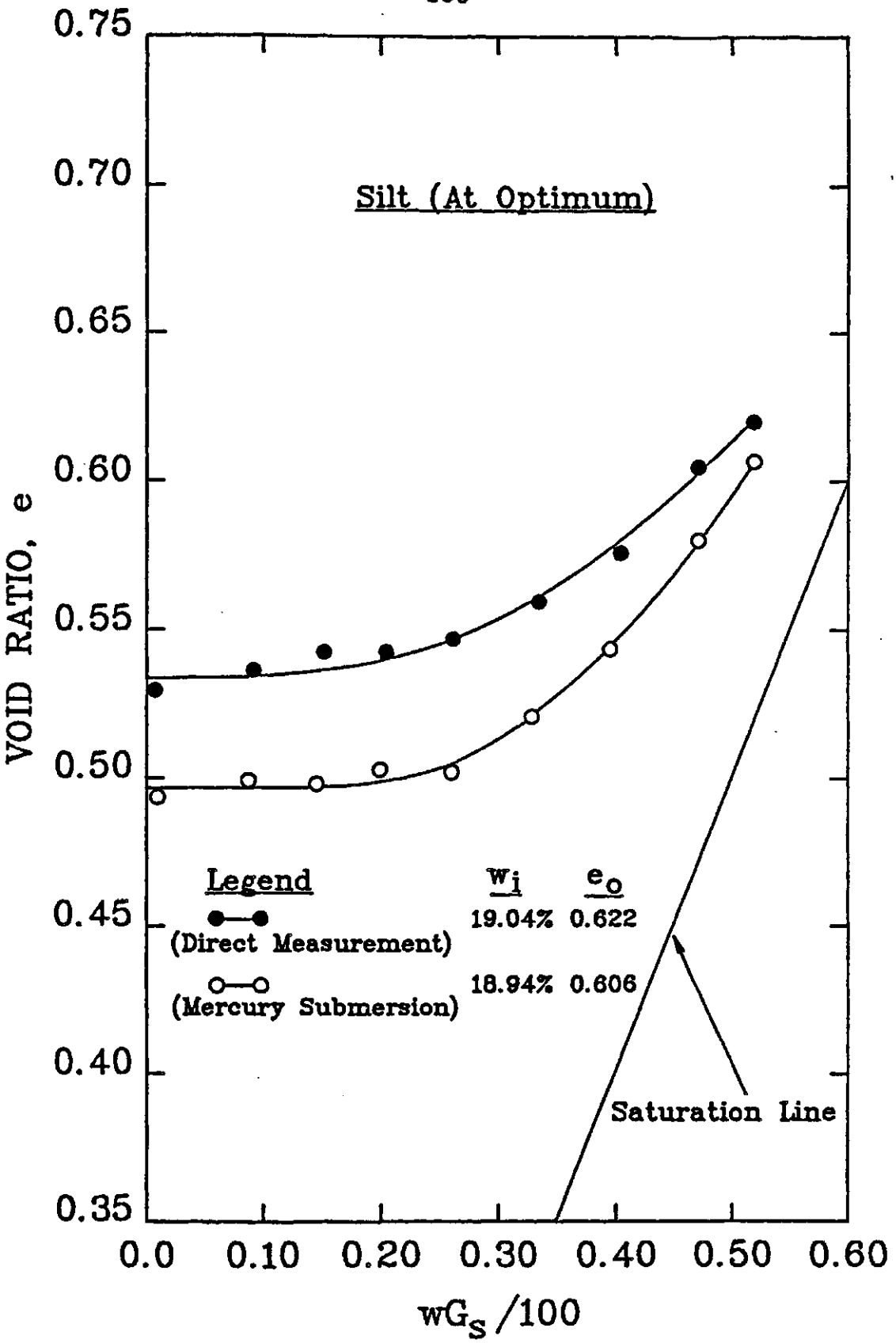

Figure 5.11 Results for Unconfined Shrinkage Test SLTDM10S

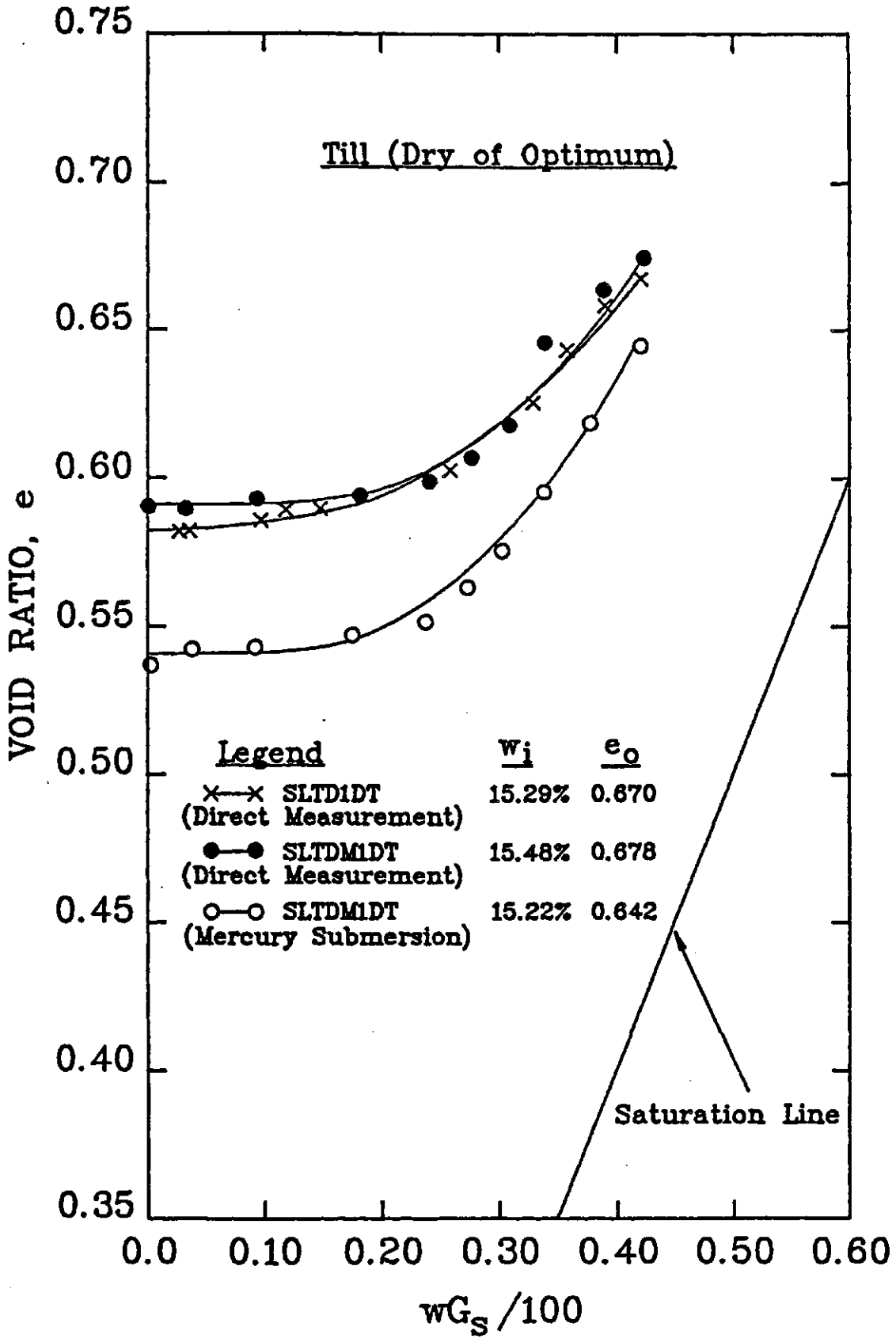

Figure 5.12 Results for Unconfined Shrinkage Tests SLTD1DT and SLTDM1DT

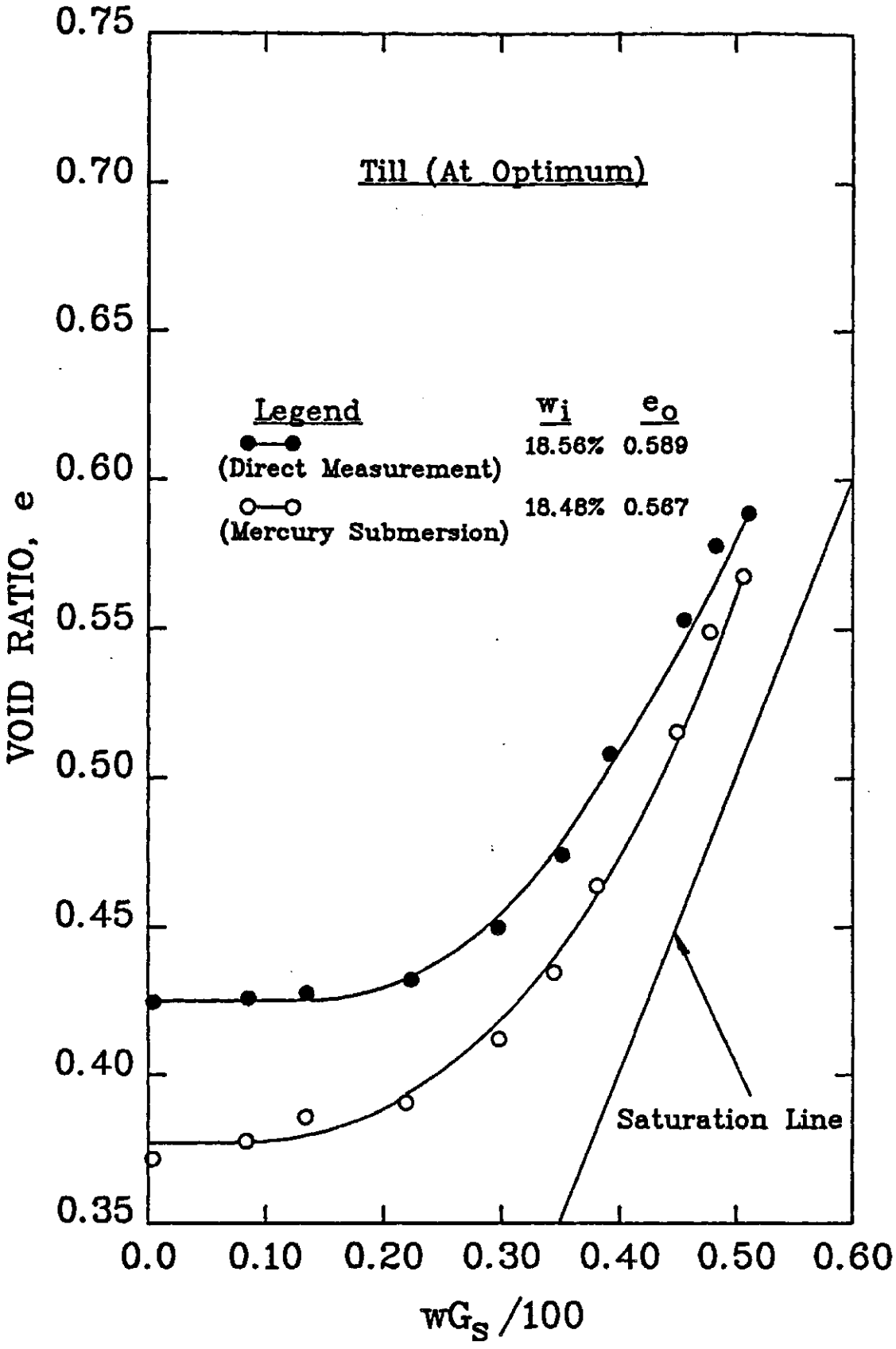

Figure 5.13 Results for Unconfined Shrinkage Test SLTDM20T

Calibration tests were performed to check the accuracy of the direct measurement method for volume. The thickness and diameter of a stainless steel plug was first measured using a micrometer. The same measurements were taken again using dial gauge and caliper as used in the direct measurement method. A comparison was made of the two techniques and the results are summarized in Table 5.2. Specimen dimensions determined using the direct measurement technique with a dial gauge and a caliper in the test program were adjusted accordingly.

Nine sets of volume measurements on oven dried silt specimens using first the direct measurement method and then the mercury submersion technique were made. Four of these specimens were initially compacted at water contents dry of optimum. Five specimens had initial water contents close to optimum. The results are presented in Figure 5.14.

5.5 One-Dimensional Constant Volume Loading and Unloading Tests

The one-dimensional constant volume loading and unloading tests were performed to establish the void ratio and water content versus net total stress relations. The oedometers were prepared as discussed in Appendix B-3.

Six one-dimensional constant volume loading and

Table 5.2 Calibration Checks for the Direct Measurement Method Using a Stainless Steel Plug

	Thickness* (cm)	Diameter* (cm)	Volume (cm^3)
Direct Measurement Method	1.6955±0.001372 (use dial gauge)	6.3107±0.002165 (use caliper)	53.0326±0.06178
Control Measurement	1.6915±0.001256 (use micrometer)	6.3071±0.001650 (use micrometer)	52.8471±0.0480
% Difference w.r.t. Control Measurements	0.2365 (over-estimate)	0.05708 (over-estimate)	0.3510 (over-estimate)

* average of 20 measurements

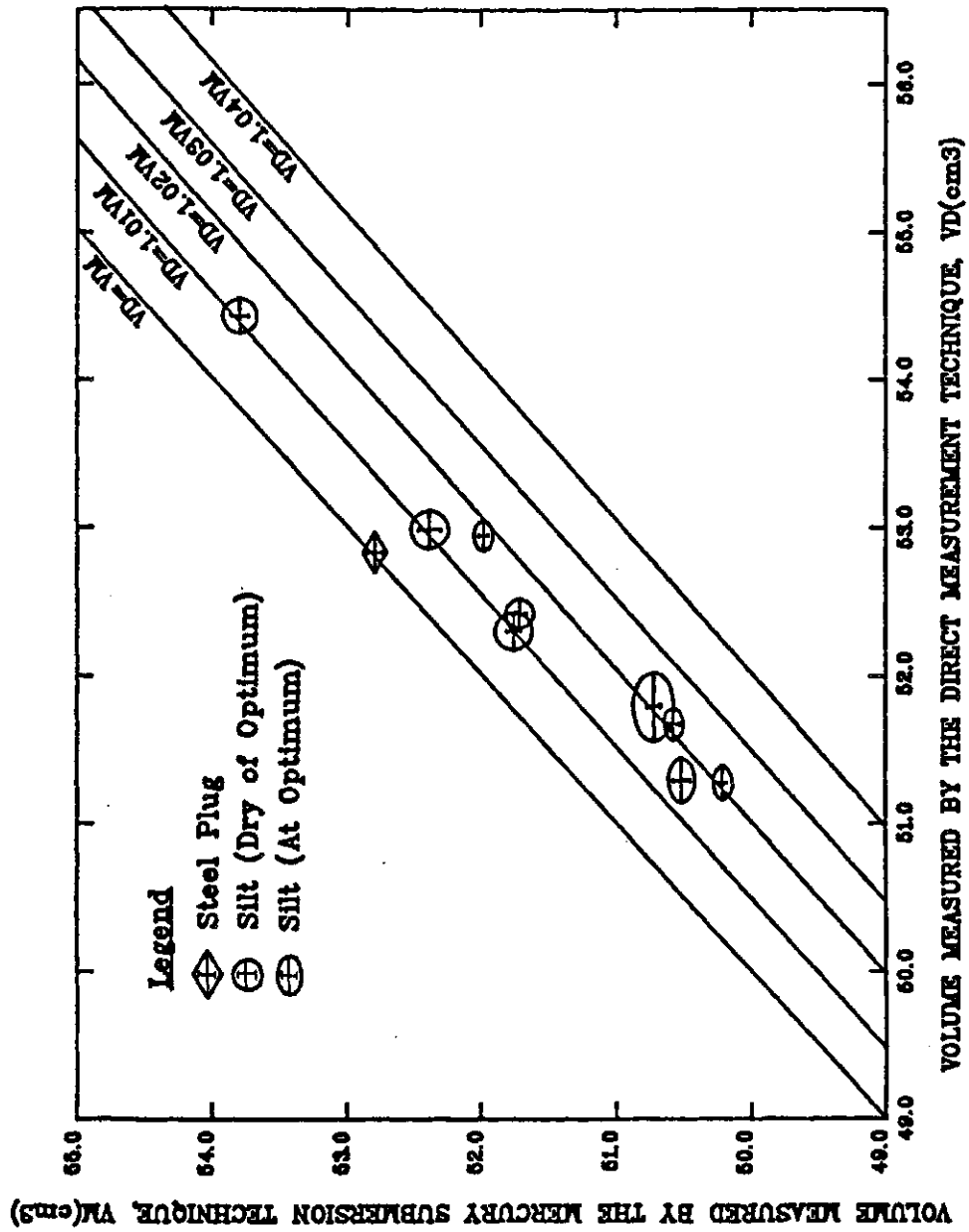

Figure 5.14 Comparsion between Volumes Measured by the Direct Measurement and Mercury Submersion Method

unloading tests (i.e., tests CVT1DS, CVT2DS, CVT3DS, CVT4DS, CVT5DS and CVT6DS) were performed on silt specimens with initial water contents dry of optimum. Tests CVT1DS and CVT2DS were trial tests. The specimens were loaded to a pressure of approximately 9000 kPa and the tests were stopped. Specimens for tests CVT3DS, CVT4DS and CVT5DS were loaded to the same stress level and unloaded to a pressure of approximately 90 kPa. The specimen for test CVT6DS was loaded to a maximum stress of 15000 kPa and unloaded to a token stress of 18 kPa. The resulting void ratio versus $(\sigma - u_a)$ curves are presented in Figure 5.15.

Four one-dimensional constant volume loading and unloading tests (i.e., tests, CVT10S, CVT20S, CVT30S and CVT40S) were performed on silt specimens with initial water contents close to optimum. The air pressure gauge on the oedometer used for test CVT10S failed when the specimen was loaded to a pressure of 500 kPa. The test was abandoned. Specimens for test CVT20S and CVT30S were loaded to a pressure of 9000 kPa and unloaded to stresses of 12.5 kPa and 73 kPa respectively. The specimen for test CVT40S was loaded to a maximum stress of 15000 kPa and unloaded to a pressure of 100 kPa. Figure 5.16 shows the resulting void ratio versus net total stress $(\sigma - u_a)$ curves.

Three one-dimensional constant volume loading and unloading tests (i.e., tests CVT1DT, CVT2DT and CVT3DT) were carried out on glacial till specimens with initial water

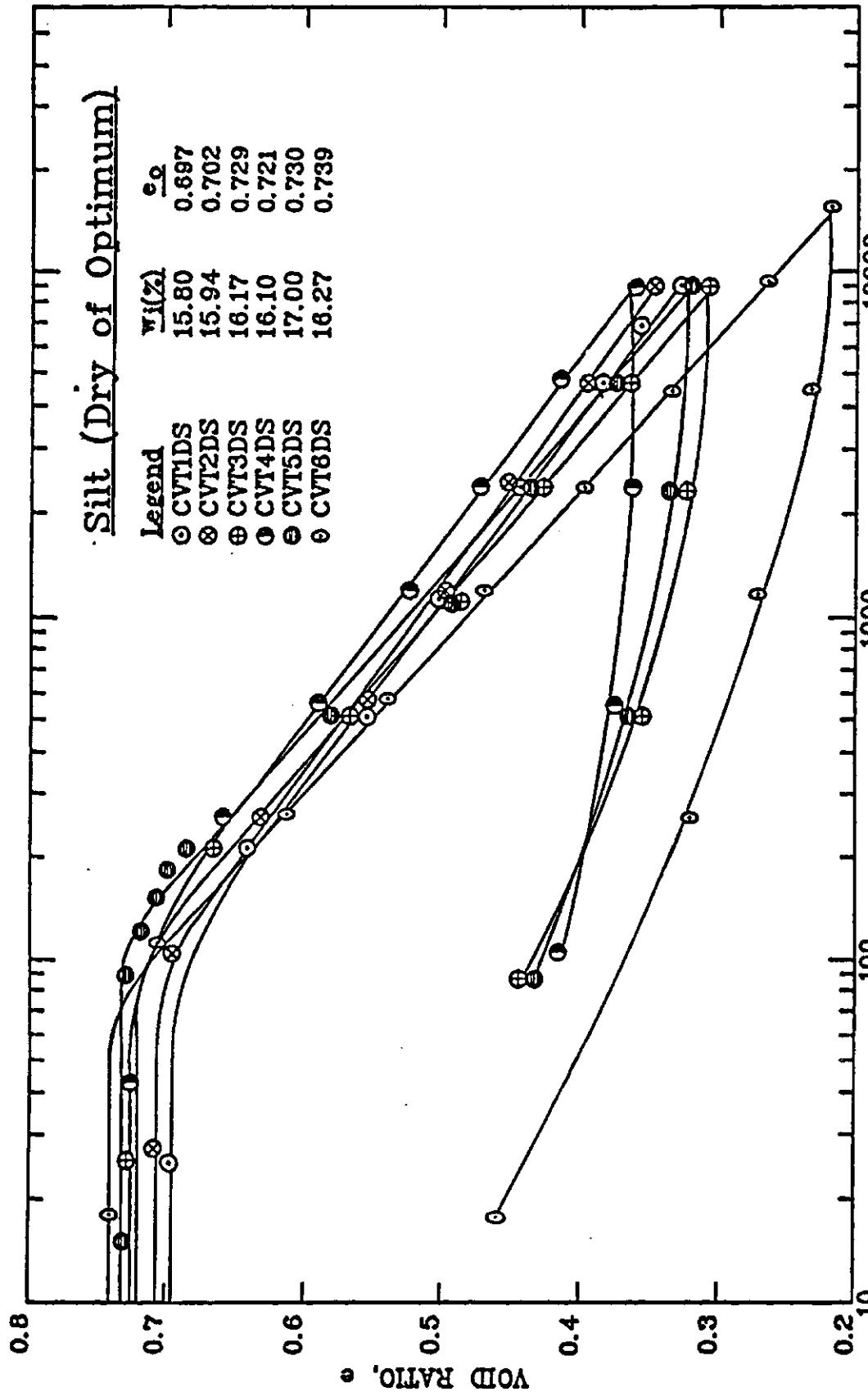

Figure 5.15 Results for One-Dimensional Constant Volume Loading and Unloading Tests CVT1DS to CVT6DS

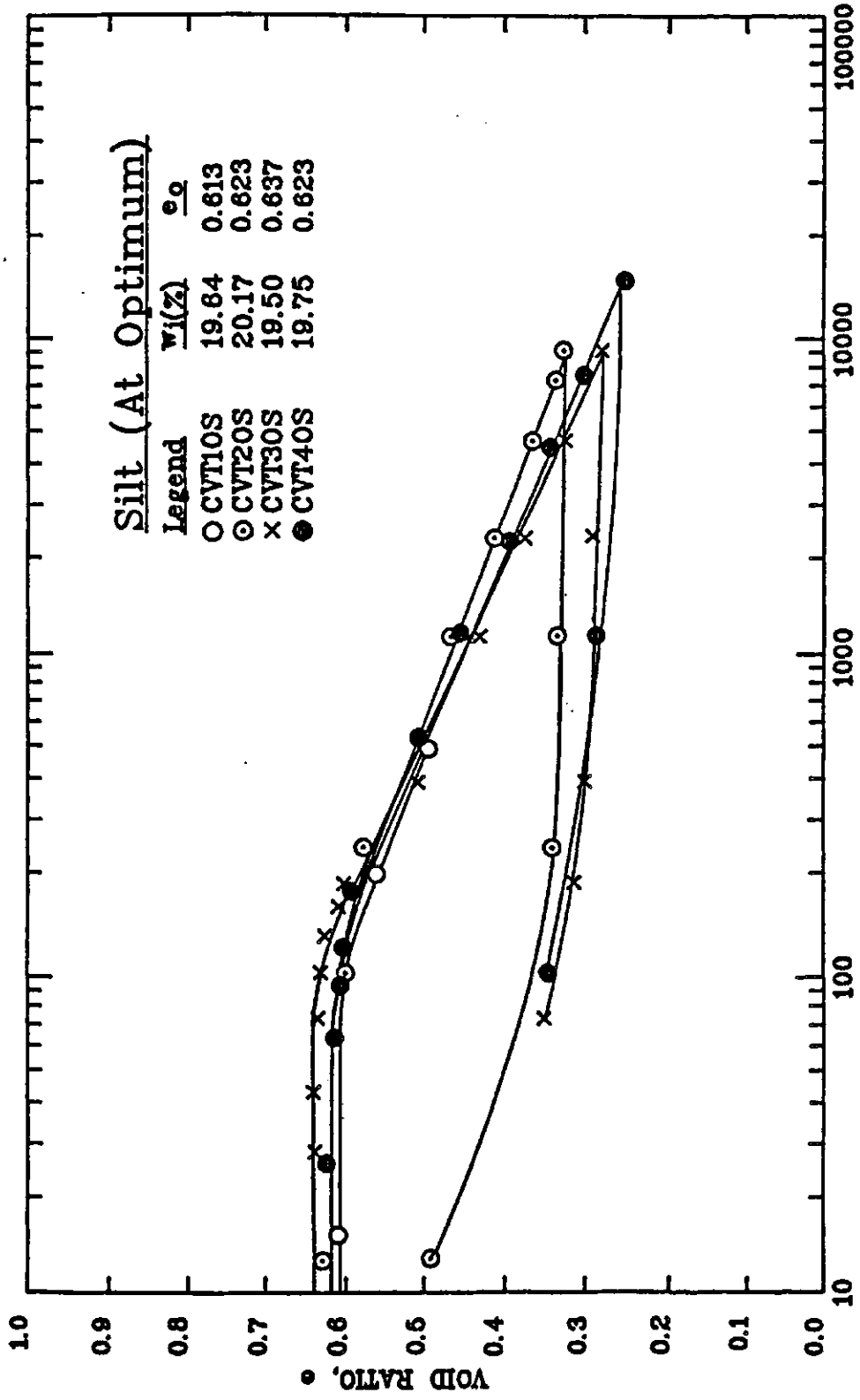

Figure 5.16 Results for One-Dimensional Constant Volume Loading and Unloading Tests CVT10S to CVT40S

contents dry of optimum. Specimens for tests CVT1DT and CVT2DT were loaded to a pressure of 9000 kPa and then unloaded to a pressure of approximately 110 kPa. The specimen for test CVT3DT was loaded to a maximum stress of 15000 kPa before it was unloaded to a pressure of 64 kPa. The resulting void ratio versus net total stress curves are presented in Figure 5.17.

Three one-dimensional constant volume loading and unloading tests (i.e., tests CVT10T, CVT20T and CVT30T) were performed on glacial till specimens with initial water contents close to optimum. specimens for tests CVT10T and CVT20T were loaded to a pressure of 9000 kPa and then unloaded to stresses of 240 kPa and 195 kPa respectively. The specimen for test CVT30T was loaded to a maximum stress of 1500 kPa and unloaded to a token load of 33 kPa. Figure 5.18 presents the resulting void ratio versus net total stress curves.

5.6 One-Dimensional Free Swell Tests

The one-dimensional free swell test was used to establish the void ratio and water content versus decreasing matric suction relations when the net total stress was equal to zero. The modified Anteus consolidometer were prepared as discussed in Appendix B-4.

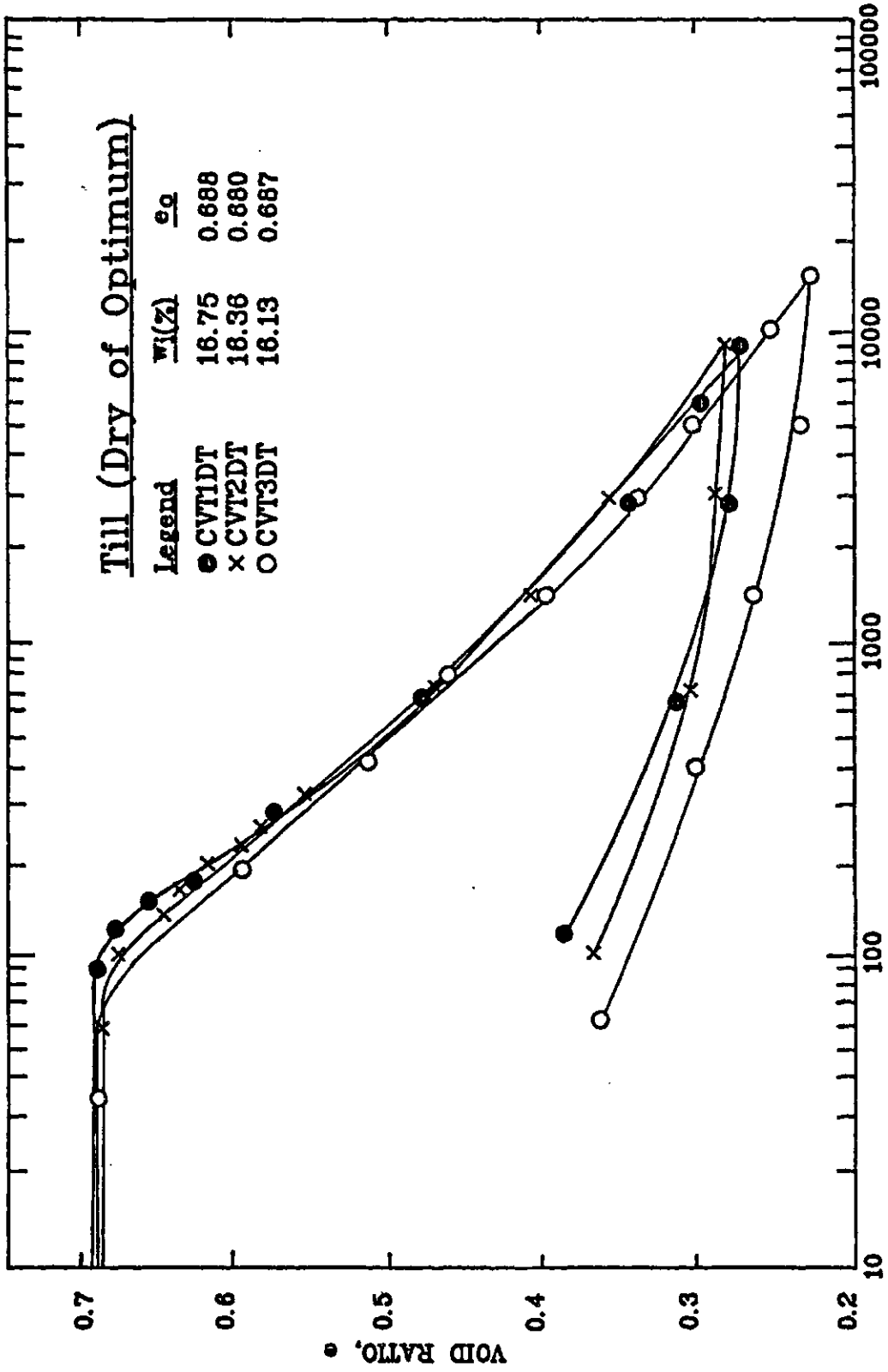

Figure 5.17 Results for One-Dimensional Constant Volume Loading and Unloading Tests CVT1DT To CVT3DT

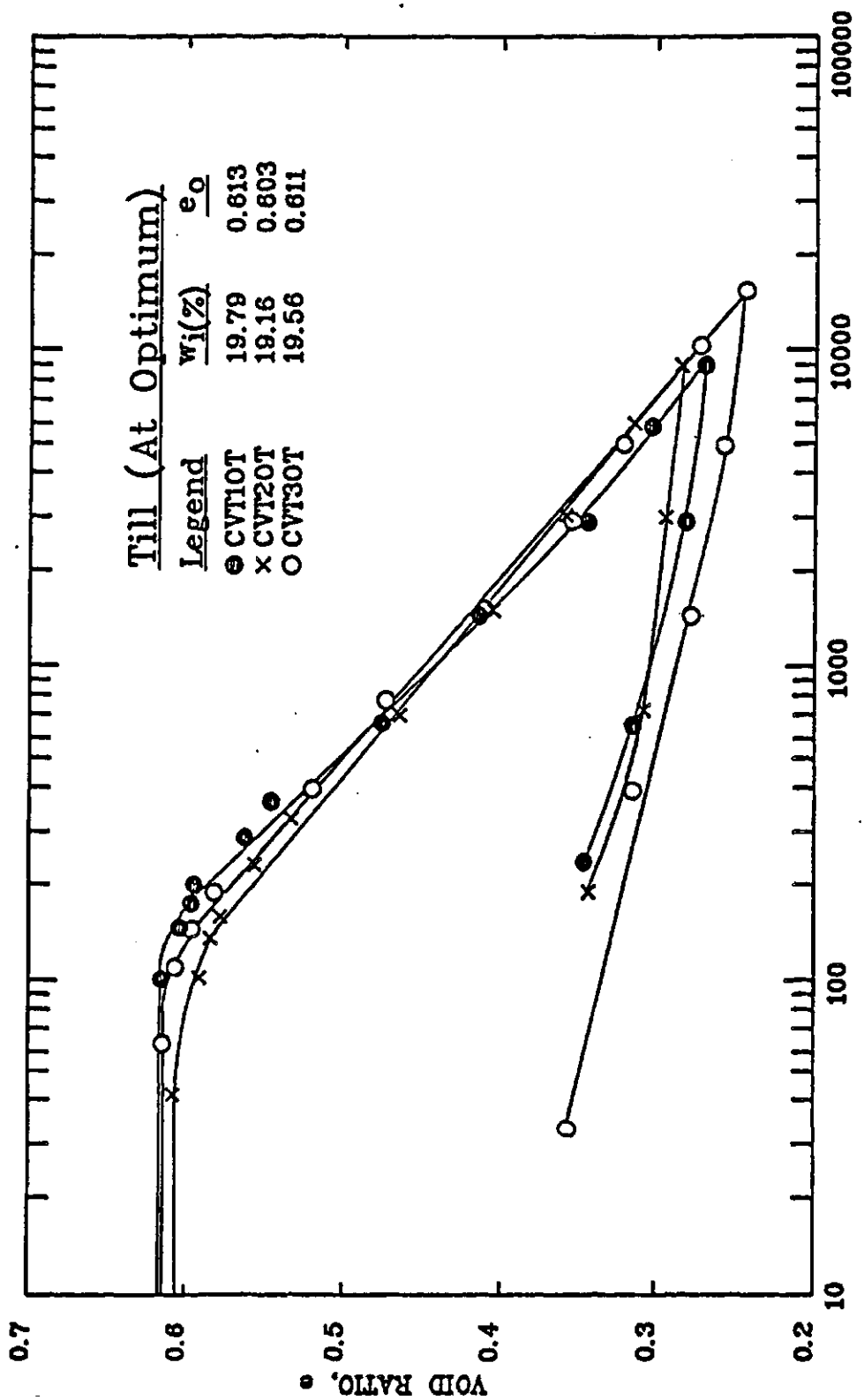

Figure 5.18 Results for One-Dimensional Constant Volume Loading and Unloading Tests CVT10T to CVT30T

Four one-dimensional free swell tests (i.e. tests FST1DS, FST2DS, FST3DS and FST4DS) were performed on silt specimens with initial water contents dry of optimum. Shortly after test FST1DS started, water was found to be leaking through the strain gauge attachment at the top of the modified Anteus consolidometer from the water chamber above the rubber diaphragm attached to the loading piston (see Figure 4.7). The test was abandoned. Approximately ten hours after test FST2DS began, water was found to be leaking from the pore-water line connector attached to the bottom of the modified Anteus consolidation. Attempt to mend the leakage failed. The test was stopped. The matric suction for specimens FST3DS and FST4DS was reduced in three stages. Specimen and water volume equilibrium curves for test FST3DS are presented in Figures 5.19 to 5.21. These equilibrium curves are found to be typical for both silt and till specimens. For test FST3DS, there was an immediate increase and subsequent decrease in specimen volume when air pressure, u_a and total stress, σ , were changed at the beginning of Stage II and III (Figure 5.20 and 5.21). It is postulated that the air pressure inside the cell chamber was momentarily higher than the load pressure above the rubber diaphragm attached to the loading piston (see Figure 4.7) during the stress adjustment. The loading piston therefore lifted slightly and then settled to equilibrium. In general, both the specimen and water volume changes were

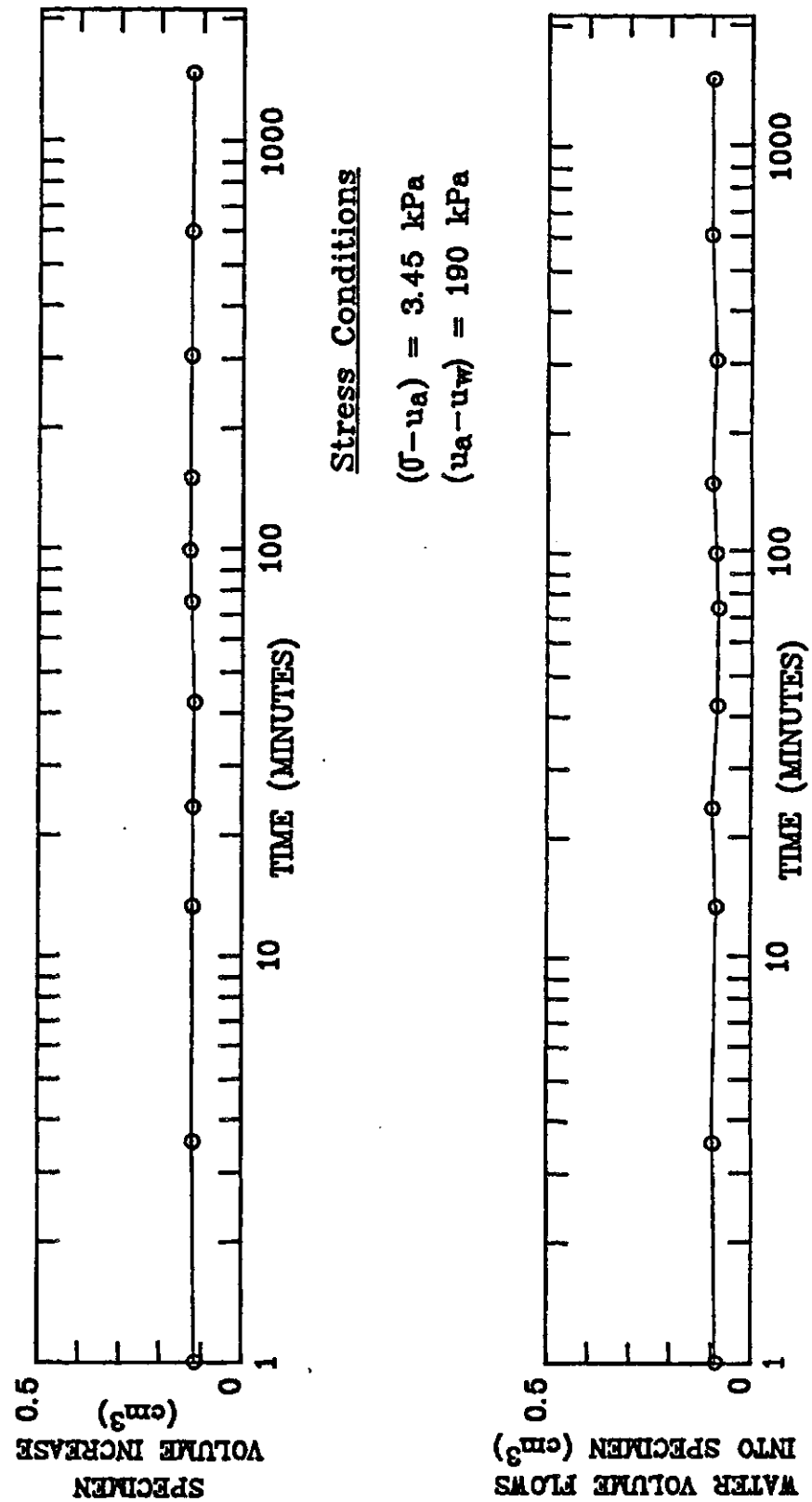

Figure 5.19 Specimen Volume and Water Volume Equilibrium Curves for Stage I of One-Dimensional Free Swell Test FST3DS

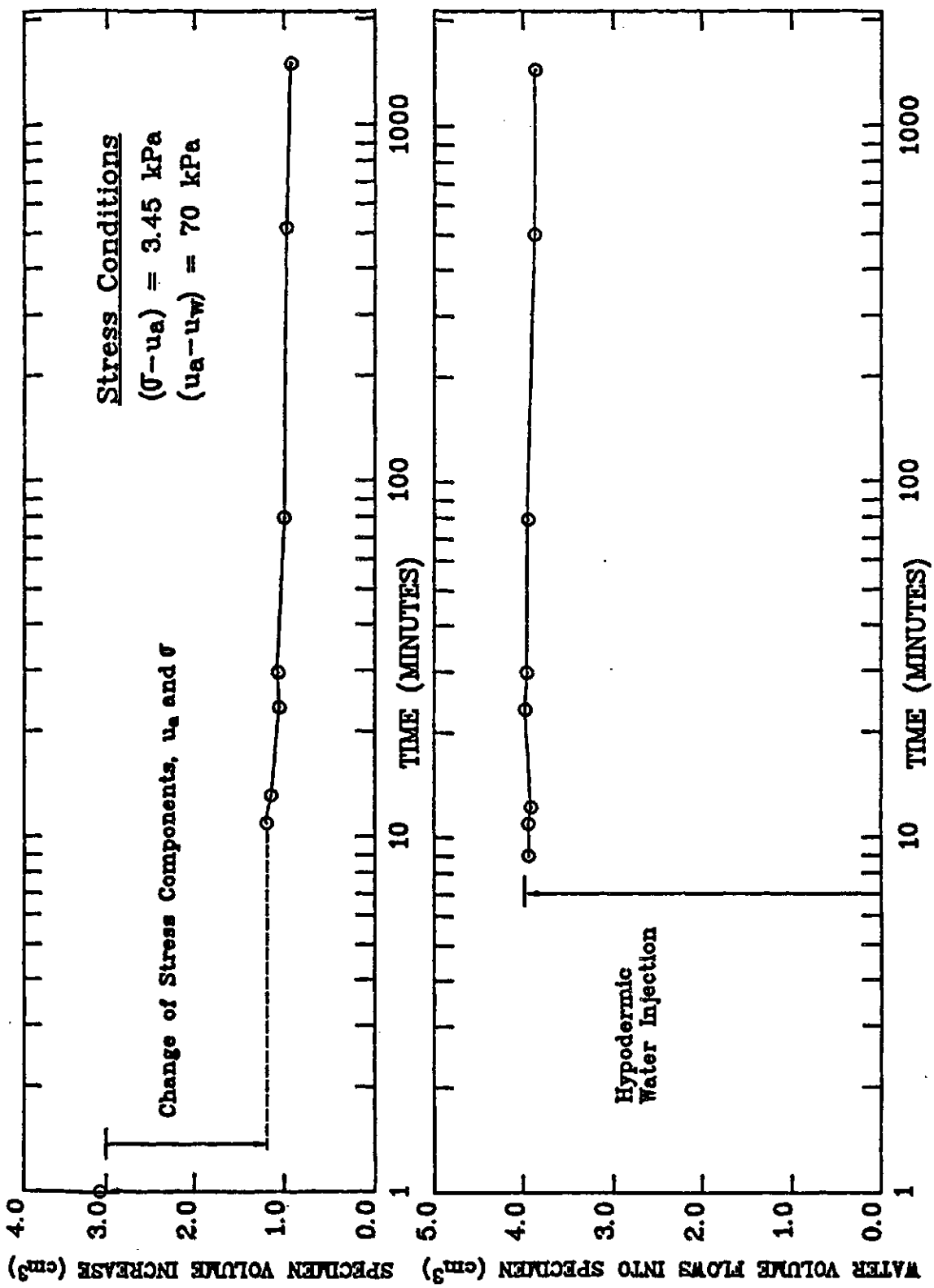

Figure 5.20 Specimen Volume and Water Volume Equilibrium Curves for Stage II of One-Dimensional Free Swell Test FST3DS

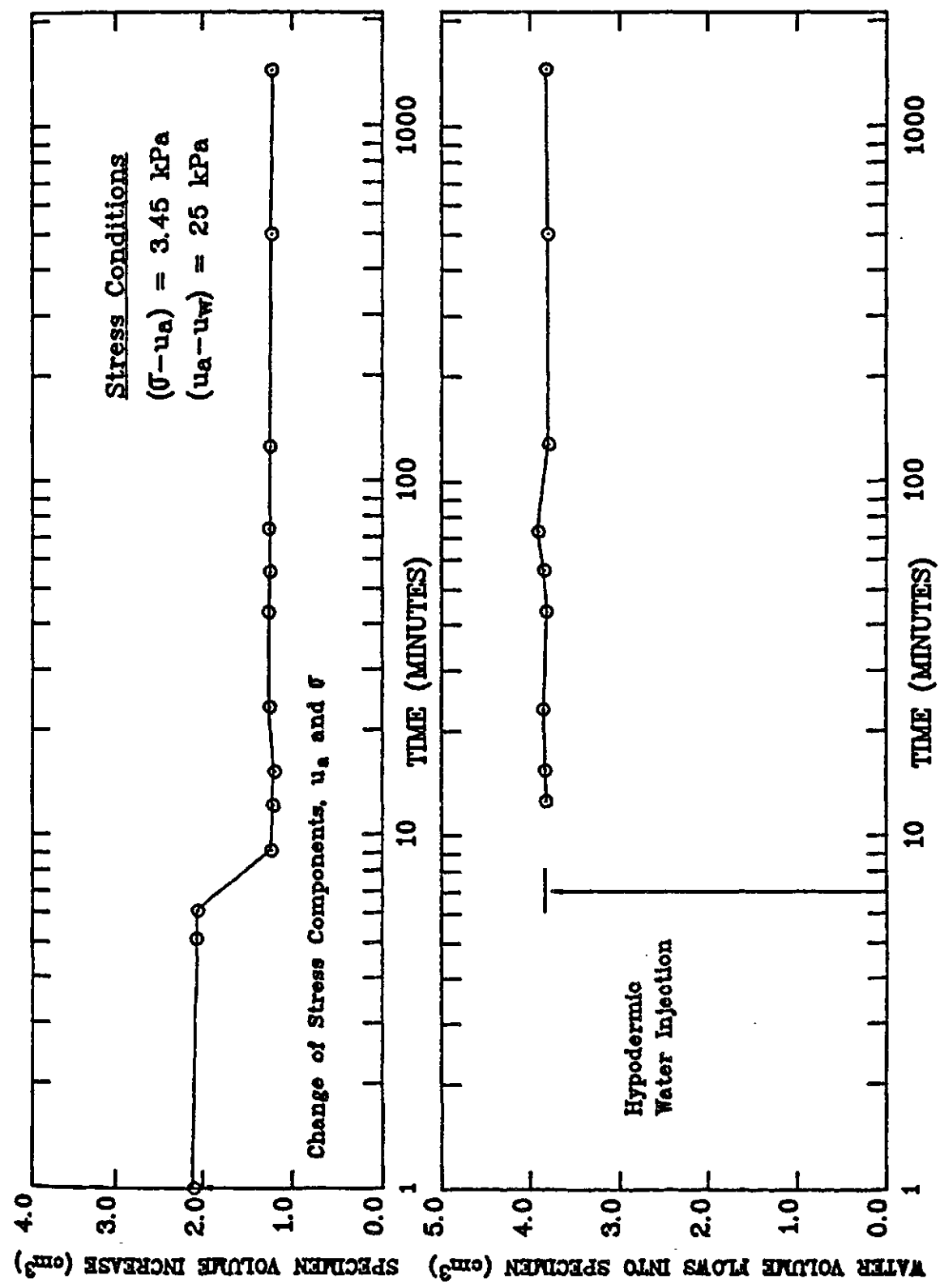

Figure 5.21 Specimen Volume and Water Volume Equilibrium Curves for Stage III of One-Dimensional Free Swell Test FST3DS

small and immediate . For test FST4DS, there was a slight decrease in both the specimen and water volume at the end of Stage I. These decreases could be due to the fact that the applied matric suction was slightly higher than the initial matric suction of the specimen. Figure 5.22 and 5.23 present the resulted matric suction versus void ratio and water content curves. A summary of the test data is shown in Table 5.3.

One one-dimensional free swell test (i.e., test FST10S) was carried out on a silt specimen with its initial water content close to optimum. The matric suction of the specimen was reduced in three stages. At the end of the stage I testing, both the specimen and water volume were found to have decreased. These volume decreases were the result of a increase in the matric suction. A summary of the test data is shown in Table 5.3. The resulting matric suction versus void ratio and water content relations are presented in Figure 5.24.

The one-dimensional free swell test, FST1DT was performed on a glacial till specimen with its initial water content dry of optimum. The matric suction of the specimen was reduced to 10 kPa in four stages. There were decreases in both the specimen and water volume at the end of the stage I of testing. These decreases could be due to the fact that the applied matric suction was actually higher than the initial matric suction of the specimen. A summary

small and immediate . For test FST4DS, there was a slight decrease in both the specimen and water volume at the end of Stage I. These decreases could be due to the fact that the applied matric suction was slightly higher than the initial matric suction of the specimen. Figure 5.22 and 5.23 present the resulted matric suction versus void ratio and water content curves. A summary of the test data is shown in Table 5.3.

One one-dimensional free swell test (i.e., test FST10S) was carried out on a silt specimen with its initial water content close to optimum. The matric suction of the specimen was reduced in three stages. At the end of the stage I testing, both the specimen and water volume were found to have decreased. These volume decreases were the result of a increase in the matric suction. A summary of the test data is shown in Table 5.3. The resulting matric suction versus void ratio and water content relations are presented in Figure 5.24.

The one-dimensional free swell test, FST1DT was performed on a glacial till specimen with its initial water content dry of optimum. The matric suction of the specimen was reduced to 10 kPa in four stages. There were decreases in both the specimen and water volume at the end of the stage I of testing. These decreases could be due to the fact that the applied matric suction was actually higher than the initial matric suction of the specimen. A summary

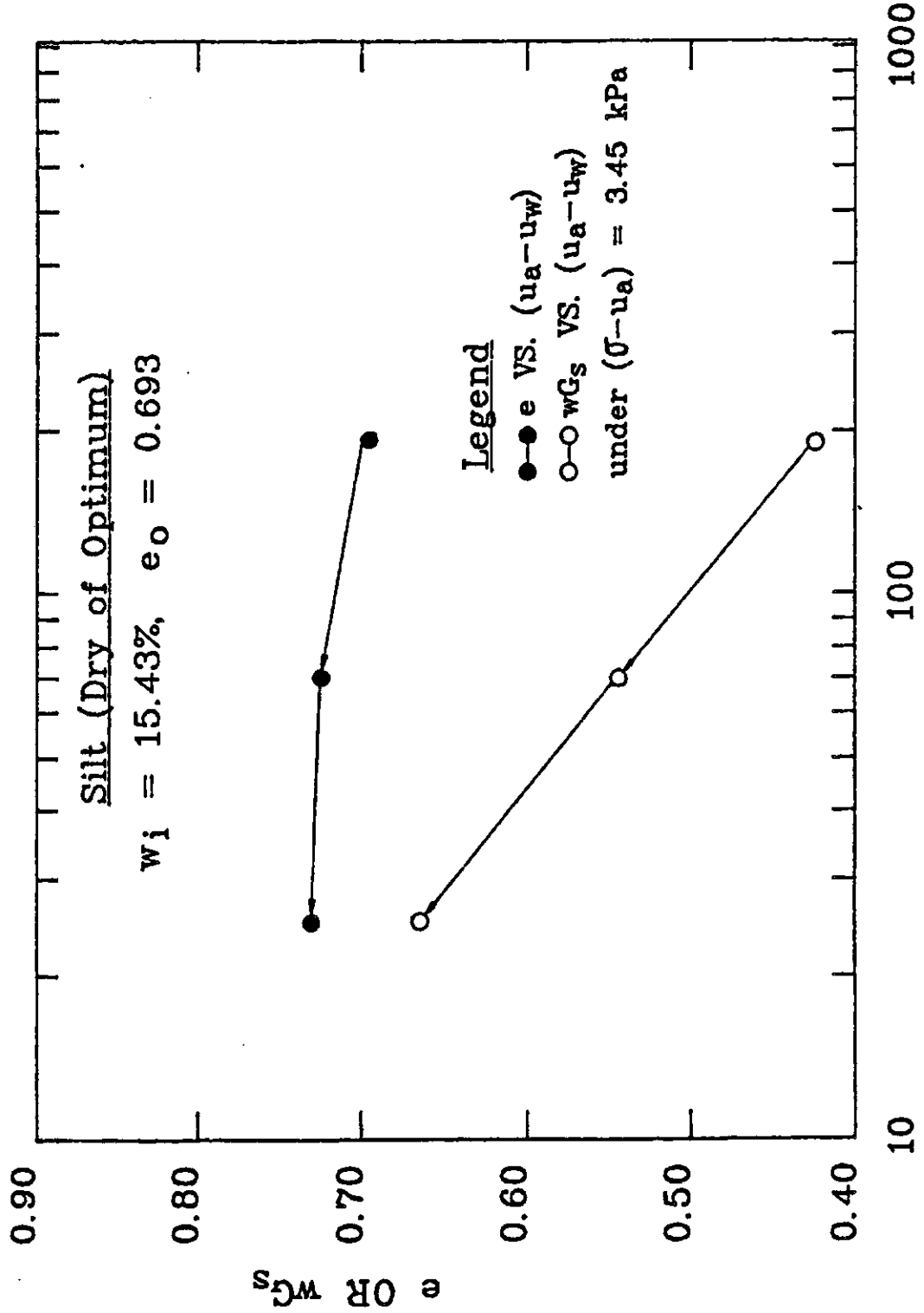

Figure 5.22 Results for One-Dimensional Free Swell Test FST3DS

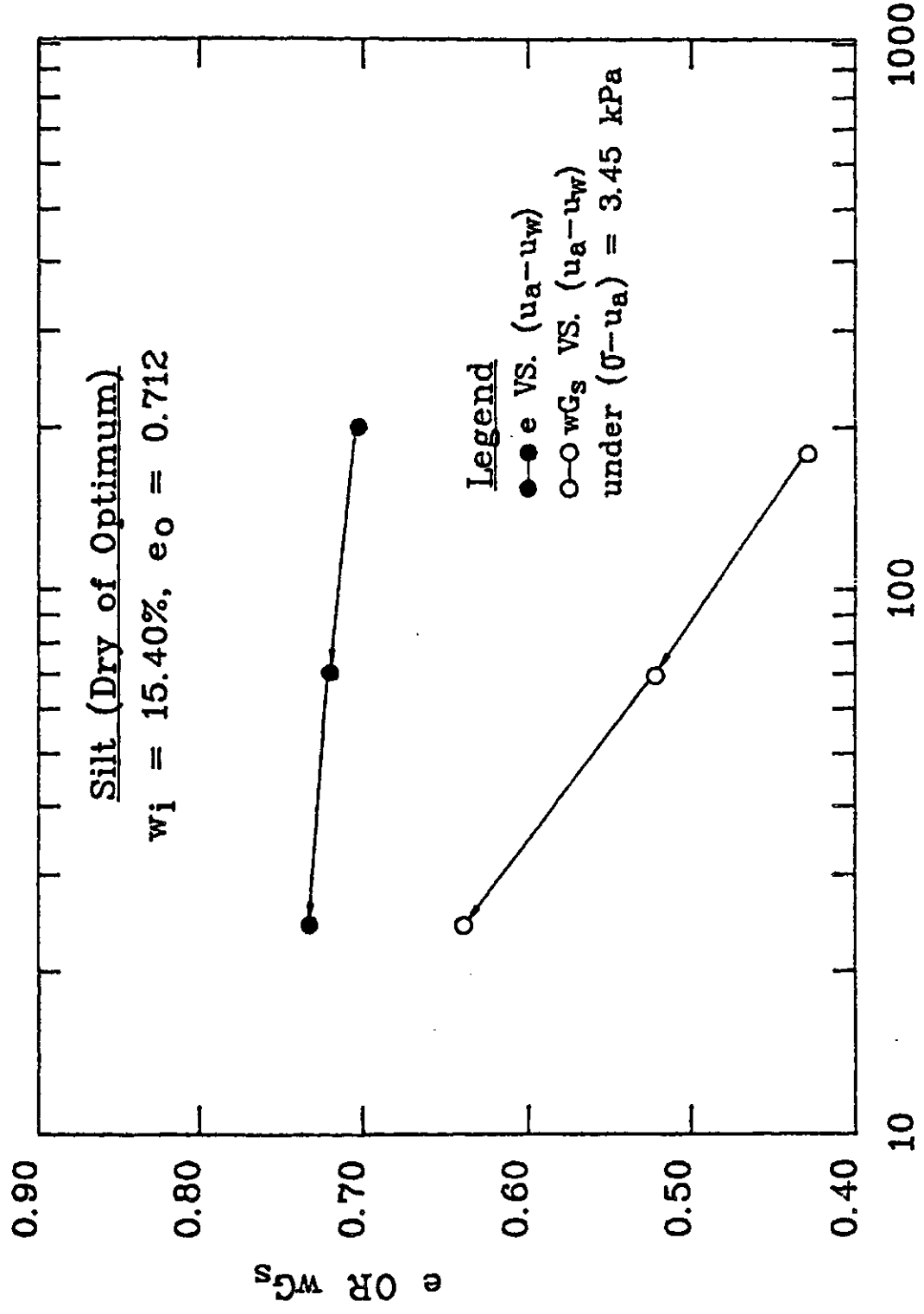

Figure 5.23 Results for One-Dimensional Free Swell Test FST4DS

Table 5.3 Summary of One-Dimensional Free Swell Test Data

TEST NO.	INITIAL e_o	INITIAL w_i (%)	INITIAL VOL.(cm^3)	INITIAL WT.(gm)	STAGE NO., SPECIMEN VOLUME CHANGE (cm^3) / $(u_a - u_w)$ (kPa) WATER VOLUME CHANGE (cm^3)							
FST3DS	0.6930	15.43	55.4053	102.70	I, +0.1284 / 190, +0.20	II, +0.9682 / 70, +3.88	III, +0.1302 / 25, +3.90					
FST4DS	0.7117	15.40	54.7762	100.40	I, -0.0099 / 190, -0.05	II, +0.2779 / 70, +3.55	III, +0.3687 / 25, +3.60					
FST10S	0.6156	19.00	54.1342	108.40	I, -0.035 / 150, -0.21	II, +1.1494 / 40.7, +1.90	III, +0.8123 / 12.9, +1.75					
FST1DT	0.6926	15.77	54.7505	103.50	I, -1.9066 / 451, -0.50	II, +0.9052 / 190, +2.00	III, +1.0554 / 50, +1.75	IV, +0.972 / 10, +3.10				
FST10T	0.5709	18.92	53.4858	111.90	I, -0.1587 / 270, -0.75	II, +0.3968 / 41.4, +1.85	III, +0.6944 / 6.2, +0.85					

* All tests were carried out under a token stress $(\sigma - u_a)$ of 3.45 kPa

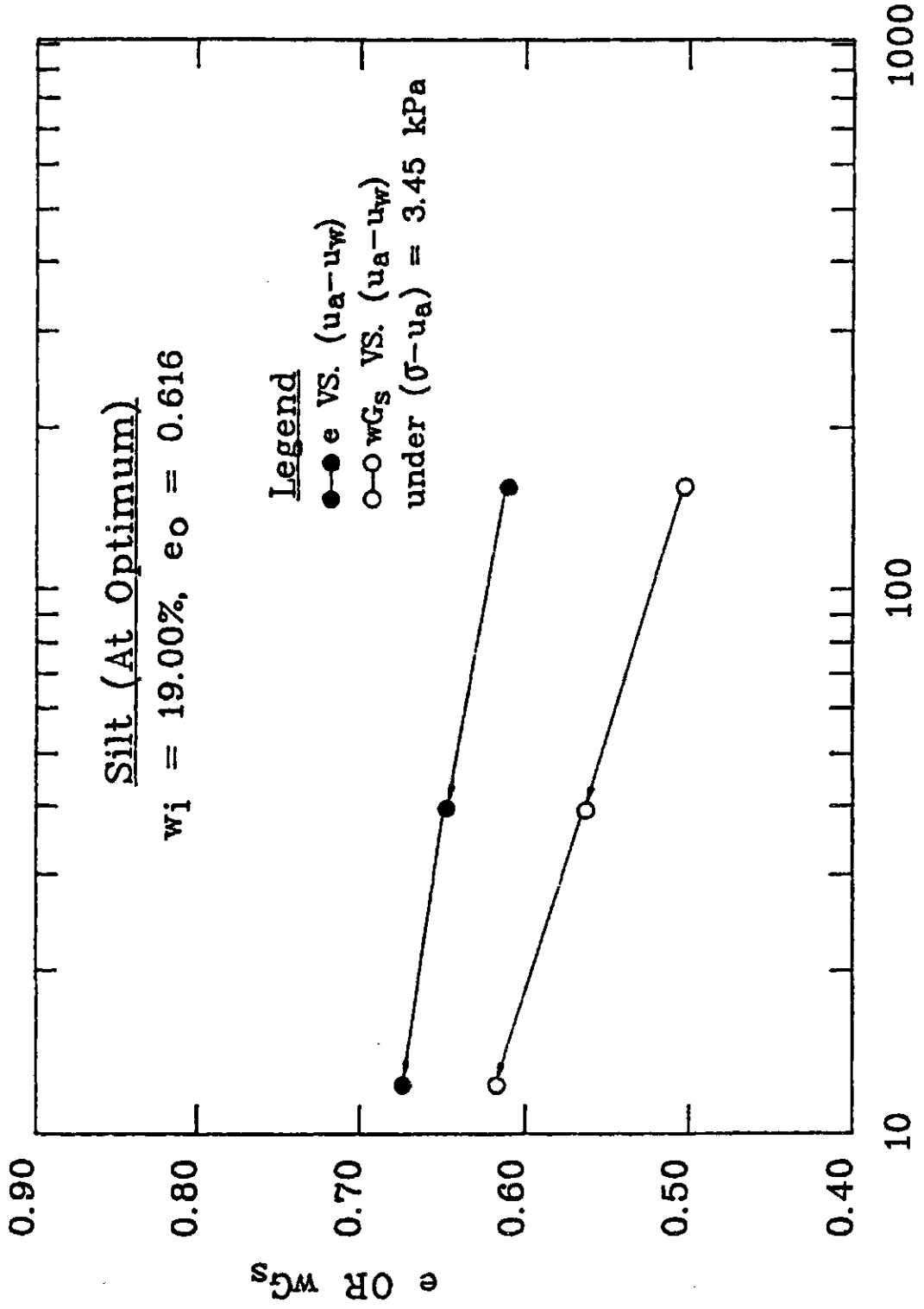

Figure 5.24 Results for One-Dimensional Free Swell Test FST10S

of the test data is given in Table 5.3. The resulting matric suction versus void ratio and water content relations are presented in Figure 5.25.

Test FST10T was the only one-dimensional free swell test carried out on a glacial till specimen with its initial water content close to optimum. The matric suction of the specimen was reduced in three stages to 6.2 kPa. The specimen was initially conditioned to a matric suction of 270 kPa during the state I of testing. Both the specimen and water volume were decreased as a result. It appears the applied matric suction was higher than the initial matric suction of the specimen. The test data are summarized in Table 5.3. The resulting matric suction versus void ratio and water content relations are shown in Figure 5.26.

5.7 Isotropic Constant Volume Loading and Unloading Tests

An isotropic constant volume loading and unloading test was used to establish the net total stress, $(\sigma - u_a)$ versus void ratio and water content relations under isotropic conditions. Specially equipped stress controlled isotropic cells were used to perform the tests. Details of the equipment set up are discussed in Appendix B-5.

Four isotropic constant volume loading and

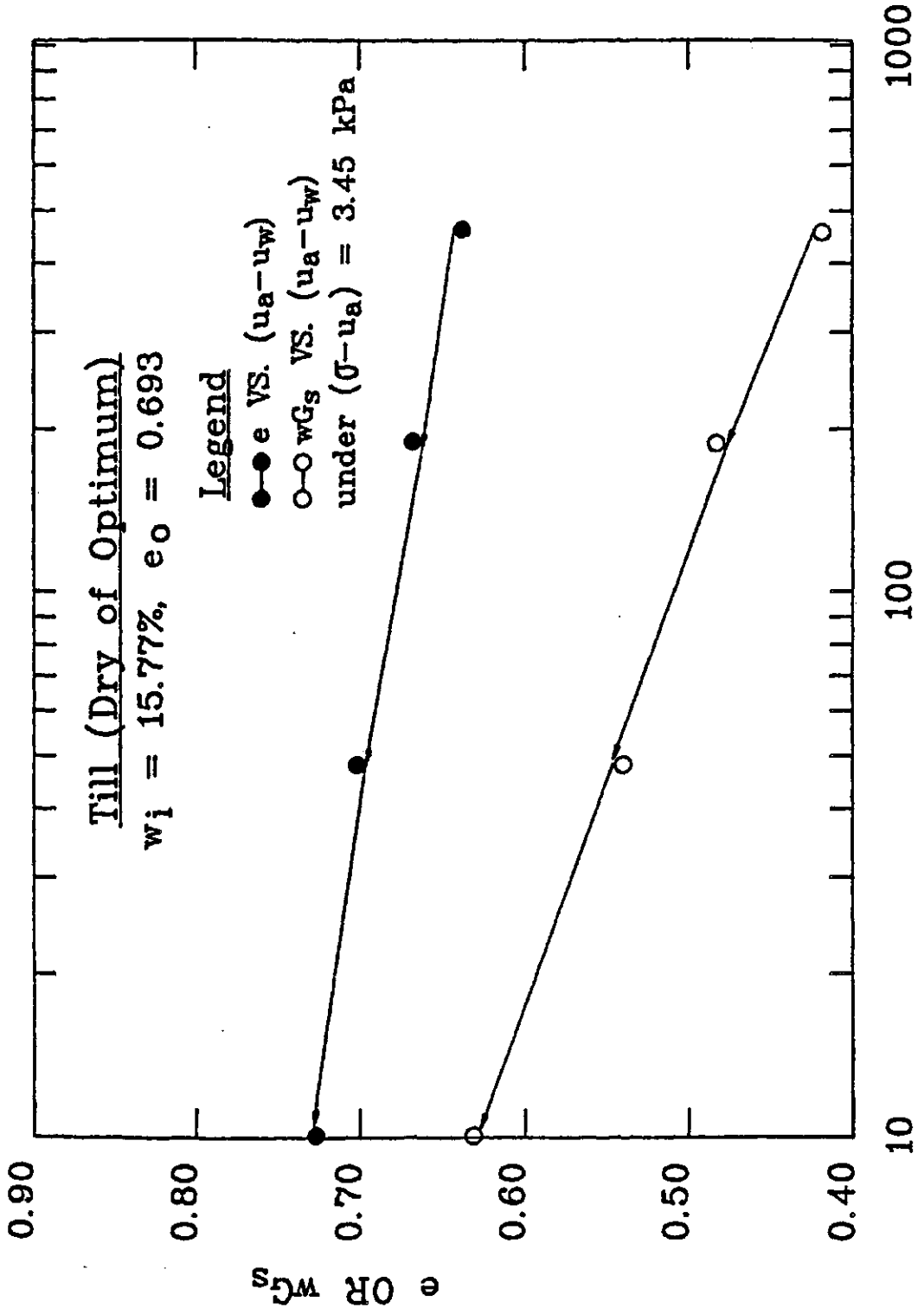

Figure 5.25 Results for One-Dimensional Free Swell Test FST1DT

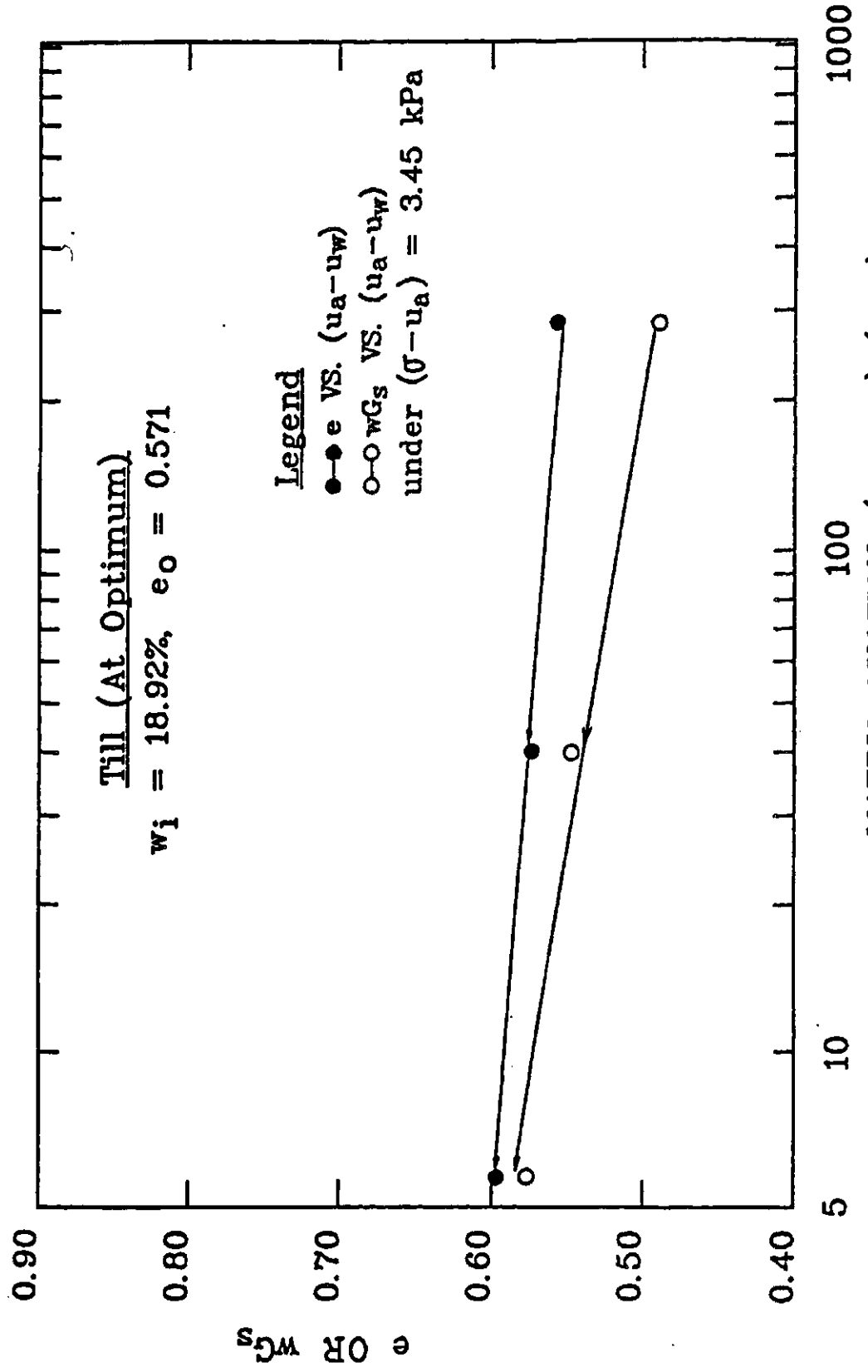

Figure 5.26 Results for One-Dimensional Free Swell Test FST10T

unloading tests (i.e., tests TCVT1DS, TCVT2DS, TCVT3DS and TCVT4DS) were performed on silt specimens with initial water contents dry of optimum. TCVT1DS was a trial test to establish the test procedure. At the beginning of the stage I testing, stresses were applied to the specimen as follows. First, the pore-air pressure was applied, then the cell pressure were applied and finally the pore-water pressure were applied. This procedure was used in order to avoid compressing the specimen unintentionally. The loading cap was found being lifted out of position. The test was abandoned. For test TCVT2DS, the cell pressure was applied to the specimen first. About two seconds later, the pore-air pressure was applied. However, the loading cap was again found to be lifted out of position. The test was abandoned. It was realized that the cell chamber would require a longer time period to pressurize because of this large volume. The stress application sequence was again revised. The cell and pore-water pressure was applied to the specimen first. About fifteen seconds later, the pore-air pressure was then applied to the specimen. The revised stress application procedure prevented the loading cap from being lifted-off. However, the subsequent specimens were found to be compressed by the cell pressure prior to the application of the pore-air and pore-water pressure. The specimen of TCVT3DS was loaded to a maximum net total stress of 605.5 kPa under a nominal matric suction of approximately

1 kPa. The cell pressure regulator failed and the test was abandoned. The specimen for test TCVT4DS was loaded to maximum $(\sigma - u_a)$ stress of 543 kPa and unloaded to 9.1 kPa under a constant matric suction of 10 kPa. The resulted void ratio versus net total stress curves are presented in Figure 5.27.

Two isotropic constant volume loading and unloading tests (i.e., TCVT10S and TCVT20S) were carried out on silt specimens with initial water contents close to optimum. During the TCVT10S test, the air pressure valve, attached to the stress controlled isotropic cell, was unintentionally closed. This error made the stress condition of the specimen during the test indeterminate. The test data are therefore disregarded. The specimen for TCVT20S was loaded to a maximum net total stress of 571 kPa and then unloaded to 10 kPa under a constant matric suction of 10 kPa. The resulting void ratio versus net total stress $(\sigma - u_a)$ curve is presented in Figure 5.28.

5.8 Isotropic Free Swell Tests

The isotropic free swell test was used to establish the void ratio and water content versus decreasing matric suction relations when net total stress, $(\sigma - u_a)$ equals to zero and under isotropic strain conditions. The stress

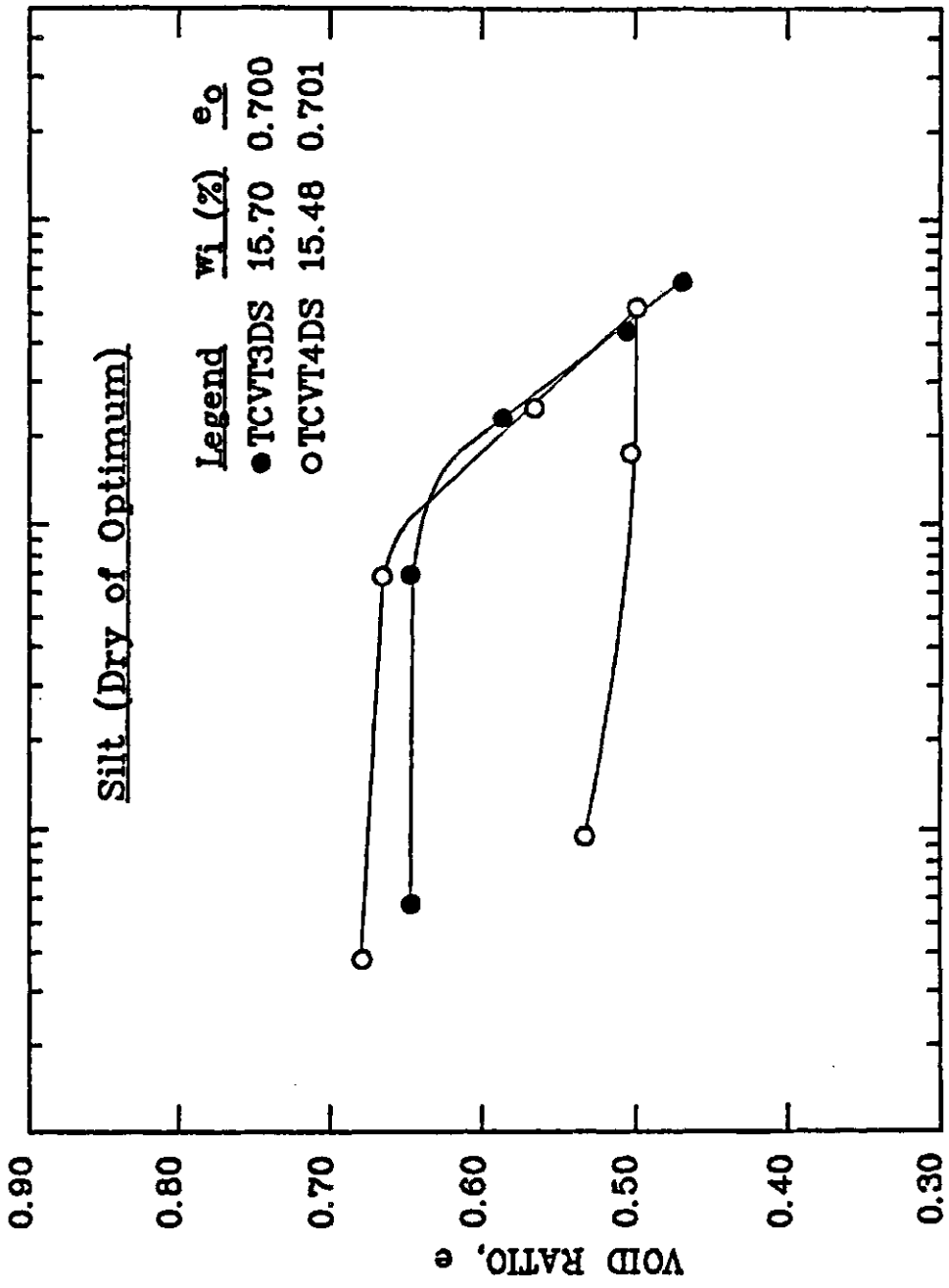

Figure 5.27 Results for The Isotropic Constant Volume Loading and Unloading Tests TCVT3DS and TCVT4DS

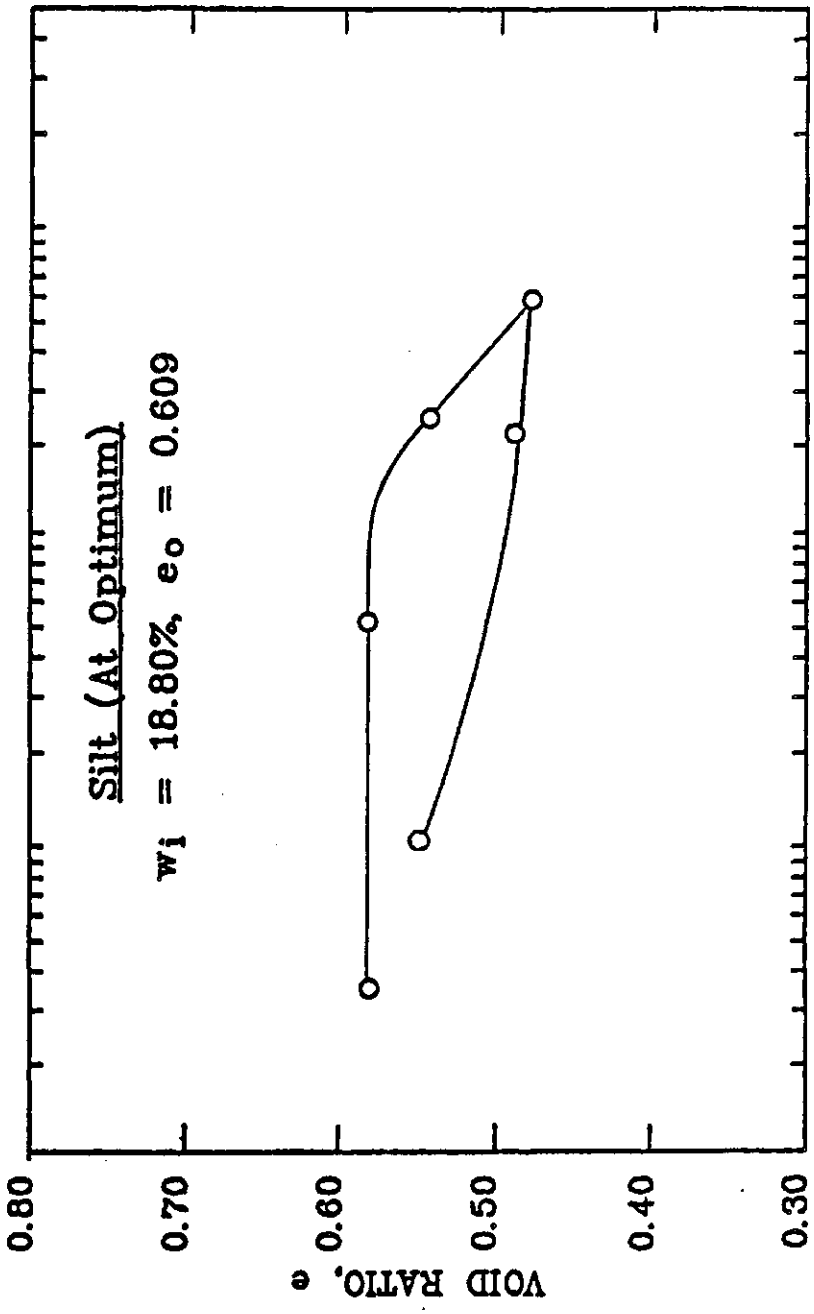

Figure 5.28 Results for The Isotropic Constant Volume Loading and Unloading Test TCVT10S

controlled isotropic cell used was prepared prior to performing the tests as discussed in Appendix B-5.

Two isotropic free swell tests (i.e., TFST1DS and TFST2DS) were carried out on silt specimens with initial water contents dry of optimum. The air pressure regulator failed shortly after test TFST1DS started. The test was abandoned. The matric suction of the specimen for test TFST2DS was reduced to 8 kPa in three stages under a token net total stress of 3 kPa. A summary of the test data is shown in Table 5.4. Both the specimen and water volume were found to have decreased at the end of the stage I testing. These decreases could be due to the fact that the applied matric suction was higher than the initial matric suction of the specimen. At the end of the stage IV testing, the data showed that the specimen had reached a degree of saturation of over 100%. This anomaly could have been caused by adding excessive water to the specimen. The extra water could have been held within the porous stone above the specimen. The last water content measurement in the test was therefore dismissed as erroneous. The void ratio is equal to the water content multiplied by the relative density when a soil approaches saturation. The last void ratio measurement in the test was then used as a control point in defining the water content versus decreasing matric suction curve. The resulting void ratio and water content versus matric suction relations are shown in Figure 5.29.

Table 5.4 Summary of Isotropic Free Swell Test Data

TEST NO.	INITIAL e_o	INITIAL w_i (%)	INITIAL VOL. (cm^3)	INITIAL WT. (gm)	STAGE NO., $(u_a - u_w)$ (kPa) / WATER VOLUME CHANGE (cm^3)							
TFST2DS	0.6991	15.48	311.79	576.08	I, -7.40	II, +2.10	III, +1.90	IV, +1.00
					190 -0.80	74 +20.20	24 +19.00	8 +25.80
TFST10S	0.6233	18.67	312.812	621.69	I, -9.30	II, +1.10		
					150 -7.50	80 +4.00		
TFST20S	0.6089	18.89	310.71	624.16	I, -6.00	II, +1.00	III, +1.70	IV, +2.50
					159 -5.50	80 +2.90	35 +5.50	10 +6.50

* All tests were carried out under a token stress $(\sigma - u_a)$ of 3.0 kPa

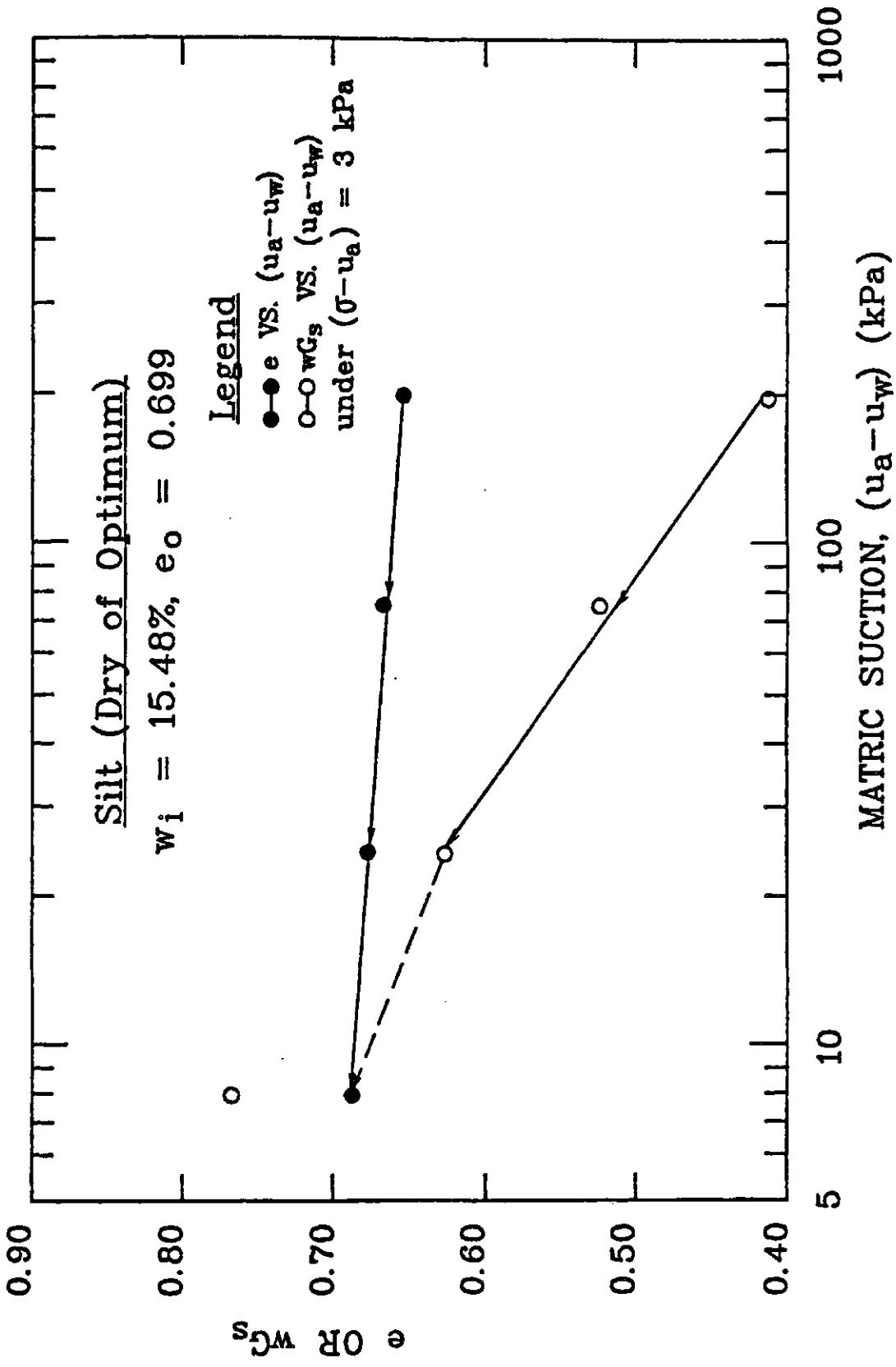

Figure 5.29 Results for The Isotropic Free Swell Test TFST2DS

Two isotropic free swell tests (i.e. TFST10S and TFST20S) were performed on silt specimens with initial water contents close to optimum. A summary of the test data is presented in Table 5.4. For both tests, the specimen and water volume were found to have decreased at the end of the stage I testing. These decreases could be caused by the applied matric suction being higher than the initial matric suction of the specimen. At the end of the stage II testing for test TFST10S, the pressure supply of the system failed. The test was stopped. The resulting void ratio and water content versus matric suction curves for both tests are shown in Figure 5.30.

5.9 Summary

Seven different types of tests were performed in the test program. A total of ninety five tests were attempted and seventy-six were successful. A summary is provided in Table 5.5.

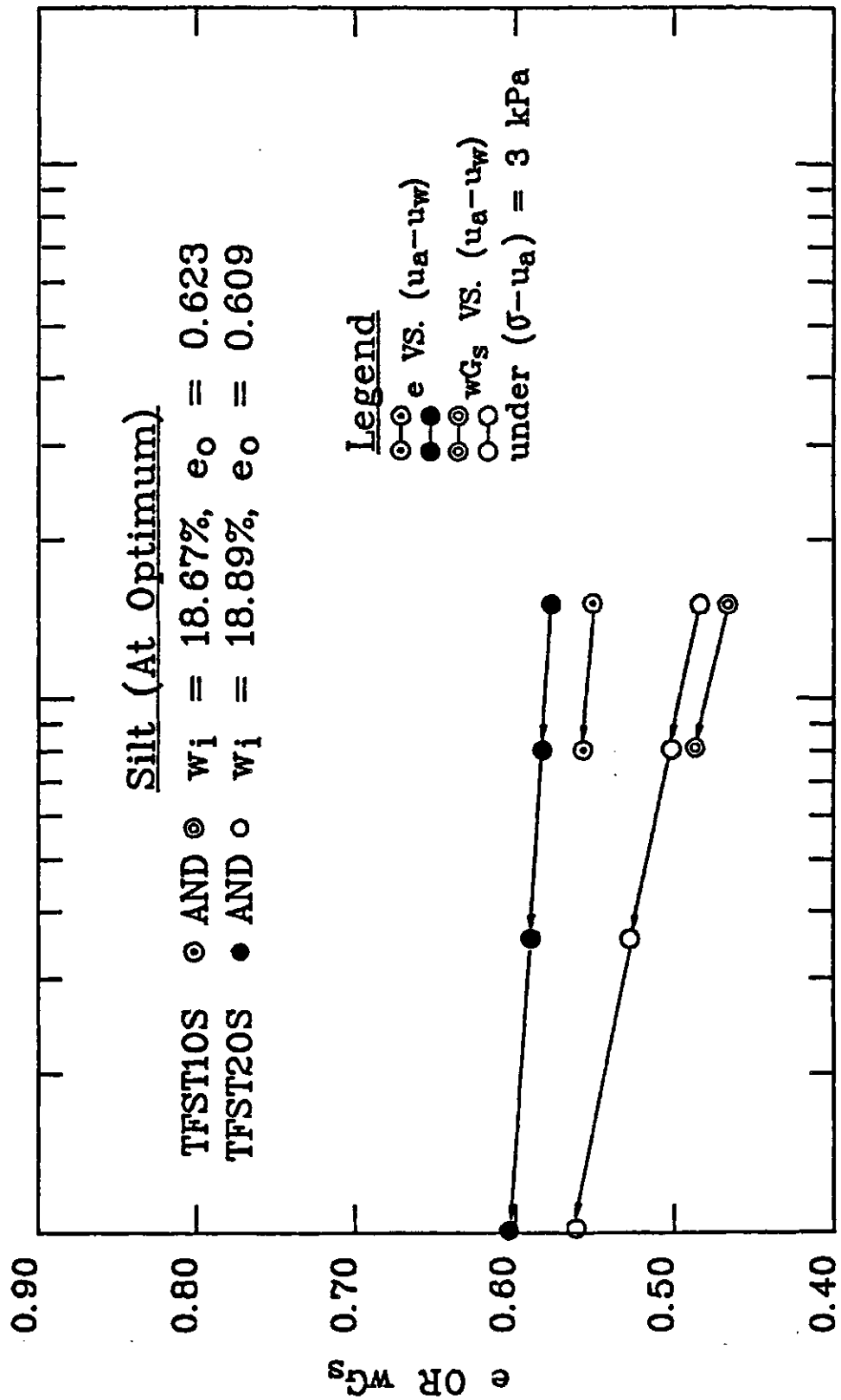

Figure 5.30 Results for The Isotopic Free Swell Test TFST10S and TFST20S

Table 5.5 A Summary of All Tests Performed

TEST TYPE	SILT DRY OF OPT.	SILT AT OPT.	TILL DRY OF OPT.	TILL AT OPT.	TOTAL NO.
Null Pressure Plate Tests, PP	3(1)	3(1)			6(2)
Suction Tests, ST	5(5)	9(9)	6(3)	6(3)	23(20)
Unconfined Shrinkage Tests, SLT					
- mercury submersion, SLTM	3(2)				3(2)
- resin-coating, SLTR	3(2)				3(2)
- direct measurement, SLTD	5(5)	5(5)	1(1)		11(11)
- combined SLTM and SLTD		1(1)	1(1)	2(1)	4(3)
- control tests, SLTM-SLTD	4(4)	5(5)			9(9)
- control tests using STEEL plug, SLTM-SLTD					3(3)
One Dimensional Constant Volume Loading and Unloading Tests,CVT	6(6)	4(4)	3(3)	3(3)	16(16)
One Dimensional Free Swell Tests, FST	4(2)	1(1)	1(1)	1(1)	7(5)
Isotropic Constant Volume Loading and Unloading Tests, TCVT	4(2)	2(1)			6(3)
Isotropic Free Swell Tests, TFST	2(1)	2(2)			4(3)
Total	39(30)	32(29)	12(9)	12(8)	95(76)

*Note: numbers in ( ) are the numbers of successful tests

CHAPTER VI

ANALYSIS AND DISCUSSION OF RESULTS

6.1 Introduction

This chapter analyses, discusses and interprets experimental results from the test program. Test results are combined to show the form of the semi-logarithmic soil structure and water phase constitutive surfaces. Section 3.5 developed and presented relationships between moduli based on the geometry of an approximated planar constitutive surfaces. These proposed relationships are examined in the latter portion of this chapter.

6.2 Analysis of Results from The Test Program

This section analyzes and discusses results from tests under the test program headings of Sub-program I and II presented in Section 4.4. Sub-program I tested soils under stress changes involving no lateral expansion. Sub-program II tested soils under isotropic changes of total stress and matric suction. Results from the same type of tests on specimens of similar initial conditions are combined and averaged. The average test results are interpreted in Section 6.3 and 6.4 to examine the proposed

relationships between the various moduli.

6.2.1 Tests to evaluate the initial matric suction

Null pressure plate tests were used to determine the initial matric suction of silt specimens compacted dry of optimum and at optimum initial water contents. Test data were shown in Figure 5.1 and 5.2. The applied air pressure under which a specimen shows no tendency to either absorb or displace water is taken as the matric suction of the specimen. The tendency of water movement was measured by the water pressure at the basal compartment underneath the high air entry disc of the pressure plate apparatus (See Figure 4.22). A summary of the test results is given in Table 6.1. The matric suction of silt specimens compacted dry of optimum and at optimum initial water contents are taken as 117.5 kPa and 100.0 kPa respectively.

In 1970, Krahn presented suction versus water content curves for different compacted soils. The glacial till used in this test program was one of the soils tested. It was found that a variation in dry density has little effect on the matric suction of remoulded compacted soils. The relation between suction and water content was concluded to be a fairly unique function, quite independent of the dry density of a soil. A similar conclusion was drawn by other researchers (Olson and Langfelder, 1965) (Sauer, 1967). In view of such findings, the suction versus water content

Table 6.1 A summary of Results from Null Pressure Plate Tests on Silt Specimens

Soil Type	Test No.	Initial Void Ratio, e_o	Initial Water Content, w_i(%)	Initial Degree of Saturation S_i (%)	Measured Matric Suction, $(u_a - u_w)$ (kPa)
DS[a]	PP3DS	0.6991	15.52	60.35	117.5
OS[b]	PP2OS	0.6060	18.98	85.15	100.0

Note: a) "DS" stands for silt at dry of optimum initial water content.
b) "OS" stands for silt at optimum initial water content.

curve for glacial till (Figure 6.1) as presented by Krahn (1970) is used to determine the matric suction of the glacial till specimens. In the test program, the averaged water contents for till specimens at dry of optimum and at optimum conditions were 15.43 % and 18.65 % respectively. The averaged matric suction for till specimens at dry of optimum and at optimum initial water contents are found to be 315.0 kPa and 64.0 kPa accordingly.

6.2.2 Tests to establish the water content versus increasing matric suction relation

The suction tests were used to establish the water content versus increasing matric suction relation. Results from suction tests on silt and till specimens at dry of optimum and at optimum initial water contents are given in Table 5.1. Published information on the characteristic shape of the water content versus increasing matric suction curves is incorporated with the test results to define the water phase loading curve. The projected matric suction at zero water content from the linear portion of the water content versus increasing matric suction curve is set to be 300,000 kPa (Croney and Coleman, 1954) (See Section 3.2). The matric suction at zero water content is assumed to be at 6.2×10^5 kPa (Arnold, 1983) (See Section 3.2).

Five suction tests were performed on silt specimens

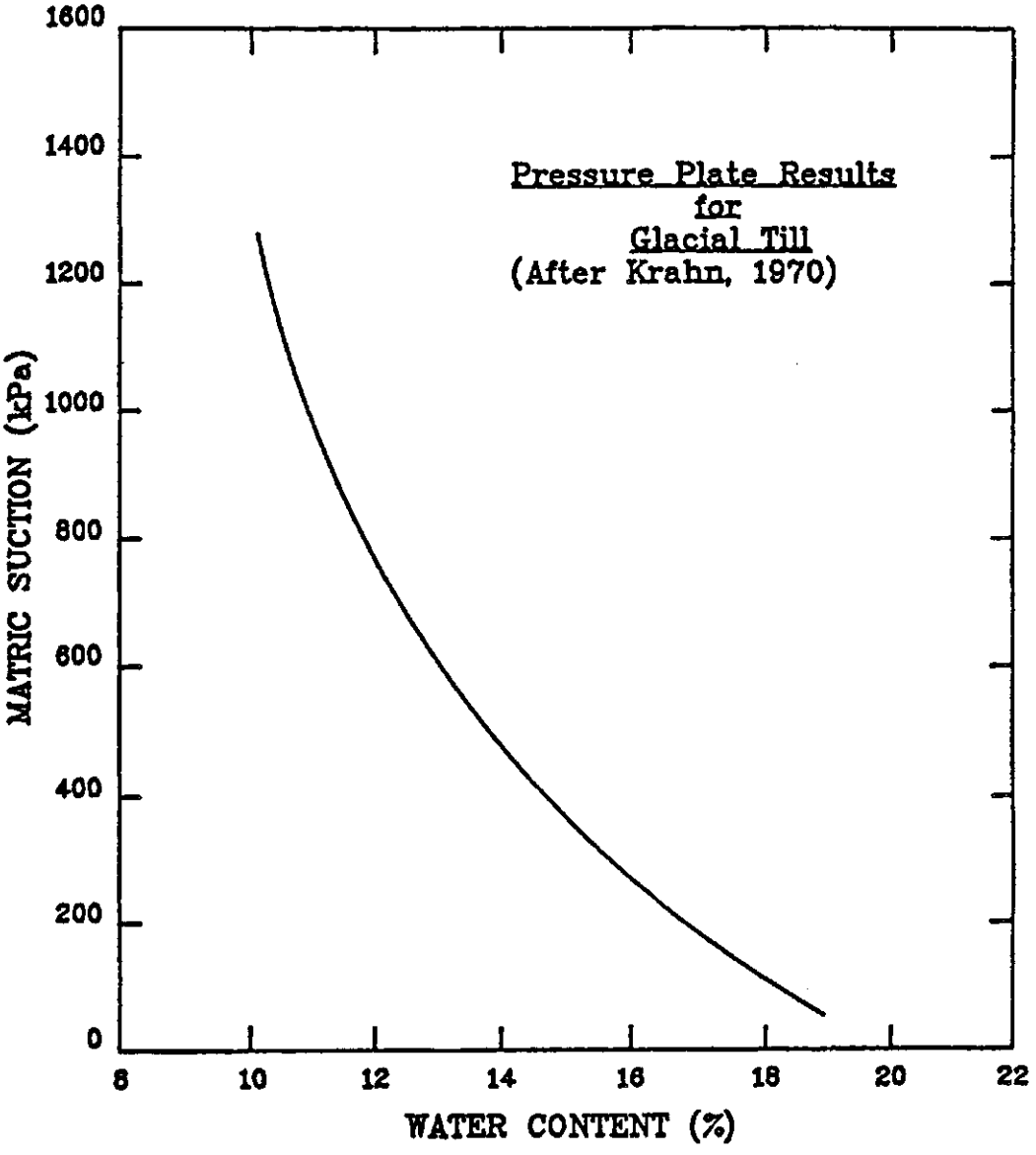

Figure 6.1 Matric Suction Versus Water Content Curve for Glacial Till (Krahn, 1970)

at dry of optimum initial water contents. The test results are combined with the result from the null pressure plate test (i.e., PP3DS) to define an average water content versus increasing matric suction curve (Figure 6.2). Similarly, results from the eight suction tests on silt specimens with optimum initial water contents are combined with the result from the null pressure plate test (i.e., PP20S) to find an average water content versus increasing matric suction curve (Figure 6.3).

In 1970, Krahn performed pressure plate tests on glacial till specimens similar to those used in this test program. The test results are shown in Figure 6.1. In 1984, Lee and Fredlund presented water content versus matric suction curves for the same glacial till (Figure 6.4). Heat dissipation sensors were used to measure the matric suction of the till specimens. These published water content versus matric suction curves are used to determine the initial matric suction of the till specimens in this test program. The so determined initial matric suction values are combined with the results from suction tests. The average water content versus increasing matric suction curves for till specimens at dry of optimum and at optimum initial water contents are shown in Figure 6.5 and 6.6. The slope of a water content versus increasing matric suction curve is equal to the water content index with respect to matric suction (i.e., D_m). A summary of the moduli determined

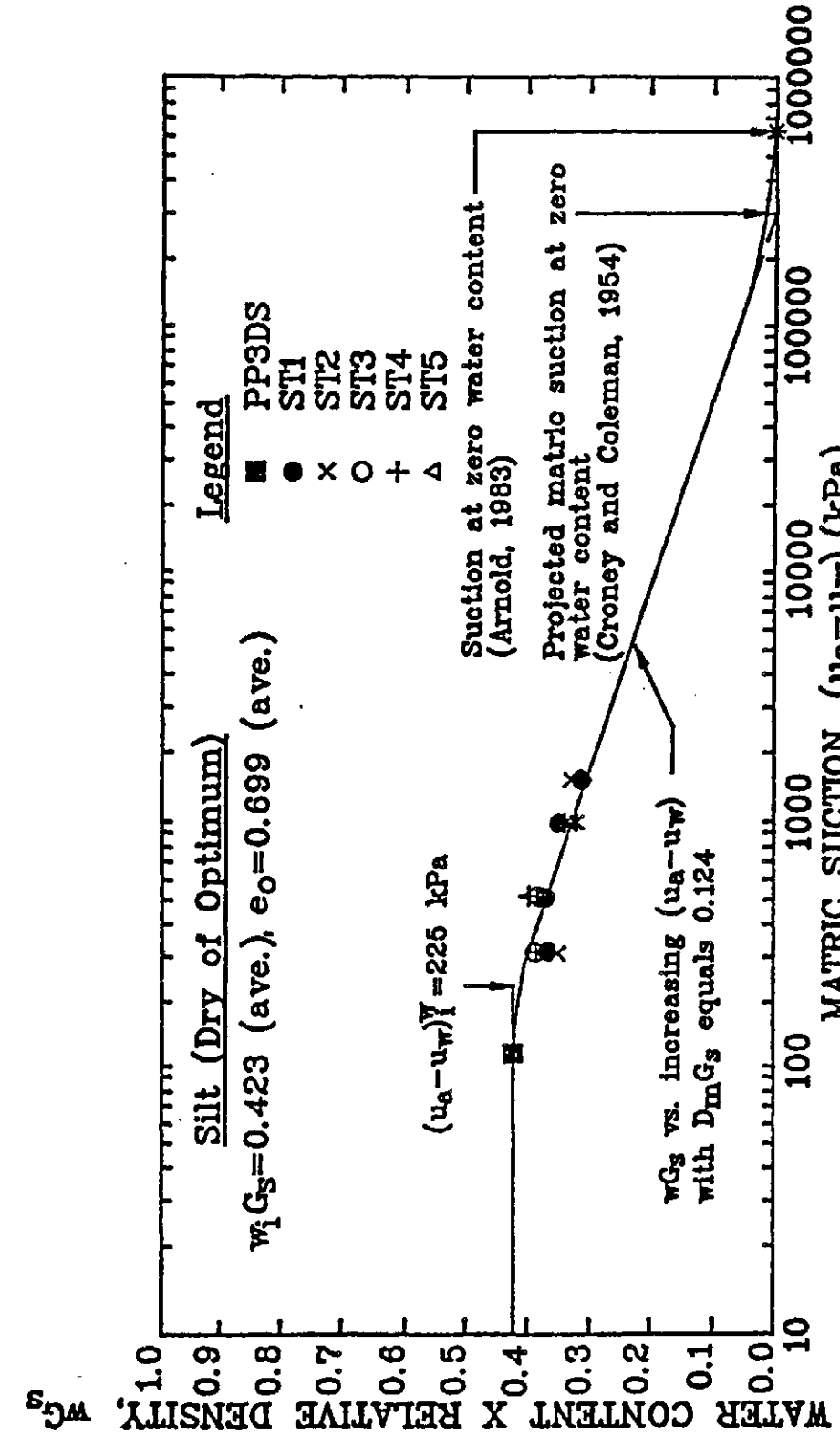

Figure 6.2 Average Water Content Versus Increasing Matric Suction Curve for Silt with Dry of Optimum Initial Water Content

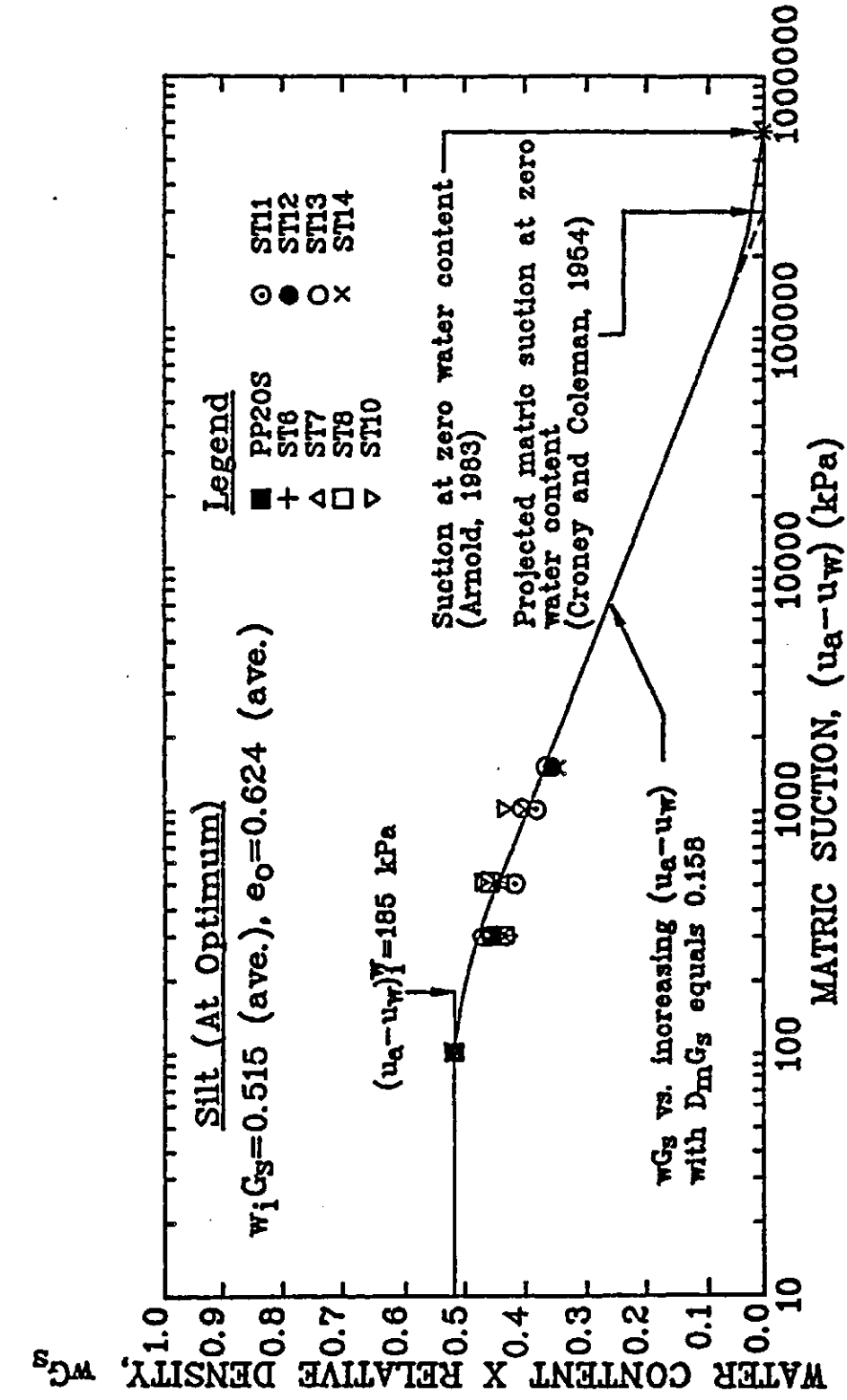

Figure 6.3 Average Water Content Versus Increasing Matric Suction Curve for Silt with Optimum Initial Water Content

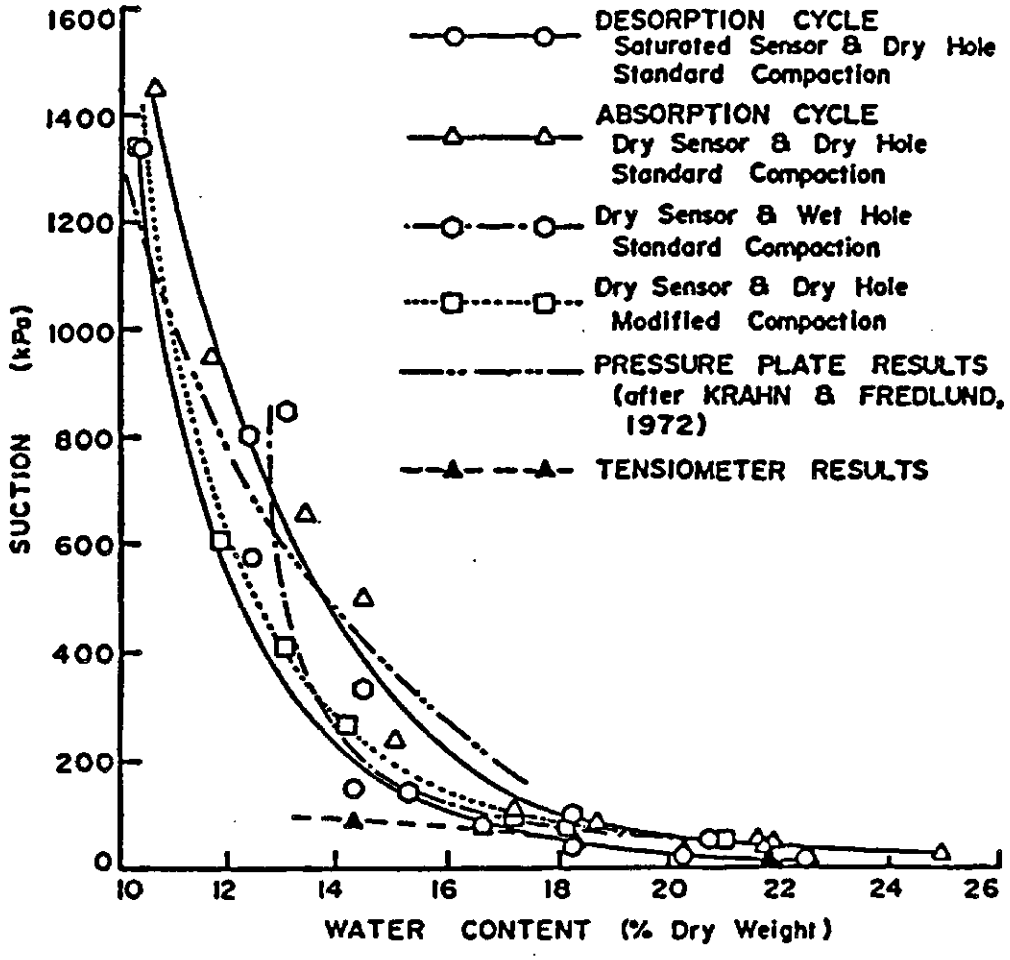

Figure 6.4 Matric Suction Versus Water Content for Glacial Till with Various Installation Methods (Lee and Fredlund, 1984)

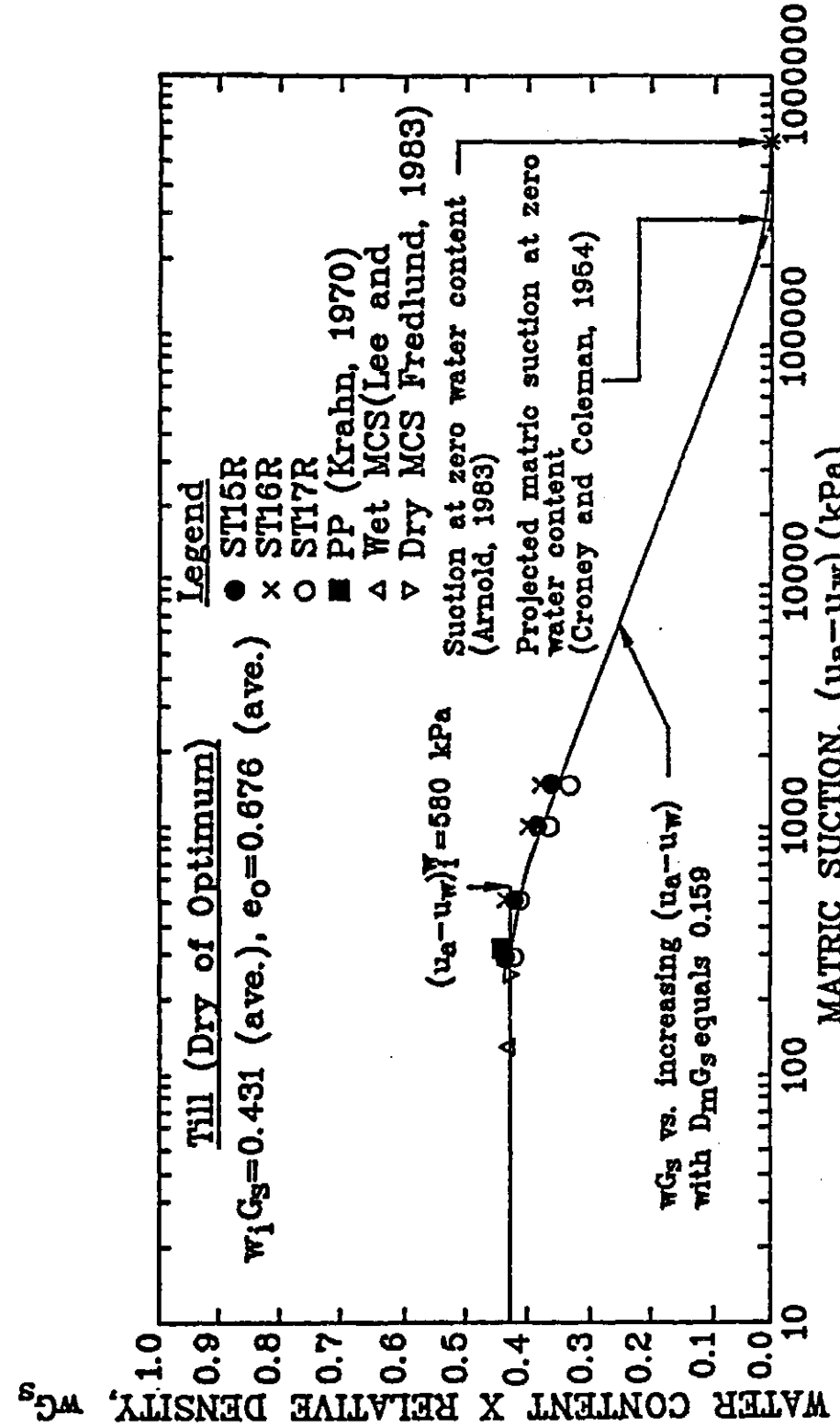

Figure 6.5 Average Water Content Versus Increasing Matric Suction Curve for Till with Dry of Optimum Initial Water Content

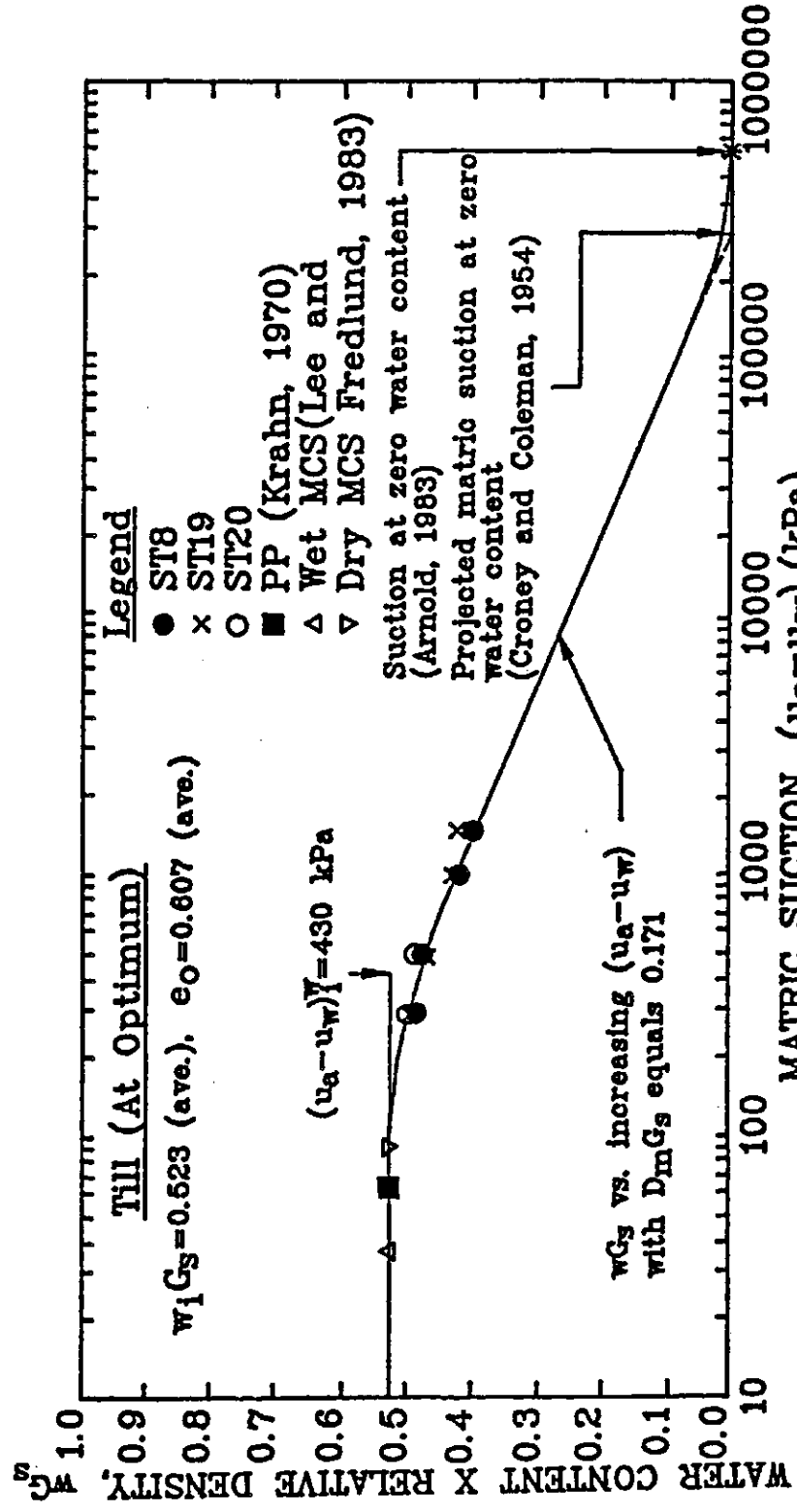

Figure 6.6 Average Water Content Versus Increasing Matric Suction Curve for Till with Optimum Initial Water Content

from the suction test results is given in Table 6.2.

In 1936, Casagrande presented a graphical procedure to estimate the preconsolidation pressure of a soil. The same procedure is used to determine the corrected initial matric suction of the specimens correcting for the effect of sample disturbance. The corrected initial matric suction for the silt specimens compacted dry of optimum and at optimum initial water contents are found to be 225.0 and 185.0 kPa respectively. The corrected initial matric suction for the till specimens compacted dry of optimum and at optimum initial water contents are found to be 580.0 and 430.0 kPa, respectively.

6.2.3 Unconfined shrinkage tests

The unconfined shrinkage test was used to establish the water content versus void ratio curve of a specimen under increasing matric suction. Three different methods were used to measure the specimen volume during the test. The three methods were the resin-coating submersion, mercury submersion and direct measurement technique. The resin-coating submersion method was abandoned after serious leaking problems with the resin coating were encountered (See Section 5.4). Volume measurements were made by the direct measurement technique with and without allowing the dial gauge tip to indent the specimen surface. A comparison

Table 6.2 A Summary of The Moduli Determined from The Average Water Content Versus Increasing Matric Suction Curves

Soil Type	Number of ST[a] Tests	e_o (ave.)	$w_i G_s$ (ave.)	S_i (%) (ave.)	$D_m G_s$
DS[b]	5	0.6989	0.4229	60.51	0.1241
OS[c]	8	0.6241	0.5153	82.57	0.1584
DT[d]	3	0.6760	0.4307	63.71	0.1588
OT[e]	3	0.6068	0.5231	86.21	0.1713

Note: a) "ST" stands for suction test
b) "DS" stands for silt at dry of optimum initial water content
c) "OS" stands for silt at optimum initial water content
d) "DT" stands for till at dry of optimum initial water content
e) "OT" stands for till at optimum initial water content

between void ratios determined from volume measurements with and without allowing the dial gauge tip to indent the specimen surface is shown in Figure 6.7. The percentage difference is small, less than three percent. The difference diminishes as the water content decreases. A comparison between water content versus void ratio curves from direct volume measurements with and without allowing the dial gauge tip to indent the specimen surface can be seen in Figure 5.6, 5.7, 5.9 and 5.10. The slope of the water content versus void ratio curve based on volume measurements allowing the dial gauge tip to indent the specimen surface is found to be less than that based on volume measurements not allowing the dial gauge tip to indent the specimen surface. The difference is insignificant for silt specimens initially compacted dry of optimum. Measurements of the volume of specimens were taken using both mercury submersion and the direct measurement technique. Direct volume measurements were made without allowing the dial gauge tip to indent the specimen surface. A comparison between void ratios determined by the two methods of measurement is presented (Figure 6.8). Void ratios determined by direct volume measurements are generally larger than those based on volumes determined by mercury submersion. The percentage difference is calculated as the difference between the void ratio determined by the direct volume measurement technique and that determined by

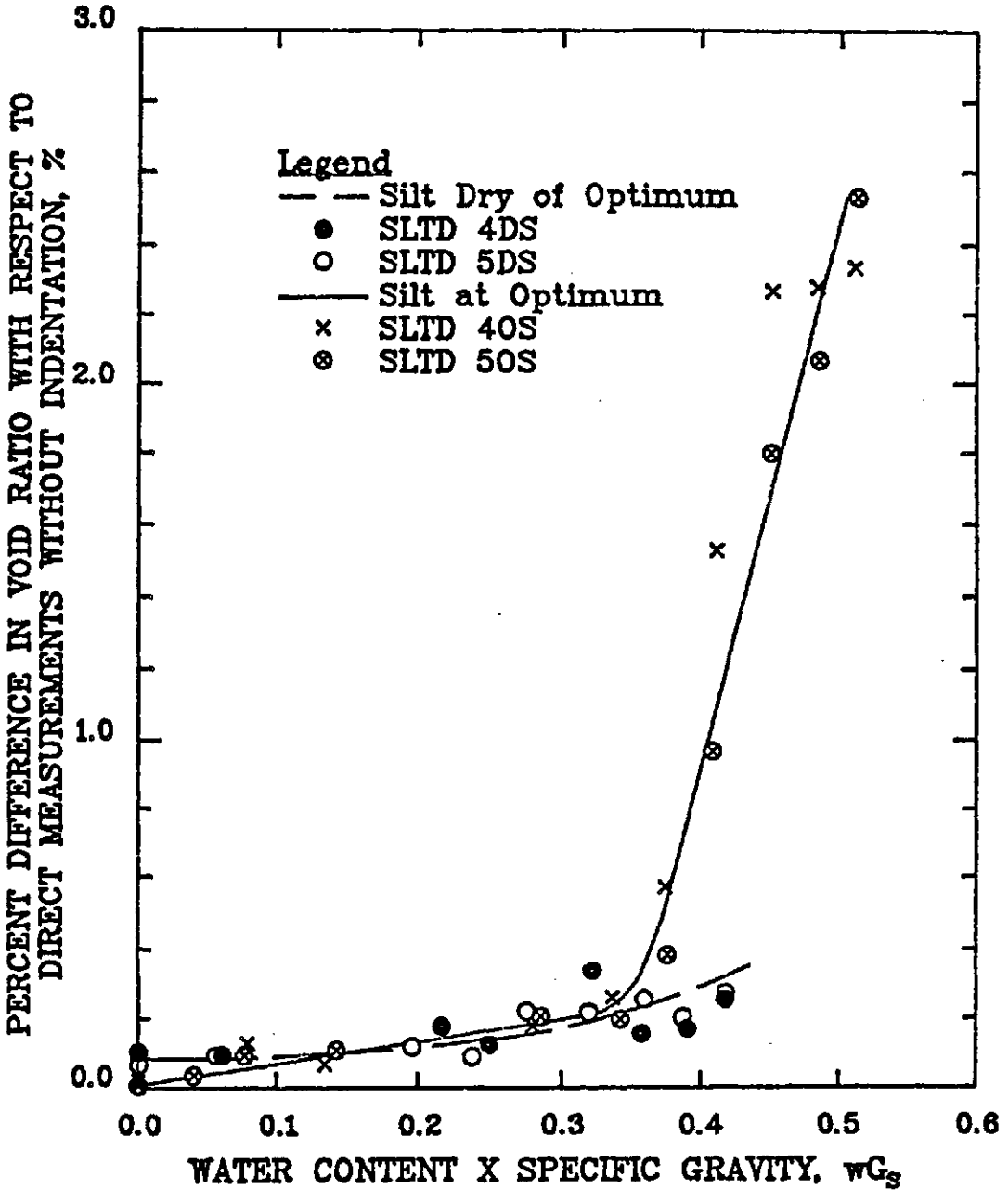

Figure 6.7 A Comparison between Void Ratios Determined by Direct Volume Measurements With and Without Surface Indentation

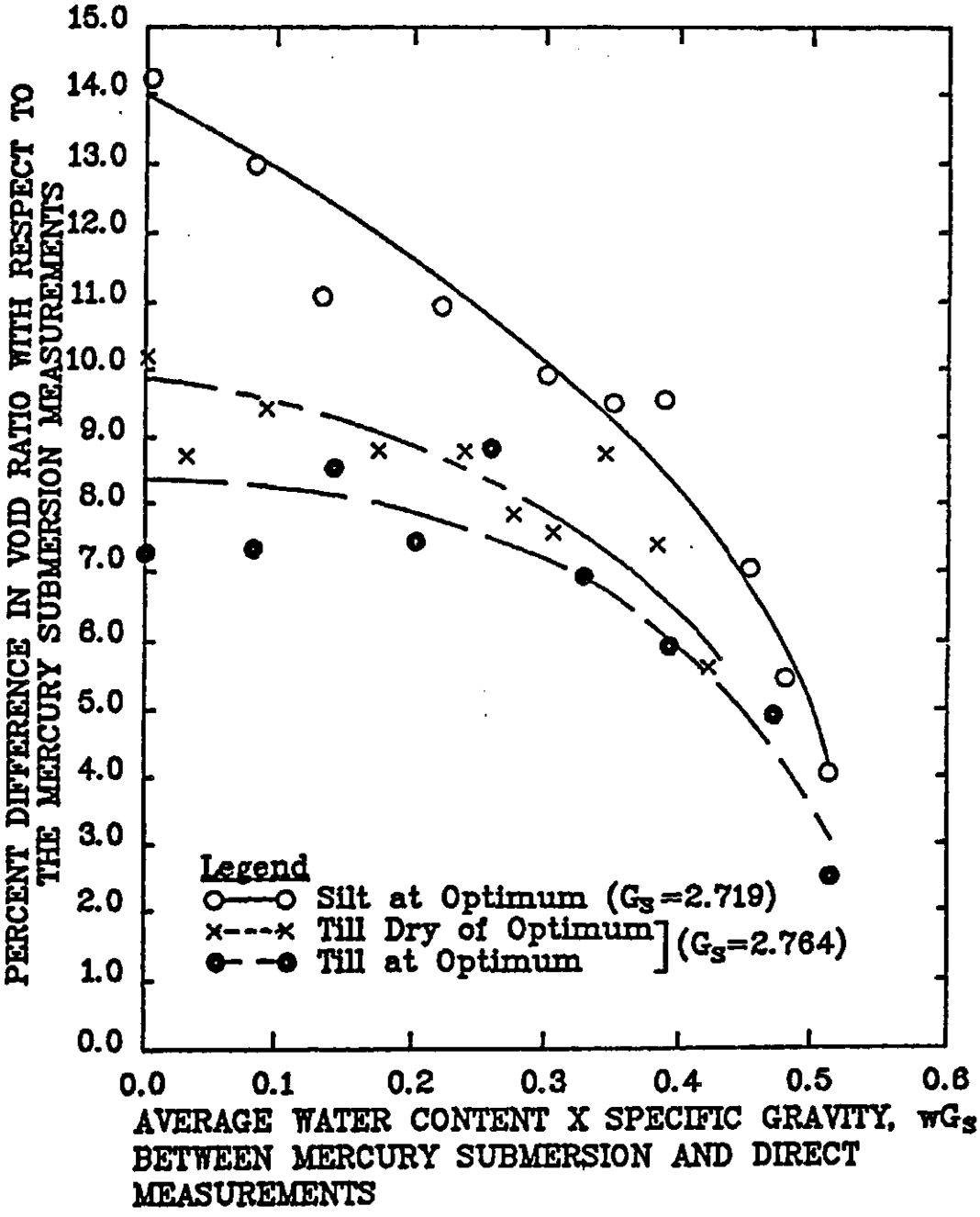

Figure 6.8 A Comparison between Void Ratios Determined by Mercury Submersion and Direct Measurements

the mercury submersion technique with the latter as the reference. The difference increases with decreasing water content, ranging from three to fifteen percents. This difference makes the slope of the water content versus void ratio curve determined by the direct measurement technique smaller than that determined by the mercury submersion method (See Figure 5.11, 5.12 and 5.13). Specimen volumes determined by the direct measurement method assume a perfectly intact specimen cylindrical in shape. The assumption over-estimates the specimen volume when the specimen surface is uneven. The unevenness may be caused by chipping due to handling. Specimen volume determined by the mercury submersion method and the resulting water content versus void ratio curve are therefore considered to be more reliable. Water content versus void ratio curves based on specimen volumes determined by the mercury submersion method are used in Section 6.3 to calculate the C_m/D_m moduli ratios.

6.2.4 One-dimensional constant volume loading and unloading tests

The one-dimensional constant volume loading and unloading test was used to establish the void ratio and water content versus net total stress relations. Test results obtained from specimens with similar initial

conditions are combined to define an average loading and unloading curve. The average loading and unloading curves for silt and till specimens compacted dry of optimum and at optimum initial water contents are shown in Figure 6.9, 6.10, 6.11 and 6.12. The slopes of the void ratio loading and unloading curves are the compressive and swelling indices with respect to the net total stress (i.e., C_t and C_{ts}) respectively. The moduli, C_t and C_{ts} are equal to $D_t G_s$ and $D_{ts} G_s$ when a soil is saturated (See Section 3.5.3). A summary of the moduli determined from the linear portions of the average loading and unloading curves is given in Table 6.3.

The loading curve of a remoulded compacted soil is characterized by the corrected swelling pressure (i.e., P_s'). The average corrected swelling pressure is determined by the Casagrande (1936) graphical procedure from the average loading curve. The average corrected swelling pressure for silt specimens compacted dry of optimum and at optimum are found to be 120.0 and 140.0 kPa. The average corrected swelling pressure for till specimens compacted dry of optimum and at optimum are found to be 90.0 and 145.0 kPa respectively.

6.2.5 One-dimensional free swell tests

The one-dimensional free swell test was used to

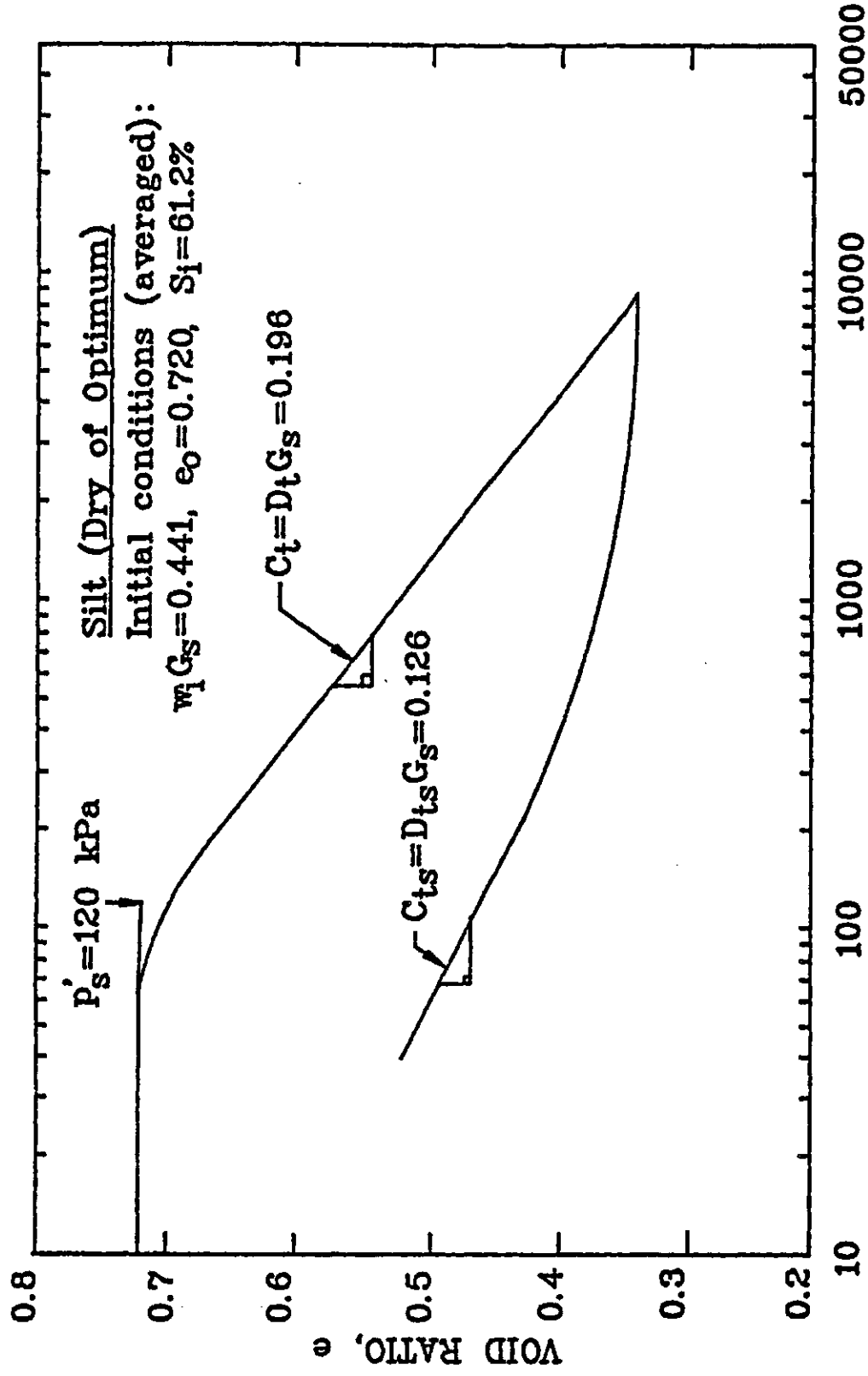

Figure 6.9 Mean Void Ratio Versus The Logarithm of Net Total Stress Curve for Silt Dry of Optimum under One-Dimensional Conditions

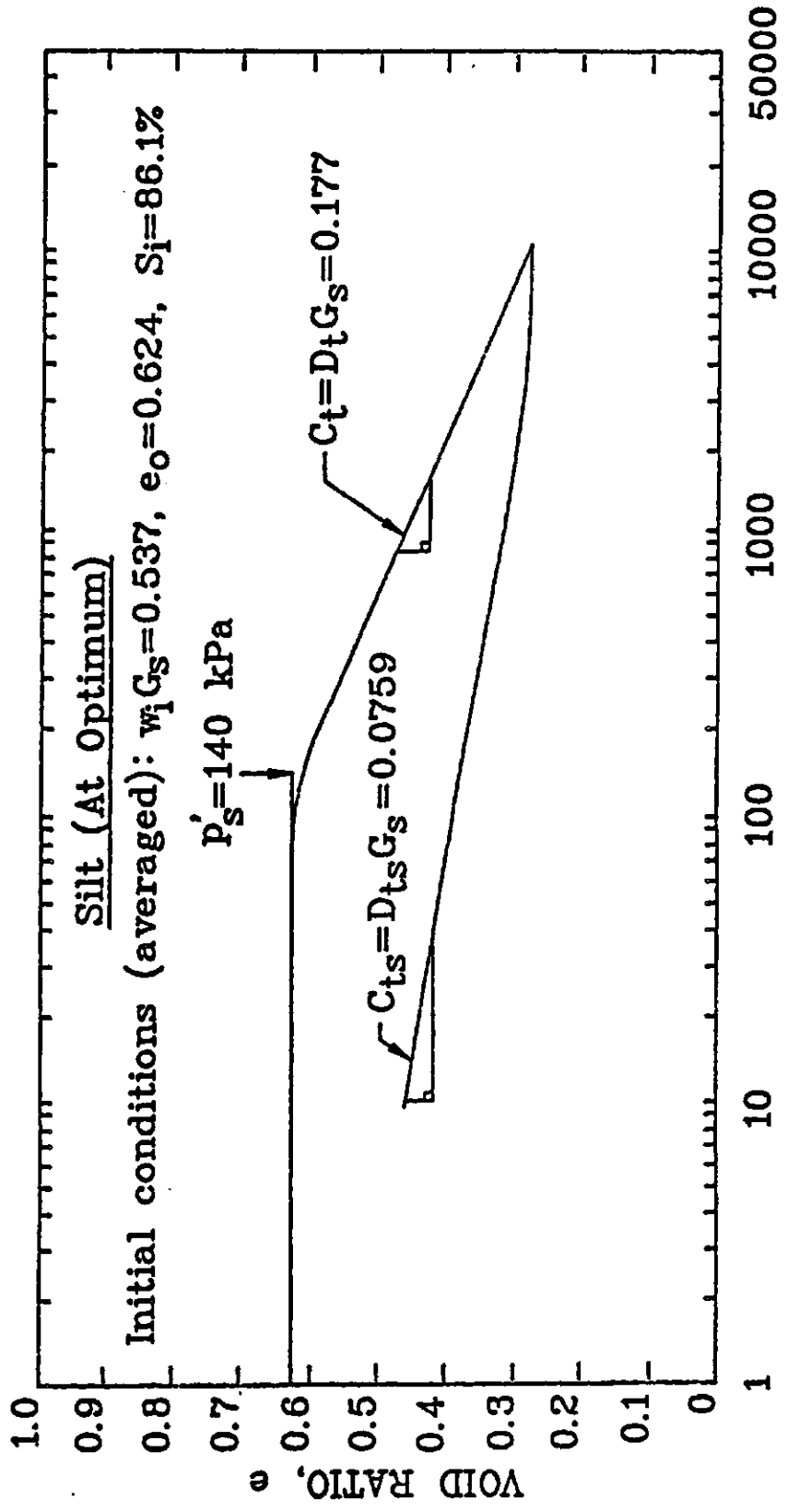

Figure 6.10 Mean Void Ratio Versus The Logarithm of Net Total Stress Curve for Silt at Optimum under One-Dimensional Conditions

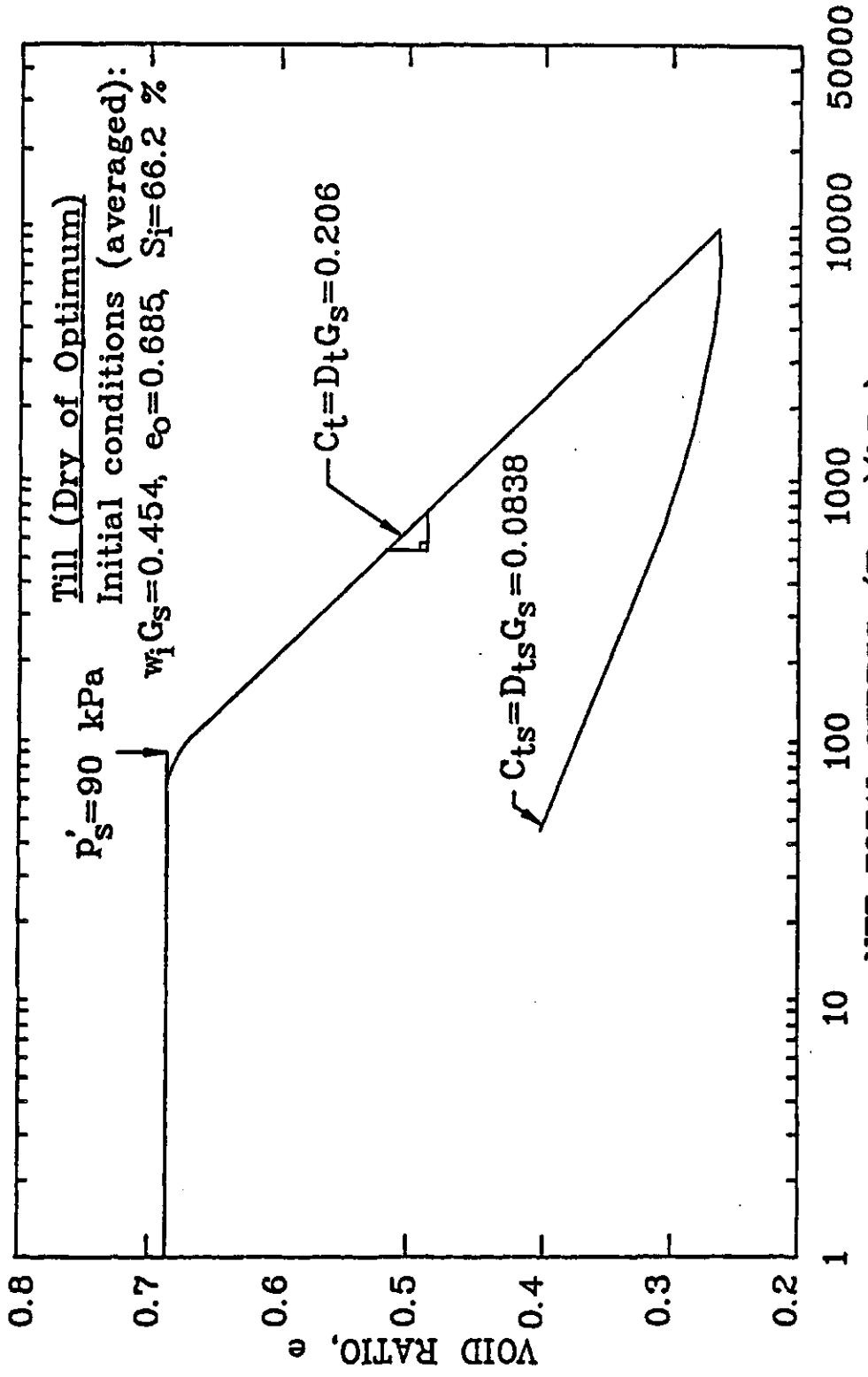

Figure 6.11 Mean Void Ratio Versus The Logarithm of Net Total Stress Curve for Till Dry of Optimum under One-Dimensional Conditions

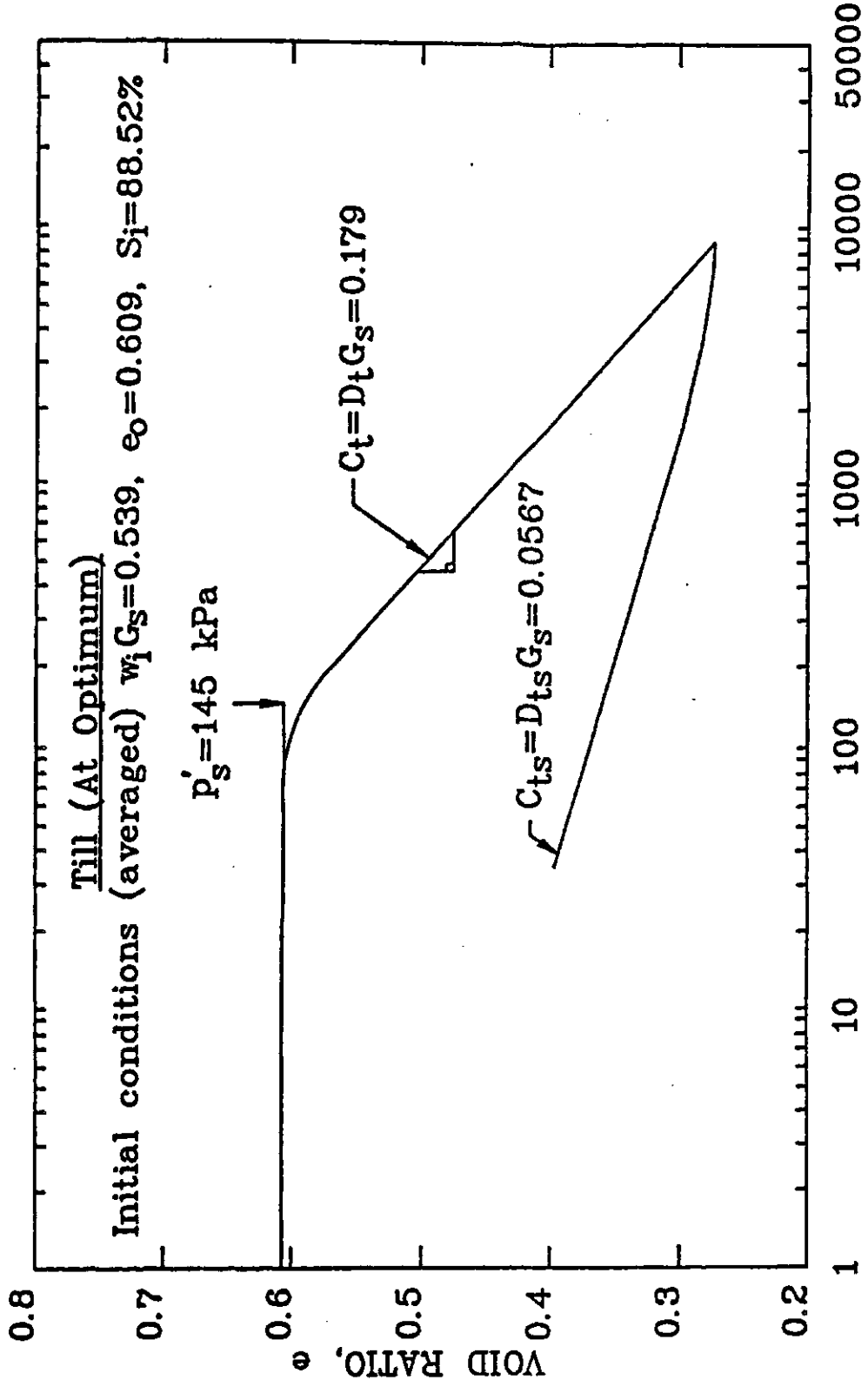

Figure 6.12 Mean Void Ratio Versus The Logarithm of Net Total Stress Curve for Till at Optimum under One-Dimensional Conditions

Table 6.3 A Summary of The Moduli Determined from The Linear Portions of The Average One-Dimensional Loading and Unloading Cuves

Soil Type	Number of CVT[a] Tests	e_o (ave.)	$w_i G_s$ (ave.)	S_i(%) (ave.)	C_t or $D_t G_s$	C_{ts} or $D_{ts} G_s$
DS[b]	6	0.7198	0.4408	61.24	0.1956	0.1256
OS[c]	4	0.6241	0.5373	86.09	0.1766	0.07593
DT[d]	3	0.6848	0.4535	66.22	0.2063	0.08384
OT[e]	3	0.6089	0.5390	88.52	0.1794	0.05671

Note: a) "CVT" stands for one-dimensional constant volume loading and unloading test.
b) "DS" stands for silt at dry of optimum initial water content.
c) "OS" stands for silt at optimum initial water content.
d) "DT" stands for till at dry of optimum initial water content.
e) "OT" stands for till at optimum initial water content.

establish the void ratio and water content versus decreasing matric suction relations when the net total stress is nominal. Results from the two one-dimensional free swell tests on silt specimens at dry of optimum initial water contents (i.e., tests FST3DS and FST4DS) are combined to obtain average void ratio and water content unloading curves with respect to matric suction (Figure 6.13). Only one one-dimensional free swell test (i.e., FST10S) was performed on a silt specimen at the optimum initial water content. The test results were presented in Figure 5.24. Single tests were performed on till specimens at dry of optimum and at optimum initial water contents. The resulting void ratio and water content versus decreasing matric suction curves were shown in Figure 5.25 and 5.26 . The slopes of the void ratio and water content versus decreasing matric suction curves are equal to the swelling index and rebound water content index with respect to matric suction (i.e., C_{ms} and D_{ms}) respectively. A summary of the moduli determined from the one-dimensional free swell test results is given in Table 6.4.

6.2.6 Isotropic constant volume loading and unloading tests

The isotropic constant volume loading and unloading test was used to establish the net total stress versus void ratio and water content relations under isotropic

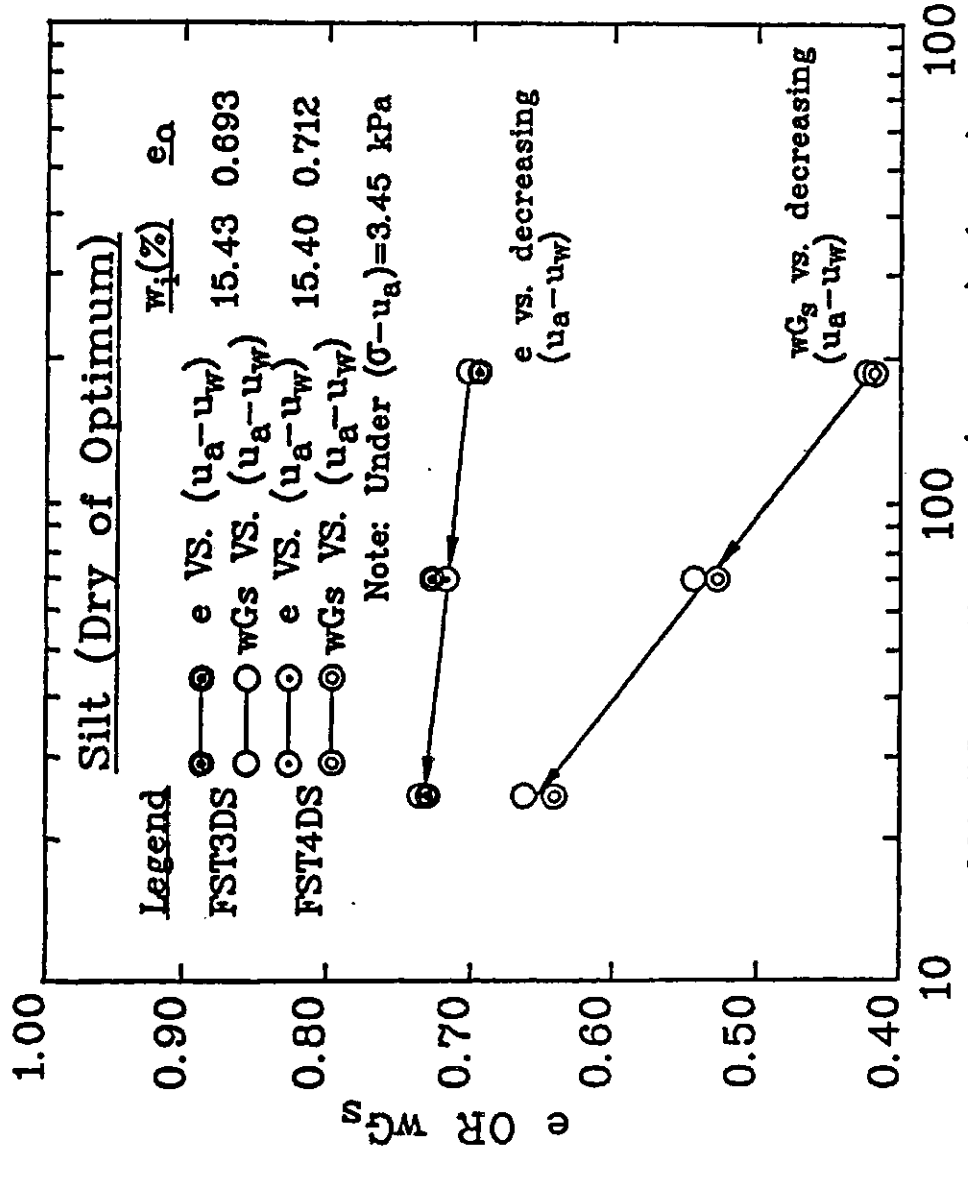

Figure 6.13 Average One-Dimensional Void Ratio and Water Content Versus Matric Suction Unloading Curves for Silt with Dry of Optimum Initial Water Content

Table 6.4 A Summary of The Moduli Determined from The One-Dimensional Free Swell Test Results

Soil Type	Number of Tests	e_o	$w_i G_s$	S_i(%)	C_{ms}	$D_{ms} G_s$
DS[b]	2	0.7024[a]	0.4192[a]	59.68[a]	0.03322[a]	0.2633[a]
OS[c]	1	0.6156	0.5165	83.91	0.05250	0.1008
DT[d]	1	0.6926	0.4359	62.93	0.05299	0.1211
OT[e]	1	0.5709	0.5229	91.59	0.02407	0.06032

Note: a) Average values
b) "DS" stands for silt at dry of optimum initial water content
c) "OS" stands for silt at optimum initial water content
d) "DT" stands for till at dry of optimum initial water content
e) "OT" stands for till at optimum initial water content

conditions. Two isotropic constant volume loading and unloading tests (i.e., Tests TCVT3DS and TCVT4DS) were successfully performed on silt specimens at dry of optimum initial water contents. One isotropic constant volume loading and unloading test (i.e., Test TCVT1DS) was carried out on a silt specimen at optimum initial water content. The resulting void ratio isotropic loading and unloading curves were presented in Figure 5.27 and 5.28. The slopes of the void ratio isotropic loading and unloading curves are the compressive and swelling indices with respect to the net total stress under isotropic conditions (i.e., C_t and C_{ts}). The moduli, C_t and C_{ts} are equal to $D_t G_s$ and $D_{ts} G_s$ when a soil is saturated (See Section 3.5.3). A summary of the moduli determined from the isotropic constant volume loading and unloading test results is presented in Table 6.5. The linear portions of the loading and unloading curves are used to calculate the various moduli.

The Casagrande (1936) graphical procedure is used to determine the corrected swelling pressure from the loading curve. The average corrected isotropic swelling pressure for silt specimens compacted dry of optimum is found to be 112.5 kPa. The average corrected isotropic swelling pressure for silt specimens compacted at optimum water content is found to be 170.0 kPa.

Table 6.5 A Summary of The Moduli Determined from The Isotropic Constant Volume Loading and unloading Test Results

Soil Type	Number of TCVT[a] Tests	e_o	$w_i G_s$	S_i(%)	C_t or $D_t G_s$	C_{ts} or $D_{ts} G_s$
DS[c]	2	0.7004[b]	0.4408[b]	60.51[b]	0.2298[b]	0.02436
OS[d]	1	0.6085	0.5111	83.99	0.1865	0.03979

Note: a) "TCVT" stands for one-dimensional constant volume loading and unloading test.
b) Average value.
c) "DS" stands for silt at dry of optimum initial water content.
d) "OS" stands for silt at optimum initial water content.
d) "DT" stands for till at dry of optimum initial water content.
e) "OT" stands for till at optimum initial water content.

6.2.7 Isotropic free swell tests

The isotropic free swell test was used to establish the void ratio and water content versus decreasing matric suction relations when the net total stress is nominal and the soil is under isotropic strain conditions. One test was performed on a silt specimen at dry of optimum initial water content (i.e., test TFST2DS). Two tests were performed on silt specimens at optimum initial water contents (i.e., test TFST10S and TFST20S). The resulting void ratio and water content versus decreasing matric suction curves were presented in Figure 5.29 and 5.30.

The slope of the void ratio and water content versus decreasing matric suction curves are the swelling index and rebound water content index with respect to matric suction (i.e., C_{ms} and D_{ms}) respectively. The water volume change data for test TST2DS indicates the specimen reached a degree of saturation over a hundred percent in the last stage (i.e., Stage IV) of testing (See Section 5.8). The last water content measurement in the test is not used in calculating the rebound water content index with respect to matric suction for the specimen. The void ratio is equal to the water content multiplied by the relative density when a soil approaches saturation. The last void ratio measurement in the test is then used as a control point in defining the water content versus deceasing matric suction curve for the test (See Figure 5.29). The rebound water content index

with respect to matric suction is calculated based on the change in matric suction and water content between the initial and final state of the specimen in the test. A summary of the moduli determined from the isotropic free swell test results is presented in Table 6.6.

6.3 The Forms of The Semi-Logarithmic Soil Structure and Water Phase Constitutive Surfaces

Section 3.4.2 presented the approximated semi-logarithmic soil structure and water phase constitutive surfaces. Section 3.5.2 developed and presented relationships between the deformation moduli of the soil structure (i.e., C_t and C_m , C_{ts} and C_{ms}) and between those of the water phase (i.e., D_t and D_m , D_{ts} and D_{ms}). These proposed relationships are written in terms of the characteristic stress states (i.e., P_s' , P_w' , $(u_a - u_w)_i^e$ and $(u_a - u_w)_i^w$, see Section 3.4.2) according to the geometry of the approximate constitutive surfaces. Results from the test program are combined to show the form of the semi-logarithmic soil structure and water phase constitutive surfaces in this section. Observations made are used to examine the proposed relationships between moduli in Section 6.4.

Table 6.6 A Summary of The Moduli Determined from The Isotropic Free Swell Test Results

Soil Type	Number of Tests	e_o	$w_i G_s$	S_i(%)	C_{ms}	$D_{ms} G_s$
DS[a]	1	0.6991	0.4208	60.20	0.02046	0.1936
OS[b]	2	0.6161	0.5106	82.87	0.02236	0.04983

Note: a) "DS" stands for silt at dry of optimum initial water content
b) "OS" stands for silt at optimum initial water content

6.3.1 The form of the semi-logarithmic soil structure and water phase constitutive surfaces for loading conditions

Average void ratio and water content loading curves are combined to show the characteristic form of the semi-logarithmic soil structure and water phase constitutive surfaces for monotonic volume decrease. The void ratio versus net total stress loading curve is obtained from the constant volume loading and unloading test results. In 1974, Rieke and Chilincarian presented a comprehensive study on the "interrelationships among density, porosity, remaining moisture content, pressure and depth" for soils. The authors reported that the void ratio of most soil would be reduced to zero at a pressure of approximately 5×10^5 psi (i.e., 3.5×10^6 kPa). This information is used as a control to define the void ratio versus net total stress loading curve at high pressure range. The void ratio versus net total stress curve is equivalent to the water content times relative density versus net total stress curve when a soil is saturated. The water content versus matric suction loading curve is obtained from suction test results. Unconfined shrinkage test results provide the water content versus void ratio curve of a soil under increasing matric suction. Cross-plotting the water content versus matric suction loading curve with the water content versus void ratio curve gives the void ratio versus matric suction

loading curve. The mercury submersion method is considered to be the most reliable volume measuring technique (See Section 6.2.3). Only water content versus void ratio curves determined by the mercury submersion method are therefore used in this analysis.

The average void ratio and water content loading curves for silt and till compacted dry of optimum and at optimum initial water contents, under one-dimensional loading conditions, are presented in Figure 6.14, 6.15, 6.16 and 6.17. Direct volume measurement over-estimates the void ratio of a soil (See Section 6.2.3). The initial void ratio of the combined void ratio loading curves is therefore assumed to be the void ratio determined by the mercury submersion technique in the unconfined shrinkage test.

The water content versus matric suction loading curves are the same for both one-dimensional and isotropic conditions. The void ratio versus net total stress loading curve for isotropic conditions is obtained from the isotropic constant volume loading and unloading test results. A comparison between the one-dimensional and isotropic void ratio versus net total stress loading and unloading curves is presented in Figure 6.18 and 6.19. Table 6.7 is a summary of moduli determined from the average loading curves for silt and till.

The characteristic stress states (i.e., P'_s, P'_w, $(u_a - u_w)^e_i$ and $(u_a - u_w)^w_i$) are determined using the

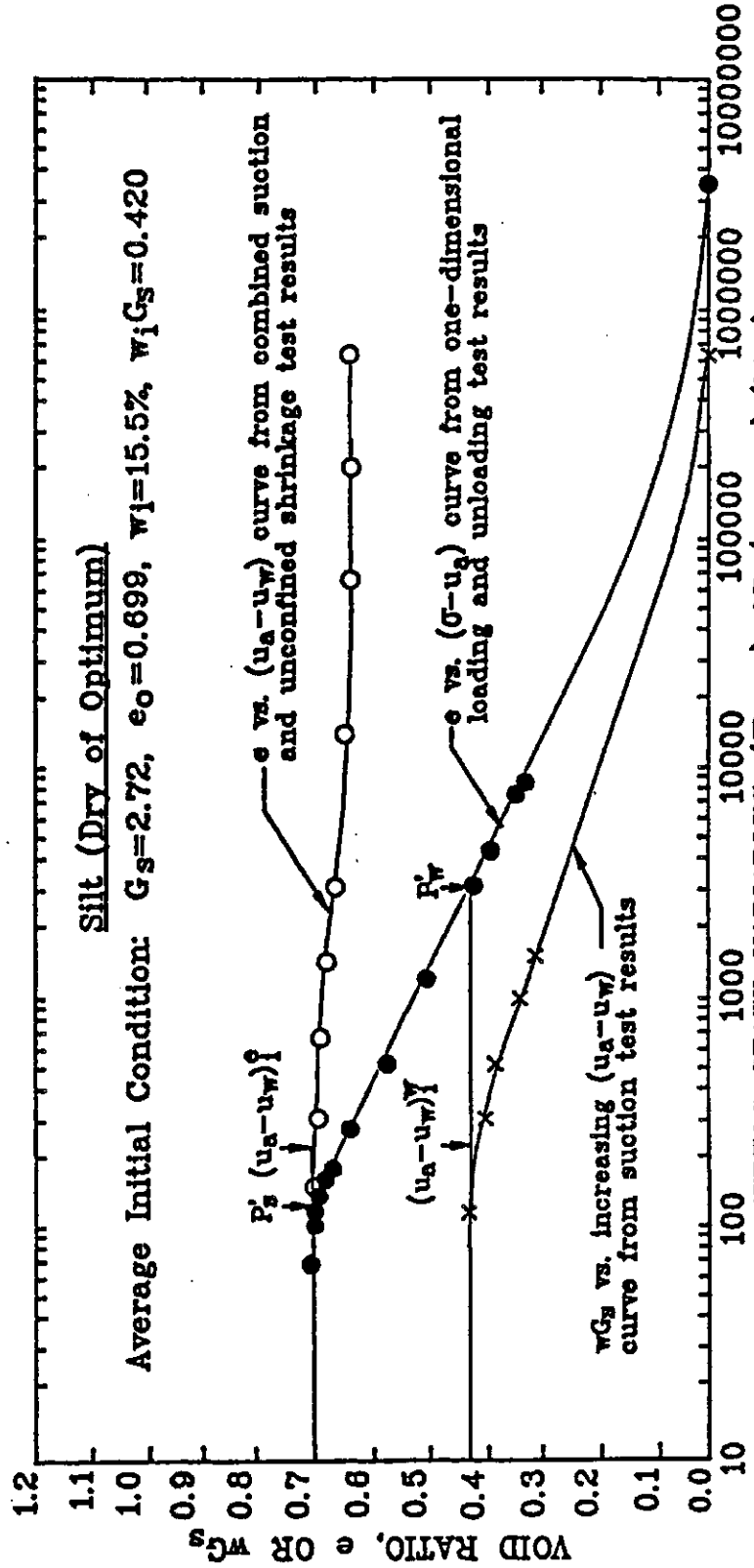

Figure 6.14 Constitutive Relations for Silt Dry of Optimum under One-dimensional Loading Conditions

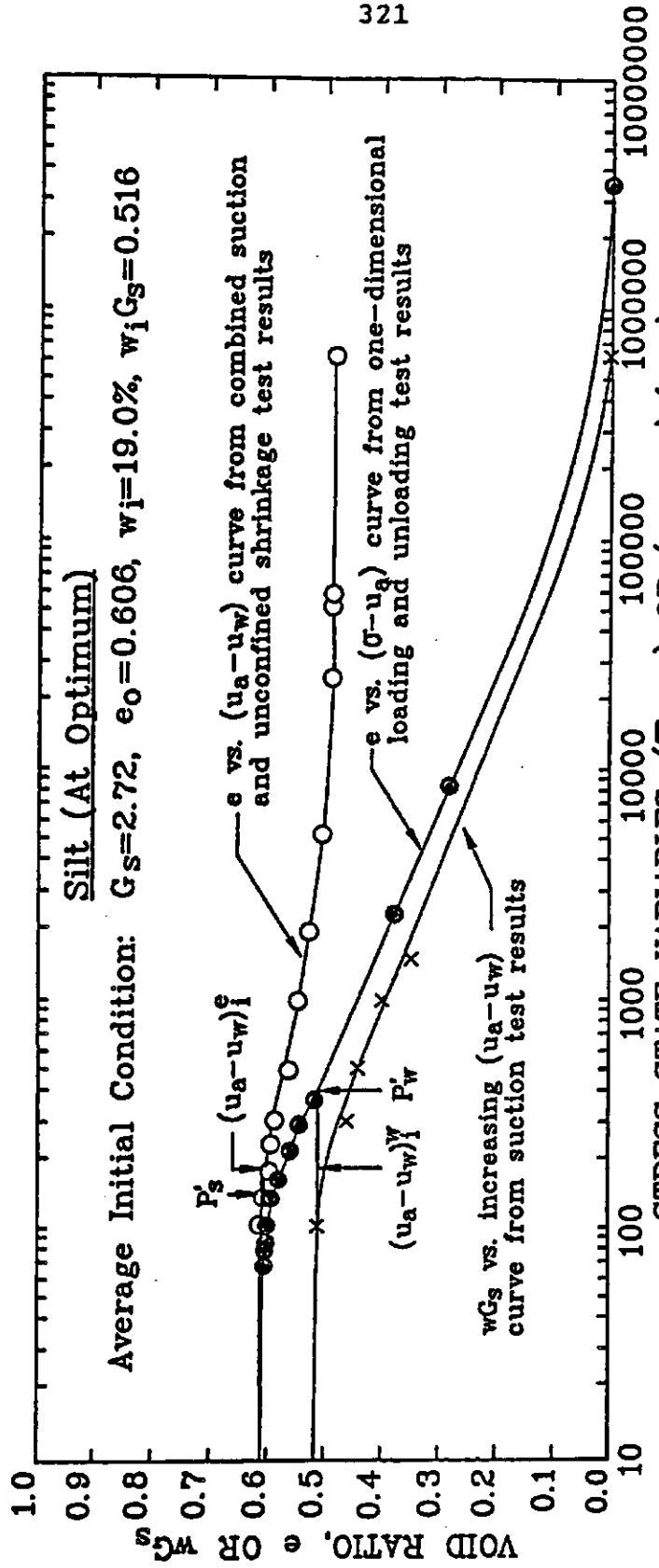

Figure 6.15 Constitutive Relations for Silt at Optimum under One-dimensional Loading Conditions

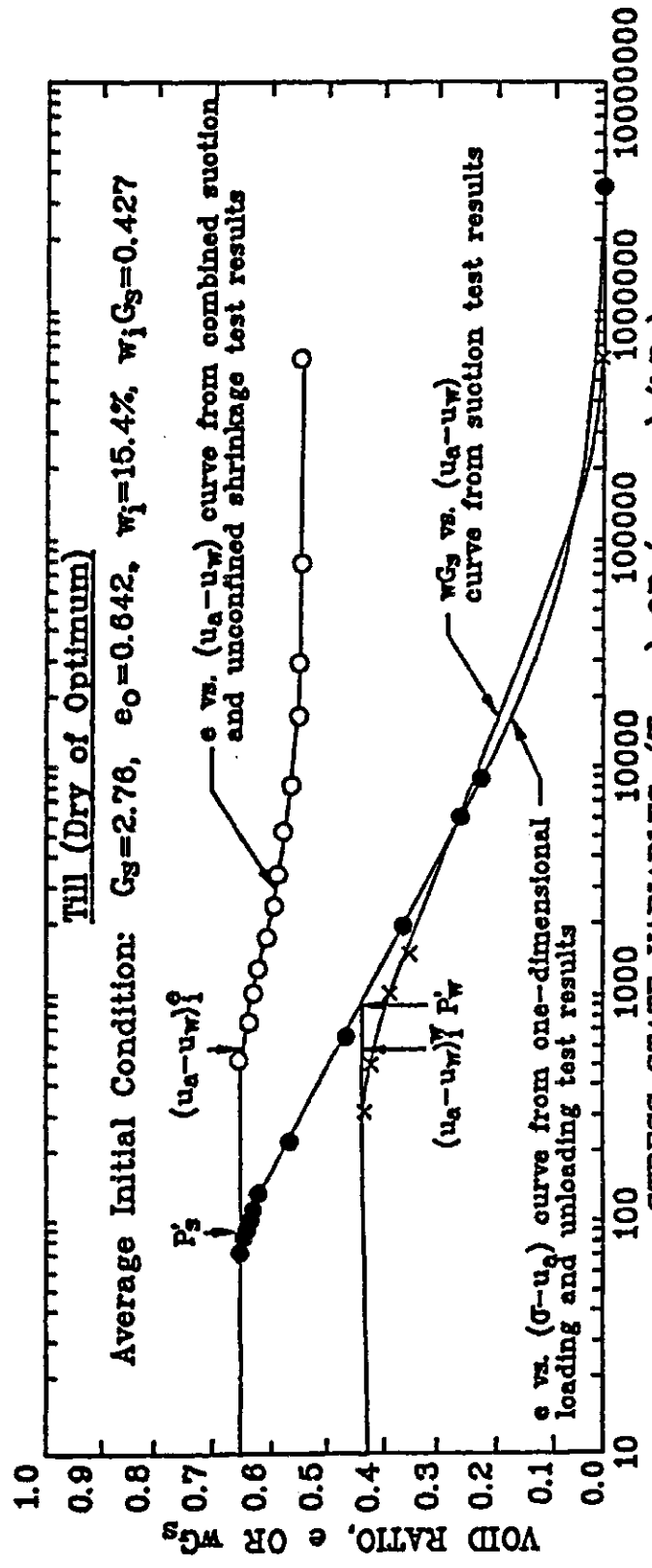

Figure 6.16 Constitutive Relations for Till Dry of Optimum under One-dimensional Loading Conditions

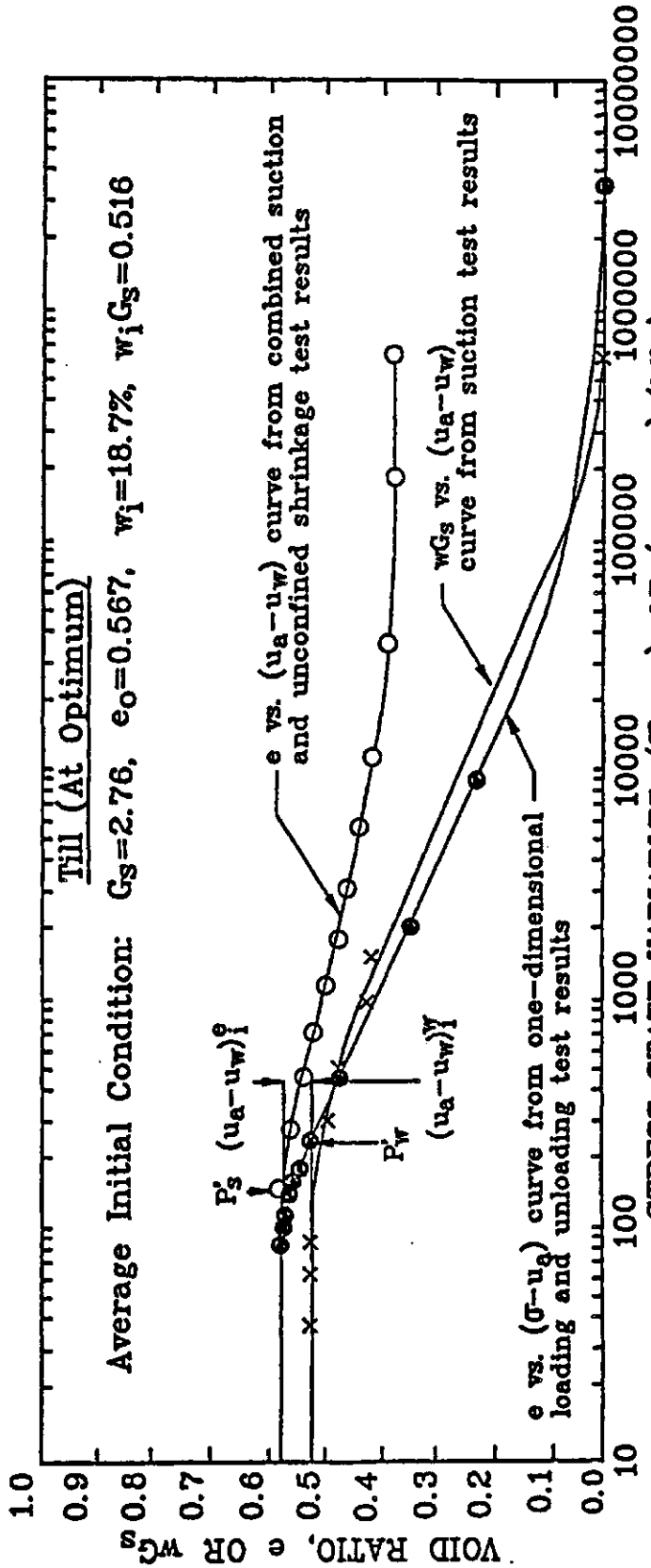

Figure 6.17 Constitutive Relations for Till at Optimum under One-dimensional Loading Conditions

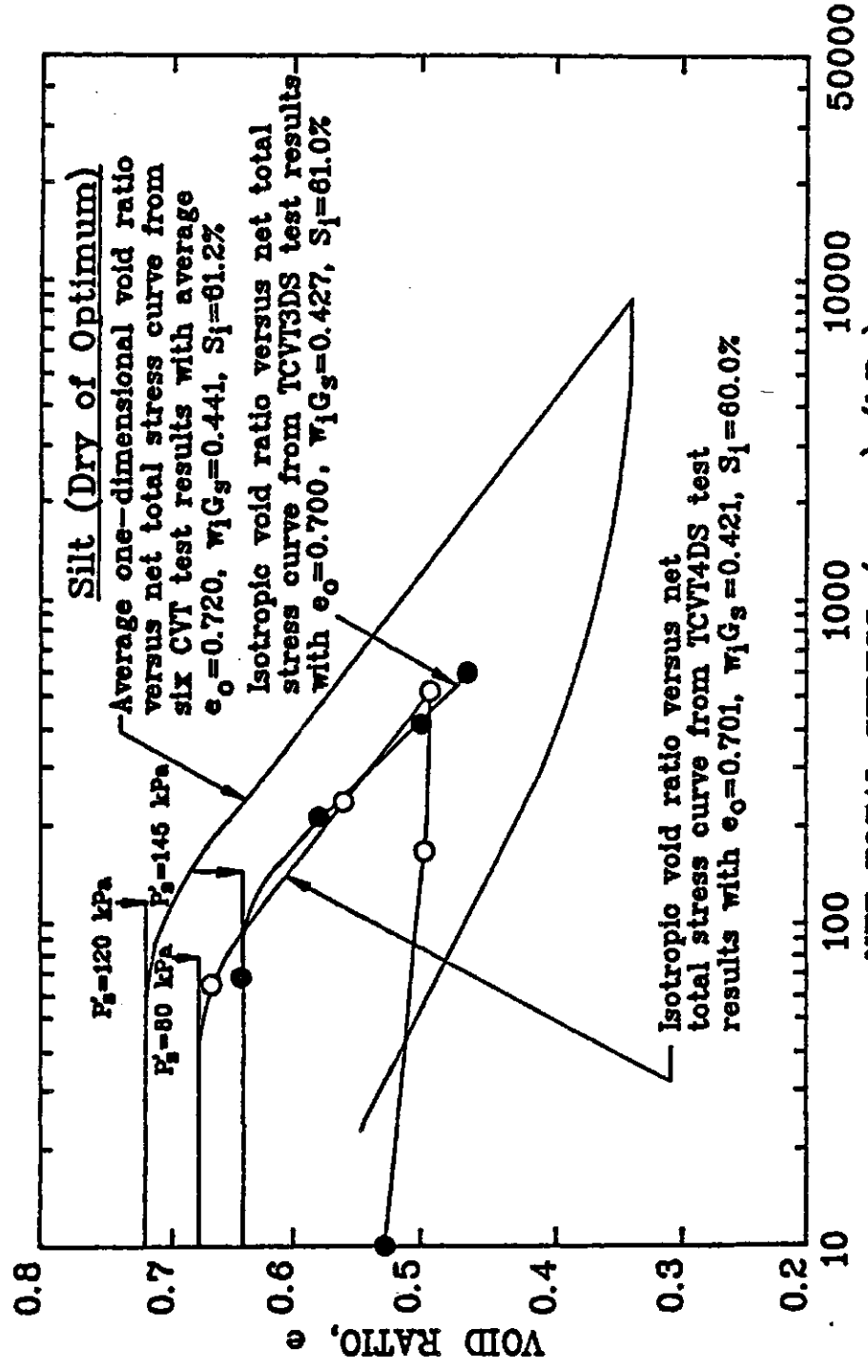

Figure 6.18 A Comparision between The One-Dimensional and Isotropic Void Ratio Versus Net Total Stress Loading and Unloading Curves for Silt with Dry of Optimum Initial Water Content

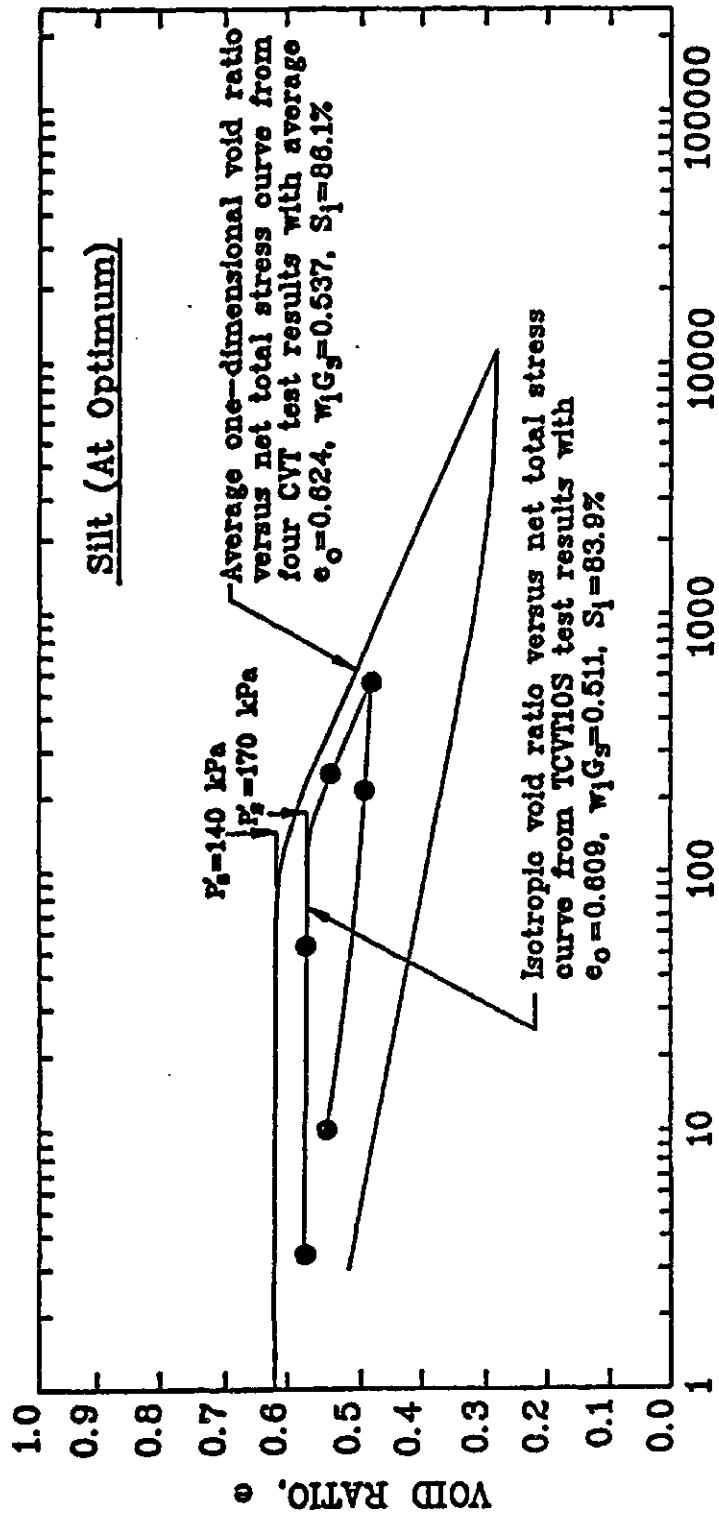

Figure 6.19 A Comparision between The One-Dimensional and Isotropic Void Ratio Versus Net Total Stress Loading and Unloading Curves for Silt with Optimum Initial Water Content

Table 6.7 A Summary of Moduli Determined from The Average Loading Curves for Silt and Till

Strain Condition	One-Dimensional				Isotropic	
Soil Type	DS[a]	OS[b]	DT[c]	OT[d]	DS[a]	OS[b]
C_t or D_tG_s	0.1956	0.1766	0.2063	0.1794	0.2298	0.1865
C_m	0.03041	0.08229	0.08943	0.1059	0.03041	0.08229
D_mG_s	0.1241	0.1584	0.1588	0.1713	0.1241	0.1584

Note: a) "DS" stands for silt at dry of optimum initial water content
b) "OS" stands for silt at optimum initial water content
c) "DT" stands for till at dry of optimum initial water content
d) "OT" stands for till at optimum initial water content

average void ratio and water content loading curves. The Casagrande (1936) graphical procedure is used to determine the corrected swelling pressure and initial matric suction of a soil from the void ratio and water content loading curves respectively (See Section 6.2.2 and 6.2.4). The initial stress state of a soil, translated to the net total stress plane following a constant water content stress path (i.e., P'_w) is determined from the average void ratio versus net total stress loading curve (See Section 3.5.4). The stress states, $(u_a - u_w)^e_i$ and $(u_a - u_w)^w_i$ are equal to the initial matric suction for an unconfined unsaturated soil (See Section 3.4.2). Table 6.8 is a summary of the characteristic stress states for silt and till compacted dry of optimum and at optimum initial water contents.

The average void ratio and water content loading curves and the characteristic stress states are combined to study the characteristic from of the semi-logarithmic soil structure and water phase constitutive surfaces for monotonic volume decrease as follows.

Form of The Semi-Logarithmic Soil Structure Constitutive Surface for Monotonic Volume Decease

The approximate semi-logarithmic soil structure constitutive surface for monotonic volume decrease is assumed to have a projected point of convergence on the void ratio axis (i.e., point EL on Figure 3.25b). This projected

Table 6.8 A Summary of The Characteristic Stress States for Silt and Till

Strain Condition	Soil Type	P'_s (kPa)	$(u_a - u_w)^e_i$ or $(u_a - u_w)^w_i$ (kPa)	P'_w (kPa)
one-dimensional	DS[a]	120	225	3000
	OS[b]	140	185	415
	DT[c]	90	580	960
	OT[d]	145	430	240
isotropic	DS	112.5	225	1050
	OS	170	185	370

Note: a) "DS" stands for silt at dry of optimum initial water content
b) "OS" stands for silt at optimum initial water content
c) "DT" stands for till at dry of optimum initial water content
d "OT" stands for till at optimum initial water content

point of convergence is assumed to be the point where the projections of the two linear void ratio versus the logarithm of net total stress and matric suction loading curves meet (See Section 3.3). The numerical value of the net total stress and matric suction at this projected point of convergence is assumed to be unity (See Section 3.4).

A graphical procedure is used to determine the net total stress and matric suction at the projected point of convergence for the silt and till specimens in the test program. The linear portions of the void ratio versus the logarithm of net total stress and matric suction loading curves are assumed to originate from the characteristic stress states, P_s' and $(u_a - u_w)_i^e$ respectively. The intersection of the projections of these loading curves gives the net total stress and matric suction at the projected point of convergence. The analysis for silt at dry of optimum initial water content and under isotropic strain conditions is presented as an illustration (Figure 6.20). Table 6.9 is a summary of the net total stress and matric suction at the projected points of convergence of the soil structure constitutive surfaces for silt and till under monotonic volume decrease. The net total stress and matric suction at the projected point of convergence are found to be in the range of 100.0 to 150.0 kPa for silt. For till, the net total stress and matric suction at the projected point of convergence are found to be in the range of 20.0 to

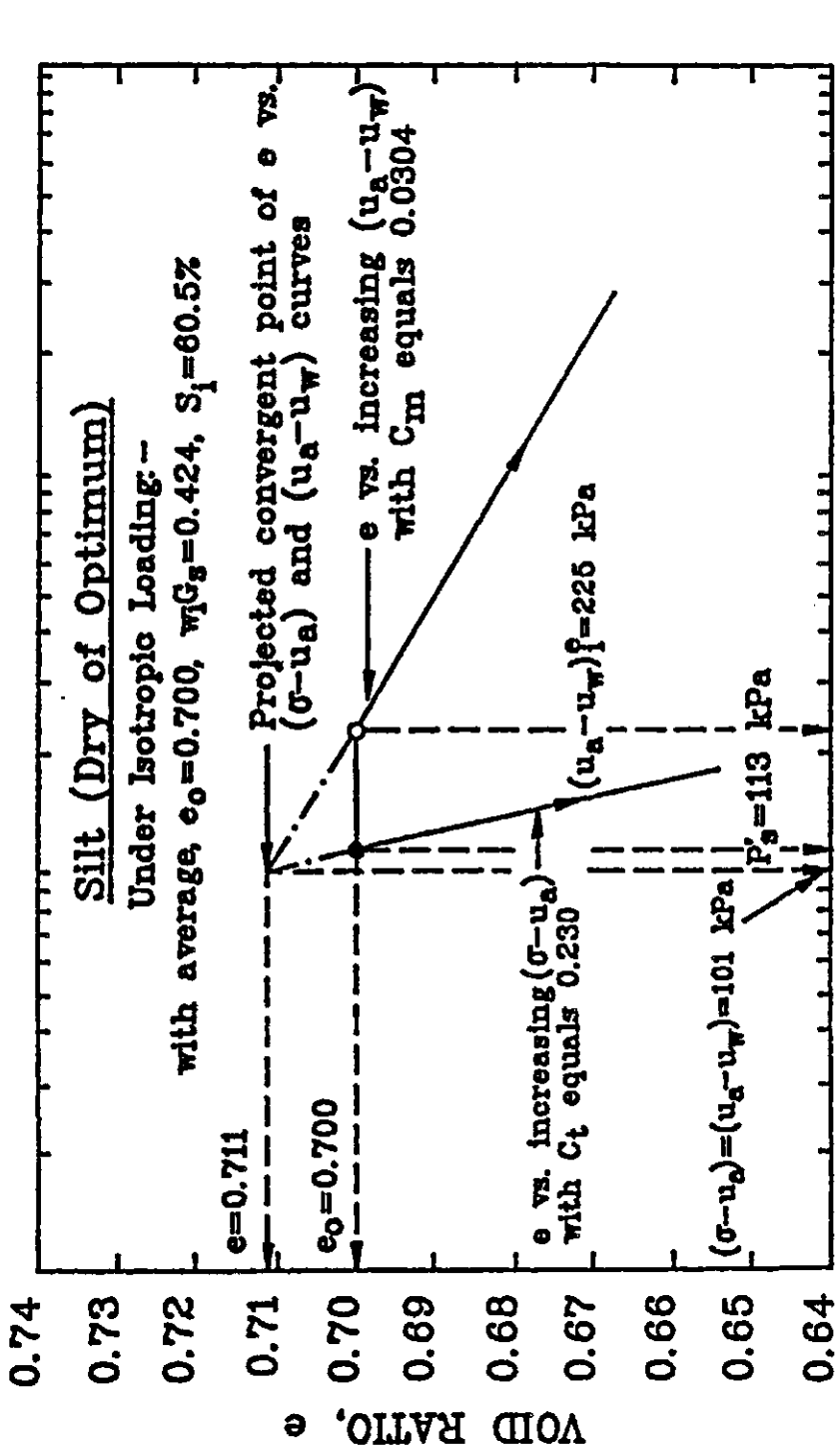

Figure 6.20 Determination of The Stress State at The Projected Point of Convergence of The Soil Structure Constitutive Surface for Silt with Dry of Optimum Initial Water Content under Isotropic Loading Conditions

Table 6.9 A Summary of The Net Total Stress and Matric Suction at The Projected Points of Convergence of The Silt and Till Soil Structure Constitutive Surfaces for Monotonic Volume Decrease

Strain Condition	One-Dimensional				Isotropic	
Soil Type	DS[a]	OS[b]	DT[c]	OT[d]	DS	OS
$p^{e}_{pr\text{-}cnv}$ (kPa)	106	110	22	30	101	159

Note: a) "DS" stands for silt at dry of optimum initial water content.
b) "OS" stands for silt at optimum initial water content.
c) "DT" stands for till at dry of optimum initial water content.
d) "OT" stands for till at optimum initial water content.
e) "$p_{pr\text{-}cnv}$" stands for the net total stress and matric suction suction at the projected point of convergence.

30.0 kPa.

Form of The Semi-Logarithmic Water Phase Constitutive Surface for Monotonic Water Content Decrease

The approximated semi-logarithmic water phase constitutive surface for monotonic water content decrease is assumed to have a projected point of convergence on the water content axis (i.e., point WL on Figure 3.26b). This projected point of convergence is assumed to be where the projections of the two linear water content versus the logarithm of net total stress and matric suction loading curves meet (See Section 3.4). The water content index with respect to matric suction (i.e., D_m) is assumed to be larger than the water content index with respect to the net total stress (i.e., D_t) (See Section 3.5.2). A summary of the water content indices with respect to net total stress and matric suction for silt and till was presented in Table 6.7. The water content indices with respect to net total stress are found to be larger than the water content indices with respect to matric suction. The projections of the water content versus the logarithm of net total stress and matric suction loading curves are found to be lines diverging from each other. The case for silt at dry of optimum initial water content and under one-dimensional loading is presented as an illustration (Figure 6.21). The observation that the water content loading curves are divergent lines contradicts

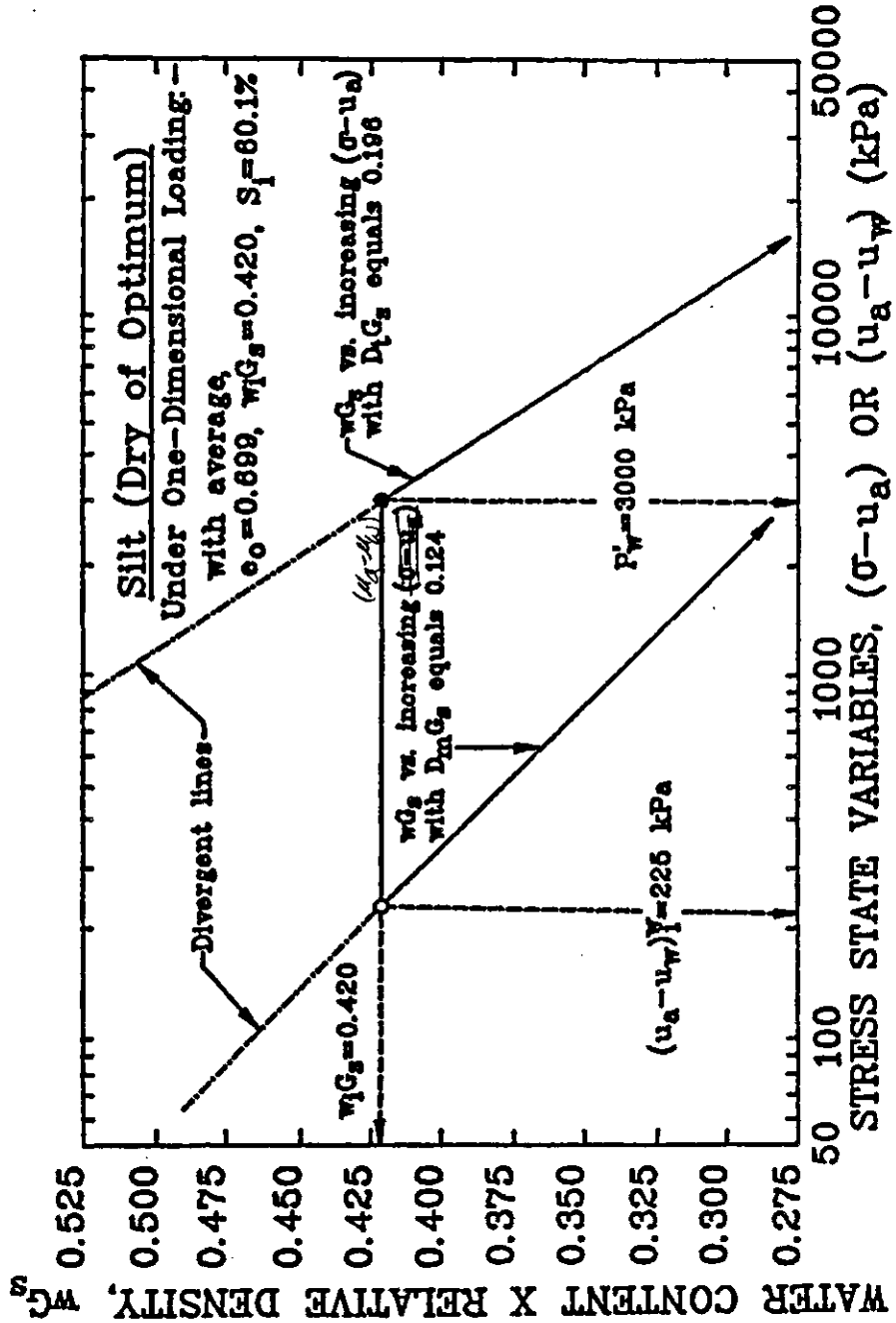

Figure 6.21 The Divergence of The Water Content Loading Curves for Silt with Dry of Optimum Initial Water Content under One-Dimensional Loading

the assumed form of the semi-logarithmic water phase constitutive surface for monotonic water content decrease. This apparent contradiction is further addressed in Section 6.4.1.

6.3.2 The form of the semi-logarithmic soil structure and water phase constitutive surfaces for unloading conditions

Average void ratio and water content unloading curves are combined to verify the assumed characteristic form of the semi-logarithmic soil structure and water phase constitutive surfaces for monotonic volume increase. The average one-dimensional void ratio versus net total stress unloading curve is obtained from one-dimensional constant volume loading and unloading test results. The average three-dimensional void ratio versus net total stress unloading curve is obtained from isotropic constant volume loading and unloading test results. Void ratio is equal to water content multiplied by the relative density when a soil is saturated. The water content versus net total stress unloading curves are derived from the void ratio unloading curves accordingly. One-dimensional free swell test results give the one-dimensional void ratio and water content versus matric suction unloading curves. Isotropic free swell test results provide the three- dimensional void ratio and water

content versus matric suction unloading curves. Average void ratio and water content unloading curves were presented in Section 6.2.4, 6.2.5, 6.2.6 and 6.2.7. Void ratio and water content unloading moduli (i.e., C_{ts}, C_{ms}, D_{ts} and D_{ms}) determined from the average unloading curves were summarized in Table 6.3, 6.4, 6.5 and 6.6. Unloading curves with respect to net total stress are approximately parallel to one another (Lambe and Whitman, 1969). Therefore, the initial void ratio and water content of the combined unloading curves are assumed to be the average initial void ratio and water content of the free swell test specimens. Specimens with near identical initial conditions were used in the test program. The characteristic stress states (i.e., P_s' , P_w' , $(u_a - u_w)_i^e$ and $(u_a - u_w)_i^w$) determined based on the average void ratio and water content loading curves are assumed to be the same for the unloading case. A summary of the characteristic stress states for silt and till at dry of optimum and at optimum initial water contents was presented in Table 6.8. The average void ratio and water content unloading curves and the characteristic stress states are combined to study the characteristic form of the semi-logarithmic soil structure and water phase constitutive surfaces for monotonic volume increase as follows.

Form of The Semi-Logarithmic Soil Structure Constitutive Surface for Monotonic Volume Increase

The approximated semi-logarithmic soil structure constitutive surface for monotonic volume increase is assumed to converge towards a point on the void ratio axis (i.e., point EU on Figure 3.25a). This point of convergence is assumed to be where the void ratio versus the logarithm of net total stress and matric suction unloading curves meet. The numerical value of the net total stress and matric suction at this point of convergence is assumed to be unity (See Section 3.4).

A graphical procedure is used to determine the net total stress and matric suction at the point of convergence for silt and till in the test program. The average void ratio versus the logarithm of net total stress and matric suction unloading curves are assume to originate from the characteristic stress states, P_s' and $(u_a - u_w)_i^e$ respectively. The intersection of these unloading curves gives the net total stress and matric suction at the point of convergence of the constitutive surface. An average swelling index with respect to the net total stress (i.e., C_{ts}) is determined between the void ratio at the corrected swelling pressure (i.e., P_s') and the void ratio at the point of convergence. This average swelling index with respect to the net total stress is used to examine the proposed relationships between moduli in Section 6.4.1. The

analyses for silt and till at dry of optimum and at optimum initial water contents are presented in Figure 6.22 to 6.27. Table 6.10 is a summary of the average swelling indices with respect to the net total stress and the net total stress and matric suction at the points of convergence of the soil structure constitutive surfaces for silt and till under monotonic volume increase. The net total stress and matric suction at the points of convergence are found to be in the range of 0.05 to 20.0 kPa.

Form of the Semi-Logarithmic Water Phase Constitutive Surface for Monotonic Water Content Increase

The approximated semi-logarithmic water phase constitutive surface for monotonic water content increase is assumed to converge towards a point on the water content axis (i.e., point WU on Figure 3.26a). This point of convergence is assumed to be where the water content versus the logarithm of net total stress and matric suction unloading curves meet (See Section 3.4). The rebound water content index with respect to matric suction (i.e., D_{ms}) is assumed to be larger than the rebound water content index with respect to the net total stress (i.e., D_{ts}). The characteristic stress state, P'_w is assumed to be larger than the characteristic stress state, $(u_a - u_w)^w_i$ (See Section 3.4.2 and 3.5.2). A summary of the characteristic stress states for silt and till was presented in Table 6.8. The

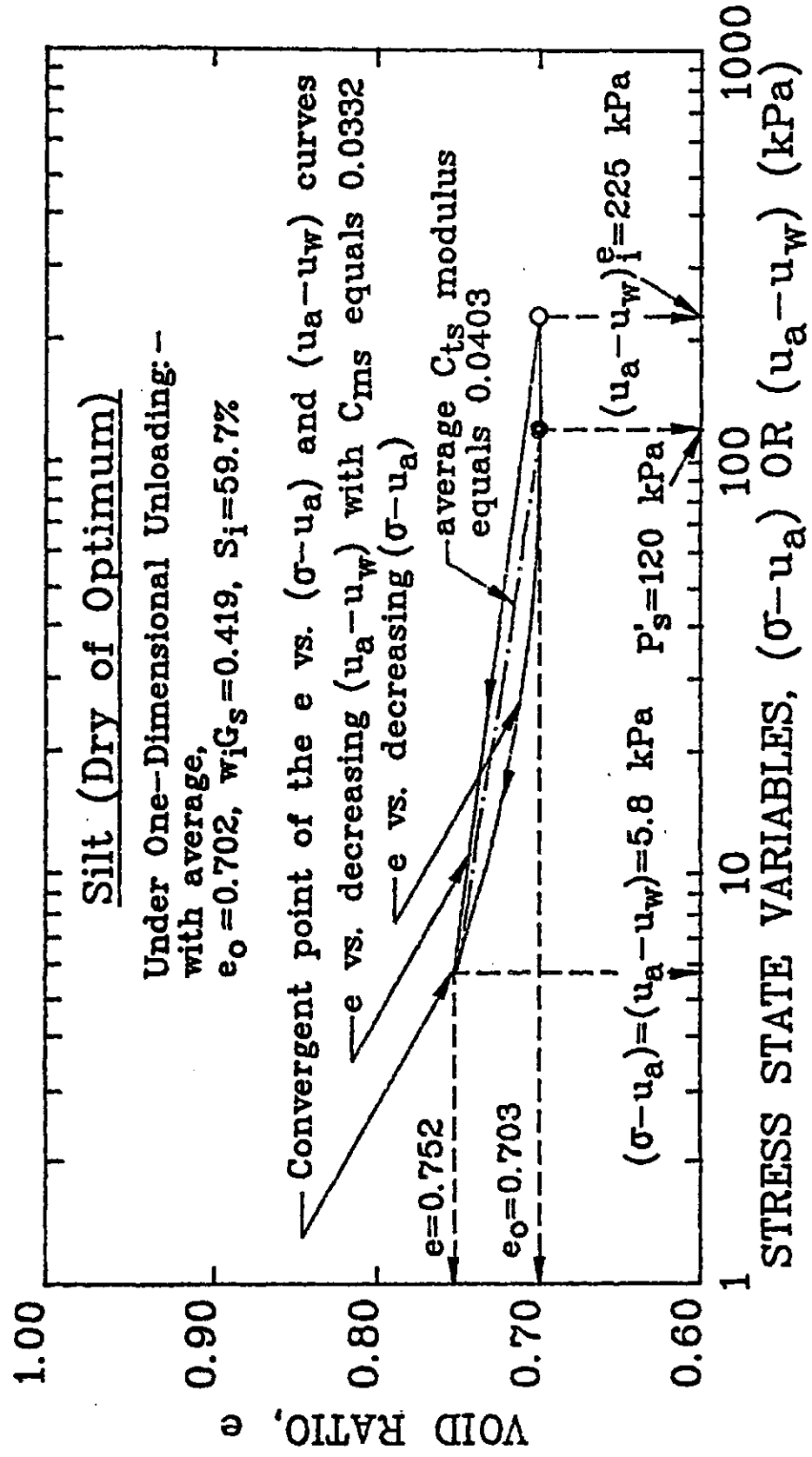

Figure 6.22 Determination of The Stress State at The Soil Structure Constitutive Surface Point of Convergence for Silt with Dry of Optimum Initial Water Content under One-Dimensional Unloading Conditions

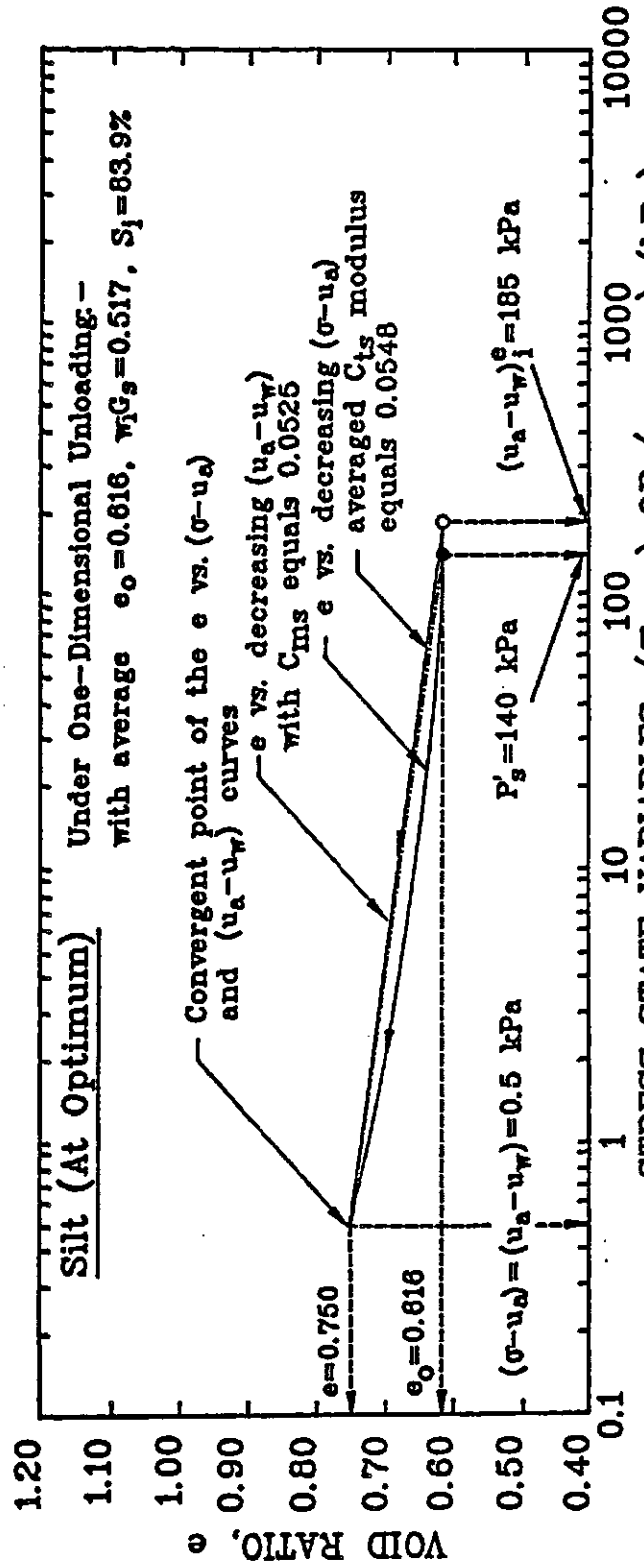

Figure 6.23 Determination of The Stress State at The Soil Structure Constitutive Surface Point of Convergence for Silt with Optimum Initial Water Content under One-Dimensional Unloading Conditions

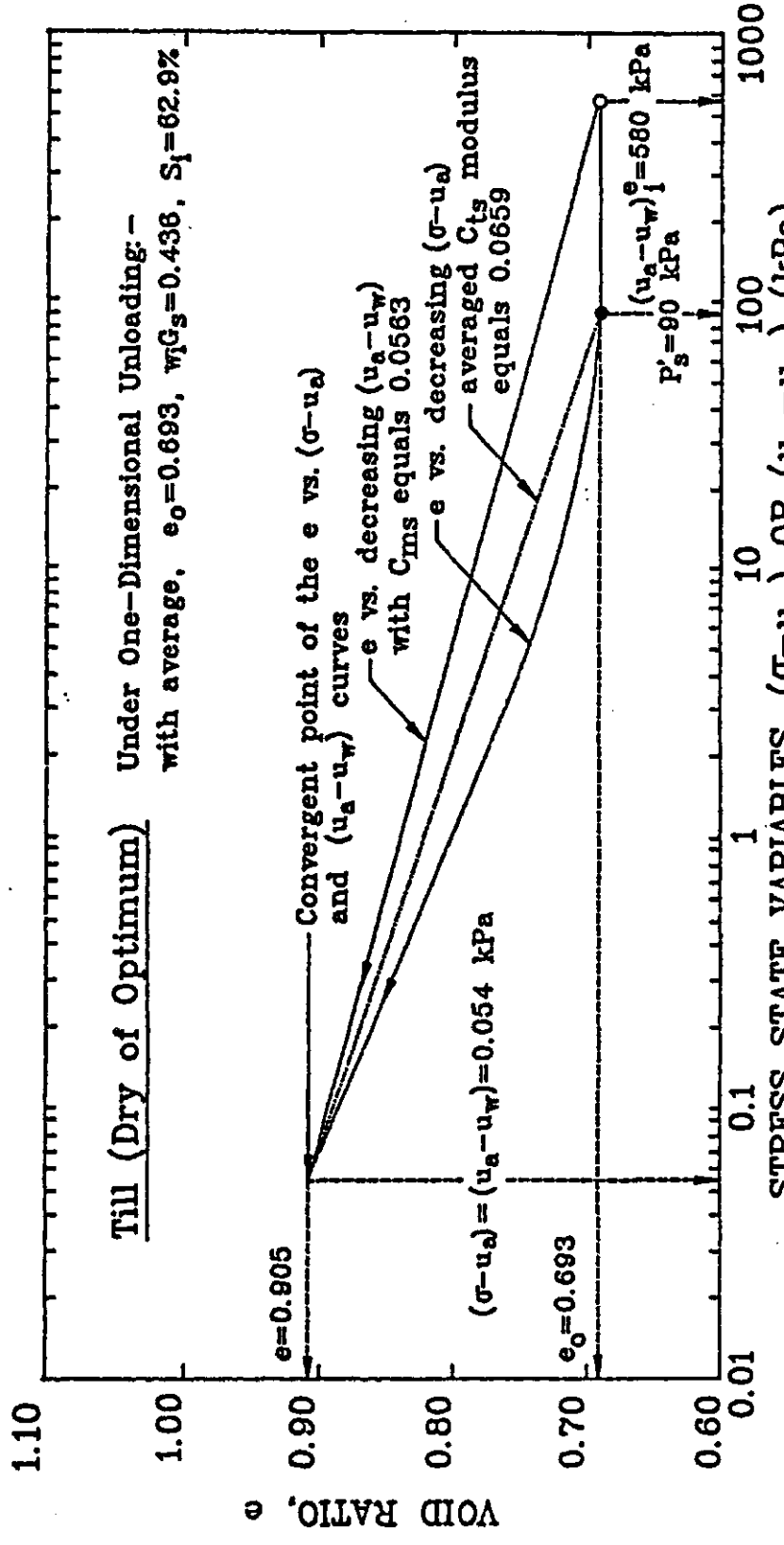

Figure 6.24 Determination of The Stress State at The Soil Structure Constitutive Surface Point of Convergence for Till with Dry of Optimum Initial Water Content under One-Dimensional Unloading Conditions

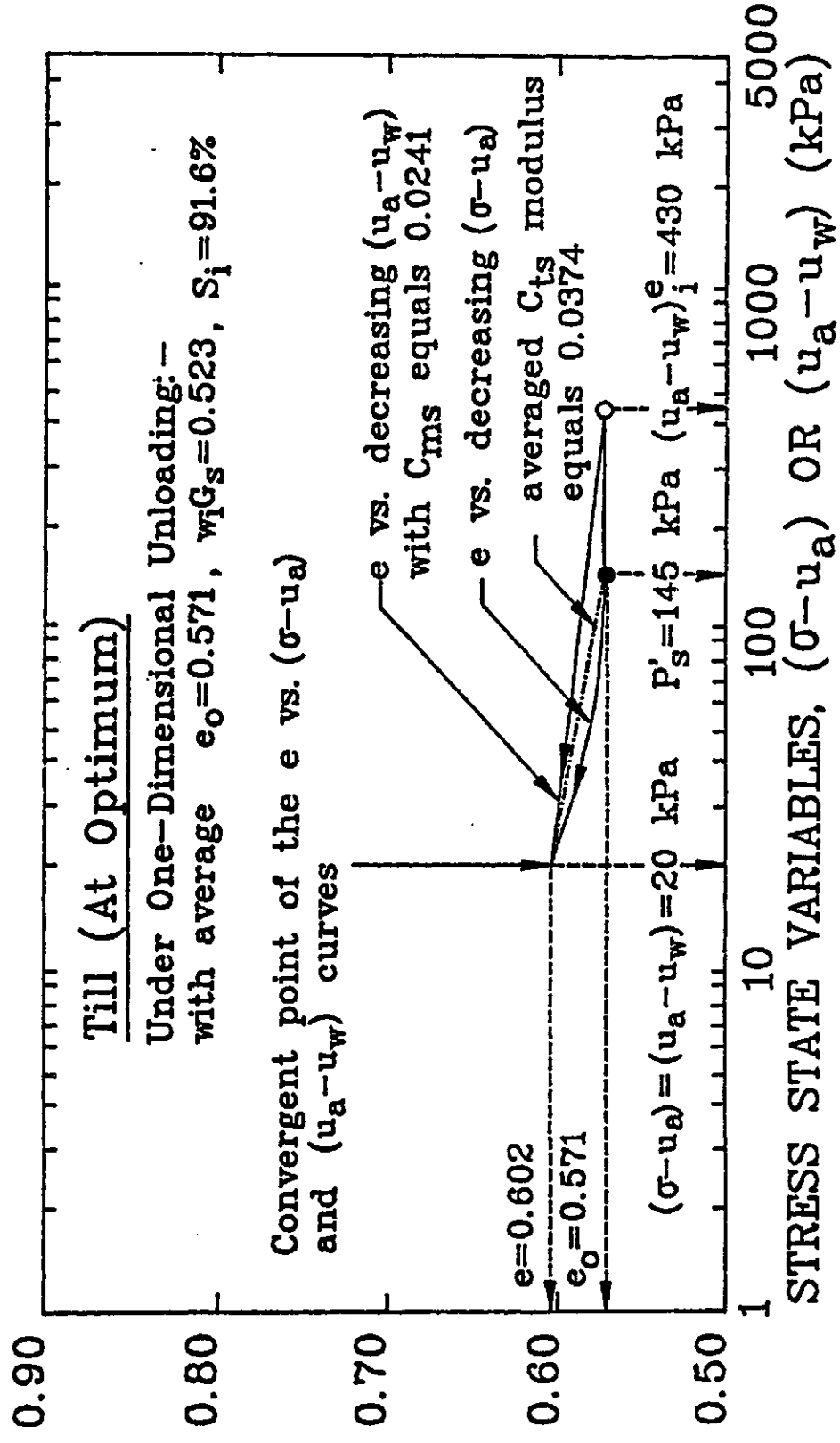

Figure 6.25 Determination of The Stress State at The Soil Structure Constitutive Surface Point of Convergence for Till with Optimum Initial Water Content under One-Dimensional Unloading Conditions

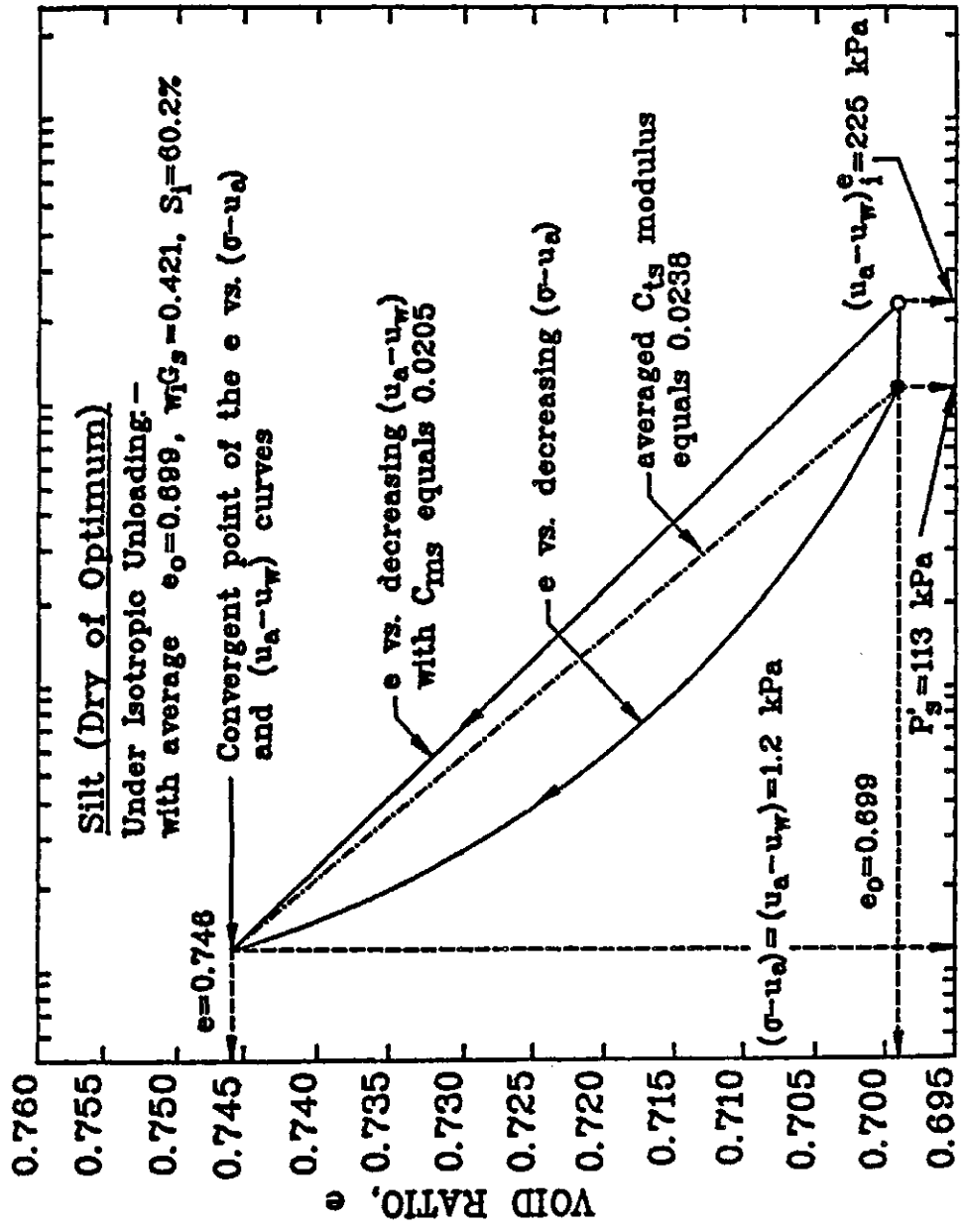

Figure 6.26 Determination of The Stress State at The Soil Structure Constitutive Surface Point of Convergence for Silt with Dry of Optimum Initial Water Content under Isotropic Unloading Conditions

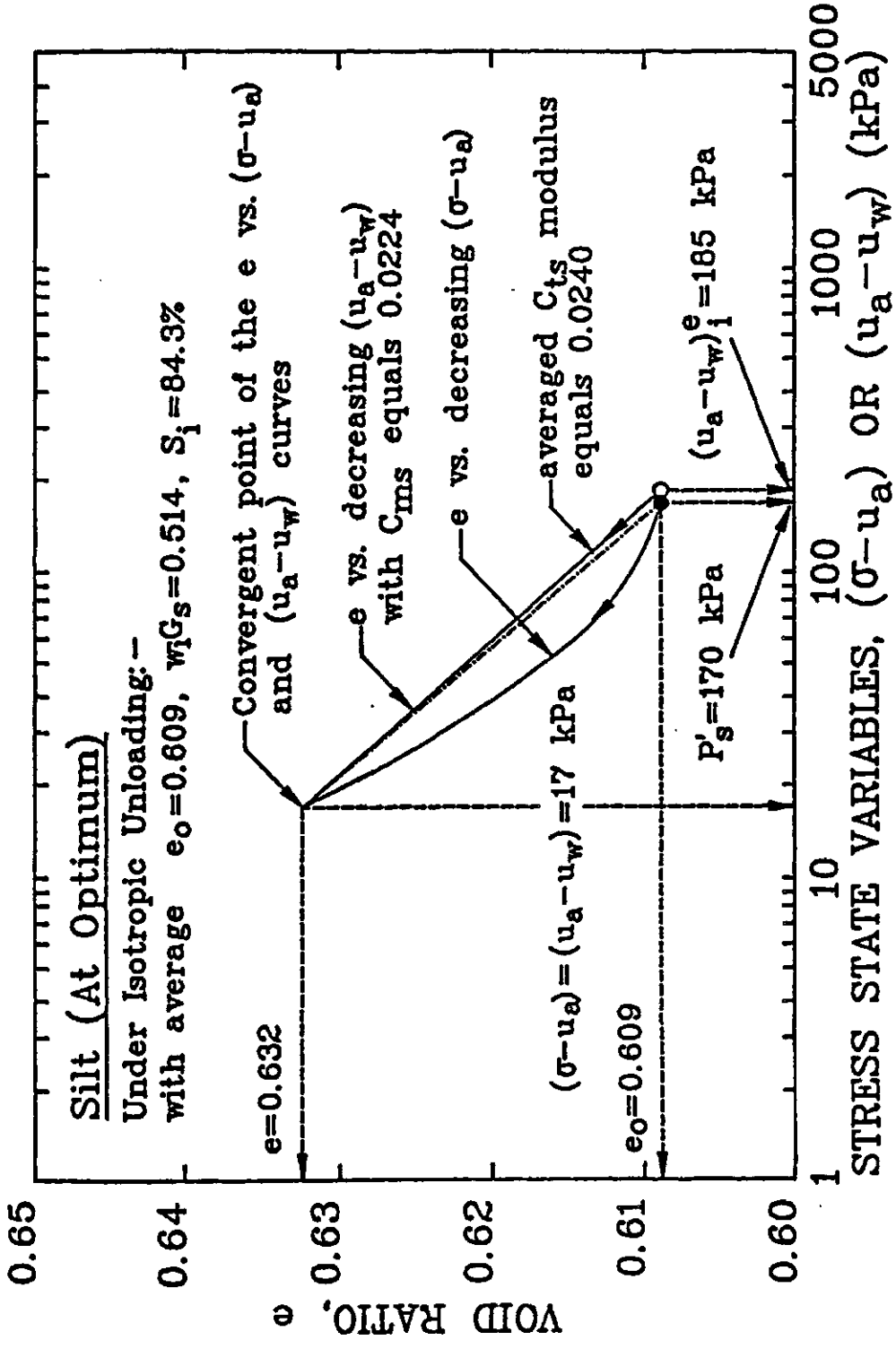

Figure 6.27 Determination of The Stress State at The Soil Structure Constitutive Surface Point of Convergence for Silt with Optimum Initial Water Content under Isotropic Unloading Conditions

Table 6.10 A summary of The Average Swelling Indices with Respect to The Net Total Stress and Matric Suction at The Points of Convergence of The Silt and Till Soil Structure Constitutive Surfaces for Monotonic Volume Increase

Strain Condition	One-Dimensional				Isotropic	
Soil Type	DS[a]	OS[b]	DT[c]	OT[d]	DS	OS
P^{e}_{cnv}(kPa)	5.8	0.5	0.054	20	1.2	17
Average C_{ts}	0.04028	0.05476	0.06592	0.03739	0.02383	0.0240
Average C_{ms}	0.03322	0.05250	0.05299	0.02407	0.02046	0.02236

Note: a) "DS" stands for silt at dry of optimum initial water content.
b) "OS" stands for silt at optimum initial water content.
c) "DT" stands for till at dry of optimum initial water content.
d) "OT" stands for till at optimum initial water content.
e) "P_{cnv}" stands for the net total stress and matric suction suction at the point of convergence.

stress state, P'_w is found to be smaller than the stress state, $(u_a - u_w)^w_i$ for till at optimum initial water content. A review of the problem indicates the assumption that the stress state, P'_w is larger than the stress state, $(u_a - u_w)^w_i$ is not always true. The void ratio of an initially unconfined unsaturated soil decreases when the soil undergoes a constant water content saturation process (Figure 6.28). There are ranges of initial water contents within which the stress state P'_w can be smaller than, equal to or larger than the stress state, $(u_a - u_w)^w_i$. The water content versus the logarithm of net total stress and matric suction unloading curves are divergent lines when the stress state, P'_w is smaller than the stress state, $(u_a - u_w)^w_i$. The case for till at optimum initial water content under one-dimensional unloading is presented as an example (Figure 6.29). The observation that the water content unloading curves may be divergent lines contradicts the assumed form of the semi-logarithmic water phase constitutive surface for monotonic water content increase. This apparent contradiction is addressed in further detail in Section 6.4.2.

6.4 Relationships between The Moduli

There are four independent moduli associated with

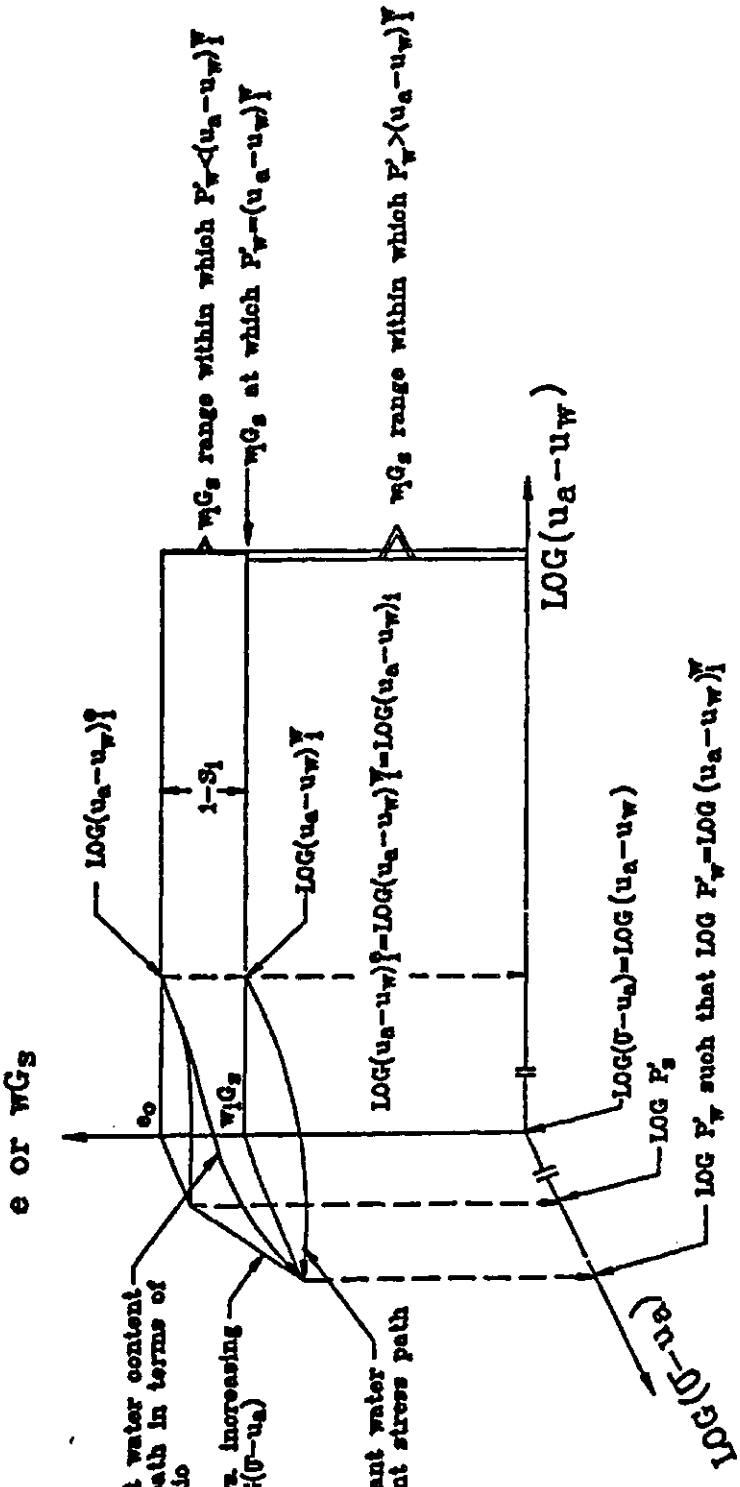

Figure 6.28 Relations between The Characteristic Stress States and Initial Soil Condition of An Unconfined Unsaturated Soil

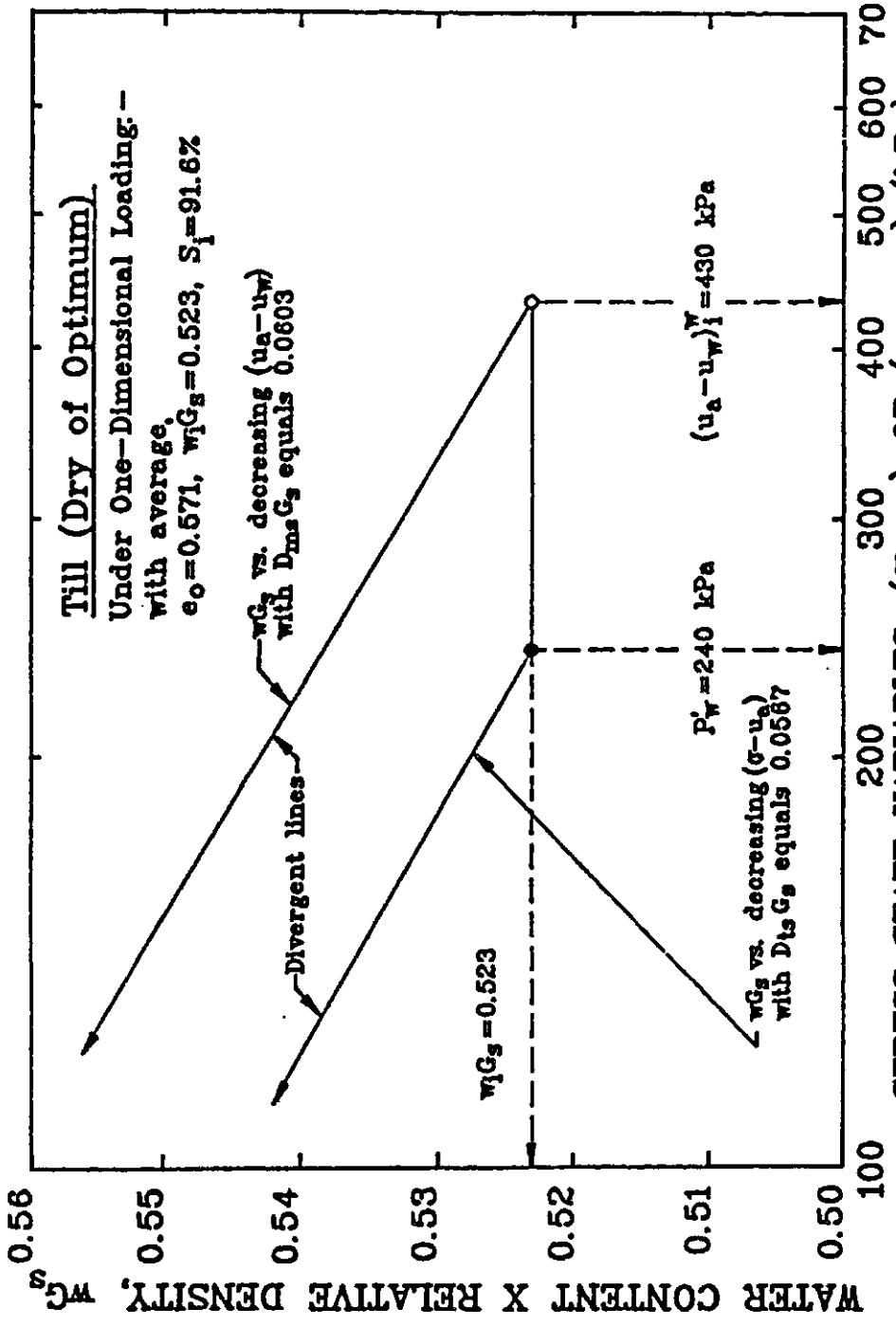

Figure 6.29 The Divergence of The Water Content Unloading Curves for Till at Dry of Optimum Initial Water Content Under One-Dimensional Unloading

the soil structure and water phase for monotonic volume change. The four moduli are C_t, C_m, D_t and D_m for monotonic volume decrease and C_{ts}, C_{ms}, D_{ts} and D_{ms} for monotonic volume increase. The prime objective of this dissertation is finding relationships between these moduli so that all can be determined if a basic few is established by conventional soil testing techniques. The moduli C_t and C_{ts} are equal to the relative density multiplied by the moduli D_t and D_{ts} respectively when a soil is saturated (See Section 3.5.3.1). The moduli, C_t and C_{ts} are the slopes of the virgin compression branch and rebound curve which can be found by conventional saturated soil tests. Approximate semi-logarithmic soil structure and water phase constitutive surfaces were presented in Chapter III. The deformation moduli, C_t, D_t, C_{ts} and D_{ts} are related to the moduli C_m, D_m, C_{ms} and D_{ms} respectively in terms of the characteristic stress states, P'_s, P'_w, $(u_a - u_w)^e_i$ and $(u_a - u_w)^w_i$. The proposed relationships are based on the geometry of the approximate semi-logarithmic constitutive surfaces. The proposed relationships are examined in this section according to the experimental results obtained from the test program.

6.4.1 Relationships between moduli of the same phase under loading conditions

The proposed relationships between C_t and C_m, D_t and D_m are examined in this section. The relationship between moduli of the soil structure undergoing monotonic volume decrease (i.e., relationship between C_t and C_m) is discussed first, followed by the relationship between moduli of the water phase undergoing monotonic water content decrease (i.e., relationship between D_t and D_m).

Relationship between Moduli of The Soil Structure Undergoing Monotonic Volume Decrease

The approximate semi-logarithmic soil structure constitutive surface for monotonic volume decrease is assumed to have a projected point of convergence on the void ratio axis (i.e., point EL on Figure 3.25b). The numerical value of the net total stress and matric suction at the projected point of convergence is assumed to be unity. Based on this assumed geometry, the compressive index with respect to the net total stress (i.e., C_t) and the compressive index with respect to matric suction (i.e., C_m) can be related as follows (see equation 3.34 in Section 3.5.2),

$$\frac{C_m}{C_t} = \frac{\log P'_s}{\log(u_a - u_w)^e_i}$$

If the numerical value of the net total stress and matric suction at the projected point of convergence is not unity,

the relationship becomes,

$$\frac{C_m}{C_t} = \frac{\log P'_s - \log P_{pr\text{-}cnv}}{\log(u_a - u_w)^e_i - \log P_{pr\text{-}cnv}} \qquad (6.1)$$

where

$P_{pr\text{-}cnv}$ = net total stress or matric suction at the projected point of convergence

The C_t and C_m moduli determined from average loading curves of silt and till were summarized in Table 6.7. A summary of the characteristic stress states determined for the same soils was presented in Table 6.8. The net total stress and matric suction at the projected points of convergence of the soil structure constitutive surfaces for silt and till were presented in Table 6.9. Table 6.11 presents a comparison between the measured moduli ratio, C_m/C_t and those predicted on the basis of the proposed relationships. The first predicted moduli ratio (i.e., $(C_m/C_t)_I$) is calculated according to the proposed relationship assuming the numerical value of the net total stress and matric suction is unity at the projected point of convergence. The predicted values overestimate the measured values by over 200% in average. The second predicted moduli ratio (i.e., $(C_m/C_t)_{II}$) is based on the same geometry of the approximated semi-logarithmic constitutive surface with the recognition that the net total stress and matric suction at the projected point of convergence may be some value, $P_{pr\text{-}cnv}$ other than unity. The resulting predictions are approximately within a 1 % difference of the measured values

Table 6.11 A Comparison between The Measured Moduli Ratio, $\frac{C_a}{C_t}$ and Those Predicted According to The Proposed Relationships

Strain Condition	Soil	P'_s (kPa)	$(u_a - u_w)^e_i$ (kPa)	C_t	C_a	P_{pr-cnv} (kPa)	$\frac{C_a}{C_t}$	$\left(\frac{C_a}{C_t}\right)$ I e	$\frac{\left(\frac{C_a}{C_t}\right)I - \frac{C_a}{C_t}}{\frac{C_a}{C_t}}$ (%)	$\left(\frac{C_a}{C_t}\right)$ II f	$\frac{\left(\frac{C_a}{C_t}\right)II - \frac{C_a}{C_t}}{\frac{C_a}{C_t}}$ (%)
One-Dimensional	DS[a]	120	225	0.1956	0.03041	106	0.1555	0.8839	+468.4	0.1648	+5.981
	OS[b]	140	185	0.1766	0.08229	110	0.4660	0.9466	+103.1	0.4638	-0.4721
	DT[c]	90	580	0.2063	0.08943	22	0.4335	0.7072	+ 63.14	0.4306	-0.6690
	OT[d]	145	430	0.1794	0.1059	30	0.5905	0.8207	+ 39.01	0.5917	+0.2032
Isotropic	DS[a]	112.5	225	0.2298	0.03041	101	0.1323	0.8720	+559.1	0.1346	+1.7380
	OS[b]	170	185	0.1865	0.08229	159	0.4412	0.9838	+123.0	0.4407	-0.1133
									χ_{ave}=+226.0%		χ_{ave}=+1.111%

Note: a) "DS" stands for silt at dry of optimum initial water content
b) "OS" stands for silt at optimum initial water content
c) "DT" stands for till at dry of optimum initial water content
d) "OT" stands for till at optimum initial water content
e) $\left(\frac{C_a}{C_t}\right)I = \frac{\log P'_s}{\log(u_a - u_w)^e_i}$

f) $\left(\frac{C_a}{C_t}\right)II = \frac{\log P'_s - \log P_{pr-cnv}}{\log(u_a - u_w)^e_i - \log P_{pr-cnv}}$

in average. The second proposed relationship (i.e., equation 6.1) is evidently a better approximation of the moduli ratio, C_m/C_t than the first proposed relationship (i.e., equation 3.34).

Relationship between Moduli of The Water Phase Undergoing Monotonic Water Content Decrease

The approximated semi-logarithmic water phase constitutive surface for monotonic water content decrease is assumed to have a projected point of convergence on the water content axis (i.e., point WL on Figure 3.26b). This projected point of convergence is assumed to be where the projections of the logarithmic water content loading curves meet. The hypothesis follows the assumption that the water content index with respect to matric suction (i.e., D_m) is larger than the water content index with respect to the net total stress (i.e., D_t). A relationship between the moduli, D_m and D_t was proposed based on the described geometry of the approximated water phase constitutive surface for monotonic water content decrease (See equation 3.35 in Section 3.5.2).

A summary of the experimentally measured water content indices for silt and till was presented in Table 6.7. The water content indices with respect to the net total stress are found to be larger than the water content indices with respect to matric suction. As a result, the

projections of the water content versus the logarithm of net total stress and matric suction loading curves are found to be lines diverging from each other (See Section 6.3.1). These findings contradict the assumed form of the semi-logarithmic water phase constitutive surface for monotonic water content decrease. Consequently, the proposed relationship between the water content indices becomes meaningless.

A change in matric suction is more effective in changing the water content of a soil than a change in net total stress (Fredlund, 1973). It is based on this concept that the water content index with respect to matric suction is assumed to be larger than the water content index with respect to the net total stress. The water content index with respect to the net total stress measures the effectiveness of decreasing the water content by an increase in net total stress when a soil is saturated. The water content index with respect to matric suction measures the effectiveness of decreasing the water content by an increase in matric suction when a soil is unsaturated. The difference in the degree of saturation between the two cases makes a direct comparison between the two water content indices improper. A better comparison is suggested to be between the water content index with respect to the net total stress and a proportioned water content index with respect to matric suction, D_m^*. The proportioned water

content index with respect to matric suction is a fictitious measure of the effectiveness of decreasing the water content by an increase in matric suction if the soil is saturated. A mathematical expression for the proportioned water content index with respect to matric suction is as follows,

$$D_m^* = \frac{D_m}{S_i} \qquad (6.2)$$

where

S_i = the degree of saturation of the soil

A comparison between the measured water content index with respect to the net total stress and the proportioned water content index with respect to matric suction for silt and till is presented in Table 6.12. As an average, there is less than a 4% difference between the two moduli (i.e., D_t and D_m^*). The net total stress acts on the soil structure whereas matric suction acts on the water phase. When a soil is saturated, the void space is completely filled with water. A volume change in the soil structure would result an equal amount of volume change in the water phase. A change in the net total stress therefore should be as effective as a change in matric suction in changing the water content. The close agreement between the proportioned water content index with respect to matric suction and the water content index with respect to the net total stress may be an illustration of the same concept. Nevertheless, the relationship that,

Table 6.12 A Comparison between The Measured Water Content Index with Respect to Net Total Stress and The Proportioned Water Content Index with Respect to Matric Suction

Strain Condition	Soil Type	e_o[e]	$w_i G_s$[f]	S_i[g] (%)	$D_t G_s$	$D_m G_s$	$D_m^* G_s$[h]	$\frac{D_m^* G_s - D_t G_s}{D_t G_s}$ (%)
One-	DS[a]	0.6993	0.4203	60.10	0.1956	0.1241	0.2065	+ 5.573
Dimensional	OS[b]	0.6060	0.5160	85.15	0.1766	0.1584	0.1860	+ 5.323
	DT[c]	0.6422	0.4265	66.41	0.2063	0.1588	0.2391	+ 15.90
	OT[d]	0.5666	0.5156	90.97	0.1794	0.1713	0.1883	+ 4.961
Isotropic	DS	0.7004	0.4238	60.51	0.2298	0.1241	0.2051	- 10.75
	OS	0.6085	0.5111	83.99	0.1865	0.1584	0.1886	+ 1.126
								$\%_{ave}$ = + 3.689%

Note: a) "DS" stands for silt at dry of optimum initial water content
b) "OS" stands for silt at optimum initial water content
c) "DT" stands for till at dry of optimum initial water content
d) "OT" stands for till at optimum initial water content
e) Average value determined by the mercury submersion method for one-dimensional conditions; average value from isotropic constant volume loading and unloading test results for isotropic conditions
f) Average value from suction test, unconfined shrinkage test and constant volume loading and unloading test results
g) $S_i = \frac{w_i G_s}{e_o}$
h) $D_m^* = \frac{D_m}{S_i}$

$$D_t = \frac{D_m}{S_i} \qquad (6.3)$$

appears to be a reliable means to estimate the water content index with respect to matric suction when the degree of saturation and the water content index with respect to net total stress are known.

6.4.2 Relationships between moduli of the same phase under unloading conditions

The proposed relationships between C_{ts} and C_{ms}, D_{ts} and D_{ms} are examined in this section. The relationship between moduli of the soil structure undergoing monotonic volume increase (i.e., relationship between C_{ts} and C_{ms}) is discussed first, followed by the relationship between moduli of the water phase undergoing monotonic water content increase (i.e., relationship between D_{ts} and D_{ms}).

Relationship between Moduli of The Soil Structure Undergoing Monotonic Volume Increase

The approximate semi-logarithmic soil structure constitutive surface for monotonic volume increase is assumed to converge towards a point on the void ratio axis (i.e., point EU on Figure 3.25a). The numerical value of the net total stress and matric suction at this point of convergence is assumed to be unity. Based on this assumed geometry, the swelling index with respect to the net total

stress (i.e., C_{ts}) and the swelling index with respect to matric suction (i.e., C_{ms}) are related as follows (See equation 3.34 in Section 3.5.2),

$$\frac{C_{ms}}{C_{ts}} = \frac{\log P'_s}{\log(u_a - u_w)^e_i}$$

If the numerical value of the net total stress and matric suction at the point of convergence is not unity, the relationship becomes,

$$\frac{C_{ms}}{C_{ts}} = \frac{\log P'_s - \log P_{cnv}}{\log(u_a - u_w)^e_i - \log P_{cnv}} \qquad (6.4)$$

where

P_{cnv} = net total stress or matric suction at the point of convergence

Values of swelling indices (i.e., C_{ts} and C_{ms}) determined from average unloading curves of silt and till were summarized in Table 6.4, 6.6 and 6.10. A summary of the characteristic stress states of silt and till was given in Table 6.8. The net total stress and matric suction at the points of convergence of the soil structure constitutive surfaces for silt and till undergoing monotonic volume increase were presented in Table 6.10. Table 6.13 presents a comparison between the measured moduli ratio, C_{ms}/C_{ts} and those predicted according to the proposed relationships (i.e., equation 3.34 and 6.4). The first predicted moduli ratio, $(C_{ms}/C_{ts})_I$ is calculated according to the proposed relationship assuming the numerical value of the net total

Table 6.13 A Comparison between The Measured Moduli Ratio, $\frac{C_{as}}{C_{ts}}$ and Those Predicted According to The Proposed Relationships

Strain Condition	Soil	P'_s (kPa)	$(u_a - u_w)^e_i$ (kPa)	C_{ts}	C_{as}	P_{cnv} (kPa)	$\frac{C_{as}}{C_{ts}}$	$(\frac{C_{as}}{C_{ts}})_I$	$\frac{(\frac{C_{as}}{C_{ts}})_I - \frac{C_{as}}{C_{ts}}}{\frac{C_{as}}{C_{ts}}}$ (%)	$(\frac{C_{as}}{C_{ts}})_{II}$	$\frac{(\frac{C_{as}}{C_{ts}})_{II} - \frac{C_{as}}{C_{ts}}}{\frac{C_{as}}{C_{ts}}}$ (%)
One-Dimensional	DS[a]	120	225	0.04028	0.03322	5.8	0.8247	0.8839	+7.178	0.8282	+0.4244
	DS[b]	140	185	0.05476	0.05250	0.5	0.9588	0.9466	-1.272	0.9529	-0.6154
	DT[c]	90	580	0.06592	0.05299	0.054	0.8038	0.7072	-12.02	0.7993	-0.5598
	DT[d]	145	430	0.03739	0.02407	20	0.6438	0.8027	+24.68	0.6457	+0.2951
Isotropic	DS[a]	112.5	225	0.02383	0.02046	1.2	0.8584	0.8720	+1.584	0.8675	+1.060
	DS[b]	170	185	0.02400	0.02236	17	0.9317	0.9838	+5.592	0.9646	+3.531
									Σ_{ave}=+4.290%		Σ_{ave}=+0.6892%

Note: a) "DS" stands for silt at dry of optimum initial water content

b) "OS" stands for silt at optimum initial water content

c) "DT" stands for till at dry of optimum initial water content

d) "OT" stands for till at optimum initial water content

e) $(\frac{C_{as}}{C_{ts}})_I = \frac{\log P'_s}{\log(u_a - u_w)^e_i}$

f) $(\frac{C_{as}}{C_{ts}})_{II} = \frac{\log P'_s - \log P_{cnv}}{\log(u_a - u_w)^e_i - \log P_{cnv}}$

stress and matric suction is unity at the point of convergence of the constitutive surface. The predicted values are within a 5% difference of the measured moduli ratios, in average. The second predicted moduli ratio, $(C_{ms}/C_{ts})_{II}$ is based on the same geometry of the approximate semi-logarithmic constitutive surface with the recognition that the net total stress and matric suction at the point of convergence may be some value, P_{cnv} other than unity. There is less than a 1 % difference between the measured and predicted values, in average. In general, both proposed relationships (i.e., equation 3.34 and 6.4) appear to give reasonable approximation of the moduli ratio, C_{ms}/C_{ts}.

Relationship between Moduli of The Water Phase Undergoing Monotonic Water Content Increase

The approximate semi-logarithmic water phase constitutive surface for monotonic water content increase is assumed to converge towards a single point on the water content axis (i.e., point WU on Figure 3.26a). This point of convergence is assumed to be where the water content versus the logarithm of net total stress and matric suction unloading curves meet. The hypothesis follows the assumption that the characteristic stress state, P'_w is larger than the characteristic stress state, $(u_a - u_w)^w_i$. At the same time, the rebound water content index with respect

to matric suction (i.e., D_{ms}) is assumed to be larger than the rebound water content index with respect to the net total stress (i.e., D_{ts}) (See Section 3.4.2 and 3.5.2). A relationship between the rebound water content indices (i.e., between D_{ms} and D_{ts}) was proposed based on the described geometry of the approximate water phase constitutive surface for monotonic water content increase (See equation 3.35 in Section 3.5.2).

A summary of the characteristic stress states for silt and till was presented in Table 6.8. The characteristic stress state, P'_w is found to be smaller than the characteristic stress state, $(u_a - u_w)^w_i$ for till at optimum initial water content. A review of the problem indicates there are conditions under which the stress state, P'_w is smaller than the stress state, $(u_a - u_w)^w_i$ (see Section 6.3.2). As a result, the water content versus the logarithm of net total stress and matric suction unloading curves would become divergent lines. The possibility that the water content unloading curves may be divergent lines contradicts the assumed form of the semi-logarithmic water phase constitutive surface for monotonic water content increase. As a result, the proposed relationship between the rebound water content indices (i.e., D_{ms} and D_{ts}) becomes meaningless.

A change in matric suction is more effective in changing the water content of a soil than a change in net

total stress (Fredlund, 1973). It is based on this concept that the rebound water content index with respect to matric suction (i.e., D_{ms}) is assumed to be larger than the rebound water content index with respect to the net total stress (i.e., D_{ts}). The rebound water content index with respect to the net total stress measures the effectiveness of increasing the water content by a decrease in the net total stress when a soil is saturated. A decrease in net total stress allows the soil structure to rebound and increase in volume. If the soil is saturated and has free access to water, the volume increase in the soil structure would result an equal volume increase in the water phase. The rebound water content index with respect to matric suction measures the effective of increasing the water content of a soil by a decrease of matric suction when a soil is unsaturated. A decrease in matric suction allows the soil structure to rebound and increase in volume. If the soil has free access to water, the volume change in the soil structure would become available to be water filled. In an unsaturated soil, only part of the void space is filled with water. Therefore, the air void within the soil before the matric suction decrease is also available to the incoming water. As a result, it is not surprising to find the rebound water content index with respect to matric suction to be larger than the rebound water content index with respect to net total stress. However, a direct comparison

between the two rebound water content indices is improper because of the difference in degree of saturation between the two cases. A better comparison is suggested to be between the rebound water content index with respect to the net total stress and a reduced rebound water content index with respect to matric suction, D^{*}_{ms}. The reduced rebound water content index with respect to matric suction is a fictitious measure of the effectiveness of increasing the water content by a decrease of matric suction in a soil disregarding the air voids within the soil. A mathematical expression for the reduced rebound water content index with respect to matric suction is as follows,

$$D^{*}_{ms} = D_{ms} \cdot S_i \qquad (6.5)$$

A comparison between the measured rebound water content index with respect to the net total stress and the reduced rebound water content index with respect to matric suction for silt and till is presented in Table 6.14. As an average, there is approximately a 6% difference between the two moduli (i.e., D_{ts} and D^{*}_{ms}). The test results for silt at dry of optimum initial water content and under isotropic strain conditions show a 380% difference. This piece of data is considered to be an "outliner" and therefore not included in calculating the average percent of difference in the comparison.

The net total stress acts on the soil structure whereas matric suction acts on the water phase. If a soil

Table 6.14 A Comparison between The Measured Water Content Index with Respect to Net Total Stress and The Reduced Rebound Water Content Index with Respect to Matric Suction

Strain Condition	Soil Type	e_o^e	$w_l G_s^e$	S_l^f(%)	$D_{ts}G_s$	$D_{ms}G_s$	$D_{ms}^* G_s^g$	$\frac{D_{ms}^* G_s - D_{ts}G_s}{D_{ts}G_s}$ (%)
One-	DS[a]	0.7025	0.4191	59.66	0.1256	0.2633	0.1571	+ 25.08
Dimensional	OS[b]	0.6156	0.5165	83.90	0.07593	0.1008	0.08457	+ 11.38
	DT[c]	0.6926	0.4359	62.94	0.08384	0.1211	0.07622	- 9.089
	OT[d]	0.5709	0.5229	91.59	0.05671	0.06032	0.05525	- 2.575
Isotropic	DS	0.6991	0.4208	60.20	0.02436	0.1939	0.1167	+ 379.1[h]
	OS	0.6089	0.5135	0.8434	0.03979	0.04983	0.04202	+ 5.621
								$\%_{ave}$=+ 6.083%

Note: a) "DS" stands for silt at dry of optimum initial water content.
b) "OS" stands for silt at optimum initial water content.
c) "DT" stands for till at dry of optimum initial water content.
d) "OT" stands for till at optimum initial water content.
e) Average value from one-dimensional free swell test results for one-dimensional conditions; average value from isotropic free swell test results for isotropic conditions
f) $S_l = \frac{w_l G_s}{e_o}$
g) $D_{ms}^* . G_s = S_l D_{ms} . G_s$
h) Data not included in calculating the average.

is saturated and has free access to water, a volume increase in the soil structure should result an equal volume increase in the water phase. A decrease in the net total stress therefore should be as effective as a decrease in matric suction in increasing the water content of a soil. The close agreement between the reduced rebound water content index with respect to matric suction and the rebound water content index with respect to the net total stress may be just a demonstration of the same concept. However, the experimental finding that,

$$D_{ts} = D_{ms} \cdot S_i \qquad (6.6)$$

appears to be a viable relationship between the rebound water content indices. Based on such a relationship, the rebound water content index with respect to matric suction can be estimated when the degree of saturation and the rebound water content index with respect to the net total stress of a soil are known.

6.4.3 Summary

The knowledge of four independent moduli is required to completely describe the behaviour of an unsaturated soil in a monotonic volume change process. A summary of the tests needed to determine the necessary moduli to describe the various types of monotonic volume changes is presented in Table 6.15. The tests involved are

Table 6.15 A Summary of Tests Needed to Determine the Necessary Moduli to Describe the Volume Change Behaviour of An Unsaturated Soil

Volume Change Process	Moduli Required	Tests Needed
Monotonic Volume decrease	C_t, C_m D_t, D_m	1) One-dimensional or isotropic constant volume loading test - C_t and D_t 2) Suction test - D_m 3) Unconfined shrinkage test - C_m/D_m
Monotonic Volume increase	C_{ts}, C_{ms} D_{ts}, D_{ms}	1) One-dimensional or isotropic constant volume unloading test - C_{ts} and D_{ts} 2) One-dimensional or isotropic free swell test - C_{ms} and D_{ms}

generally sophisticated and require special equipment to run. The main objective of this study is the development of relationships between the moduli in order that all required moduli can be determined from a few basic conventional soil tests.

Relationships are proposed for the four independent moduli associated with the soil structure and water phase undergoing monotonic volume change (i.e., C_t , C_m, D_t and D_m or C_{ts}, C_{ms}, D_{ts} and D_{ms}). The moduli C_t and C_{ts} are equal to the relative density multiplied by the moduli, D_t and D_{ts} respectively. Both moduli, C_t and C_{ts} can be found by conventional saturated soil tests. The following relationships are proposed to relate moduli C_m and C_t, C_{ms} and C_{ts}, D_m and D_t, D_{ms} and D_{ts}.

$$\frac{C_m}{C_t} = \frac{\log P'_s - \log P_{pr\text{-}cnv}}{\log(u_a - u_w)^e_i - \log P_{pr\text{-}cnv}}$$

$$\frac{C_{ms}}{C_{ts}} = \frac{\log P'_s}{\log(u_a - u_w)^e_i}$$

$$D_t = \frac{D_m}{S_i}$$

and

$$D_{ts} = D_{ms} \cdot S_i$$

As a result, moduli C_m , D_m, C_{ms} and D_{ms} can be estimated from the proposed relationships with the knowledge of the two basic moduli, C_t and C_{ts} and the characteristic stress states, P'_s and $(u_a - u_w)^e_i$.

CHAPTER VII

CONCLUSIONS AND RECOMMENDATIONS

7.1 Conclusions

Eight independent volume change moduli are required to describe the volume change behaviour of an unsaturated soil, four for monotonic volume increase and four for monotonic volume decrease. Sophisticated tests are needed to determine these moduli. The one-dimensional or isotropic constant volume compression test, the suction and unconfined shrinkage tests are required to determine moduli necessary for solving settlement problems. The one-dimensional or isotropic constant volume unloading test and the one-dimensional or isotropic free swell test are required to determine moduli necessary for solving swelling problems.

The main objective of this investigation was to measure and develop relationships between volume change moduli of an unsaturated soil. The form of the semi-logarithmic soil structure and water phase constitutive surfaces was studied from information available in the research literature. Approximate planar semi-logarithmic constitutive surfaces were proposed. Relationships between moduli associated with a particular phase were developed based on the geometry of the approximate semi-logarithmic constitutive surfaces. These relationships were tested

using the results of an experimental program on compacted silt and till specimens. The conclusions arrived at are based on the theoretical and experimental studies conducted as part of this dissertation, as well as previous studies.

1) Four independent moduli associated with the soil structure and water phase can be used to define monotonic volume change. The four moduli are C_t, C_m, D_t and D_m for monotonic volume decrease and C_{ts}, C_{ms}, D_{ts} and D_{ms} for monotonic volume increase. These are all "index" type properties measured on a semi-logarithmic scale. It is possible to measure all these moduli experimentally. The tests required are as follows:

i) One-dimensional or isotropic constant volume loading test to determine C_t and D_t.

ii) Suction test to determine D_m.

iii) Unconfined shrinkage test to determine the moduli ratio, C_m/D_m.

iv) One-dimensional or isotropic constant volume unloading test to determine C_{ts} and D_{ts}.

v) One-dimensional or isotropic free swell test to determine C_{ms} and D_{ms}.

2) The moduli, C_t and C_{ts}, are the slopes on the compression branch and rebound curves which can be found using conventional saturated soil tests (i.e., the application of a total stress with the specimens saturated).

3) When the soil is saturated, the soil structure moduli, C_t and C_{ts} are equal to the relative density (i.e., G_s) multiplied by the water phase moduli D_t and D_{ts} respectively.

4) An approximate semi-logarithmic soil structure constitutive surface for monotonic volume increase is proposed. The approximate constitutive surface is assumed to converge towards a single point on the void ratio axis. The numerical value of the net total stress and matric suction at the point of convergence was assumed to be unity. The use of a logarithmic scale for the abscissas makes the specification of units for the stress variables unnecessary. A relationship between the moduli, C_{ts} and C_{ms}, is proposed.

$$\frac{C_{ms}}{C_{ts}} = \frac{\log P'_s}{\log(u_a - u_w)^e_i}$$

The proposed relationship was found to predict the moduli ratio, $\frac{C_{ms}}{C_{ts}}$ to within an average of 5% difference of the measured values for silt and till. The proposed equation is more accurate if the point of convergence is known for the soil. In that case, the proposed relationship becomes,

$$\frac{C_{ms}}{C_{ts}} = \frac{\log P'_s - \log P_{cnv}}{\log(u_a - u_w)^e_i - \log P_{cnv}}$$

The term, P_{cnv} is the net total stress or matric suction at the point of convergence. This refined relationship was

found to predict the moduli ratio, $\frac{C_{ms}}{C_{ts}}$ to within an average of 1 % difference of the measured values for silt and till.

5) An approximate semi-logarithmic soil structure constitutive surface for monotonic volume decrease is proposed. The approximate constitutive surface is assumed to have a projected point of convergence on the void ratio axis. The relationship between the moduli, C_m and C_t is suggested to be as follows,

$$\frac{C_m}{C_t} = \frac{\log P'_s - \log P_{pr\text{-}cnv}}{\log(u_a - u_w)^e_i - \log P_{pr\text{-}cnv}}$$

The net total stress and matric suction at the projected point of convergence (i.e., $P_{pr\text{-}cnv}$) were found to be in the range of 100 to 150 kPa for the silt and 20 to 30 kPa for the till. The proposed relationship was found to predict the moduli ratio, $\frac{C_m}{C_t}$ to within an average of 1 % difference of the measured values for silt and till.

6) A relationship between the water phase moduli, D_{ms} and D_{ts} is proposed in accordance with the experimental data from the test program. The suggested relationship is as follows.

$$D_{ts} = D_{ms} S_i$$

Measured D_{ms} and D_{ts} moduli values for silt and till were found to be within a 6% difference of the proposed relationship.

7) Based on experimental evidence from the laboratory test data, the following relationship between the

water phase moduli, D_m and D_t is proposed.

$$D_t = \frac{D_m}{S_i}$$

Measured D_m and D_t moduli values for silt and till were found to be within a 4 % difference of the proposed relationship.

7.2 Recommendations

The prime objective of this thesis was to develop relationships between the volumetric deformation moduli for unsaturated soils. Future research is needed to corroborate the observations and conclusions presented in this dissertation. A number of suggestions are made.

1) Relationships are proposed for the four independent moduli associated with the soil structure and water phase undergoing monotonic volume change (i.e., C_t, C_m, D_t and D_m; C_{ts}, C_{ms}, D_{ts} and D_{ms}). The moduli, C_t and C_{ts} are regarded as "basic" moduli which can be found using conventional saturated soil testing equipment. The proposed relationships can then be used to estimate the values of the other moduli, D_t, D_{ts}, C_m, D_{ms}, D_m and D_{ms}, once there is a knowledge of the two basic moduli and the characteristic stress states, P_s' and $(u_a - u_w)_i^e$. More documented data for different soils should be collected to further examine and test the proposed relationships.

2) Approximate semi-logarithmic soil structure constitutive surfaces are presented for monotonic volume changes. These approximate constitutive surfaces, along with the knowledge of the moduli, can be used to solve unsaturated soil volume change problems. Further studies should be carried out to verify the form of soil structure constitutive surfaces for different unsaturated soils.

3) The approximate semi-logarithmic constitutive surface for the soil structure undergoing monotonic volume decrease is assumed to have a projected point of convergence on the void ratio axis. The net total stress and matric suction at the projected points of convergence are found to be different for silt and till. Further research is needed to study factors affecting the net total stress and matric suction value at the projected point of convergence.

4) Little information is available about the form of the water phase constitutive surfaces. Such information is useful when solving unsaturated soil volume change problems involving water content changes. Knowledge about the form of the water phase constitutive surfaces is required in order to completely understand the volume change behaviour of unsaturated soils.

5) Limited information is available in the research literature on the volume change constitutive relations for collapsing soils. More research is required in order to establish the form of the constitutive surfaces for

collapsing soils. The idea of approximating a curved constitutive surface by a composite planar constitutive surface may be a viable means to relate the moduli of a collapsing soil. Further studies on collapsing soils, within this context, could prove fruitful.

LIST OF REFERENCES

AITCHISON, G. D. (1965), "Soil Properties, Shear Strength and Consolidation", Proc. of the 6th Int. Conf. on soil Mech. Fdn. Engng., Montreal, Canada, Volume 3, pp. 318-321.

AITCHISON, G. D. (1973), "The Quantitative Description of the Stress - Deformation Behaviour of Expansive Soils - Preface to set of papers", Proc. of the 3rd Int. Conf. on Expansive soils, Haifa, Israel, Volume 2, pp. 79-82.

AITCHISON, G. D. and MARTIN, R. (1973), "A Membrane Oedometer for Complex Stress-Path Studies in Expansive Clays", Proc. of the 3rd Int. Conf. on Expansive Soils, Haifa, Israel, Volume 2, pp. 83-88.

AITCHISON, G. D., PETER, P. and MARTIN, R. (1973), "The Instability Indices I_{Pm}" and I_{Ps}" in Expensive Soils", Proc. of the 3rd Int. Conf. on Expansive Soils, Haifa, Israel, Volume 2, pp. 101-104.

AITCHISON, G. D. and WOODBURN, J. A. (1969), "Soil Suction in Foundation Design", Proc. of the 7th Int. Conf. Soil Mech. Found. Eng., Mexico, Vol. 2, pp. 1-8.

ALONSO E. E. and LLORET, A. (1982), "Behaviour of Partially Saturated Soil in Undrained Loading and Step by Step Embankment Construction", Proc. of the IUTAM Conf. on Deformation and Failure of Granular Materials, Delft, pp. 173-180.

ARNOLD M. (1983), "The Moisture Characteristic", Unpublished Research Report.

BARDEN, L., MADEDOR, A. O. and SIDES, G. R. (1969), "Volume Change Characteristics of Unsaturated Clay", ASCE, J. Soil Mech. Found. Div., 95(SMI), pp. 33-51.

BEAL, N. S. (1984), "Direct Determination of Linear Dimension Versus Moisture Content Relationship in Expansive Clays", Proc. of the 5th Int. Conf. on Expansive Soils, Adelaide, Australia, pp. 62-66.

BIOT, M. A. (1941), "General Theory of Three Dimensional Consolidation", J. App. Phys, 12, pp. 155-164.

BISHOP, A. W. (1959), "Principle of Effective Stress", TEK. UKEFLAD, No. 39, PP. 859-863.

BISHOP, A. W. (1960), "The Measurement of Pore Pressure in Triaxial Test", Proc. of Conf. on Pore Pressure and Suction in Soils, Butterworth, London, pp. 38-46.

BISHOP, A. W. and BLIGHT, G. E. (1963), "Some Aspects of Effective Stress in Saturated and Unsaturated Soils", Geotechnique, Vol. 13, pp. 177-197.

BRACKLEY, I. J. A. (1971), "Partial Collapse in Unsaturated Expensive Clay", Proc. 5th Reg. Conf. Soil Mech. Found. Eng., South Africa, pp. 23-30.

CASAGRANDE, A. (1936), "The Determination of the Pre-Consolidation Load and Its Practical Significance", Discussion D-34, Proc. of the 1st Int. Conf. on Soil Mech. Fdn. Engng., Cambridge, Vol. III, pp. 60-64.

CHEN, F. H. (1975), "Foundations on Expansive Soils" Elsevier Scientific Publishing Co., New York, 1st Edition.

COLEMAN, J. D. (1962), "Stress/Strain Relations for Partly Saturated Soils", Correspondence, Geotechnique, 12(4), pp. 348-350.

CRONEY, D. and COLEMAN, J. D. (1954), "Soil Structure in Relation to Soil Suction (pF)", J. of Soil Science, 5(1), pp. 75-84.

DAKSHANAMURTHY, V. and FREDLUND, D.G, (1980), "Moisture and Air Flow in An Unsaturated Soil", Proc. of the 4th Int. Conf. on Expansive Soils, ASCE, Vol. 1. pp. 514-532.

ESCARIO, V. (1969), "Swelling of Soils in Contact with Water at A Negative Pressure", Proc. of the 2nd Int. Research and Engng. Conf. on Expansive Clay Soils, Texas A & M University, College Station, U.S.A., pp. 207-218.

FREDLUND, D. G. (1964), "Comparison of Soil Suction and One-Dimensional Characteristics of a Highly Plastic Clay", National Research Council of Canada, Division of Building Research, Technical Report No. 245.

FREDLUND, D. G. (1973), "Volume Change Behaviour of Unsaturated Soils", Ph.D. Dissertation, University of Alberta, Edmonton.

FREDLUND, D. G. (1974), "Engineering Approach to Soil Continua". Proceedings of the Second Symposium on the Application of Solid Mechanics, Hamilton, Ontario, Canada, pp. 46-59.

FREDLUND, D. G. (1975), "A Diffused Air Volume Indicator for Unsaturated Soils". Canadian Geotechnical Journal, Vol. 12, No. 4, pp. 533-539.

FREDLUND, D. G. (1979), "Second Canadian Geotechnical Colloquium: Appropriate Concepts and Technology for Unsaturated Soils". Canadian Geotechnicla Journal, Vol. 16, No. 1, pp. 121-139.

FREDLUND, D. G. (1982), "Consolidation of Unsaturated Porous Media", Nato Advance Study Institute , Mechanics of Fluids in Porous Media, University of Delaware, U.S.A.

FREDLUND, D. G. (1983), "Prediction of Ground Movements in Swelling Clays", Proc. of the 31st Annual Soil Mech. and Fdn. Engng. Conf., University of Minnesota, Minneapolis, Minnesota, U.S.A.

FREDLUND, D. G. (1985a), "Soil Mechanics Principles That Embrace Unsaturated Soils", Proc. of the 11th Int. Conf. on Soil Mech. Fdn. Engng., San Francisco.

FREDLUND, D. G. (1985b), "Theory Formulation and Application for Volume Change and Shear Strength Problems in Unsaturated Soils", Proc. of the 11st Int. Conf. on Soil Mech. Fdn. Engng., San Francisco.

FREDLUND, D. G., HASAN, J. U. and FILSON, H. L. (1980), "The Prediction of Total Heave", Proc. of the 4th Int. Conf. on Expansive Soils, ASCE Denver, U.S.A.

FREDLUND, D. G. and MORGENSTERN, N. R. (1976), "Constitutive Relations for Volume Change in Unsaturated Soils". Canadian Geotechnical Journal, Vol. 13, No. 3, pp. 261-276.

FREDLUND, D. G. and MORGENSTERN, N. R. (1977), "Stress State Variables for Unsaturated Soils". Journal of the Geotechnical Engineering Division, ASCE, Vol. 103, G75, pp. 447-466.

FREDLUND, D. G., MORGENSTERN, N. R. and WIDGER A. (1978), "Shear Strength of Unsaturated Soils", Can. Geot. J., Vol. 15, No. 3, pp. 313-321.

GILCHRIST, H. G. (1963), "A Study of Volume Change of a Highly Plastic Clay", M. Sc. Dissertation, University of Saskatchewan, Saskatoon, Canada.

HAINES, W. B. (1923), "The Volume Changes Associated with Variations of Water Content in Soil", J. of Agricultural Science, Vol. XIII, pp. 296-310.

HARDY, F (1923), "The Shrinkage Coefficient of Clays and Soils", J. of Agricultural Science, Vol. XIII, pp. 244-264.

HOLTZ, W. G. and GIBBS, H. J. (1956), "Engineering Properties of Expansive Clays", Transactions of the ASCE, Vol. 121, pp. 641-663.

JENNINGS, J. E. and BURLAND, J. B. (1962), "Limitations to the Use of Effective Stresses in Partly Saturated Soils", Geotechnique, London, England, Vol. 12, No. 2, pp. 125-144.

JUSTO, J. L., DELGADO, A. and RUIZ, J. (1984) "The Influence of Stress-Path in The Collapse-Swelling of Soils at The Laboratory", Proc. of the 5th Int. Conf.(on Expansive Soils, Adelaide, Australia, pp. 67-71.

KRAHN, J. (1970), "Comparison of Soil Pore Water Potential Components", M. Sc. dissertation, University of Saskatchewan, Saskatoon, Canada.

LAMBE, T. W. (1951), "Soil Testing For Engineers", 1st edition, John Wiley Sons, Inc., New York, pp. 74-88.

LAMBE, T. W. and WHITMAN, R. V. (1979), "Soil Mechanics", John Wiley Sons, Inc., New York.

LEE, R. K. C. and FREDLUND, D. G. (1984) "Measurement of Soil Suction Using the MCS 6000 Sensor", Proc. of the 5th Int. Conf. on Expansive Soils, Adelaide, Australia, pp. 50-54.

LIDGREN, R. A. (1970), "Volume Change Characteristics of Compacted Till", M.Sc. thesis, University of Saskatchewan, Saskatoon, Canada.

LLORET A. AND ALONSO, E. E. (1985), "State Surfaces for Partially Saturated Soils", Proc. of the 11th Int. Conf. on Soil Mech. and Fdn. Engng., San Francisco, Vol. 2, pp. 557-562.

MASE, G. E. (1970), "Continuum Mechanics", McGraw-Hill Book Company, New York, U.S.A.

MATYAS, E. L. and RADHAKRISHNA, H. S. (1968), "Volume Change Characteristics of Partially Saturated Soils", Geotechnique, 18(4), pp. 432-448.

McWHORTER, D. B. and NELSON, J. D. (1979) "Unsaturated Flow Beneath Tailings Impoundments", J. of the Geot. Engng. Div., ASCE, Vol. 105, pp. 1317-1334.

MITCHELL, P. W. and AVALLE, D. L. (1984), "A Technique to Predict Expansive Soil Movements", Proc. of the 5th Int. Conf. on Expansive Soils, Adelaide, Australia, pp. 124-130.

NOBLE, C. A. (1966), "Swelling Measurements and Prediction of Heave for A Lacustrine Clay", Can. Geot. J., Vol. 3, pp. 32-41.

OLSEN, R. E. and LANGFELDER, L. J. (1965), "Pore Pressures in Unsaturated Soils", Journal of the Soil Mech. and Fdn. Div., ASCE, Vol. 91, SM4.

POPESCU, M. (1980), "Behaviour of Expansive Soils with A Crumb Structure", Proc. of the 4th Int. Conf. on Expansive Soils, ASCE, Vol. 1, pp. 158-171.

PUFHAL, D. (1970), "Evaluation of Effective Stress Components in Non-Saturated Soils", M. Sc. thesis, University of Saskatchewan, Saskatoon, Canada.

RICHARDS, B. G., PETER, P. and MARTIN R. (1984), "The Determination of Volume Change Properties in Expansive Soils", Proc. of the 5th Int. Conf. on Expansive Soils, Adelaide, Australia, pp. 179-186.

RIEKE, H. H. and CHILINGARIAN, G. V. (1974), "Compaction of Argillaceous Sediments", Development in Sedimentology No. 16, Elsevier Scientific Publishing Co., Amsterdam, pp. 31-86.

SAUER, E. K. (1967), "Application of Geotechnical Principles to Highway Engineering", D. Eng. thesis, University of California, Berkely, U.S.A.

SEKER E. (1983), "The Study of Deformation for Unsaturated Soils", Ph. D. Thesis, Ecole Polytechnique Fédérale of Lausanne, Spain.

SMITH, G. N. (1978), "Elements of Soil Mechanics for Civil and Mining Engineers", fourth edition, Granada Publishing Limited, London, pp. 5-6.

TERZAGHI, K. (1936), "The Shearing Resistance of Saturated Soils", Proceedings of the First International Conference on Soil Mechanics, Vol. 1.

TERZAGHI, K. and PECK, R. B. (1967), "Soil Mechanics in Engineering Practice", John Wiley Sons, Inc., New York, N.Y.

WOOLTORTON, F. L. D. (1954), "The Scientific Basis of Road Design", Edward Arnold Publishers Ltd., London.

YOSHIDA, R., FREDLUND, D. G. and HAMILTON, J. J. (1981). "The Prediction of Total Heave of a Slab-on-Ground Floor on Regina Clay". Proceedings of the Thirty-Fourth Canadian Geotechnical Conference held in Fredericton, New Brunswick, Canada.

APPENDIX A

Listings of The Programs for

a) Sensor Calibrations

b) Data Processing

```
1 REM*************************************
2 REM** THIS IS A MODIFIED VERSION    **
3 REM** OF THE STANDARD BASIC 8066A/ **
4 REM** PET/CS4 SOFTWARE FOR CALIBRA(**
5 REM** -IONS IN THE TEST PROGRAM OF **
6 REM** D.HO'S PH.D THESIS-AUGUST,86.**
7 REM*************************************
8 GOSUB54000:REM INITIALIZE VARIABLES
9 :
20 PRINT"ENTER:-"
30 PRINT"SENSOR TYPE SELECTION:-"
40 PRINT"    1--PRESSURE TRANSDUCER"
50 PRINT"    2--LVDT OR PROXIMETER"
60 INPUT"SENSOR TYPE";ST%
70 INPUT"NO.OF CHNL.";NC%
80 IF ST%=1 GOTO 100
90 IF ST%=2 GOTO 200
100 C=NC%
110 G=2
120 GOSUB 50000
130 PRINT M
140 GET PS$
150 IF PS$="S" THEN 5000
160 GOTO 100
200 C=NC%
210 G=0
220 GOSUB 50000
230 PRINT M
240 GET PS$
250 IF PS$="S" THEN 5000
260 GOTO 200
5000 CLOSE 1
5100 END
49900 END
49990 END
49997 :
49999 REM VOLTS
50000 POKEBA,(PEEK(BA)AND243):BF=0:GOSUB55010:M=VO/(G(G)*1000)
50010 RETURN
50098 :
50099 REM AUTOVOLTS
50100 G=-1
50110 G=G+1:GOSUB50000:IF(G=3)THEN50130
50120 IF(ABS(M)<(4.096/G(G+1)))THEN50110
50130 RETURN
50198 :
50199 REM AMPS
50200 BF=1:GOSUB55010:M=VO/(G(G)*R2*1000)
50210 RETURN
50298 :
50299 REM OHMS
50300 C=INT(C):RA=INT(RA)
50310 IF((C<0)OR(C>63))THENER=7:ER$="C":GOSUB54800:GOTO50370
50320 IF((RA<1)OR(RA>3))THENER=7:ER$="RA":GOSUB54800:GOTO50370
50330 POKEBA,((PEEK(BA)AND240)+4*RA):POKEBA+1,128+C:BF=2
50340 IF(RA=3)THENFORZZ=0TO400:NEXTZZ:REM TIMING LOOP
50350 GOSUB55010:M=FNB(VO*RA(RA)/2048):POKEBA+1,AZ%:POKEBA,(PEEK(BA)AND240)
50360 IF(MK0)THENER=6:GOSUB54800
50370 RETURN
```

Figure A-1-1 Listing of The Program, C1-DH8082A for Sensor Calibrations

```
50399 :
50399 REM AUTOOHMS
50400 RA=4
50410 RA=RA-1:GOSUB50300:IF(RA=1)THEN50430
50420 IF(MK*1.95*RA(RA-1))THEN50410
50430 RETURN
50599 :
50599 REM HERTZ
50600 M=0:Z1%=0:FP=1000825:C=INT(C.):BF=3
50610 IF((C<0)OR(C>63))THENER=7:ER$="C":GOSUB54800:GOTO50680
50615 POKEBA+3,0:IF(PEEK(BA+3)<>0)THENER=1:GOSUB54800:GOTO50680
50620 POKEBA+2,191:POKEBA+3,255:POKEBA+1,(192ORC):POKEBA+11,(PEEK(BA+11)OR224)
50630 POKEBA,(PEEK(BA)AND207):POKEBA+4,Z1%:POKEBA+5,0:POKEBA+6,255
50640 POKEBA+9,255:POKEBA,PEEK(BA)OR32:ZZ=TI:ZX=65536*2*(Z1%+2)/FP*60
50650 IF((PEEK(BA+13)AND16)<>16)AND((TI-ZZ)(ZX)THEN50650
50660 IF((TI-ZZ))ZX)OR((PEEK(BA+13)AND32)=32)THEN50690
50670 M=FNC(FP/(65536-256*PEEK(BA+9)-PEEK(BA+8))/(2*Z1%+4))
50680 RETURN
50798 :
50799 REM LEVEL
50800 IF((C<0)OR(C>15))THENER=7:ER$="C":GOSUB54800:GOTO50820
50805 ZX=C:ZZ=18:IFZX>7THENZX=ZX-8:ZZ=19
50810 M=0:IF((PEEK(BA+ZZ)AND(2↑ZX))=0)THENM=1
50820 RETURN
50998 :
50999 REM THERMOCOUPLE
51000 GOSUB51200:G=3:VC=K0(TY)+RE*(K1(TY)+RE*(K2(TY)+RE*K3(TY))):GOSUB50000
51010 V=M*1000+VC:M=C0(TY)+V*(C1(TY)+V*(C2(TY)+V*C3(TY)))
51020 RETURN
51198 :
51199 REM REFTEMP
51200 ZZ=TI-RT:OC%=C:IFZZ<0THENZZ=ZZ+5184000
51210 IF((ZZ>RD)OR(RE=0))THENOG%=G:C=CR%:GOSUB51400:RE=M:RT=TI:C=OC%:G=OG%
51220 RETURN
51398 :
51399 PROC THERMISTOR
51400 RA=2:GOSUB50300:IF(IK=0)THENER=5:GOSUB54800:GOTO51420
51410 ZZ=LOG(M):M=1/(A0+ZZ*(A1+ZZ*(A2+ZZ*A3)))-273.15
51420 RETURN
51598 :
51599 REM AD590
51602 G=1:GOSUB50200:M=0.039*G(G)*M*:E6-269.44
51610 RETURN
51795 :
51796 REM INITIALIZATION
51800 BA=35840 :REM 8082A BASE ADDRESS
54010 PRINT"....CHECKING 8082A REGISTERS"
54014 GOSUB54600:IF(ER=0)THEN54625
54016 PRINT"8082A REGISTERS FAILED:";ER$
54018 PRINT"(CHECK POWER/CABLES/SWITCHES/BASE ADDRESS)":STOP
54025 GOSUB 54710
54030 :
54035 REM.....8082A PARAMETERS - SERIAL NUMBER ; ######.....
54037 PRINT".....INITIALIZING 8082A CONSTANTS"
54040 AZ%=0  :REM SHORTED CHANNEL (AUTO ZERO)
54042 CR%=33 :REM REFERENCE TEMP CHANNEL
54044 VR=2048:REM 8082A REFERENCE VOLTAGE VALUE (MV)
54046 RD=1000:REM REF TEMP UPDATE FREQUENCY IN 1/60'S OF A SEC
54048 ZT=1000:REM AUTOZERO UPDATE FREQUENCY IN 1/60'S OF A SEC
54050 G(0)=1.000:G(1)=10.027:G(2)=100.5:G(3)=503.321
54052 RA(1)=1002.0:RA(2)=10030.0:RA(3)=632100:R2=1002.1
54053 :
54054 REM.....FUNCTIONS
54055 BF$(0)="VOLTS":BF$(1)="AMPS":BF$(2)="OHMS":BF$(3)="HERTZ"
```

Figure A-1-1 (continued)

```
54059 :
54060 REM.....ERROR MESSAGES
54065 DIM ER$(7)
54070 ER$(0)="NO ERRORS DETECTED"
54071 ER$(1)="VIA INOPERATIVE"
54072 ER$(2)="A/D CONVERTER INOPERATIVE"
54073 ER$(3)="SIGNAL OUT OF RANGE"
54074 ER$(4)="A/D CONVERTER TIMED OUT
54075 ER$(5)="A/D DIGITAL READ PROBLEM
54076 ER$(6)="RESISTANCE < 6 ERROR"
54077 ER$(7)="BAD CHANNEL OR RANGE PARAMETER"
54080 :
54100 REM.....ROUNDOFF FUNCTION DEFINITIONS
54110 DEFFNA(X)=INT(X+.5):DEFFNB(X)=INT(10*X+.5)/10
54112 DEFFNC(X)=INT(100*X+.5)/100:DEFFND(X)=INT(1000*X+.5)/1000
54120 :
54130 REM.....TRANSDUCER EQUATION COEFFICIENTS
54132 REM...YSI 44005 THERMISTOR
54135 A0=1.403E-3:A1=2.373E-4:A2=-3.188E-8:A3=1.066E-7
54140 REM...THERMOCOUPLES--V=F(T) K'S; FOR T=F(V) C'S; TY=TYPE
54145 REM...TYPE T THERMOCOUPLES  (TY=0)
54150 K0(0)=-0.00119:K1(0)=0.038619:K2(0)=4.3658E-5:K3(0)=-2.0671E-8
54155 C0(0)=-.0099:C1(0)=25.9527:C2(0)=-.89648:C3(0)=.02613
54160 REM...TYPE E THERMOCOUPLES  (TY=1)
54165 K0(1)=2.5577E-4:K1(1)=.05855:K2(1)=4.92145E-5:K3(1)=-3.0384E-8
54170 C0(1)=-0.02636:C1(1)=17.07668:C2(1)=-.23002:C3(1)=.00538
54175 REM...TYPE J THERMOCOUPLES  (TY=2)
54180 K0(2)=8.33345E-4:K1(2)=.05037:K2(2)=2.85715E-5:K3(2)=-5.7363E-8
54185 C0(2)=-.031617:C1(2)=19.84916:C2(2)=-.21026:C3(2)=8.96989E-3
54190 RETURN
54199 :
54597 REM REG-TEST
54600 EZ$="":ZZ=BA+2:ER$="DDB ":GOSUB54650:ZZ=BA+3:ER$="DDA ":GOSUB54650
54605 POKEBA+2,255:POKEBA+3,255
54610 ZZ=BA+11:ER$="ACR ":GOSUB54650:ZZ=BA+12:ER$="PCR ":GOSUB54650
54615 POKEBA+11,0:POKEBA+12,0
54620 ZZ=BA:ER$="PB ":GOSUB54650:ZZ=BA+1:ER$="PA ":GOSUB54650
54625 ER$=EZ$:IFER=0THENER$=""
54630 RETURN
54637 :
54640 REM BITLOOP
54650 FOREX=0TO7:ZX=2^EX:POKEZZ,ZX:IF(PEEK(ZZ)<>ZX)THENEZ$=EZ$+ER$:ER=1:EX=8
54655 NEXTEX:RETURN
54695 :
54700 REM VIA-INIT
54710 POKEBA+2,0:POKEBA+3,0:POKEBA+11,0:POKEBA+12,204:POKEBA+14,128
54720 POKEBA+2,191:POKEBA+3,255
54730 RETURN
54737 :
54738 REM ERROR
54740 IFEP=0THEN54950
54810 IFER=1THENFORZQ=1TO3:GOSUB54710:NEXTZQ
54830 M=-9999:EZ$=BF$(BF)+" "+ZX=(PEEK(BA+1)AND192)/64
54840 IF(ZX<>BF)THENEZ$=EZ$+" (ACTUALLY:"+BF$(ZX)+")"
54850 ER$=EZ$+ER$(ER)+ER$+" (CH="+STR$(PEEK(BA+1)AND63)+") TIME:"+TI$
54880 PRINTER$:ER$="":ER=0
54950 RETURN
```

Figure A-1-1 (continued)

```
54997 :
54998 REM ATOD1
55010 ER=0:POKEBA+12,204:C=INT(C):G=INT(G):BF=INT(BF)
55020 IF((BF(0)OR(BF)2))THENER=7:ER$="BF":GOSUB54800:GOTO55100
55030 IF((C(0)OR(C)63))THENER=7:ER$="C":GOSUB54800:GOTO55100
55035 IF((G(0)OR(G)3))THENER=7:ER$="G":GOSUB54800:GOTO55100
55040 ZZ=TI-ZL:IF((ZZ(ZT)OR(BF=2))THEN55070
55050 OG%=G:POKEBA+1,AZ%:FORG=0TO3:POKEBA,((PEEK(BA)AND240)+G)
55060 GOSUB 55510:AZ(G)=VO:NEXTG:G=OG%:ZL=TI
55070 POKEBA+1,(64*BF+C):IF(ER(>0)THEN55100
55080 IF(BF=2)THENPOKEBA,(PEEK(BA)AND252):GOSUB55510:GOTO55100
55090 POKEBA,(((PEEK(BA))AND240)+G):GOSUB55510:VO=VO-AZ(G)
55100 POKEBA+1,AZ%:RETURN
55200 :
55500 REM ATOD2
55510 IF(PEEK(BA+12)(>204)THENER=1:GOSUB 54800:GOTO55610
55520 POKEBA+12,206:POKEBA+12,204
55530 ZZ=TI+15:IFZZ)5184000THENZZ=ZZ-5184000
55540 IF((TI(=ZZ)AND(PEEK(BA+13)AND2)(>2)THEN55540
55550 IF(TI>ZZ)THENER=4:GOSUB 54800:GOTO55610
55560 VL%=PEEK(BA+16):VH%=PEEK(BA+17)
55570 IF((VL%(>PEEK(BA+16))OR(VH%(>PEEK(BA+17)))THENER=5:GOSUB 54800:GOTO55610
55580 IF((VH%AND16)=16)THENER=3:GOSUB 54800:GOTO55610
55590 VO=256*(VH%AND15)+VL%:IF(VH%AND32)=0THENVO=-VO
55600 ZZ=PEEK(BA+1):IF((PEEK(BA+13)AND2)=2)THENER=2:GOSUB 54800
55610 RETURN
```

Figure A-1-1 (continued)

```
0 REM ************************************************
1 REM*********************************
2 REM** THIS IS A MODIFIED VERSION OF**
3 REM** THE STANDARD BASIC 8082A/PET/**
4 REM** C64 SOFTWARE FOR COLLECTING  **
5 REM** DATA IN THE TRIAXIAL TEST    **
6 REM** PROGRAM OF D.HO'S PH.D THESIS**
7 REM**         AUGUST,1986          **
8 REM*********************************
9 GOSUB54000:REM INITIALIZE VARIABLES/8082A
10 :
11 REM** FROM 11 TO 490 INCLUSIVE IS**
12 REM** THE DECLARATION SUBROUTINE **
20 OPEN 2,4
30 DIM DAT(30)
40 DIM AQ(30)
50 DIM SQ(30)
490 REM** FROM 500 TO 690 INCLUSIVE **
490 REM** IS THE INPUT SUBROUTINE   **
500 INPUT "DATE=";DT
510 INPUT "TIME= ";TI$
520 INPUT"PT-CHNL RANGE FOR A=";P1%,P2%
530 INPUT"PX-CHNL RANGE FOR A=";X1%,X2%
540 INPUT"NO. OF LVDT CHNL FOR A=";LA%
550 INPUT"PT-CHNL RANGE FOR B=";Q1%,Q2%
560 INPUT"PX-CHNL RANGE FOR B=";Y1%,Y2%
570 INPUT"NO. OF LVDT CHNL FOR B=";LB%
580 INPUT"INITIAL DIA.OF A (CM)=";A0
590 INPUT"INITIAL HT. OF A (CM)=";H1
600 INPUT"INITIAL DIA.OF B (CM)=";B0
610 INPUT"INITIAL HT. OF B (CM)=";H2
691 REM** FROM 700 TO 1090 INCLUSIVE **
692 REM** IS THE INITIAL PROXIMETER &**
693 REM** LVDT'S SCREENING SUBROUTINE**
700 FOR Y=X1% TO X2%
710 C=Y
720 G=0
730 GOSUB 50000
740 AQ(Y)=M
750 NEXT Y
760 C=LA%
770 G=0
780 GOSUB 50000
790 L1=M
800 FOR J=Y1% TO Y2%
810 C=J
820 G=0
830 GOSUB 50000
840 BQ(J)=M
850 NEXT J
860 C=LB%
870 G=0
880 GOSUB 50000
890 L2=M
900 PRINT"INITIAL RDG.FOR PXA1=";AQ(13)
910 PRINT#2,"INIT.RDG.FOR PXA1=";AQ(13)
920 PRINT"INITIAL RDG.FOR PXA2=";AQ(14)
930 PRINT#2,"INIT.RDG.FOR PXA2=";AQ(14)
940 PRINT"THE INITIAL LVDT-A RDG.=";L1
950 PRINT#2,"INIT.RDG.FOR LVDT-A=";L1
960 PRINT"INITIAL RDG.FOR PXB1=";BQ(19)
970 PRINT#2,"INIT.RDG.FOR PXB1=";BQ(19)
980 PRINT"INITIAL RDG.FOR PXB2=";BQ(20)
990 PRINT#2,"INIT.RDG.FOR PXB2=";BQ(20)
1000 PRINT"THE INITIAL LVDT-B RDG.=";L2
```

Figure A-1-2 Listing of The Program, R9-DH8082A for Data Processing

```
1010 PRINT#2,"INIT.RCG.FOR LVDT-B=";L2
1020 VA=((AD*0.5)↑2)*3.1416*H1
1030 PRINT"INIT.VOL.OF A (CM↑3)=";VA
1040 PRINT#2,"INIT.VOL.OF A(CM↑3)=";VA
1050 VB=((BD*0.5)↑2)*3.1416*H2
1060 PRINT"INIT.VOL.OF B (CM↑3)=",VB
1070 PRINT#2,"INIT.VOL.OF B (CM↑3)=";VB
1091 REM**FROM 1100 TO 1450 INCLUSIVE**
1092 REM**IS THE TIME SCREENING SUB- **
1093 REM**-ROUTINE                  **
1100 LET F=0
1105 LET B=0
1110 PRINT"TIME INTERVAL CHOICE:-"
1115 PRINT"   1---1 MIN. INTERVAL"
1120 PRINT"   2---10 MIN. INTERVAL"
1125 INPUT"TIME INTERVAL?";T%
1130 GOTO 1135
1135 IF T%=1 GOTO 1145
1140 IF T%=2 GOTO 1210
1145 GOTO 1150
1150 A=VAL(MID$(TI$,5,2))
1155 D=VAL(TI$)
1160 IF D=F GOTO 1175
1165 IF D=235959 THEN DT=DT+1
1170 LET F=D
1175 GET PS$
1180 IF PS$="S" THEN 1110
1185 IF A=B GOTO 1145
1190 IF A=INT(A/59)*59 GOTO 1500
1195 GET PS$
1200 IF PS$="S" THEN 1110
1205 GOTO 1145
1210 GOTO 1215
1215 A=VAL(MID$(TI$,3,2))
1220 D=VAL(TI$)
1225 IF D=F GOTO 1240
1230 IF D=235959 THEN DT=DT+1
1235 LET F=D
1240 GET PS$
1245 IF PS$="S" THEN 1110
1250 IF A=B GOTO 1210
1255 IF A=INT(A/10)*10 GOTO 1500
1260 GET PS$
1265 IF PS$="S" THEN 1110
1270 GOTO 1210
1451 REM** FROM 1500 TO 2490 INCLU-  **
1452 REM** SIVE IS THE CHANNEL SCREE-**
1453 REM** NING SUBROUTINE           **
1500 FOR X=P1% TO P2%
1510 C=X
1520 G=2
1530 GOSUB 50000
1540 DAT(X)=M
1550 NEXT X
1600 FOR Y=X1% TO X2%
1610 C=Y
1620 G=0
1630 GOSUB 50000
1640 DAT(Y)=M
1650 NEXT Y
1700 C=LA%
```

Figure A-1-2 (continued)

```
1710 G=9
1720 GOSUB 50000
1730 Z=M
1800 FOR I=Q1% TO Q2%
1810 C=I
1820 G=2
1830 GOSUB 50000
1840 DAT(I)=M
1850 NEXT I
1900 FOR J=Y1% TO Y2%
1910 C=J
1920 G=0
1930 GOSUB 50000
1940 DAT(J)=M
1950 NEXT J
2000 C=LB%
2010 G=0
2020 GOSUB 50000
2030 K=M
2491 REM** FROM 2500 TO 3390          **
2492 REM** INCLUSIVE IS THE DATA      **
2493 REM** REDUCTION & PRINTOUT       **
2494 REM** SUBROUTINE                 **
2500 PRINT"DATE=";DT;"TIME=";TI$
2510 PRINT#2,"DATE=";DT;"TIME=";TI$
2520 FOR X=P1% TO P2%
2530 IF X=10 GOTO 2560
2540 IF X=11 GOTO 2620
2550 IF X=12 GOTO 2680
2560 WA=(53586.96*DAT(X))-2.2375
2570 PRINT"CHNL#10=";DAT(X)
2580 PRINT#2,"CHNL#10=";DAT(X)
2590 PRINT"PWP OF CELL A(KPA)=";WA
2600 PRINT#2,"PWP OF CELL A(KPA)=";WA
2610 GOTO 2740
2620 AA=(54233.85*DAT(X))+5.8270
2630 PRINT"CHNL#11=";DAT(X)
2640 PRINT#2,"CHNL#11=";DAT(X)
2650 PRINT"PAP OF CELL A(KPA)=";AA
2660 PRINT#2,"PAP OF CELL A(KPA)=";AA
2670 GOTO 2740
2680 CA=(53970.28*DAT(X))-3.0049
2690 PRINT"CHNL#12=";DAT(X)
2700 PRINT#2,"CHNL#12=";DAT(X)
2710 PRINT"CELL P.OF CELL A(KPA)=";CA
2720 PRINT#2,"CELL P.OF A(KPA)=";CA
2730 GOTO 2740
2740 NEXT X
2800 FOR Y=X1% TO X2%
2810 IF Y=13 GOTO 2630
2820 IF Y=14 GOTO 2870
2830 PRINT"CHNL#13=";DAT(Y)
2840 PRINT#2,"CHNL#13=";DAT(Y)
2850 R1=(AQ(13)-DAT(13))*0.9714
2852 GOTO 2910
2870 PRINT"CHNL#14=";DAT(Y)
2880 PRINT#2,"CHNL#14=";DAT(Y)
2890 R2=(AQ(14)-DAT(14))*0.3571
2900 GOTO 2910
2910 NEXT Y
2920 AF=AD+((R1+R2)*0.1)
2930 PRINT"CHNL#15=";Z
2940 PRINT#2,"CHNL#15=";Z
2950 CH=(Z-L1)*1.5659
2960 HA=H1+(CH*0.1)
2970 V1=((AF*0.5)^2)*3.1416*HA
```

Figure A-1-2 (continued)

```
2980 V2=V1-VA
2990 PRINT"VOL.CHANGE IN A(CM13)=";V2
3000 PRINT#2,"VOL.CHG. IN A(CM13)=";V2
3010 FOR I=Q1% TO Q2%
3020 IF I=16 GOTO 3050
3030 IF I=17 GOTO 3110
3040 IF I=18 GOTO 3170
3050 WB=(53893.90*DAT(I))-3.7092
3060 PRINT"CHNL#16=";DAT(I)
3070 PRINT#2,"CHNL#16=";DAT(I)
3080 PRINT"PWP OF CELL B(KPA)=";WB
3090 PRINT#2,"PWP OF CELL B(KPA)=";WB
3100 GOTO 3220
3110 AB=(53853.78*DAT(I))+3.6021
3120 PRINT"CHNL#17=";DAT(I)
3130 PRINT#2,"CHNL#17=";DAT(I)
3140 PRINT"PAP OF CELL B(KPA)=";AB
3150 PRINT#2,"PAP OF CELL B(KPA)=";AB
3160 GOTO 3220
3170 CB=(53940.35*DAT(I))-14.2872
3180 PRINT"CHNL#18=";DAT(I)
3190 PRINT#2,"CHNL#18=";DAT(I)
3200 PRINT"CELL P.OF CELL B(KPA)=";CB
3210 PRINT#2,"CL.P.OF CELL B(KPA)=";CB
3220 GOTO 3230
3230 NEXT I
3300 FOR J=Y1% TO Y2%
3310 IF J=19 GOTO 3330
3320 IF J=20 GOTO 3370
3330 PRINT"CHNL#19=";DAT(J)
3340 PRINT#2,"CHNL#19=";DAT(J)
3350 S1=(BQ(19)-DAT(19))*2.5417
3360 GOTO 3400
3370 PRINT"CHNL#20=";DAT(J)
3380 PRINT#2,"CHNL#20=";DAT(J).
3390 S2=(BQ(20)-DAT(20))*2.6667
3400 GOTO 3410
3410 NEXT J
3420 BF=BD^((S1+S2)*0.1)
3430 PRINT"CHNL#21=";K
3440 PRINT#2,"CHNL#21=";K
3450 CH=(K-1.2)*1.5831
3460 HB=H2*(CH*0.1)
3470 V3=((BF*0.5)↑2)*3.1416*HB
3480 V4=V3-VB
3490 PRINT"VOL.CHANGE OF B(CM13)=";V4
3500 PRINT#2,"VOL.CHE.OF B(CM13)=";V4
3991 REM** FROM 4000 TO  49000          **
3992 REM** INCLUSIVE IS THE ROUND-UP    **
3993 REM** SUBROUTINE                   **
4000 LET B=A
4010 GET PS$
4020 IF PS$="S" THEN 1110
4030 GOTO 1130
49990 END
49997 !
49998 REM VOLTS
50000 POKEBA,(PEEK(BA)AND243):BF=0:GOSUB50101:M=VO/(G(G)*1000)
50010 RETURN
50098 !
50099 REM AUTOVOLTS
50100 G=-1
50110 G=G+1:GOSUB50000:IF(G=3)THEN50130
50120 IF(ABS(M)<(4.096/G(G+1)))THEN50110
50130 RETURN
50199 !
```

Figure A-1-2 (continued)

```
50198 REM AMPS
50200 BF=1:GOSUB55010:M=VO/(G(0)*R2*1000)
50210 RETURN
50298 :
50299 REM OHMS
50300 C=INT(C):RA=INT(RA)
50310 IF((C<0)OR(C>63))THENER=7:ER$="C":GOSUB54800:GOTO50370
50320 IF((RA<1)OR(RA>3))THENER=7:ER$="RA":GOSUB54800:GOTO50370
50330 POKEBA,((PEEK(BA)AND218)+4*RA):POKEBA+1,128+C:BF=2
50340 IF(RA=3)THENFORZZ=0TO400:NEXTZZ:REM TIMING LOOP
50350 GOSUB55010:M=FNB(VO*RA(RA)/2048):POKEBA+1,AZ%:POKEBA,(PEEK(BA)AND240)
50360 IF(M(0)THENER=6:GOSUB54800
50370 RETURN
50398 :
50399 REM AUTOOHMS
50400 RA=4
50410 RA=RA-1:GOSUB50300:IF(RA=1)THEN50430
50420 IF(MK=1.95*RA(RA-1))THEN50410
50430 RETURN
50598 :
50599 REM HERTZ
50600 M=0:Z1%=0:FP=1000825:C=INT(C):BF=3
50610 IF((C<0)OR(C>63))THENER=7:ER$="C":GOSUB54800:GOTO50680
50615 POKEBA+3,0:IF(PEEK(BA+3)<>0)THENER=1:GOSUB54800:GOTO50680
50620 POKEBA+2,191:POKEBA+3,255:POKEBA+1,(192ORC):POKEBA+11,(PEEK(BA+11)OR224
50630 POKEBA,(PEEK(BA)AND240):POKEBA+4,0:POKEBA+5,0:POKEBA+8,255
50640 POKEBA+9,255:POKEBA,PEEK(BA)OR32:ZZ=TI:ZX=65536*2^(Z1%+2)/FP*60
50650 IF((PEEK(BA+13)AND16)<>16)AND((TI-ZZ)<ZX)THEN50650
50660 IF((TI-ZZ)>ZX)OR((PEEK(BA+13)AND32)=32)THEN50690
50670 M=FNC(FP/(65536-256*PEEK(BA+9)-PEEK(BA+8)))/(2^Z1%+4))
50680 RETURN
50798 :
50799 REM LEVEL
50800 IF((C<0)OR(C>15))THENER=7:ER$="C":GOSUB54800:GOTO50820
50805 ZX=C:ZZ=16:IFZX>7THENZX=ZX-8:ZZ=16
50810 M=0:IF((PEEK(BA+ZZ)AND2^ZX)>0)THENM=1
50820 RETURN
50998 :
50999 REM THERMOCOUPLE
51000 GOSUB51200:G=3:VC=K0(TY)+RE*(K1(TY)+RE*(K2(TY)+RE*K3(TY))):GOSUB50000
51010 V=M*1000+VC:M=C0(TY)+V*(C1(TY)+V*(C2(TY)+V*C3(TY)))
51020 RETURN
51198 :
51199 REM REFTEMP
51200 ZZ=TI-RT:OC%=C:IFZZ<0THENZZ=ZZ+5184000
51210 IF((ZZ>RD)OR(RE=0))THENOG%=G:C=CR%:GOSUB51400:RE=M:RT=TI:C=OC%:G=OG%
51220 RETURN
51398 :
51399 PROC THERMISTOR
51400 RA=2:GOSUB50300:IF(MK=0)THENER=8:GOSUB54800:GOTO51420
51410 ZZ=LOG(M):M=1/(A0+ZZ*(A1+ZZ*(A2+ZZ*A3)))-273.15
51420 RETURN
51598 :
51599 REM AD590
51600 G=1:GOSUB50200:M=0.098*G(3)*M*:E6-269.44
51610 RETURN
53995 :
53996 REM INITIALIZATION
54000 BA=35840:REM 8082A BASE ADDRESS
54010 PRINT"....CHECKING 8082A REGISTERS"
54014 GOSUB54600:IF(ER=0)THEN54025
54016 PRINT"8082A REGISTERS FAILED:";ER$
54018 PRINT"(CHECK POWER/CABLES/SWITCHES/BASE ADDRESS)":STOP
54025 GOSUB 54710
54030 :
54035 REM.....8082A PARAMETERS - SERIAL NUMBER : ######.....
```

Figure A-1-2 (continued)

```
54037 PRINT".....INITIALIZING 8052A CONSTANTS"
54040 AZ%=0   :REM SHORTED CHANNEL (AUTO ZERO)
54042 CR%=1   :REM REFERENCE TEMP CHANNEL
54044 VR=2049:REM 8052A REFERENCE VOLTAGE VALUE (MV)
54046 RT=1000:REM REF TEMP UPDATE FREQUENCY IN 1/60'S OF A SEC
54048 ZT=1000:REM AUTOZERO UPDATE FREQUENCY IN 1/60'S OF A SEC
54050 G(0)=1.000:G(1)=10.027:G(2)=100.024:G(3)=503.321
54052 RA(1)=1000:RA(2)=10000:RA(3)=65.1000:R2=1000
54053 :
54054 REM.....FUNCTIONS
54056 BF$(0)="VOLTS":BF$(1)="AMPS":BF$(2)="OHMS":BF$(3)="HERTZ"
54058 :
54060 REM.....ERROR MESSAGES
54065 DIM ER$(7)
54070 ER$(0)="NO ERRORS DETECTED"
54071 ER$(1)="VIA INOPERATIVE"
54072 ER$(2)="A/D CONVERTER INOPERATIVE"
54073 ER$(3)="SIGNAL OUT OF RANGE"
54074 ER$(4)="A/D CONVERTER TIMED OUT"
54075 ER$(5)="A/D DIGITAL READ PROBLEM"
54076 ER$(6)="RESISTANCE < 0 ERROR"
54077 ER$(7)="BAD CHANNEL OR RANGE PARAMETER"
54080 :
54100 REM.....ROUNDOFF FUNCTION DEFINITIONS
54110 DEFFNA(X)=INT(X+.5):DEFFNB(X)=INT(10*X+.5)/10
54112 DEFFNC(X)=INT(100*X+.5)/100:DEFFND(X)=INT(1000*X+.5)/1000
54120 :
54130 REM.....TRANSDUCER EQUATION COEFFICIENTS
54133 REM...YSI 44005 THERMISTOR
54135 A0=1.403E-3:A1=2.373E-4:A2=-3.168E-8:A3=1.006E-7
54140 REM...THERMOCOUPLES--V=F(T) K'S; FOR T=F(V) C'S; TY=TYPE
54145 REM...TYPE T THERMOCOUPLES  (TY=0)
54150 K0(0)=-0.00119:K1(0)=0.038613:K2(0)=4.3656E-5:K3(0)=-2.0671E-8
54155 C0(0)=-.0099:C1(0)=25.6827:C2(0)=-.69646:C3(0)=.02613
54160 REM...TYPE E THERMOCOUPLES  (TY=1)
54165 K0(1)=2.5577E-4:K1(1)=.05853:K2(1)=4.9214E-5:K3(1)=-3.0384E-6
54170 C0(1)=-0.02636:C1(1)=17.07666:C2(1)=-.23092:C3(1)=.00538
54175 REM...TYPE J THERMOCOUPLES  (TY=2)
54180 K0(2)=8.39345E-4:K1(2)=.05037:K2(2)=2.85715E-5:K3(2)=-5.7363E-8
54185 C0(2)=-.031617:C1(2)=19.84918:C2(2)=-.21026:C3(2)=8.96989E-3
54190 RETURN
54195 :
54597 REM REG-TEST
54600 EZ$="":ZZ=BA+2:ER$="DDB ":GOSUB54650:ZZ=BA+3:ER$="DDA ":GOSUB54650
54605 POKEBA+2,255:POKEBA+3,255
54610 ZZ=BA+11:ER$="ACR ":GOSUB54650:ZZ=BA+12:ER$="PCR ":GOSUB54650
54615 POKEBA+11,0:POKEBA+12,0
54620 ZZ=BA:ER$="PB ":GOSUB54650.ZZ=BA+1:ER$="PA ":GOSUB54650
54625 ER$=EZ$:IFER=0THENER$=""
54630 RETURN
54637 :
54640 REM BITLOOP
54650 FOREX=0TO7:ZX=2^EX:POKEZZ,ZX:IF(PEEK(ZZ)<>ZX)THENEZ$=EZ$+ER$:ER=1:EX=8
54655 NEXTEX:RETURN
54695 :
54700 REM VIA-INIT
54710 POKEBA+2,0:POKEBA+3,0:POKEBA+11,0:POKEBA+12,204:POKEBA+14,128
54720 POKEBA+2,191:POKEBA+3,255
54730 RETURN
```

Figure A-1-2 (continued)

```
54797 :
54798 REM ERROR
54800 IFER=0THEN54950
54910 IFER=1THENFORZ=1TO3:GOSUB54710:NEXTZ:
54930 M=-9999:E2$=BF$(BF)+" ":ZX=(PEEK(BA+1)AND192)/64
54940 IF(ZX<>BF)THENE2$=E2$+" (ACTUALLY:"+BF$(ZX)+") "
54950 ER$=E2$+ER$(ER)+ER$+" (CH="+STR$(PEEK(BA+1)AND63)+") TIME:"+TI$
54960 PRINTER$:ER$="":ER=0
54970 RETURN
54997 :
54999 REM ATOD1
55010 ER=0:POKEBA+12,204:C=INT(C):G=INT(G):BF=INT(BF)
55020 IF((BF<0)OR(BF>2))THENER=7:ER$="BF":GOSUB54800:GOTO55100
55030 IF((C<0)OR(C>63))THENER=7:ER$="C":GOSUB54800:GOTO55100
55035 IF((G<0)OR(G>3))THENER=7:ER$="G":GOSUB54800:GOTO55100
55040 ZZ=TI-ZL:IF((ZZ<ZT)OR(BF=2))THEN55070
55050 OG%=0:POKEBA+1,AZ%:FORG=0TO3:POKEBA,((PEEK(BA)AND240)+G)
55060 GOSUB 55510:AZ(G)=VO:NEXTG:G=OG%:ZL=TI
55070 POKEBA+1,(64*BF+C):IF(ER<>0)THEN55100
55080 IF(BF=2)THENPOKEBA,(PEEK(BA)AND252):GOSUB55510:GOTO55100
55090 POKEBA,(((PEEK(BA))AND240)+G):GOSUB55510:VO=VO-AZ(G)
55100 POKEBA+1,AZ%:RETURN
55250 :
55500 REM ATOD2
55510 IF(PEEK(BA+12)<>204)THENER=1:GOSUB 54800:GOTO55610
55520 POKEBA+12,206:POKEBA+12,204
55530 ZZ=TI+15:IFZZ>5184000THENZZ=ZZ-5184000
55540 IF((TI<=ZZ)AND(PEEK(BA+13)AND2)<>2)THEN55540
55550 IF(TI>ZZ)THENER=4:GOSUB 54800:GOTO55610
55560 VL%=PEEK(BA+16):VH%=PEEK(BA+17)
55570 IF((VL%<>PEEK(BA+16))OR(VH%<>PEEK(BA+17)))THENER=5:GOSUB 54800:GOTO55610
55580 IF((VH%AND16)=16)THENER=3:GOSUB 54800:GOTO55610
55590 VO=256*(VH%AND15)+VL%:IF(VH%AND32)=0THENVO=-VO
55600 ZZ=PEEK(BA+1):IF((PEEK(BA+13)AND2)=2)THENER=2:GOSUB 54800
55610 RETURN
```

Figure A-1-2 (continued)

APPENDIX B

B-1) Equipment Preparation for The Null Pressure Plate Tests

B-2a) Equipment Preparation for The Suction Tests

B-2b) Estimation of Equalization Time for Suction Tests

B-3) Equipment Preparation for The One-Dimensional Constant Volume Loading and Unloading Tests

B-4) Equipment Preparation for The One-Dimensional Free Swell Tests

B-5) Equipment Preparation for The Isotropic Free Swell and Constant Volume Loading and Unloading Tests

APPENDIX B-1 Equipment Preparation for The Null Pressure Plate Tests

The high air entry disc installed at the base pedestal of the pressure plate apparatus was saturated. The saturated permeability of the disc was measured and compared to published value. The comparison was used to reveal the presence of cracks in the disc. The procedure is briefly described as follows.

a) The chamber of the pressure plate was filled with deaired water.

b) The water inside the chamber was subjected to a pressure of 550 kPa (i.e. 80 psi). Water was allowed to flow through the high air entry disc. The volume of water passing through was monitored to check the saturated coefficient of permeability of the disc. A back pressure of 70 kPa (i.e. 10 psi) was applied during the process which continued for several hours.

c) Diffused air collected underneath the disc was flushed out through the flush-port by the applied back pressure.

d) The values at the base of the pressure plate was closed for about an hour. During which time, water underneath the disc was under a pressure of 480 kPa (i.e. 70 psi) which would dissolve any air within the disc.

e) Water was then allowed to flow through the disc for

about 10 minutes.

f) The basal compartment underneath the disc was flushed again.

g) Procedure from (b) onward was repeated for at least six times to ensure the high air entry disc was saturated.

Suggested saturated coefficients of permeability for ceramic discs of different high air entry values are presented in Table B(1).1 (Fredlund, 1973). Table B(1).2 presents the results of one permeability check on the 15 bar high air entry disc of the pressure plate apparatus used for the null pressure plate tests.

A double burette volume charge indicator was used to measure the water volume change. The unit was checked for leakage by a procedure described as follows.

a) A back pressure of 345 kPa (i.e., 50 psi) was applied to the double burette volume change indicator unit. Volume change readings were taken every few hours for two days or more.

b) The flow direction valves of the unit were reversed and the check repeated. Fredlund (1973) suggested that the recorded volume change "should not be more than a few hundredths of a cubic centimetre over a two day period". Table B(1).3 presents the results of the leakage check on the double burette volume change indicator used for the pressure plate apparatus.

Valves attached to the base plate of the pressure

Table B(1).1 Physical Properties of The High Air Entry Discs[a] (Fredlund, 1973)

Air Entry Value (bars)	Air Entry Value (kPa)	Porosity (%)	Saturated Permeability (cm/sec)	Bubbling Pressure (kPa)
3	304	36	1.73×10^{-7}	> 317
5	507	34	1.21×10^{-7}	> 552
15	1520	32	2.60×10^{-9}	> 1517

Note: a) The high air entry ceramic discs used in this thesis are manufactured by Soilmoisture Equipment Corporation, Santa Barbara, California

Table B(1).2 Test Results of The Permeability Check for The Pressure Plate Apparatus

Chamber pressure : 550 kPa (i.e., 80 psi)

Back Pressure : 69 kPa (i.e., 10 psi)

Diameter of the 1520 kPa (i.e., 15 bar) high air entry disc : 6.23 cm

Thickness of the 1520 kpa (i.e., 15 bar) high air entry disc : 0.635 cm

Elpsed Time (min.)	Vw[a] (cm^3)	Measured q[b] (cm^3/sec)	Measured k_{sat}[c] (cm/sec)
34	2.05	0.0010050	4.25×10^{-9}
43	2.05	0.0007945	3.36×10^{-9}
63	3.00	0.0007936	3.36×10^{-9}
79	3.25	0.0006856	2.90×10^{-9}
93	4.10	0.0007347	3.11×10^{-9}
123	5.70	0.0007723	3.27×10^{-9}
164	7.85	0.0007977	3.38×10^{-9}
342	15.80	0.0007699	3.26×10^{-9}

Note: a) Vw = volume of water passed through
b) q = measured flow rate
c) k_{sat} = measured saturated coefficient of permeability

Table B(1).3 Test Results of The Leakage Check for The Double Burette Volume Change Indicator, VCI unit #3

Double burette volume change indicator, VCI : unit #3

Capacity of the unit : 25 cm^3

Back pressure : 345 kPa (i.e., 50 psi)

Elpsed time (days)	Direction of the Flow Valves	Measured Volume Change, (cm^3)
2	<---	0.00
3	--->	0.00
1	<---	0.40
2	--->	1.25

* Replaced all the O-rings and the base block of the double burette volume change indicator (unit #3)

2	<---	0.00
7	--->	0.00

plate apparatus were checked for leakage. The test procedure is as follows.

a) The chamber was filled with de-aired water.

b) The double burette volume change indicator was connected to the outlet of each valve.

c) A back pressure of 69 kPa (i.e., 10 psi) was applied to the volume change indicator while the chamber pressure was kept at 550 kPa (i.e., 80 psi).

d) The volume change indicator was monitored for leakage for a one day period.

APPENDIX B-2a Equipment Preparation for The Suction Tests

A 30.48 cm diameter 507 kPa (i.e., 5 bar) high air entry disc was placed at the top compartment of the multi-layered pressure plate apparatus. Prior to running the test, the disc was saturated. The saturated permeability of the disc was measured (Table B(2).1) and compared to published value (Table B(1).1) to check for cracks in the disc. The procedures are as follows.

a) A film of distilled de-aired water (approximate 300 cm^3) was left on the surface of the high air entry disc.

b) A chamber pressure of 138 kPa (i.e., 20 psi) was applied.

c) Water passed through the disc over a 15 minute time period was collected and measured.

d) Steps (a) to (c) were repeated 6 times to ensure the high air entry disc was saturated.

The pressure membrane apparatus was checked for leakage before it was used. The procedures are as follows.

a) A cellulose membrane with a high air entry value of 1520 kPa (i.e., 15 bar) was thoroughly soaked in de-aired distilled water.

b) The cellulose membrane was placed inside the pressure membrane apparatus.

c) An air pressure of 1520 kPa (i.e., 15 bar) was applied

Table B(2).1 Test Results of The Permeability Check for The Multi-Layered Pressure Plate Apparatus

Chamber pressure : 138 kPa (i.e., 20 psi)

Diameter of the 507 kPa (i.e., 5 bar) high air entry disc : 30.48 cm

Thickness of the 507 kpa (i.e., 5 bar) high air entry disc : 0.635 cm

Elpsed Time (min.)	Vw[a] (cm^3)	Measured q[b] (cm^3/sec)	Measured k_{sat}[c] (cm/sec)
15	160	0.1777	1.10×10^{-7}
15	263	0.2924	1.81×10^{-7}
15	270	0.2989	1.85×10^{-7}
15	266	0.2956	1.83×10^{-7}
15	267	0.2972	1.84×10^{-7}
15	276	0.3069	1.90×10^{-7}

Note: a) Vw = volume of water passed through
b) q = measured flow rate
c) k_{sat} = measured saturated coefficient of permeability

to the chamber for approximately 4 hours. Air leakage through the membrane to the bottom exit of the apparatus was checked.

APPENDIX B-2b Estimation of the Equalization Time for Suction Tests

The 500 kPa high air entry disc of the pressure plate apparatus impedes water drainage from the soil specimens after each matric suction increment. The equalization time required for 90% of pore-water pressure dissipation within the specimens was estimated according to the theoretical model presented by Ho and Fredlund (1982).

$$t_q = \frac{h^2}{n\, c_v^w (1-U_f)} \qquad \text{(B1)}$$

where

t_f = equalization time required

h = thickness of the specimen

U_f = average degree of dissipation of the induced pore-water pressure

c_v^w = coefficient of consolidation with respect to the water phase $\frac{K_w}{\gamma_w m_2^w}$ Gardner (1958) equation $K_w = \frac{K_{sat}}{1 + \left(\frac{\psi}{a}\right)^n}$

$n = \frac{0.75}{(1 + 3/\lambda)}$ for one way drainage

$\lambda = \frac{k_d\, h}{k_w\, h_d}$

k_d = coefficient of permeability of the high air entry disc

k_w = coefficient of permeability of the specimen with respect to the water phase

h_d = thickness of the high air entry disc

Table B(2).2 summarizes the input data for the estimation of the equalization time. Saturated soil parameters available at the time of preparing for the suction tests were used in

Table B(2).2 Input data for the Estimation of The Equalization Time Required Between Matric suction Changes for Suction Tests

Soil Type	h (cm)	U_f	C_v^w (cm^2/sec)	k_d (cm/sec)	k_v (cm/sec)	h_d (cm)	λ	n	t_f (hour)
silt	1.70	0.9	53.8[a]	1.21×10^{-7}	1×10^{-3}[b]	0.635	3.24×10^{-4}	8.1×10^{-5}	1.84
till	1.70	0.9	5×10^{-4}[a]	1.21×10^{-7}	8×10^{-9}[b]	0.635	40.5	0.698	22.9

Note: a) Averaged saturated coefficient of consolidation from one-dimensional consolidation tests on specimens at dry of optimum initial water contents

b) Averaged saturated coefficient of permeability obtained from one-dimensional consolidation tests on specimens at dry of optimum initial water contents

the calculations. The amount of equalization time required between matric suction changes was estimated to be 1.84 and 22.9 hours for 1.70 cm thick silt and glacial till specimens respectively. A 48 hour equalization period was used to account for the uncertainties of the soil parameters used in the estimation. Part way through the suction tests, the specimen thickness was further reduced to 1.0 cm to reduce the equalization time needed.

The same 48 hour equalization period was used when the specimens were placed inside the pressure membrane apparatus. The readiness of the cellulose membrane to allow water flow provided free drainage to the specimens. The 48 hour equalization time was therefore considered to be adequate.

APPENDIX B-3 Equipment Preparation for The One-Dimensional Constant Volume Loading and Unloading Tests

Three Conbel pneumatic oedometers were used to perform the one-dimensional constant volume loading and unloading tests. The pressure gauges on each oedometer were calibrated against proving rings for accuracy. The compressibility of each apparatus was determined by proceeding through the loading and unloading cycles with a stainless steel plug in the consolidometer pot. Two cycles were run on each apparatus to check the reproducibility of compression of the apparatus. There is little variation between cycles for each apparatus. Figure B-3-1, B-3-2 and B-3-3 present the average compressibility curves for the three oedometers used in the test program. the compressibility of the apparatus was subtracted form the measured compression of the specimen in the data analysis.

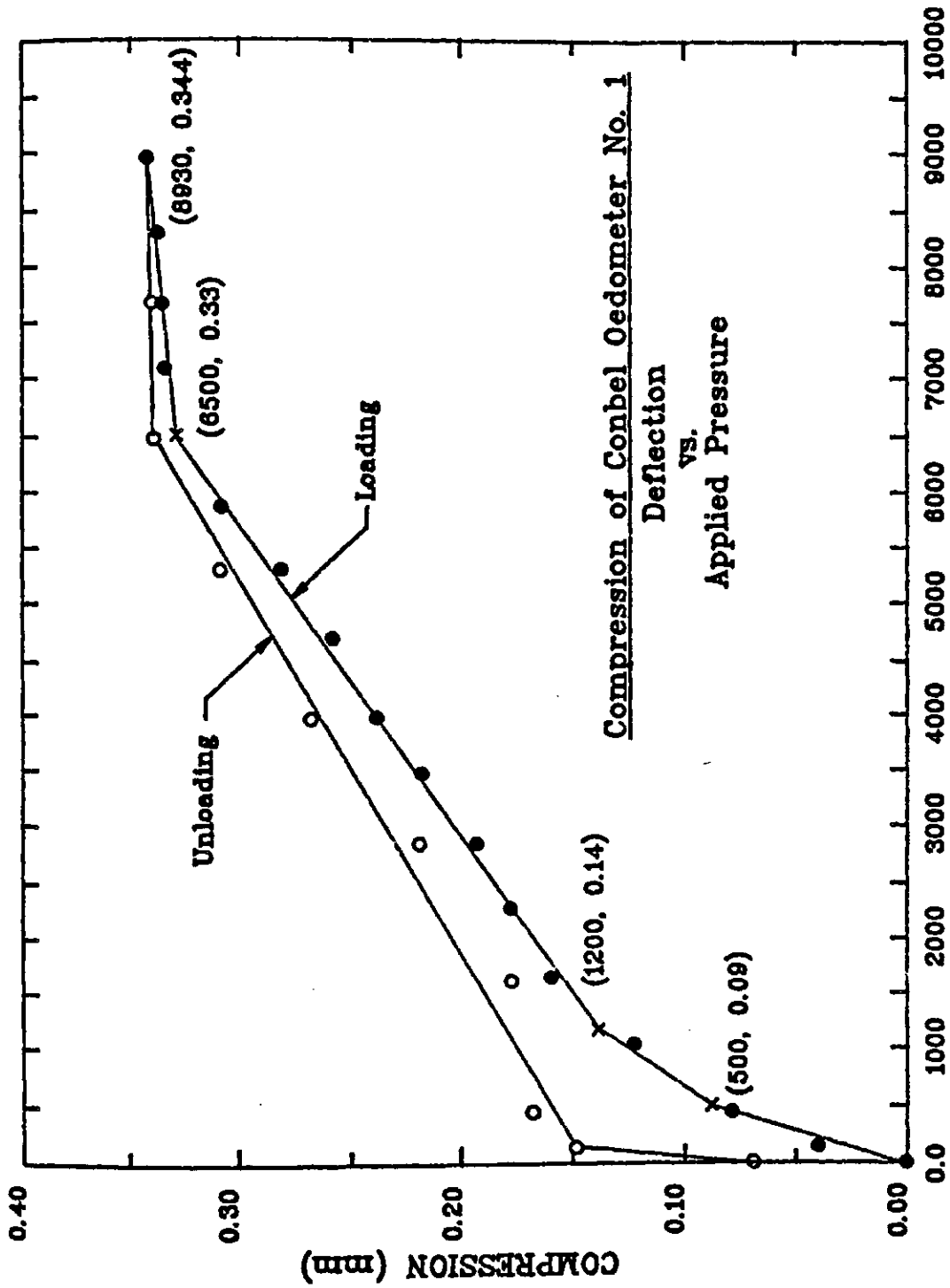

Figure B-3-1 Compressibility Curve for The Conbel Pneumatic Oedometer Number one

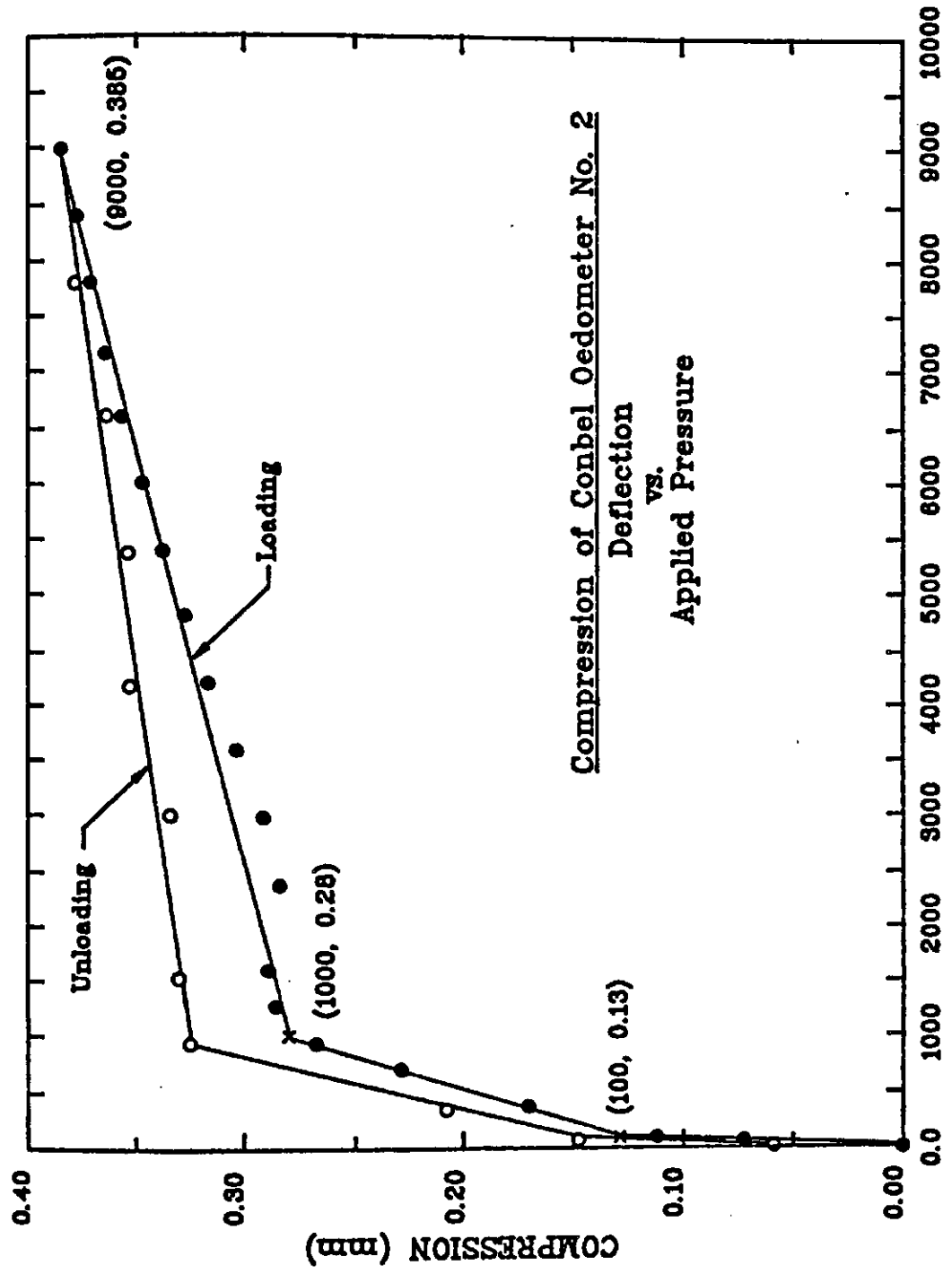

Figure B-3-2 Compressibility Curve for The Conbel Pneumatic Oedometer Number Two

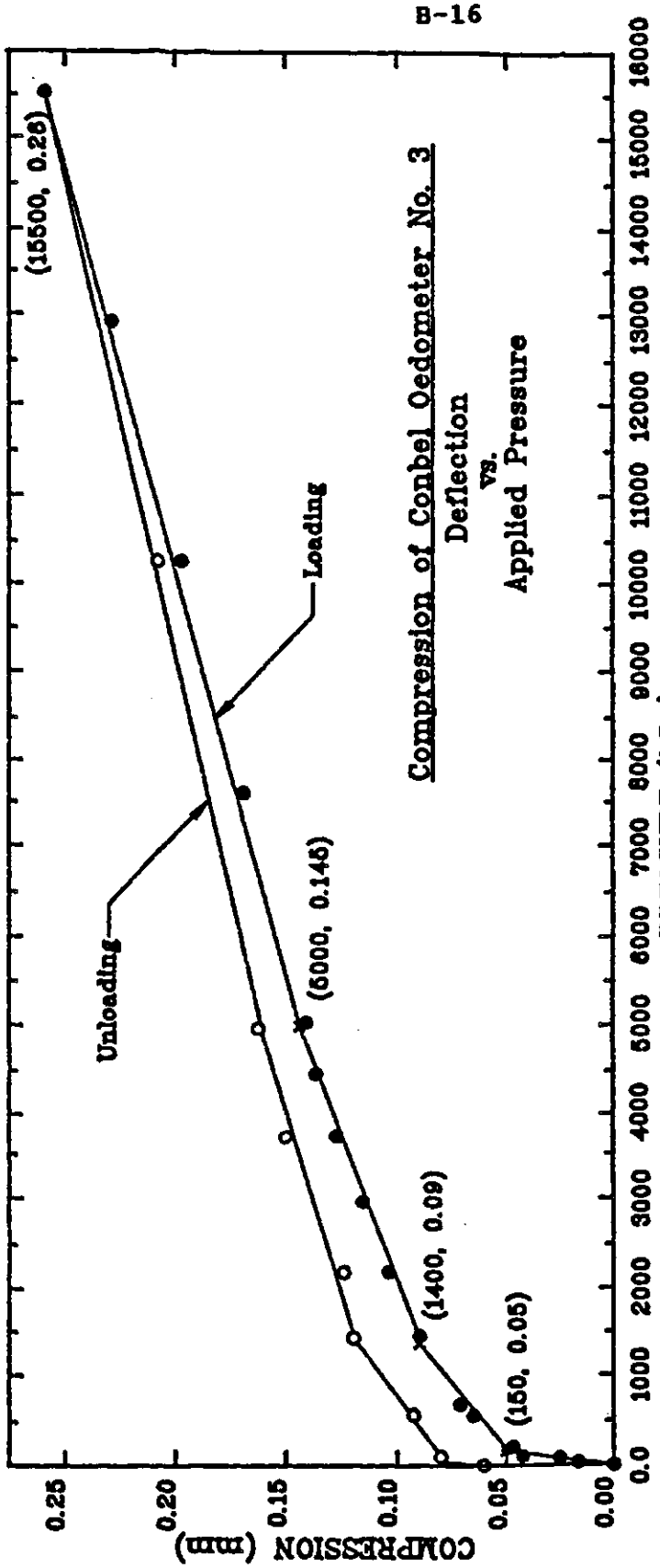

Figure B-3-3 Compressibility Curve for The Conbel Pneumatic Oedometer Number Three

APPENDIX B-4 Equipment Preparation for The One-Dimensional Free Swell Tests

Two modified Anteus consolidometers were used to perform the one-dimensional free swell tests. The high air entry disc installed at the base pedestal of each modified Anteus consolidometer was saturated prior to being used. The saturated permeability of the disc was measured and compared to published value (see Table B(1).1). the comparison was used to reveal the presence of cracks in the disc. The procedure for the permeability check is similar to that described in Appendix B-1. A summary of the results of the permeability checks for the modified Anteus consolidometers is presented in Table B(4).1 and B(4).2. The measured saturated coefficients permeability of both high air entry discs are an order of magnitude larger than the published value for a 1520 kPa (i.e, 15 bar) high air entry disc. The manufacturer of the high air entry disks suggested the saturated permeability of the disks may vary from one batch of products to another. The high air entry disc was installed to separately control the air and water pressure within a specimen. In the test program, the maximum air water pressure differential applied to a specimen was approximately equal to 600 kPa. Each saturated high air entry disc was subjected to an air-water pressure differential of 690 kPa for twenty-four hours. No sign of

Table B(4).1 Test Results of The Permeability Check for The Modified Anteus Consolidometer Unit No. 1

Chamber pressure : 413.7 kPa (i.e., 60 psi)

Back Pressure : 69 kPa (i.e., 10 psi)

Diameter of the 1520 kPa (i.e., 15 bar) high air entry disc : 6.35 cm

Thickness of the 1520 kpa (i.e., 15 bar) high air entry disc : 0.635 cm

Elpsed Time (min.)	V_w[a] (cm^3)	Measured q[b] (cm^3/sec)	Measured k_{sat}[c] (cm/sec)
11	2.10	0.003182	1.82×10^{-8}
30	6.45	0.003583	2.04×10^{-8}
60	13.31	0.003698	2.11×10^{-8}
120	26.50	0.003681	2.10×10^{-8}
240	54.26	0.003768	2.15×10^{-8}
360	80.26	0.003716	2.12×10^{-8}

Note: a) V_w = volume of water passed through
b) q^w = measured flow rate
c) k_{sat} = measured saturated coefficient of permeability

Table B(4).2 Test Results of The Permeability Check for The Modified Anteus Consolidometer Unit No. 2

Chamber pressure : 413.7 kPa (i.e., 60 psi)

Back Pressure : 69 kPa (i.e., 10 psi)

Diameter of the 1520 kPa (i.e., 15 bar) high air entry disc : 6.35 cm

Thickness of the 1520 kpa (i.e., 15 bar) high air entry disc : 0.635 cm

Elpsed Time (min.)	V_w[a] (cm^3)	Measured q[b] (cm^3/sec)	Measured k_{sat}[c] (cm/sec)
8	3.60	0.007500	4.28×10^{-8}
19	8.13	0.007132	4.07×10^{-8}
60	25.81	0.007168	4.09×10^{-8}
120	52.12	0.007239	4.13×10^{-8}
240	103.73	0.007203	4.11×10^{-8}
360	155.22	0.007186	4.10×10^{-8}

Note: a) V_w = volume of water passed through
b) q_w = measured flow rate
c) k_{sat} = measured saturated coefficient of permeability

air leaking through the disc was detected. The disks were therefore assumed to be functionally capable.

A double burette volume change indicator was used to measure the water volume change in the specimen during the test. The two double burette volume change indicators used for the two modified Anteus consolidometer units were checked for leakage prior to performing the tests. The procedure used was previously described in Appendix B-1. A summary of the results of the leakage checks for the double burette volume change indicators is presented in Table B(4).3 and B(4).4.

Valves attached to the based plate of each modified Anteus consolidometer unit were checked for leakage prior to being used. The test procedure was described in Appendix B-1.

Table B(4).3 Test Results of The Leakage Check for The Double Burette Volume Change Indicator, VCI unit #1

Double burette volume change indicator, VCI : unit #1
Capacity of the unit : 10 cm^3
Back pressure : 345 kPa (i.e., 50 psi)

Elpsed time (days)	Direction of the Flow Valves	Measured Volume Change (cm^3)
1	<---	0.00
2	<---	0.01
3	--->	0.00
4	--->	0.01
5	<---	0.00
6	--->	0.00

Table B(4).4 Test Results of The Leakage Check for The Double Burette Volume Change Indicator, VCI unit #2

Double burette volume change indicator, VCI : unit #2
Capacity of the unit : 10 cm^3
Back pressure : 345 kPa (i.e., 50 psi)

Elpsed time (days)	Direction of the Flow Valves	Measured Volume Change (cm^3)
1	<---	0.00
2	<---	0.02
3	--->	0.00
4	--->	0.00
5	<---	0.00
6	<---	0.01
7	--->	0.00
8	--->	0.00

APPENDIX B-5 Equipment Preparation for The Isotropic Free Swell and Constant Volume Loading and Unloading Tests

Two stress controlled isotropic cells were used to perform the isotropic free swell and constant volume loading and unloading tests. The compressibility of each apparatus was determined by proceeding through the loading and unloading cycles with a stainless steel plug in place of a soil specimen. The volume change was measured by a combination of radial and vertical deformation measurements. Radial deformation measurements were made by using a "None-Contacting Displacement Measuring System" described in section 4.3.2. The vertical deformation was measured by a linear variable differential transformer (i.e., LVDT). Two cycles were run on each apparatus to check the reproducibility of compression of the apparatus. There is little variation between cycles for each apparatus. Figure B-5-1 presents the average compressibility curves for the two stress controlled isotropic cells used in the test program. The compressibility of the apparatus was subtracted from the measured compression of the specimen in the data analysis.

The high air entry disc installed at the base pedestal of each stress controlled isotropic cell was saturated prior to being used. The saturated permeability

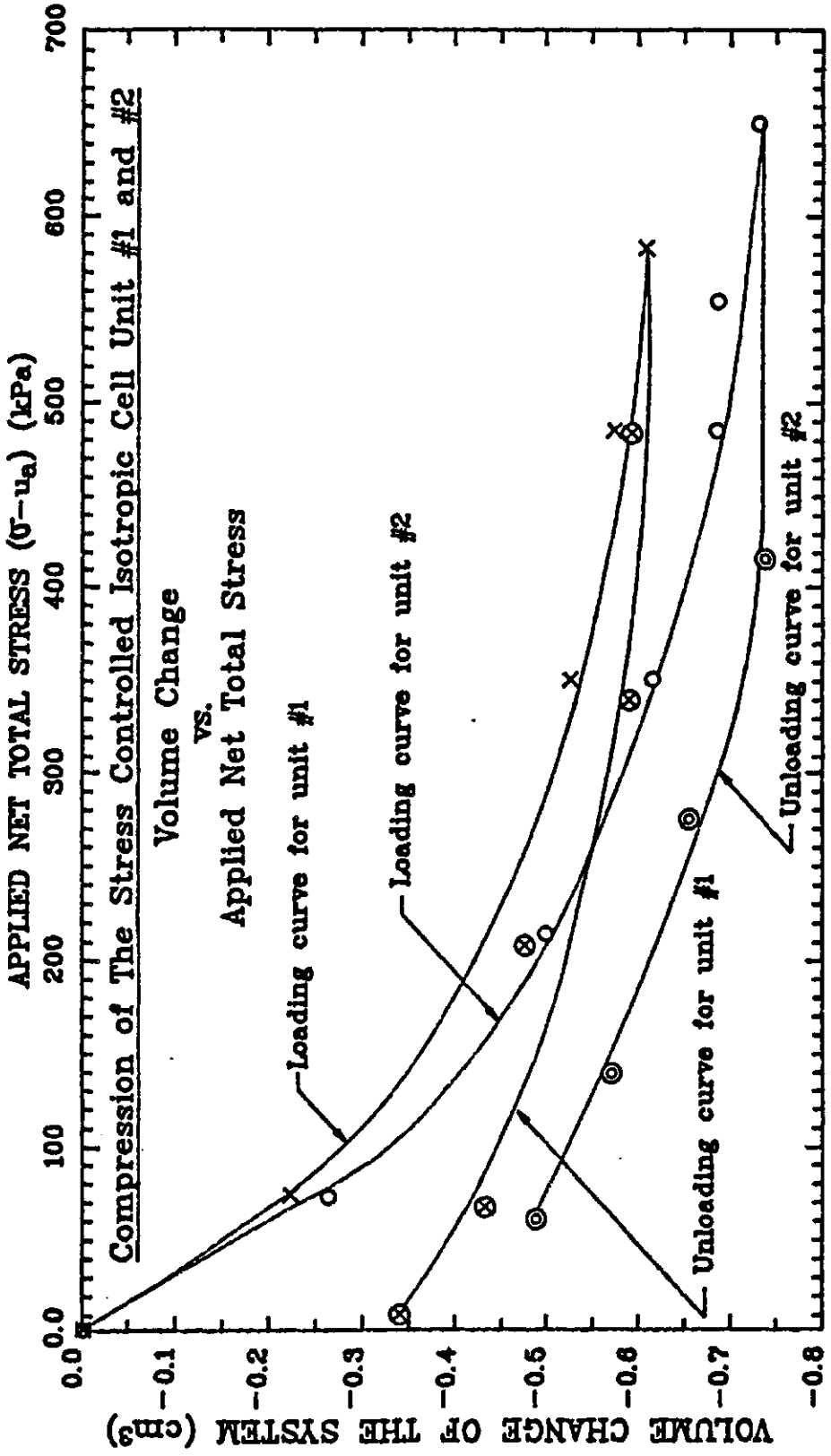

Figure B-5-1 Average Compressibility Curves for The Stress Controlled Isotropic Cell Unit Number One and Number Two

of the disc was measured and compared to published value (see Table B(1).1). The comparison was used to detect the presence of cracks in the disc. The procedure of the permeability check is similar to that described in Appendix B-1. A summary of the results of the permeability checks for the stress controlled isotropic cells is presented in Table B(5).1 and B(5).2.

Two double burette volume change indicators were used in conjunction with the stress controlled isotropic cells to measure the water volume change in the specimens during the tests. These double burette volume change indicators were checked for leakage prior to being used. The same two double burette volume change indicators were used for the modified Anteus consolidometers and the stress controlled isotropic cells. The procedure and results of the leakage checks for these volume change indicators were presented previously in Appendix B-4.

Valves attached to the base plate of each stress controlled isotropic cell were checked for leakage prior to performing the tests. The test procedure was similar to that described in Appendix B-1. all faulty valves were either repaired or replaced prior to the tests.

Table B(5).1 Test Results of The Permeability Check for The Stress Controlled Isotropic Cell Unit No. 1

Chamber pressure : 551.6 kPa (i.e., 80 psi)

Back Pressure : 69 kPa (i.e., 10 psi)

Diameter of the 1520 kPa (i.e., 15 bar) high air entry disc : 10.16 cm

Thickness of the 1520 kpa (i.e., 15 bar) high air entry disc : 0.635 cm

Elpsed Time (min.)	V_w[a] (cm^3)	Measured q[b] (cm^3/sec)	Measured k_{sat}[c] (cm/sec)
11	2.39	0.003621	5.76×10^{-9}
30	6.22	0.003455	5.50×10^{-9}
60	12.32	0.003423	5.45×10^{-9}
120	25.33	0.003518	5.60×10^{-9}
240	49.48	0.003436	5.47×10^{-9}
360	74.62	0.003455	5.50×10^{-9}

Note: a) V_w = volume of water passed through
b) q^w = measured flow rate
c) k_{sat} = measured saturated coefficient of permeability

Table B(5).2 Test Results for The Permeability Check on The Stress Controlled Isotropic Cell Unit No. 2

Chamber pressure : 344.8 kPa (i.e., 50 psi)

Back Pressure : 69 kPa (i.e., 10 psi)

Diameter of the 507 kPa (i.e., 5 bar) high air entry disc : 10.16 cm

Thickness of the 507 kpa (i.e., 5 bar) high air entry disc : 0.635 cm

Elpsed Time (min.)	V_w[a] (cm^3)	Measured q[b] (cm^3/sec)	Measured k_{sat}[c] (cm/sec)
1	3.55	0.05917	1.70×10^{-7}
15	53.95	0.05994	1.67×10^{-7}
30	109.19	0.06066	1.69×10^{-7}
60	220.97	0.06138	1.71×10^{-7}
120	434.18	0.06030	1.68×10^{-7}
	* restart the test *		
2	7.10	0.05917	1.65×10^{-7}
120	436.77	0.06066	1.69×10^{-7}

Note: a) V_w = volume of water passed through
b) q^w = measured flow rate
c) k_{sat} = measured saturated coefficient of permeability